

# Coastal Eye: Monitoring Coastal Environments Using Lightweight Drones

Submitted by James P. Duffy

to the University of Exeter as a thesis for the degree of

Doctor of Philosophy in Physical Geography

in November 2018



This thesis is available for library use on the understanding that it is copyright material and that no quotation from the thesis may be published without proper acknowledgement.

I certify that all material in this thesis which is not my own work has been identified and that no material has previously been submitted and approved for the award of a degree by this or any other University.

Signature: .....



## Abstract

Monitoring coastal environments is a challenging task. This is because of both the logistical demands involved with *in-situ* data collection and the dynamic nature of the coastal zone, where multiple processes operate over varying spatial and temporal scales. Remote sensing products derived from spaceborne and airborne platforms have proven highly useful in the monitoring of coastal ecosystems, but often they fail to capture fine scale processes and there remains a lack of cost-effective and flexible methods for coastal monitoring at these scales. Proximal sensing technology such as lightweight drones and kites has greatly improved the ability to capture fine spatial resolution data at user-dictated visit times. These approaches are democratising, allowing researchers and managers to collect data in locations and at defined times themselves. In this thesis I develop our scientific understanding of the application of proximal sensing within coastal environments. The two critical review pieces consolidate disparate information on the application of kites as a proximal sensing platform, and the often overlooked hurdles of conducting drone operations in challenging environments. The empirical work presented then tests the use of this technology in three different coastal environments spanning the land-sea interface. Firstly, I use kite aerial photography and uncertainty-assessed structure-from-motion multi-view stereo (SfM-MVS) processing to track changes in coastal dunes over time. I report that sub-decimetre changes (both erosion and accretion) can be detected with this methodology. Secondly, I used lightweight drones to capture fine spatial resolution optical data of intertidal seagrass meadows. I found that estimations of plant cover were more similar to *in-situ* measures in sparsely populated than densely populated meadows. Lastly, I developed a novel technique utilising lightweight drones and SfM-MVS to measure benthic structural complexity in tropical coral reefs. I found that structural complexity measures were obtainable from SfM-MVS derived point clouds, but that the technique was influenced by glint type artefacts in the image data. Collectively, this work advances the knowledge of proximal sensing in the coastal zone, identifying both the strengths and weaknesses of its application across several ecosystems.

# Contents

Abstract .....	3
List of figures .....	11
List of tables .....	23
Declaration of authorship.....	25
Acknowledgements .....	26
Table of abbreviations .....	28
1 Introduction.....	29
1.1 The global importance of coastal environments .....	29
1.2 The challenges of coastal monitoring .....	30
1.3 Remote sensing of coastal environments.....	32
1.3.1 Satellite platforms .....	32
1.3.2 Airborne platforms .....	33
1.3.3 Terrestrial <i>in-situ</i> sensing .....	34
1.3.4 Issues and drawbacks with remote sensing methods.....	36
1.4 The rise of drone technology .....	39
1.5 How are drones being used at the coast? .....	41
1.6 Kite-based proximal sensing at the coast.....	45
1.7 The land-sea interface explored in this thesis .....	46
1.8 Coastal dunes .....	48
1.8.1 Extent and importance.....	48
1.8.2 The pressures on coastal dune environments.....	49
1.8.3 <i>In-situ</i> monitoring of coastal dunes.....	50
1.8.4 Monitoring coastal dunes with remote sensing.....	50
1.8.5 How can proximal sensing be used to monitor coastal dunes? .	53
1.1 Seagrass meadows.....	56
1.1.1 Extent and importance.....	56
1.1.2 The future of seagrass meadows: threats and pressures.....	57
1.1.3 <i>In-situ</i> monitoring of seagrass .....	59

1.1.4	Monitoring seagrass with remote sensing .....	59
1.8.6	How can proximal sensing be used to monitor seagrass habitats? .....	63
1.2	Tropical coral reefs.....	67
1.2.1	Extent and importance.....	67
1.2.2	The future of tropical coral reefs: threats and pressures .....	67
1.2.3	<i>In-situ</i> monitoring of reefs .....	69
1.2.4	Monitoring reefs with remote sensing .....	69
1.2.5	How can proximal sensing be used to monitor reefs? .....	72
1.9	Summary.....	77
2	Research Aims .....	78
3	Methods.....	82
3.1	Hardware.....	82
3.1.1	Drones.....	82
3.1.2	Kites .....	85
3.1.3	3D printing .....	86
3.1.4	Canon hack development kit (CHDK).....	88
3.2	Data capture.....	90
3.2.1	Drone operations (legal framework) .....	90
3.2.2	Drone operations (practical) .....	90
3.2.3	Kite operations (practical).....	91
3.3	Data processing & analysis .....	92
3.3.1	Photogrammetry.....	92
4	Operating drones in challenging environments.....	95
4.1	Abstract.....	97
4.2	Introduction .....	98
4.3	Considerations for safe deployment.....	102
4.3.1	Pre-flight planning .....	102
4.3.2	Making decisions about when and where it is safe to fly .....	104
4.3.3	Establishing safe locations for take-off and landing & identifying obstructions .....	104

4.3.4	International, regional and local legislation.....	106
4.3.5	Flight operations.....	107
4.3.6	Site-specific flight planning considerations.....	109
4.3.7	Weather and local environment considerations.....	112
4.4	Dust, damage and redundancy.....	114
4.5	Data quality.....	115
4.5.1	Spatial constraint.....	115
4.5.2	Shadows and sun angle effects.....	117
4.5.3	Wind and motion blur.....	120
4.6	Batteries.....	120
4.7	Social and ethical considerations, challenges and mitigation.....	122
4.8	Conclusions.....	126
4.9	Acknowledgements.....	127
5	The renaissance of kites in proximal sensing.....	128
5.1	Abstract.....	129
5.2	Introduction.....	130
5.3	A renaissance in proximal remote sensing.....	133
5.3.1	The need for fine-grained data.....	133
5.3.2	Drones, blimps and balloons.....	134
5.3.3	Kites as an alternative.....	136
5.3.4	The 21 <sup>st</sup> century technology boom.....	137
5.4	Kites as platforms for proximal sensing in physical geography.....	139
5.4.1	Basic mapping.....	139
5.4.2	3D landscape reconstruction.....	141
5.4.3	Ecology and agriculture.....	142
5.4.4	Democratic mapping and teaching.....	143
5.5	Conclusions.....	144
6	Sand dune dynamics.....	146
6.1	Abstract.....	147
6.2	Introduction.....	148

6.3	Materials and methods .....	154
6.3.1	Study system .....	154
6.3.2	Data capture .....	157
6.3.3	Data processing .....	162
6.3.4	Analysis .....	163
6.4	Results .....	164
6.4.1	Drone versus KAP survey .....	167
6.4.2	KAP Surveys .....	172
6.4.3	Intra-annual variation.....	172
6.4.4	Inter-annual variation.....	176
6.4.5	Change within specific features.....	176
6.5	Discussion.....	177
6.5.1	Drone versus KAP survey .....	178
6.5.2	KAP surveys.....	180
6.5.3	KAP as a tool for coastal monitoring .....	181
6.5.4	Other sources of uncertainty .....	182
6.6	Conclusions.....	183
6.7	Acknowledgements .....	185
7	Seagrass meadow spatial variability.....	186
7.1	Abstract.....	187
7.2	Introduction .....	188
7.3	Methods .....	192
7.3.1	Study species: <i>Zostera noltii</i> .....	192
7.3.2	Study sites.....	193
7.3.3	Drone & sensor equipment.....	196
7.3.4	Ground based surveys .....	197
7.3.5	Processing & analysis .....	198
7.3.6	Unsupervised classification with optical bands.....	200
7.3.7	Unsupervised classification with optical bands and texture .....	201
7.3.8	Segmentation & support vector machine classification .....	203
7.3.9	Analysis of classified maps.....	203

7.3.10	Feature detection .....	205
7.3.11	Quadrat sampling bias.....	205
7.4	Results .....	205
7.4.1	Areal coverage and perimeter estimates .....	209
7.4.2	Feature detection .....	210
7.5	Discussion.....	217
7.5.1	Coverage estimates & assessment of quadrat sampling .....	218
7.5.2	Meadow boundary detection .....	219
7.5.3	Feature detection .....	219
7.5.4	Ecosystem dynamics and blue carbon .....	221
7.6	Conclusions.....	222
7.7	Acknowledgements .....	223
8	Coral reef structure .....	224
8.1	Abstract.....	225
8.2	Introduction .....	226
8.2.1	Measuring reef complexity.....	228
8.2.2	Remote sensing .....	229
8.2.3	Aims and scope .....	231
8.3	Methods .....	232
8.3.1	Study system.....	232
8.3.2	Drone and sensor equipment .....	234
8.3.3	Ground control, image resampling & photogrammetry workflow ... .....	236
8.3.4	<i>In-situ</i> structural complexity surveys.....	237
8.3.5	Calculating structural complexity across multiple axes from point clouds .....	238
8.3.6	Collating published rugosity values .....	242
8.3.7	Zoning and areal measurements of the reef environment .....	242
8.4	Results .....	242
8.4.1	Drone flights and photogrammetry data products.....	242

8.4.2	Structural complexity variations across simulated altitudes/ground sampling distance .....	245
8.4.3	Comparing point clouds made with and without oblique image data .....	249
8.4.4	Comparing point cloud derived structural complexity to literature derived rugosity values .....	252
8.4.5	Scaling up with whole reef system zonation .....	254
8.4.6	Comparing <i>in-situ</i> transects to point cloud derived structural complexity estimations.....	256
8.5	Discussion.....	257
8.5.1	Building on existing published work.....	258
8.5.2	Variations in ground sampling distance and the addition of oblique image data .....	261
8.5.3	Differences between morphometric types/cover classes.....	262
8.5.4	<i>In-situ</i> transects .....	263
8.5.5	Future work .....	264
8.6	Conclusions.....	265
9	Discussion .....	267
9.1	Research aims .....	267
9.2	General remarks .....	268
9.2.1	Drones and kites – different platforms for different situations..	268
9.2.2	The coast as a ‘natural’ laboratory .....	269
9.2.3	Integrating proximal sensing with other remote sensing data products .....	270
9.2.4	The sky’s the limit – or is it? .....	271
9.3	The renaissance of kites and the logistical challenges surrounding drone operations .....	272
9.4	Empirical discussion and future research questions.....	273
9.4.1	Coastal dunes .....	273
9.4.2	Intertidal seagrass .....	276
9.4.3	Coral reefs.....	278
9.5	Technology – challenges and opportunities .....	281

9.5.1	Hardware.....	281
9.5.2	Software .....	282
9.6	Concluding remarks .....	284
10	Appendices.....	285
10.1	The CAA approved operations manual – manuscript.....	285
10.1.1	Abstract .....	286
10.1.2	Introduction.....	287
10.1.3	Airspace regulations.....	290
10.1.4	Flying drones for research and CAA permission .....	291
10.1.5	The operations manual (OM).....	295
10.1.6	Conclusion.....	296
10.1.7	Acknowledgements .....	297
10.2	The CAA approved operations manual .....	298
10.3	Appendix for Chapter 8 – St. Gothian sands dune system, Cornwall, UK .....	350
10.3.1	Agisoft photoscan and M3C2-PM workflow .....	350
10.3.2	Figures .....	352
10.3.3	Tables.....	358
10.3.4	Photoscan reports .....	361
10.4	Appendix for chapter 7 – intertidal seagrass meadows, Pembrokeshire, UK .....	418
10.4.1	Supplementary methods.....	418
10.4.2	Supplementary results.....	420
10.4.3	Photoscan reports .....	424
11	References .....	439

## List of figures

- Figure 1.1: DEM of two coastal dune blowouts based on a TLS survey in May 2011. The lines show the position of the rim of the bowl blowout (A) and of the saucer blowout (B) in each survey period. Figure reproduced from Smith et al. (2017)...... 36**
- Figure 1.2: (A) Orthomosaic representing a sandy coast with underwater formation of reef-building tube worm *Sabellaria alveolata*. (B) Thematic map of the same areas generated after image segmentation and classification through an OBIA algorithm. Figure reproduced from Ventura et al. (2018). ..... 44**
- Figure 1.3: Conceptual diagram of the land-sea interface explored in this thesis. Three ecosystems are represented – coastal sand dunes, intertidal seagrass meadows and tropical coral reefs. The proximal sensing techniques used in each environment are also indicated with a kite, and two lightweight drones. Vector icons from [www.vecteezy.com](http://www.vecteezy.com)..... 47**
- Figure 1.4: (A) Alongshore profile of a backbarrier dune pre- and post-storm Ivan, created with data from airborne LiDAR surveys. (B) A photograph of the dune showing erosion on the eastern side. Figure reproduced from Houser et al. (2008). ..... 52**
- Figure 1.5: Two potential uses of kites to monitor changes in coastal sand dunes. A-C) show that collection of data before and after a storm event is possible with a sensor on a kite. D-F) shows that impacts of human activity can be monitored by collecting data with a kite before and after a particular period of disturbance. Vector icons from [www.vecteezy.com](http://www.vecteezy.com). ..... 55**

**Figure 1.6: Maps of the Eastern Banks, Moreton Bay, Australia derived from field data and fine spatial resolution satellite imagery (2 m × 2 m pixel size) using OBIA analysis for dominant seagrass species (left), and, seagrass percentage cover (centre) for June 2012. (right) Above ground biomass map. The lower panels indicate the level of detail in each classification, the area of which is defined by the yellow box. Figure reproduced from (Roelfsema et al., 2014)..... 63**

**Figure 1.7: The benefits of remote sensing with a drone. A) Sub optimal conditions include a high sun angle, rough sea surface, causing sunglint, where data collected with a satellite platform may lack quality for remotely sensing seagrass and B) Optimal conditions with the sun at a low sun angle, and calm waters/low tide. When these conditions occur a drone can opportunistically be flown to collect data. Vector icons from www.vecteezy.com..... 66**

**Figure 1.8: (A)The inner lagoon of Tiahura, Moorea, French Polynesia (aerial image from WorldView-2, DigitalGlobe). (B) Aerial view of the boat used as landing/take-off base for the drone flight. (C) Location of one ground control point (GCP) in the surveyed area; the circle indicates the approximate area represented in D. (D) Detail of C, example of GCP and scale bar used to georeference the image data. (E) Composite ortho-rectified photo obtained from structure from motion. (F) Bathymetric raster obtained from SfM-MVS, with indication of GCPs. Figure reproduced from (Casella et al., 2017). ..... 75**

**Figure 1.9: The potential benefits of using a drone in coral reef environments. A) Manual transect undertaken by snorkeller/diver using a**

chain and tape approach. Transect is limited in its spatial extent. B) Nadir and off-nadir positioning of optical sensor captures more data on the structure of the reef. Also undertaken with a low sun angle to reduce glint on the water. Vector icons from [www.vecteezy.com](http://www.vecteezy.com). ..... 76

Figure 2.1: Conceptual diagram showing the structure of the thesis. .... 81

Figure 3.1: The 3 research drones used during this thesis. A) A 3DR Y6 hexacopter “Yeti”, B) A QuadH<sub>2</sub>O quadcopter “Henrietta”, C) A 3DR Solo quadcopter “Duffolo”..... 85

Figure 3.2: Examples of the 3D printed mounting system used to attach the Ricoh GR II to the 3DR Solo. .... 87

Figure 3.3: Examples of the KAP setup with the picavet mount attached. 87

Figure 3.4: Typical workflow in the production of georeferenced dense point clouds from image sets and ground control points. Inputs and outputs are shown in dark red. In the top right, as a demonstration, matches determined to be valid are shown in red, while matches determined to be invalid are given in blue. Figure reproduced from (Smith et al., 2015)..... 93

Figure 4.1: The geographical diversity of locations where we have successfully or unsuccessfully deployed lightweight drones for collection of proximal remote sensing data, including (A) arctic, (B) desert, (C) coastal and (D) tropical forest. .... 101

Figure 4.2: The challenges of drone fieldwork in four key environments. .... 109

Figure 4.3: Issues with optical imaging. (A) Sun glint over coral reefs in the Maldives, (B) ripples in the water’s surface caused by a boat in Greece and

<b>(C) Marram grass (which is easily moved by wind) on sand dunes in the UK</b> .....	119
<b>Figure 5.1: The box kite used in the study by Dines in 1903. Reprinted by permission from Macmillan Publishers Ltd. (Dines, 1903).</b> .....	132
<b>Figure 5.2: Custom-designed lightweight picavet mount for Canon Powershot D30. Model constructed in OpenSCAD (<a href="http://www.openscad.org/">http://www.openscad.org/</a>) and available to download from Thingiverse (<a href="http://www.thingiverse.com/thing:1372969">http://www.thingiverse.com/thing:1372969</a>).</b> .....	138
<b>Figure 5.3: Author (JPD) flying 1.6 m HQ KAP single-line kite over seagrass meadows in northern Greece (A) and resulting aerial photograph (B)...</b>	141
<b>Figure 7.1: A) The location of St Ives bay and Gwithian Towans within the UK and Cornwall. B) The location of St Gothian Sands Local Nature Reserve. C) An aerial image (courtesy of Channel Coastal Observatory, <a href="https://www.channelcoast.org/">https://www.channelcoast.org/</a>) with the dune study system (area of interest) indicated by dashed line. D) The study system annotated with features of interest.</b> .....	155
<b>Figure 7.2: Wind profile characterising the study system using weather data from Camborne weather station (located approximately 5km east of St Gothian Sands nature reserve). Histogram displays average hourly wind speed (grouped by week) throughout the study period, and wind roses indicate average hourly wind speed and direction during the periods between pairs of the six KAP and drone surveys used in analysis (indicated by number labels). Weather data obtained from Met Office DataPoint Service (<a href="https://www.metoffice.gov.uk/datapoint">https://www.metoffice.gov.uk/datapoint</a>; contains public sector information licensed under the Open Government Licence).</b> .....	156

**Figure 7.3: Data collection, processing and analysis workflow for KAP and drone surveys..... 160**

**Figure 7.4: A) Orthomosaic constructed with data from survey 4 conducted on 20/01/2017. B) Digital Elevation Model (DEM) of survey 4. C) Screenshot of dense point cloud made with data from survey 4. D) Orthomosaic constructed with data from survey 6 conducted on 12/01/2017. E) DEM of survey 6. F) Screenshot of dense point cloud made with data from survey 6. Scale bar in A) also applied to B, D & E. .... 166**

**Figure 7.5: A) Orthomosaic constructed with data from survey 5 (conducted on 16/06/2017) overlaid with a transect. B) Elevation profiles of the transect constructed with data from DEMs of all 6 KAP surveys. .... 167**

**Figure 7.6: Comparisons between KAP survey 6 and the drone survey A) An orthomosaic created from images captured in KAP survey 6. B) Image overlap for the KAP survey (taken from Photoscan report). C) Image overlap for the drone survey (taken from Photoscan report). Black dots show estimated camera positions. D) Digital elevation model (DEM) for the KAP survey. E) DEM for the drone survey. F) A DEM of difference between the KAP and drone DEMs. G) Rasterised representation (spatial resolution of 0.1 m for display purposes) of significant results from M3C2-PM change analysis between point clouds created with data from KAP and drone surveys (overlaid on orthomosaic (at 50% transparency) from panel A). Non-significant change points are absent from G. .... 169**

**Figure 7.7: Distribution of M3C2 distances between the kite survey and drone survey. Main figure shows data cropped to 5% and 95% quantiles with inset histogram showing all data. Points falling outside the common**

area between surveys have been removed, as they cannot be used in M3C2 analysis. Point cloud exported at native resolution of drone derived point cloud. Light grey shows all points in the change cloud and darker grey indicates significant changes in distance. Dashed lines indicate the positive (128 mm) and negative (-56 mm) median values of significant changes..... 170

Figure 7.8: Significant differences indicated by M3C2-PM comparisons between pairs of dense clouds. Changes were mostly between -2 and 2 m as indicated by the split colour ramps. Rasters were created from change clouds at a resolution of 0.75 m, with the mean of intersecting points in horizontal space assigned as the value in each cell. and cropped to the area of interest (Figure 7.1)..... 174

Figure 7.9: Analysis of M3C2 change clouds for specific features within the study system. Change was calculated between surveys 4 and 6 (12 month timespan). Histograms show the distribution of all points (light grey) overlaid with the distribution of significant change points (dark grey) for each of the three features (beach, foredune, path) analysed. .... 177

Figure 8.1: The location of the study sites within the context of west Wales, UK A) and Pembrokeshire B). Flight paths are shown with dashed lines for Angle Bay C) and Garron Pill D)..... 195

Figure 8.2: Data collection, processing and analysis workflow..... 202

Figure 8.3: Mosaicked RGB imagery of *Zostera noltii* habitat in Angle Bay. The 50 x 50 m plot is show in A), with two finer spatial scale examples shown in B) and C)..... 207

**Figure 8.4: Mosaicked RGB imagery of *Zostera noltii* habitat at Garron Pill. The ~25 x 100 m plot is shown in A), with three finer spatial scale examples shown in B), C) and D). ..... 208**

**Figure 8.5: The relationship between observed and classified seagrass coverage observed within quadrats. Unsupervised classifications with red, green and blue bands shown in A), with added texture layers in B) and supervised object-based image analysis results are shown in C)..... 213**

**Figure 8.6: Box and whisker plots showing the distribution of bootstrapped overall uncertainty calculations (n = 1000), calculated from the differences between observed and classified seagrass cover in quadrats. Lower and upper hinges refer to 25% and 75% percentiles respectively. Central lines represent the median, whiskers represent 5% and 95% quantiles and points represent outliers. .... 214**

**Figure 8.7: Orthomosaic of *Zostera noltii* meadow boundary at Garron Pill. Images captured at 50 m altitude. No ground control targets were deployed at this site due to the inaccessible nature of the river channel. .... 215**

**Figure 8.8: Three examples of ecological features found in *Zostera noltii* meadows. A) Shows two Lugworm (*Arenicola sp.*) mounds, B) Cockle (*Cerastoderma edule*) shells surrounded by seagrass shoots and C) on non-vegetated substrate..... 216**

**Figure 9.1: Location of the study system. A) Location of the Huvadhu Atoll within the Maldives. B) Location of Kandahalagala within the Huvadhu atoll. C) The island of Kandahalagala. D) The path of one drone flight used in this study. Axis units in A) are in degrees, and units in D) are in meters, WGS 84 / UTM Zone 43N. .... 233**

**Figure 9.2: Methodological flowchart demonstrating the data capture and processing workflow..... 235**

**Figure 9.3: The position of each of the 8 snorkelled ReefBudget transects (yellow lines) within the study system. Orthomosaic created with native 30 m altitude images..... 238**

**Figure 9.4: The calculation of point cloud structural complexity from dense point clouds. This figure shows a conceptualized version of the methodology in 2D, whereas the extraction of data came from the dense point clouds. A) The mixed reef AOI subset from the whole orthomosaic. B) 1 m × 1 m fishnet grid overlaid on AOI orthomosaic with a single cell highlighted in yellow. C) 4 × 1 m transects oriented to the 8 major compass directions overlaid on the orthomosaic cropped to the extent of the yellow cell in B. D) Manually delineated cover classes for the whole mixed reef AOI, with the single cell identified in B, highlighted in yellow. E) 2 cover classes located within area cropped to the extent of the yellow cell in D. F + G) 4 transects oriented to the 8 major compass directions intersecting the centre point of a cover class segment, cropped to the boundaries of the segment..... 241**

**Figure 9.5: Example photogrammetry data products using nadir images captured at 30 m altitude. A) Subset of the DEM. B) Screenshot of the point cloud with a similar extent to A. C) An example of structure in a dense point cloud over sandy substrate Note view of point cloud captured at an angle to help visualise z-axis differences in B. 1) Shows an example of an individual coral bommy, 2) A set of structures with varying topography,**

surrounded by sand and 3) A shallow sandy area surrounded by coral structures..... 244

Figure 9.6: Orthomosaics of subset areas and associated structural complexity calculations on point clouds created with different resolution (resampled altitude) images. Calculated using a 1 m<sup>2</sup> grid over each area of interest (AOI)..... 248

Figure 9.7: The distribution of structural complexity (see Equation 1) calculations across native and resampled altitudes in each subset area. Values below 1 are erroneous, representing virtual transects with too few data points in the dense cloud. Central lines in boxes represent median, upper and lower bounds of boxes represent 0.25 and 0.75 quantiles respectively and ends of whiskers represent 0.05 and 0.95 quantiles. ... 249

Figure 9.8: Surface structural complexity calculations (see Equation 1) derived from dense point clouds created with 30 m altitude images using both nadir only and nadir & oblique images. Difference estimations calculated using 1 m<sup>2</sup> grid for each AOI..... 251

Figure 9.9: Thematic maps showing cover classes in each AOI, and associated distributions. A-F) Cropped orthomosaics and associated manually delineated cover classes. G-I) Proportion of each cover class found within each of the AOIs..... 253

Figure 9.10: Distribution of estimated structural complexity for all cover/morphometric types from the 30 m native point cloud. Data shown are a sum across each of the three AOIs. .... 254

**Figure 9.11: Kandehalagala island reef system and manually delineated zones. .... 255**

**Figure 9.12: Comparison of structural complexity calculations over 10 m transects using data collected from ReefBudget transects, and values derived from dense point clouds. .... 257**

**Figure 9.13: Subset of a single image captured from ~30 m altitude over a mixture of sandy substrate and hard coral structures. .... 260**

**Figure 11.1: A schematic representation of where the operations manual fits into the typical accreditation process for ‘aerial work’ according to the UK Civil Aviation Authority. Please note that we show two routes for its use. The left-hand part of the flow chart shows the process for CAA accreditation of aerial work which permits RPAS use for commercial operation. However, as we argue in the manuscript, any researcher could use (following adaptation for their specific aircraft and procedures) our operations manual within their flight protocols, to demonstrate to collaborators a competency and safe protocol for drone flights outside of those operations requiring special permission from the CAA for ‘aerial work’. .... 294**

**Figure 11.2: Timeline for PFAW certification experienced by the authors. .... 296**

**Figure 11.3: (A) The KAP equipment in the field, with the picavet mount (containing camera) suspended from the single kite line using two carabiners. (B) 3D model of the picavet mount that can be produced with a 3D printer. .... 352**

**Figure 11.4: The subset area of interest (AOI) used for the drone and kite comparison analysis. Dark grey shaded area shows whole study system AOI..... 353**

**Figure 11.5: Orthomosaics constructed with images from each of the six KAP surveys. Products from surveys 1-6 represented by A-F respectively. All mosaics cropped to the study area of interest (Figure 7.1). ..... 354**

**Figure 11.6: Digital elevation models (DEMs) for each of the six KAP surveys. Products from surveys 1-6 represented by A-F respectively. All models colour scaled to the minimum and maximum found across models. All rasters cropped to the study area of interest (Figure 7.1)..... 355**

**Figure 11.7: The distribution of estimated altitudes of the camera when images were captured for each of the six surveys. Additional drone survey altitude included with KAP survey six. Altitude estimates calculated in Agisoft Photoscan after sparse cloud construction. Darker grey bars show each surveys bins, whereas distribution incorporating all six surveys is shown in lighter grey. .... 356**

**Figure 11.8: Pitch estimations for each camera position as calculated by Photoscan for both the drone and KAP survey 6 data..... 357**

**Figure 11.9: Roll estimations for each camera position as calculated by Photoscan for both the drone and KAP survey 6 data..... 357**

**Figure 11.10: Ten photographs of quadrats were split into two classes and the % coverage of seagrass compared to observed coverage estimations. .... 420**

**Figure 11.11: Angle Bay orthomosaic A), unsupervised classification using RGB B), unsupervised classification using RGB and texture layers C) and OBIA based classification D)..... 421**

**Figure 11.12: Garron Pill orthomosaic A), unsupervised classification using RGB B), unsupervised classification using RGB and texture layers C) and OBIA based classification D). Non-seagrass class encompasses substrate, macroalgae and gravel cover types..... 422**

## List of tables

<b>Table 1.1: The major classifications of types of coastal environments. Adapted from Burke et al. (2001). .....</b>	<b>31</b>
<b>Table 3.1: Overview of the key equipment used throughout the thesis. ...</b>	<b>89</b>
<b>Table 4.1: Challenges faced during drone operations and the environments in which they can occur.....</b>	<b>103</b>
<b>Table 4.2: Social concerns associated with using drones. ....</b>	<b>124</b>
<b>Table 7.1: Details of each KAP and drone survey undertaken and associated wind conditions. Times (in GMT) are estimations based on the first and last photos that are deemed useable in the photogrammetry workflow. Wind data from Camborne weather station (located approximately 4.7 km ESE from the study system). Weather data obtained from Met Office DataPoint Service (<a href="https://www.metoffice.gov.uk/datapoint">https://www.metoffice.gov.uk/datapoint</a>; contains public sector information licensed under the Open Government Licence). ....</b>	<b>161</b>
<b>Table 7.2: M3C2-PM derived precision estimations for the points contained in the KAP versus drone subset area of interest (Figure 11.4). ....</b>	<b>171</b>
<b>Table 7.3: Proportions of total number of significant points in M3C2-PM change rasters between pairs of surveys. Rasters were created from change clouds at a resolution of 0.75 m, with the mean of intersecting points in horizontal space assigned as the value in each cell. ....</b>	<b>175</b>
<b>Table 8.1: Accuracy assessment of unsupervised classifications including both RGB and RGB and Texture, and OBIA classifications. Root mean squared deviation (RMSD) and standard deviation (SD) and bias calculated on the percentage difference between observed and classified seagrass</b>	

cover in quadrats. Bootstrapped SE was calculated in the bootstrapping process. Overall uncertainty calculated from bias, SD and bootstrapped SE using the equation described in section 8.3.9. Coverage estimates calculated by totalling the number of pixels classed as seagrass at each site. .... 212

**Table 9.1: Image dimensions for resampled photographs used to simulate variation in altitude. .... 245**

**Table 9.2: Total count of points from dense point clouds constructed with native and resampled images in Agisoft Photoscan. NA present in 200 m data as mosaicking did not produce a sufficiently dense point cloud product to cover the whole area of interest. .... 247**

**Table 9.3: Literature derived rugosity estimates. \*Mean taken of small and medium massive rugosity values. .... 252**

**Table 11.1: Number of Monte Carlo sparse cloud iterations and accuracy values used as seeds in Agisoft Photoscan for each dataset. Marker and tie point accuracy set as the same values within each processing set. This process is part of the workflow presented in (James et al., 2017). .... 358**

**Table 11.2: Check point (n=4) errors for each survey. Check points were a subset of GCPs positioned within the SfM-MVS model, but excluded from the point cloud creation stages in the photogrammetry workflow. .... 359**

**Table 11.3: Specifications for sensors used in the study. .... 423**

## Declaration of authorship

Chapters 4, 5, 6, 7, 8 have been published or written for publication as co-authored academic papers.

I co-conceived the idea for chapter 4 with Andrew Cunliffe (AC) and Karen Anderson (KA). AC and I co-wrote the manuscript, with major contributions from KA and minor contributions from Leon DeBell (LD), Chris Sandbrook, Serge Wich, Jamie Shutler (JS), Isla Myers-Smith and Miguel Varela.

I conceived the idea for chapter 5 and wrote the manuscript with major contributions from KA.

I designed all the fieldwork for chapter 6 with advice from KA. I led the fieldwork with assistance from KA and others (acknowledged within the chapter). I processed and analysed the data with advice from LD, JS and KA. I obtained weather data with help from Matthew Witt (MW). I led the writing of the manuscript and developed it using comments from JS, MW, LD and KA.

I designed all the fieldwork for chapter 7 with assistance from Laura Pratt (LP). I led the fieldwork with assistance from JS and LP. I processed and analysed the data with advice from Peter Land (PL), KA and JS. I led the writing of the manuscript and developed it using comments from KA, PL and JS.

I designed all the fieldwork for chapter 8 with assistance from KA, Chris Perry (CP) and Jonathan Crocker (JC). I processed and analysed the data with guidance from CP, KA and JS. I led the writing of the manuscript and developed it using comments from CP, KA and JS.

## Acknowledgements

This thesis is the product of much encouragement and support from both people inside and outside the academic world. Firstly, I would like to thank my supervisor Karen Anderson. I count myself very fortunate to have had such a supportive, approachable and motivated mentor during this process. Your sense of humour, patience and involvement in all parts of this project have made undertaking this PhD a genuinely enjoyable experience. Also, founding the Dronelab alongside my PhD work has been an amazing opportunity, and I thank you for allowing me on-board that particular train. Thank you also to my supervisor Jamie Shutler for your support and guidance throughout these past 4 years. Your attention to detail, and also willingness to join in with fieldwork have been very helpful in creating this body of work. Keeping a cool head in tricky fieldwork situations was much appreciated. Thanks both to Karen and Jamie for your wise words, willingness to read multiple iterations of manuscripts and guidance throughout. Matthew Witt and Peter Land have also provided sage advice and expertise for various parts of this thesis, thank you both for your help. Also thank you Matt for the opportunity to test drones for seal pup monitoring in the Scillies. Maybe we'll crack it in the future! Thank you to Chris Perry for giving me the opportunity to travel to the Maldives and undertake fieldwork. I also wish to acknowledge everyone else that has helped me with fieldwork. Without your willingness to give up your time to help out, some of this work would not have been possible.

Next, I would like to thank Leon DeBell for your continued friendship. Not only do you have buckets of patience, but you taught me a lot of what I know about drones and without your generosity, I would not have been able to achieve as much during these past 4 years. I will always remember the joy of 'tidy Fridays' and the

Funk, Soul, Disco soundtrack. Also, thank you to Andrew Cunliffe for the fun times, especially relating to drone licencing exams, and also introducing me to drone flying on day one of my PhD. Thanks also to Dominic Fawcett and Joel Forsmoo for being great DroneLab colleagues.

A mixture of friends I've made whilst on the Penryn campus and those outside the academic bubble have made 'work life' and beyond during the hard times, ok, and during the good times, great fun. Thank you Sam Barton, Amy Campbell, Ricky Coleman, Maria Correa-Cano, Ned Crowley, Sarah Crowley, Lynda Donaldson, Paz Durán, Helen Fielding, Ed Firth, David Fisher, Colin Gardiner, Cecily Goodwin, Rich Inger, Darren Jones, Chris Kay-Ayling, Anne Leonard, Marina Maier, Cat McNicol, Sean Meaden, Daniel Padfield, Beth Robinson, Nigel Sainsbury, Katie Shanks, Rich Sherley, Matthew Silk, George Swan, Carl Wimhurst, Oliver Wright and my fellow GW4+ cohort – Lewis Bartlett, Beth Clarke, Paula Marjamaki, Sara Mynott, Ian Skicko, & Alice Williams.

A special thank you to Nicole Parr for being a babe. You've been incredibly supportive and patient with me throughout this journey. We've had some great times in the past 4 years, and I hope we'll have many more. My parents Amanda and Howard, brother Jonathan and nannie Ann, have been extremely supportive and have always backed me in whatever career choices I have made (including undertaking this PhD). I count myself fortunate to have such a great loving family. Thanks for your help along the way.

Lastly, I would like to acknowledge my funders the Natural Environment Research Council (NERC) and Plymouth Marine Laboratory (PML) for funding my studentship.

## Table of abbreviations

3DR	3D Robotics
ABS	Acrylonitrile butadiene styrene
APM	ArduPilot Mega
AOI	Area of Interest
ATC	Air Traffic Control
CAA	Civil Aviation Authority
CAD	Computer Aided Design
CAP	Civil Aviation Publication
CHDK	Canon Hack Development Kit
CMOS	Complementary Metal-Oxide-Semiconductor
DEM	Digital Elevation Model
DoD	Difference of DEMs
ESC	Electronic Speed Controller
GPS	Global Positioning System
GRASS	Geographic Resources Analysis Support System
GNSS	Global Navigation Satellite System
ICAO	International Civil Aviation Organization
KAP	Kite Aerial Photography
LiDAR	Light Detection and Ranging
LiPo	Lithium Polymer
M3C2-PM	Multiscale Model to Model Cloud Comparison – Precision Mapping
NDVI	Normalised Difference Vegetation Index
OBIA	Object Based Image Analysis
OM	Operations Manual
PfAW	Permission for Aerial Work
PfCO	Permission for Commercial Operations
PPK	Post Processing Kinematics
RGB	Red, green, blue
RMSD	Root Mean Squared Deviation
RPAS	Remotely Piloted Aircraft System
RTK	Real-time Kinematics
SfM-MVS	Structure-from-Motion Multi-View Stereo
TLS	Terrestrial Laser Scanner
UAV	Unmanned Aerial Vehicle
VLOS	Visual Line of Sight

# 1 Introduction

## 1.1 The global importance of coastal environments

More than 50% of coastal countries have over 80% of their population living within 100 km of the coast (Martínez et al., 2007), with the average human population density in these regions nearly three times of that found elsewhere globally (Small and Nicholls, 2003). Furthermore, the magnitude of this situation is likely to increase (McGranahan et al., 2007). It is estimated that the world has 1,634,701 km of coastline (Burke et al., 2001), which encompasses diverse ecosystems, varying greatly in structure and function. They are often classified by their physical characteristics and grouped by their position in relation to land and sea (see **Table 1.1**). These coastal environments are highly dynamic and productive areas which are of environmental, economic and social importance (Martínez et al., 2007). They offer places to live and ecosystem goods and services; such as food provision (e.g. fishing and aquaculture (Holmlund and Hammer, 1999; Liqueste et al., 2013)), storm protection (Costanza et al., 2008), erosion control (Barbier et al., 2011) and areas for recreational activities (Ghermandi and Nunes, 2013) among many others. Biodiversity is also a fundamental coastal ecosystem service, with coastal regions providing a rich habitat for organisms (Jennerjahn, 2012). However, due to increasing pressure from human activity as described above and the evolution of weather patterns and climate change, pressing issues with the coastal environment have arisen, such as pollution, species invasions, overfishing, habitat modification (Halpern et al., 2008) and most notably those driven by climate change including ocean acidification (McGranahan et al., 2007). In order to understand and potentially mitigate or reverse changes in coastal environments, monitoring efforts and new methods that are able to evolve and

adapt with this important but changing environment are required to detect change over time.

## 1.2 The challenges of coastal monitoring

To understand these changes at the coast requires environmental monitoring, both to detect inter-annual trends and shifts, and to monitor dynamics which can arise as a result of intra- and inter-annual variations in stressors (e.g. storms). Additionally, it is important to establish baselines with regards to the structure and function of the natural environment, in order to quantify responses to environmental change and increased anthropogenic stressors. With knowledge of how environmental processes operate naturally, the effects of anthropogenic pressures can be characterised more accurately. If targeted and well-planned, environmental monitoring can be a cost-effective method to protect natural resources and scientifically rigorous enough to influence policy makers, in turn delivering effective management and protection (Lovett et al., 2007). While in recent decades, huge progress has been made towards operational environmental monitoring at the coast, the ability to collect scale-appropriate data, at appropriate times, capable of resolving processes of interest, is hampered by several problems. *In-situ* data collection is often unviable or logistically challenging and costly (Brewin et al., 2015), due to restricted access at the land-sea interface or complexities with the upkeep and maintenance of equipment in these environments. Coastal zones are often harsh with the presence of sand, salt-water and windy conditions making it challenging to undertake some forms of research. For reasons such as these, remote sensing is becoming a tool of choice for monitoring coastal processes and change.

**Table 1.1: The major classifications of types of coastal environments. Adapted from Burke et al. (2001).**

<b>Coastal Zone</b>	<b>Habitat/Environment</b>
Near-shore terrestrial	Dunes, cliffs, rocky and sandy shores, xeromorphic habitats, human modified landscapes
Intertidal	Estuaries, deltas, lagoons, mangrove forests, mudflats, salt marshes, salt pans, other wetlands, ports, marinas, aquaculture beds
Benthic	Kelp forests, seagrass beds, coral reefs, soft bottom environments above the continental shelf, artificial reefs and structures
Pelagic	Open waters above the continental shelf, fish farms

### 1.3 Remote sensing of coastal environments

The following sections give an overview of remote sensing science in the coastal zone, encompassing techniques that utilise data from satellite, airborne and more proximal platforms, as well as *in-situ* approaches. This synopsis focuses mainly on optical and light detection and ranging (LiDAR) based approaches.

#### 1.3.1 Satellite platforms

Data products from satellite platforms vary greatly in their spectral, spatial and temporal (i.e. revisit time) resolutions. Some of the more widely utilised satellite platforms for coastal monitoring include the Landsat program, IKONOS and Quickbird (Klemas, 2011). The fine temporal resolution (e.g. regular revisit times) and ease-of-access (e.g. Landsat data freely available since 2008) of some satellite derived datasets have made them a suitable choice for studying coastal processes over long timescales and over large areas. For example, Landsat images have been used for multi-decadal landcover change detection at the landscape scale (~100 km of coastline analysed; Shalaby and Tateishi, 2007). The recent launch of Sentinel 2 satellites (which are a Landsat continuation mission) have increased revisit times to approximately 3 days when considering a combination of the Landsat and Sentinel 2 programs (Li and Roy, 2017). In contrast to the 30 m spatial resolution data available from the Landsat program, <1 m spatial resolution data are provided by commercially operated systems such as Quickbird and IKONOS. This finer spatial resolution allows for more detailed investigation of coastal ecosystems (e.g. delineating different species within mangrove habitat (Wang et al., 2004). Another alternative is Planet Labs Dove program, which utilises more numerous lower cost platforms to achieve greater

sampling rates. For example, data from 55 Dove satellites provided daily revisit capability at a spatial resolution of ~3.7 m, which has been used to monitor coral reef atoll development by the Chinese government (Asner et al., 2017).

### 1.3.2 Airborne platforms

Airborne platforms such as light aircraft have been used with a multitude of sensors for monitoring coastal environments. They are useful platforms for acquiring data over relatively large spatial scales (10s-100s km<sup>2</sup>) and provide data at finer spatial resolutions than is typically available from satellite platforms. Of particular note, LiDAR sensors have been used to understand structural patterns in coastal landscapes (e.g. to monitor topographic changes in beach environments (Sallenger et al., 2003) or map coastal habitats (Chust et al., 2008)). Aside from active sensors such as LiDAR, optical sensors have also been utilised on airborne platforms, including red, green, blue (RGB), multispectral and hyperspectral imaging systems. Both panchromatic and colour aerial photography have been combined with fine-grained mapping products (e.g. Ordnance Survey data in the UK) and LiDAR surveys to track intra-decadal change in shoreline position at 100 m intervals along a 74 km stretch of coastline. (Burningham and French, 2017). Airborne multispectral sensors have provided data to help delineate coastal water types (e.g. river, fresh water marsh, salt marsh drainage; Huh et al., 1996) and map intertidal seaweed communities (Brodie et al., 2018). Hyperspectral sensors have increased spectral resolution meaning that a greater number of contiguous bands in the electromagnetic spectrum are sampled during data acquisition. More advanced hyperspectral scanners such as the Compact Airborne Spectrographic Imager (CASI) have been deployed to aid in the estimation of seagrass standing stock (Mumby et al.,

1997), mapping mangrove extent (Green et al., 1998) and tracking invasive marine alga (Theriault et al., 2006).

### 1.3.3 Terrestrial *in-situ* sensing

Time-lapse photography using sensors mounted at near-ground based positions has been used successfully to monitor dynamic processes in the coastal zone. Thermal erosion of permafrost coastline has been tracked using this technique (Wobus et al., 2011), at a temporal resolution of 2 hours over a 6 week period using time-lapse cameras. Time-lapse photos have also been used to quantify the pressures and carrying capacity in beach zones; the daily number of beach users was calculated (Pereira da Silva et al., 2016). An alternative application of time-lapse photography has been assessment of the efficacy of coastal engineering projects, such as beach drainage (Bowman et al., 2007).

Another terrestrial sensing technique also involves the use of cameras, but also some processing of the data using a Structure-from-Motion-Multi-View-Stereo (SfM-MVS) workflow. This form of data processing is made possible by the ability to obtain overlapping images from optical sensors. The resultant data products are most commonly orthomosaics, digital elevation models and point clouds, the latter two of which can be used to describe topographic variation of a particular environment. This technique has only recently emerged as considerable processing developments in digital photogrammetry and SfM have only emerged within the past 5 years (Smith et al., 2015). More about this technique can be found in section 3.3.1. This technique has been used to measure beach shoreline positional changes and rotation (Pikelj et al., 2018). Cameras on poles have been used to capture images from proximal aerial positions, (e.g. to produce fine-

spatial resolution, 10 mm in this case, digital surface models used to investigate turtle nest site selection (Kelly et al., 2017). As well as over relatively small extents (i.e.  $\sim 250 \text{ m}^2$ ; Kelly et al., 2017), ground-based SfM-MVS has also been applied over larger spatial domains, such as a  $\sim 1 \text{ km}$  stretch of cliff face, for erosion monitoring purposes (Westoby et al., 2018).

Terrestrial laser scanning (TLS) is a technique used to rapidly capture the distance of objects and surfaces in a given scene, resulting in a 2.5D/3D model of the surveyed environment. At the coast, TLS is commonly used for quantifying the size of terrestrial features such as sand dunes (Feagin et al., 2014), their development over time (Smith et al., 2017; **Figure 1.1**) and assessing the erosion processes on cliffs (Westoby et al., 2018). Data captured in this way can provide fine spatial and temporal resolution point clouds (e.g. revisit times within days or weeks) are useful for quantifying topographic changes in coastal environments (Smith et al., 2017).

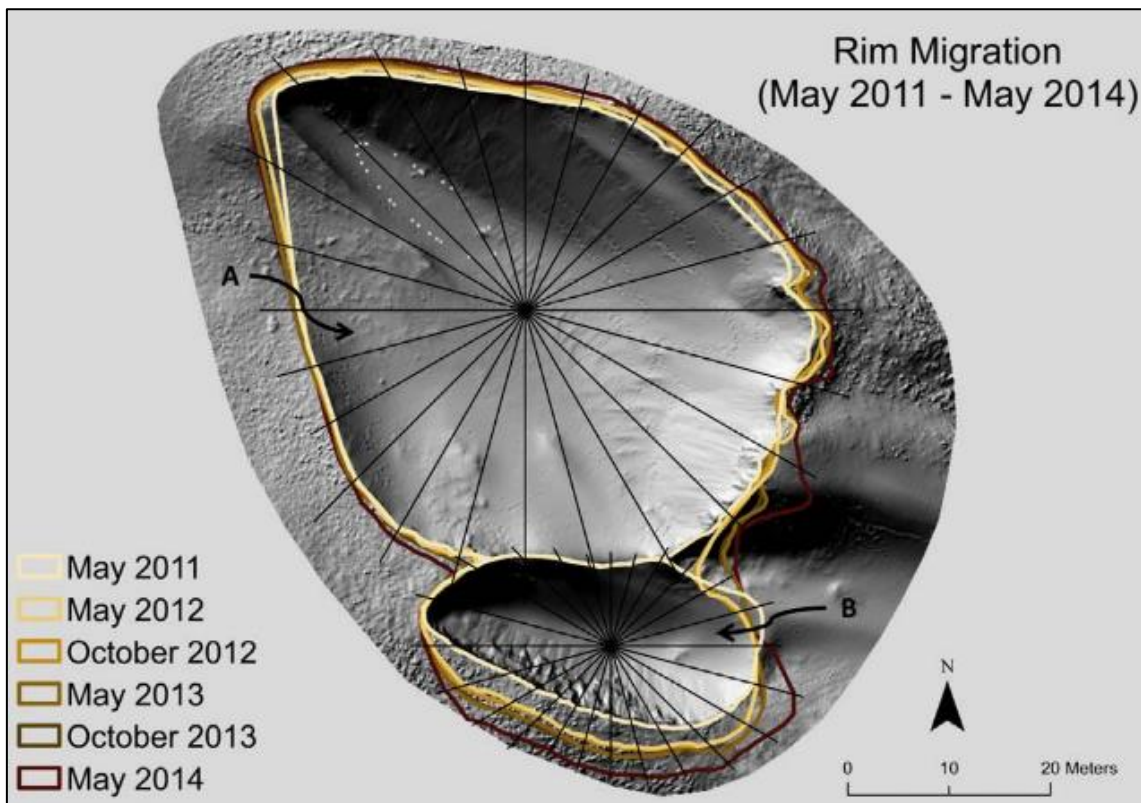


**Figure 1.1: DEM of two coastal dune blowouts based on a TLS survey in May 2011. The lines show the position of the rim of the bowl blowout (A) and of the saucer blowout (B) in each survey period. Figure reproduced from Smith et al. (2017).**

#### 1.3.4 Issues and drawbacks with remote sensing methods

Although data captured from satellite platforms have been hugely beneficial for coastal monitoring, there remain issues and barriers which can limit the success of its application. Firstly, regarding intertidal and shallow submerged environments, the state of the tide is critical to how useful the data are. For example, filtering Landsat data for low tide state images will result in a coarser temporal resolution than using the full dataset (Sagar et al., 2017). As a result, data at desired times (e.g. weekly intervals) may not be achievable using satellite derived data from one platform (or set of platforms) alone. Another issue, which affects all optical remote sensing from space is the presence of clouds (Ju and Roy, 2008). Clouds effectively mask pixels in optical and some infra-red remote

sensing data, meaning the true reflectance signal is greatly reduced or completely absent. Even if cloud free data are regularly available, the temporal revisit times of many of the most widely used satellites are often too infrequent (e.g. Landsat – 16 days) to monitor highly dynamic coastal processes (Thomas et al., 2002). In combination with the limited windows in which tide times might be optimal, this further reduces the pool of likely useful data. Data outputs from Landsat, MODIS, Sentinel (2 & 3), and other satellite programs are currently freely available which is a huge benefit in terms of cost-effectiveness for coastal monitoring. However, spatial resolutions in these free datasets are usually not fine enough for monitoring dynamic processes and heterogenous coastal zones. This in turn leads to issues such as the mixing of pixels between land and sea and contamination of data due to the adjacency effect (Minomura et al., 2001). One alternative is to use commercial data from platforms such as WorldView-2 (with a spatial resolution of 0.5 m RGB), but, as stated previously, this comes at a relatively high financial cost ~\$20 per km<sup>2</sup> (with further costs for multiple user licenses), and coarser temporal resolutions than freely available alternatives, unless the user is willing to compromise by requesting off-nadir acquisitions which can be delivered from the pointable platforms (e.g. NASA-MISR). These costs can preclude the use of such data in time series monitoring or for projects where financial constraints limit the purchase of data.

The quality issues caused by environmental conditions for satellite derived data can have similar effects on data acquired from airborne platforms. However, there is more control over when surveys are undertaken, and so optimal tide states and cloud coverage can be factored in to a certain extent. However, airborne campaigns are logistically complex, often involving multiple individuals and

organisations (e.g. pilots, aviation authorities, instrument operators), and its unlikely flights can be undertaken at very short notice (if optimal conditions arise). The associated costs with piloted aircraft operations means that this form of data capture is relatively expensive (e.g. £1000s per survey). This cost alone can limit the use of airborne remote sensing for projects with small budgets or in areas of the world without national survey capabilities. Whilst some airborne data are now available in the UK and other countries as open access datasets (e.g. LiDAR archive from UK Environment Agency (<https://environment.data.gov.uk/ds/survey>)), these data only document past change and may not be suitable for answering questions where timing of acquisitions is critical. Furthermore, gaining clearance from relevant aviation authorities (if applicable) may also hinder the ability to undertake regular flights making airborne remote sensing a less viable source of data for routine coastal monitoring.

The drawbacks of TLS are that the operational range of the equipment is limiting (i.e. 50 m (Kandrot et al., 2016)), and is also cumbersome to move around sites (a requirement to obtain optimal viewing angles for the capture of laser returns). This means that the spatial extent over which a scanner can capture data is limited, realistically, to areas of less than a hectare per survey, in turn restricting the types of processes that can be monitored over time. Also, the equipment is expensive, one estimation stating that new scanners cost between 30,000 and 80,000 euros (Liang et al., 2016). Other terrestrial sensing methods such as handheld photography and time-lapse photography are certainly more cost-effective than the aforementioned techniques, but can lack the nadir perspective that other remote sensing products can provide. This means that quantitative

analysis is more challenging due to the potential lack of coverage (i.e. feature omission) and differing perspectives in images and data captured during a single collection period and across multiple collection periods. Like TLS, these ground based techniques are also lacking in their spatial extent. Large volumes of data and associated computer power are required for the processing of TLS and ground-based photography (for SfM-MVS) data. Resources and expertise to efficiently handle such data may not be readily available therefore potentially restricting the use of these techniques for some projects.

#### 1.4 The rise of drone technology

Drone is a broad term used to describe remotely piloted, powered aircraft, often with autonomous capabilities that can carry a payload (e.g. a sensor). Lightweight drones are typically <7 kg. Recently, there has been a rapid uptake of drone technology in ecological and environmental research. The ability to take scale-appropriate measurements with fine spatial resolution and control over revisit times has made drone platforms an increasingly popular choice for collecting spatial data (Anderson and Gaston, 2013). Applications are wide-ranging and encompass fields from geomorphology to ecology, with users applying drone-based data collection methods to map habitats to delineate landcover types (Chabot and Bird, 2013), quantify vegetation cover (Breckenridge et al., 2011) to inform management decisions or conservation efforts (Chabot et al., 2014), and monitor the location and estimated populations of wildlife (Jones et al., 2006).

The flexibility to deploy drones at times suited to the user and environmental conditions has allowed for data collection in extreme environments such as Antarctica, where alternative approaches are unviable (Goebel et al., 2015). The

user-controlled revisit times that can be managed with drone-based remote sensing surveys is also attractive for monitoring change in dynamic systems such as fragile farmland prone to erosion (Eltner et al., 2015). The potential to achieve fine temporal resolution and flexibility in when data are collected is unmatched by satellite platforms and comes at a much lower cost (approximately 10 times cheaper) than airborne data acquisition (Jones et al., 2006), with the caveat that each drone survey at present tends to be limited by policy or battery life, restricting each survey to relatively small spatial extents of a few hectares per survey. Along with the potential for fine temporal resolution data collection, drones also offer a platform for optical, near infra-red and thermal cameras to collect fine spatial resolution data with ground sampling distances of sub-decimeter (i.e. 10 mm from a multicopter drone system flown at 25 m altitude with a 12 megapixel red, green, blue (RGB) digital camera (Puttock et al., 2015)). This can provide new insights into environmental processes when compared to existing remote sensing products such as Landsat observations which are collected at a spatial resolution of 30 m (Kovalskyy and Roy, 2013). Also, the miniaturisation of sensor technology such as LiDAR sensors (which are now a viable payload for larger drone systems) provides new opportunities for coastal monitoring, such as quantifying the size of aeolian dunes (Solazzo et al., 2018). The nature of drone based data collection means that issues such as cloud contamination (Asner, 2001) are less of a problem (eliminated if non-radiometric data are sufficient for the application) and the need for atmospheric correction (Chavez, 1996) is greatly reduced or eliminated due to the low altitudes at which they fly.

In line with the technological developments which have converged to make drones viable and widely applicable research tools (e.g. hardware miniaturisation & accessible computer processing power), kite based proximal sensing has also seen a renaissance. A review of the resurgence of this approach can be found in chapter 5.

### 1.5 How are drones being used at the coast?

Lightweight drones are already being used for research (and recreation) at coasts across the globe. There are many opportunities to apply drone technology for research and monitoring in coastal environments, including wildlife monitoring, 2D, and 2.5D habitat mapping (Joyce et al., 2018). Given the flexibility in design and ability to carry a variety of payloads, this form of proximal sensing is being synergistically applied across multiple areas of marine science and conservation (Johnston, 2019). The advantages of very fine spatial resolution data (e.g. sub-decimeter optical data) and user-controlled revisit times (e.g. at optimal tide states) make lightweight drones a well-suited proximal sensing platform for dynamic coastal environments. This section will focus on coastal applications and highlight published work which demonstrates the strengths of drone technology at the land-sea interface.

Drone-mounted optical sensors have been used as a census tool in shallow marine areas, for example to count organisms such as elasmobranchs (Kiszka et al., 2016; Rieucau et al., 2018), jellyfish (Raoult and Gaston, 2018) and in terrestrial coastal areas (e.g. to count penguins (Ratcliffe et al., 2015). Furthermore, non-optical sensor payloads have been applied novelly to collect biological samples such as whale sputum (Geoghegan et al., 2018) for further

virological analysis. These examples demonstrate the ways in which drones can reduce the effort involved in sampling, counting, or collecting data and also illustrate the way in which previously limiting methods have been replaced by methodologies with a potential to deliver higher sampling rates or greater sample sizes.

The fine spatial resolution available from optical sensors on board drones has been utilised for 2D habitat mapping, both in the terrestrial realm (e.g. to classify broad coastal and wetland landcover types (Sturdivant et al., 2017), and also in shallow marine areas to identify suitable nursery habitat for fish (**Figure 1.2**; Ventura et al., 2018, 2016). All of these examples have undertaken classifications using object based image analysis (OBIA), a technique increasing in popularity, due mostly to the fine spatial resolution optical data available from sensors mounted on drones. Beyond optical sensing, infrared sensors have been used to detect contamination of coastal waters (Lega et al., 2012).

Structural and topographic change investigations are being undertaken in a variety of coastal environments, most commonly with the use of data derived from SfM-MVS workflows. More about this technique can be found in section 3.3.1. Examples of this form of analysis at the coast include the study of the topography of coastal dunes (Gonçalves et al., 2018; Mancini et al., 2013), changes in beach topography (Casella et al., 2016), in relation to both natural and artificial changes to the environment (Gonçalves and Henriques, 2015). In the intertidal zone, fine spatial resolution topographic and multi-spectral data have been used to link geomorphological variables to the presence of biotic features such as macroalgae (Murfitt et al., 2017). Beyond terrestrial coastal applications, drones

have also been used to produce bathymetric data (comparable to airborne LiDAR measurements) in shallow tropical coral reefs (Casella et al., 2017).

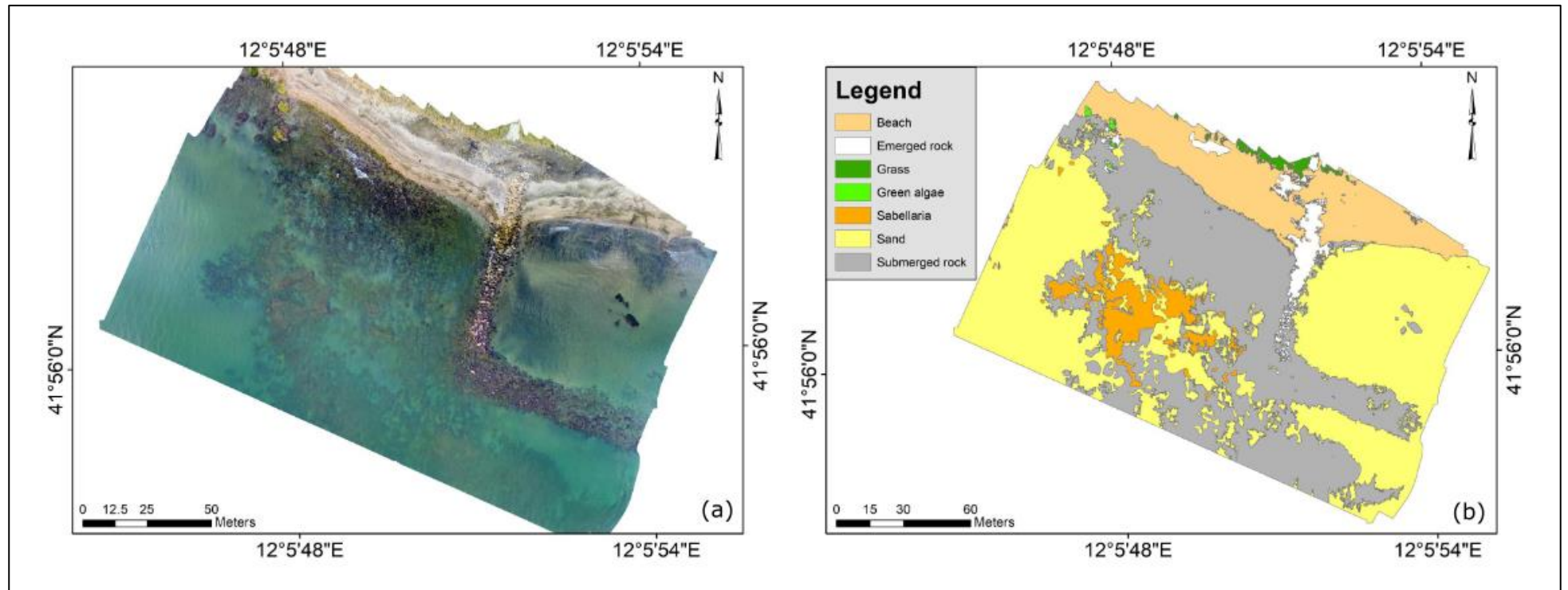


**Figure 1.2: (A) Orthomosaic representing a sandy coast with underwater formation of reef-building tube worm *Sabellaria alveolata*. (B) Thematic map of the same areas generated after image segmentation and classification through an OBIA algorithm. Figure reproduced from Ventura et al. (2018).**

## 1.6 Kite-based proximal sensing at the coast

Kite-based proximal sensing is well suited for coastal environments due to the abundance of a natural fuel source in the form of wind. Furthermore, the minimal number of moving mechanical parts (none if a fixed sensor mount is used) makes them suitable for operations in coastal zones where salt and sand can cause degradation of electronic components. As seen with the application of lightweight drones at the coast, a variety of work utilising kites as proximal sensing platforms has been published in recent years.

The high altitude (~250 m) safely obtainable with a tethered device such as a kite has allowed for comprehensive seabird population counts (Delord et al., 2015). Habitat and land cover mapping has also been undertaken using optical sensors such as consumer grade cameras (Currier, 2015). Multispectral sensors have been used to map invasive vegetation species (Madurapperuma and Dellysse, 2018) and map the presence of algae in the intertidal zone (Bryson et al., 2013) by using the Normalised Difference Vegetation Index (NDVI). Kites have also been used to obtain data for SfM-MVS processing in order to quantify the movement of boulders in response to storm events (Autret et al., 2018), and changes in rubble and sediment topography on a coral cay (Bryson et al., 2016).

## 1.7 The land-sea interface explored in this thesis

As described in section 1.1, the coastal zone harbours a huge diversity of ecosystems, which can be broadly grouped by their position within the land-sea interface. In this thesis, three key coastal environments were empirically studied; coastal dunes, intertidal seagrass meadows and coral reefs (**Figure 1.3**). Each of these environments present their own unique challenges and opportunities (for both data capture and processing) with regards to proximal sensing with drones and kites. Between them, a range of environmental conditions and complexities are found, including differing levels of water presence, and types of vegetation and substrate. Accessibility is highly variable across these three ecosystems, with dunes accessible on foot, seagrass only exposed at low tide and reefs fully submerged. The following sections introduce each of these three environments in turn, giving an overview of their importance, the pressures they face, how they are monitored, and what opportunities proximal sensing utilising lightweight drones and kites could unlock.

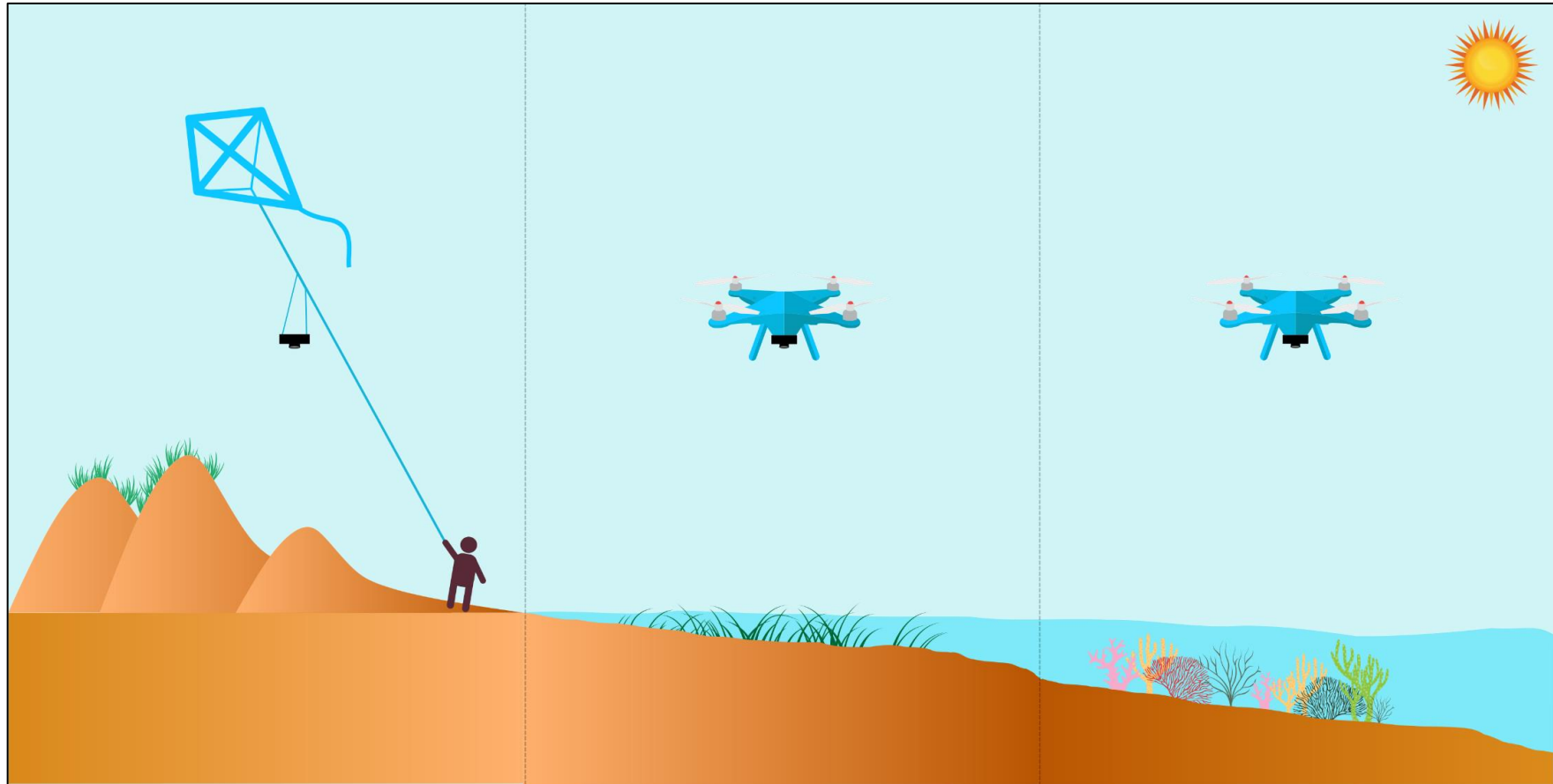


**Figure 1.3: Conceptual diagram of the land-sea interface explored in this thesis. Three ecosystems are represented – coastal sand dunes, intertidal seagrass meadows and tropical coral reefs. The proximal sensing techniques used in each environment are also indicated with a kite, and two lightweight drones. Vector icons from [www.vecteezy.com](http://www.vecteezy.com).**

## 1.8 Coastal dunes

Coastal dune systems are highly dynamic environments, susceptible to change caused by weather events and anthropogenic pressures. Like many other coastal environments remote sensing is already employed for monitoring purposes. However, the spatial scale of these remote sensing approaches has often been coarse, with large (i.e. annual) gaps between sampling. Frequent data collection using a drone or kite platforms could be combined with SfM-MVS techniques, algorithms which have become more powerful with the availability of more powerful computer systems. These algorithms can effectively be used to create 2.5D models of dune systems, potentially allowing for the detection of fine spatial and temporal scale changes in dune form, through erosion and deposition (Mancini et al., 2013).

### 1.8.1 Extent and importance

Coastal dune systems are a global phenomenon, found on coastlines from high latitude polar regions to the tropics (Martinez et al., 2004). They occur in intertidal zones where there is a supply of sand and prevailing winds capable of transporting sediment (Everard et al., 2010). Some of the ecosystem services provided by sand dunes include raw materials, coastal protection, erosion control, habitat for biological diversity and tourism/recreation (Barbier et al., 2011). Despite their close proximity to the sea, dunes also serve as catchments, with aquifers able to provide drinking water (van der Meulen et al., 2004). Like other coastal habitats, the process of carbon sequestration provided by dunes has also been explored, with the value of CO<sub>2</sub> sequestration currently valued at £9 million per year in the UK alone (Beaumont et al., 2014).

Coastal protection has been one of the more well studied services that dunes provide. If these dune ecosystems and associated sand dominated environments are managed well, then they can offer a sustainable defence against storm damage (Hanley et al., 2014). In relation to the effects of storm conditions on sandy coastlines, three important roles have been identified: sand reservoirs, energy dissipation and barriers to storm waves and swash (Leatherman, 1979). The importance of dune presence was demonstrated during the 2004 Asian tsunami where it was observed that beachside properties with in-tact dunes were less effected than those that had removed them (in this case for aesthetic purposes; Liu et al., 2005). Linked closely to storm protection is the erosion control dunes provide through the trapping of sediment (Barbier et al., 2011). The reduction of the movement of sediment in this way can protect sandy coastal habitats and the ecosystem services such as recreation that they provide (Huang et al., 2007).

#### 1.8.2 The pressures on coastal dune environments

Sandy shores are naturally harsh dynamic environments, but are expected to be under increasing pressure from both natural storm events and numerous anthropogenic pressures such as pollution, mining and tourism (Brown and McLachlan, 2002). There are examples of inappropriate management leading to urban development in dune environments, in turn having a strong effect on these ecosystems (Carboni et al., 2009). The continuous development of coastal areas, and implementation of hard defences to mitigate storm damage has, in some European places, led to the loss of dunes and their associated natural protection (Hanley et al., 2014). In a study of 26 different sites along 902 km of coast in Mexico, 81% of dune systems showed vulnerability levels of concern (Martínez

et al., 2006). An emphasis was put on management in this study, showing that monitoring is required to quantify the stress on dune systems, often exacerbated by human disturbance.

### 1.8.3 *In-situ* monitoring of coastal dunes

*In-situ* dune monitoring can involve measurements of dune structure and vegetation coverage using levels and quadrats (Hesp, 2013). With a focus on dune vegetation, biotope maps have been drawn by hand and digitized (Lee et al., 2012). These manual methodologies are time consuming and costly, when put into context of the size of area covered. *In-situ* data collection at dune sites can also be logistically challenging, due to the variable weather conditions in these areas and topography of the landscape. Yearly vegetation transects have also been performed in dune systems to quantify species composition and the effects of invasive species in dune ecosystems (Stanisci et al., 2014). Although fine-grained and repeatable, transects are limited in their scope, and only provide a snapshot of the ecosystem in time and space.

### 1.8.4 Monitoring coastal dunes with remote sensing

Compared to other coastal environments, published studies utilising optical data from satellite platforms to study coastal dune processes are limited in number. This is presumably because the environment is a challenging one, with mixtures of plants and sand/sediment giving rise to mixed pixels in satellite data. To provide some examples, multispectral data from the Landsat program has been used to identify spectral differences in sand colour which indicates the presence of freshwater ponds within the dune ecosystem (Levin et al., 2007). Finer spatial

resolution WorldView-2 data have also been used to delineate landcover types in a mixed dune and marsh environment (Rapinel et al., 2014).

Airborne LiDAR has been used to look at the volumetric change in coastal dunes, for example in response to storm events (**Figure 1.4**; Houser et al., 2008). Woolard and Colby (2002) found that data at a spatial scale of 1 m was best for describing the change in dune structure over time. Beyond 2 m, the resolution, the estimations of volumetric change spiralled, highlighting the need for fine spatial resolution data when studying dune form.

Digital photogrammetry techniques have been used with paired aerial photographs of dune systems to detect blowouts and other processes of dune development (Brown and Arbogast, 1999), and to quantify volumetric changes in dune systems (Ojeda et al., 2005). Although successful digital elevation models were created in the latter, the study was constrained by the availability of aerial data, which were collected at different spatial resolutions. Inconsistencies such as this in remote sensing data are likely to lead to error in analyses so there is a need to use consistent workflows for both data capture and processing. For example, capturing images with the same sensors, from the same altitudes and accounting for lighting conditions.

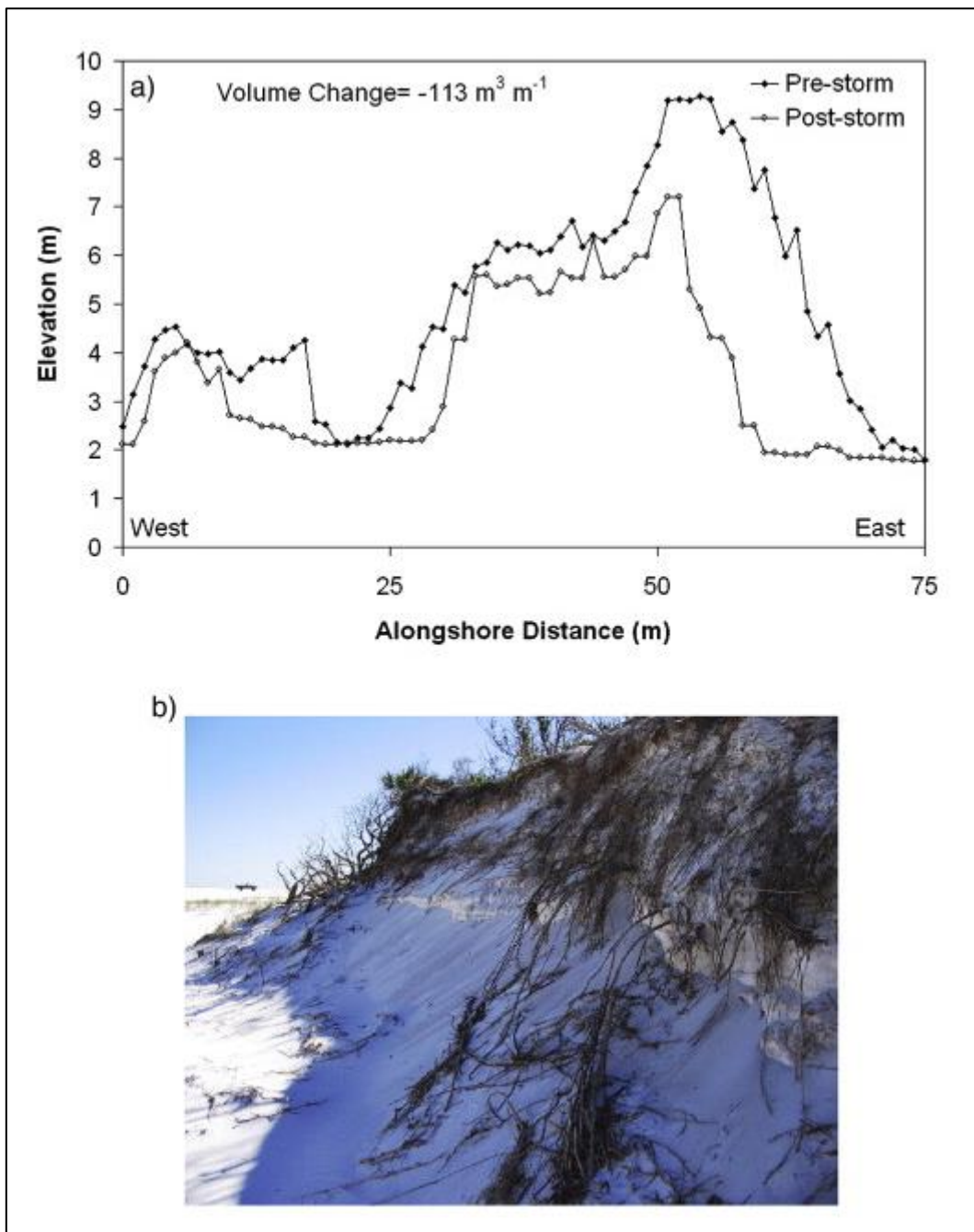


**Figure 1.4: (A) Alongshore profile of a backbarrier dune pre- and post-storm Ivan, created with data from airborne LiDAR surveys. (B) A photograph of the dune showing erosion on the eastern side. Figure reproduced from Houser et al. (2008).**

### 1.8.5 How can proximal sensing be used to monitor coastal dunes?

Drone technology has been used to reconstruct topography of a beach dune system using SfM-MVS processing in Italy. Results were compared to a TLS survey of the same features and the SfM-MVS derived model using data collected with a drone platform, with no more than a 50 mm error between vertical distances detected (Mancini et al., 2013). In order to understand the changes in dune structure over time, a quasi-3D approach is required (Andrews et al., 2002), and with data collected from a drone or kite, this is a lot more easily achieved than with existing methods such as utilising airborne or satellite data or *in-situ* techniques. SfM-MVS works best with a combination of oblique and nadir aerial data in most structured systems (James and Robson, 2014) because multiple viewing angles lead to a greater number of tie points in the processing workflow. From the ground, one cannot readily deliver the oblique data necessary to construct topographic models of dune systems due to the elevational range that coastal dunes can span. The issue with satellite or airborne image data is the lack of variation in view angles at temporally similar points in time. However, with a drone (especially multirotors) or kite platform, the flexibility in both the way in which payloads can be mounted, along with the manoeuvrability of the device means that data of the preferred specifications can be collected, but at the expense of large spatial coverage.

One potential application of proximal sensing in these systems is to deliver new understanding of the way in which storms modify dune structure and vegetation. For example, proximal sensing data could be used to build a topographic model before and after a storm event, allowing for a process-specific investigation of erosion and depositional processes (**Figure 1.5A-C**). This could also be applied

to other disturbances, such as those caused by human activity, allowing the impact to be studied post-activity. (**Figure 1.5D-F**). Another application relates to tracking vegetation dynamics on dunes. The presence and volume of various species can vary seasonally, and fine spatial resolution optical data could be used to quantify these temporal changes. The control over revisit times makes drones and kites highly desirable tools for environmental monitoring and for supporting the management of these ecosystems.

Like most coastal environments, sand dunes are challenging places to conduct research. In particular, sand poses a major challenge for access and maintenance of equipment. Although drone platforms are used in the air, take-off and landing must take place from a stable surface. Spinning propellers can set sand in motion, causing potential damage to components and the camera on board (Mancini et al., 2013). This operational constraint must be carefully considered when using drone technology in such sandy environments. On the contrary, kite platforms excel in these environments, using the often-abundant lift from the wind and the absence of moving mechanical parts.

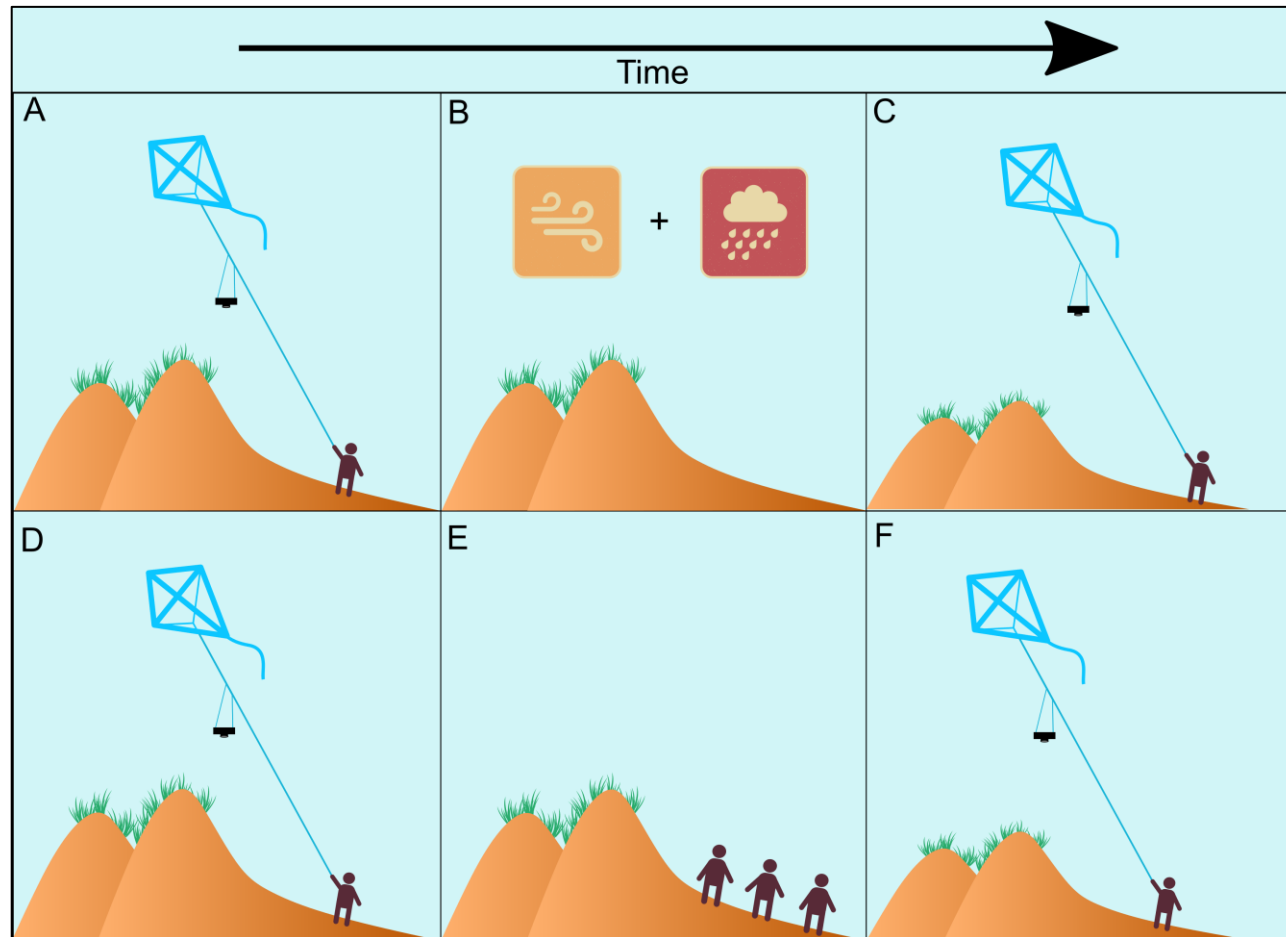


Figure 1.5: Two potential uses of kites to monitor changes in coastal sand dunes. A-C) show that collection of data before and after a storm event is possible with a sensor on a kite. D-F) shows that impacts of human activity can be monitored by collecting data with a kite before and after a particular period of disturbance. Vector icons from [www.vecteezy.com](http://www.vecteezy.com).

## 1.1 Seagrass meadows

### 1.1.1 Extent and importance

There are 60 seagrass species found globally, in both temperate and tropical waters, covering approximately 0.1-0.2% of the global ocean (Duarte, 2002). The highest species diversity occurs in south-east Asia and the western coast of Australia (Tittensor et al., 2010). Seagrasses are described as ecological engineers (Orth et al., 2006), and foundation species that, through their physical characteristics, provide habitat for other species or ecosystems (Hughes et al., 2009). Most seagrass species grow subtidally, to depths where ~11% of sunlight reaches the bottom (Duarte, 1991), although some do grow in intertidal zones (Duarte, 2002). Seagrass habitats provide a variety of ecosystem services such as raw materials, food, coastal protection, erosion control, water purification, carbon sequestration, maintenance of fisheries and recreational services (Barbier et al., 2011). The direct exploitation of seagrasses have declined with time, although they are still harvested for agricultural fertilizer (de la Torre-Castro and Rönnbäck, 2004), and in the Solomon Islands used for more symbolic social purposes (Lauer and Aswani, 2010). Other benefits include coastal protection, which has been cited as an important service due to their ability to dampen wave energy (Barbier et al., 2011). However, the level of protection varies depending on factors such as species, density, location and tidal regime (Koch et al., 2009). Stabilization of sediment is also provided by their plant root and rhizome structures, reducing the removal of sediment from the ecosystem (McGlathery et al., 2012).

Seagrasses are among the most effective natural ecosystems for sequestering carbon (Macreadie et al., 2014), with global burial of carbon in seagrass meadows estimated between 48 and 112 Tg yr<sup>-1</sup> (Kennedy et al., 2010). The plants absorb carbon from the seawater, mainly in the form of dissolved aqueous carbon dioxide (CO<sub>2</sub>) during photosynthesis but they also use bicarbonate (HCO<sub>3</sub>) from the water during growth (Barbier et al., 2011). They play, therefore, a significant role in the marine carbon cycle, by burying carbon in the sediment and creating a carbon sink (Duarte et al., 2005). With increasing awareness regarding the effectiveness of seagrasses in sequestering and burying carbon, concerns have grown over the potential impact to climate of the global loss of seagrass habitat. Although the plants can be replanted, much like terrestrial species, the environmental conditions (i.e. water quality and light availability) which can cause the loss of seagrass beds are more difficult to restore than on land (Fourqurean et al., 2012). Restored seagrass meadows of *Zostera marina* are estimated to accumulate carbon at levels similar to natural stocks within 12 years of initial seeding (Greiner et al., 2013).

#### 1.1.2 The future of seagrass meadows: threats and pressures

Despite their fundamental roles in marine environments, seagrass habitats, are in decline globally with 29% of known areal extent having disappeared between 1879-2009 (Waycott et al., 2009). Described as uncharismatic compared to other coastal ecosystems such as coral reefs, proportionally less attention is paid both by the scientific community (e.g. 5 times the number of scientific papers published on coral reefs compared to seagrass) and the media (Duarte et al., 2008). The causes of such declines in seagrass habitats are due to disturbances. These can generally be broken down into natural events (e.g. geological, meteorological and

biological) and anthropogenic related issues (e.g. reduction in water clarity, physical damage and pollution) (Short and Wyllie-Echeverria, 1996). Rapid environmental change driven by increased anthropogenic pressure in the coastal zone is a major threat to seagrasses (Orth et al., 2006). Whilst, the addition of physical structures to the coastal environment can prevent the shoreward migration which is necessitated by sea level rise (Orth et al., 2006). This demonstrates that pressures rarely work in isolation and it is often a more complex mixture of natural and human-derived threats that ultimately reduce their coverage, with negative implication for the wider ecosystems in which they grow (Waycott et al., 2009).

The reduction in water quality is one of the major factors causing seagrass declines globally (Duarte, 2002). It is often linked to development in and around catchments which physically connect to seagrass habitats. Multi-decadal decline in multiple seagrass species has been attributed to industrial development and the addition of plant rich nutrients to the marine environment (Cambridge and McComb, 1984). Changes in turbidity and disruption to the environment through the process of dredging, have also been cited as factors for long term declines in seagrass meadows, with processes such as wasting disease potentially caused by degradation in environmental conditions (Giesen et al., 1990).

Seagrass ecosystems are likely to be affected by further climate change. The key effects of climate change on seagrasses have been identified as sea temperature rise (Koch et al., 2013), sea level rise, increasing CO<sub>2</sub> within the oceans, and increases in UV-B radiation (Short and Neckles, 1999). Furthermore, the introduction of non-native species can impact delicate seagrass ecosystems. For example, the introduction of seaweed farming and associated macroalgae

species led to decreases in seagrass coverage and associated macrofaunal abundance (Eklöf et al., 2005).

#### 1.1.3 *In-situ* monitoring of seagrass

Monitoring of seagrass often requires *in-situ* sampling with quadrats and snorkels (Downing and Anderson, 1985), usually to verify larger scale approximations (Kutser et al., 2007). Surveys are also undertaken from hovercraft (Dumbauld and McCoy, 2015). More recently, the availability of robotics technology for environmental monitoring has led to a number of innovative applications. The effectiveness of autonomous underwater vehicles were compared to traditional snorkel based surveys, concluding that they are highly useful tool in deeper waters where snorkelling was not feasible (Roelfsema et al., 2015). This style of surveying is often localised and requires up-scaling up to obtain data appropriate to seagrass meadows as a whole.

#### 1.1.4 Monitoring seagrass with remote sensing

Monitoring of seagrass habitat is critical to track changes in its extent, but it can also be used as a proxy or sentinel for the condition of the environment in which it grows (Dennison et al., 1993). The coastal habitats in which seagrasses reside are often challenging environments for extensive *in-situ* data collection. Considering this challenge, remote sensing has been employed as an effective mapping technique both in terms of cost and time (Armstrong, 1993; Mumby et al., 1999). The research effort in this area is echoed by the availability of resources such as spectral libraries detailing seagrass species (Fyfe, 2003).

Aerial photography has been used to track the changes in seagrass cover within Tampa Bay, Florida, although the coarse spatial resolution (minimum mapping unit of seagrass was 2.5 h), was attributed to potential error within the study (Robbins, 1997). Whereas, colour aerial photography has been utilised to track changes in eelgrass in relation to pressure from nitrogen loading (Short and Burdick, 1996). This work demonstrated overall declines in seagrass cover over time, with variations between sub-basins. Products such as Landsat data, aerial photographs have still played a role as reference data for these analyses (Ferguson and Korfmacher, 1997). When available, archived aerial photography can provide multi-decadal time series. A dedicated flight in optimal conditions was used to collect rectification base imagery from which to analyse older data (Kendrick et al., 2002). The opportunistic nature of data collection in this study demonstrates an advantage of using aircraft to obtain spatial data; minimal winds, an incident sun angle of 20-30° and maximum water quality were cited as factors making the conditions optimal (Kendrick et al., 2002).

Optical Earth observation data obtained by the Landsat program have proven to be a popular choice for monitoring seagrass meadows, with a range of examples in the published literature (Armstrong, 1993; Ferguson and Korfmacher, 1997; Gullström et al., 2006; Macleod and Congalton, 1998; Schweizer et al., 2005; Wabnitz et al., 2008; Ward et al., 1997). Multiple band combinations have been used with just the visible bands (Armstrong, 1993), visible and near-infrared (Ferguson and Korfmacher, 1997) and a six band configuration (Gullström et al., 2006) all used to map seagrass meadows. The 30 m spatial resolution of Landsat data have been appropriate for studies over large extents such as 50 km<sup>2</sup> (Gullström et al., 2006), but its associated lack of detail has not been able to

detect finer features such as smaller seagrass patches (Wabnitz et al., 2008) because seagrass shoots are very small features (e.g. *Zostera noltii* leaves are ~0.1 m long) and will exhibit a low spectral contrast against the substrate when viewed from above. Favourable environmental conditions are also required to coincide with the exact time that satellite data are collected. This is often not the case, and factors such as wind can render Landsat data unsuitable for subtidal seagrass habitat mapping, due to movement on the water's surface (Ferguson and Korfmacher, 1997). Furthermore, issues with optical remote sensing in the marine environment include varying water depth and the effects this has on light attenuation. Using Landsat data, transformation of the spectral bands including a depth variable has been applied (by linearising the exponential depth dependence of the signal) to minimize the variance associated with depth, when using bottom surface reflectance (Armstrong, 1993).

One solution to the inability to resolve features of interest in Landsat data products is to use sensors capable of finer spatial resolutions such as those on board the IKONOS satellite constellation. Despite the ground sampling distance of 1-4 m achievable with IKONOS imagery, a comprehensive study focussing on coastal environments found that it was still not possible to discriminate broad habitat categories such as coral, seagrass and algae (Mumby and Edwards, 2002). However, with the addition of finer spatial resolution data from systems such as Quickbird and WorldView, seagrass habitat maps have been successfully constructed (Roelfsema et al., 2014). Multiple biomass and coverage maps of six seagrass species were created using a combination of fine spatial resolution satellite data and *in-situ* samples (**Figure 1.6**). Despite this successful landscape level approach, an estimated 30% increase in the cost of

the monitoring project was attributed to the remote sensing component which uses commercial image products, limiting its large-scale applicability. IKONOS has also been used to map a heterogeneous habitat of seagrass, algae, sand and rock (Malthus and Karpouzli, 2003). The authors of this study were enthusiastic about the promise of finer spatial resolution data achieved with IKONOS, but highlight that limited spectral resolution means it remains difficult to discriminate between submerged cover types with similar properties. Again the incorporation of *in-situ* data was evident, with use of the empirical line method (Karpouzli and Malthus, 2003) for radiometric correction of the data to remove atmospheric effects.

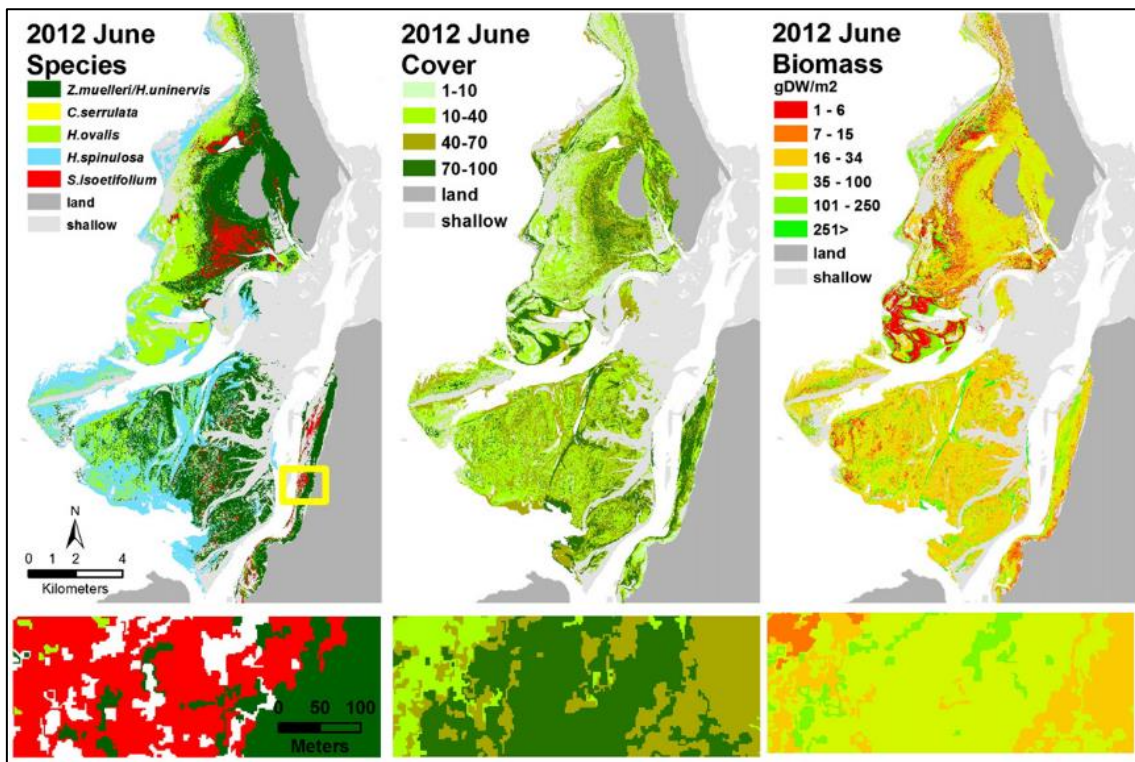


**Figure 1.6: Maps of the Eastern Banks, Moreton Bay, Australia derived from field data and fine spatial resolution satellite imagery (2 m × 2 m pixel size) using OBIA analysis for dominant seagrass species (left), and, seagrass percentage cover (centre) for June 2012. (right) Above ground biomass map. The lower panels indicate the level of detail in each classification, the area of which is defined by the yellow box. Figure reproduced from (Roelfsema et al., 2014).**

#### 1.8.6 How can proximal sensing be used to monitor seagrass habitats?

Within seagrass habitats, proximal sensing will allow for mapping in the realms of individual shoots as opposed to just the extent of meadows as a whole. This will further the understanding of seagrass life history and habitat, both important factors for meadow management, especially when considering whether they are transitory or enduring (Kilminster et al., 2015). As stated previously (see section 1.8.5), fine scale proximal sensing data overcomes issues with other remote sensing workflows both in the temporal and spatial domains. As a result, data could prove useful for tracking seagrass response to disturbance events, monitoring die-off events. For example, a rapid dieback event in Australia was

only successfully mapped months after it occurred using aerial imagery (Seddon et al., 2000). With repeat monitoring on a weekly or even daily basis, a greater understanding of the location and cause of the issue can be achieved. In turn, mitigation could be put in place to try and control the source of die-off (e.g. pollution) protecting seagrass habitat. Monitoring at these fine scales has not yet been demonstrated and remains unexplored.

Some seagrass species are intertidal, whilst the majority grow in fully submerged environments. The permanent presence of water causes issues with both sunglint and light attenuation when collecting remote sensing data. Sunglint is the specular reflection of solar radiation on non-flat water surfaces (Hedley et al., 2005). Techniques have been developed to remove it from remote sensing data (e.g. (Kay et al., 2009)), but post-processing can be time consuming and costly. Drone platforms offer the ability to determine when data are collected, and therefore optimal environmental conditions can be chosen as the time to map seagrass meadows. In many cases, satellites are on fixed orbits and therefore there is no control over revisit times. This can affect the quality of data collected with sub-optimal conditions such as a rough sea surface and a high sun angle, causing sun glint in the captured images (**Figure 1.7**). Whereas, waiting for when the water is in a calm state, or the tide is out, the sun is low in the sky and then collecting data using a drone platform can produce data of a higher quality with minimal sun glint issues (**Figure 1.7**). The relationship between time of day and glint occurrence in data collected with a drone has been discussed in a study researching dugongs (Hodgson et al., 2013). They found that early afternoons were the least favourable time to be collecting data with an optical digital SLR

camera because the sun angle in relation to the sensors position created a greater amount of glint in the captured images.

Multispectral imagery has been utilised in both airborne and satellite based remote sensing of seagrass meadows. Most commonly, the red, green, blue and near-infrared spectral bands have been processed to classify the benthic environment in which the plants grow. Sensors with the capability of collecting spectral data at relatively narrow and spectrally precise wavelengths have now been miniaturised so that they drone mountable (e.g. the Tetracam Micro MCA - [http://www.tetracam.com/Products-Micro\\_MCA.htm](http://www.tetracam.com/Products-Micro_MCA.htm)). Combined, with the all the aforementioned benefits, our understanding of seagrass habitats is set to improve greatly with this technology.

Despite the benefits that drone based data collection can provide, it is important to consider their limiting factors. Light attenuation through water is a well-established issue in coastal remote sensing, and data collection in this way does nothing to try and solve this issue. Flight times are also limited due to the way in which drones are powered. Multicopter drones can typically fly for no longer than 20 minutes and fixed wings for no more than a few hours. This means that the areal coverage is small compared to that achievable in satellite and airborne data. Therefore, the use of drones for seagrass monitoring must be tailored to situations where the benefits of fine temporal and spatial resolution can achieve the biggest gains.

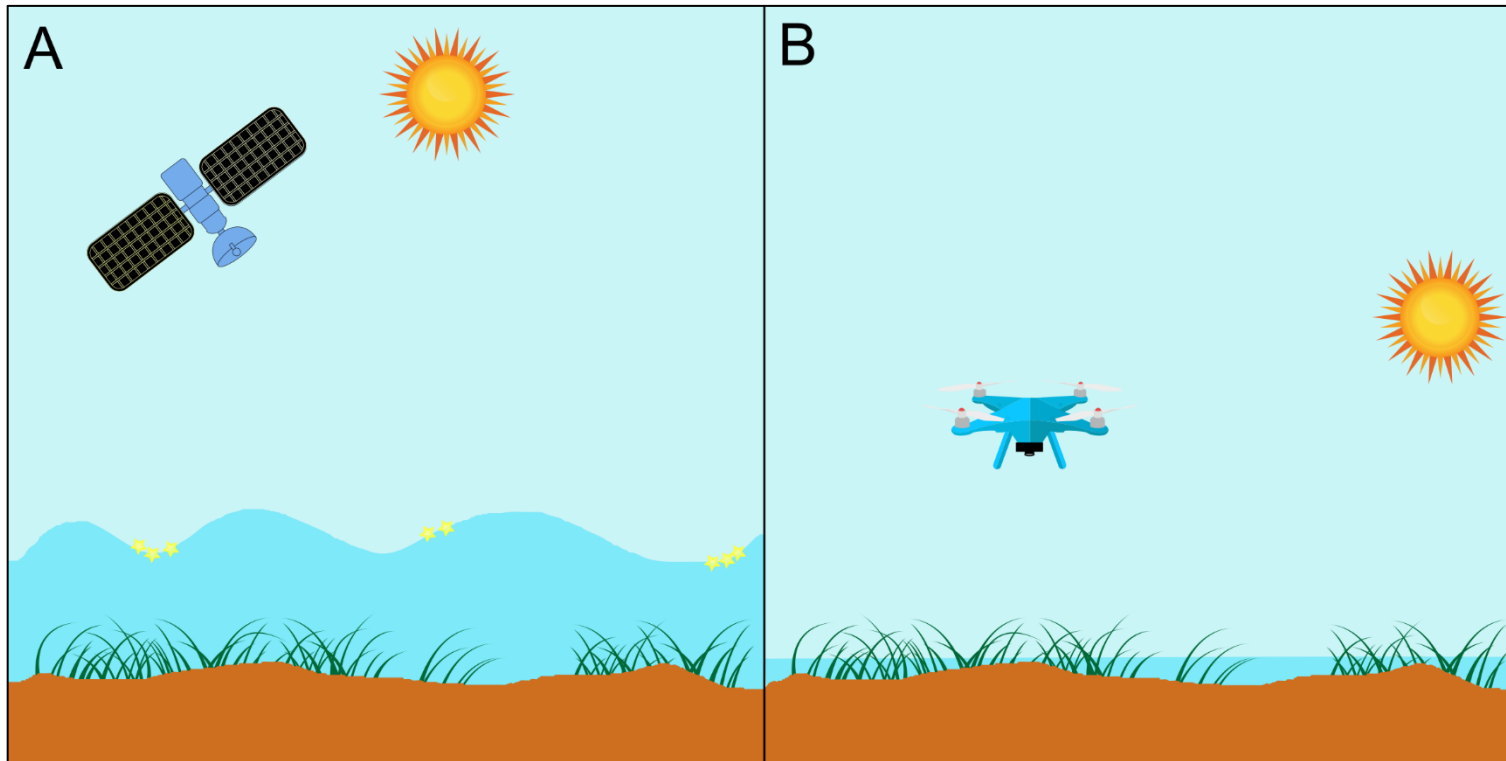


**Figure 1.7: The benefits of remote sensing with a drone. A) Sub optimal conditions include a high sun angle, rough sea surface, causing sunglint, where data collected with a satellite platform may lack quality for remotely sensing seagrass and B) Optimal conditions with the sun at a low sun angle, and calm waters/low tide. When these conditions occur a drone can opportunistically be flown to collect data. Vector icons from [www.vecteezy.com](http://www.vecteezy.com).**

## 1.2 Tropical coral reefs

### 1.2.1 Extent and importance

Tropical coral reefs grow in shallow water environments where photosynthetic activity, (which is critical to their continued growth and survival) is possible (Sheppard et al., 2018a). They are complex self-building ecosystems, where coral species (symbiotically living with algae) deposit limestone as they grow, in turn creating habitat for other sea dwelling organisms such as fish. Globally, they cover an estimated 284,300 km<sup>2</sup> of coastline, with the majority occurring in the Indo-Pacific region (Spalding et al., 2001). These highly productive coastal ecosystems are hugely beneficial to human populations. Some of the key services that they provide include a source of tourism attraction and therefore associated monetary income (Davenport and Davenport, 2006) and coastal protection by buffering shorelines from severe weather and in turn protecting human populations and infrastructure (Barbier et al., 2011). Tropical reefs are some of the most biodiverse coastal regions in the world (Roberts et al., 2002) and as a result are productive environments supporting and sustaining fisheries beneficial to human populations (Russ et al., 2004). Furthermore, reefs play a role in global carbon cycling, taking carbon from the water and depositing it in their hard skeletons as they grow (Sheppard et al., 2018b).

### 1.2.2 The future of tropical coral reefs: threats and pressures

Compared to other coastal environments, tropical coral reefs receive the majority of attention in the literature (i.e. five times the number of scientific publications on reef habitats compared to seagrass meadows due to their perceived greater levels of charisma (Duarte et al., 2008)). In recent decades, a major emerging

threat to tropical reefs has been the increase in bleaching events (e.g. in the Indian Ocean (Obura et al., 2018; Perry and Morgan, 2017a). Bleaching is caused by increases in water temperature (e.g. ocean heat waves), which in turn expel the symbiotic algae from their coral hosts, leaving them unable to survive. In 2018, the average time period between these excessive temperature events is was 6 years, compared to a time period of 25-30 years in 1980 (Hughes et al., 2018).

As well as bleaching, degradation in water quality and anthropogenic activity are cited as threats and causes of coral reef decline. Terrestrial run-off, especially from agriculture (Fabricius, 2005) and also from direct sources such as sunscreen (Danovaro et al., 2008), and the effects of sedimentation (Rogers, 1990) have been studied, each found to have negative impacts on coral functioning and ultimately survival. Other threats to coral reefs include physical damage from fishing practices which involve anchor scraping and explosives used to stun fish (Mcmanus et al., 1997) and disease which can target particular species and/or their symbiotic zooxanthellae (e.g. white band disease on Caribbean coral reefs; Aronson and Precht, 2001). Hurricanes and tropical cyclones, which are natural processes but that are thought to be increasing in occurrence due to climate change, have long been recognized as natural pressures on reef ecosystems, that can alter the structure of reefs in a relatively short period of time, with long lasting effects as phase-shifts or recovery take place (Gardner et al., 2005). Monitoring and mapping coral reefs is crucial to understand their composition, their health, stability, and to detect phase-shifts to more productive or degraded states. Techniques for this include both *in-situ* methodologies and remote sensing, overviews of which are provided in the following sections.

### 1.2.3 *In-situ* monitoring of reefs

Snorkel and scuba equipment are used frequently to collect data from underwater transects in reef environments. For example, across coral reef, seagrass and mangrove habitat, the suitability of nursery habitat for juvenile fish has been assessed with visual estimations (Jaxion-Harm et al., 2012), and diver collected underwater transects have been used to describe the differing geomorphic zones and types of coral (Rajasuriya et al., 1998).

Describing the structural complexity of coral reefs is of interest to researchers and managers alike, as structure can be used as a proxy for reef health and state (Graham and Nash, 2013). Measuring complexity is non-trivial and has been undertaken using a variety of methods including a variable sized wheel system (Wilding et al., 2007), chain-and-tape (McCormick, 1994), and digital gauges (Dustan et al., 2013). Various measures such as rugosity and fractal dimensions have been derived from data collected in these ways in an attempt to describe the complexity of the reef environment. One such application of this data are for calculating the carbonate budgets of coral reefs, where growth rates are incorporated with measures of benthic cover types to calculate net carbonate gains or losses (Perry et al., 2012).

### 1.2.4 Monitoring reefs with remote sensing

Given their positioning in shallow waters, challenging logistics, accessibility issues and their spatial extent, remote sensing has been a useful tool for those researching, monitoring and managing coral reefs (Hamyton, 2017; Mumby et al., 2004). The cost-effectiveness of remote sensing approaches has made it favoured data capture technique for ecosystem assessments (Mumby et al.,

1999), especially with freely available satellite image products such as the Landsat archive (Roelfsema et al., 2018), but relatively little has been achieved using airborne surveys due to cost constraints (Hedley et al., 2012). In one airborne campaign, data collected with an optical sensor yielded true-colour photographs at a spatial resolution of 0.4 m and was subsequently used to describe and map the main bottom elements in a stony reef environment (Cuevas-Jimenez et al., 2002). Also, multispectral airborne images have been captured with the Compact Airborne Spectrographic Imager (CASI) platform (8 spectral bands and a spatial resolution of 1 m) and used to classify distinct types of habitat defined by dominant coral species (Mumby et al., 1998).

The use of satellite derived remote sensing products for coral reef monitoring is well documented and reviewed in detail by Hamylton, (2017); Hedley et al., (2016) and Mumby et al. (2004), and therefore this section will highlight examples from the literature. Some of the most commonly used data products in the published literature are derived from the Landsat, Sentinel and Worldview-2 Earth observation systems. Landsat and Sentinel data are favoured for time series analysis, where the benefits of revisit times of 16 days (Landsat only), which increases in frequency when combined with sentinel products (Li and Roy, 2017). Furthermore, the temporal resolution (Landsat archive spanning back to 1972) of these data also make them valuable for multi-decadal monitoring programs. The benefits of data from systems such as Worldview-2 are a much finer spatial resolution (~0.5 m), which can be used to further advance the understanding of shallow reef complexity and processes. As mentioned in section 1.3.4, using fine spatial resolution data is not a cost effective approach for monitoring. One such example using Landsat products involved multi-decadal benthic cover type

change detection in the Red Sea (El-Askary et al., 2014). Alternatively, fine spatial resolution data provided by the Worldview-2 platform have been used with a focus on habitat mapping for conservation mapping (Selgrath et al., 2016).

Recently, OBIA has become a popular classification tool in coral reef remote sensing studies. OBIA is well suited when features of interest consist of multiple pixels as opposed to individual pixels containing a mixture of features or classes (i.e. a H-resolution case; Blaschke, 2010; Strahler et al., 1986). This scenario is becoming more common with the availability of fine spatial resolution data (e.g. Quickbird-2 images at ~0.6 m used to create benthic cover maps of reefs in the western Pacific (Phinn et al., 2012). However, OBIA has also been shown to work with coarser spatial resolution data of reef environments. For example, Landsat data products at a spatial resolution of ~30 m have been used to classify broad reef cover classes such as sand rubble and coral (Wahidin et al., 2015; Xu et al., 2016), and geomorphologically distinct parts of the reef system e.g. lagoon and forereef (Leon and Woodroffe, 2011) since these features exhibit length scales that are larger than the resolution of the pixels. Despite the variety of successful studies found in the literature, there are limitations to the use of satellite data products for some reef monitoring purposes. For example, Hedley et al. (2018) have shown that bleaching is detectable from Sentinel-2 data, but further work is required to develop bleaching detection methods. The 10 m spatial resolution data allow for relatively coarse bleaching assessments, but are not able to resolve finer scale regions of potentially healthy reef.

With advancements in sensor and processing technology several hybrid methodologies incorporating both *in-situ* data and remote sensing have emerged. Using waterproof or underwater housed consumer grade cameras, Dumas et al.

(2009) categorized different reef cover types such as foliose, encrusting and massive corals. More recently, with the increases in high performance computing hardware, SfM-MVS has been used to create benthic dense point clouds. Handheld underwater photography has been used to create very fine scale (~10 mm spatial resolution) 2.5D representations of the benthic environment (e.g. (Leon et al., 2015). This technique is particularly useful for quantifying the structural complexity of reefs at limited spatial extents (e.g. ~ 1.5 × 200 m; Leon et al., 2015).

#### 1.2.5 How can proximal sensing be used to monitor reefs?

There are already some published examples detailing the application of lightweight drones for capturing data in tropical coral reef environments. Coral bleaching extent has been quantified using an RGB sensor on a consumer grade DJI Phantom 2 drone (Levy et al., 2018), and DEMs produced in a photogrammetry workflow have been shown to produce similar estimates of reef topography to LiDAR measurements (Casella et al., 2017). This study was conducted over a sparsely colonised lagoon (**Figure 1.8**), with near-perfect environmental conditions. Application of this technique in more structurally complex reef areas and in more challenging environmental conditions remains to be tested. This is a growing field of research and examples in the literature are limited, but there is great potential for proximal sensing techniques to progress remote sensing in tropical reef settings. This new methodology could be a crucial tool for monitoring reefs and understanding their response to various pressures such as ocean warming, heatwaves and damage from hurricanes and tropical cyclones.

Logistically, the deployment flexibility available with drone technology, would help capture data in optimal environmental conditions. Wind, tide, cloud, and sun angle can all impact the quality of optically sensed data of submerged features. For example for coastal investigations, Landsat data needs to be carefully chosen so that images captured at high tide are excluded (Sagar et al., 2017). In contrast, with a drone, data can be collected at the desired tidal state. This is also the case with sun glint which has been described in section 1.8.5. The resultant data will be of finer spatial resolution compared to airborne or satellite acquired data and have minimal effects from environmental conditions. The low flying altitude of drones and fine spatial resolution data available from on-board sensors, mean that in coral reef environments, there will be the potential to identify individual colonies in the resultant data. This would be progressive in a field that has been dominated by broad category thematic maps which have identified geomorphologically distinct areas of the reef such as flats, crests and slope from satellite and airborne image data (Capolsini et al., 2003; Roelfsema et al., 2018).

Drones can acquire data at larger spatial extents than is typically possible with *in-situ* reef transects. Incorporating greater parts of the reef in surveys is vital for moving towards a more representative picture of these heterogenous habitats. With careful flight planning and sensor mounting at oblique angles, one can achieve varying view angles of features on the ground/in the sea. This variation in view angles is optimal for SfM-MVS processing to produce dense point clouds (James et al., 2017a). These dense point clouds can inform us of the structural complexity of reef environments, a key proxy for their health. Compared to underwater transects, conducted by hand (**Figure 1.9A**), data captured with a lightweight drone and processed in a photogrammetry workflow could provide

information for much greater spatial extents (**Figure 1.9B**). Lastly, tropical reefs can be logistically challenging areas to work in. In some cases, diving and snorkelling may not be feasible due to boat access limitations. In these situations, drones can collect data from remote areas, quickly and safely.

Despite the large range of potential applications for drones in reef environments, there are still issues to take into consideration when capturing and processing data in this way. There are often very few suitable launch and landing terrestrial areas near reefs, and operating from a boat may be required. Launching and landing from/to a vessel can be challenging and requires an experienced pilot to undertake such manoeuvres and a correctly configured drone as many drones have fail safes that disable their use on a non-stationary platform. Low sun angles are optimal for sensing reefs with drones (Casella et al., 2017), and therefore access to the reef at/before sunrise/sunset needs to be taken into consideration and/or the ability to alter the flight path and sensor configuration accordingly. Furthermore, the salt and sand in these environments can accelerate the degradation of drone components, so extra checks and maintenance routines are necessary. Considering the data collected of submerged features, as mentioned for satellite and airborne data, signal attenuation through the water column remains an issue. Also, refraction and reflections can cause artefacts in images collected from proximal sensing platforms.

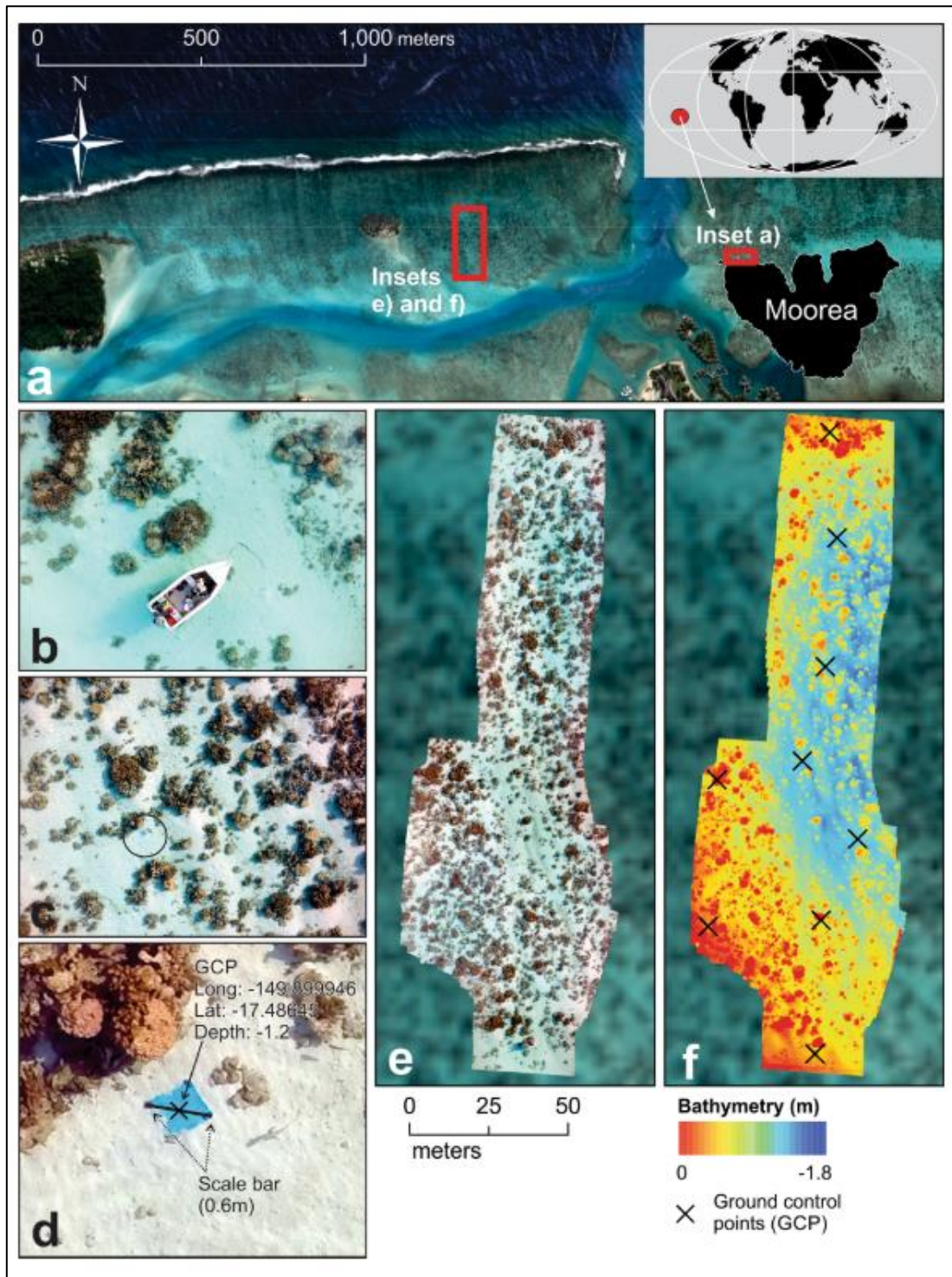


**Figure 1.8: (A)The inner lagoon of Tiahura, Moorea, French Polynesia (aerial image from WorldView-2, DigitalGlobe). (B) Aerial view of the boat used as landing/take-off base for the drone flight. (C) Location of one ground control point (GCP) in the surveyed area; the circle indicates the approximate area represented in D. (D) Detail of C, example of GCP and scale bar used to georeference the image data. (E) Composite orthorectified photo obtained from structure from motion. (F) Bathymetric raster obtained from SfM-MVS, with indication of GCPs. Figure reproduced from (Casella et al., 2017).**

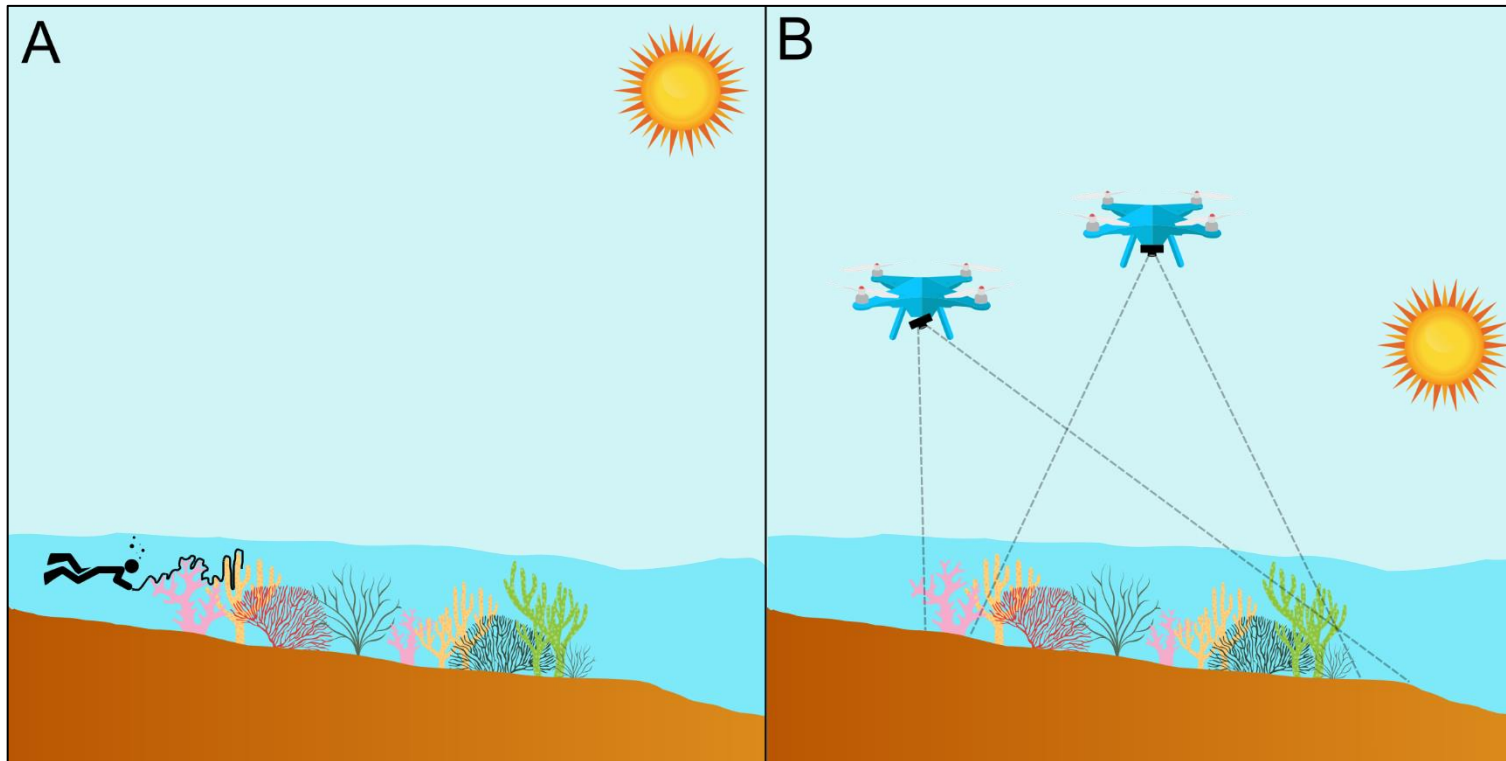


**Figure 1.9: The potential benefits of using a drone in coral reef environments. A) Manual transect undertaken by snorkeller/diver using a chain and tape approach. Transect is limited in its spatial extent. B) Nadir and off-nadir positioning of optical sensor captures more data on the structure of the reef. Also undertaken with a low sun angle to reduce glint on the water. Vector icons from [www.vecteezy.com](http://www.vecteezy.com).**

## 1.9 Summary

There are no shortage of examples demonstrating how remote sensing is being utilised in the complex and highly heterogeneous coastal environments. The development of new remote sensing methodologies and availability of data have revolutionized monitoring efforts in the highly dynamic, structurally and biologically complex coastal zone. This has mainly been driven by the acquisition of images from sensors on-board satellite and airborne platforms, along with ground-based sensing equipment such as TLS. However, there are still some fundamental drawbacks when using these approaches, including those related to weather conditions, tidal state and accessibility. Proximal sensing utilising drones and kites are poised to resolve some of these issues due to the ability to flexibly deploy and customize their payloads for data acquisition. Although many different coastal environments could and have begun to be explored in relation to proximal sensing data, the acquisition and analysis of fine grained data are still largely unexplored. Coastal, sand dunes, intertidal seagrass meadows and tropical coral reefs provide a novel and interesting set of test environments for this new form of data capture. Each of these three ecosystems face diverse threats and pressures ranging from global to local in scale and provide logistically challenging environments in which to undertake proximal sensing data capture. Furthermore, the types of research questions that can be explored, are diverse and can be used to highlight some of the key strengths of using drones and kites for monitoring the highly important coastal environments.

## 2 Research Aims

**The overall aim of this thesis is to develop new approaches using novel proximal sensing platforms such as lightweight drones and kites, that could deliver advances in the quantitative understanding of coastal processes.** The following aims are more focussed in their scope and addressed throughout the thesis:

- i. **Critically evaluate the challenges of operating lightweight drones in logistically demanding environments including the coast [Chapter 4].** The rapid uptake of drones for environmental and ecological research has seen a surge in the number of studies using this technology for data capture. While reported methodologies are often detailed regarding image processing, there is often a lack of information about the hurdles involved with data capture, especially in locations such as coasts, tropical forests and polar environments. To increase the success rate and collaboratively improve the efficiency of drone-based research, a synthesis of challenges and solutions is required to share with the academic community. The early stages of work towards this thesis involved a series of methodological experiments with drones in coastal settings, some more successful than others. It was these experiences, set against a backdrop of a lack of transparency within scientific literature describing experimental pitfalls and complexities, that was used to inform the scope and some of the content of this piece.
- ii. **Review the historical and current use of kites for proximal sensing and assess their feasibility as a modern data capture tool for empirical research [Chapter 5].** The technological advances fuelling the

rapid uptake of drones are also set to benefit other proximal sensing platforms such as blimps, balloons and kites. In particular settings drones will not be the most affordable or suitable proximal sensing platform, whereas kites may provide an optimal solution for data capture. There is a need to review published studies to understand how kites are being used, and explore how kites can be used for empirical research moving forward.

- iii. Investigate the ability of kite aerial photography and SfM-MVS processing techniques to quantitatively assess topographic changes in terrestrial coastal dune systems [Chapter 8].** Coastal dunes are dynamic environments, experiencing spatially and temporally heterogeneous processes of erosion and accretion over time. Limited options exist for cost-effective monitoring of coastal dune environments at fine intra- and inter-annual temporal resolutions. LiDAR data can provide information on dune topography, but such data are often costly and logistically challenging to acquire, and therefore not feasible for regular monitoring purposes. SfM-MVS photogrammetry processing of data captured from optical sensors on a kite platform could be used to assess sub-decimeter changes in coastal topography over time, yet the implications of the variable kite platform on data quality are not evaluated within the literature. Combining time-series analysis with consideration of point-cloud uncertainty will deliver new insights towards the operationalization of kite-based survey protocols in sand dune systems and elsewhere.

**iv. Explore the effectiveness of consumer grade optical sensors on-board lightweight drones to map seagrass coverage within intertidal meadows [Chapter 9].**

Remote sensing of seagrass meadows is currently heavily focussed on quantifying the spatial extent of these habitats alone. A knowledge gap exists relating to the heterogeneity of plants within meadows due to the lack of fine spatial and temporal resolution Earth observation data. Such observations can be indicative of the health of these ecosystems. Drones are well positioned to enable observations which capture within meadow variability, and therefore there is a need to test the ability of these platforms to deliver such data. New work in this sphere targeted at managers and conservation practitioners will deliver new insights into seagrass growth dynamics and indicators of meadow health.

**v. Further develop proximal sensing methodology to quantitatively measure the structural complexity of coral reefs with consumer grade optical sensors [Chapter 10].**

Currently, measurements of structural complexity within coral reef habitats are highly limited in their spatial extent. This is due to the way in which data are captured, typically by snorkel or diver surveys, or through using active sensors attached beneath vessels. Therefore, estimations typically lack representation of the wider reef environment. Proximal sensing and SfM-MVS processing offers the opportunity to up-scale these measurements over greater spatial extents. This has been demonstrated by Casella et al. (2017), but only with a limited set of flight parameters and in a geomorphologically homogenous reef setting. The limits of this technique in reef environments require exploration and

characterisation, to assist in optimising methodologies and understanding how the approach can be successfully applied.

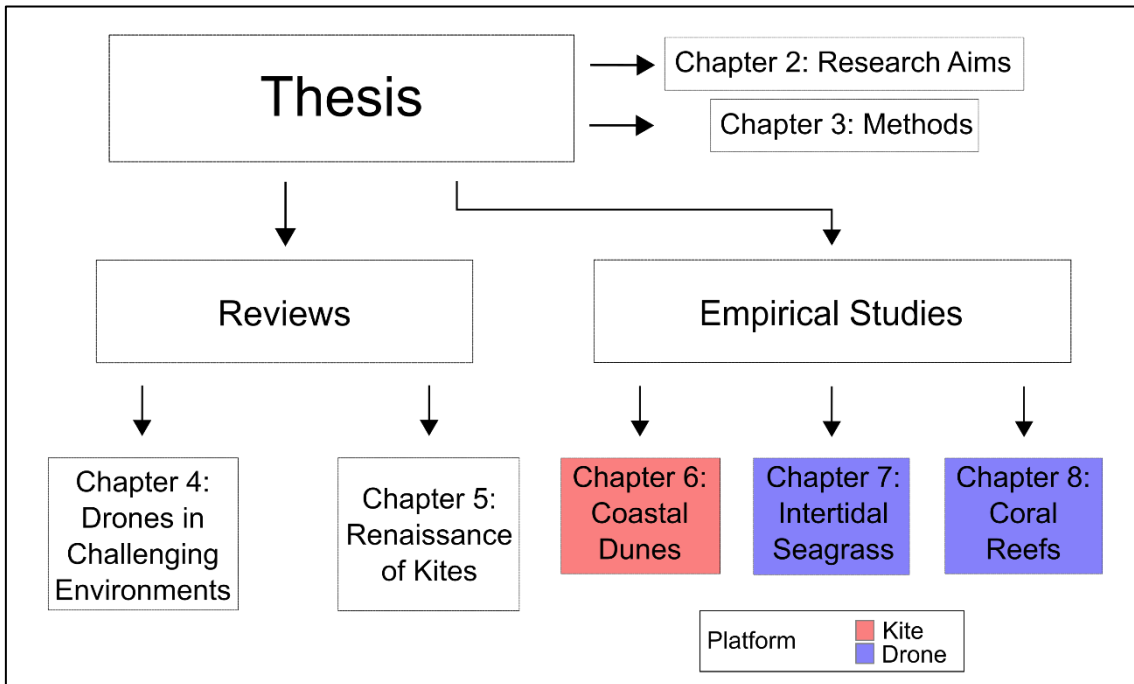


**Figure 2.1: Conceptual diagram showing the structure of the thesis.**

## 3 Methods

Empirical data collection undertaken for this project spanned multiple different environments, but shared commonalities in the equipment, methods and processing/analysis technology used. While each of the empirical investigations (see chapters 6, 7, & 8) contain methods sections relevant to those particular studies, details that were omitted are explored in this section. This chapter also serves to explore some of the broader methodological details found throughout the thesis. Firstly, hardware utilised for data capture and associated modifications are described, followed by a description of the processes involved in deploying drones and kites for data capture. Thirdly, processing techniques including an overview of software packages used to manipulate and analyse empirical data are described.

### 3.1 Hardware

#### 3.1.1 Drones

Airframe design and associated electronic components are rapidly evolving technology realms and even since the start of this PhD project (December 2014) much has changed. However, all of the data captured for this thesis has been undertaken using lightweight multirotor drones (sub 7 kg) using the open source Pixhawk autopilot system (which runs the ArduPilotMega (APM) flight stack (<http://www.ardupilot.org/>)). The main reasons for this choice of autopilot were threefold. Firstly, Pixhawk is open-source hardware running open-source software allowing for customization and user-dictated choice of components (e.g. GPS modules, electronic speed controllers (ESCs) and telemetry). This gives flexibility in the design of a drone and the adaptation for scientific data collection.

Secondly, the multitude of sensors on board the autopilot and those attached to it, record at high temporal frequency (e.g. tens of readings per second) are made easily available for post-flight analysis. This metadata from each flight can aid in the process and analysis of data collected by on-board sensors such as consumer-grade cameras. Lastly, the flight modes available with the firmware, especially the 'Auto' mode, that allows for grid-based mapping. Automated waypoint guided flying allows for user-dictated flight speed, altitude, position and direction to achieve more uniform coverage of a given area. As a result, for example with optical sensors, similar overlap can be achieved between images, than would typically be possible with manual flying modes. At the start of this research project, the autonomous flight capabilities provided by APM firmware were more advanced when compared to other available autopilot systems. Three types of drone (all using Pixhawk or Pixhawk 2 autopilots) were utilised for this project (**Figure 3.1**). They are described as follows:

### **3D Robotics Y6 co-axial hexacopter "Yeti"**

This drone was acquired pre-constructed and 'ready-to-fly'. The following modifications were made, making it better suited for scientific data capture:

- Pixhawk autopilot replaced due to issues with the previous one. 3D printed vibration dampened mount added for Pixhawk autopilot designed, printed and installed.
- FrSky X8R receiver (Rx) installed to allow for more channels for communication. This was to enable a greater number of modes to be assigned to switches on the Taranis transmitter (Tx).

- 3D printed housing for LiPo battery and integrated camera mount for Canon Powershot D30 or Canon S110, designed, printed and installed.

### **QuadH<sub>2</sub>O custom built quadcopter “Henrietta”**

This drone was acquired pre-constructed and ‘ready-to-fly’. It was designed to protect the electronics from water ingress and also has the ability to take-off from and land on calm water. The following modifications were made, making it better suited for scientific data capture:

- DJI NAZA autopilot replaced with Pixhawk autopilot. 3D printed internal vibration dampened housing for electronics designed, printed and installed.
- FrSky X8R receiver (Rx) installed to allow for more channels for communication. This was to enable a greater number of modes to be assigned to switches on the Taranis transmitter (Tx).
- 3D printed vibration dampened camera mount for GoPro Hero 3 and Canon Powershot D30, designed, printed and installed.
- Additional buoyancy installed on the underside of the body with foam strips cut from swimming pool buoyancy device (pool noodle).

### **3D Robotics Solo quadcopter “Duffolo”**

This drone was acquired ‘off-the-shelf’ and ‘ready-to-fly’. No modifications were made to the internal electronics. However, the following additions were made to the external body of the drone:

- Universal vibration dampened sensor mount designed, printed and installed.

- Multiple sensor mounts (e.g. Ricoh GR II (**Figure 3.2**), Agrocam, Canon Powershot D30), both nadir and oblique designed, printed and installed.
- Extended leg mounts (to allow for greater clearance of drone underside from the ground), designed, printed and installed.

Only the 3DR Solo was utilised for empirical data capture as seen in chapters 7 & 8 (**Table 3.1**), but I have included the details of the other two drones as they were pivotal in my development of skills to build, maintain and operate drones for scientific research. Also, many of the lessons learned, which feature in chapter 4 occurred while operating these airframes.

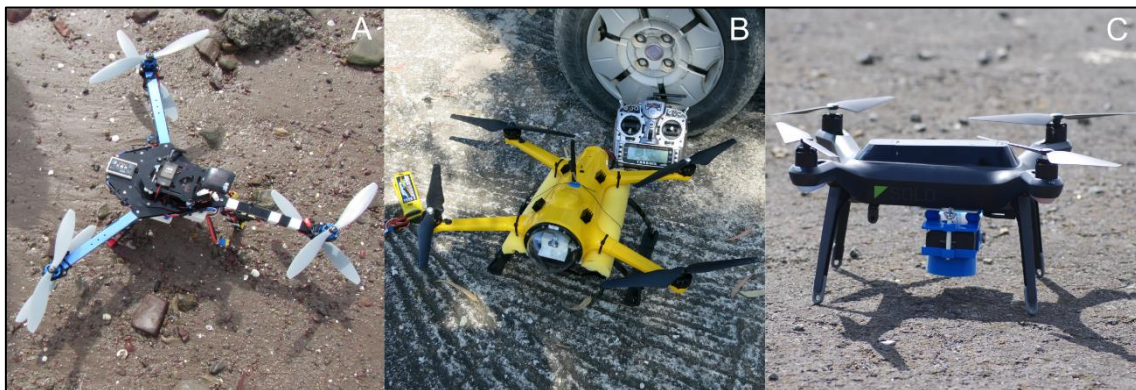


**Figure 3.1: The 3 research drones used during this thesis. A) A 3DR Y6 hexacopter “Yeti”, B) A QuadH<sub>2</sub>O quadcopter “Henrietta”, C) A 3DR Solo quadcopter “Duffolo”.**

### 3.1.2 Kites

The kite Aerial Photography (KAP) setup consisted of two main parts. Firstly, was the kite itself, which was a single line design, created specifically for KAP and was therefore stable and easy to operate (**Figure 3.3A**). For the majority of the KAP data capture an HQ KAP Foil 1.6 was used. For one survey, an HQ KAP Foil 5 was used. During data capture, hanging from the single line of the kite was a picavet, self-levelling mount (**Figure 3.3**). Inspiration for this design was taken

from an easy to build example found at <http://www.instructables.com/id/Kite-Aerial-Photography-Picavet-System-Fun-Simple-/>. A modified version to house a Canon Powershot D30 compact camera was designed and printed using a 3D printer. Nylon kite line and a yo-yo winder were used with the kite. The nylon line was marked with marker pen every 1 m so that an estimated altitude could be obtained during launch and operation.

### 3.1.3 3D printing

3D printing using materials such as Acrylonitrile butadiene styrene (ABS) plastics has democratised the building process of drone components and modifications. In tandem to the physical printer technology (which has been made readily available to the consumer), a plethora of software and online services have also made creating, sharing and modifying computer aided design (CAD) products easier. For design, open source software such as OpenSCAD (<http://www.openscad.org/>) and Blender (<https://www.blender.org/>) make creating designs to print a viable option for many. Beyond this, sharing and modifying can be facilitated with services such as Thingiverse (<https://www.thingiverse.com/>) and Tinkercad (<https://www.tinkercad.com/>). All of these have been used to create and share CAD designs during this project. Using a Stratasys uPrint SEPlus 3D printer (<http://www.stratasys.com/3d-printers/uprint-se-plus>) rapid prototyping was undertaken, allowing for design modifications in short periods of time. Designs ranged in complexity from custom sized washers, to camera mounts. All designs were created in OpenSCAD, toolpaths created and printer operations performed in Catalyst EX 4.4 (the software licensed with the 3D printer).

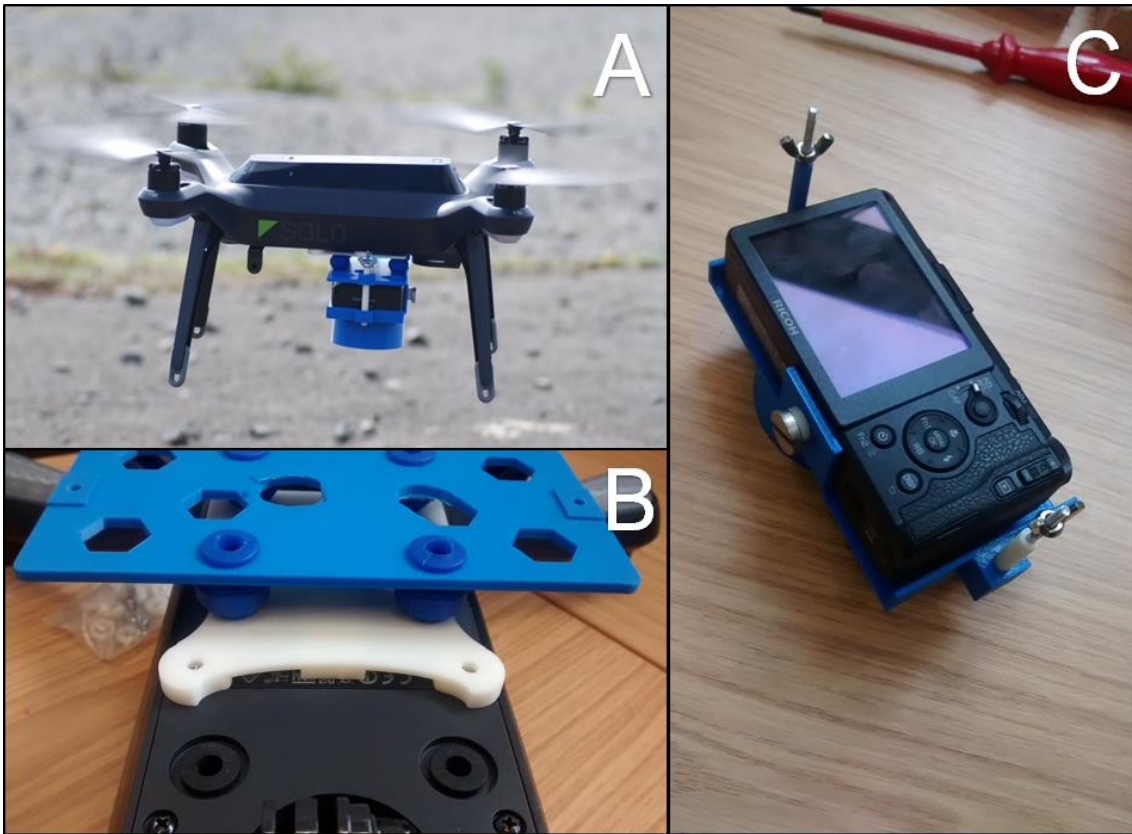


**Figure 3.2: Examples of the 3D printed mounting system used to attach the Ricoh GR II to the 3DR Solo.**

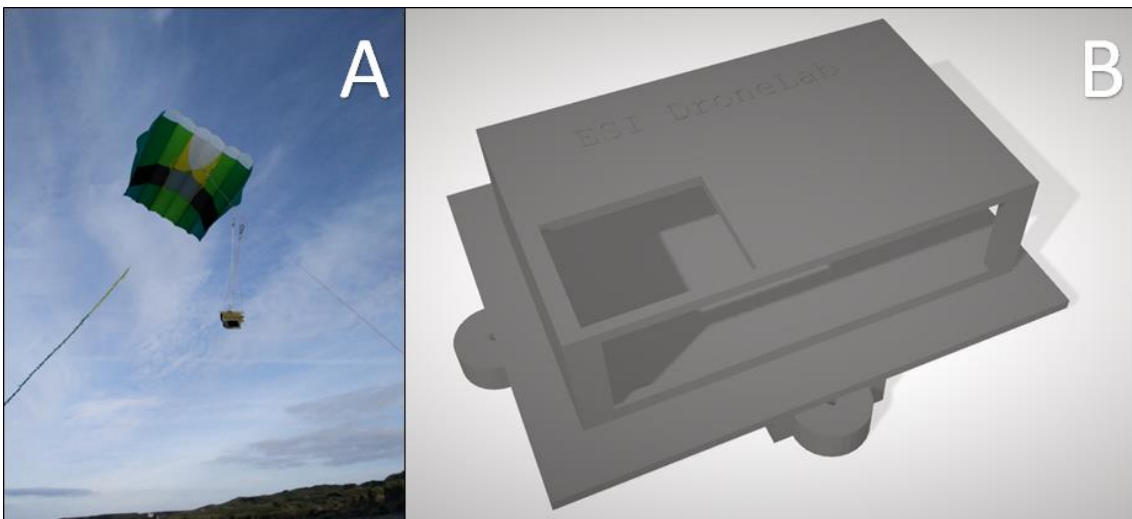


**Figure 3.3: Examples of the KAP setup with the picavet mount attached.**

#### 3.1.4 Canon hack development kit (CHDK)

CHDK is freely available software which can be used to modify the behaviour of some models of Canon compact cameras. One of the main benefits is increased functionality, allowing user control over settings such as shutter speed, ISO, aperture, and the time intervals at which photos are taken. For some models, the ability to capture photos in RAW as well as native JPEG format can be activated. This is especially useful in scientific data capture settings, given that one may want to recover information from the uncompressed 'digital negative' or correct for exposure if images are too under- or over-exposed post data capture. The software is non-destructive and boots from an SD card that has been formatted for CHDK use. Once running on the camera, user-created scripts can be executed, causing the camera to automatically trigger with designated settings. More information about installation and the full features of CHDK can be found at <http://chdk.wikia.com/wiki/CHDK>. This software was used to manipulate the Canon Powershot D30 used with some drone systems and the KAP setup during data collection.

**Table 3.1: Overview of the key equipment used throughout the thesis.**

<b>Equipment</b>	<b>Training and Testing</b>	<b>Sand Dunes - UK</b>	<b>Seagrass - UK</b>	<b>Corals - Maldives</b>
<b>3DR Y6 “Yeti”</b>	X			
<b>QuadH20 “Henrietta”</b>	X			
<b>3DR Solo “Duffolo”</b>	X		X	X
<b>Garmin GPS</b>	X	X		X
<b>Leica D-GNSS</b>	X	X	X	
<b>Kite</b>	X	X		

## 3.2 Data capture

### 3.2.1 Drone operations (legal framework)

The safe and legal application of lightweight drone technology in scientific research is shaped by two factors. Firstly, safety and risk assessment considering both the researchers involved and other individuals and their property in the immediate area. Secondly legal constraints, requiring conformation to rules and regulations often stipulated by a country's aviation authority (e.g. the civil aviation authority (CAA) in the UK).

In the UK, a permission for commercial operations (PfCO) (formerly permission for aerial work (PfAW)) is only required if one is to financially gain from work undertaken with drone technology (e.g. videography at a wedding or inspecting roofing on a property). For research purposes, this permission is not mandatory. However, as preparations for data collection progressed throughout the project, it appeared that major landowners in the UK requested a PfCO even though there would be no remuneration for the data captured. As part of the PfCO application, an operations manual is required for submission to the CAA. Drone operations throughout the project followed those laid out in the ESI DroneLab operations manual (see chapter 10.1 and section 10.2).

### 3.2.2 Drone operations (practical)

All drone operations presented in this thesis followed a similar methodology which I will outline here. As aforementioned the ardupilot autopilot was chosen for its flexibility and ability to plan complex autonomous missions. These missions were created in either Mission Planner (Osborne, 2016) on a Windows machine or Tower on an Android tablet (Huya-Kouadio, 2016). Missions were created in the

field, where hazards and other obstacles can be more readily identified. Planned missions can control airframe speed, altitude and position, as well as take off and landing routines. Once a mission was planned it was uploaded via Wi-Fi to the drone. The drone was restarted, and the mission downloaded, to check that the correct mission was loaded onto the drone. Next, if GCPs were used, they were positioned pre-flight, drone safety checks were undertaken (as outlined in the operations manual) and the sensor (i.e. Ricoh GR II) were set up. In this case the built-in intervalometer was activated. Finally, the drone was launched, and the mission undertaken. Post-flight, data was backed-up onto a laptop, drone battery was changed, and if multiple flights were planned, further missions were uploaded, and the process repeated.

### 3.2.3 Kite operations (practical)

Kite operations are strongly weather dependant, even more so than drone surveys, so weather forecast checking was critical in the build-up to planned fieldwork. Once in the field, the site was checked for potential hazards and an assessment of wind conditions was made based by observation of vegetation and/or using an anemometer. The tail was attached to the kite whilst on the ground, and then the kite was launched with two people. One would hold the foil, and the other would hold the yo-yo winder. The foil was held at arm's length and let go into the wind, with the line let out as the kite gained altitude. Next, the camera was set up, with an intervalometer and fixed settings, and attached to the picavet mount. Then, with the kite in the air, the picavet mount was attached to the kite line using carabiners ~ 1 m apart. Depending on the wind conditions, the kite line was released to gain altitude, and the line operator walked around the survey site ensuring the platform was over areas of interest. After ~30 minutes

the kite was brought down or lowered, and the SD card/battery changed if necessary.

### 3.3 Data processing & analysis

#### 3.3.1 Photogrammetry

With the increasing availability of low-cost computing power and improvements in software such as computer vision SfM-MVS has become a viable tool for modelling environments in three dimensions using only two-dimensional images. A seminal application of this approach utilising the many images available on the internet is the reconstruction of famous buildings in Rome (e.g. the Trevi Fountain) using photographs taken by visitors to these locations (Snavely et al., 2008). Beyond the proof of concept approach, researchers have been applying SfM-MVS to produce data at spatial and temporal scales that have been previously unachievable e.g.in the geosciences (Westoby et al., 2012). The applications of SfM-MVS in Physical Geography and environmental science are well documented in **Figure 3.3** (Smith et al., 2015). The authors describe the origins of SfM-MVS, typical workflows and some example applications. Agisoft Photoscan was used for all SfM-MVS processing in this thesis, to create dense point clouds, DEMs and orthomosaics. All these products were georeferenced, using either GCPs or aerial control in the form of geotagged input images.

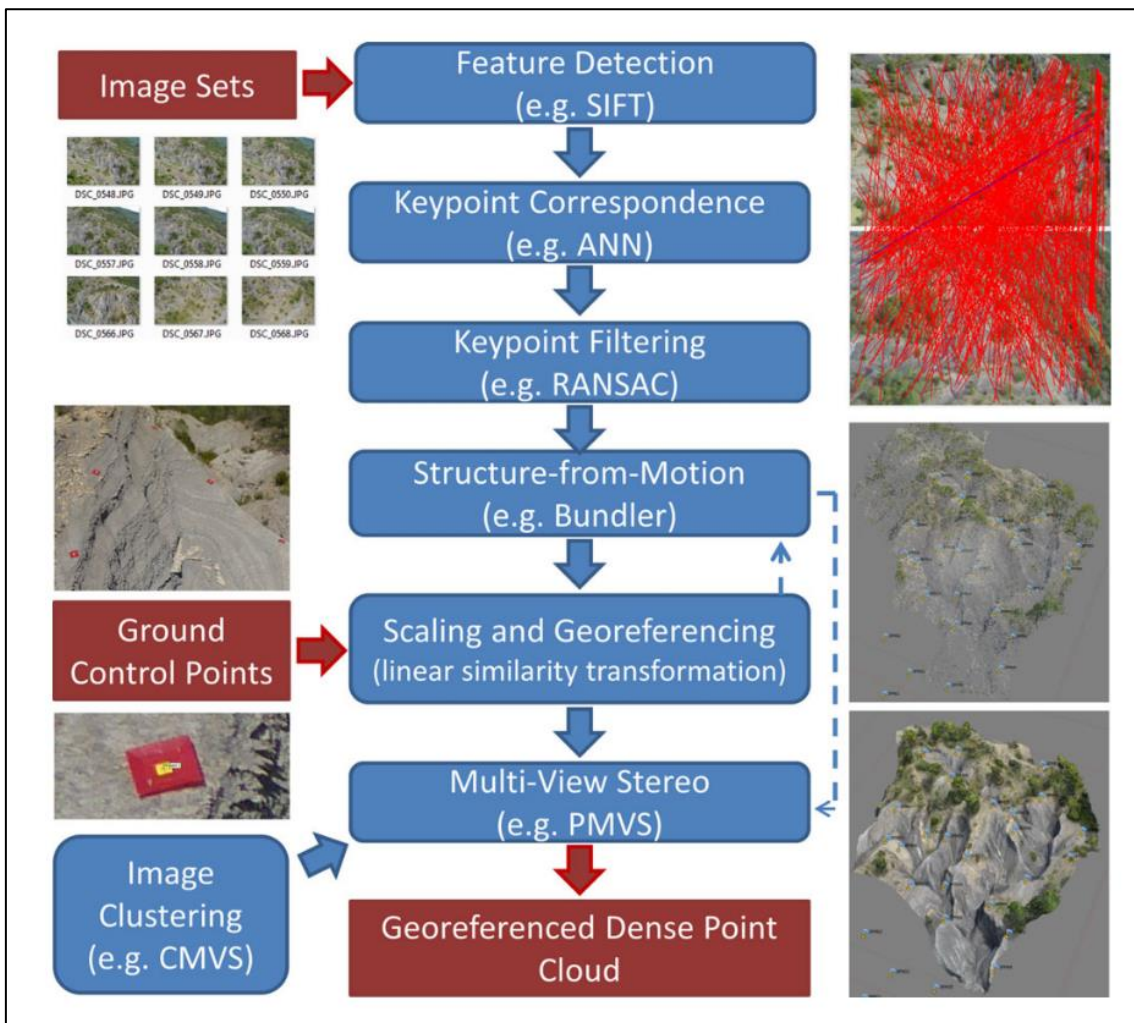


**Figure 3.4: Typical workflow in the production of georeferenced dense point clouds from image sets and ground control points. Inputs and outputs are shown in dark red. In the top right, as a demonstration, matches determined to be valid are shown in red, while matches determined to be invalid are given in blue. Figure reproduced from (Smith et al., 2015)**

The proceeding parts of the thesis can be broadly split into two types. Firstly, chapters 4 and 5 are focussed on the techniques of drone and kite based remote sensing with environmental applications. They include reviews of the literature and discussion of the technology and techniques used within these fields. Following on from these two pieces are three empirical chapters (6,7 and 8). Empirical data collection was undertaken in three different environments that fall along a land-sea continuum in the coastal zone using lightweight drones and kite

platforms. Firstly, the changes in geomorphological structure on terrestrial beach dune systems were studied using kite aerial photography (KAP) and structure-from-motion photogrammetry processing techniques. Secondly, a study investigating the ability to capture and analyse fine spatial resolution data of intertidal seagrass meadows in Pembrokeshire, Wales. Lastly, a study to investigate the ability of proximal sensing from a drone to measure surface roughness on subtidal coral reefs in the Maldives.

## 4 Operating drones in challenging environments



This paper was published in *Remote Sensing in Ecology and Conservation* in 2018:

Duffy, J.P., Cunliffe, A.M., DeBell, L., Sandbrook, C., Wich, S. A., Shutler, J.D., Myers-Smith, I.H., Varela, M.R. & Anderson, K. (2018) Location, location, location: considerations when using lightweight drones in challenging environments. *Remote Sensing in Ecology and Conservation*, 4, 7-19.

## **Location, location, location: Considerations when using lightweight drones in challenging environments.**

James P. Duffy<sup>1±\*</sup>, Andrew M. Cunliffe<sup>2±</sup>, Leon DeBell<sup>1</sup>, Chris Sandbrook<sup>3,4</sup>, Serge A. Wich<sup>5,6</sup>, Jamie D. Shutler<sup>7</sup>, Isla H. Myers-Smith<sup>2</sup>, Miguel R. Varela<sup>8</sup> & Karen Anderson<sup>1</sup>

*± These authors contributed equally to the work.*

*\*Corresponding author*

1. DroneLab Research Group, Environment and Sustainability Institute, University of Exeter, Penryn Campus, Penryn, Cornwall, TR10 9FE, UK

2. School of GeoSciences, University of Edinburgh, Edinburgh, EH9 3FF, UK

3. UN Environment World Conservation Monitoring Centre, 219 Huntingdon Road, Cambridge, CB3 0DL, UK

4. Department of Geography, University of Cambridge, Downing Place, Cambridge, CB2 3EN, UK

5. School of Natural Sciences and Psychology, Liverpool John Moores University, Liverpool, UK

6. Institute for Biodiversity and Ecosystem Dynamics, University of Amsterdam, Amsterdam, The Netherlands

7. Centre for Geography, Environment and Society, University of Exeter, Penryn Campus, Penryn, Cornwall, TR10 9FE, UK

8. Centre for Ecology and Conservation, Biosciences, College of Life and Environmental Sciences, University of Exeter, Penryn Campus, Penryn, Cornwall, TR10 9FE, UK

#### 4.1 Abstract

Lightweight drones have emerged recently as a remote sensing survey tool of choice for ecologists, conservation practitioners and environmental scientists. In published work, there are plentiful details on the parameters and settings used for successful data capture, but in contrast there is a dearth of information describing the operational complexity of drone deployment. Information about the practices of flying in the field, whilst currently lacking, would be useful for others embarking on new drone-based investigations. As a group of drone-piloting scientists, we have operated lightweight drones for research on over 25 projects, in over 10 countries, in polar, desert, coastal and tropical ecosystems, with many hundreds of hours of flying experience between us. The purpose of this manuscript is to document the lesser-reported methodological pitfalls of drone deployments so that other scientists can understand the spectrum of considerations that need to be accounted for prior to, and during drone survey flights. Herein, we describe the most common challenges encountered, alongside mitigation and remediation actions that increase the chances of safe and successful data capture. Challenges are grouped into the following categories: (i) pre-flight planning, (ii) flight operations, (iii) weather, (iv) redundancy, (v) data quality, (vi) batteries. We also discuss the importance of scientists undertaking ethical assessment of their drone practices, to identify and mitigate potential conflicts associated with drone use in particular areas. By sharing our experience, our intention is that the manuscript will assist those embarking on new drone

deployments, increasing the efficacy of acquiring high quality data from this new proximal aerial viewpoint.

## 4.2 Introduction

Lightweight drones are now firmly established as part of a remote sensing surveying methodology and the scientific literature is replete with examples of drone technology being used for a multitude of purposes including conservation (Koh and Wich, 2012), wildlife monitoring (Christie et al., 2016), plant inventory mapping (Husson et al., 2016), biomass estimation (Cunliffe et al., 2016), coastal morphological mapping (Long et al., 2016), coral reef monitoring (Casella et al., 2017), disaster response (Nedjati et al., 2016) and precision agriculture (Bukart et al., 2018). Many environmental science, ecology and conservation applications of drone technology will inherently encounter and have to overcome common challenges and problems. Despite this, these communities lack a common understanding and shared protocols for addressing these challenges, often making the acquisition of drone data collection more problematic and open to error, particularly for those less familiar with the technology.

The ability to deploy drones in a variety of different environments leads to site-specific and user-specific data collection methods. This in turn creates a plethora of methodological challenges, many of which remain unreported in the scientific literature. This is because the style of scientific papers is such that it is rarely required, or indeed attractive to share the broader considerations of drone deployments with the reader; instead the focus is placed on describing flight parameters or details of image capture and data processing. As a group of scientists who are well practiced in deploying lightweight drones, we can attest

that even in low-risk deployment scenarios, methodological issues are experienced regularly, requiring a change in approach or compromise. The frequency and severity of such issues are amplified when deploying drones in challenging environments and in parts of the world where drone operations are not well-understood by local communities and resources are limited. This dearth of detailed, practice-based methodological insight into drone deployment considerations means that scientific drone users are likely to be duplicating efforts and it also presents a barrier to those wishing to begin using drone technology, since many helpful operational details remain buried in user forums of online drone groups (e.g. <http://diydrones.com/>).

Drawing on our extensive collective experiences using lightweight (sub-7 kg take-off-weight) drones in diverse locations such as deserts in the USA, Arctic tundra in Canada, coral atolls in the Maldives, and tropical rainforests in Indonesia and Brazil (**Figure 4.1**), this manuscript provides a practice-based overview of the methodological challenges faced by drone operators in field settings. Alongside, we present some of our tested solutions to these methodological issues to aid scientists working in ecological, conservation and environmental research, to support the efficient deployment of drone technology and underpin the collection of high quality scientific data. Our work has been exclusively with optical sensors, although many of the challenges faced are not sensor specific. We also provide sections on environment specific challenges, however many challenges may be encountered in more than one type of environment (**Table 4.1**). We do not cover the specific considerations for drone operations around wildlife as this has already been discussed by others (e.g., Ditmer et al., 2015; Hodgson and Koh, 2016; Pomeroy et al., 2015; Vas et al., 2015). Additionally, scientists rarely write

about the cultural and ethical implications of their practices, and therefore we discuss the importance of considering ethical issues prior to undertaking drone operations and offer some guidance for ethical assessment of drone operations. It is too difficult to cover every type of drone-sensor operation, so this manuscript is primarily focused on discussing lightweight (< 7 kg take-off-weight) fixed wing and multicopter drones equipped with photographic equipment for ortho-mosaic (e.g. Husson et al., 2014) and structure-from-motion (SfM) photogrammetry (e.g. Smith et al., 2015) type applications. We begin this paper by providing several key operational guidelines that will assist scientists working in most field settings.

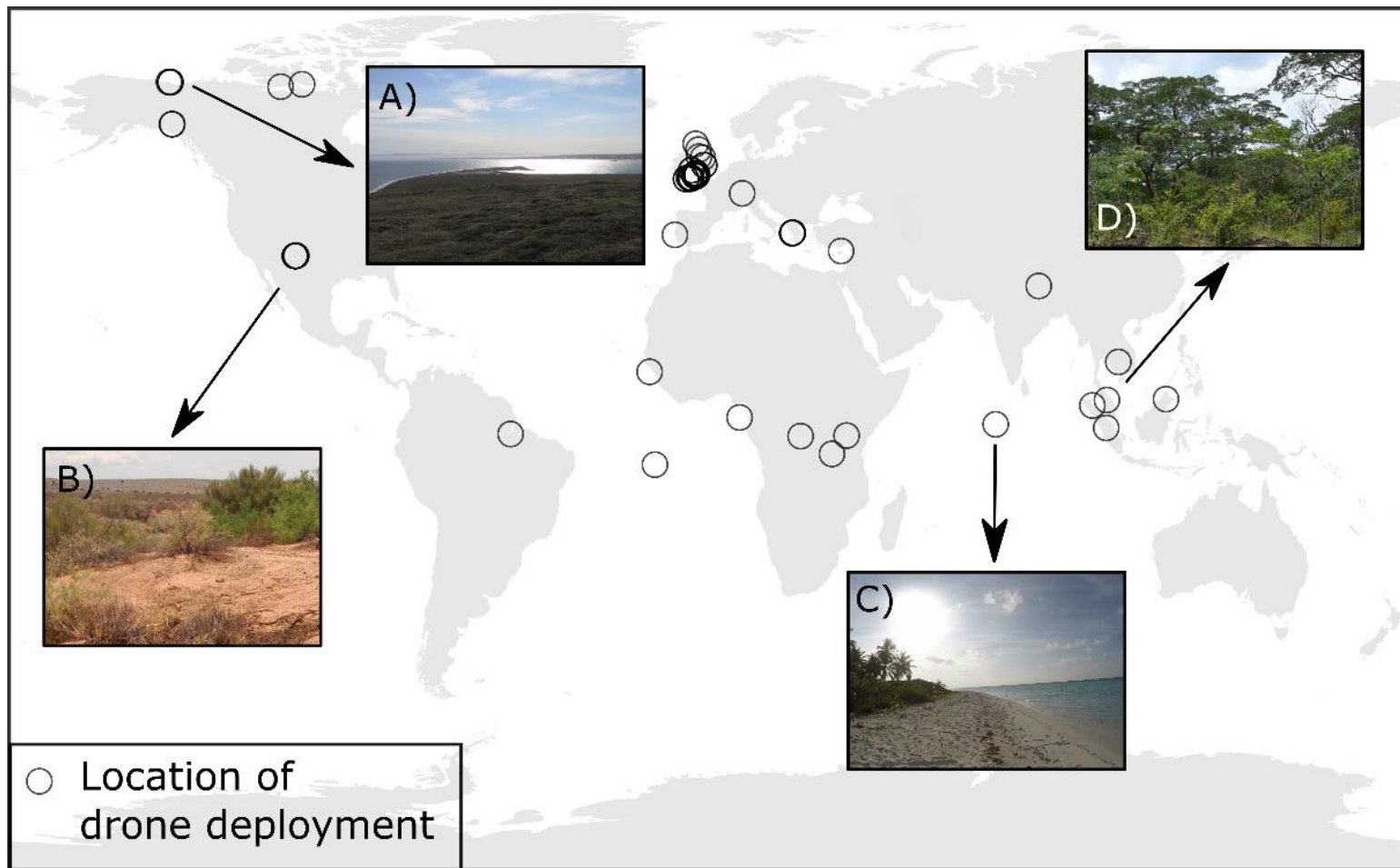


**Figure 4.1: The geographical diversity of locations where we have successfully or unsuccessfully deployed lightweight drones for collection of proximal remote sensing data, including (A) arctic, (B) desert, (C) coastal and (D) tropical forest.**

## 4.3 Considerations for safe deployment

### 4.3.1 Pre-flight planning

Safety of drone operations is paramount to researchers, for the obvious reasons of minimising risks to participants, bystanders and other organisms, but also to ensure delivery of useable scientific data and safe return of equipment. A key stage in safe deployment of drone technology is pre-flight planning, which is a relatively simple procedure but, as we have found, can involve considerations of complex issues in some settings. All drone operations should involve a critical pre-flight site check, usually initiated as a desk-based assessment and supported by a survey of the immediate surroundings once on-site. Pre-flight planning is very easy to achieve using various tools to assist the operator in (a) making optimal decisions about where and when it is safe to fly, (b) identifying safe locations for take-off and landing, and (c) becoming conversant with the regulations governing drone operations, which can differ between countries and sites.

**Table 4.1: Challenges faced during drone operations and the environments in which they can occur.**

	Specific Challenge							
<b>Operating environment</b>	Safety and regulation	Societal considerations	Wind	Fine particles	Solar effects (glint, shadows, albedo)	Spatial constraint of data products (Difficulties deploying/locating GCPs)	Telemetry issues	Topography issues
Coastal	X	X	X	X	X	X		X
Dryland	X	X	X	X				X
Polar	X	X	X		X			X
Dense forest	X	X	X			X	X	X
High altitude	X	X	X					X

#### 4.3.2 Making decisions about when and where it is safe to fly

In many developed countries, online databases exist detailing information on airspace restrictions, e.g. Notices to Airmen (NOTAMs). Increasingly, mobile applications can provide near-real-time information on the location of other airspace users (e.g. <http://notaminfo.com>, <http://dronesafe.uk/drone-assist>). During drone operations, we commonly establish contact with regional civilian and military air traffic control (ATC). It can often take time to identify the appropriate contacts for relevant authorities such as ATC, but doing so can help alleviate interruptions in data collection and prevent near misses with aircraft. For example, when flying near Land's End Airport in Cornwall, UK (but outside of an official aerodrome traffic zone), we obtained the number of the airport ATC tower from the internet and liaised with them. This allowed them to create a temporary restricted zone around our operations and to notify any incoming aircraft. On completion of flight operations, we again informed the ATC and the restriction was removed. In summary, a key to safe flying anywhere in the world is to keep other air users informed; in our experience, local ATC managers would rather know of drone operations so that appropriate measures can be enacted (e.g. NOTAMs). Even if official channels are difficult to access or identify (i.e. in remote areas), drone operators may wish to contact other airspace users directly to inform them of their planned operations (e.g. local charter flight companies).

#### 4.3.3 Establishing safe locations for take-off and landing & identifying obstructions

Experience suggests that extensive site reconnaissance prior to flight operations allows obstructions to be identified and increases the chances of successful data

capture. Given this, we strongly advise a 'virtual' site assessment prior to fieldwork using freely available map services such as Google Earth (<https://earth.google.co.uk/>) or apps such as *Altitude Angel* (<https://www.altitudeangel.com/>). Google Earth's terrain layer or an alternative local terrain model (e.g. Shuttle Radar Topography Mission 90 m resolution DEM) can be used to understand local topography. These pre-flight activities will reveal some hazards, but problems posed by objects such as varying tree heights and overhead pylons will be difficult to identify. Therefore, exploring the proposed area of flight operations and beyond (to allow for unexpected deviations) later by foot will give the drone operator a more complete idea of which altitudes are safe to fly and the location of hazards should an alternative flight scenario arise. In addition, a site risk assessment is often conducted and will help identify such hazards.

Other airspace users should also be considered, and an air navigation chart can be used to assist with flight planning. When planning work in remote areas we advise that this stage should be undertaken when in reach of internet connectivity, caching (storing) maps within flight planning software for offline usage within the field. The requirements of the chosen aircraft also need to be considered. Fixed wing systems require larger, flatter areas for take-off and landing in comparison to multi-rotor systems capable of vertical take-off and landing (VTOL). Fixed wing aircraft typically glide to a descent, requiring tens of meters of flat landing space to ensure incident-free landing although alternative retrieval techniques such as parachutes and nets (e.g. Williams et al., 2016) reduce the requirement for a large landing area and in our own practice have found parachute landings greatly facilitate the safe retrieval of fixed wing drones.

The covering and stability of the landing surface should also be considered. A landing pad (**Figure 4.2**) can help to provide a stable surface for landing multi-rotor systems and to reduce generation of dust by downdraft. Alternatively, a member of the team (other than the remote pilot) could use appropriate personal protective equipment to catch the aircraft during landing.

Insight gained through flights above rainforest canopies show that pre-flight assessments may not reveal all of the potential risks. In areas with dense tree canopies, small hills and topographic ridges may exist that are not easily identifiable from pre-flight efforts. Emergent trees can reach up to 70 m above ground level in some ecosystems, presenting themselves as obstructions of varying heights. In these circumstances it is advisable to first perform a flight over the area of interest at an appropriate altitude to avoid such obstructions and then examine the image data in the field to determine whether flying lower is safe. Quickly carrying out a first flight like this using a multi-rotor, allowing the aircraft to hover parallel to the obstructions, can provide a fast way to obtain their altitude.

#### 4.3.4 International, regional and local legislation

Scientific drone operators must consult the legislation regulating drone operations in the country of intended use. DeBell et al. (2016) provide useful guidance on general operational protocols and provide details of the legislative complexity, stating “there is a huge diversity in the legislative framework governing UAV (Unmanned Aerial Vehicle) use globally, and coupled with diverse cultural attitudes to UAVs this can make the decision of where and how to fly quite difficult”. Some countries have established rules of operation (e.g. UK, USA, Canada, Australia) and others have no restrictions or regulations (e.g. Guinea

Bissau). It may be difficult to establish what rules and regulations exist for a particular country and so as a starting point we recommend consulting community collated information which can be found at <https://www.droneregulations.info>. Along with the need for landowner's permission, authority for airspace usage is often required. From experience we have found that engaging with local groups and/or partnering with them has enabled smoother drone deployments with reduced concern from local communities (e.g. in Greece, we liaised with a local conservation agency who negotiated airspace use on our behalf). Regardless of the country, it is important to contact local authorities when flying close to military areas or airfields, even for countries with no drone legislation. For example, on Ascension Island, where no formal restrictions exist, we had to submit pilot identification and comprehensive flight plans to local authorities two months prior to flights and constant contact with a local ATC had to be maintained during the fieldwork. With all locations it is critical to perform a pre-deployment check of the permitted radio frequencies (e.g. 433 MHz, 915 MHz, 2.4 GHz or 5.8 GHz etc.) and power settings for radio transmissions, as these can vary according to regulatory jurisdictions.

#### 4.3.5 Flight operations

Once the appropriate pre-flight checks and permissions have been sought, a robust field procedure should be followed, for which Cunliffe et al. (2017) provide advice and an operations manual for other users to use as a guide. Importantly the operational procedure outlined therein should be modified according to the specific aircraft being used and methodology being followed. We have found that it is useful to have a prior-agreed operational protocol, with one pilot-in-command and a 'spotter/ground control station operator' to assist. Drone pilots are strongly

advised to maintain their own comprehensive flight logs, as a record of both deployments and experience; such records can prove invaluable when presenting a safety case to institutions, regulators, collaborators and landowners. This can be achieved manually or using third party services such as AirData UAV (DJI specific; <https://airdata.com/>).



**Figure 4.2: The challenges of drone fieldwork in four key environments.**

#### 4.3.6 Site-specific flight planning considerations

Specific operational issues can arise in particular settings such as coastal or over-water, forest, or in remote regions. Planning operations at coastal sites is challenging since it can often be hard to find (and then access) a suitable take-off and landing area. For example, in recent fieldwork in the UK Scilly Isles, it was necessary to transfer equipment from a ship to an island using a small dinghy. Alternatively, launching from land may not be feasible for some missions, and

therefore boat-launches can be used as an alternative. Managing drone operations from the deck of a moving boat can be very challenging, but not impossible; there is evidence of success in achieving this (e.g. Casella et al., 2016; Christiansen et al., 2016; Williams et al., 2016). From our own experience with Pixhawk flight controllers (<https://pixhawk.org/>), it is necessary to perform the drone's pre-flight accelerometer and compass calibration on stable ground before deploying from the boat (which wobbles, disrupting the normal pre-flight calibration procedure of flight control sensors). Failure to do this can result in the loss of aircraft control shortly after take-off as it is likely to crash into the water. This was the case during our work in Greece, where a drone and on-board sensor were downed after an attempted boat launch. However, it is important to note that calibration procedures can vary between different flight systems.

In tropical rainforest settings, where drone-based data can provide information about forest structure (e.g. Kachamba et al., 2016; Zahawi et al., 2015), and biodiversity (Van Andel et al., 2015), it is often difficult to identify sufficiently large areas for fixed wing drones to land. Fixed wing systems in these areas are generally preferred over multi-rotors because they provide greater areal coverage necessitating that flights often start and end from the edge of forest blocks, utilising openings in the canopy (**Figure 4.2**). Where forest blocks are large, often only the edge of the forest can be surveyed which may bias observations. If flights have to be made within visual line-of-sight (VLOS), a pilot standing at the edge of a wall of trees will have very limited VLOS, thus limiting the area that can be surveyed. Dense forest canopies can also impede the transmission of Global Navigation Satellite System (GNSS) signals to the drone, and radio signals between the drone and the ground controllers due to the vegetation attenuating

and/or scattering the radio signal. The impact of the vegetation is also dependent upon the geometry of communications link and the vegetation and so it can vary in space and time (e.g. Ndzi et al., 2012).

Most lightweight drones now contain positional receivers to guide the drone during automatic flight and to provide a failsafe if the radio link with the remote pilot is broken, but in high latitude environments this can cause operational issues. At high latitudes some drone operators have reported difficulties with obtaining positional lock, caused by poor visibility of geostationary equatorial GNSS satellites and issues with magnetometers and gyroscopes on-board the drone (Jensen and Sicard, 2010; Williams et al., 2016). By default, some flight controllers require a minimum number of satellite GNSS connections or 'fixes' which provide a minimum accuracy of positional data (lock) before they allow take off. Obtaining a 'lock' can be difficult when the horizon is obscured, for example when working in small spaces in forests. These restrictions can be overridden by the operator on many drone systems, where appropriate, but it is useful to anticipate this potential issue and a method to resolve it in the field. In the future we expect these issues to reduce as the constellations of GNSS increase. The ability to operate drones in flight modes relying on magnetometers can be severely hampered when close to magnetic poles and manual flight may be the only option in such environments. Note, that while conducting ~200 flights at 70° N 139° W in the Canadian Arctic where the inclination of the magnetic field was ~84°, we never encountered problems with the GNSS lock but did occasionally encounter errors with magnetometers and gyroscopes.

In remote settings (e.g. polar regions and deserts), drone based operations can also be challenging due to reduced airspace control. Less formal control does not

necessarily mean that there will not be air traffic. For example, for Arctic field sites aircraft are the main method of access and lightweight drones can pose major risks to other air users. Thus, establishment of lines of communication with local pilots may be required to maintain airspace safety. Additionally when operating in extreme or remote conditions we plan the flight missions to start at the furthest survey point away from base camp and finish close to base camp (i.e. the flight follows a transect of some sort). This provides extra security for landing in an emergency due to battery issues as drones may otherwise land in a location where recovery is difficult. Depending on the drone pilot's preference and regulator requirements, a 'kill-switch' or sequence of commands can be programmed, so that the motors can be shut down in the event of an imminent collision with other airspace users.

#### 4.3.7 Weather and local environment considerations

Whilst weather forecasts can be useful for choosing optimal times for drone surveys, it is always necessary to check weather conditions at the site on arrival, particularly wind and be aware that they can change. For wind, we suggest carrying a handheld anemometer to check that wind conditions are within operational ranges e.g. maximum permissible wind speed including gusts of  $13.4 \text{ m s}^{-1}$  is recommended for a 3DR Y6 hexacopter (Cunliffe et al., 2017).

In many environments, drone operators must be mindful of complex wind profiles and these can occur in all types of terrain. Our flight operations in the Arctic have been constrained by weather, especially by high wind speeds. At the coast complex winds can arise from sea breezes (land/ocean temperature differences) or from topographic landforms that alter air flow. Similar complex and localised

wind effects can occur in tree canopies. When operating drones from clifftops we have encountered atmospheric turbulence (wind shear) which affects launch and landing procedures. Resultantly we have adopted a methodology where we fly high whilst the drone moves inland over the cliff edge before bringing it down to a pre-identified safe landing area some distance from the cliff edge. For coastal surveys, we sometimes supplement drones with kites as part of our contingency - in high winds a single-line kite can be used to carry a camera to perform some survey tasks, although variable flying height can degrade data reproducibility (Duffy and Anderson, 2016).

When working in the Chihuahuan desert (USA), we have experienced extreme localised heating of the ground surface, giving rise to rotating columns of high-intensity wind, known as dust devils. These can interfere catastrophically with drone flight operations, but are often visible when approaching survey areas. Such encounters reinforce the value of utilising a spotter to support the remote pilot in monitoring the environment (Cunliffe, 2016). When working at altitude, one must also consider issues relating to air density, a factor that is fundamental to the flight operation of all aerial vehicles (air density is inversely related to both altitude and air temperature). In the Chihuahuan desert, we were flying 1800 m above sea level, with ground level air temperatures exceeding 45°C. Here, we observed that the performance envelope of multirotor aerial vehicles was affected, reducing flight endurance, manoeuvrability and payload capacity. Such issues should be considered when planning flights at high altitude sites.

Working in tropical and coastal areas with drones carries specific risks as the humidity of these environments is often high and there is a need to ensure that all electronic components stay dry. Sensors can be stored or housed in

watertight cases with a desiccant, but this is often not a feasible for the drone itself. In tropical environments, areas of open canopy are often less humid and remaining in these locations can help avoid the negative effects of humidity. Foam and/or glue on components may start to become soft in hot environments, which might compromise the integrity of sensors and/or aircraft. This may be exacerbated if the aircraft has low albedo and/or exposed to direct sunlight. In these cases we advise covering the drone and components with a white textile or reflective material before arming and initiating the flight.

#### 4.4 Dust, damage and redundancy

A common difficulty when operating drones is the ingress of small particles into moving parts of both aircraft and sensors, which can accelerate mechanical erosion of moving parts and damage sensors (Cunliffe, 2016). We have encountered these difficulties most severely in dryland ecosystems and sandy beaches. Drylands typically have high levels of dust due to low levels of soil cohesion and vegetation cover, which are exacerbated when undertaking near-ground operations with multi-rotor aircraft (RAF, 2011; Wadcock et al., 2008). Working in the Chihuahuan desert, we destroyed several lightweight cameras due to dust ingress into lenses, prior to arriving at a low-tech solution (**Figure 4.2**) whereby cameras were sealed inside dust-proof enclosures. At the coast, exposed electronics (e.g. motors, cable connectors and ports) can be easily clogged or corroded by sand and salt and good maintenance of drone equipment post-flight becomes very important. Possible mitigation strategies to overcome these difficulties include: i) using landing pads to minimise generation of dust during take-off and landing operations with multi-rotor drones; ii) cleaning moving parts after each flight, using a can of compressed air iii) coating electronics in

anti-corrosion spray and iv) using dust-sealed cameras or other sensors (e.g. using sealed cases or ruggedized waterproof cameras such as the Canon PowerShot D30; **Figure 4.2**).

One critical aspect of deploying lightweight drones in any environment is the importance of contingency and redundancy in all aspects of the system. This is pertinent in very remote parts of the world, where there may be no options for obtaining replacement hardware or software (Zahawi et al., 2015). During recent fieldwork in the Canadian Arctic, we carried comprehensive sets of spare parts for all platform components; however, even this level of redundancy was not sufficient for our needs over a two-month field campaign. As a minimum we advise drone operators to carry multiple replacement batteries (drone and controllers), a battery voltage checker, replacement propellers, basic toolkit, soldering kit, electrical tape and cable ties. In more remote locations, there is a stringent need for the hardware (particularly airframes) to be sufficiently robust to operate in these environments and to choose the right drone(s) and sensor(s) for the operational setting. Ideally, one will have an entire fully operational drone available at the field base to provide full redundancy. This is more attainable with low cost lightweight drone systems.

## 4.5 Data quality

### 4.5.1 Spatial constraint

A key challenge with most forms of drone acquired data is that of a relatively poor spatial accuracy, as compared to, sub-decimeter spatial resolution data. The GNSS positional receivers on-board drones provide data that can be harnessed within image processing toolboxes (e.g. Cunliffe et al., 2016). However, the

positional accuracy of these aircraft systems (typically  $\pm 2-10$  m), is often not sufficient for some remote sensing applications and to improve the spatial accuracy of derived products, ground control markers are commonly deployed *in-situ* across the scene. The locations of the markers can be independently surveyed e.g. using a differential GPS to an accuracy of ca.  $\pm 0.02$  m and reconstructions of the drone sensor data can then be constrained spatially using these markers (e.g. James et al., 2017a; Puttock et al., 2015). When used, markers should be designed in accordance with (i) the spatial resolution (i.e. being at least 6-8 pixels in diameter (James et al., 2017a)), and (ii) the electromagnetic sensitivity of the sensor (i.e. identifiable in all spectral bands, particularly when working with non-visible spectrum data). However, markers can be time-consuming to deploy, and cannot be used in all locations, such as dense forests. As we write, new GNSS systems are becoming increasingly available for drones which can yield higher precision estimates of the drone position as it flies, e.g. Real Time or Post Processing Kinematic (RTK or PPK) GNSS systems. While uptake of these systems has not yet been widespread, we anticipate that within a few years these may replace current methodologies employing *in-situ* markers, although we advise that independent ground validation should remain a critical requirement for remote sensing investigations. Furthermore, newer low-cost receivers support recording of raw GNSS observations (if base stations are close) that can be post-processed to improve accuracy for incorporation into any data product, but this capability often needs to be enabled prior to any flights taking place.

#### 4.5.2 Shadows and sun angle effects

It is generally preferable to collect data when illumination conditions are relatively consistent. In any areas with structured surfaces, for example those covered by vegetation or with coarse sediment, there may be issues associated with temporally variant shadows. When working in dryland ecosystems, for example, the vegetation cover is commonly spatially discontinuous and feature matching algorithms can be confused by inconsistent shadows between images (Carrivick et al., 2016), particularly where the bare soils have high albedo. To minimise changes in shadows between different images, it can be useful to undertake aerial surveys close to solar noon, thus minimising shadows and significant changes in illumination angles (Cunliffe et al., 2016; MicaSense, 2017; Puttock et al., 2015). In polar regions, even at solar noon, sun angles are usually low, potentially requiring drone operators to experiment with varying exposure settings on sensors to optimise image quality. For example, flying on days with variable cloud cover can lead to changes in illumination in imagery, thus influencing the homogeneity of spectral signatures influencing derived spectral, structural or classification-based data products.

Artefacts caused by the reflectance of light from water based surfaces have been a long-standing issue in remote sensing data products created from visible spectrum satellite and airborne sensors (Kay et al., 2009). A detailed explanation about the occurrence of sunlight or skylight glitter on surface waters (often referred to as glint) in aerial photography, its geometry manifestations and distributions can be found in Cox and Munk (1954) and Aber et al., (2010). In any data collection scenario over water bodies, the drone operator must be mindful of such issues, because they manifest themselves in complex forms in fine-

grained data (**Figure 4.3A**). During fieldwork in the Maldives when using drones to map coral reefs (i.e. attempting to view through the water), we found sun glint issues caused major problems with image data quality (**Figure 4.3A**). Capturing image data when the sun is lower on the horizon (avoiding midday sun) (as suggested by Casella et al., 2016 and Hodgson et al., 2013) helped us to achieve data through water free of sun glint. We also programmed the drone to always point the camera north, so that whilst following a typical 'lawnmower' flight pattern, the impact of glint on the sensor data was minimised as the viewing zenith was approximately 90 degree to the sun. In addition to sun glint, disturbance to the water's surface (i.e. caused by boats) was an issue during our work in the Amvrakikos Gulf, Greece (**Figure 4.3B**). Careful timing of flights can aid in minimising these issues.

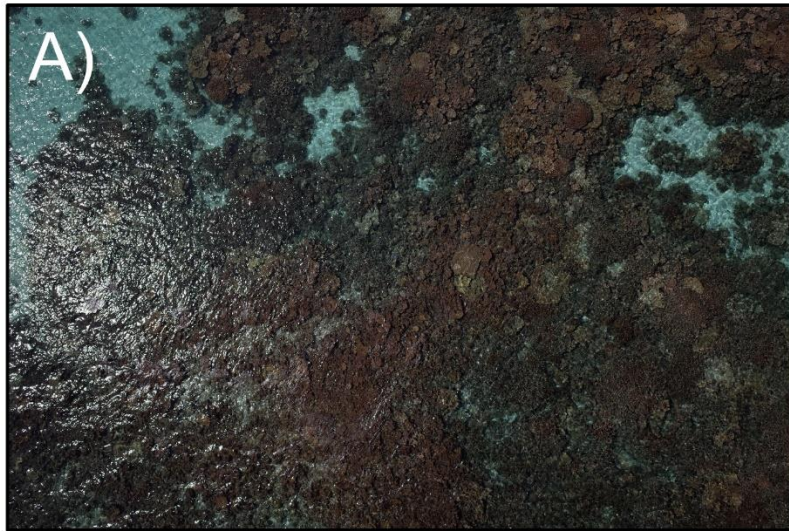


**Figure 4.3: Issues with optical imaging. (A) Sun glint over coral reefs in the Maldives, (B) ripples in the water's surface caused by a boat in Greece and (C) Marram grass (which is easily moved by wind) on sand dunes in the UK**

### 4.5.3 Wind and motion blur

In areas with high wind, movement of features of interest (e.g. vegetation), can cause problems with feature matching between images. Vegetated sand dunes (**Figure 4.3C**) are an ecosystem where vegetation movement is a particular issue. Beyond environmental conditions, movement in the sensor gimbal or the sensor itself during data capture can lead to motion blur in imagery influencing data quality. Poorly designed or fitted camera mounts/gimbals may exacerbate problems with motion blur from wind buffeting of aircraft, due to insufficient vibration dampening and movement of the sensor during flight. Where applicable, in order to avoid/reduce motion blur, shutter speeds of optical sensors should be set with consideration of the intended speed of the aircraft (i.e. higher speeds require a faster shutter). We recommend planning test flights to assess such issues with initial assessment of data quality in the field. Changing to a fixed mount and/or altering camera mounts and orientations (i.e. reducing aerodynamic drag) may help to solve such issues. This approach was needed whilst working in constant wind speeds of  $10 \text{ ms}^{-1}$  on Ascension Island.

Conducting flight operations during low wind conditions will help to mitigate both of these issues, but workflows for data analysis may need to address variable data quality. Software tools such as PixelPeeper (<https://pixelpeeper.com/>) allow for the screening of data, aiding in the removal of images that are likely to introduce error further into the processing workflow (e.g. blurry photographs).

## 4.6 Batteries

Most lightweight drone systems used for environmental research are powered by lithium polymer (LiPo) batteries, which represent one of the most troublesome

and potentially hazardous components of drone operations (Salameh and Kim, 2009; Scrosati et al., 2001). The overriding issue here is that LiPo's represent a significant fire risk, particularly if they are (i) over-(dis)charged, (ii) (dis)charged too rapidly, or (iii) the physical integrity of the cells is compromised. Because of this fire risk, the transportation of LiPos is strictly regulated. For transport by air, the International Civil Aviation Organization (ICAO) determines these regulations, and many state jurisdictions impose additional controls on the transportation of LiPos under dangerous goods regulations (e.g. Canada). ICAO currently prohibits the transport of Lithium ion batteries as cargo on passenger aircraft, although LiPos within passenger luggage are still permitted within strict limits. But these restrictions can preclude the transport of LiPos above a certain size (currently determined by watt hours (Wh) or lithium content), which can impede field deployments, particularly with larger drone systems.

LiPo batteries are a relatively expensive component in drone systems, and do have a finite lifespan (Salameh and Kim, 2009) and there is often a degree of reluctance by users towards replacing older, less effective LiPos. Older LiPos can pose a safety issue, particularly when undertaking endurance flight operations. Users are strongly encouraged to keep logs for individual batteries, to allow declining battery performance to be monitored; such recording is commonly also mandated by regulators. For safe storage and transport, we suggest that LiPos be (dis)charged to 50-60% and placed within individual fire-resistant bags. Damaged LiPos should never be transported and should be safely disposed of as soon as possible. We have used a lightbulb to assist in full discharge when operating in remote areas. To ensure the long life and stability of cells, they should be charged with a balance charger, and a maximum charge rate of 1C is

recommended (i.e. maximum charge rate of 5A for a 5000 mAh battery). LiPo efficacy is usually impeded when cell temperatures are below 0 °C (Salameh and Kim, 2009), and we have observed problems with sudden voltage drops in flight when using LiPos that have not been adequately warmed; ideally above approximately 10 °C prior to use. It is essential to plan for the charging requirements of LiPos, especially when travelling to remote places. For example, low voltage photovoltaic arrays may not be adequate to charge LiPos comprising of many cells.

#### 4.7 Social and ethical considerations, challenges and mitigation

Until this point, we have considered some of the challenges relating to deploying drones in particular physical environments, and the equipment itself. However, it is important also to consider the social environment within which drones are deployed, and the associated challenges and opportunities, especially given ethical assessment increasingly required in scientific research. In some circumstances the use of drones can have positive influences on people, for example by empowering local people to monitor their resources more effectively (Paneque-Gálvez et al., 2014) or by fostering improved relationships with stakeholders through conversations around the drones themselves and associated visually attractive data products. However, there are several ways in which drones may cause real or perceived harm to people, which can in turn create difficulties for drone users. Here we first identify some of the possible social and ethical challenges that can exist, and then identify possible strategies to mitigate these challenges.

A range of potential social challenges associated with using drones are detailed

in **Table 4.2**, many of which have been identified previously (e.g Boucher, 2015; Klauser and Pedrozo, 2015; Sandbrook, 2015). If not appropriately mitigated, these challenges can lead to conflict. Such conflicts could result in damage to equipment and/or undermine stakeholder relations, impacting or undermining the wider scientific or applied objectives of the work.

**Table 4.2: Social concerns associated with using drones.**

<b>Nature of social interaction</b>	<b>Description of social challenge</b>
Safety	In some circumstances drones could be dangerous for people on the ground, particularly if used in crowded places or at very low altitude. For this reason such usage is not legal without special permission from the national aviation authority in many jurisdictions
Disturbance	Drones can be noisy, potentially distracting or alarming for those who are not used to them. This could be dangerous (e.g. if people are operating machinery), annoying or upsetting (e.g. if they are wanting to enjoy the quiet of the natural environment).
Privacy	People may feel that drones are collecting data that violates their privacy, for example by taking photographs of them or their belongings (their home, their land, their trees, their pets etc.). This concern can occur even when no such data are being collected.
Fear	Drones can insight fear in people. This fear can be related to safety, disturbance, privacy or may just relate to a lack of familiarity with the technology. People may be afraid of drones because they associate the technology with military applications or intelligence gathering
Data access and usage	People may request or feel that they should be given access to the data collected, because it relates to them personally (e.g. images in which they feature) or regarding environmental features that were surveyed by the drones (e.g. locations of animals). They may worry that drones are being used to collect data that will be used against their interests, such as the creation of a National Park.

<p>Changing perceptions of environmental management</p>	<p>Flying drones to collect data about a particular environment and the wildlife therein may change perceptions about the appropriate use and management of that environment. For example, collecting data about a dangerous animal may lead to people assuming that those using the drones should be responsible for controlling the animal. This could lead for demands for compensation and associated conflict</p>
---	--

We now provide suggestions to help mitigate the potential social challenges identified in **Table 4.2**, based on a combination of reviewed literature, the experience of the authors, and common sense.

First, it is essential to recognise that social problems might occur. A recent review of the published literature on the use of drones for conservation and ecology found a remarkable lack of engagement with these issues (Sandbrook, 2015), although in our own experience most drone users do recognise their importance. Second, as discussed earlier, it is essential to comply with local regulations. In most jurisdictions, there will be rules regarding flying drones in proximity to people and the collection of data and these must always be obeyed.

Third, when data on humans (including their land or property) are to be collected, projects should go through a human ethics review process. Such processes are designed to identify potential problems and help researchers develop mitigation strategies. For example, it may be appropriate (or mandated by law) to seek consent from key stakeholders before collecting data relating to them. It may also be necessary to think in advance about how human data will be stored and shared (e.g. will images showing illegal behaviour be shared with law enforcement authorities? What action would you take if somebody demands to

see any data relating to them?). In many cases ethical reviews are already required for drone research, and we encourage universal adoption of this practice.

Finally, ensuring good communication with stakeholders is essential. In many cases problems can be avoided by explaining how and why drones are being used to key stakeholders in advance. Indeed, in our experience drones (and the conversations they prompt) can underpin new opportunities for engagement and outreach, allowing for greater dissemination of scientific understanding and research findings.

#### 4.8 Conclusions

The pace of development of both the technological and regulatory sides of drone operations makes it difficult to be overly prescriptive about how to successfully undertake drone operations. The peer-reviewed literature often fails to capture the finer details of methodology such as how to prepare for and overcome issues that affect safety or data capture. Scientists should not underestimate the wealth of knowledge available in the 'grey literature' and from on-line forums: although these 'hobbyist' sites can be easily regarded as being separate to scientific operations, they have provided us with great insight when pioneering new drone deployments in challenging places (we credit the helpful community that reside in [DIYdrones.com](http://DIYdrones.com) with much that we have learned). Here, we have provided practical advice aimed at increasing the success of any environmental scientist, ecologist or conservation practitioner wishing to use drones for research purposes, especially in more challenging environmental settings. We believe careful consideration of the issues raised herein will promote the success of

drone-based research applications both with regards to data collection and the social perceptions of such research.

#### 4.9 Acknowledgements

This work was supported by the Natural Environment Research Council [NE/K570009815], [NE/K500902/1] (to AMC), [NE/M016323/1] (to IHM-S), [NE/570009815] (to JPD) and the UK Technology Strategy Board [TS/K00266X/1] (to KA). JS and KA were partly supported by the European Space Agency contract No. 4000117644/16/NL/FF/gp. Thanks to two anonymous reviewers and the associate editor for constructive feedback on an earlier version of this paper.

## 5 The renaissance of kites in proximal sensing



This paper was published in Progress in Physical Geography in 2016:

Duffy, J.P. & Anderson, K. (2016) A 21<sup>st</sup>-century renaissance of kites as platforms for proximal sensing. Progress in Physical Geography, 40, 352-361.

# **A twenty-first century renaissance of kites as platforms for proximal sensing**

James P. Duffy<sup>1\*</sup> and Karen Anderson<sup>1</sup>

1. Environment and Sustainability Institute, University of Exeter, Penryn Campus, Cornwall, UK

*\*Corresponding author*

## **5.1 Abstract**

In 1903, W. H. Dines first proposed kites as platforms from which scientific measurements could be captured. This early paper was focused on collection of atmospheric measurements but later on, kites were used widely as platforms for aerial photography – a memorable example is the aerial survey of San Francisco captured from a kite platform after the 1906 earthquake. In this paper, we begin by providing a brief overview of this early scientific and remote sensing work from kite platforms. We then discuss the resurgence of kite use within modern geography and environmental science research using examples from published work in the past 20 years. We discuss how the use of kites in these disciplines has expanded in recent years, with a renewed focus on collection of proximal remote sensing data. Also, we present a variety of contemporary examples of kite-based sensing (including basic mapping, ecological survey, population counts and humanitarian mapping) and discuss the merits of kites compared to drone-based platforms which have captured much of the public and scientific attention as proximal sensing platforms in recent times. The beauty of kite based proximal sensing lies in the simplicity and low-cost nature of data capture, as highlighted by Dines' 1903 paper. This simplicity supported by the wide array of

modern complex data processing capabilities means that kites are now in a position to deliver fine-grained spatial data to the modern geographer. Furthermore, in today's world, there are many situations where kites can fly freely, but drones cannot.

## 5.2 Introduction

In 1903, (Dines, 1903) provided one of the first scientific papers explaining the methodological framework that could be employed to turn simple long-line kites into platforms for collection of scientific data. The major focus of Dines' work was empirical measurement of atmospheric conditions. The 'rhombus' kites (**Figure 5.1**) he described using were launched from the deck of a small tug boat and were capable of "reaching 1500 feet elevation", with a potential for attaining elevations of "5000 feet" with a "sufficient relative motion" of the boat and favourable winds. His work showed the impact of pressure-driven weather systems on local temperatures, where he commented that "upper air in the neighbourhood of a cyclone is relatively warm" and that "cyclones are convectional effects" with varying conditions over water and land. Around the same time, others were experimenting with kites as platforms for other types of environmental measurement. The most notable was George Lawrence in 1906 who famously used a stack of conyne (a modified form of box kite) kites to capture aerial images of San Francisco in the immediate aftermath of the devastating earthquake. This was a technique he had pioneered in the years before, where his Chicago-based company coined the slogan, "The Hitherto Impossible in Photography is Our Specialty". Piloted aviation was still in its infancy at this time, and air ships were expensive and cumbersome. In response to this, George Lawrence devised and patented an ingenious system that he named "the captive

airship” of multiple kites and wires that could lift a 46-pound panoramic camera 2000 feet into the air. Lawrence launched the kite stack half a mile above the city and then “tripped the shutter with an electrical impulse generated by an old style telephone magneto” (Arrowsmith, 2002). The image of the city was then exposed onto a “22 by 55 inch negative” (Arrowsmith, 2002).

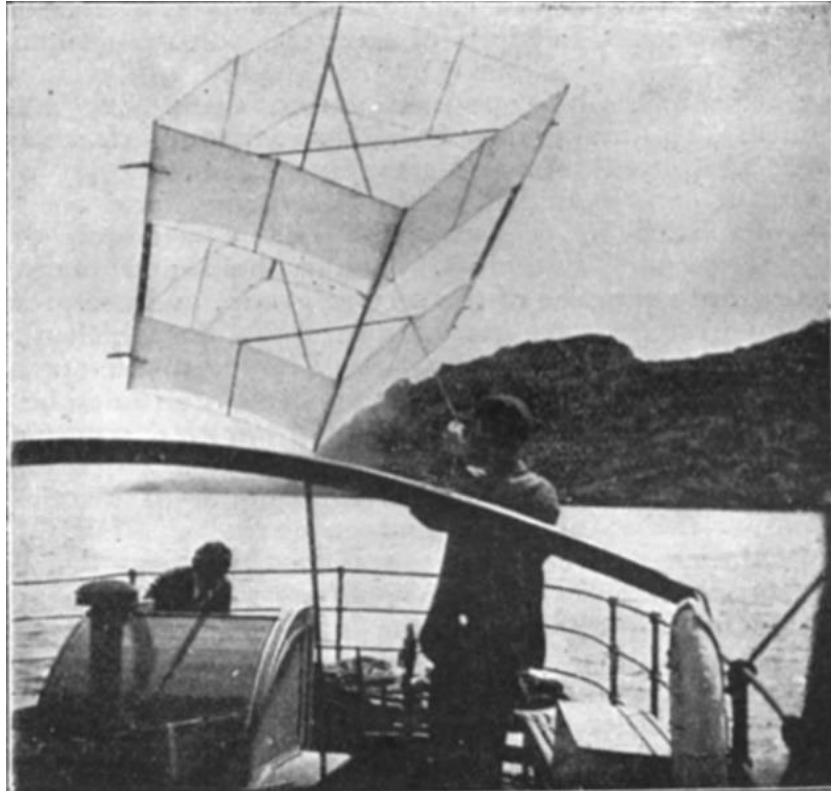


**Figure 5.1: The box kite used in the study by Dines in 1903. Reprinted by permission from Macmillan Publishers Ltd. (Dines, 1903).**

Both of these early studies, although vastly different in their complexity, showed that within the realm of science and engineering the spirit of self-service data capture was alive and well at the start of the 20<sup>th</sup> century. Dines (1903) stated that “kite flying is an art of which we were then without previous experience”. The simplicity of the technique was highlighted by Dines’ (1903) study in which he stated that, “no difficulty was experienced” when operating the equipment and capturing atmospheric data from the kite platform.

With a long hiatus in their documented use within scientific literature, the past couple of decades have seen a renaissance of kite flying for scientific data capture (Aber and Gałazka, 2000). The atmospheric and meteorological science area initially explored by (Dines, 1903) has had little traction with kite platforms since this early work. This scientific community has adopted balloons instead of

kites as a more robust platform for empirical measurements because they can aid data capture at higher elevations (this opportunity was in fact highlighted by Dines (1906) in a later paper published in Nature. There are relatively few contemporary examples of meteorological studies using kites. A review of meteorological research throughout the 20<sup>th</sup> century is provided by Balsley et al. (1998), detailing early work and more recent research investigating electric fields, temperature, ozone and humidity.

In recent times, research in physical geography has particularly benefited from kite-based optical remote sensing, and the rest of this manuscript will explain the reasons for that renaissance and justify the utility of kites as scientific tools supporting environmental research. We will also compare kites to their powered counterparts (lightweight drones) which are widely hailed as modern self-service platforms for data capture across the geosciences and ecology, and we will provide a balanced view of kites against drones as alternative platforms. This manuscript will also visit a range of scientific and non-scientific applications of kite based proximal sensing to demonstrate the progression and renaissance of this method for field survey.

### 5.3 A renaissance in proximal remote sensing

#### 5.3.1 The need for fine-grained data

Recent years have seen an upsurge in the application of proximal remote sensing from a range of platforms including, but not limited to, kites. This has been driven by the recognition of the need for fine-grained and responsive data in both time and space, and the need to bridge the gap in scale between in situ measurements and those collected by coarser resolution satellite sensors. For example, in soil

erosion studies D'Oleire-Oltmanns et al. (2012) argues that proximal sensing allows for the monitoring of processes at the “speed of change within a landscape”. Barrell and Grant (2015) writing recently on intertidal habitats state that “while the spatial resolution of satellite and aerial photography has improved it remains insufficient for detecting fine-scale structure”. Fine-grained data from proximal platforms can certainly provide sub-decimeter resolution models for addressing science questions in diverse fields including ecology (Dandois et al., 2015), forestry (Chianucci et al., 2016), geomorphology (Eltner et al., 2015; Westoby et al., 2012), archaeology (Verhoeven, 2009) and environmental management (Torres-Sánchez et al., 2013).

### 5.3.2 Drones, blimps and balloons

With a wide variety of papers documenting their use in supporting geographical, ecological and geoscience research there is no doubt that lightweight drones (sometimes called unmanned aerial vehicles) appear to be the most disruptive technological advancement in this field of proximal sensing (Anderson and Gaston, 2013; Jones et al., 2006; Woodget et al., 2015). The opportunity to obtain fine spatial and temporal resolution data, along with user controlled revisit times has made drones a popular self-service research platform. They come in a variety of shapes and sizes, catering for differing types of ‘mission’ but despite the long list of advantages that they bring to scientific data collection, they are not without their operational limitations. Firstly, drones are complex to operate and maintain, requiring a skilled pilot for safe and successful operation. In short, it is unlikely one can successfully operate a drone platform without first investing significant amounts of time. Secondly, drone costs can be prohibitive: although most lightweight drones fall into a “low-cost” bracket (Koh and Wich, 2012), they

usually cost at least £1000 which may be out of reach for those with limited budgets. Thirdly, flights of drones are heavily controlled and regulated in most countries of the world, with drone use in some settings illegal (e.g. in urbanised zones in the UK drone flights are illegal without first obtaining special permission from the civil aviation authority). Fourthly, battery technology somewhat limits the use of drones for particular types of scientific data capture with typical flight times from lightweight multirotors being between 8 and 20 minutes per flight. For surveying larger sites, this can be limiting, requiring pilots to take-off and land multiple times to achieve good spatial coverage. Finally, small lightweight drones struggle to operate consistently in high winds which make surveying in some situations problematic. With these limitations in mind it is therefore important to recognise the alternatives to drone platforms which in some situations can offer significant advantages for proximal sensing. Options include balloons, blimps and kites. Balloons and helium blimps have been employed as remote sensing platforms, offering low altitude perspectives of vegetation (Bar Massada et al., 2008; Jiao and Zhou, 2014; Miyamoto et al., 2004) and shorelines (Eulie et al., 2013). These offer a low cost self-service data collection platform, but they require a source of fuel in the form of helium which is costly. Blimps have allowed for greater coverage than balloons or kites, but they are often complex and require a team of people to operate them safely (Ries and Marzloff, 2003). Like balloons, the logistics of inflation with helium at sites with restricted access is a major limitation, only making them suitable in particular situations (Guichard et al., 2000). In comparison, kites have a variety of operational and cost advantages over drones, blimps and balloons and resultantly there are a wide variety of reasons why their use has expanded in geographical and environmental research in recent times.

### 5.3.3 Kites as an alternative

The aforementioned issues posed by drone technology and gas-filled platforms such as balloons and blimps are largely absent or less pronounced with kites. Firstly, operational complexity is lower, with launch and landing procedures simplified and the tethered nature of the equipment making it easy and safe to operate. A natural fuel source in the wind means safety issues with batteries or helium fuel are also avoided. Maintenance is often minimal, with robust materials such as nylon popular choices for kite foil material. Kites are easy and cheap to repair, and often adaptable allowing for flexibility in the range of materials that can be used. Secondly, kites are low-cost pieces of equipment. For example a full operational kite kit including a camera is estimated by Delord et al (2015) to cost ~£600. Our own research utilises a fixed line kite (Kite Aerial Photography (KAP) HQ 1.6 m Foil) fitted with a ruggedized Global Positioning System (GPS)-enabled camera, costing much less (~£350). Although prices are in constant flux, for comparison, a fully operational drone platform and associated equipment and training can cost up to ~£30,000 (Woodget et al., 2015).

The issue of legality is where kites greatly excel in comparison with drones. Safety is far less of an issue due to the absence of an autonomous component. Concerns around privacy are still present if cameras are being used, but one is more likely to permissively fly a kite due to the traceability of the equipment and fewer associated safety concerns. In today's world, there are many situations in which kites can fly, but drones cannot. Battery life limitations that regularly affect drones do not hinder kite based operations. Apart from those required for sensors on board the platform (i.e. in a camera), the natural source of wind allows for unconstrained data capture. Kite design has also developed to allow for flight in

the most minimal wind conditions (e.g. large foil-based single line kites with wing areas of 8-12 m<sup>2</sup> (such as those manufactured by HQ) can allow take off in winds as low as 3 mph).

#### 5.3.4 The 21<sup>st</sup> century technology boom

We argue that the renaissance of kite based remote sensing is being fuelled in large, by a technology boom. Several technological developments in the past decades have joined forces to allow kite-based sensing to emerge and grow again. These parallel developments include: the miniaturisation of digital sensors (i.e. compact multispectral imaging systems (Shaw et al., 2012) and thermal imagers (Zarco-Tejada et al., 2012)), and software development (i.e. the Canon Hack Development Kit (CHDK)) which are providing new ways to collect data. Sensors are also vastly more affordable, with a digital infrared camera costing \$10,000 in 2001 (Aber et al., 2001) and now more in the region of £220 (<http://www.mapir.camera/>). Increased coverage from global navigational satellite systems (i.e. GPS, Galileo, GLONASS (the Russian satellite navigation system)) and the inclusion of GPS capabilities in mobile phones and digital cameras also allows for more geographically meaningful observations to be captured from kites. On the ground, differential Global Navigation Satellite System (GNSS) with Real Time Kinematic (RTK) techniques can complement the capture of proximal remote sensing data with centimetre accurate measurements (Eulie et al., 2013; Puttock et al., 2015) for product validation or geospatial model derivation. Researchers are also offered a range of new ways to process the data captured from kite-based platforms. Computing power is readily obtainable at low costs, whether it be locally (e.g. desktop or laptop), remotely on the cloud (i.e. Amazon

web service) or somewhere in between for scientists based at universities or research institutes (i.e. Beowulf clusters (Meredith et al., 2003)).

Kite rig design can now be readily achieved with the aid of twenty first century technology. Techniques such as 3D printing allow for fully customisable rigs to be constructed to allow sensors to be hung from kite lines (e.g. in **Figure 5.2** we demonstrate a bespoke picavet mount designed to house a Canon Powershot D30 camera (author's own design)). Luckily the compact and lightweight nature of camera equipment and sensors today does not require the complexity of rigs used in early kite-based aerial photography. Pendulum and picavet mounts are the two most popular forms of camera mounting designs for kites and the internet has become a comprehensive source of tutorials on DIY designs (e.g. (Silver, 2013)) and ready created models to be printed with a 3D printer (e.g. (Fastie, 2014)).

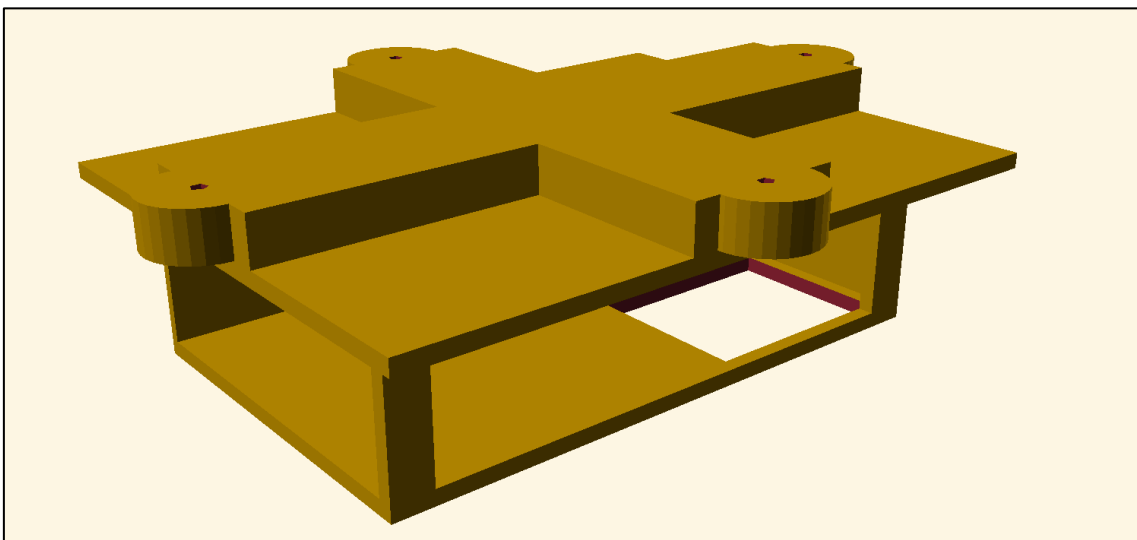


**Figure 5.2: Custom-designed lightweight picavet mount for Canon Powershot D30. Model constructed in OpenSCAD (<http://www.openscad.org/>) and available to download from Thingiverse (<http://www.thingiverse.com/thing:1372969>).**

There is a high-tech revolution underway in kite-based aerial photography, and a prime example is the intelligent kite aerial photography platform (iKAPP) platform which provides a comprehensive example of how robotics, on-board micro-processors and imaging capabilities can be combined into a sophisticated surveying platform (Murray et al., 2007). Additions of a real time data link via an on-board computer and functions to automate the coverage of a site are a true demonstration of the fusion between the humble kite similar to that used by Dines and 21<sup>st</sup> century technology. One step further than iKAPP is the AUTOKITE, a hybrid model plane, with autopilot and kite components attached (McGarey and Saripalli, 2014). The designers of this system claim greater flight times, lower required pilot experience, lower costs and more wind tolerance than multicopter drones. However, the incorporation of a lithium battery and loss of the tethered component bring into question its labelling as a true kite platform.

#### 5.4 Kites as platforms for proximal sensing in physical geography

Over 100 years after Dines' original publication there is a range of new work emerging that shows how kites continue to evolve as platforms for data capture in physical geography. The following sections will discuss the variety of applications where kites have been used to capture fine-scale data describing environmental or geographical phenomena.

##### 5.4.1 Basic mapping

Kites serve as an ideal tool for basic mapping purposes. The nadir view provided from the kite perspective has proven useful for describing the location of ice-wedge polygons in Alaska (Boike and Yoshikawa, 2003). Further geomorphological study has been conducted on sand dunes (Lorenz and

Scheidt, 2014) and surface features relevant to Quaternary studies (Aber and Gałazka, 2000). Kites have been used successfully to obtain aerial data over coastal or coral reef environments (Currier, 2015; Scoffin, 1982). Indeed, coastal environments are often difficult places in which to fly drones owing to complex wind conditions, and yet these environments are perfect for kite flying, with more consistent wind conditions allowing for good kite survey opportunities. **Figure 5.3A** shows the author flying a 1.6m HQ KAP kite over a seagrass habitat in Greece alongside a resultant aerial image (**Figure 5.3B**) captured from a Canon Powershot D30 camera tethered below the kite using a 3D printed rig similar to that shown in **Figure 5.2**. The image of the coastal habitat was captured from a flying height of ~20m. The conditions at this coastal site were too windy and unsafe to allow a drone to be flown, demonstrating the important complementary role of kite platforms in supporting fine-grained data capture.

Archaeology is one of the areas where there is more long-term evidence of their use as surveying tools. The literature contains three decades of evidence of kite use for local scale surveys with the main focus being mapping and site documentation (Verhoeven, 2009). Perhaps the reason for kite use being more prominent in this field is that archaeological sites tend to be contained within relatively small geographical areas and kites are therefore an ideal tool to capture the required aerial data in an easy low-cost and safe manner.



**Figure 5.3: Author (JPD) flying 1.6 m HQ KAP single-line kite over seagrass meadows in northern Greece (A) and resulting aerial photograph (B).**

#### 5.4.2 3D landscape reconstruction

Photogrammetry and more specifically Structure from Motion (SfM) has become an increasingly prominent data processing technique within physical geography (Smith et al., 2015). Its roots are in computer vision and ultimately it allows for 3D reconstruction of a scene using unordered 2D images (Dandois and Ellis, 2013; Westoby et al., 2012). There are many platforms from which to collect 2D photographs to be used in a SfM workflow, including, balloons, gyrocopters, drones and kites (Smith et al., 2015). One key requirement of data collected for SfM processing is the acquisition of photographs with overlapping, multiple viewpoints of the same scene or object of interest. From kites, this can be achieved relatively easily with the ability to move the kite slowly over complex

features allowing for optimal photographic overlap, or by variations in camera orientation provided by natural movement of the kite, or by more intelligently designed camera rigs (i.e. radio controlled camera mount) (Marzloff and Poesen, 2009; Smith et al., 2009). In typically poorly surveyed environments such as mountainous landscapes, kites provide a simple lightweight solution for proximal data capture, and in places where power supplies are limited kites are the perfect low-tech platform for aerial photography. For example (Wundram and Löffler, 2008) working in a remote region in the Norwegian mountains, used a 4MP camera attached to a kite to generate a 0.25m digital elevation model of an alpine mountain landscape.

An interesting example where kite-based mapping procedures were used to great effect was in a study of an Australian intertidal rocky shore (Bryson et al., 2013). The work in this study followed a low-cost theme throughout, with consumer grade digital cameras, a small number of ground control points and a consumer grade handheld GPS device for validation. With great attention to detail in the design of the study, multispectral terrain models with sub-centimeter resolution were created, describing elevation, slope, aspect and land cover type. This work is a prime example of how kite-based mapping can generate fine-spatial resolution proximal sensing data of the natural environment.

#### 5.4.3 Ecology and agriculture

Population counting of bird colonies has been demonstrated as a suitable application for kites in ecological research. Adélie Penguin (*Pygoscelis adeliae*) colonies have been surveyed with longline kites, with logistical complexities and cost savings cited as the key reasons for the choice of remote sensing platform

(Fraser et al., 1999). A similar method but with improved camera technology has been employed over Guanay Cormorant (*Phalacrocorax bougainvillii*), Macaroni penguin (*Eudyptes chrysocome*) and King penguin (*Aptedonytes patagonicus*) colonies (Delord et al., 2015). The resulting images were mosaicked and contained estimated counts of up to 140,000 breeding pairs. Presumably, kites offer a lower risk option than drones in these settings, being quieter and with reduced risk of animal disturbance (Vas et al., 2015).

In agricultural settings where fine-grained information on crop health, soil condition and water availability are critical determinants of yield, there are great opportunities and proven capabilities for kite platforms. Kites have been used as a feasible platform from which to monitor growth rates over bean and banana plantations (Oberthür et al., 2007). The calculation of above ground biomass of desert vegetation has also been tested with some success in China (Siebert et al., 2004). Although this work was conducted to track degradation of the environment, the principles of biomass estimation could also be useful for commercial purposes.

#### 5.4.4 Democratic mapping and teaching

Outside the realm of scientific research, it is also our view that kites will play a critical future role in democratic mapping and teaching based activities. The minimal required training, robustness of the equipment and safety of operation have made kites a welcome addition to practical field study in higher education (Sander, 2014). With kites being ubiquitous in most regions of the world, there is a great opportunity to see these, as combined with basic sensor technologies (i.e. cameras in widely available mobile phone devices) as tools for democratic

mapping. This has been tested with drones in the city of Lima (<http://remaplima.blogspot.co.uk/>) but in our view, the basic simplicity of kite flying offers an even more accessible toolkit for communities across the world to engage with new self-service mapping in an affordable fashion. This leads to the role of fine-grained spatial data in assisting with humanitarian work, and the potential role of kites in making this more accessible. For example kites have been used to assess the magnitude of a humanitarian emergency in Chad (Sklaver et al., 2006). The position of infrastructure features such as latrines and counts of the number of people in a refugee camp were obtained from aerial photographs. This study demonstrates that the choice of a kite is ideal in environments with no/limited fuel, where alternative proximal platforms such as drones or balloons are unviable. The flexibility of the parts and tethered nature also makes it a safer option for obtaining aerial photographs in what is described as a crowded environment (Sklaver et al., 2006). The aforementioned technology boom has also brought with it innovative and accessible ways to share data and software for analysis purposes. Open aerial map (<https://github.com/hotosm/OpenAerialMap>) is one such example, where tools are provided to aid in the sharing of aerial data for use in disaster relief situations.

## 5.5 Conclusions

The renaissance in kite based proximal sensing has its foundations in the amateur world, with much scientific work citing public open-source publications such as the 'Areal Eye' as a source of information of kite and rig design (e.g. (Wundram and Löffler, 2008)). Whether in paper format, or more recently online, resources such as Public Lab (<https://publiclab.org/wiki/kite-mapping>) and the Drachen Foundation (<http://www.drachen.org/learn/kite-basics>) are a key source

of information for design and operation of kite platforms. This is very much a grassroots movement enabling users to collect data (often in a participatory fashion) when they want and where they want. With the increase in available technology, kites can continue to be successful and reliable proximal remote sensing platforms, playing an important role in validating complimentary datasets such as satellite observation data (Thayn, 2012).

The kite was part of one of the earliest proximal sensing scientific studies and is set to be a key part of the modern geographer's toolkit. The low-tech, and often open source nature of the equipment involved offers a complementary and in some cases, better platform for proximal remote sensing than a drone. In an age where drones are in the news every week, let's not forget the humble yet viable alternative that is the kite.

## 6 Sand dune dynamics

### *St. Gothian sands dune system, Cornwall, UK*



This paper was published in Remote Sensing in 2018:

Duffy, J.P., Shutler, J.D., Witt, M.J., DeBell, L & Anderson, K. (2018) Tracking Fine-Scale Structural Changes in Coastal Dune Morphology Using Kite Aerial Photography and Uncertainty-Assessed Structure-from-Motion Photogrammetry. Remote Sensing, 10, 1494.

# Tracking Fine-Scale Structural Changes in Coastal Dune Morphology Using Kite Aerial Photography and Uncertainty-Assessed Structure-from-Motion Photogrammetry

James P. Duffy<sup>1\*</sup>, Jamie D. Shutler<sup>2</sup>, Matthew J. Witt<sup>3</sup>, Leon DeBell<sup>1</sup> and Karen Anderson<sup>1</sup>

1. DroneLab Research Group, Environment and Sustainability Institute, University of Exeter, Penryn Campus, Penryn, Cornwall TR10 9FE, UK

2. Centre for Geography, Environment and Society, University of Exeter, Penryn Campus, Penryn, Cornwall TR10 9FE, UK

3. College of Life and Environmental Sciences, Environmental Biology Group, Hatherly Laboratories, University of Exeter, Exeter, EX4 4PS, UK

*\*Corresponding author*

## 6.1 Abstract

Coastal dunes are globally-distributed dynamic ecosystems that occur at the land-sea interface. They are sensitive to disturbance both from natural forces and anthropogenic stressors, and therefore require regular monitoring to track changes in their form and function ultimately informing management decisions. Existing techniques employing satellite or airborne data lack the temporal or spatial resolution to resolve fine-scale changes in these environments, both temporally and spatially whilst fine-scale in-situ monitoring (e.g., terrestrial laser scanning) can be costly and is therefore confined to relatively small areas. The rise of proximal sensing-based Structure-from-Motion Multi-View Stereo (SfM-MVS) photogrammetric techniques for land surface surveying offers an

alternative, scale-appropriate method for spatially distributed surveying of dune systems. Here we present the results of an inter- and intra-annual experiment which utilised a low-cost and highly portable kite aerial photography (KAP) and SfM-MVS workflow to track sub-decimetre spatial scale changes in dune morphology over timescales of between 3 and 12 months. We also compare KAP and drone surveys undertaken at near-coincident times of the same dune system to test the KAP reproducibility. Using a Monte Carlo based change detection approach (Multiscale Model to Model Cloud Comparison (M3C2)) which quantifies and accounts for survey uncertainty, we show that the KAP-based survey technique, whilst exhibiting higher x,y,z uncertainties than the equivalent drone methodology, is capable of delivering data describing dune system topographical change. Significant change (according to M3C2); both positive (accretion) and negative (erosion) was detected across 3, 6- and 12-month timescales with the majority of change detected below 500 mm. Significant topographic changes as small as ~20 mm were detected between surveys. We demonstrate that portable, low-cost consumer-grade KAP survey techniques, which have been employed for decades for hobbyist aerial photography, can now deliver science-grade data, and we argue that kites are well-suited to coastal survey where winds and sediment might otherwise impede surveys by other proximal sensing platforms, such as drones.

## 6.2 Introduction

Sand dune ecosystems are globally distributed (Barbier et al., 2011), covering approximately 34% of the world's ice-free coastlines (Hardisty, 1994), and they form on many types of shores and under a variety of climatic conditions (Hesp, 2002). They deliver critical ecosystem services such as coastal protection (Sigren

et al., 2018) as well as providing environmental heterogeneity which promotes ecological diversity (Acosta et al., 2009). Other services include nutrient cycling, well-being and recreation, and mineral extraction (Everard et al., 2010). Whilst these services are beneficial to human populations at the coast and beyond, coastal sand dune environments face pressures. The threats to sandy beach ecosystems and their associated dunes are wide ranging from local to global in scale (Defeo et al., 2009). Dune systems worldwide are under threat from increased storm damage and human interference such as pollution, and human disturbance (e.g. off-road vehicles and trampling (Brown and McLachlan, 2002; Santoro et al., 2012)). There is a pressing need to monitor these sensitive environments in order to inform management decisions for preserving their integrity and averting irreversible damage (Lemauviel and Rozé, 2003).

A wide range of scientific work has used field, laboratory and spatial modelling approaches to understand the fine-scale dynamics of sand dune systems, and to identify which physical processes shape them (e.g. 2D profiles to understand how sediment budgets influence foredune structure (Davidson-Arnott et al., 2018)). Numerical modelling approaches incorporating wave dynamics have also been utilised to understand the response of coastal dunes to environmental change such as storm events and hurricanes (Roelvink et al., 2009). Monitoring of dune condition is critical to ensure the provision of the services they provide, to complement understanding of the natural processes shaping coastal dunes. The task of monitoring can be greatly aided by data from remote sensing systems. To date, a variety of both remote and proximal sensing techniques have been used to answer questions about dune morphology, dynamics and change, and for the management of dune systems. For example, terrestrial laser scanning (TLS) has

proven useful for quantifying coastal dune morphology (Feagin et al., 2014), and repeat TLS has been used successfully to monitor the evolution of erosion features such as dune blowouts (Smith et al., 2017). TLS has also been deployed to track erosion and predict overtopping of anthropogenic berms on the coast (Schubert et al., 2015). Despite the very high precision (<10 mm) and fine spatial resolution (~7 mm at 50 m range; (Buckley et al., 2008)) data that TLS systems can provide, the equipment is expensive, complex and time consuming to operate (Westoby et al., 2012). The spatial extent over which it can be employed is also limited as positioning of the equipment has to be carefully considered to avoid gaps in the data collected, and the most beneficial positions for the equipment may not always be accessible (Buckley et al., 2008). From commercial satellite systems, relatively fine spatial (0.61 m panchromatic) resolution data such as those delivered by Quickbird, we argue, are poorly suited for cost-effective monitoring of dynamic systems such as those found in coastal environments. This is because dune systems are highly dynamic and repeat surveys are often required to gain understanding of the processes at work in the coastal zone, necessitating the purchase of multiple data sets, which can become very costly, sometimes, prohibitively so for long-term monitoring programs (Westoby et al., 2018; Zhang and Kovacs, 2012). Furthermore, despite their fine spatial resolution, issues such as mixed pixels can still arise in dune environments due to a high degree of habitat heterogeneity and mixtures of vegetation and sand (Hugenholtz et al., 2012). Alternatives to Quickbird include data provided by the Landsat and Sentinel 2 sensors for which global median revisit times are approximately 3 days (Li and Roy, 2017). However, their coarser spatial resolution (>10 m) are unsuitable for monitoring the heterogeneous environments found at the land-sea boundary, where the mixing of terrestrial and marine realms

again can give rise to mixed pixels, ultimately reducing the success of delineating key landcover types. Aside from satellite platforms, data collected during airborne campaigns both with Light Detection and Ranging (LiDAR) and optical sensors have been utilised for coastal monitoring (Rader et al., 2018). For example, LiDAR data have been used to aid the estimation of shoreline slope and position over hundreds of kilometers of coastline (Stockdon et al., 2002), to conduct shoreline change analysis on centennial and intra-decadal scales (Burningham and French, 2017), and to complement ground based vegetation surveys to identify major habitat types to improve understanding of the relationship between dune structure and plant species occurrence (Bazzichetto et al., 2016). In combination with airborne multispectral data, LiDAR data have shown promise for classifying coastal habitats (Chust et al., 2008). However, high costs of piloted aerial surveys prohibit the commissioning of airborne campaigns for regular monitoring (Mumby et al., 1999), and are not feasible in countries where such survey resources are unavailable.

Proximal sensing from low-cost lightweight drone and kite platforms has seen a recent rapid uptake within the geosciences and biosciences for environmental monitoring purposes (Anderson and Gaston, 2013; Duffy and Anderson, 2016). Reasons for this include the low cost of the technology, ease of use, user-dictated surveys both in time and space and the ability to customise the payloads (e.g. sensors) that are attached to the platforms. In parallel, the increased availability of high performance computers and development of photogrammetry software means that Structure-from-Motion Multi-View Stereo (hereafter: SfM-MVS) techniques are now easily employable using images collected from consumer grade cameras (Cunliffe et al., 2016; Westoby et al., 2012). SfM-MVS has been

used to study geomorphological features such as glacially sculpted ridges (Westoby et al., 2012), estimate biomass in tropical forest environments (Ota et al., 2015) and create digital surface models of coastal dune environments (Mancini et al., 2013). Fine spatial resolution data (typically sub-centimeter) have been used to quantify the heterogeneity of seagrass meadows (Duffy et al., 2018), conduct coastal vulnerability assessments (Sturdivant et al., 2017), map mangroves (Otero et al., 2018) and quantify changes in vegetation within dune ecosystems (Madurapperuma et al., 2018; Nolet et al., 2018). Although these prior experiments have demonstrated the opportunities for this new approach to be adopted widely in coastal environments, drone operations specifically are not without their risks in these settings. First, coastal environments have a tendency to be windy and this makes both operating drones and capturing high quality data here more challenging (Duffy et al., 2018). Second, the presence of loose sediment such as sand particles poses a risk to mechanical drone parts such as motors, and parts of the on-board payloads (e.g. camera lenses). One alternative that mitigates some of these issues is kite aerial photography (KAP). The natural fuel source of the wind in coastal systems makes KAP a cost-effective and accessible method with which to collect proximal sensing data (Duffy and Anderson, 2016). Kites have been used for data capture in ecological studies, e.g. to monitor penguin population sizes (Fraser et al., 1999), for geomorphological applications such as the catchment scale gully detection (Feurer et al., 2018) and intertidal landscape mapping (Bryson et al., 2013), but there are no similar studies documenting the use of kites for sand-dune mapping and topographic change mapping over time.

The self-service nature of proximal sensing from KAP platforms facilitates data capture at high temporal resolution (i.e. possibility of multiple surveys in one day) and fine spatial resolution. Alongside, the emergence of high performance and affordable computing power allows for the analysis of SfM-MVS data outputs. Analysing the changes in the structure of features represented in such data (e.g. point clouds), whilst also taking account of data uncertainty, can now be achieved with the Multiscale Model to Model Cloud Comparison (M3C2) technique (Lague et al., 2013). This method improves on the difference of DEM (DoD) technique by incorporating 95% confidence intervals into change detection between the points in two clouds, also allowing for the detection of very small changes and indicating whether they are statistically significant. Building on this, the M3C2-Precision Mapping (M3C2-PM) technique has been developed; incorporating Monte Carlo creation of multiple point clouds to derive precision estimates for each point in the cloud (James et al., 2017b). This type of analysis can readily be applied to the outputs of SfM-MVS workflows. To our knowledge, the combination of KAP and SfM-MVS techniques involving multi-temporal surveys has not been undertaken to date using M3C2-PM methods. Neither has the method been demonstrated robustly for coastal monitoring over time. We address the following research questions to explore these knowledge gaps:

**1) How do data from a KAP system processed with SfM-MVS methodology compare to the same data captured from a more stable drone system for sand-dune morphological assessment at a single point in time?** Given existing work that allows robust estimates of spatial uncertainty to be obtained for SfM-MVS derived point clouds (e.g. M3C2-PM), we apply such methods to the

data produced from the drone survey and a single KAP survey to understand differences in the data produced.

**2) To what extent can a KAP + SfM-MVS methodology capture fine spatial scale (sub-decimeter) changes in sand-dune morphology over time?**

Applying M3C2-PM analysis techniques, we aim to determine the extent to which significant changes can be detected in sand-dune morphology from multi-temporal KAP-SfM-MVS data products, focussing on three-, six- (intra-annual) and twelve-month (inter-annual) timescales.

**3) Employing such methods, how do beach, dune fronts/foredunes, and footpaths change over time?**

## 6.3 Materials and methods

### 6.3.1 Study system

The study system used for this proof-of-concept work was located within St Gothian Sands Local Nature Reserve (50.226, -5.392) on the north coast of Cornwall in south-west England (**Figure 6.1**). A stretch of foredunes measuring approximately 180 m in length was selected for data collection. Although now protected, the site was exploited for sand extraction until 2005 (Natural England, 2018). It is now a popular recreational site with dog walkers, and other beach goers throughout the year. The predominant wind direction at the site is westerly followed closely by southerly winds (**Figure 6.2**).

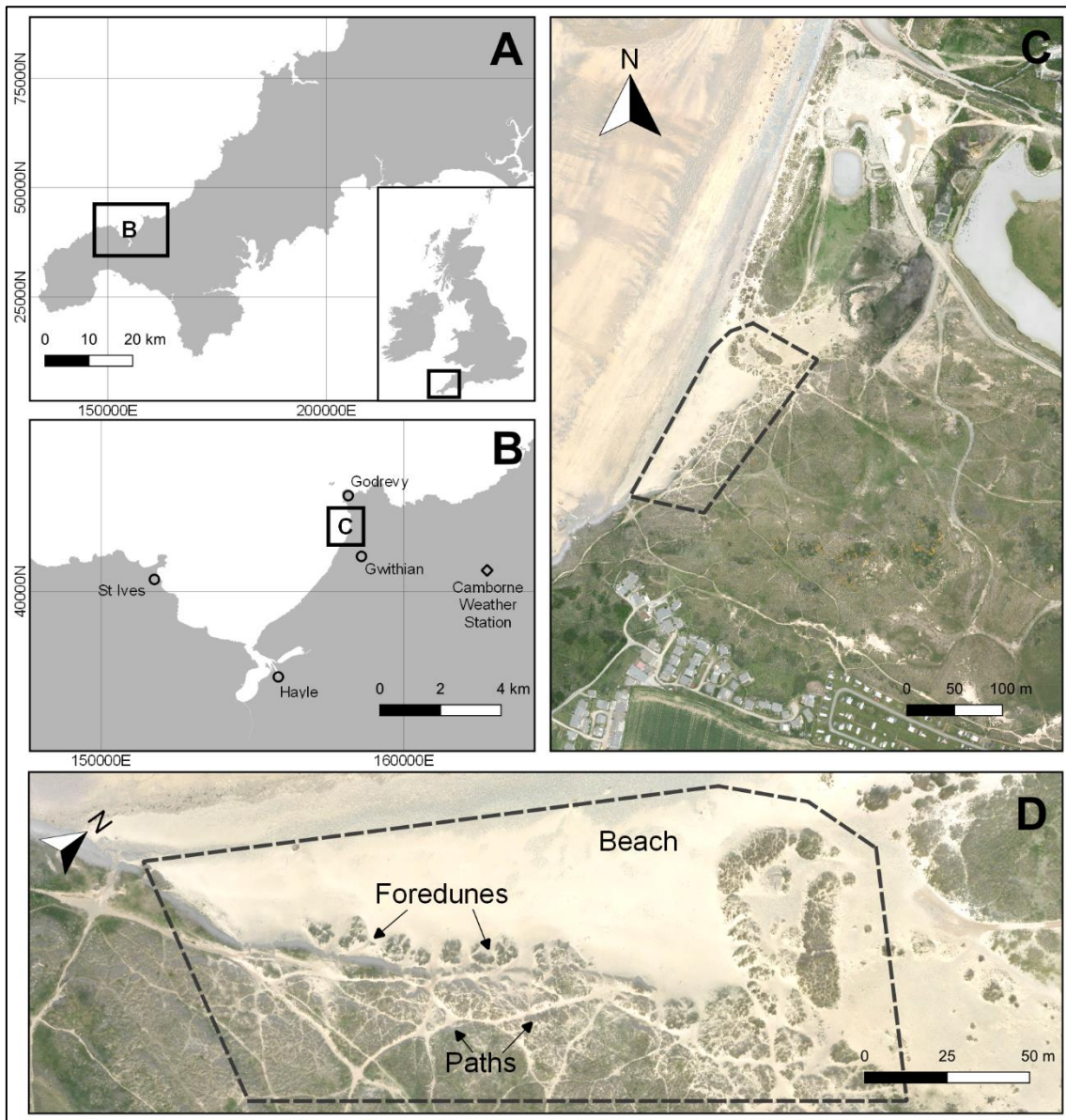


**Figure 6.1: A) The location of St Ives bay and Gwithian Towans within the UK and Cornwall. B) The location of St Gothian Sands Local Nature Reserve. C) An aerial image (courtesy of Channel Coastal Observatory, <https://www.channelcoast.org/>) with the dune study system (area of interest) indicated by dashed line. D) The study system annotated with features of interest.**

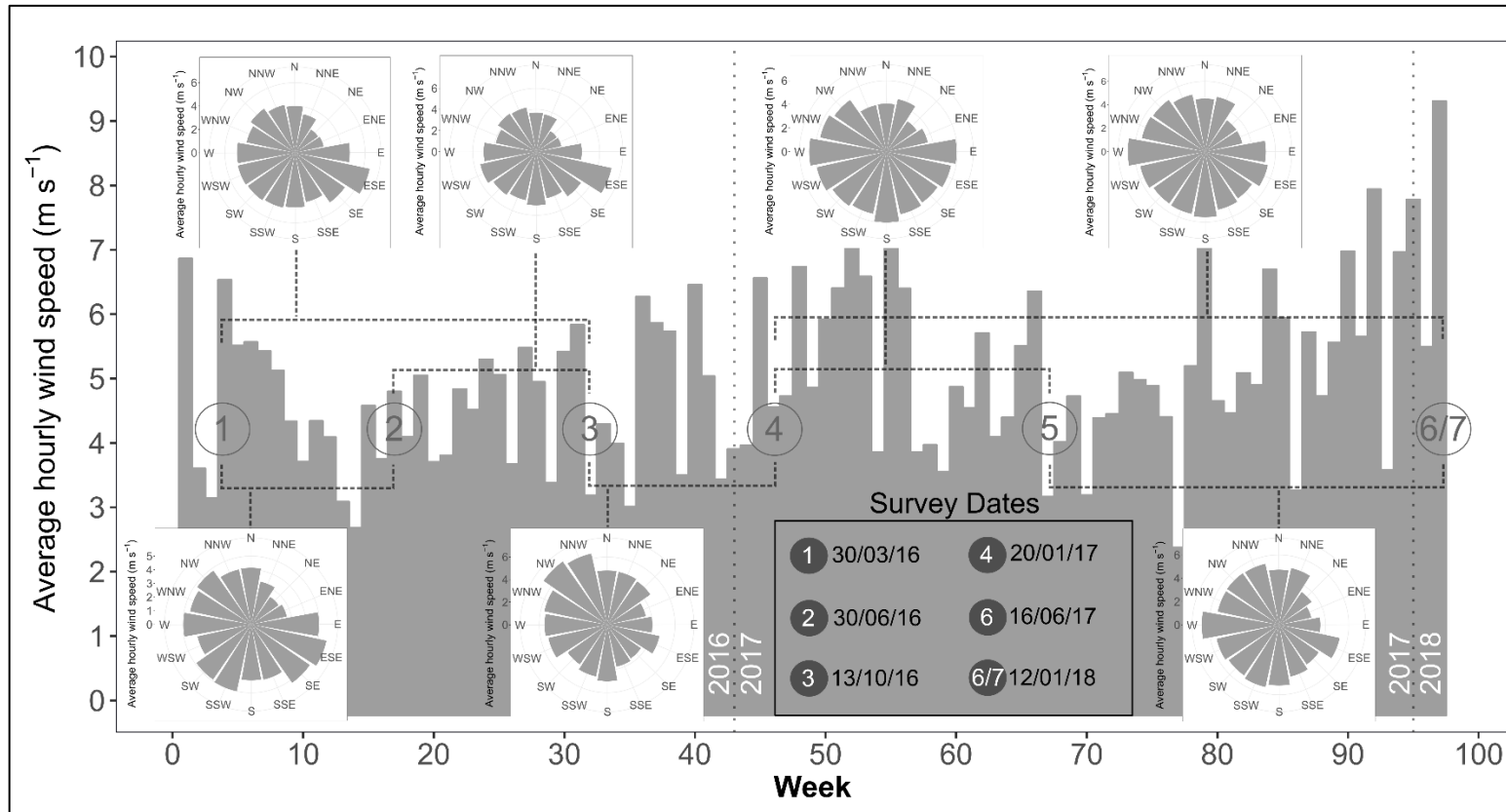


**Figure 6.2: Wind profile characterising the study system using weather data from Camborne weather station (located approximately 5km east of St Gothian Sands nature reserve). Histogram displays average hourly wind speed (grouped by week) throughout the study period, and wind roses indicate average hourly wind speed and direction during the periods between pairs of the six KAP and drone surveys used in analysis (indicated by number labels). Weather data obtained from Met Office DataPoint Service (<https://www.metoffice.gov.uk/datapoint>; contains public sector information licensed under the Open Government Licence).**

### 6.3.2 Data capture

KAP was used to collect aerial images of the site. Two variants of the same kite were used, depending on weather conditions, but both were single line foil systems (HQ KAP Foil 1.6 m<sup>2</sup> and HQ KAP Foil 5.0 m<sup>2</sup>) that are renowned for providing stable aerial platforms. The 5.0 m<sup>2</sup> model was suitable for lower wind conditions (1.79-8.94 m s<sup>-1</sup>), whilst the 1.6 m<sup>2</sup> model was suitable for higher wind conditions (3.13-13.86 m s<sup>-1</sup>), which were more typical at the site. A custom 3D printed picavet mount (created by author JPD: <https://www.thingiverse.com/thing:1372969>) was used to carry a ruggedized, waterproof and dustproof Canon D30 compact digital camera with a 5-20 mm focal length lens and 12.1 effective megapixel sensor (**Figure 10.3**). Picavet refers to a system of cords and/or pulleys designed to keep a platform stable. The camera also has an internal GPS sensor, recording positional information and storing it as metadata on each image captured. The Canon Hacking Development Kit (CHDK; (CHDK Development Team, 2018)) was loaded onto the SD card inside the camera to allow for manual control of settings such as shutter speed, aperture, ISO and the time interval between consecutive image capture. The majority of surveys were conducted before 13.00 (GMT), but exact times varied depending on light availability and wind conditions at different times of year (Table 1). Wind conditions dictated the altitude of the kite, and sufficient line was deployed until the platform was deemed stable to commence surveying: typically this was between 20 m and 40 m of line, but the angle between the kite and the ground varied during and between surveys due to temporally variant wind speeds, resulting in variations in spatial resolution both within and between surveys. The variation in sensor altitude was calculated as part of the SfM-MVS

workflow. Six surveys were conducted between 30/03/2016 and 12/01/2018, to capture potential structural change at 3, 6 (intra-annual) and 12 month (inter-annual) periods (**Table 6.1**).

To deliver an independent dataset for comparison to the KAP-SfM-MVS data, a single additional survey was undertaken using a 3DR Solo lightweight multirotor drone on the same date as survey 6 (**Table 6.1**) over a small sub-area of the dune study system, specifically to answer research question 1 (**Figure 10.4**). This type of drone has been previously used to collect high quality remote sensing observations of coastal seagrass environments (Duffy et al., 2018). A short ~4-minute flight with a fixed altitude of 40 m and speed of  $\sim 3 \text{ ms}^{-1}$  was undertaken ~30 minutes after survey 6 (**Table 6.1**). Resulting data allowed for the direct comparison of point clouds constructed with images from the kite platform to those from the drone platform. The same sensor and setup (Cannon D30 with CHDK) was used with the multirotor drone as was used with the KAP methodology, with identical camera settings.

To provide independent ground control for spatial constraint of the SfM-MVS model (James et al., 2017a), 14 black and white chequered 300 mm × 300 mm plastic ground control points (GCPs) were distributed across the area of interest (except for survey 1, where 14 were deployed but only 12 successfully measured due to technical issues with field equipment). A laminated card with a letter (a unique identifier, e.g. "A") and a notice to ask beachgoers not to interfere with the target was placed alongside. The position of these GCPs was measured both with a handheld GPS device (Garmin GPSMap 64) and using a Leica GS-08 differential Global Navigation Satellite System (D-GNSS). The D-GNSS system uses a base and rover to deliver a differentially corrected geospatial location

dataset with approximately 10 mm accuracy in x,y,z dimensions. Geospatial data collected with these two devices were recorded in the British National Grid projection (EPSG:27700). A cross was etched into on a concrete platform within the dunes, marking a single point to be used throughout the study period, and used as the base location for each repeat survey (easting = 158199.7 m, northing = 41825.74 m, altitude = 6.34 m). Ground-based photos were also taken of this point and its surroundings to aid in its relocation at the beginning of each survey. To minimise the distribution of error across the dataset, GCPs were placed in approximately the same positions according to their position from survey 1, using the handheld GPS as a guide to locate these positions during each revisit to the site. The data collection, processing and analysis workflow can be seen in **Figure 6.3**.

Weather data were obtained from the Met Office DataPoint Service (<https://www.metoffice.gov.uk/datapoint> which provides public sector information licensed under the Open Government Licence). The nearest Met Office weather station to the study site with hourly recordings of weather conditions including wind speed and direction was Camborne in Cornwall (latitude: 50.218, longitude: -5.327), which is approximately 4.7 km ESE from the study system (**Figure 6.1B**). This data assisted in characterising the general wind conditions within the study system and between survey dates (**Figure 6.2**).

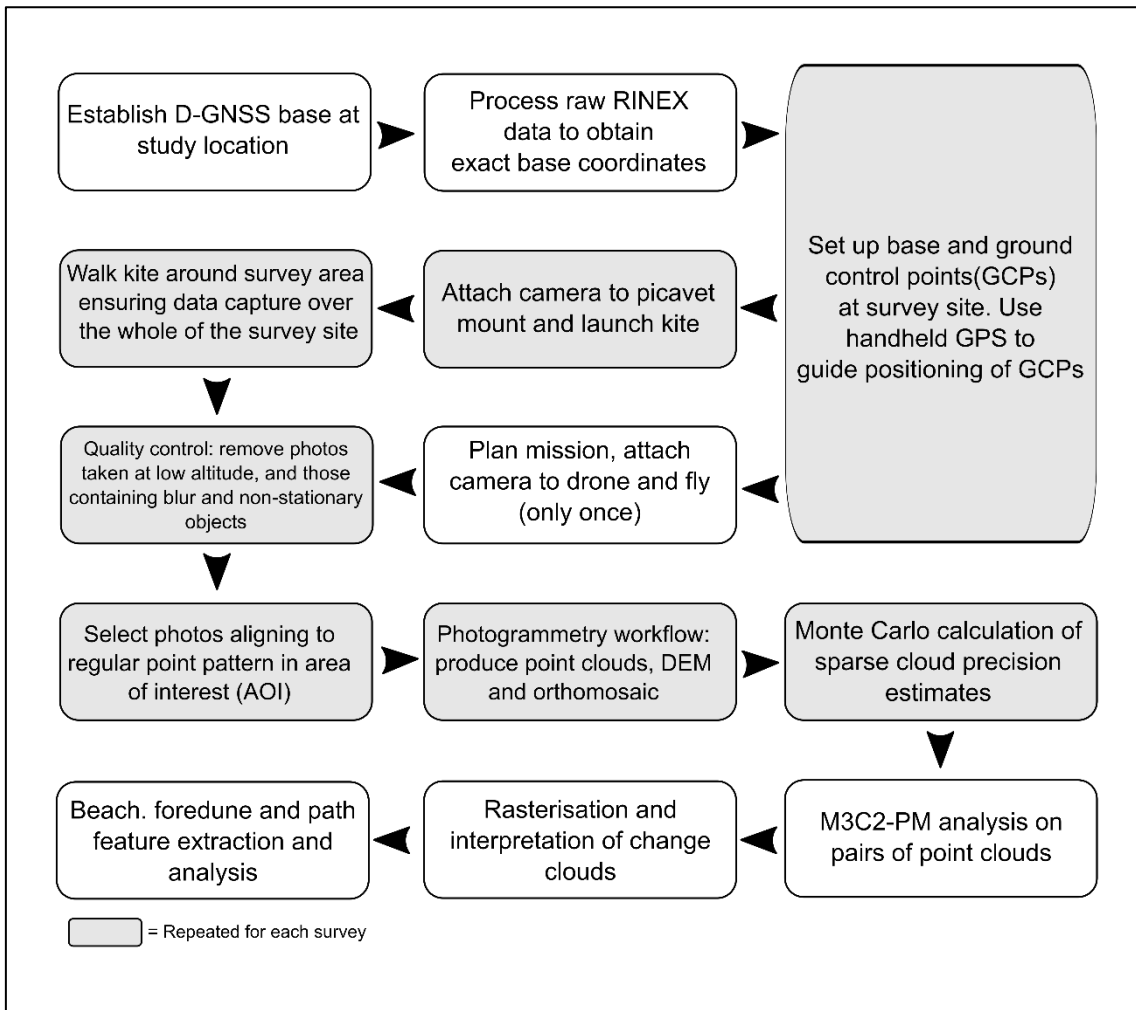


**Figure 6.3: Data collection, processing and analysis workflow for KAP and drone surveys.**

**Table 6.1: Details of each KAP and drone survey undertaken and associated wind conditions. Times (in GMT) are estimations based on the first and last photos that are deemed useable in the photogrammetry workflow. Wind data from Camborne weather station (located approximately 4.7 km ESE from the study system). Weather data obtained from Met Office DataPoint Service (<https://www.metoffice.gov.uk/datapoint>; contains public sector information licensed under the Open Government Licence).**

Survey ID	Date	Survey Duration (GMT)	Platform	Predominant Wind Direction	Wind speed range (m s <sup>-1</sup> )
1	30/03/2016	10:45-11:35	KAP HQ 1.6	WNW	3.6-4.5
2	30/06/2016	08:05-11:50	KAP HQ 1.6	W	4-6.3
3	13/10/2016	10:25-11:00	KAP HQ 1.6	E	6.7
4	20/01/2017	13:50-14:20	KAP HQ 1.6	E	4-4.5
5	16/06/2017	07:45-08:35	KAP HQ 1.6	W	4.5-4.9
6	12/01/2018	10:30-12:00	KAP HQ 1.6 & 5	S	5.8-7.2
7	12/01/2018	12:30:12:55	3DR Solo Quadcopter	S	7.2

### 6.3.3 Data processing

#### **Sub-setting images**

Images from each survey were manually filtered. First, those with visible blur, non-stationary objects (e.g. humans and dogs), and “low-altitude” images (e.g. captured during take-off and landing) were removed. A copy of all remaining images were imported to Photoscan and a ‘low-quality’ alignment procedure conducted. This process estimates a camera position in the x,y and z dimensions for each image. These positions were then tagged to the metadata of each image using the freely available exiftool software package (Harvey, 2018). Given the level of processing required in the SfM-MVS workflow and the number of images collected during each survey, 300 was chosen as a suitable number of images to include for photogrammetry processing. Using the spatstat package (Baddeley et al., 2015) in R 3.3.3 (R Core Team, 2017), a regular point pattern ( $n = 298$ , spacing between points  $\sim 7.70$  m) was constructed within the bounds of the area of interest, and then a nearest neighbour procedure was conducted to find the closest image to each point. The nearest neighbour analysis was conducted iteratively, recording the identity of the image with the shortest Euclidean distance, removing the image and regular point from the selection and repeating. This resulted in a subset of 298 images for each survey. These subsets were then used as ‘raw data’ for the photogrammetric workflows (**Figure 6.3**).

#### **Photogrammetry workflow**

Point clouds and associated elevation models and orthomosaics were built using Agisoft Photoscan (v 1.3) (Agisoft LLC, 2017). Processing reports for each build can be found in the supplementary information. Using the subset of 298 images

from the sub-setting procedure as an index, the images containing metadata with positional information captured by the sensors internal GPS (original images) were assigned for the SfM-MVS workflow. Prior to processing, the latitude and longitude metadata values were converted from WGS84 (EPSG:4326) to British National Grid (EPSG:27700) format to match the co-ordinate system which was used for surveying ground control points with the D-GNSS. This conversion was undertaken in the statistical software R (version 3.3.3) (R Core Team, 2017), using the `sp` package (Pebezma et al., 2018) and image metadata were modified with `exiftool` (Harvey, 2018). Once initial alignment was undertaken, and a mesh constructed based on the sparse cloud, GCPs were located within the images and positional information from the D-GNSS attached. Further details on the full processing workflow in Photoscan can be found in section 10.3.1.

#### 6.3.4 Analysis

To investigate morphological change between surveys, a modified M3C2 approach which incorporates precision estimates for the point clouds was used (James et al., 2017b; Lague et al., 2013). This technique is well-suited to multi-temporal KAP topographic change estimation, where variation in data capture between surveys requires consideration within the analysis. Precision estimates for each point in the sparse clouds were calculated with Monte Carlo iterative processing in Photoscan, utilising pseudo-random offsets applied to the image observations and control measurements on each iteration. Full details can be found in the supplementary information of (James et al., 2017b). Given that the clouds varied in size between surveys, the number of iterations in the process varied (restricted by computer memory availability), with the estimated maximum possible number rounded down to the nearest 100 (**Table 10.1**). The estimates

were then mapped (with a nearest neighbour approach) to the associated dense clouds and the M3C2-PM approach used to calculate changes in distance between pairs of clouds using the M3C2-PM plugin in CloudCompare (CloudCompare, 2017; James et al., 2017b). The M3C2 change detection was then conducted on the two clouds and their precision estimates, and a change cloud derived as a result for pairs of surveys. Within the change cloud, points that changed significantly in position were flagged to differentiate them from other points in the cloud. Change clouds were exported scaled down, reducing their density to approximately 0.5 m between points, so they could be analysed and rasterised for visualisation more effectively.

For the specific features (beach, foredunes, paths), polygons were manually constructed with guidance of the orthomosaics produced with images from surveys 4 and 6. The polygons were then used as masks to extract relevant parts of the dense cloud, and the M3C2-PM process was repeated in Cloud Compare as was applied for the full clouds. Change clouds were exported at the native resolution of the dense cloud of survey 4. From this, the proportions and distributions of the data were analysed in R (R Core Team, 2017).

## 6.4 Results

Using an SfM-MVS workflow (**Figure 6.3**), point cloud, DEM and orthomosaic products (**Figure 10.5 & Figure 10.6**) were produced for each of the six KAP surveys and one drone survey undertaken at the study site (**Table 6.1**). **Figure 6.4** shows examples of these photogrammetry products for two of the six KAP surveys. A single transect was taken across the dune system to show elevational changes (derived from DEMs) across the six surveys (**Figure 6.5**). Changes in

elevation between surveys are generally in the decimeter range, and quantifying differences at this spatial scale is a suitable application of M3C2-PM (see section 2.4). The proceeding results sections describe analysis using this technique, rather than calculating differences between DEMs over time.

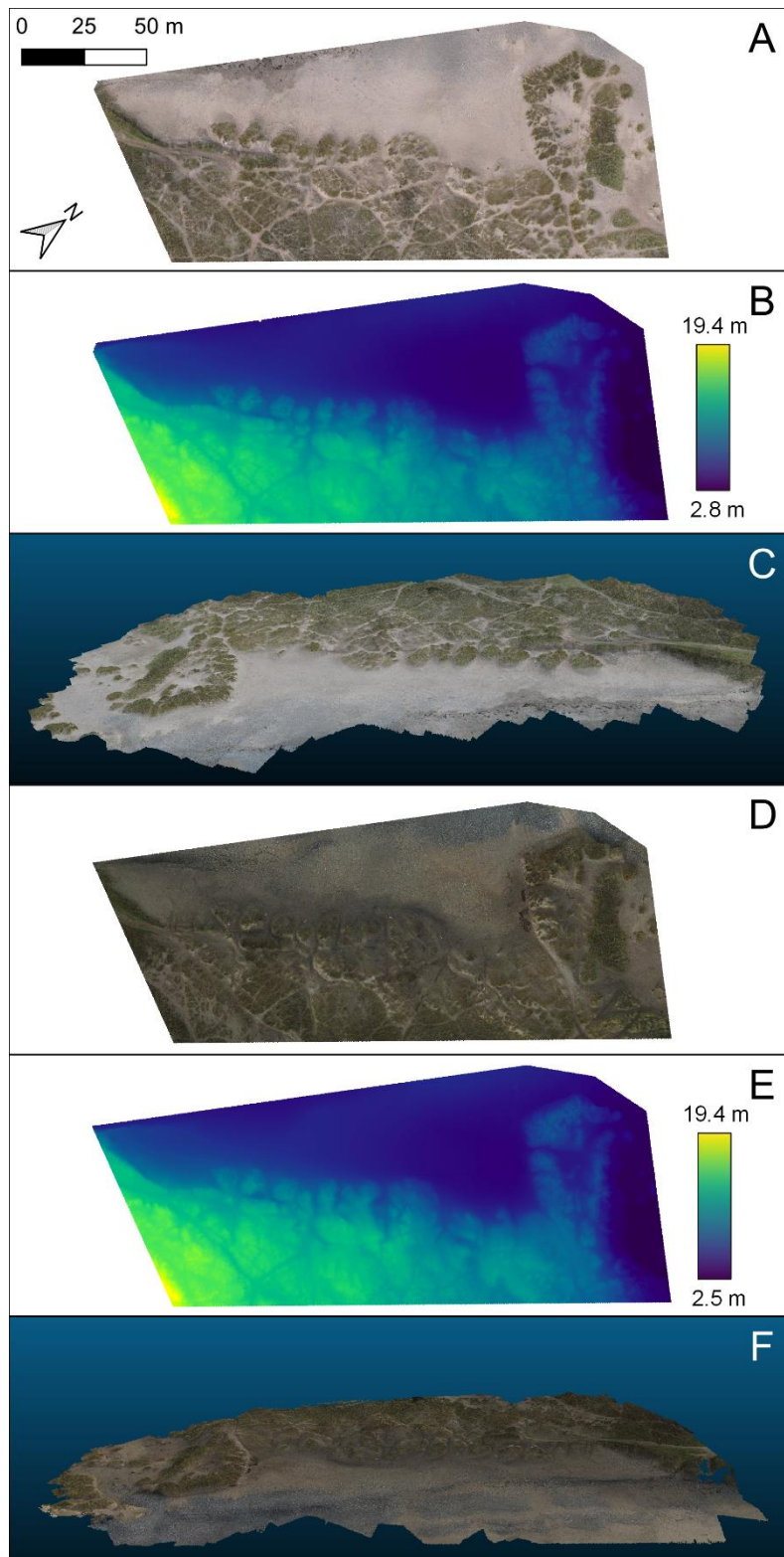


**Figure 6.4: A) Orthomosaic constructed with data from survey 4 conducted on 20/01/2017. B) Digital Elevation Model (DEM) of survey 4. C) Screenshot of dense point cloud made with data from survey 4. D) Orthomosaic constructed with data from survey 6 conducted on 12/01/2017. E) DEM of survey 6. F) Screenshot of dense point cloud made with data from survey 6. Scale bar in A) also applied to B, D & E.**

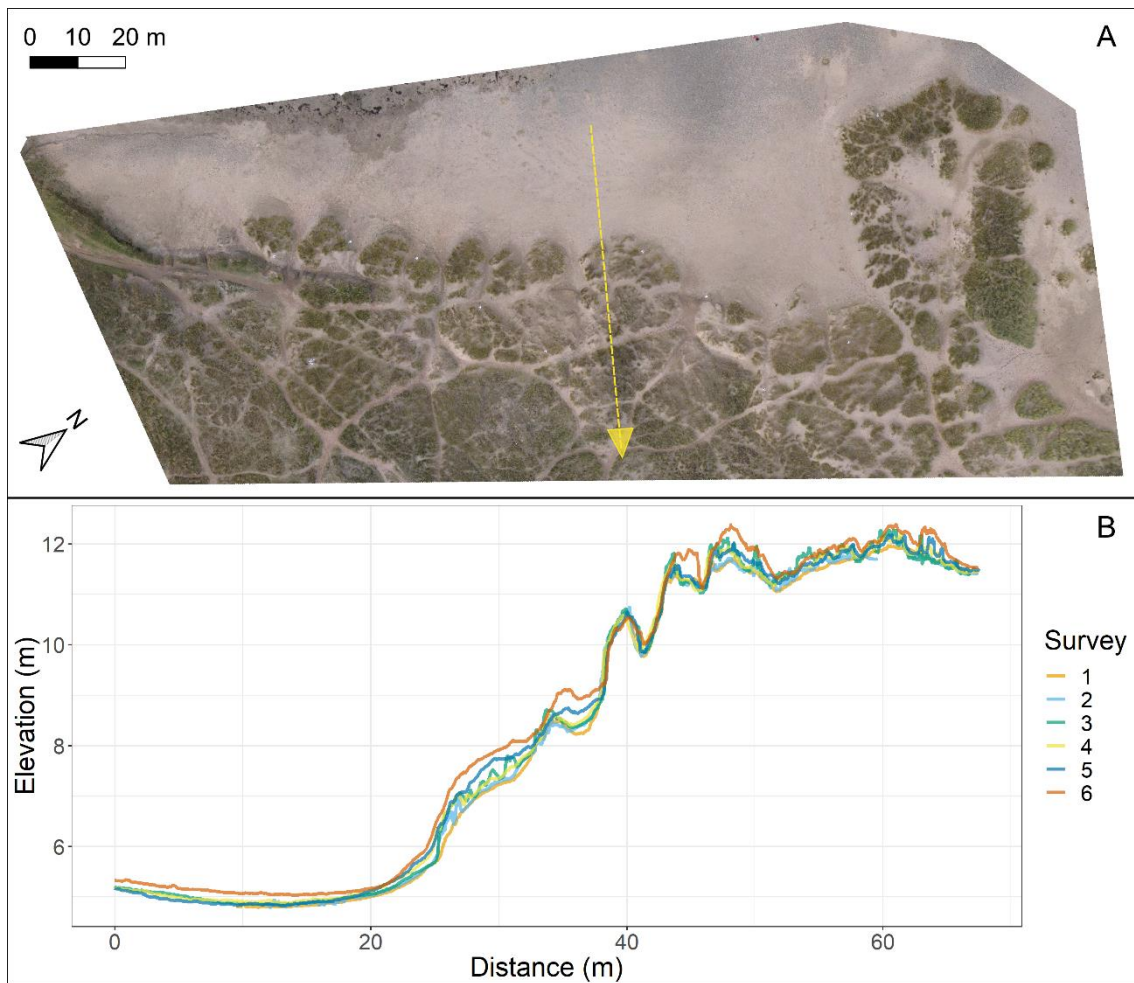


**Figure 6.5: A) Orthomosaic constructed with data from survey 5 (conducted on 16/06/2017) overlaid with a transect. B) Elevation profiles of the transect constructed with data from DEMs of all 6 KAP surveys.**

#### 6.4.1 Drone versus KAP survey

Survey 6 with the KAP setup and the drone survey were undertaken on the same day and within one hour of each other. The drone flight covered part but not all of the area of interest (**Figure 6.6A & Figure 10.4**). The two surveys were compared to evaluate the relative uncertainties within both the drone and KAP methods, especially as the positioning of the sensor and resulting image overlap varied between the two (**Figure 6.6B & C**). In  $x$ ,  $y$  and  $z$  dimensions, M3C2-PM precision estimations were smaller for the sparse dense cloud constructed with data from the drone survey compared to the KAP survey (**Table 6.2**). Mean precision

estimates were approximately 6 times greater for points in the KAP cloud in x and y dimensions (e.g. 31.3 mm and 29.5 mm respectively). For the z axis, mean precision estimations were almost 10 times greater in the KAP cloud at 87.9 mm (**Table 6.2**). DEMs created for the subset area used for this comparison show overall elevational range of 9.8 m, with sandy beach areas on the western edge and foredunes running approximately SW-NE (**Figure 6.6D & E**). The mean difference between the two DEMs was 30.7 mm, and the 5% and 95% quantiles were - 41 mm and 177.3 mm respectively (**Figure 6.6F**). Beyond differences between DEMs, M3C2-PM was conducted using the dense clouds from each survey, to create a change point cloud (**Figure 6.6G**). Within this change cloud, 19% of points had significant differences, of these 89% were positive (showing greater elevation in the kite survey than the drone survey) and 11% negative (**Figure 6.7**). The distribution of significant change points was bi-modal, falling either side of 0 (no change; **Figure 6.7**), with a mean of 160 mm. The greatest differences between the point clouds derived from the KAP survey and drone survey were on stabilised and mostly vegetated parts of the dunes (**Figure 6.6G**), the positive differences greater (median: 128 mm; maximum: 313.6 mm) than negative differences (mean: -56 mm; maximum: -48 mm).

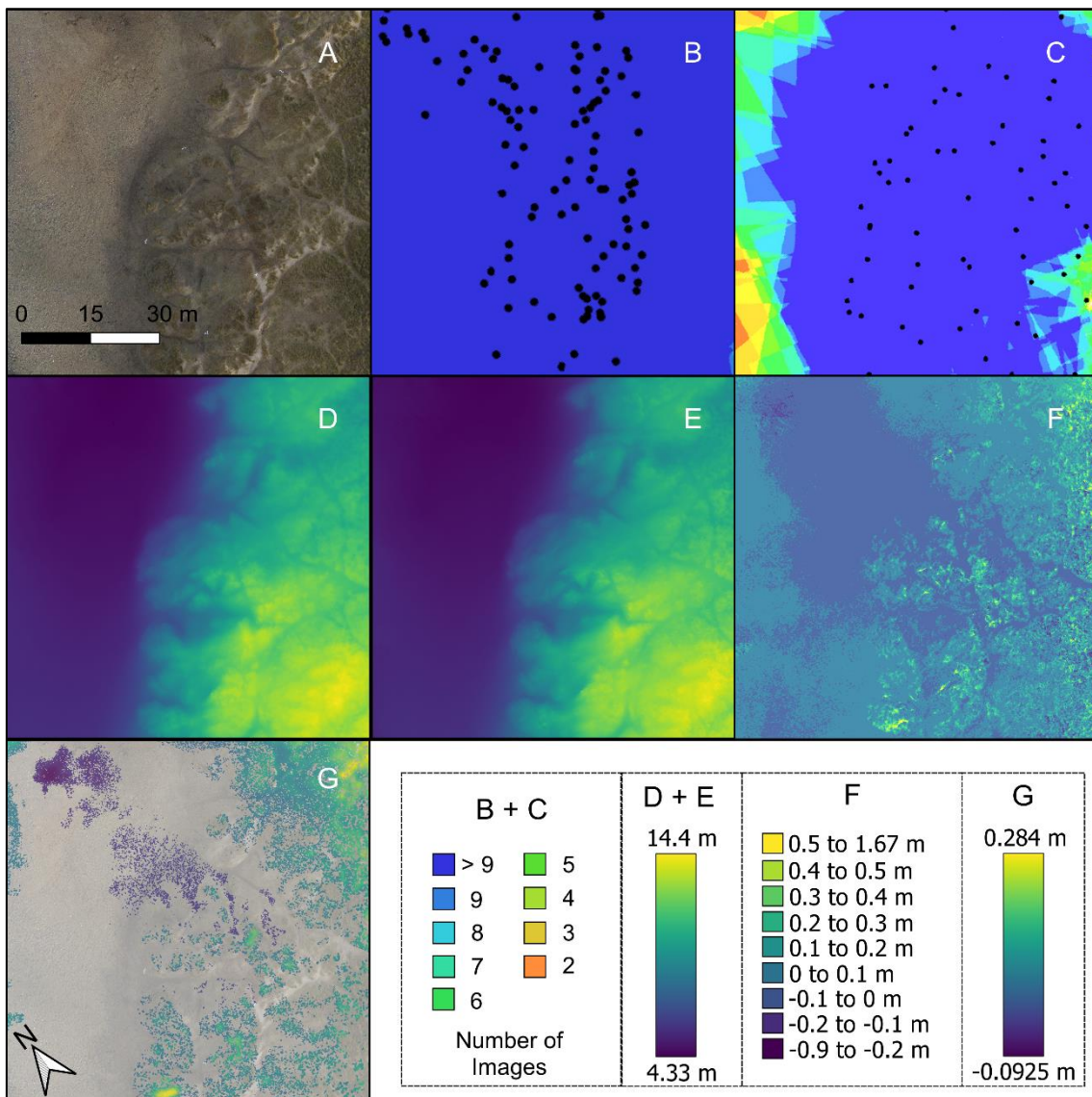


**Figure 6.6: Comparisons between KAP survey 6 and the drone survey** A) An orthomosaic created from images captured in KAP survey 6. B) Image overlap for the KAP survey (taken from Photoscan report). C) Image overlap for the drone survey (taken from Photoscan report). Black dots show estimated camera positions. D) Digital elevation model (DEM) for the KAP survey. E) DEM for the drone survey. F) A DEM of difference between the KAP and drone DEMs. G) Rasterised representation (spatial resolution of 0.1 m for display purposes) of significant results from M3C2-PM change analysis between point clouds created with data from KAP and drone surveys (overlaid on orthomosaic (at 50% transparency) from panel A). Non-significant change points are absent from G.

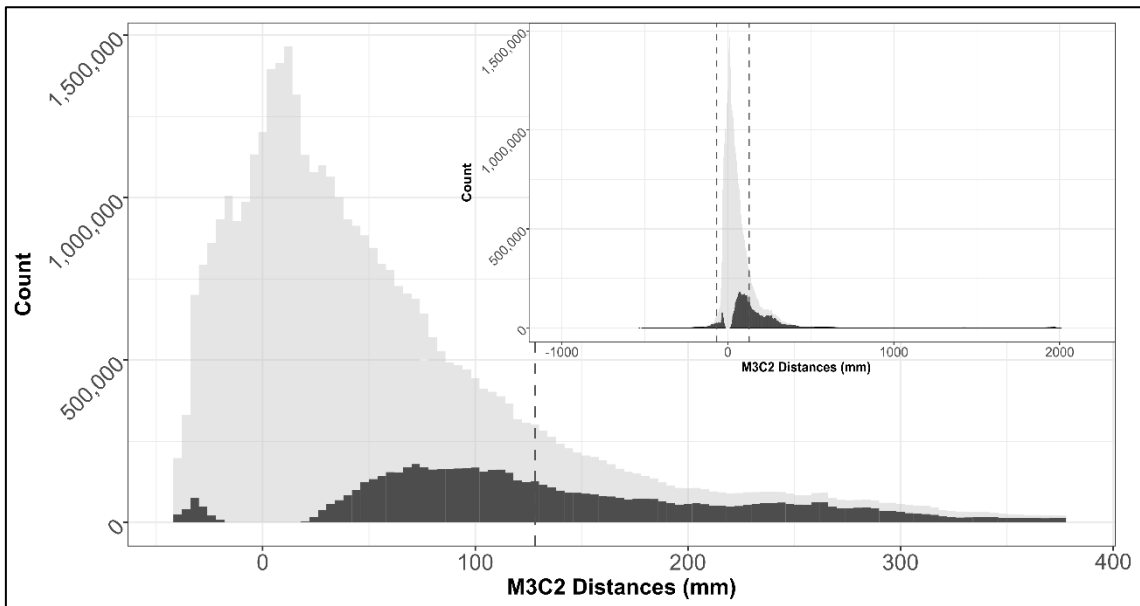


**Figure 6.7: Distribution of M3C2 distances between the kite survey and drone survey. Main figure shows data cropped to 5% and 95% quantiles with inset histogram showing all data. Points falling outside the common area between surveys have been removed, as they cannot be used in M3C2 analysis. Point cloud exported at native resolution of drone derived point cloud. Light grey shows all points in the change cloud and darker grey indicates significant changes in distance. Dashed lines indicate the positive (128 mm) and negative (-56 mm) median values of significant changes.**

**Table 6.2: M3C2-PM derived precision estimations for the points contained in the KAP versus drone subset area of interest (Figure 10.4).**

		Precision Estimates			Number of Points
		X (mm)	Y (mm)	Z (mm)	
<b>KAP</b>	<b>Minimum</b>	3.9	3.8	5.6	467784
	<b>Mean</b>	31.3	29.5	87.9	
	<b>Maximum</b>	11505	8013.5	12242.1	
<b>Drone</b>	<b>Minimum</b>	3.5	3.6	5	250787
	<b>Mean</b>	4.9	5	9	
	<b>Maximum</b>	317.7	851.5	1517.6	

#### 6.4.2 KAP Surveys

Considering all KAP surveys, the number of useable (e.g. non-blurry and without humans/animals) images collected in each survey varied from 374 (52% of the total collected during survey 6) to 774 (64% of the total collected during survey 2). Camera positions were calculated in Agisoft Photoscan, (rather than using the camera's internal GPS unit) providing estimated x and y positions alongside the altitude at which each image was captured. The mean altitude was 36.9 m with 5% and 95% quartiles showing as 19 m and 56.8 m respectively (**Figure 10.7**). The accuracy of the point clouds when compared to check points for validation varied between surveys. Four ground control points were withheld for validation in each survey dataset, to assist in understanding the total error in products produced by the SfM-MVS workflow (compared to the D-GNSS measurements). Root mean square error (RMSE) calculated across x, y and z dimensions for all check points for each survey show that error was higher in surveys 4 and 5 (39.7 and 44.0 mm) than the other four surveys (ranged 15.9 – 18.9 mm; **Table 8.2**). The higher RMSE in survey 4's check points was driven mainly by one point, especially in the z dimension (117.4 mm), whereas for survey 5, z dimension RMSE were higher for all points than seen in the other surveys (**Table 8.2**). Total RMSE calculated with error from all check points for all surveys was 19.7 mm in the horizontal (x/y), 39.4 mm in the vertical (z) and 27.9 across all (x/y/z) domains.

#### 6.4.3 Intra-annual variation

Three pairs of surveys (1 & 2 (pair 1), 2 & 3 (pair 2) and 3 & 4 (pair 3)) were undertaken approximately 3 months apart (**Table 6.1**). In all 3 pairs of surveys, the majority of significant change across the dune system was positive

(accretion), indicating elevational gain in the survey undertaken at the later date of the 2 in a pair. For all 3 surveys, more of the significant change was positive than negative (**Table 6.3**). Whilst most of the change in pairs 1 and 2 was between 0-500 mm, 40% points in pair 3 showed negative change (erosion) of between 0-500 mm (**Table 6.3**). Significant changes in elevation between surveys 1 & 2 were distributed across the whole area of interest whereas they were more concentrated in results from surveys 2 & 3 (**Figure 6.8**). There was far less significant change in pair 3 compared to pairs 1 and 2, with most of it negative and situated in areas of foredune. The mean positive change for each of the 3 month comparisons was pair 1: 121.8 mm, pair 2: 218.3 mm and pair 3: 197.7 mm.

Three pairs of surveys (1 & 3 (pair 1), 4 & 5 (pair 2) and 5 & 6 (pair 3)) were undertaken approximately 6 months apart (**Table 6.1**). Significant gain in sand dune elevation (accretion) was seen in the M3C2 results for pair 1, both in foredune areas and further inland (**Figure 6.8**). For pair 2, the north-eastern and south-western sides of the area of interest were concentrated areas of significant reduction in elevation, generally between 0-500 mm. For pair 3, elevational changes were almost exclusively positive and seen across the whole area of interest (**Figure 6.8**). Most of this change (97% of significantly changed points) was between 0-500 mm (**Table 6.3**). The mean significant positive change for pair 1 and pair 3 was 199.8 mm and 229.1 mm respectively. The mean negative change (erosion; as these were more numerous than positive changes) in survey pair 2 was -178.1 mm.

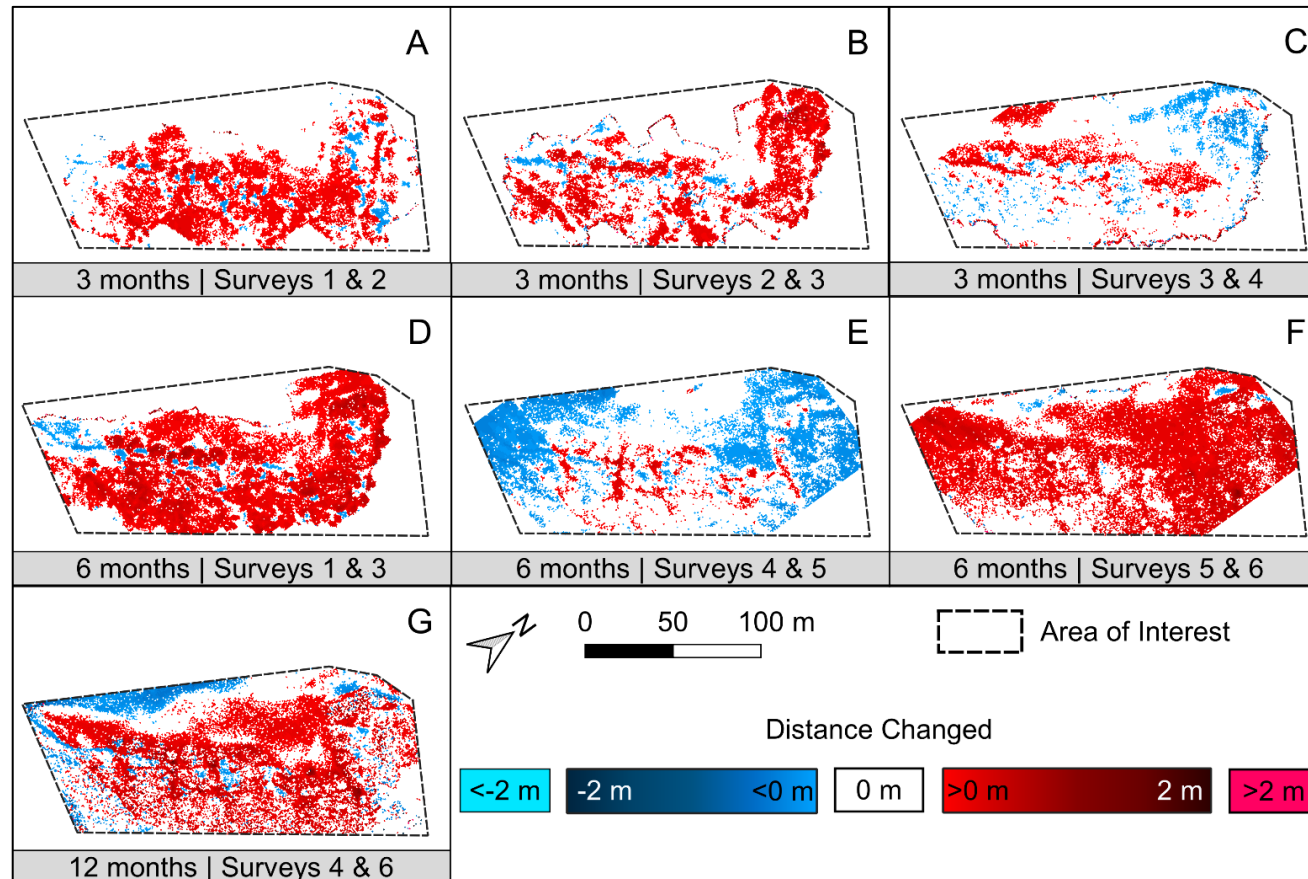


**Figure 6.8: Significant differences indicated by M3C2-PM comparisons between pairs of dense clouds. Changes were mostly between -2 and 2 m as indicated by the split colour ramps. Rasters were created from change clouds at a resolution of 0.75 m, with the mean of intersecting points in horizontal space assigned as the value in each cell, and cropped to the area of interest (Figure 6.1).**

**Table 6.3: Proportions of total number of significant points in M3C2-PM change rasters between pairs of surveys. Rasters were created from change clouds at a resolution of 0.75 m, with the mean of intersecting points in horizontal space assigned as the value in each cell.**

Change Period (months)	Survey Pair	M3C2 Distance (mm)								
		-7000 to -2000	-2000 to -1000	-1000 to -500	-500 to 0	0 to 500	500 to 1000	1000 to 2000	2000 to 7000	7000 to 15000
3	1 & 2	0.12	0.03	0.13	9.86	89.37	0.27	0.12	0.09	0
	2 & 3	0.2	0.26	0.29	10.52	84.57	2.19	1.23	0.69	0.01
	3 & 4	0.43	0.27	0.54	39.48	55.64	1.53	1.23	0.74	0.03
6	1 & 3	0.03	0.02	0.03	7.85	88.64	3.19	0.16	0.09	0
	4 & 5	0	0	0.12	81.6	18.25	0.03	0	0	0
	5 & 6	0.09	0.02	0.03	1.7	96.88	0.89	0.21	0.15	0.02
12	4 & 6	0.12	0.21	0.69	19.7	74.25	4.44	0.37	0.08	0.04

#### 6.4.4 Inter-annual variation

Surveys 4 and 6 were conducted in January of 2017 and 2018 respectively (**Table 6.1**) providing an opportunity to explore change over a period of 12 months. The majority of significant change in this period was positive (accretion), with nearly 74% of points in the change cloud in the 0-500 mm category (**Table 6.3**). Some negative change (erosion) was also detected, with approximately 20% of points showing elevation reduction of between 0 to -500 mm (**Table 6.3**). The majority of negative changes were on the seaward side of the area of interest, whereas positive changes were seen along the dune fronts and further back towards the more stabilised part of the ecosystem (**Figure 6.8**).

#### 6.4.5 Change within specific features

In order to further understand how specific components of the dune ecosystem changed in topography of time, beach, foredune and path areas were investigated on an inter-annual timescale. Of the three chosen features, points in beach areas experienced the lowest proportion of significant change compared to the total number of points sampled (42%). The majority of points in foredune and path environments changed significantly over 12 months, with 72% in foredunes and 83% on paths (**Figure 6.9**). Within beach features, significant change was exclusively positive with a mean of 130 mm change (**Figure 6.9**). For foredunes, the distribution was bimodal (median positive = 254 mm, median negative = -75 mm), although the majority of change was still positive (**Figure 6.9**). Change on footpaths was also bimodal (median positive = 388 mm, negative = -164 mm), but the distances (amount of change) were much greater than the other two features, with a range of -290 mm to 980 mm (**Figure 6.9**).

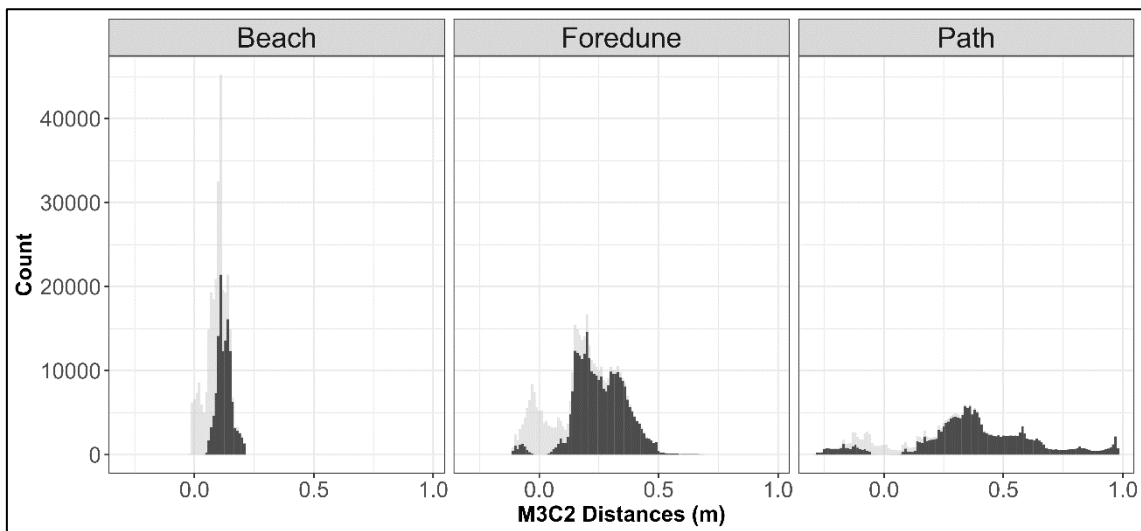


**Figure 6.9: Analysis of M3C2 change clouds for specific features within the study system. Change was calculated between surveys 4 and 6 (12 month timespan). Histograms show the distribution of all points (light grey) overlaid with the distribution of significant change points (dark grey) for each of the three features (beach, foredune, path) analysed.**

## 6.5 Discussion

Here we have described the novel coupling of KAP for data capture with M3C2-PM analysis to track fine spatial scale changes in a coastal dune environment. We also provide a direct comparison of point clouds created with data from a lightweight multirotor drone and a KAP setup. The experimental design applied here, employing M3C2 analysis has allowed for consideration of repeatability (KAP versus drone) on the same date, assuming a consistent measurand, and between-date reproducibility to be quantified and taken into account (intra- and inter-annual KAP surveys). We argue that this is particularly important when the survey methodology (KAP) is likely to be affected by differing conditions at the time of each survey (wind, kite height, angular acquisition properties) such that consistent survey grid designs (as could be delivered from a drone or other aerial platform) are not guaranteed. In the subsequent sections, we discuss the major

findings of the experiment and place these in the broader context of coastal monitoring using KAP based proximal sensing.

#### 6.5.1 Drone versus KAP survey

First, the assessment of the point cloud precision estimates (**Table 6.2**) showed that individual drone and KAP surveys captured on the same date exhibited precision estimates below 90 mm in all dimensions across both techniques. Precision estimates for the drone-derived point cloud were exceptionally small, and whilst the KAP precision estimates were greater they were still small at ~30 mm horizontally and 90 mm vertically. Even though the precision estimates of the KAP are higher (**Table 6.2**) the overall uncertainties are still small in magnitude. Comparing these results to one of the most commonly used methods for coastal topographic monitoring (airborne LiDAR), we have demonstrated that the KAP method can deliver orthomosaics with ~6 mm spatial resolution and point clouds with greater accuracy (x/y: 19.7 mm, z: 39.4 mm (see **Table 10.2**)). This exceeds the current typical capability of a the UK Environment Agency LiDAR system which generally have a spatial resolution of approximately 250 mm, and poorer z (150 mm) and x/y (400 mm) RMSE derived accuracy estimations (Environment Agency, 2016). Importantly, the level of precision shown in the KAP data is still suitable from a dune management point of view, where topographic change upwards of the decimeter scale is likely to be of interest.

Second, our results show that despite data collection at very similar periods of time (less than 60 minutes between flights), M3C2-PM analysis still highlighted topographical differences between the point clouds. On the more stabilised vegetated parts of the dune system, topography in the drone survey was more

elevated than data from the KAP survey. The predominant type of vegetation in this zone of the dune system is Marram grass, which is easily moved in windy conditions, most likely explaining differences seen in these areas. Negative differences between the drone and KAP point clouds (5% quantile -42 mm) were of a smaller magnitude than positive differences (95% quantile 380 mm) (**Figure 6.7**). Most of these points were located within the foredune and beach zones, which although had high estimated image overlap (>9; **Figure 6.6B & C**), the KAP survey contained more images in this area compared to the drone. The differences seen between the drone and the KAP survey also highlight the presence of methodological uncertainty in proximal sensing techniques. The position of the sensor when it captured images of the study system most likely drove this difference between the resultant point clouds. The drone survey was flown with a 'cross-hatch' pattern meaning that parallel lines 90 degrees from each other were used as a flight path, with the aim to increase the number of viewing angles of features on the ground, and the drone camera geometry was fixed at nadir. The kite survey was walked across the study system with a less control resulting in less evenly spaced camera positions than the drone survey (after image quality checks and subsequent removal) (**Figure 6.6B & C**). Furthermore, the design of the picavet mount meant that the sensor could swing, naturally providing varying viewing angles during data capture with the KAP system, whereas the drone provided a more level platform. We also acknowledge that lighting conditions would have varied between these two surveys, driven by both sun angle and the level of cloud at the time of survey (see also section 6.5.4). Despite these identified differences in methodology, there was a far greater proportion of cloud points that were not significantly different between the KAP and drone surveys (81%), compared to those that were (19%).

### 6.5.2 KAP surveys

The time-series analysis of intra- and inter-annual KAP survey data evidenced that the majority of change in the dune system, both positive and negative topographic change, was small in absolute magnitude (less than 500 mm accretion or erosion; **Table 6.3**). Furthermore, despite the measurement uncertainties, the M3C2 analysis showed that the KAP survey method was capable of measuring these changes since they were highlighted as being significant (i.e. exceeding the point-based uncertainty measures). Finally, the mixture of 3-, 6- and 12-month comparisons demonstrate how KAP can be used to monitor change in coastal systems over different timescales and at different times of year where pressures on the system may differ. For example, within the 3 month datasets, the period between pairs 1 and 2 was characterised by enhanced tourist activity, when visitor numbers, and thus, trampling pressures were higher. In contrast the inter-annual survey encompasses change from a multitude of sources throughout the season including weather events and human activity.

The variety in camera positions (in x,y,z) between the 6 KAP surveys resulted in irregular spatial extent in the point cloud, orthomosaics (**Figure 10.5**) and DEMs (**Figure 10.6**) produced from the SfM-MVS workflow. Given that the majority of the area of interest was covered in each survey, the irregularity in coverage found with the KAP survey method was not an issue for M3C2-PM analysis. Furthermore the M3C2-PM technique does not require the exact matching of data points in space to conduct change analysis between point clouds, and also provides more spatially heterogeneous error assessment compared to difference of DEM techniques (James et al., 2017b). The technique is therefore well suited

for survey-to-survey variable measurement uncertainty, such as comparing methodologies or multi-temporal change analysis as is presented in this study.

The presence of Marram grass and other dune vegetation likely drove the changes in elevation detected in stabilised parts of the dune system between pairs of surveys. For example, the difference between surveys 1&2 exhibited positive elevational changes in areas behind the foredunes, where Marram grass is present (**Figure 6.8 & Figure 10.5**). These surveys were conducted in March and June 2016, a period of Spring to Summer transition where vegetation in the dune environment 'greens up'. In this experiment we used only a RGB sensor so vegetation metrics (e.g. normalised difference vegetation index (NDVI)) could not be determined. However, we suggest that including infra-red based vegetation index data such as NDVI could be used to further enhance the M3C2-PM analysis by separating vegetation from bare sand areas to improve identification of the more dynamic parts of the dune environment, as has been shown by (Nolet et al., 2018).

### 6.5.3 KAP as a tool for coastal monitoring

Conducting proximal sensing topographic surveys in coastal dune environments is not a trivial task. First, with reference to the positioning of GCPs, there are very few static features that can be utilised as known points in space between surveys. In this case we managed to measure the positioning of two fixed features (concrete base and an entrance stone). Leaving GCPs for more than half a day was not a feasible option due to the risk of human interference. For one survey presented in this study, one GCP was removed by a member of the public only hours after being placed. However, the financial gains (compared to other coastal

monitoring techniques) and fine temporal resolution offered with proximal sensing make this a valuable tool for monitoring the coastal environment (Gonçalves and Henriques, 2015).

The windy conditions found at the coast (**Figure 6.2**) make KAP a useful alternative proximal sensing technique when compared to drones (which are more difficult to operate in windy conditions). Their ease-of-use, low-cost (Conlin et al., 2018) and less strict regulation surrounding their use make the technique a democratic and appropriate technology (Duffy and Anderson, 2016). When collecting data for an SfM-MVS workflow, we have shown that KAP can be an advantageous platform for optical sensors due to the variation in camera position created by movement of the kite, shown by the larger precision estimations calculated in the Monte Carlo processing stage (**Table 6.2**). This in turn offers oblique viewing angles of features on the ground which helps reproduce steep sided features (such as those found in dunes) which may be absent in nadir images, especially when the features are orthogonal to the sensors orientation. Furthermore oblique imagery reduces the doming effect sometimes visible in SfM-MVS data products (James and Robson, 2014).

#### 6.5.4 Other sources of uncertainty

As we stated at the beginning of the discussion, the method followed allowed us to consider various sources of measurement uncertainty, both within (i.e. precision/repeatability; **Table 6.2**) and between surveys (i.e. reproducibility (e.g. **Figure 6.8 & Table 6.3**), and with reference to independent checkpoints surveyed with a D-GNSS (**Table 10.2**). The M3C2-PM technique takes into account sources of calibration (e.g. internal camera sensor calibration), equipment

(specific camera performance) and method (e.g. accuracy of GCP locations) uncertainty relating to the collection and processing of SfM-MVS data and propagates these through the analysis. However, other sources should also be considered including operator and environment related uncertainties. Here the same operator (author JPD) conducted all surveys and so we cannot quantify this within our experiment, but we suggest that it would be important to consider if multiple kite operators were used. This may be particularly pertinent in the event that KAP surveys were used as a crowdsourcing data collection effort. Uncertainties related to the environmental conditions under which the measurements were collected can manifest as differences in i) sky illumination (potentially explaining differences between the KAP and drone survey in this study), ii) reflectance of wet/dry surfaces relating to weather conditions prior to and during the survey, iii) wind conditions affecting the position of vegetation, and iv) the presence of aerosols (airborne sand or salt particles). We argue that these scene- and site-dependent environmentally-driven uncertainties will have been captured to some extent within the large dataset analysed and so are likely accounted for within the M3C2-PM results. Disaggregating their individual impacts is impossible without undertaking a series of separate experiments where those parameters are varied individually, and the impacts quantified. This lies outside of the scope of our work but could form the basis of a series of interesting follow-up studies.

## 6.6 Conclusions

It is in the interest of coastal communities and populations in general to maintain high quality sand dune systems, especially in vulnerable coastal environments. Dunes and their associated vegetation communities can help form part of a

realistic and sustainable coastal protection system (Feagin et al., 2015). The impacts of disturbances in dune systems such as trampling until now have focused largely on the changes in plant communities (Santoro et al., 2012), but less on changes to dune structure. Given that trampling can lead to the destabilization of dune systems (Barbier et al., 2011), there is a need to monitor change in topography over time. Sand dunes are highly dynamic and change rapidly over time, and thus a flexible method that allows for data capture at user-dictated times makes KAP a well-suited method for dune monitoring efforts. Furthermore, the technique presented in this study can be readily deployed by others to monitor changes in dune topography in relation to anthropogenic disturbance events alongside the monitoring of natural change over time. From a management point of view, one could perform KAP surveys before and after interventions such as fencing or signposting to understand their effectiveness in preserving environmental integrity. This approach lends itself to the implementation of proactive rather than reactive interventions, allowing managers to monitor coastal environments at temporal scales tailored to their specific needs. Our approach also shows that specific areas (i.e. foredune) can be specifically analysed to aid in the understanding of change in specific parts of dune systems. This work develops that of (Autret et al., 2018; Bryson et al., 2016; Seymour et al., 2018; Westoby et al., 2018) but takes a more robust quantitative approach to multi-temporal monitoring by accounting for many forms of uncertainty with the M3C2-PM methodology.

Beyond monitoring natural dynamic coastal environments, the technique could also be used to monitor movement and/or damage to structures such as jetties, rock defences, sea walls and other property. For example, the effects of storm

damage to sea walls could be detected immediately post storm in a cost-effective manner that doesn't require airborne LiDAR or TLS capabilities, in turn reducing the cost of surveying. KAP is a low-cost, self-service, highly-portable technique that has lower barriers to entry than other proximal sensing techniques (e.g. drone technology). When applied at relevant spatial and temporal scales KAP is a powerful data capture method well suited for monitoring coastal environments.

## 6.7 Acknowledgements

We would like to thank Colin Anderson, Jonathan Crocker, Ned Crowley, Sarah Crowley, Joel Forsmoo, Cecily Goodwin, Darren Jones, Nicole Parr, and Polly Shutler for their assistance with data collection. Also, thank you to Cornwall Council for allowing us to conduct research on the St Gothian Sands Local Nature Reserve. We are grateful to Mike James (Lancaster University) for his guidance with data processing and analysis and Peter Land (Plymouth Marine Laboratory) for constructive comments on the manuscript. We also thank three anonymous reviewers and the editor for their constructive comments which have improved the manuscript.

## 7 Seagrass meadow spatial variability

### *Intertidal seagrass meadows, Pembrokeshire, UK*



This paper was published in *Estuarine, Coastal and Shelf Science* in 2018:

Duffy, J.P., Pratt, L., Anderson, K., Land, P.E. & Shutler, J.D. (2018) Spatial assessment of intertidal seagrass meadows using optical imaging systems and a lightweight drone. *Estuarine Coastal and Shelf Science*, 200, 169-180.

## **Spatial assessment of intertidal seagrass meadows using optical imaging systems and a lightweight drone**

James P. Duffy<sup>1\*</sup>, Laura Pratt<sup>2,3</sup>, Karen Anderson<sup>1</sup>, Peter E. Land<sup>4</sup>, & Jamie D. Shutler<sup>5</sup>

1. Environment and Sustainability Institute, University of Exeter, Penryn Campus, Penryn, Cornwall, TR10 9FE, UK

2. Project Seagrass, Sustainable Places Research Institute, Cardiff University, Cardiff, CF10 3BA, UK

3. School of Biosciences, Cardiff University, The Sir Martin Evans Building, Museum Avenue, Cardiff, CF10 3AX, UK

4. Plymouth Marine Laboratory, Prospect Place, The Hoe, Plymouth, PL1 3DH, UK

5. Centre for Geography, Environment and Society, University of Exeter, Penryn Campus, Penryn, Cornwall, TR10 9FE, UK

*\*Corresponding author*

### **7.1 Abstract**

Seagrass ecosystems are highly sensitive to environmental change. They are also in global decline and under threat from a variety of anthropogenic factors. There is now an urgency to establish robust monitoring methodologies so that changes in seagrass abundance and distribution in these sensitive coastal environments can be understood. Typical monitoring approaches have included remote sensing from satellites and airborne platforms, ground based ecological

surveys and snorkel/scuba surveys. These techniques can suffer from temporal and spatial inconsistency or are very localised making it hard to assess seagrass meadows in a structured manner. Here we present a novel technique using a lightweight (sub 7 kg) drone and consumer grade cameras to produce very high spatial resolution ( $\sim 4$  mm pixel<sup>-1</sup>) mosaics of two intertidal sites in Wales, UK. We present a full data collection methodology followed by a selection of classification techniques to produce coverage estimates at each site. We trialled three classification approaches of varying complexity to investigate and illustrate the differing performance and capabilities of each. Our results show that unsupervised classifications perform better than object-based methods in classifying seagrass cover. We also found that the more sparsely vegetated of the two meadows studied was more accurately classified - it had lower root mean squared deviation (RMSD) between observed and classified coverage (9 to 9.5 %) compared to a more densely vegetated meadow (RMSD 16 to 22 %). Furthermore, we examine the potential to detect other biotic features, finding that lugworm mounds can be detected visually at coarser resolutions such as 43 mm pixel<sup>-1</sup>, whereas smaller features such as cockle shells within seagrass require finer grained data ( $< 17$  mm pixel<sup>-1</sup>).

## 7.2 Introduction

Seagrass ecosystems have a global distribution, and they play an integral role in delivering multiple ecosystem services to coastal regions (Barbier et al., 2011; Orth et al., 2006), including the provision of nursery ground for commercial fish species (Beaumont et al., 2008; Bertelli and Unsworth, 2014), sediment stabilization (McGlathery et al., 2012), pathogen reduction in coastal waters (Lamb et al., 2017) and carbon sequestration (Fourqurean et al., 2012; Macreadie

et al., 2014). Despite their evident ecological importance, seagrass ecosystems have been in decline for three decades (Waycott et al., 2009), with one in five seagrass-habitat associated species at some risk of extinction according to International Union for the Conservation of Nature (IUCN) categorisation (Short et al., 2011). With threats such as human disturbance (e.g. mechanical damage and release of toxic compounds (Short and Wyllie-Echeverria, 1996)), changes in water quality (Duarte, 2002) and warming of seas (Marbà and Duarte, 2010) likely causing such declines, there is a clear need to develop methods to monitor the extent and health of seagrass meadows.

Monitoring efforts to date have been conducted using a range of *in situ* approaches, including scuba/snorkelling surveys (Gotceitas et al., 1997), ground-based sampling (Moore et al., 2000), and hovercraft-based mapping (Mckenzie, 2003). Active and passive remote sensing approaches are also used frequently to estimate the coverage and quality of seagrass habitats. Using active acoustic remote sensing methods such as side scan sonar, it has been shown to be possible to quantify the coverage of seagrass meadows (Barrell et al., 2015; Hossain et al., 2014), whilst passive spectral sensors on-board platforms such as satellites or light aircraft have proven useful for quantifying seagrass meadow dynamics (e.g. Baumstark et al., 2016 and Cunha et al., 2005). For example, using freely available multi-spectral Landsat data (with a spatial resolution of ~30 m per pixel), changes in seagrass meadow extent have been charted (Knudby et al., 2010), and so have fluctuations in biomass (Misbari and Hashim, 2016). Finer spatial resolution optical and infra-red satellite data from systems such as IKONOS and Quickbird (with a spatial resolution finer than 4 m) have also generated useful biomass estimates for multiple seagrass species (Lyons et al.,

2015; Roelfsema et al., 2014). Beyond the commonly used four-band spectral approach (blue, green, red, infra-red), multi-spectral data with 16 spectral bands have been captured from airborne sensors and used to estimate seagrass coverage, biomass and species composition (Phinn et al., 2008). The limit of many such remote sensing techniques is the spatial resolution, which restricts the focus of studies to identification and mapping of seagrass areal extent only: even in fine spatial resolution satellite data, individual seagrass plants or shoots cannot be resolved. Additionally, the ability to detect features such as seagrass from satellite observations is frequently affected by cloud cover and variable tide states (Stekoll et al., 2006), limiting the utility and applicability of such data for time-series investigations. Furthermore, the inability of satellite measurements to capture the fine spatial patterns in the distribution of plants and biomass within seagrass meadows, particularly in sparsely vegetated areas (Valle et al., 2015), means that current scientific understanding of seasonal growth patterns and the causes of meadow decline is highly uncertain.

The recent rapid growth in deployment of lightweight low-cost drone technology has been mooted as a revolutionary addition to the toolkit of ecological and environmental researchers (Anderson and Gaston, 2013). Drones offer a low-flying platform from which fine-grained (sub-decimetres spatial resolution) remote sensing observations can be captured, and such approaches are already being used widely in fields such as hydrology (DeBell et al., 2016), forestry science (Inoue et al., 2014), polar studies (Ryan et al., 2015) and wildlife monitoring (Chabot et al., 2015; Hodgson et al., 2013). The flexibility of the lightweight drone platform, both in deployment capabilities and customization (i.e. payload options) has led to their utilisation in coastal environments including studies monitoring

beach and dune topography (Gonçalves and Henriques, 2015), classifying habitats used as nurseries for fish (including seagrass) (Ventura et al., 2016) and mapping coral reefs (Chirayath and Earle, 2016). Additionally, the self-service nature of data collection and the ability to replicate data collection with the aid of GPS navigation, make drones very useful tools for monitoring dynamic environments such as the intertidal zone. In environments such as this, other remote sensing technologies, such as low spatial resolution satellite sensors, find retrievals challenging. Reasons for this may include a large temporal gap between image acquisitions, fixed orbit patterns causing data capture at different tidal states and therefore differing effects from the water column, presence of sun glint (Kay et al., 2009), mixed pixels (Suominen and Tolvanen, 2016) and land-sea adjacency issues (Sterckx et al., 2011).

Given the extensive loss of seagrass in the British Isles in recent years (Jones and Unsworth, 2016), developing new and scale-appropriate methods for quantifying and monitoring changes in this ecosystem should improve the way that drivers of change are understood, and allow for improved management. The work presented herein uses a lightweight drone fitted with consumer grade cameras to capture aerial data of intertidal seagrass (*Zostera noltii*) meadows at low tide. We explicitly sought to address the following research questions:

- i) Can a consumer grade camera and lightweight drone be used to collect proximal remote observations of intertidal seagrass meadows?
- ii) How effective are different image classification techniques for mapping the distribution of intertidal *Zostera noltii* meadows?

iii) How accurate are *Zostera noltii* coverage estimates derived from drone-based photographic data?

iv) Are other biotic features (e.g. gastropod shells and lugworm mounds) detectable in the image data?

The study utilised two intertidal seagrass meadow sites with differing plant density to test a further question:

v) To what extent can the drone-based methodology capture differences in plant density using a standardised survey protocol?

In this manuscript, we demonstrate a full workflow including data capture, processing and some example classification schemes, and combine this information to obtain meadow coverage estimates at two intertidal seagrass meadow sites in Wales, UK.

## 7.3 Methods

### 7.3.1 Study species: *Zostera noltii*

*Zostera noltii* (commonly known as dwarf eelgrass) has an extensive distribution, and it is found throughout the British Isles, parts of Scandinavia, the western Mediterranean, parts of west and north Africa and in the Black Sea (Pergent-Martini et al., 2015). Although assigned a status of 'Least Concern' on the IUCN red list, the overall population status is assumed to be declining (Short et al., 2010). Furthermore, apart from reports of meadow expansion in Wales (Bertelli et al., 2018), local declines in Europe have been observed in recent decades,

e.g. in France (Bernard et al., 2007), the Wadden Sea (Philippart and Dijkema, 1995), Spain (Hernandez et al., 1997) and Portugal (Martins et al., 2005).

Like many seagrass species, *Z. noltii* grows in an ecological niche, requiring specific environmental conditions (e.g. substrate slope and grain size Valle et al., 2011) to successfully grow and survive. It is easily disrupted by changes in water quality and light attenuation in the water column. Multiple studies have found that sediment input into *Zostera noltii* habitat has detrimental effects on shoot density and ultimately survival, both *in-situ* (Han et al., 2012) and in a laboratory setting (Cabaço et al., 2007).

### 7.3.2 Study sites

The research was focused on two sites in Pembrokeshire in Wales, the United Kingdom (**Figure 7.1**) both of which have *Zostera noltii* meadows. One of the meadows is located in Angle Bay (51°40'50.42"N; 5°02'35.10"W) and the other at Garron Pill (51°44'05.80"N; 4°52'55.39"W). Angle Bay is an extensive intertidal habitat covering approximately 2 km<sup>2</sup> at low tide. *Zostera noltii* grows in the majority of this area and was particularly dense at the time of data collection (mean percentage cover of quadrats was 54% in July 2016). The sediment at the site is relatively firm and therefore accessible (although not easily so) on foot at low tide. Garron Pill is a more sheltered site located further upstream along the Pembroke River. It is one of several tidal inlets in the area, and when drained at low tide reveals an intertidal habitat of approximately 0.5 km<sup>2</sup>. Seagrass was less dense at this site (mean percentage cover of quadrats was 17.6%) There is also a mixture of macroalgae-dominated, and salt marsh habitats at this site. The sediment is much less stable than at Angle Bay, and therefore only small sections

of the site were accessible on foot. One plot (of approximately 50 m<sup>2</sup> in size) was surveyed at each site (Angle Bay and Garron Pill).

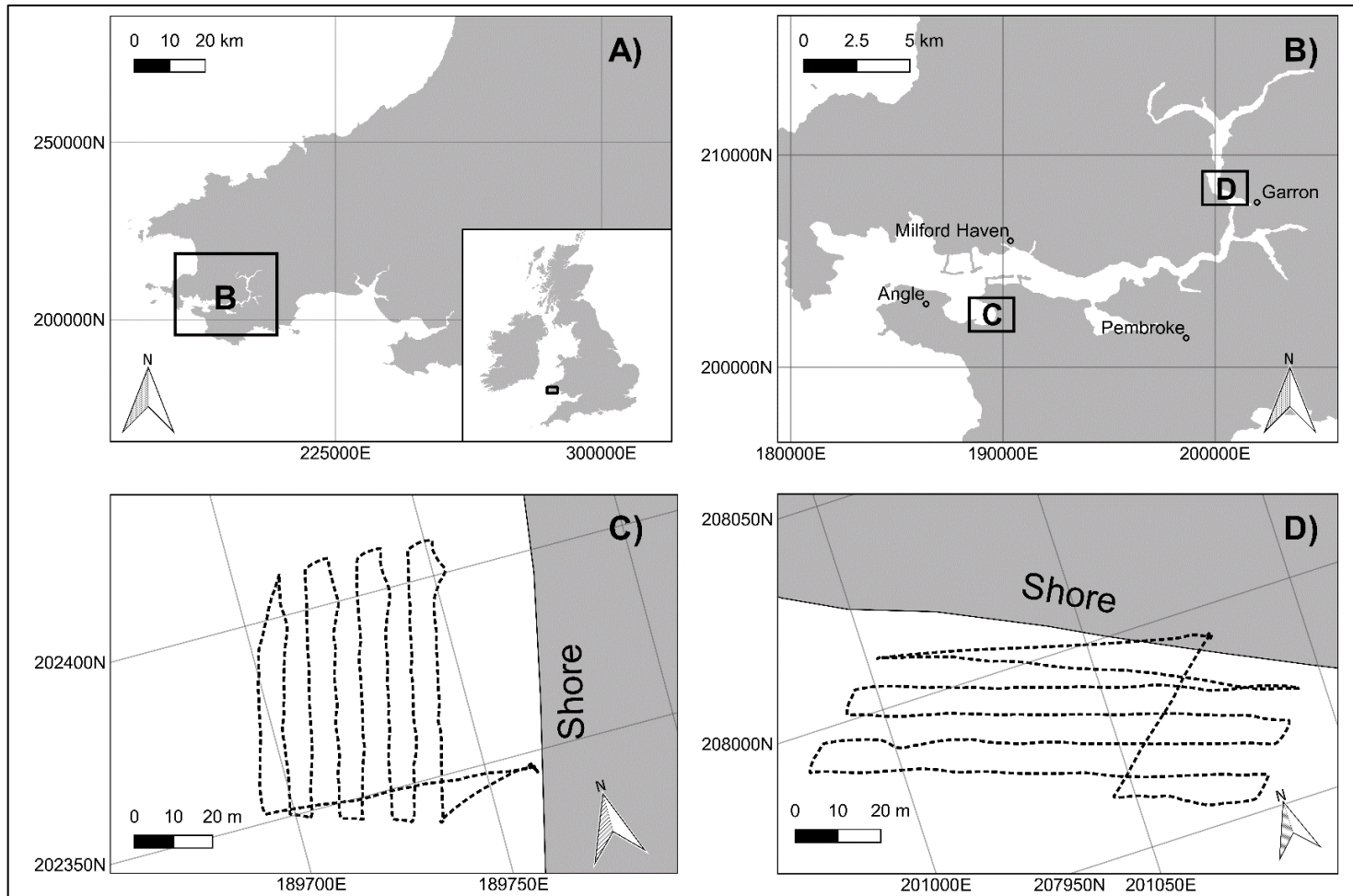


**Figure 7.1: The location of the study sites within the context of west Wales, UK A) and Pembrokeshire B). Flight paths are shown with dashed lines for Angle Bay C) and Garron Pill D).**

### 7.3.3 Drone & sensor equipment

A 3D Robotics Solo (<https://3dr.com/>) multi-rotor drone was used with a custom designed vibration-dampened 3D-printed sensor mount (by the author JPD) (<http://www.thingiverse.com/thing:1964056>). The mount allowed for the attachment of a nadir-viewing Ricoh GR II compact digital camera that captures images with 16.2 effective megapixels and encompasses a complementary metal-oxide semiconductor (CMOS) sensor and prime lens with a fixed focal length of 28 mm. It can capture images in both uncompressed (RAW) and lossy (JPEG) formats, and also includes a built-in intervalometer. This allows the shutter to capture images at given time intervals, which is useful for data capture from autonomous vehicles such as lightweight drones. Camera specifications can be found in **Table 10.3**. In combination with flight planning software, ideal intervals can be calculated based on the sensors field of view, altitude and flight speed, allowing optimal image overlap to be determined, thus permitting production of good quality orthomosaics and digital terrain models (Dandois et al., 2015).

Arducopter firmware (APM:Copter solo-2.0.20) running on the Pixhawk 2 autopilot system located inside the drone allows for waypoint-guided flights. Control over position (in all three dimensions) and speed of the vehicle allow for structured surveying with user-dictated overlaps in the image data given the altitude of the drone and the field of view of the sensor. Flight missions (i.e. way point guided flight paths) were designed in Mission Planner (Osborne, 2016) and in the field, flights were conducted using the Android application Tower (Huya-Kouadio, 2016).

At both sites, two flights were conducted at 15 m altitude and a speed of 2 ms<sup>-1</sup> (**Figure 7.1C & D**). This altitude gave a ground sampling distance of ~4 mm when using the Ricoh GR II sensor (see **Table 10.3**). The speed and altitude combinations provided sufficient overlap (~70% frontlap and ~70% sidelap) between each image so that image matching and mosaicking was optimised. Further details of the mosaicking process can be found in section 2.5: Processing and Analysis. At Angle Bay, the data collection flight was undertaken at 16:30 GMT on 21/07/2016. Weather conditions were dry, with windspeeds averaging 4.5 ms<sup>-1</sup>, light cloud cover and intermittent sunshine. At Garron Pill, the flight was conducted at 14:00 GMT on 23/07/2016. Weather conditions were dry with windspeeds averaging 7.5 ms<sup>-1</sup>, and it was generally overcast. An additional two flights at 50 m altitude were undertaken at Garron Pill with an AgroCam RGB sensor (ground sampling distance of ~14 mm; **Table 10.3**), with the aim of capturing data to identify meadow boundaries. More details about these flights can be found in section 10.4.3.

#### 7.3.4 Ground based surveys

Quadrat sampling was used to collect *in-situ* information about the seagrass meadows so that drone-based observations could be validated (**Figure 7.2**). Twenty-seven 500 mm × 500 mm quadrats were randomly placed in each of the two ~50 m<sup>2</sup> plots. The following observations were recorded for each quadrat by the author (LP) trained in conducting the standard Seagrass-Watch protocols (Mckenzie et al., 2001): estimated percentage cover, shoot lengths and densities, estimated number of gastropods and algal/epiphytic cover. We acknowledge that these estimations have their own inherent uncertainties, but for the purpose of

this study assume they are truth in order to evaluate the image classification procedures presented.

Given the very high spatial resolution data capture capabilities of the camera payload on board the drone, high precision ground-truth data were required so as to georectify resulting orthomosaics and accurately locate quadrat sampling areas and features of interest within the study sites (Cunliffe et al., 2016). The position of all four quadrat corners were recorded with approximately 10 mm accuracy in  $x,y,z$  dimensions using a differential Global Navigation Satellite System (D-GNSS) Leica GS-08 plus survey system (comprising a base and rover). To assist with the mosaicking process, chequered targets (300 × 300 mm in size) were used as ground control points, placed at ~25 m intervals around the perimeter of the ~50 m<sup>2</sup> study areas (**Figure 7.3C**). To secure them in the soft substrate, two metal pegs were used on opposite corners. A laminated A4 sheet with a unique letter of the alphabet was pegged next to each target to assist in identification within the aerial photographs. Due to the shape of the plots at each site, 8 ground control points were used at Angle Bay, and 10 at Garron Pill. The central points of these black and white targets were recorded as the exact ground control points using the Leica GS-08 plus survey system.

#### 7.3.5 Processing & analysis

Photogrammetric workflows have emerged as the most popular way to collate and stitch aerial photographic image data into georectified orthomosaics (Gross and Heumann, 2016; Smith et al., 2015). For this study, Agisoft Photoscan (v 1.2.5) (Agisoft LLC, 2016) was used to generate orthomosaic models from the aerial data collected, using the positions of the ground control markers to optimize

camera positions during the point cloud formation stage. They were also used to orientate and georeference the data.

The very high spatial resolution and spectral complexity of the data makes classification challenging, because of the “H resolution” problem as defined by Strahler et al. (1986). Coupled with the multitude of techniques developed for analysing and classifying cover types using optical remote sensing data, an aim of this paper was to explore three methods with differing complexity for image-based classification. In turn, we demonstrate the potential use and application of these drone-based optical imaging data for seagrass meadow assessment.

The varying complexities in the three techniques used in this study give an overview of approaches commonly used in remote sensing analyses. First, we explored the use of a basic unsupervised optical classification, which is the simplest of approaches. Using only the red, green and blue spectral bands from the camera, we show what can be achieved with minimal processing of the data once it has been stitched via photogrammetry workflow. Building on this, we explored the effect of adding optical texture layers to the unsupervised classification workflow. This process shows that more information can be derived (than just the red, green and blue bands) from data captured with consumer grade cameras, that can in turn potentially help discriminate seagrass from its surrounding environment. Third, object-based techniques are increasingly applied to segment and classify very fine spatial resolution data. This is because objects of interest are constructed of multiple pixels as opposed to the representation of multiple objects within a single pixel (Myint et al., 2011), as is the case with coarser spatial resolution data. Given the fine spatial resolution of our data, we applied object based image analysis (OBIA) as a third classification

approach (containing a 'supervised' stage) to determine whether this could be used to meaningfully improve the quality of the seagrass mapping products. We purposefully did not try to use a pixel-based supervised classifier to produce the mapping products because this would rely on the identification of individual 'pure' pixels containing either seagrass or bare substrate. Due to the data having a spatial resolution of less than 1 cm per pixel, we considered it a more robust approach to test a supervised classification that first used a segmentation algorithm to automate the identification of clusters of pixels that had similar spectral properties. A schematic describing data collection, processing and analysis is shown in **Figure 7.2**. The classifications used are described in the following sections.

#### 7.3.6 Unsupervised classification with optical bands

The first type of classification performed incorporated the red, green and blue (RGB) spectral bands. An unsupervised approach using K-means (Hartigan-Wong algorithm; Hartigan and Wong, 1979) clustering was performed using the ``unsuperClass`` function in the ``RStoolbox`` (Leutner and Horning, 2016) package in R (R Core Team, 2016a). Maps with two, three, four and five discrete classes were produced for each site. These classes represented seagrass and non-seagrass cover types (e.g. substrate and macroalgae). Where more than two classes were used, they were combined to create a binary result. Next, the areas coinciding with quadrat placement were extracted, and pixel counts recorded. Every possible combination of the discrete classes was tested, and that with the lowest RMSD score when comparing classified and observed seagrass coverage was then chosen as the best candidate classifier for each site.

### 7.3.7 Unsupervised classification with optical bands and texture

Further to the spectral data alone, textural bands were also added to the classification process. Image texture can be used to describe patterns in images that are naturally identified and interpreted by humans but more difficult for computers to understand. Given that the dominant colour of seagrass is green, texture layers were calculated for this band only. Textural layers were calculated using moving windows on spectral data (Haralick et al., 1973). Grey level co-occurrence matrices were calculated for each orthomosaic using the ``gldm`` (Zvoleff, 2016) package in R (R Core Team, 2016a) with a window size of  $3 \times 3$  pixels. From these matrices, eight different measures were calculated (mean, variance, homogeneity, contrast, dissimilarity, entropy, second moment and correlation). Next, every possible combination of these layers were combined with the RGB layers, and two, three, four and five class unsupervised classifications (as described in section 7.3.6) were performed. The same selection procedure to find the combination with the lowest RMSD was followed as was performed with optical bands.

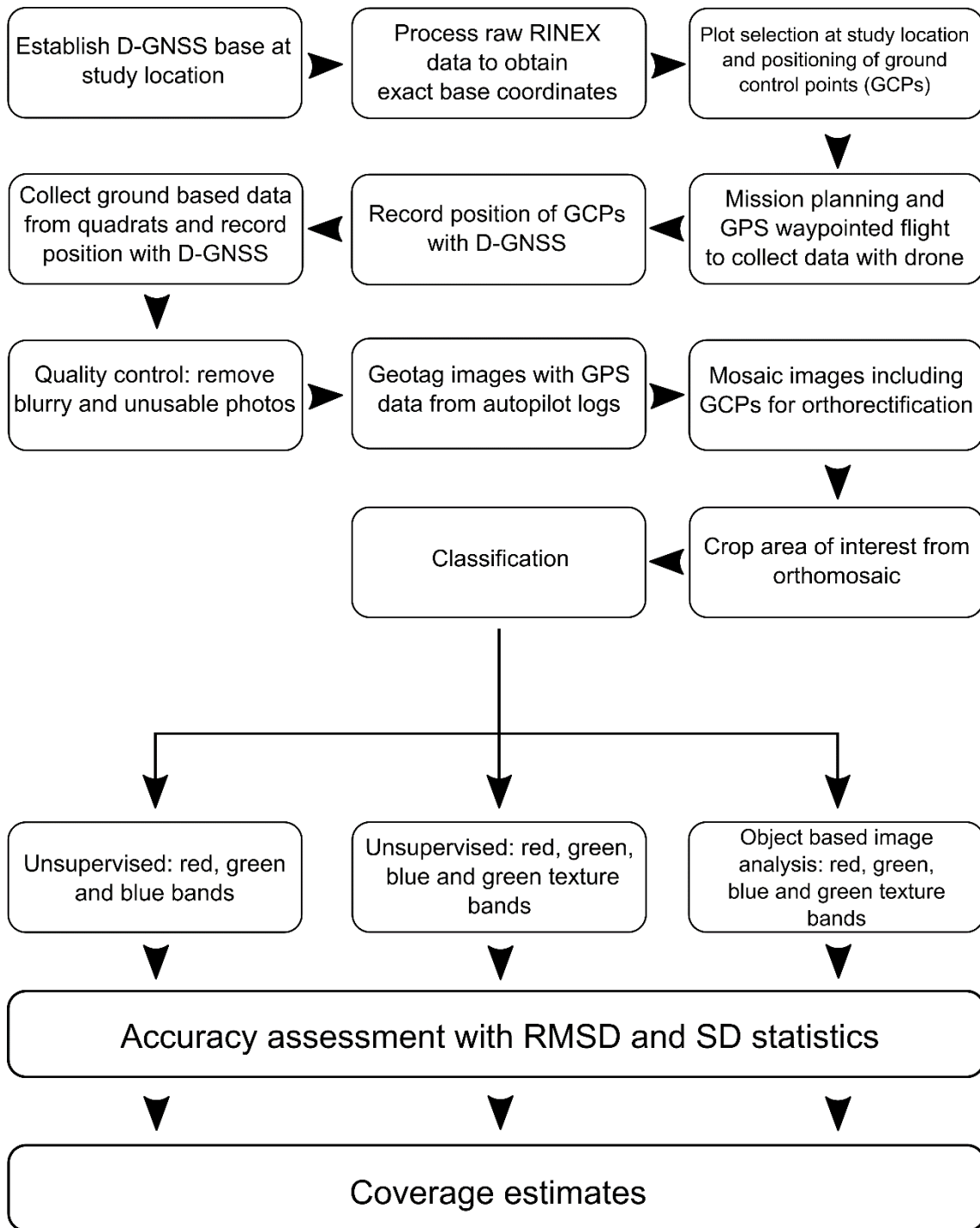


**Figure 7.2: Data collection, processing and analysis workflow.**

### 7.3.8 Segmentation & support vector machine classification

The third classification approach used the method of OBIA. This technique has seen increasing usage in the analysis of remote sensing data (Blaschke, 2010). A typical OBIA workflow involves firstly image segmentation and secondly classification of the segmented data (Myint et al., 2011). In order to keep the analysis of these data as open-source and replicable as possible, the ``i.segment.uspo``, ``i.segment`` and ``i.segment.stats`` and ``v.class.mlR`` functions were used in the Geographic Resources Analysis Support System (GRASS) 7.0 (GRASS Development Team, 2015) software package. Both the optical and optimum texture layers were used in these classifications. Each orthomosaic was segmented and classified with supervised training data (subset from the segmented data). Given the knowledge obtained from visual inspection of the mosaics, a two-class classification (seagrass and substrate) was applied to data from Angle Bay and five-class (seagrass, substrate, macroalgae species 1, macroalgae species 2, rock) classification for Garron Pill. More detailed information on the OBIA procedures used can be found in the supplementary information (section 10.4.1).

### 7.3.9 Analysis of classified maps

All analysis of classified maps and graphing of data took place in the statistical package R 3.3.1 (R Core Team, 2016a). Data manipulation and analysis were conducted using the `dplyr` (Wickham and Francois, 2016), `raster` (Hijmans, 2015) and `tidyr` (Wickham, 2017) packages. Graphs were created using `ggplot2` (Wickham, 2009) and `gridExtra` (Auguie, 2016).

Coverage within each quadrat was estimated by cropping the mosaic to the area defined by the D-GNSS system for each quadrat. The pixels in the cropped image were then counted and a coverage estimate derived by dividing the number of pixels classed as seagrass by the total number of pixels. This was repeated for each quadrat.

Bootstrapping was used to explore the variation between estimated and observed coverage within quadrats at both sites. This enabled the investigation of classification performance by describing over- or under- estimation of seagrass coverage. Firstly, the difference between estimated and observed percent coverage was calculated for each of the 27 quadrats. Then, a random selection ( $n=27$ ) of these differences was selected (with replacement enabled, meaning quadrats could be chosen more than once in each iteration) and the mean and standard deviation calculated from the selection. These statistics were stored and the process was then repeated for 1000 iterations, resulting in a selection of 1000 sets of mean, standard deviation and iteration standard error (equal to standard deviation divided by  $\sqrt{27}$ ) per site. From these, three overall statistics were calculated: the mean and standard deviation of the 27 measured differences, and the overall standard error as the standard deviation of iteration means. The combined uncertainty was then calculated both for each iteration and in total with the following equation:

$$uncertainty = \sqrt{m^2 + \sigma^2 + se^2} \quad (1)$$

where  $m$  is the mean,  $\sigma$  is the standard deviation and  $se$  is the standard error.

### 7.3.10 Feature detection

To test the effect of the spatial resolution of the data on the ability to resolve biotic features other than seagrass in intertidal meadows, samples from the mosaics were rescaled to different spatial resolutions. This was performed using the `gdalUtils` package (Greenberg and Mattiuzzi, 2015) in R (R Core Team, 2016a). The `'gdalwarp'` function was used to output at resolutions 2,4,6,8 and 10 times coarser than the native resolution of 4.36 mm pixel<sup>-1</sup>. The output pixel values were calculated as the mean of the corresponding input pixels.

### 7.3.11 Quadrat sampling bias

A further analysis exploring the potential biases in quadrat sampling using photos taken at the time of data collection was also conducted. The methods and results of this procedure are presented in the supplementary information (sections 10.4.1 & 10.4.2).

## 7.4 Results

Data collection at Angle Bay yielded 220 useable images during a flight that lasted 10'57". At Garron Pill, 191 useable images were collected during a flight 08'43" in length. Upon visual inspection that stitching had worked, the mosaics were then cropped so that ground control targets and associated tape measures were not included in the imagery, reducing complications during the classification phase (**Figure 7.3 & Figure 7.4**). Mosaics for both sites had a ground resolution of 4.31 mm pixel<sup>-1</sup> with a re-projection error (calculated by the software) of 0.32 pixels at both sites.

For the RGB classifications optimum classifications were as follows: Angle Bay optical – four classes, two of which were combined for the seagrass class, Garron Pill optical – five classes, one assigned as seagrass. Contrast, dissimilarity and variance were combined with optical data for Angle Bay, and classified with five discrete classes. Three of these were labelled as seagrass. For Garron Pill, contrast, homogeneity and second moment were the optimum texture layers along with the RGB data. Two of the five classes in the optimum classification were combined to make a seagrass class. For the OBIA analysis the combined RGB and texture layers described here were used. Thematic maps were created showing these classifications (**Figure 10.11 & Figure 10.12**).

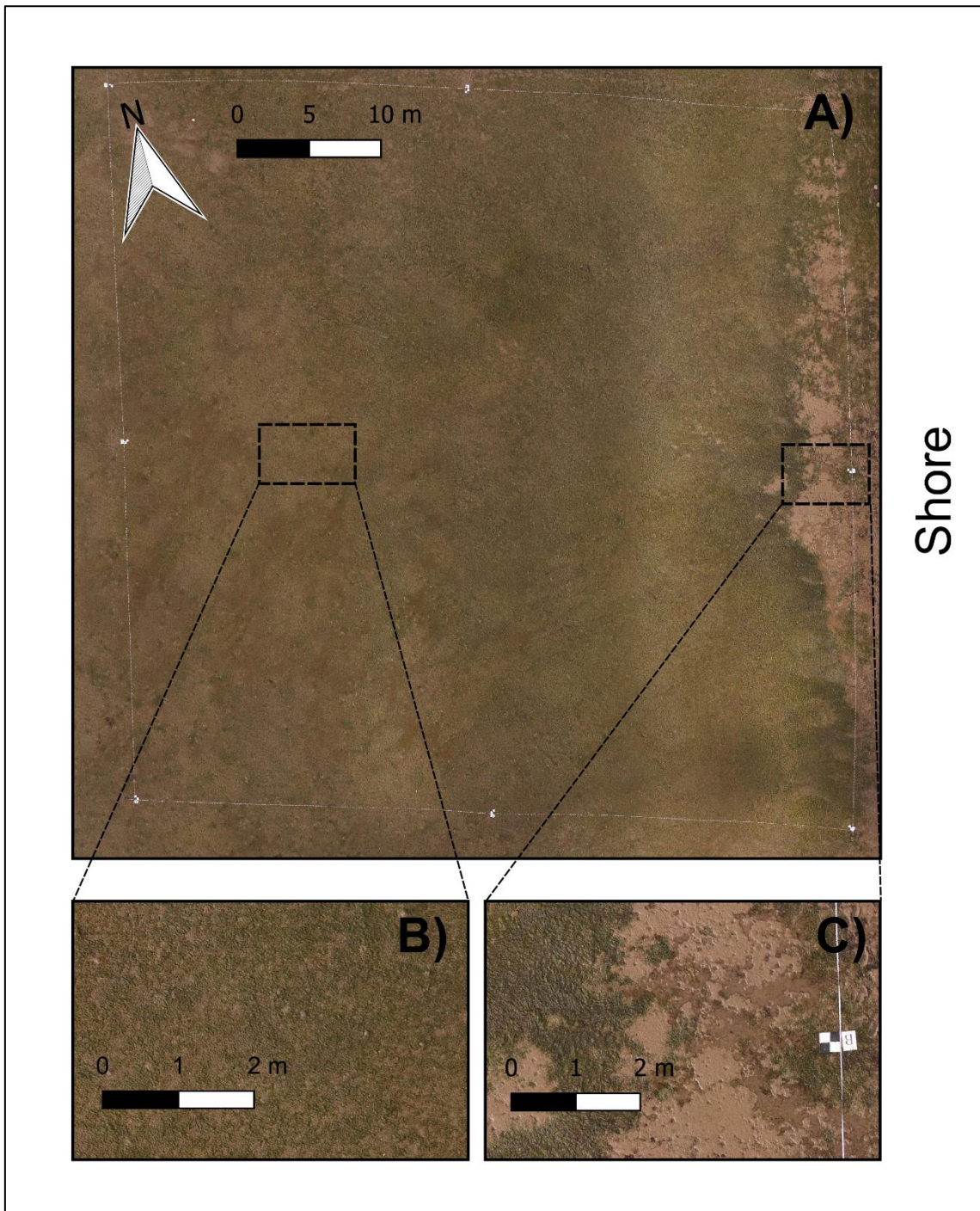


Figure 7.3: Mosaicked RGB imagery of *Zostera noltii* habitat in Angle Bay. The 50 x 50 m plot is shown in A), with two finer spatial scale examples shown in B) and C).

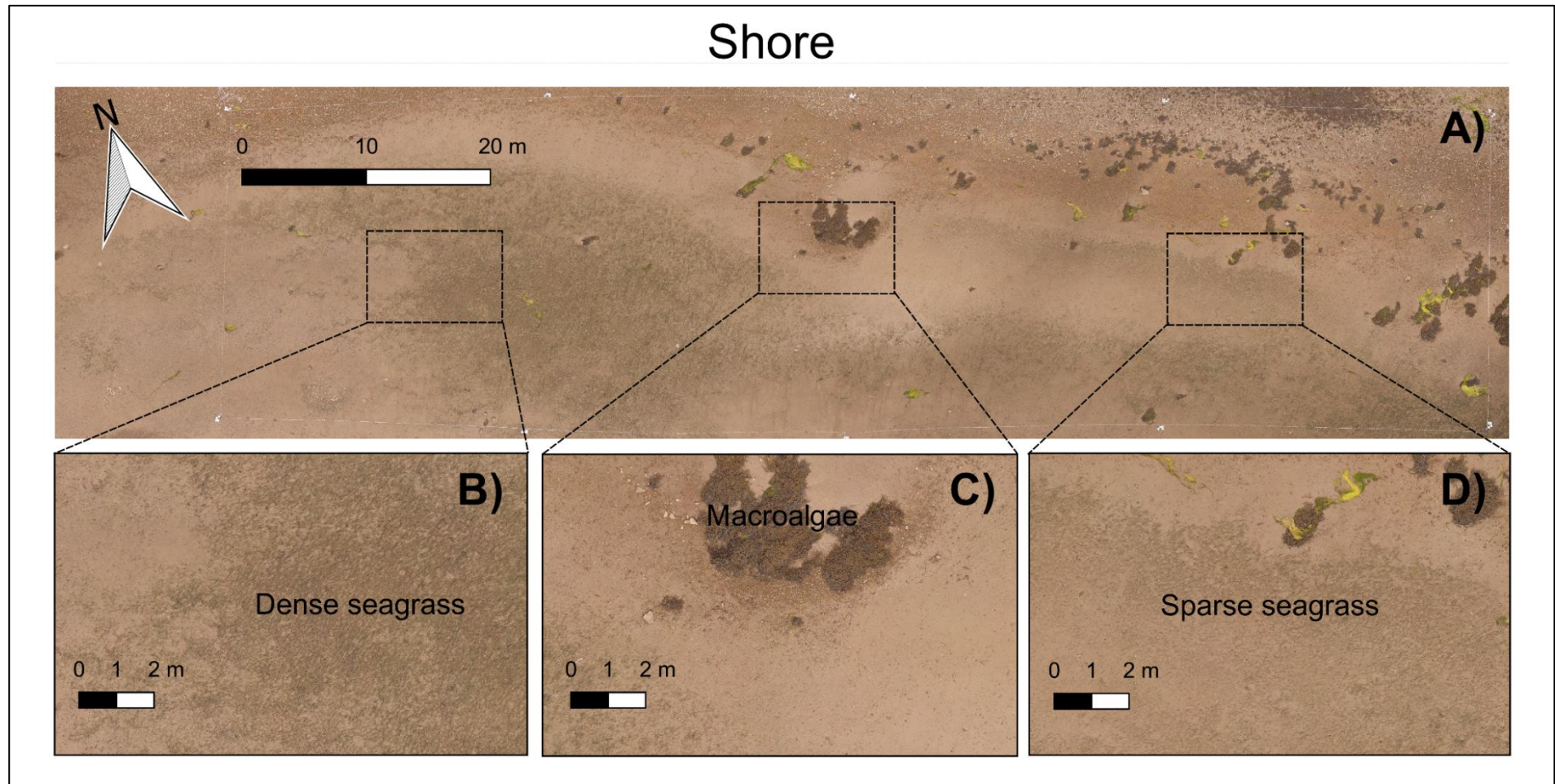


Figure 7.4: Mosaicked RGB imagery of *Zostera noltii* habitat at Garron Pill. The ~25 x 100 m plot is shown in A), with three finer spatial scale examples shown in B), C) and D).

The RMSD values calculated from classifications on the data from Garron Pill were all lower than their corresponding results for Angle Bay (**Table 7.1**). For Angle Bay, the addition of texture layers increased the RMSD by 5.7 with units of % coverage and SD by 4.3% (i.e. the fit was poorer), whereas for Garron Pill, RMSD was reduced by 0.2% and SD by 0.5%. Object based image analysis did not improve on either of the RGB or RGB & Texture classifications at either site with RMSD and SD values generally much higher. For both of the unsupervised classifications, both under- and overestimations were seen across the 27 quadrats (**Figure 7.5A & B**), whereas for OBIA, it appears the majority of quadrats were overestimated by the classifier (**Figure 7.5C**). Additionally, quadrat sampling bias was explored, and a mean difference of 15% between observed and classified ground-based photos was found (**Figure 10.10**).

The bootstrapped overall uncertainty values show relatively little variation in the unsupervised classifications with and without texture for Garron Pill (**Figure 7.6**). Angle Bay, the more densely vegetated of the two meadows had over double the mean overall uncertainty when compared to Garron Pill for the RGB & texture classification (**Table 7.1**). Along with the high RMSD and SD values, the OBIA classifications also showed both high mean overall uncertainty, (the highest being 33% for Angle Bay).

#### 7.4.1 Areal coverage and perimeter estimates

Combining the known ground sampling distances (4.36 mm) in the orthomosaics with counts of pixels in each classified raster allowed for seagrass areal coverage estimates to be made. For Angle Bay, estimates ranged from 1110 m<sup>2</sup> (47 % of the surveyed areas) produced by the RGB & texture classification to 1967 m<sup>2</sup>

(83%) calculated from the OBIA classification (**Table 7.1**). Overall, Garron Pill had smaller estimations with the lowest at 555 m<sup>2</sup> (22%) and highest at 904 m<sup>2</sup> (36%) produced with data from the OBIA classifier. OBIA classifications at both sites resulted in greater numbers of pixels being labelled as seagrass, which in turn has driven the higher areal coverage estimates. The two flights at 50 m altitude used to collect data from the river channel area yielded total of 258 useable images. These flights were 11' 45" and 12' 01" in duration. No ground control points were deployed or used here due to the inaccessibility of the river channel by foot. The images collected were then stitched with the same procedure mentioned earlier in this manuscript, but without the inclusion of GCPs, so therefore relying on GNSS information from the flight log (tagged to images) to produce a georeferenced orthomosaic (**Figure 7.7**). The resulting image demonstrates the capability of this form of data collection to visualise the boundaries of seagrass meadows in terrain that is not accessible by foot (e.g. soft muddy intertidal river beds). Other broad category vegetation features such as macroalgae are also detectable in these data (**Figure 7.7C**).

#### 7.4.2 Feature detection

Within intertidal seagrass meadows, some features can be detected with optical remote sensing data indicating the presence of biotic features other than seagrass that co-habit these environments. At both sites cockles (*Cerastoderma edule*) and Lugworm (*Arenicola sp.*) mounds were found on the sediment surface in high abundance. **Figure 7.8** displays three example features both at native and multiple resampled resolutions. Lugworm mounds are generally round features approximately 50 – 100 mm in diameter. They were clearly visible at the native resolution in the data and remained detectable even at 43 mm pixel<sup>-1</sup> (× 10)

spatial resolution. Cockles on sediment appeared more detectable than those within seagrass (**Figure 7.8**). The shells remained detectable in the absence of seagrass when viewed at 43 mm pixel<sup>-1</sup> spatial resolution, but when found within *Zostera noltii* shoots they become undetectable at 17.2 mm pixel<sup>-1</sup> (× 4) spatial resolution (**Figure 7.8**).

**Table 7.1: Accuracy assessment of unsupervised classifications including both RGB and RGB and Texture, and OBIA classifications. Root mean squared deviation (RMSD) and standard deviation (SD) and bias calculated on the percentage difference between observed and classified seagrass cover in quadrats. Bootstrapped SE was calculated in the bootstrapping process. Overall uncertainty calculated from bias, SD and bootstrapped SE using the equation described in section 7.3.9. Coverage estimates calculated by totalling the number of pixels classed as seagrass at each site.**

Site	Layers	No. Classes	RMSD (%)	SD	Bias (%)	Bootstrapped SE	Overall Uncertainty	Estimated Coverage (m <sup>2</sup> )	Estimated Coverage (%)
Angle Bay	RGB	4	16.12	16.33	-1.78	0.5	16.71	1224.07	51.93
	RGB & Texture	5	21.85	20.65	-8.19	0.63	22.54	1110.33	47.10
	RGB & Texture (OBIA)	2	32.74	20.53	25.81	0.63	33.2	1967.14	83.45
Garron Pill	RGB	5	9.45	9.62	-0.4	0.29	9.8	554.92	21.86
	RGB & Texture	5	9.22	9.06	2.44	0.28	9.54	661.77	26.07
	RGB & Texture (OBIA)	5	26.42	20.95	16.59	0.65	27.01	904.35	35.62

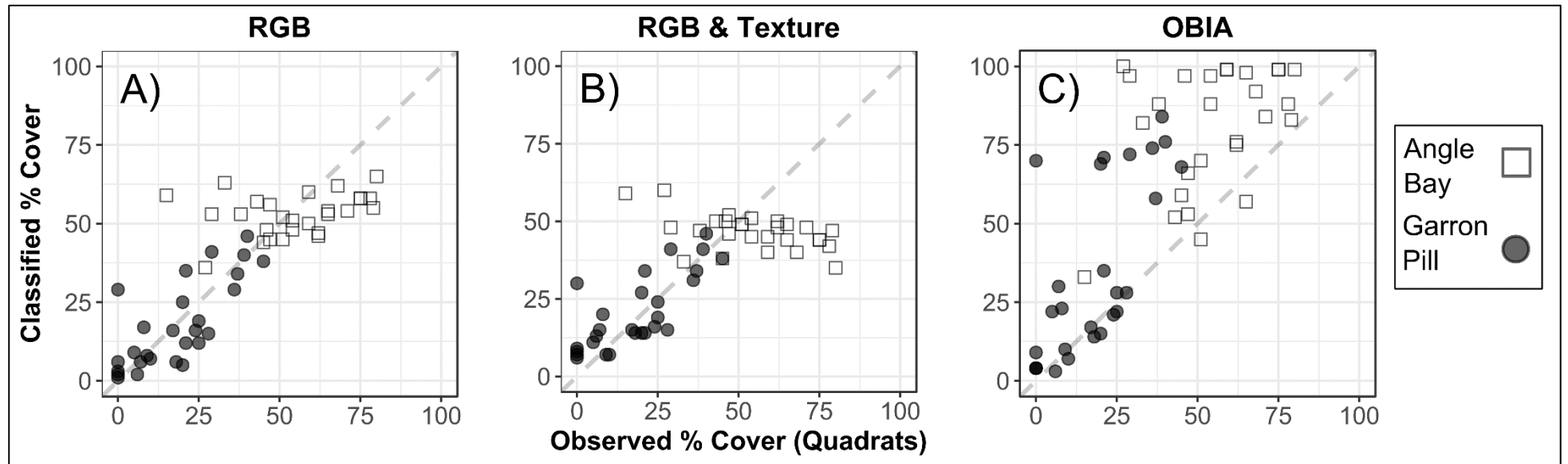


**Figure 7.5: The relationship between observed and classified seagrass coverage observed within quadrats. Unsupervised classifications with red, green and blue bands shown in A), with added texture layers in B) and supervised object-based image analysis results are shown in C).**

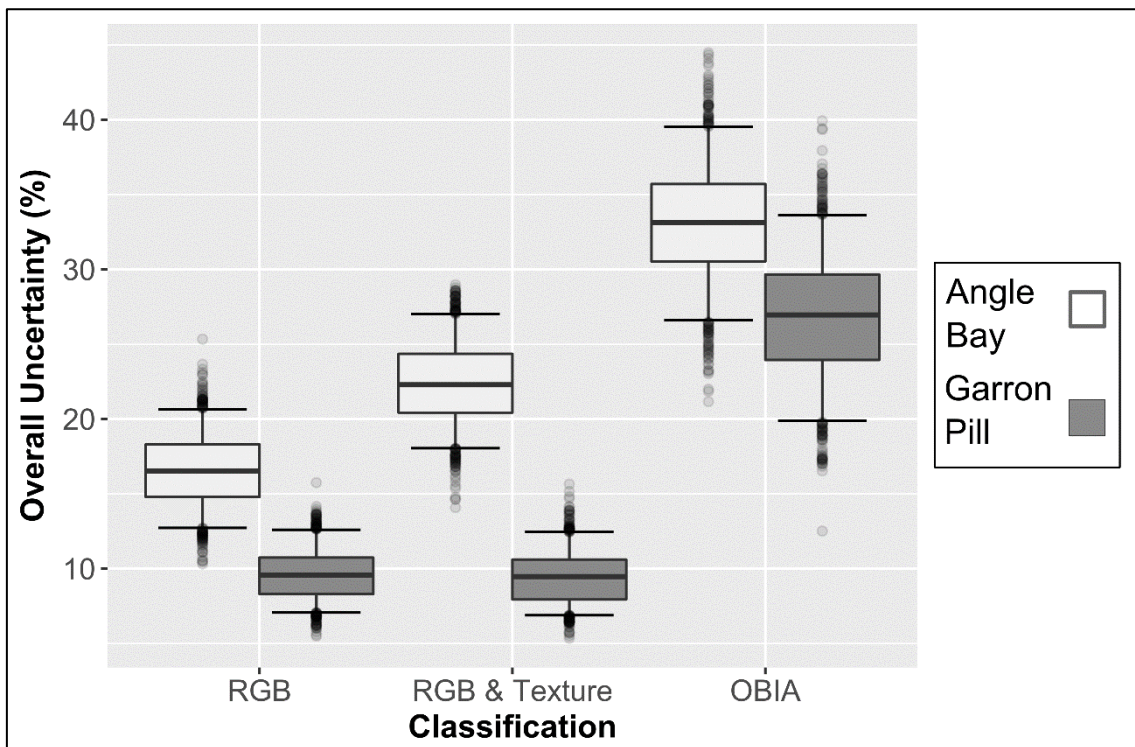


**Figure 7.6: Box and whisker plots showing the distribution of bootstrapped overall uncertainty calculations (n = 1000), calculated from the differences between observed and classified seagrass cover in quadrats. Lower and upper hinges refer to 25% and 75% percentiles respectively. Central lines represent the median, whiskers represent 5% and 95% quantiles and points represent outliers.**

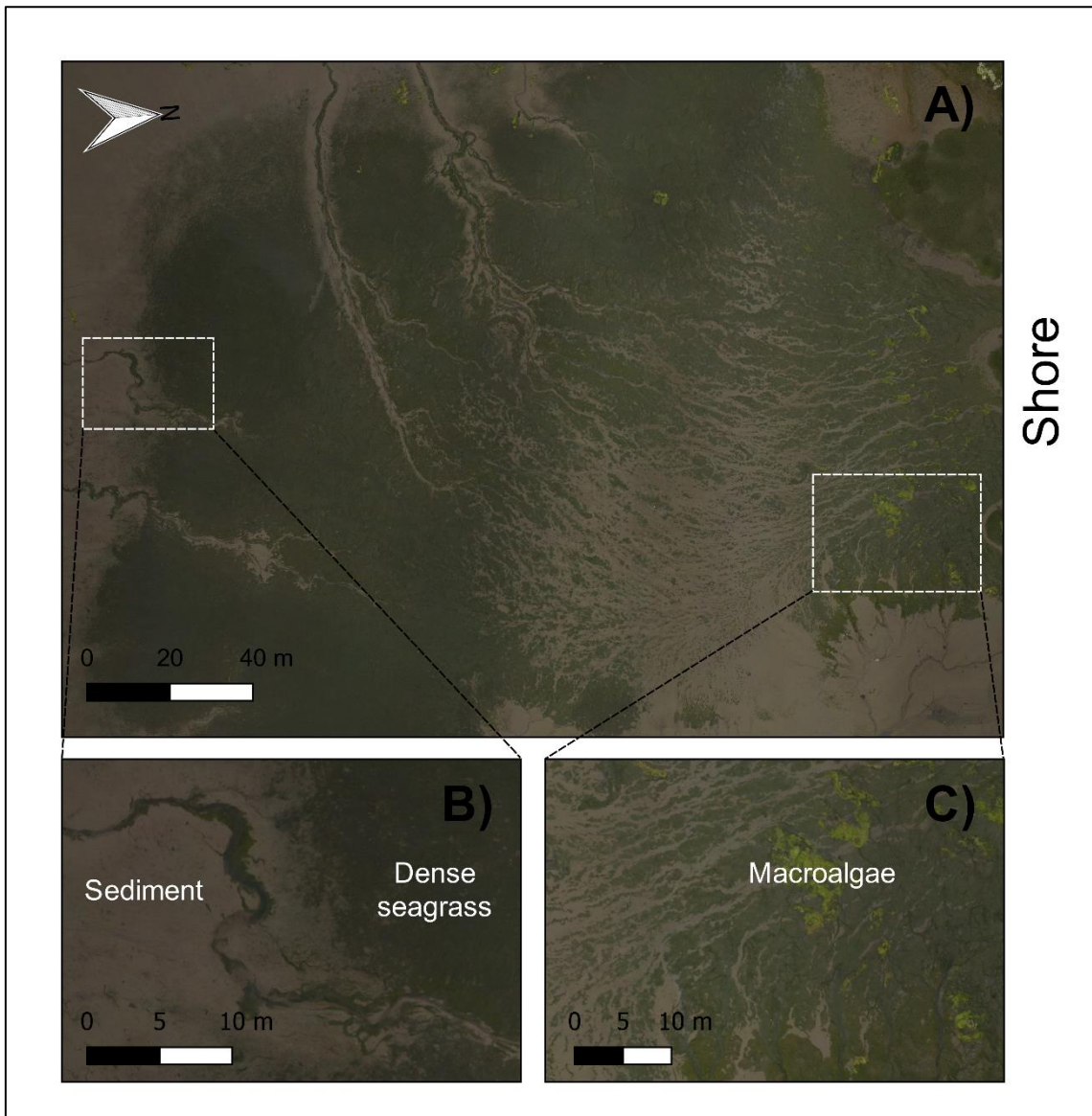


**Figure 7.7: Orthomosaic of *Zostera noltii* meadow boundary at Garron Pill. Images captured at 50 m altitude. No ground control targets were deployed at this site due to the inaccessible nature of the river channel.**

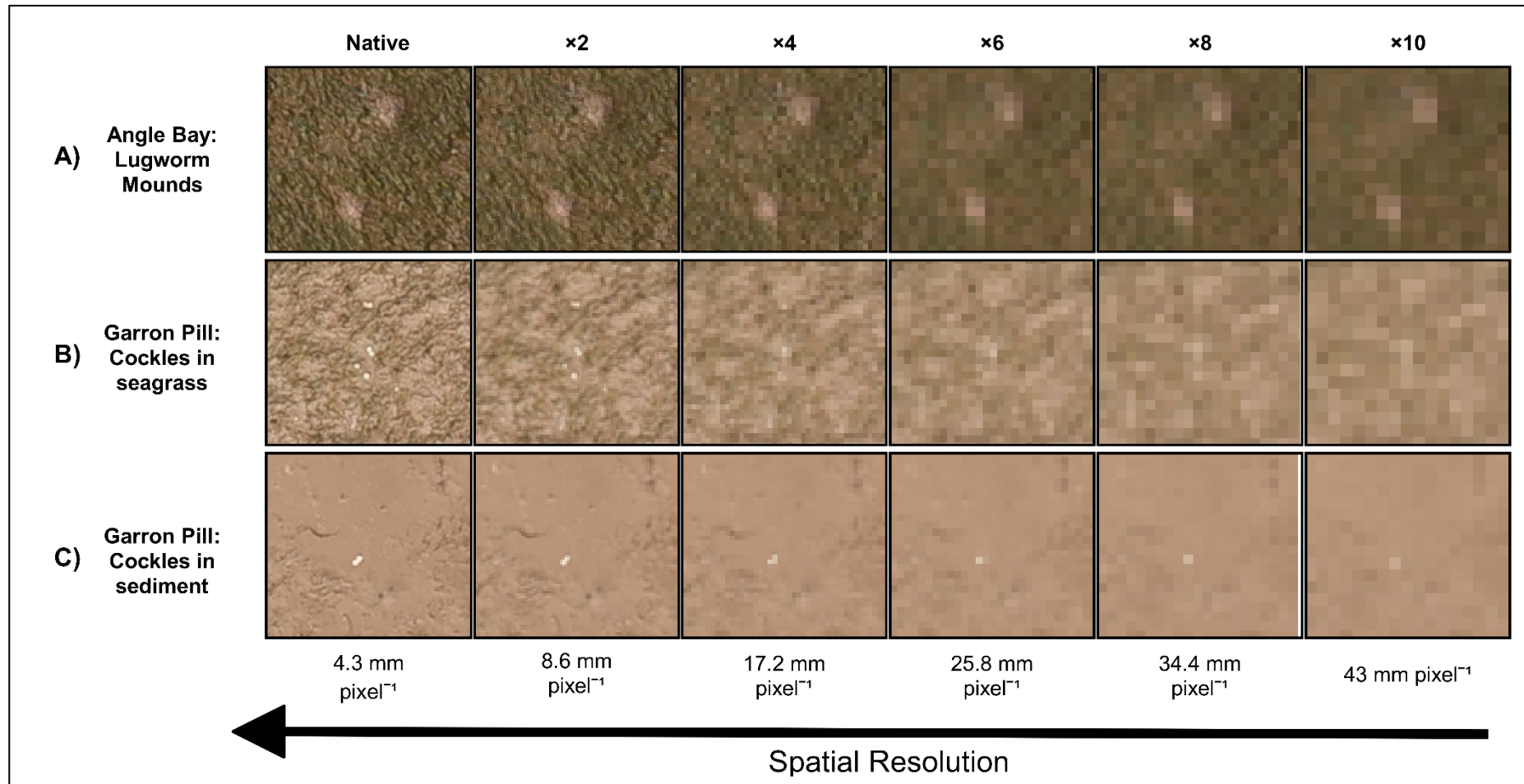


Figure 7.8: Three examples of ecological features found in *Zostera noltii* meadows. A) Shows two Lugworm (*Arenicola sp.*) mounds, B) Cockle (*Cerastoderma edule*) shells surrounded by seagrass shoots and C) on non-vegetated substrate.

## 7.5 Discussion

This study describes for the first time an approach to intertidal seagrass mapping using a lightweight drone to obtain very fine grained, high spatial resolution data. We found wide variation between classifications when measuring the differences between classified and observed cover within the quadrat samples collected (**Table 7.1**). Given that the addition of texture layers has improved classification accuracy in the past in similar habitats such as salt marsh (Kim et al., 2011), we expected to see reduced RMSD scores in this study. It may be that the classification of the very fine spatial resolution data shown in this study can only be improved by the addition of more spectral (e.g. near infra-red) rather than textural layers. The spectral complexity found in hyperspectral optical remote sensing studies on *Zostera noltii* leaves (Bargain et al., 2013) suggests that the addition of further spectral bands may produce a better discrimination between seagrass shoots and background sediment. Different texture measures were selected during the layer selection phase for each site. This highlights the importance of treating each mosaic individually when selecting layers to input to a classification scheme. Variables such as the spatial resolution of the images, and the meteorological conditions (e.g. cloud cover) during data collection can strongly influence the type of data collected, and in turn which texture measures may highlight differences between seagrass and non-seagrass features.

OBIA has been increasingly employed to analyse fine grained data such as that collected from sensors on board drones (e.g. Husson et al., 2016 and Ventura et al., 2016). In this case, the unsupervised classifications performed better than the support vector machine algorithms used on the segmented data. Despite the very high spatial resolution of the data, *Zostera noltii* shoots still appear as very fine

and complex features within the input bands. The segmentation process applied struggled to properly define the edges between seagrass and non-seagrass features, and therefore non-vegetated areas were also captured within the objects labelled as seagrass. This over-estimation is reflected in the comparisons with quadrat data at both sites (**Figure 7.5**). Furthermore, OBIA is notoriously subjective and its poor performance in this scenario may have been caused by the choice of 'training' segments during pre-classification. New segmentation algorithms (e.g. SLIC super pixels; Csillik, 2017), are emerging and in future as these mature, there may be promise to further test these on fine spatial resolution intertidal orthomosaics.

#### 7.5.1 Coverage estimates & assessment of quadrat sampling

The variation in coverage estimates produced from the classified data in this study is caused by uncertainty in the classifications themselves. Working at such fine spatial scales allows for the consideration of within-meadow variation and in turn more representative predictions of overall coverage. However, working at such fine spatial scales brings new challenges for data interpretation. Underestimation, seen more commonly for quadrats at Angle Bay (**Figure 7.5**) could be due to the high density of seagrass in parts of this site and the differences between what a sensor captures and what a human observer interprets. This could be caused by a saturation effect also seen in optical remote sensing studies of other vegetated ecosystems (Mutanga et al., 2012). Positive bias, seen in some quadrats at both sites, could potentially be explained by an observer effect. Estimations of coverage by a human observer could take into consideration the fact that seagrasses stand vertically when suspended in water, whereas a sensor, in this case on board a lightweight drone, simply counts the

proportion of pixels covered by seagrass. The hypothesis that observer bias was present during ground-based sampling was investigated by examining photographs of the quadrats (see supplementary information; **Figure 10.10**). Observer bias and variability of cover estimations, regardless of experience, has been raised as an issue with quadrat sampling in terrestrial systems (Sykes et al., 1983). It may be the case that in this study similar issues were causing underestimation, combined with the knowledge that a given number of seagrass shoots change their coverage of a quadrat when suspended in water compared to laid flat at low tide. Although ground based photographs were taken in this study, their quality was variable, and therefore we recommend a standardised approach (i.e. using a fixed height (Luscier et al., 2006) in future investigations.

#### 7.5.2 Meadow boundary detection

Meadow boundaries were clearly visible in the mosaic created with images captured at 50 m altitude. Information of this type provides a cost-effective approach to *Zostera noltii* meadow mapping, especially in tidal channels where the logistics of boat or hovercraft surveying are non-trivial. The distinction between seagrass and macroalgae was clearly visible in the resulting orthomosaic (**Figure 7.7C**), which from a management point of view provides a useful tool to quantify the invasion of other species such as macroalgae in seagrass-dominated habitats (Thomsen et al., 2012).

#### 7.5.3 Feature detection

The very fine spatial resolution data produced in this study (4.36 mm pixel<sup>-1</sup>) allowed for the identification of meadow features such as lugworm (*Arenicola sp.*) mounds and cockle shells (*Cerastoderma edule*). The ability to capture this

information within images containing seagrass shoots could allow questions regarding lugworm presence/density effects on *Zostera noltii* density to be revisited (Philippart and Dijkema, 1995). The presence of bivalve shells is also a crude but useful indicator of the health and diversity of the below-surface intertidal environment (Lohrer et al., 2016). With regards to the spatial resolution of the data captured in this study, these features were all identifiable at coarser resolutions than the native data. This indicates that a higher- altitude flight could be conducted resulting in a coarser ground sampling distance, therefore allowing for data collection from a larger area without compromising the ability to capture fine scale biotic features.

In future work, other users should consider monitoring conditions. In this study, conditions were generally overcast and therefore favourable when collecting imagery at Garron Pill, but for Angle Bay, the meteorological conditions were mixed with intermittent sunshine amongst the cloud. As the drone flew with a variable heading, the sensors viewing angle changed in relation to the sun's position on alternate legs of the drone's way-pointed path (**Figure 7.1C & D**). As a result, the attitude of the drone and therefore the attached sensor, manipulated the presence of glint and shadow in the imagery. Due to the gridded pattern of flight, artefacts have developed at overlapping areas between images during the image stitching process. We recommend in future, to conduct flights with a constant heading, to ensure the sensors view angle remains fixed in relation to sun angle. We would also encourage other users to consider image calibration if time-series monitoring is being undertaken.

#### 7.5.4 Ecosystem dynamics and blue carbon

The potential of coastal ecosystems and more specifically the plants that live within them to capture and sequester carbon (known as blue carbon) has been a growing field of scientific research (Fourqurean et al., 2012; Macreadie et al., 2014). The coverage estimates that we present here can be complementary to allometric data such as above- and below-ground biomass calculations to ultimately produce more accurate estimations. This has been demonstrated in terrestrial systems with drone-based data (Cunliffe et al., 2016). This can then be combined with information about carbon capture in a particular species such as *Zostera noltii*, quantifying the amount of carbon stored in a given meadow and allowing its monetary value to be estimated. Monetary valuation such as this is likely to give great value to policy decision making (Turner et al., 2003). Aside from monetary valuation, fine-scale data such as these can potentially improve the performance of predictive habitat modelling approaches which have been applied to understand seagrass distribution (Grech and Coles, 2010).

For another species of seagrass, seasonality has been shown to create changes of up to 35% in coverage estimates of seagrass meadows on the coast of Reunion Island (Cuvillier et al., 2016). *Zostera noltii* is a perennial species that grows in spring and summer, flowers, and then dies back to about half its peak density in autumn and winter (Auby and Labourg, 1996). While this variation in above ground biomass is an issue with ground based surveying (Mckenzie et al., 2001), using drones with user-dictated data collection, allows for repeatable data collection at the same stage of the annual phenological cycle of a seagrass species such as this. The case for repeat studies at the same time of year is also strengthened by the discovery of a seasonal variation in pigment concentration

in *Zostera noltii* leaves, which in turn can influence measurements derived from remote sensing products (Bargain et al., 2013).

## 7.6 Conclusions

In this study we have demonstrated the potential of low-cost, flexible, drone-based data collection techniques for monitoring intertidal seagrass meadows. Working on foot in an intertidal environment can be challenging and one clear advantage of drone technology is the flexibility in deployment and the utility of data, as we have demonstrated here. Time-series monitoring is critical to understand the dynamics of seagrass meadows, especially when it comes to disentangling the natural variation from changes that are human-induced (Cunha et al., 2005).

The understanding of within-meadow seagrass heterogeneity is a complementary approach to more traditional boundary mapping which has often been conducted using satellite and airborne imagery (e.g. Phinn et al., 2008). Drones bring the ability to capture data useful for within environment variation analysis, which has also been demonstrated in wetlands (Zweig et al., 2015). With threats such as reduced water quality and wasting disease, the decline in meadow quality may be more nuanced than a simple shrinking in overall extent, highlighting the need to understand the more complex matrix of plants and sediment in the intertidal environment. It is therefore crucial to investigate the fragmentation within meadows, which can inform researchers and managers whether a meadow is potentially degrading or recovering. The combination of this previously unobtainable data and the cost-effective, self-service nature of drone

based remote sensing gives great promise to the application of drones for seagrass conservation efforts.

Moving forward, we feel that the rapidly developing field of lightweight drones and miniaturisation of sensors for optical remote sensing will soon allow for more detailed measurements of meadow quality such as plant health and presence of wasting disease based on the spectral signatures obtained from seagrass shoots.

### 7.7 Acknowledgements

We would like to thank Benjamin Leutner, Moritz Lennert and Chris Kay-Ayling for assistance with the analysis of this data. We are grateful to two anonymous reviewers whose advice and comments helped improve this work. This work was supported by the Natural Environment Research Council [grant number 570009815 to JPD].

## 8 Coral reef structure

### *Kandehalagala coral reef system, Maldives*



This chapter is in preparation for publication. Potential outlets include 'Coral Reefs', and 'Marine Ecology Progress Series'.

## **Towards Drone-Derived Structure-from-Motion Point Clouds for Characterising the Structural Complexity of a Submerged Coral Reef**

James P. Duffy<sup>1\*</sup>, Chris T. Perry<sup>2</sup>, Jonathan Crocker<sup>2</sup>, Jamie D. Shutler<sup>3</sup> & Karen Anderson<sup>1</sup>

1. DroneLab Research Group, Environment and Sustainability Institute, University of Exeter, Penryn Campus, Penryn, Cornwall, TR10 9FE, UK

2. Geography, College of Life and Environmental Sciences, University of Exeter, Streatham Campus, Exeter EX4 4RJ, UK

3. Centre for Geography, Environment and Society, University of Exeter, Penryn Campus, Penryn, Cornwall, TR10 9FE, UK

*\*Corresponding author*

### **8.1 Abstract**

Tropical coral reefs are structurally complex and deliver a wealth of ecosystem goods and services. Monitoring efforts in these environments are often informed by *in-situ* surveys, satellite and airborne remote sensing datasets. These methods either lack representativeness, temporal or spatial resolution. Structure-from-Motion Multi-view-stereo (SfM-MVS) processing of data from drone-based sensors has been used to measure structural complexity on finer spatial scales. We test a variety of drone flight parameters across a range of topographically diverse reef environments, to understand their influence on SfM-MVS derived structural complexity estimations. Images acquired above the water column at 30 m altitude with a 3DR Solo and Ricoh GR II camera successfully produced dense point clouds, gridded elevation products and orthomosaics. Virtual transects were conducted to calculate structural complexity estimations as a function of the ratio

between 3D surface distance and planar distance. We found that across the reef environment, differences in complexity were most pronounced in lagoon areas with mixtures of bare sand and individual coral bommies. In denser reef areas, complexity measures became homogenous despite the presence of heterogenous complex structures, implying aliasing in the ability of the approach to resolve subtle details. We found that data captured at 30 m produced denser point clouds (up to 71%) than using simulated higher altitude (50 m) data with greater ground sampling distances, as expected due to a reduced ability to match benthic features. Complexity estimations derived from the point clouds for different cover types (e.g. sand, tabular coral, branching coral) did not correlate with colony level rugosity estimates derived from the literature. We also found no relationship between *in-situ* transects describing submerged topography and cloud derived measures. In summary, the techniques shown here show promise as some variation in reef structure was measured, but finer spatial resolutions and robust corrections to deal with the presence of water are required to improve the methodology.

## 8.2 Introduction

Coral reef ecosystems are globally distributed complex environments that provide a multitude of ecosystem services such as coastal protection (van Zanten et al., 2014), tourism (Weijerman et al., 2018) nutrient cycling and maintenance of fisheries (Barbier et al., 2011). Tropical reefs form in coastal waters typically, with a heterogenous mix of species and associated morphological diversity providing a structurally complex habitat (Richardson et al., 2017). Structural complexity is closely linked to the productivity and health of coral reefs with more complex habitats deemed more able to support a greater diversity of species and

individuals than those harbouring simpler architecture (Graham and Nash, 2013). This is because they provide more niches from which organisms can exploit resources (e.g. territory for reproduction (Catano et al., 2015)). Furthermore, complexity is a strong predictor of fish abundance, biomass, species richness and trophic structure (Darling et al., 2017). Recent degradation of both local and global environmental conditions has led to the collapse of reef architecture or 'flattening' of some reefs (Alvarez-Filip et al., 2009) in turn reducing the total species richness in these habitats (Newman et al., 2015). The shift to degraded states can also alter reef carbonate budgets - effectively balances between constructive processes (such as reef calcification/building) and destructive processes (erosion from physical, biological or chemical forces). A reduction in coral calcification rates and changes in associated turnover of carbonate from bioeroders such as urchins and parrotfish could shift reefs from positive to negative carbonate budget states meaning a reduction in coral cover over time (Perry et al., 2014). The loss of structural complexity also leads to a reduction in the reef's capacity to deliver coastal protection, leaving tropical coastlines more vulnerable to increased impacts from waves (Harris et al., 2018). Due to changes in reef composition (e.g. a shift to a more algal-dominated habitat) resource availability for native organisms is reduced, in turn affecting ecosystem services such as fisheries provision (Rogers et al., 2018, 2014). In order to quantify the impacts of reef morphometric change on delivery of aforementioned ecosystem services, there is an urgency for new approaches that can identify and map the fine-grained structures of reef systems so as to inform improved management or mitigation strategies. Although bleached reefs can eventually collapse, leading to a decline in structural complexity and associated biological diversity, the process can occur over many years (Garpe et al., 2006). Therefore, there is a need to

understand submerged topographic change over time on both healthy and degrading reefs.

### 8.2.1 Measuring reef complexity

Measuring complexity in reef environments is a non-trivial task empirically – for example it is challenging to capture data describing the spatially extensive structural attributes of the reef using scuba or snorkel surveys (Nash et al., 2013). Also, training individuals to undertake such surveys is a costly and time-consuming process, limiting the number of skilled people available to conduct benthic surveys (Gutierrez-Heredia et al., 2016). Measurement techniques include the use of a variable size wheel system (Wilding et al., 2007) and an analogue chain and tape method (McCormick, 1994), which has been adopted due to its low cost and relative ease of use (Dustan et al., 2013), but data from such systems are two-dimensional and deliver transect-based data only, limiting abilities to monitor reef-extent changes in habitat structure. Alternatively, digital level gauges have also been used to obtain millimetre spatial scale measurements across reef transects, but these are also reliant on scuba approaches (Dustan et al., 2013). Scuba and snorkel based surveys are expensive, time intensive and can be high risk, meaning for some monitoring purposes they are a sub-optimal way in which to capture data. Also, despite the ability of *in-situ* measurements to provide information about the topography of reef substrate, the resulting sample sizes can be small and the spatial representativeness of samples uneven, which can introduce uncertainty or biases when upscaling measurements to the wider reef environment.

### 8.2.2 Remote sensing

Satellite and airborne remote sensing have long been explored as information sources for coral reef monitoring programs. Satellite-derived seafloor maps have been used to thematically map tropical reef ecosystems (Teixeira et al., 2016) and estimate carbonate production rates across reef environments at the regional scale (Hamilton et al., 2017) but require *in-situ* validation data owing to their coarser spatial grain. Whilst quantifying structural complexity from optical satellite and aerial data products is difficult to achieve (e.g. the lack of suitable overlapping data required for a photogrammetric based workflow), some success has been achieved through using airborne bathymetric light detection and ranging (LiDAR) to quantify structural complexity (Brock et al., 2006, 2004; Pittman et al., 2009). However, for many regions of the world with a large proportion of the global coral reef resource, LiDAR is either unavailable or too costly a technology to deploy for repeat data collection. At more local and low-cost scales, acoustic sensors such as 'RoxAnn' (an echo sounding device that maps the sea bottom) mounted underneath the hulls of small boats can be used to deliver structural complexity estimates (Bejarano et al., 2011) and such approaches have proven useful for categorizing reef habitat type and attaining habitat metrics, although these methods are limited to deeper areas where boats can safely operate over the reef (Hedley et al., 2016). To accurately survey shallow reef systems, an easily deployable and non-invasive method is required to provide data with finer spatial and temporal resolutions and at larger spatial extents than those currently used to quantify reef structure. There is now potential to achieve this with proximal sensing platforms such as drones and kites (Duffy et al., 2018; Duffy and Anderson, 2016). Drone platforms and their on-board sensors can collect optical

data useful for assessing coral health (Levy et al., 2018) and also provide estimations of topographic variation with Structure-from-Motion-Multi View Stereo (SfM-MVS) techniques. SfM-MVS is a technique that estimates the position and size of three-dimensional structures from two-dimensional images (e.g. photographs). Features located in multiple images from a single survey are matched and their position in space estimated. For tropical reefs, Casella et al., (2017) were the first to demonstrate that maps of bathymetric structure (with SfM-MVS) can be delivered from overlapping drone photographs, and they used these as indicators of structural complexity within the reef environment and compared them to LiDAR data. Of particular note in the Casella et al., (2017) study were the optimal surveying conditions, with minimal wind and clear water with no evidence of artefacts on the sea surface. Furthermore, the study was conducted in a bommie dominated lagoon, with few continuous coral structures. Aside from this single published study, the exploration of SfM-MVS using drone acquired data is largely unexplored and requires further investigation if it is to become a robust monitoring technique. On the contrary to the lack of above water data capture, many papers have demonstrated the promise of SfM-MVS using images captured underwater. Off the shelf hardware such as consumer grade cameras have been used to calculate the structural complexity of individual coral colonies in a lab environment (Figueira et al., 2015) and also to undertake transects in the field (Leon et al., 2015). *In-situ* SfM-MVS measurements of individual coral bommies have been shown to be robust over time and between observers (Raoult et al., 2017), making it a technique that may eventually replace more traditional methods such as chain and tape (Storlazzi et al., 2016). Efforts are also being made to develop techniques that ensure user-defined overlap between images (beneficial for SfM-MVS workflows; Pizarro et al., 2017a), and also with

the use of autonomous underwater vehicles for data capture (Friedman et al., 2012). These studies are however, often limited in their spatial scale, and still require a significant time investment to capture images. They do not consider the complexities of scaling up measurements in order to better understand the structural complexity of reef systems on larger extents (>100 m).

### 8.2.3 Aims and scope

This work was undertaken to test a simple question that develops the limited existing SfM-MVS work undertaken previously in reef systems. Broadly, the aim of the experiment was to establish the information content of drone-derived SfM-MVS point clouds acquired over submerged reef systems and to examine the potential of aerial SfM-MVS derived point clouds to deliver information about reef structural complexity (a proxy for surface roughness, also known as surface complexity (Burns et al., 2015)), at different spatial extents and grains. Working within a fringing tropical coral reef environment in the Maldives, we set out to answer the following questions surrounding flight planning, data capture and comparisons to both *in-situ* and literature derived complexity metrics:

- 1) Can drone-based SfM-MVS data capture changes in submerged reef topography?**
- 2) Do measurements of structural complexity change in relation to the ground sampling distance of the SfM-MVS derived data?**
- 3) Does inclusion of oblique image data affect spatial estimations of structural complexity, compared to just using nadir images?**

4) How do such measures vary between lagoon, mixed and continuous reef parts of the ecosystem?

5) Making comparisons with literature derived rugosity values, how do point-cloud derived measures of structural complexity compare for different coral classes (branching, compact branching, massive, plate, sand and other types of coral)?

6) How similar are *in-situ* chain-and-tape transects to structural complexity estimations derived from SfM-MVS point clouds?

### 8.3 Methods

#### 8.3.1 Study system

Data collection was conducted on a fringing coral reef ecosystem surrounding the small island of Kandehalagala (~0.063 km<sup>2</sup>), located north-east of Faaresmathooda in the southern part of the Huvadhu atoll in the Maldives (0°13'31.65"N; 73°13'00.45"E; **Figure 8.1**). The island is found within the interior of the atoll and is currently uninhabited by humans. At the time of survey, a large proportion of the reef was in a degraded state due to a bleaching event in 2016 (Perry and Morgan, 2017a, 2017b). The island and reef system are ~0.4 km<sup>2</sup>, encompassing both a shallow lagoon with sparsely distributed coral colonies and a more densely populated fringing reef. One part of the reef system was surveyed for this study (**Figure 8.1D**). This area was selected due to its inclusion of the major distinctly topographically different densities of reef structures across a gradient from beach to reef wall (in deeper water) in a relatively small area. Also, despite large areas of the reef system appearing bleached, the coral structures

in this part of the reef were more in-tact than many other areas around Kandahalagala. This meant that there was a variety of morphometric types against which to test our research questions. Lastly, it was also chosen for logistical reasons - it was located parallel to the area of beach at which boat landings for kit and personnel were possible.

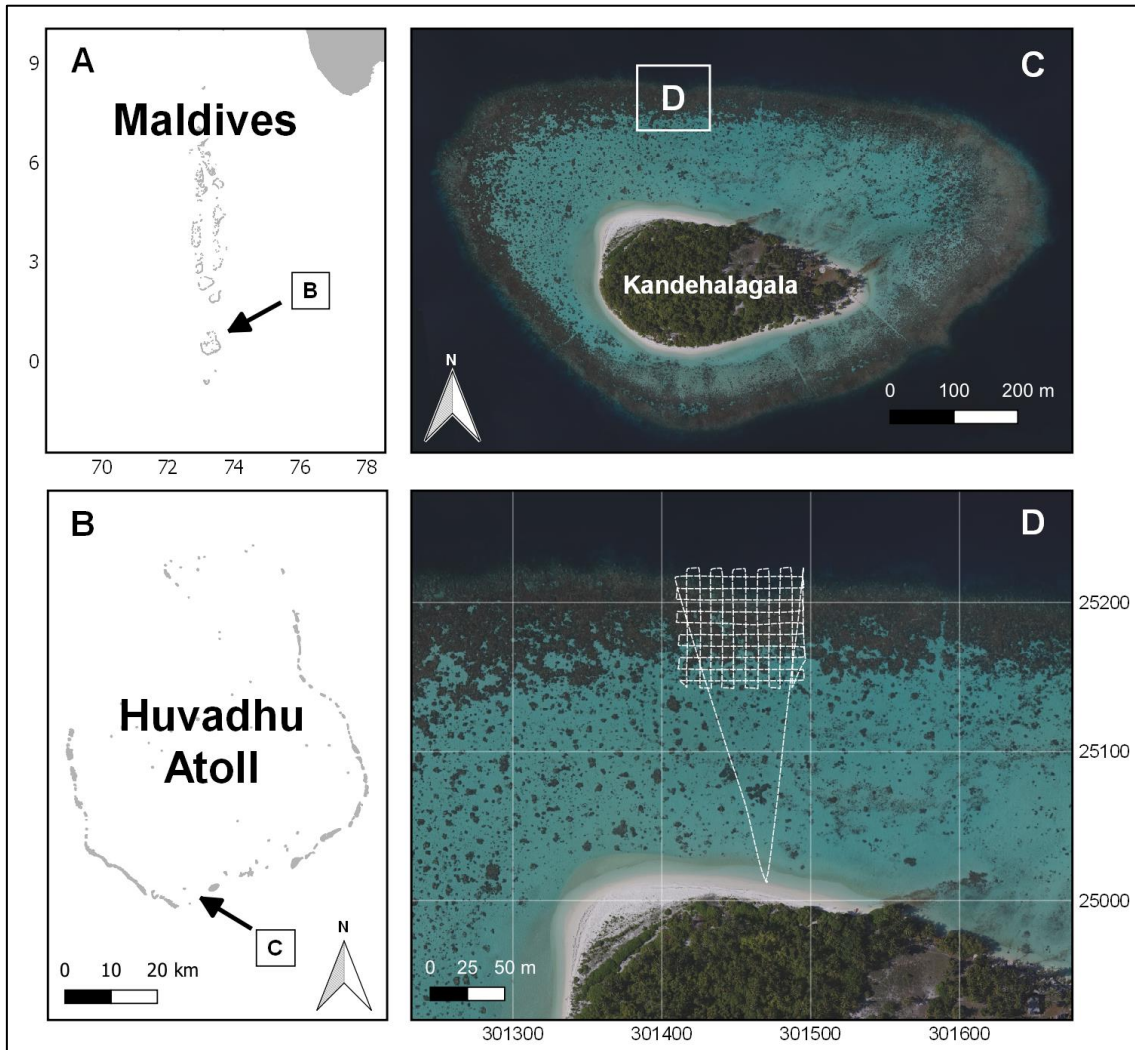


**Figure 8.1: Location of the study system. A) Location of the Huvadhu Atoll within the Maldives. B) Location of Kandahalagala within the Huvadhu atoll. C) The island of Kandahalagala. D) The path of one drone flight used in this study. Axis units in A) are in degrees, and units in D) are in meters, WGS 84 / UTM Zone 43N.**

### 8.3.2 Drone and sensor equipment

A 3D Robotics Solo quadcopter drone was used with two custom designed vibration-dampened 3D-printed sensor mounts (by the author JPD) (<http://www.thingiverse.com/thing:1964056>). Both mounts allowed for the attachment of a Ricoh GR II compact digital camera that captures images at 16.2 effective megapixels in both uncompressed (RAW) and lossy (JPEG) formats. This system has previously been used to capture data in coastal settings (Duffy et al., 2018). One mount positioned the sensor as nadir and another at an angle ( $20^\circ$ ) to obtain oblique image data (with the potential of seeing underneath or around objects in the water). Only one mount was attached at a time, so capturing data at both angles required the use of two replicated survey flights following an identical flight plan. The camera has a built-in intervalometer allowing automated triggering at set time intervals, and for these surveys a two second interval was used.

Each flight was pre-programmed using Mission Planner software (Osborne, 2016) in conjunction with the Pixhawk 2 (APM:Copter solo-2.0.20 firmware) autopilot onboard the drone. This allowed for Global Navigation Satellite System (GNSS)-guided flying and control of the position (in all three dimensions) and speed of the vehicle. This way, structured surveys could be designed ensuring that image overlap was controlled - the image overlap parameter is crucial for effective scene reconstruction when processing images with SfM-MVS algorithms (James and Robson, 2014). Two flights were conducted at an altitude of  $\sim 30$  m between 8:00am and 8:40am on 11/03/2017, one with the nadir mount and another with the oblique mount fitted both at a speed of  $\sim 4$  m s<sup>-1</sup>. Both flights used the same flight plan – a cross grid pattern (**Figure 8.1**) with a minimum of 80% frontlap and

sidelap. Flights were conducted early in the day (i.e. before 09:00) to minimise sun glitter in the image data. At this time of day, wind conditions were typically calmer, reducing surface water roughness and sun angles were lower, which due to the chosen camera angles minimises the potential of light to be reflected straight into the camera sensor. One further flight at an altitude of ~220 m at 5:30pm on 12/03/2017 was undertaken with the nadir mount, covering the whole reef system and island of Kandahalagala (**Figure 8.2**).

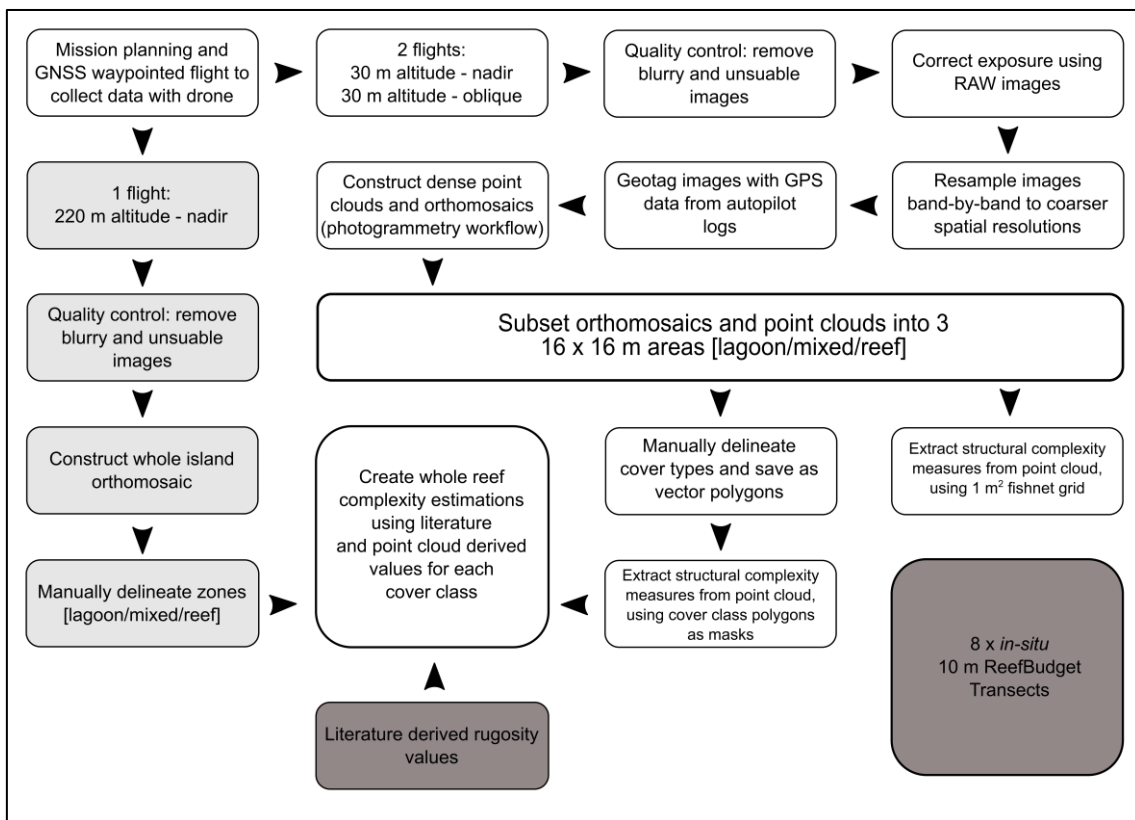


**Figure 8.2: Methodological flowchart demonstrating the data capture and processing workflow.**

### 8.3.3 Ground control, image resampling & photogrammetry workflow

The remote nature of the field site meant that it was not possible to follow the standard methodology as advocated by Gonçalves and Henriques, (2015) & James et al., (2017a), where one would distribute ground-control markers around the scene extent and survey them using a high accuracy GNSS system. However, to answer our research questions, this methodology was not required because georectification between datasets was not needed. Instead, we selected a single dataset (a combination of one set of both nadir and oblique images) collected at 30 m altitude and downsampled the images to simulate data collected at higher altitudes / coarser ground sampling distances. This meant that sensor positions between simulated surveys were identical and therefore the georeferencing of resulting photogrammetry products was the same. The RAW image files were converted to lossless .TIF files, exposure was increased (number of stops varied depending on how dark the images were (O'Connor et al., 2017)), and each of the red, green and blue bands were resampled using a nearest neighbour approach to match the desired image height and width of images at coarser resolutions (**Table 8.1**). A ground sampling distance calculator was used to attain the image height and width that would achieve a similar spatial resolution as if the drone was flown at higher altitudes (**Table 8.1**). This process was undertaken in Python 3, utilising `ufRaw` (<http://ufraw.sourceforge.net/>) to change exposure, Python Image Library (<https://python-pillow.org/>) to resample, and `exiftool` (Harvey, 2018) to re-tag the photos with image metadata. The resampled images were processed in Agisoft Photoscan Professional 1.3.2 (Agisoft LLC, 2017). Dense point clouds and orthomosaics were created for each data set using the same settings.

#### 8.3.4 *In-situ* structural complexity surveys

Eight 10 m long underwater transects were surveyed for structural complexity (Crocker, 2017), following the ReefBudget methodology for calculating the carbonate budgets in reef environments (Perry et al., 2012; **Figure 8.3**). These surveys used a tape measure-based methodology to quantify the surface area of the benthic environment over a given single transect distance. This results in both a 2D and 3D distance, of which a ratio can be derived as a measure of structural complexity. A handheld GPS (Garmin GPSMap 64) was used to mark the start and end points of each transect. Given that the position measurements from the GPS are only accurate to several meters, underwater videos (using a GoPro Hero 4) of each transect were used to assist in the georeferencing of the transects so that they appeared in the correct locations in relation to the photogrammetry products.

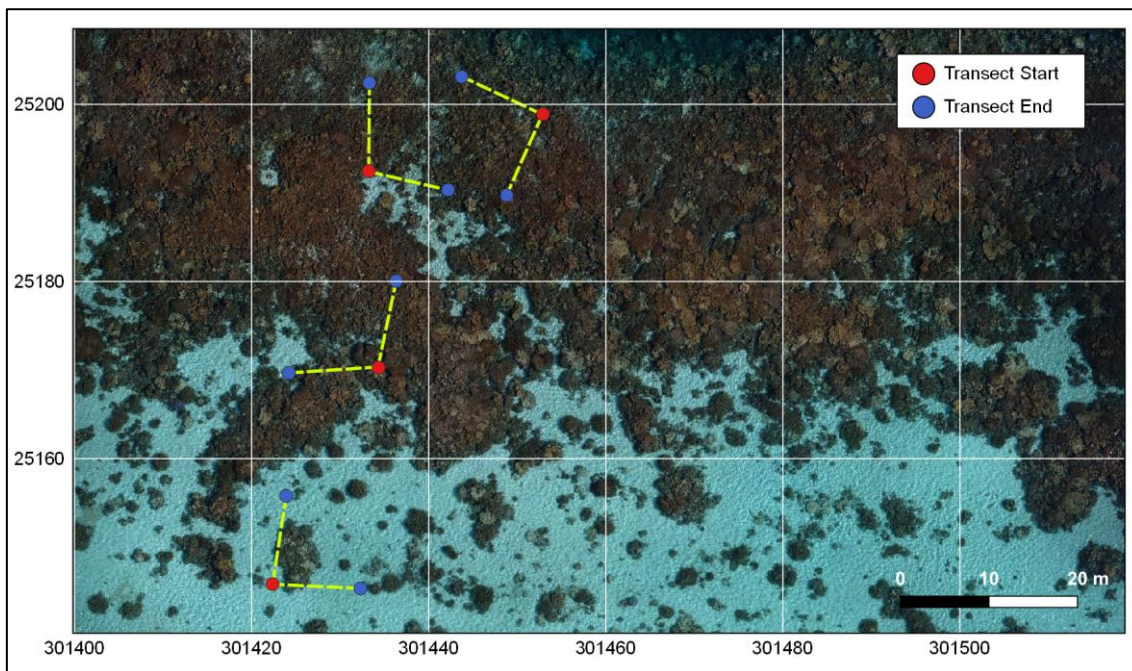


**Figure 8.3: The position of each of the 8 snorkelled ReefBudget transects (yellow lines) within the study system. Orthomosaic created with native 30 m altitude images.**

### 8.3.5 Calculating structural complexity across multiple axes from point clouds

Building on the ReefBudget transect methodology, we sought to automate measurements from the dense point clouds. All data manipulation and extraction was undertaken in R (R Core Team, 2017), using the following packages: ‘data.table’ (Dowle and Srinivasan, 2017) to rapidly read and write point cloud data, ‘dplyr’ (Wickham and Francois, 2016), ‘raster’ (Hijmans, 2015), ‘rgdal’ (Bivand et al., 2017), ‘rgeos’ (Bivand and Rundel, 2017), ‘sp’ (Pebesma and Bivand, 2005) and ‘spatstat’ (Baddeley et al., 2015) to manipulate and analyse point cloud data. To produce structural complexity estimations, the following procedure was applied to the orthomosaic and associated dense point cloud created using only nadir, and nadir & oblique images. Three areas of interest (AOIs) were manually defined (16 × 16 m) by vector polygons, each representing a topographically different part of the reef system (e.g. **Figure 8.4A**). The first

was a lagoon area with a sparse distribution of coral colonies and mainly sandy substrate, the second a mixture of sandy substrate and densely packed colonies, and the third an area with almost exclusively dense coral colonies. The dense point clouds and orthomosaics were then cropped to each of the AOIs. Within each of these 3 AOIs, the following procedures were undertaken. A regular fishnet grid was created over the extent of the AOI at a spatial resolution of 1 m × 1 m (**Figure 8.4B**). This resulted in a vector consisting of 256 square polygon cells. For each cell in the fishnet grid, 4 × 1 m virtual transects oriented to the 8 major compass directions and intersecting the centre point of the cell were created (**Figure 8.4C**). Next, the dense point cloud was sampled at regular points (n=256) along each transect, with the nearest point in *x/y* space in the dense cloud to each point along the transect selected, and the *z* coordinate recorded. Once 256 *z* values had been extracted for each virtual transect, the total 3D distance between each consecutive point was calculated. Given that the length of the transect is known (1 m planar distance), equation 1 was used to calculate the difference between 2D and 3D surface (structural complexity) along each transect:

$$\text{structural complexity} = \frac{3D \text{ transect distance}}{\text{planar distance}} \quad (1)$$

The mean structural complexity value of the four transects was then used as the overall complexity value for each cell in the fishnet grid. Building on this technique we sought to calculate the structural complexity of different morphometric types (hereafter called cover classes) within the AOIs. The following was applied to the nadir dataset only. Using the orthomosaics cropped to the AOIs, cover classes were manually delineated in QGIS (QGIS Development Team, 2018). Six classes

were defined: branching coral, compact branching coral, massive coral, plating coral, sand and other coral. Cover classes that could not be confidently assigned one of the morphometric types or sand, were assigned as other coral. Once delineated, each of these classes were saved as vector polygons (**Figure 8.4D**). One AOI at a time, each cell in the fishnet grid was selected and used to crop out the relevant cover classes in that cell (**Figure 8.4E**). For each continuous segment of cover class within that cell, the centre point was located, and 4 virtual transects following the 8 major compass directions were used to extract points from the dense cloud (**Figure 8.4F/G**). The same technique as described for the non-cover class approach was used to produce structural complexity estimations (using equation 1), but this time for each cover class segment within each cell of the fishnet. Due to the irregular shape of cover class segments, the length of transect lines within them varied (e.g. **Figure 8.4F/G**) and therefore proportional structural complexity was calculated for each transect considering the total length of transects within each segment (rather than a mean of each transect, which is only feasible when transect lengths are equal). This resulted in a structural complexity estimation per cover class segment, per cell (of fishnet), per AOI.

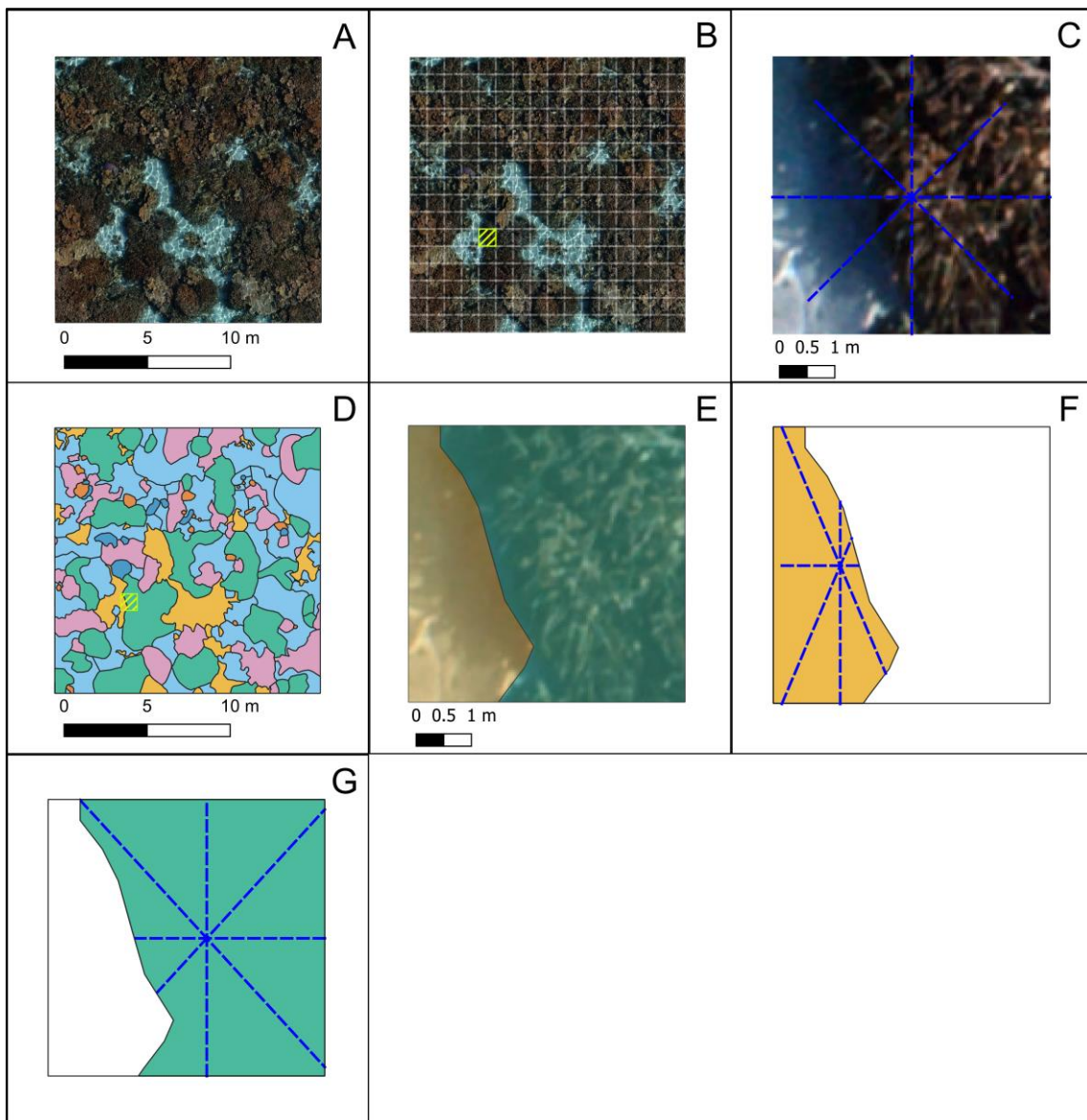


**Figure 8.4: The calculation of point cloud structural complexity from dense point clouds. This figure shows a conceptualized version of the methodology in 2D, whereas the extraction of data came from the dense point clouds. A) The mixed reef AOI subset from the whole orthomosaic. B) 1 m × 1 m fishnet grid overlaid on AOI orthomosaic with a single cell highlighted in yellow. C) 4 × 1 m transects oriented to the 8 major compass directions overlaid on the orthomosaic cropped to the extent of the yellow cell in B. D) Manually delineated cover classes for the whole mixed reef AOI, with the single cell identified in B, highlighted in yellow. E) 2 cover classes located within area cropped to the extent of the yellow cell in D. F + G) 4 transects oriented to the 8 major compass directions intersecting the centre point of a cover class segment, cropped to the boundaries of the segment.**

### 8.3.6 Collating published rugosity values

We sought to compare structural complexity estimations to published rugosity values at the colony scale. Given the similarity of morphometric types of colonies within the Indo-Pacific region, estimated rugosity values were gathered from published sources that reported rugosity values. Scientific literature was provided using the expertise of author CP and also through searches of web of science using the terms “coral”, “rugosity”, “measurements”. Published data in this format is very limited and our results show the total obtained from a basic collation of this information.

### 8.3.7 Zoning and areal measurements of the reef environment

Using an orthomosaic (~0.5 m spatial resolution) which included Kandahalagala reef in its entirety within QGIS (QGIS Development Team, 2018) three zones (matching aforementioned AOIs: lagoon, mixed, dense reef) were manually delineated and saved as vector polygons.

## 8.4 Results

### 8.4.1 Drone flights and photogrammetry data products

During the nadir flight at 30 m altitude, 331 useable images were captured, and for the flight with the oblique mount 338 useable images were captured. Orthomosaics, DEMs and point clouds (e.g. **Figure 8.5**) were created using the nadir only dataset and also with the addition of the oblique images. The dense point cloud created with nadir images contained 12,902,413 points, which increased to 12,941,612 when oblique images were added to the photogrammetry process. The nadir only orthomosaic was produced at a spatial

resolution of 7.82 mm pixel<sup>-1</sup> and the combination of nadir and oblique images resulted in a spatial resolution of 8.13 mm pixel<sup>-1</sup>. For the 220 m altitude flight covering the whole reef system, 231 images were captured, and a resulting orthomosaic with a spatial resolution of 57.8 mm pixel<sup>-1</sup> was produced. In relation to research question 1, visible inspection of the DEM and dense point clouds produced with the nadir images (**Figure 8.5**), it is evident that drone-based SfM-MVS data is capable of capturing changes and variation in submerged reef topography, with an elevational range from -0.54 m to 0.98 m.

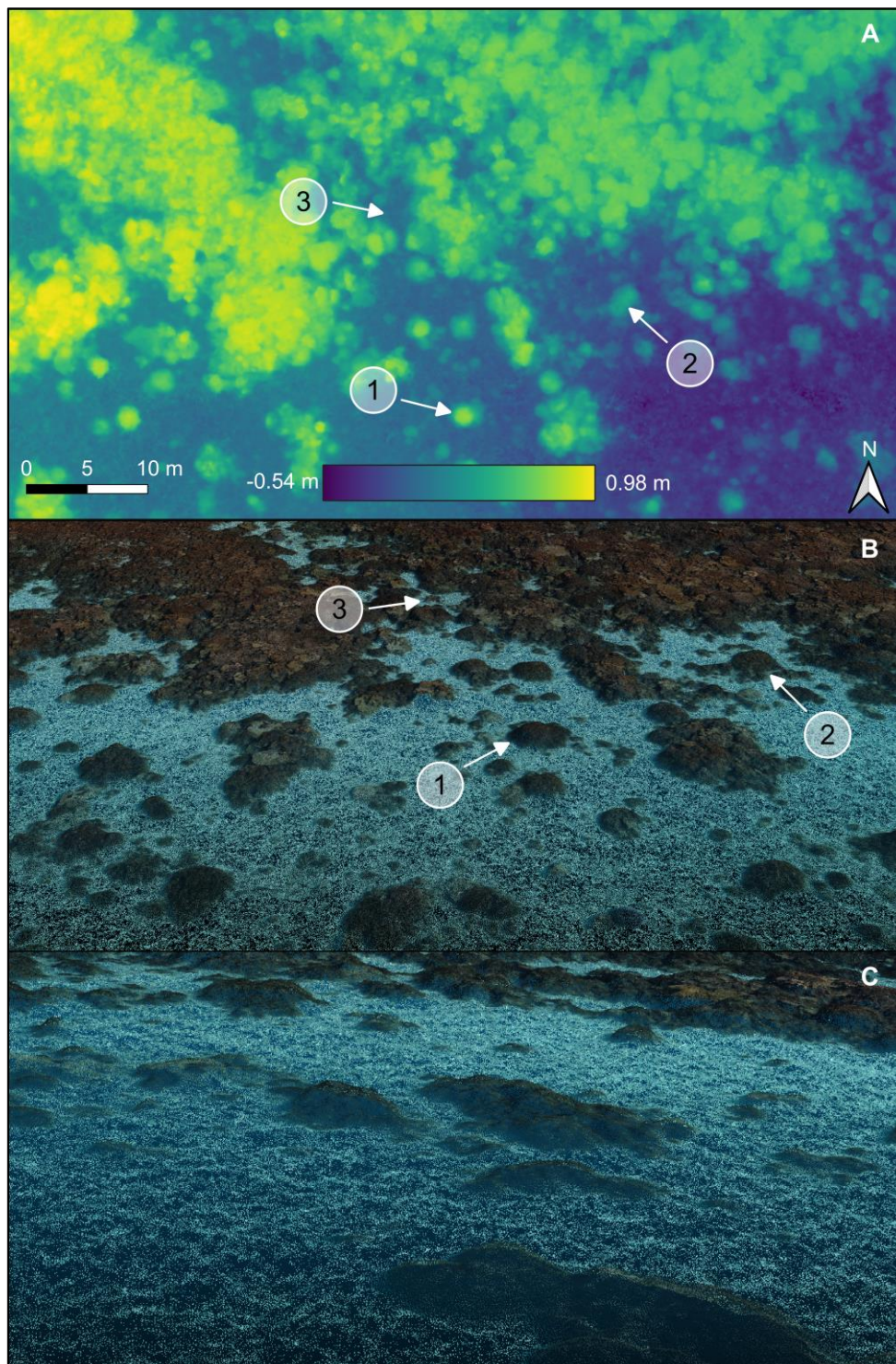


**Figure 8.5: Example photogrammetry data products using nadir images captured at 30 m altitude. A) Subset of the DEM. B) Screenshot of the point cloud with a similar extent to A. C) An example of structure in a dense point cloud over sandy substrate Note view of point cloud captured at an angle to help visualise z-axis differences in B. 1) Shows an example of an individual coral bommy, 2) A set of structures with varying topography, surrounded by sand and 3) A shallow sandy area surrounded by coral structures.**

#### 8.4.2 Structural complexity variations across simulated altitudes/ground sampling distance

The native resolution of images captured at 30 m altitude was ~16 megapixels. When resampled, this decreased to approximately 10, 5 and 2.5 for 50, 100 and 200 m simulated altitudes respectively (**Table 8.1**). The resulting differences in ground sampling distance obtained after processing the images can be seen in **Table 8.1**.

**Table 8.1: Image dimensions for resampled photographs used to simulate variation in altitude.**

Altitude	Image Width (pixels)	Image Height (pixels)	Approx. megapixels	Ground Sampling Distance (mm pixel <sup>-1</sup> )
30 m (native)	4928	3264	16	7.9
50 m	3080	2040	10	13.1
100 m	1540	1020	5	26.3
200 m	770	510	2.5	52.6

Changes in point clouds across different simulated altitudes were measured in the three areas of interest (AOI; lagoon, mixed and dense reef; **Figure 8.6**) using nadir images only. Point clouds reduced in density as image pixel size (simulated altitude) increased. Between 30 m and 50 m the number of points reduced on average by 54%, with the mixed AOI seeing a much greater reduction of 71%. Further decreases are apparent as image resolution decreases, with an average (across subset areas) of 8% of points in the 100 m cloud compared to clouds

created at the native 30 m resolution. Very sparse point clouds were produced at the simulated 200 m altitude with the lowest number of points found in the mixed subset area (n=4467; **Table 8.2**).

**Table 8.2: Total count of points from dense point clouds constructed with native and resampled images in Agisoft Photoscan. NA present in 200 m data as mosaicking did not produce a sufficiently dense point cloud product to cover the whole area of interest.**

	<b>Altitude</b>							
<b>AOI</b>	<b>30 m (Native)</b>		<b>50 m</b>		<b>100 m</b>		<b>200 m</b>	
	<b>Nadir</b>	<b>Nadir+Oblique</b>	<b>Nadir</b>	<b>Nadir+Oblique</b>	<b>Nadir</b>	<b>Nadir+Oblique</b>	<b>Nadir</b>	<b>Nadir+Oblique</b>
Lagoon	172035	189481	98783	83149	16828	15141	6049	6646
Mixed	303518	199170	90166	102688	19221	14317	4467	NA
Reef	184512	266330	93734	104635	16009	13510	5307	878

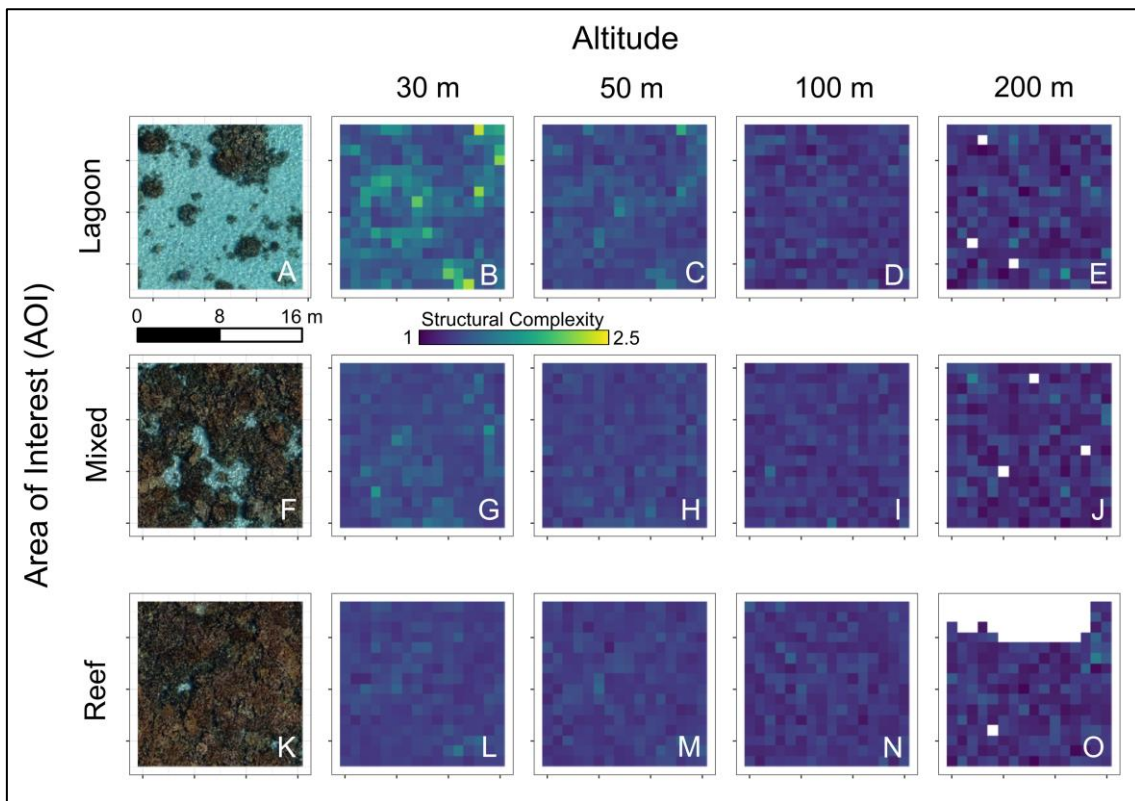


**Figure 8.6: Orthomosaics of subset areas and associated structural complexity calculations on point clouds created with different resolution (resampled altitude) images. Calculated using a 1 m<sup>2</sup> grid over each area of interest (AOI).**

Generally, measures of structural complexity (see Equation 1) decreased as altitude increased, and at 200 m altitude in all AOIs, erroneous measures below 1 occurred indicating too few points available to sample in the point clouds (white pixels in **Figure 8.6**), identifying the most coarse spatial resolution for this methodology. At the native resolution of 30 m the mean structural complexity (see equation 1) across all three AOIs was 1.38. Also, at the native resolution, complexity was greater in the lagoon AOI compared to the mixed and dense reef AOIs, with the same applying to 50 m resolution but not for 100 m and 200 m resolutions (**Figure 8.6, Figure 8.7**). The areas with highest structural complexity estimates were over sandy substrate and at the edge of the coral colonies

(Figure 8.6B/G). The magnitude of erroneous values was far greater in the reef AOI at 200 m resolution than the other parts of the reef (Figure 8.7).

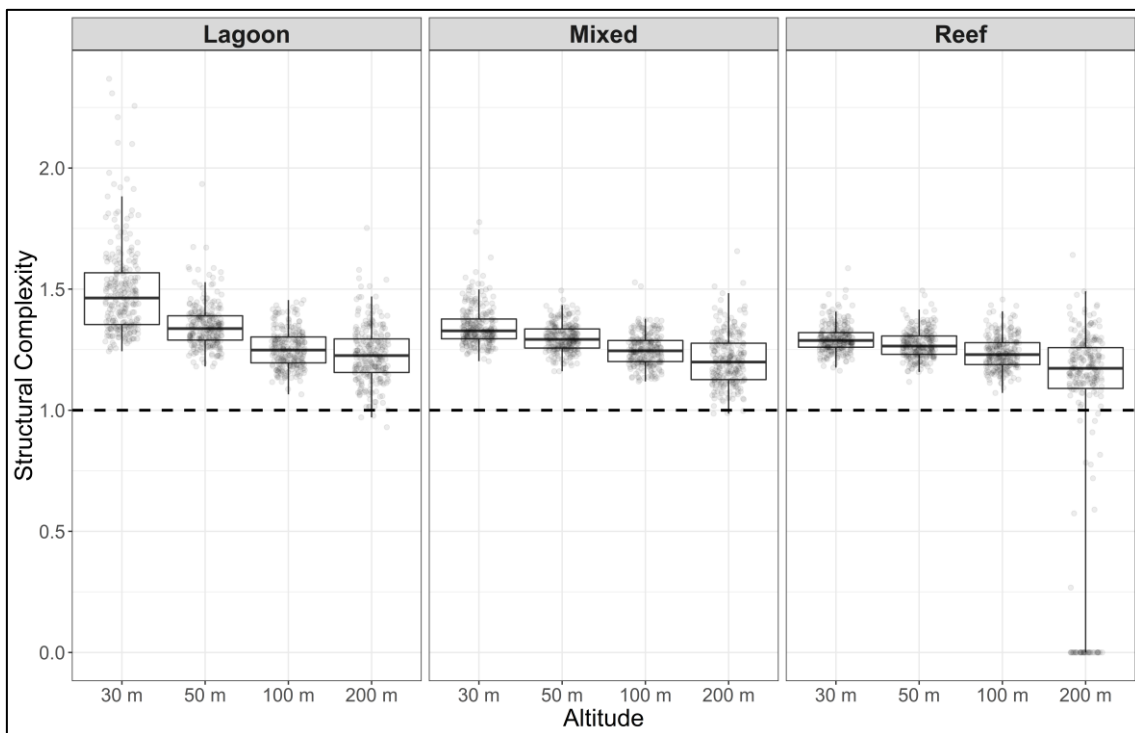


**Figure 8.7: The distribution of structural complexity (see Equation 1) calculations across native and resampled altitudes in each subset area. Values below 1 are erroneous, representing virtual transects with too few data points in the dense cloud. Central lines in boxes represent median, upper and lower bounds of boxes represent 0.25 and 0.75 quantiles respectively and ends of whiskers represent 0.05 and 0.95 quantiles.**

#### 8.4.3 Comparing point clouds made with and without oblique image data

The dense point cloud constructed with data from only the nadir survey had a similar total point counts to the cloud constructed with the addition of oblique images (see section 8.4.1 for details). These datasets were explored in relation to research question 3. Gridded structural complexity estimates were calculated across the 3 AOIs using the native 30 m altitude images. In the lagoon AOI, structural complexity estimates were generally greater when only nadir images were used (Figure 8.8). For the mixed and reef subset areas, calculated

structural complexity differed spatially, but were not as great as measured in the lagoon subset (**Figure 8.8**). The number of points within the dense clouds were similar in the lagoon AOI but differed greatly in the mixed and dense reef AOIs. At the native 30 m resolution, in the mixed AOI, there were ~52% more points without the inclusion of oblique image data, whereas there were ~30% fewer points in the dense reef AOI (**Table 8.2**).

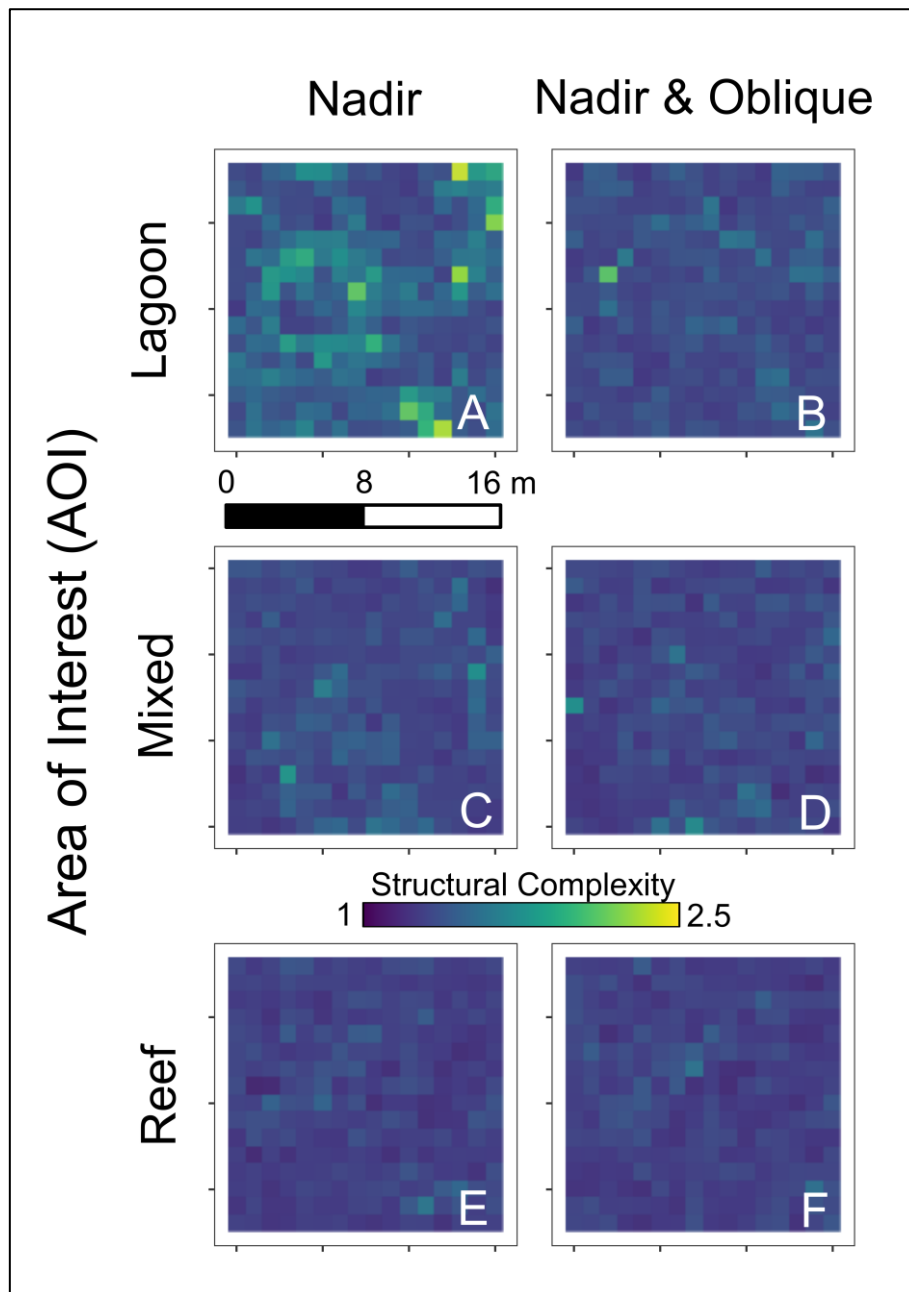


**Figure 8.8: Surface structural complexity calculations (see Equation 1) derived from dense point clouds created with 30 m altitude images using both nadir only and nadir & oblique images. Difference estimations calculated using 1 m<sup>2</sup> grid for each AOI.**

#### 8.4.4 Comparing point cloud derived structural complexity to literature derived rugosity values

Literature searches for rugosity values at the colony scale and for benthic sand cover classes revealed that sand has a measured rugosity of 1.05 and massive corals have the greatest of the morphometric types explored in this study with a value of 2.3 (**Table 8.3**). Manually delineated cover classes show that in the lagoon AOI, sand was the most dominant cover type (71% of total cover; **Figure 8.9B/G**). In the mixed AOI, other (unidentified) morphometric types were most dominant (38% of total cover), followed by branching morphologies (29% of total cover; **Figure 8.9D/H**). Major cover classes in the reef subset area were branching corals (39%) and plate type corals (32%; **Figure 8.9F/I**). Structural complexity estimations across the 3 AOIs were combined for each of the six cover classes (**Figure 8.10**). The mean surface difference values were similar across all cover types (1.17-1.27) except for sand which had a mean of 1.39 (**Figure 8.10**).

**Table 8.3: Literature derived rugosity estimates. \*Mean taken of small and medium massive rugosity values.**

Cover Type	Rugosity Value	Source
Branching	2.25	Knudby and Ledrew (2007)
Compact Branching	1.8	Knudby and Ledrew (2007)
Massive	2.30	Figueira et al. (2015)*
Other	mean of other coral classes	NA
Plate	1.50	Figueira et al. (2015)
Sand	1.05	Knudby and Ledrew (2007)

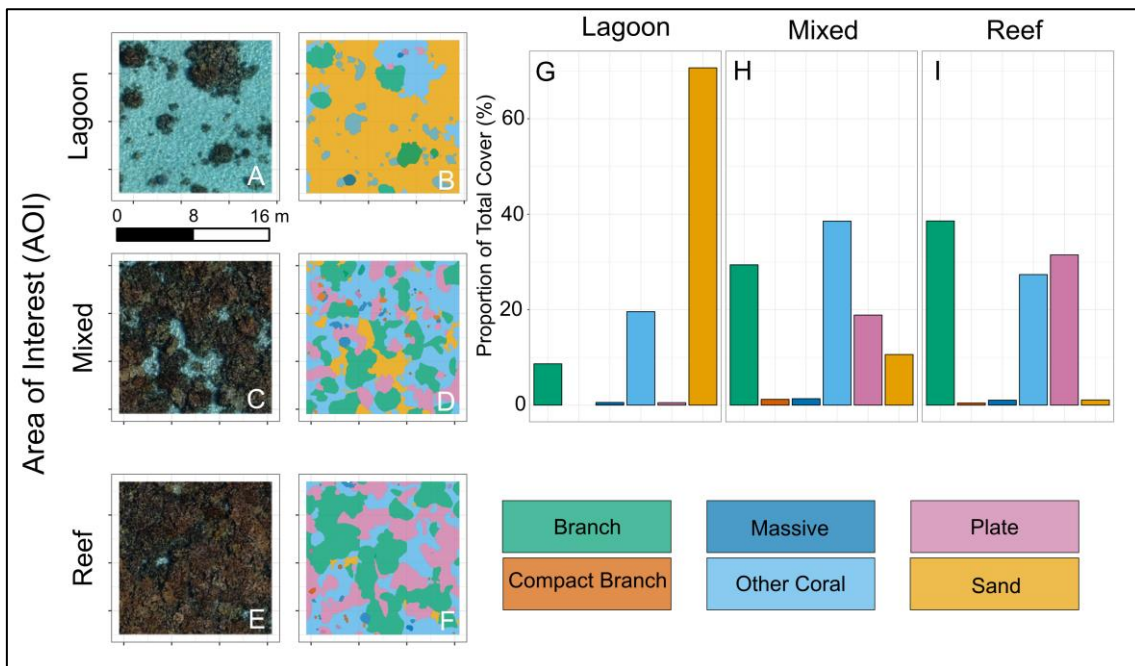


**Figure 8.9: Thematic maps showing cover classes in each AOI, and associated distributions. A-F) Cropped orthomosaics and associated manually delineated cover classes. G-I) Proportion of each cover class found within each of the AOIs.**

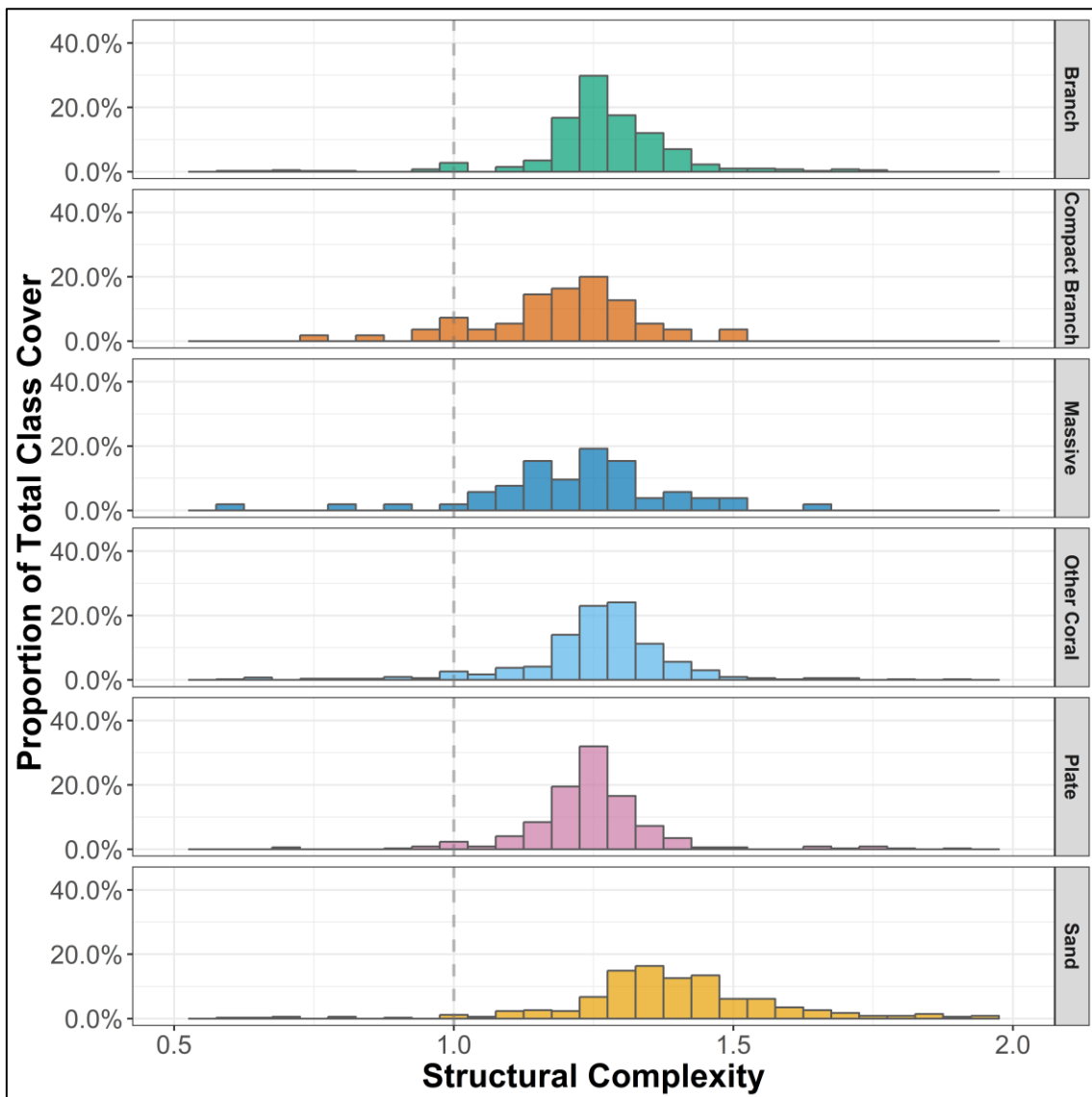


**Figure 8.10: Distribution of estimated structural complexity for all cover/morphometric types from the 30 m native point cloud. Data shown are a sum across each of the three AOIs.**

#### 8.4.5 Scaling up with whole reef system zonation

Combining the proportion of cover classes in each of the AOIs (**Figure 8.9**) with mean structural complexity values derived from dense point clouds (**Figure 8.10**) we produced structural complexity values per AOI. These were calculated as 1.35 for the lagoon, 1.26 for the mixed and 1.25 for the reef. In comparison, literature derived estimations were also used to produce a single structural complexity

value (incorporating proportion of cover classes) for each AOI. These values were 1.35 for the lagoon, 1.88 for the mixed and 1.93 for the dense reef.

Across the whole of Kandahalagala reef, lagoon was the most prominent of the three delineated zones, encompassing ~46% of the total mapped area (**Figure 8.11**). The dense/outer reef zone covered ~32% of the reef system and the mixed area covered 21% (**Figure 8.11**). A final combination of the whole reef zone estimations and single AOI complexity estimations was made to produce a single whole reef complexity estimate based on both dense cloud and literature derived values. These were 1.3 (cloud) and 1.65 (literature).

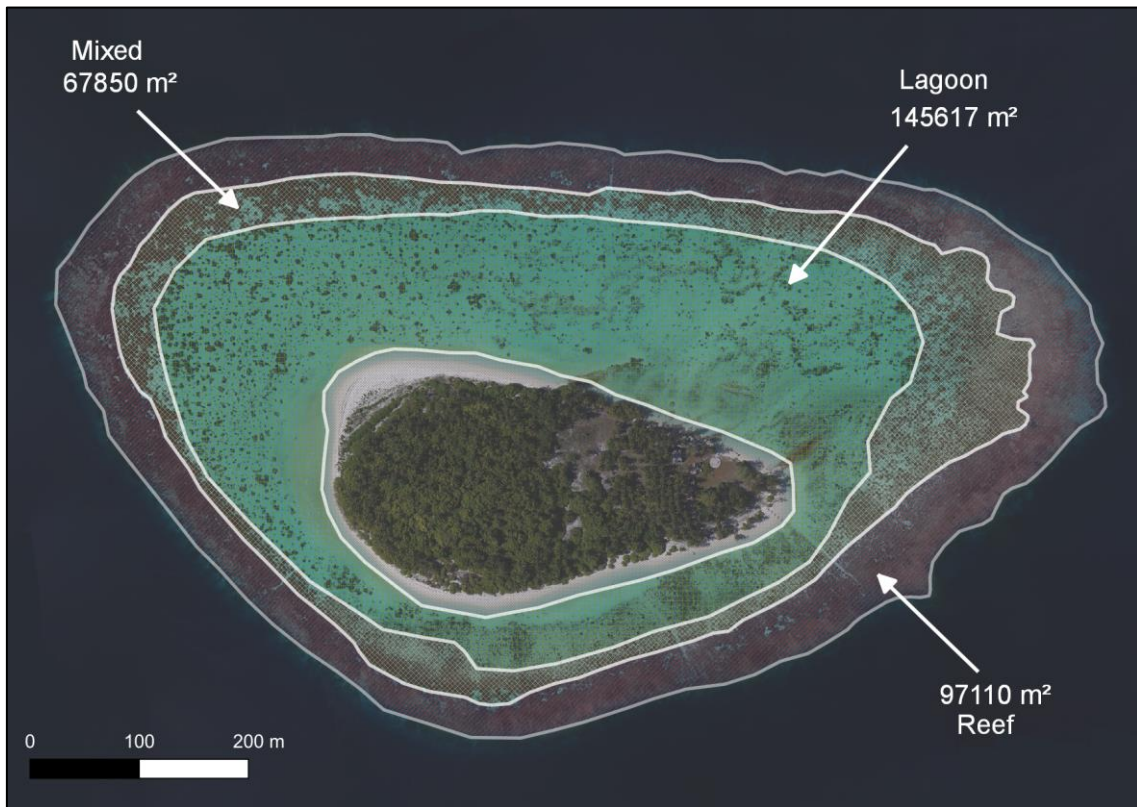


**Figure 8.11: Kandahalagala island reef system and manually delineated zones.**

#### 8.4.6 Comparing *in-situ* transects to point cloud derived structural complexity estimations

Structural complexity estimations derived from the ReefBudget surveys (**Figure 8.4**) varied between 1.16 and 2.53. In comparison, the values obtained from 2D/3D difference calculations (see section 8.3.4) on the dense point clouds generally yielded much lower values. For the native 30 m altitude dataset, one transect produced similar values with both methods (*in-situ* = 1.24 & cloud derived = 1.25), whereas for all other transects, the point cloud method were underestimates compared to the *in-situ* method (**Figure 8.12**). The relationship was similar for all altitudes, except for the resampled data at 100 m, where for one transect the point cloud structural complexity was greater than the *in-situ* measurement (**Figure 8.12**). For the 200 m data, four of the transects were not sampled due to insufficient points in the cloud (**Figure 8.12**).

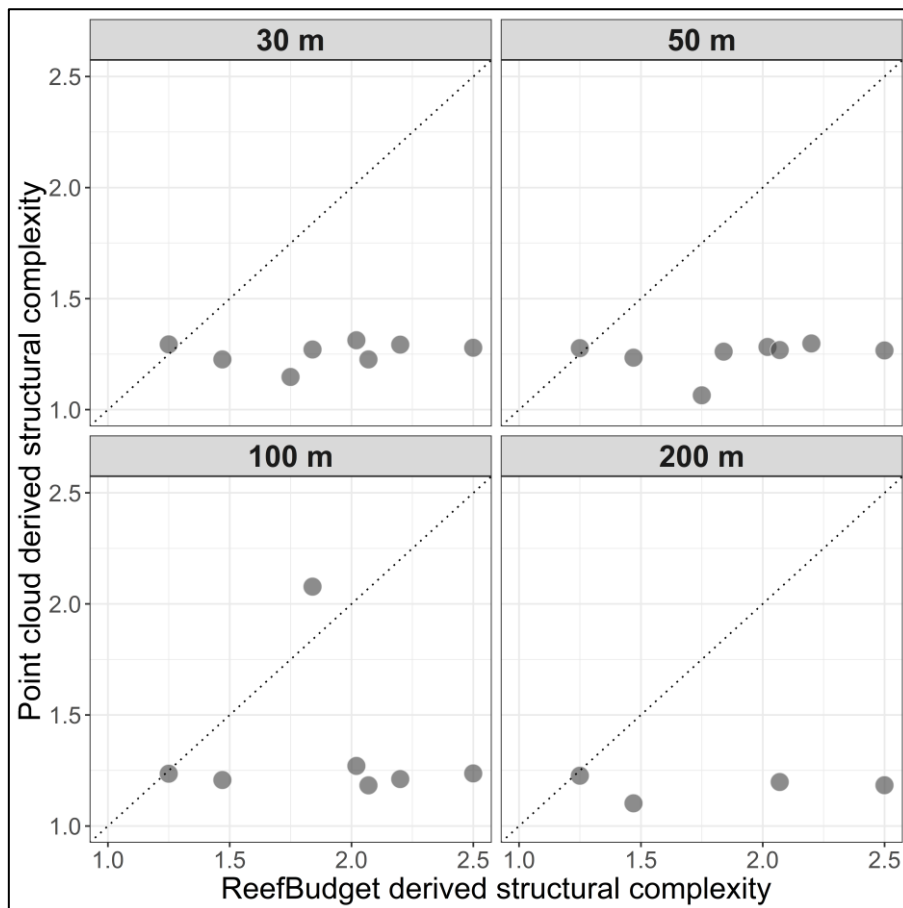


**Figure 8.12: Comparison of structural complexity calculations over 10 m transects using data collected from ReefBudget transects, and values derived from dense point clouds.**

## 8.5 Discussion

As several authors recently have evidenced (e.g. Johnston, 2019; Ventura et al., 2018; Westoby et al., 2018), drone technology shows great promise for the monitoring of many coastal environments by virtue of its flexible deployment capabilities (e.g. user dictated revisit times and GNSS-enabled aerial positioning). With regards to tropical coral reefs, very little work has been done to explore, quantify and characterise the capability of drone-based proximal sensing techniques to deliver measurements of the benthic topography. Due to this lack of application of drones in reef environments, there is a deficiency of understanding in how to quantify structural complexity of reef systems with optical

data collected with drone platforms. Here we have described multiple approaches to measure the structural complexity of tropical reefs using drone-acquired photographic data and SfM-MVS processing techniques. Overall, we found that virtual transects capturing structural complexity measurements can be applied to point clouds to produce proxy measurements of structural complexity. As expected, we found that data captured at 30 m altitude with a 16MP resolution optical sensor, produced more diverse measurements of topographic variation, and coarser resolution resampled images performed more poorly in this regard. We also found that generally, complexity measurements from point clouds for different cover classes/morphometric types were not directly comparable to *in-situ* measurements describing reef rugosity reported in the literature. However, this methodology shows promise, in that it can detect some level of structural variation in the benthic environment. With image data collected in more suitable conditions (where water surface movement is minimal), or corrected image data there is a possibility more representative structural complexity measures could be derived from dense point clouds.

#### 8.5.1 Building on existing published work

To our knowledge, there is only a single peer-reviewed piece of work investigating the ability of drone-derived image data and SfM-MVS processing to measure the structural complexity of tropical coral reef environments. The work by Casella et al. (2017) focussed primarily on bommie dominated lagoon areas of the coral reef ecosystem. They showed that when comparing drone derived DEMs to LiDAR data, there were z axis differences ranging from -1.4 to 1.4 m with a standard deviation of 0.45 m.

The work we have presented here builds on this pioneering work in several ways. Firstly, we explore methodological variation in both the resolution of the photos and the position of the sensor during data capture (exploring nadir and oblique positioning). Secondly, we investigated SfM-MVS measurements in other parts of the reef (with differing densities of coral structures (**Figure 8.6**). In these AOIs (in this manuscript referred to as lagoon, mixed and dense reef), our estimates of structural complexity were largely similar regardless of the type of cover found within the measured areas. The lagoon subset area did show detectable differences between hard structures and sandy substrate, although some of this was driven by artefacts in the data (**Figure 8.6**). Within areas of sandy substrate some points in the dense point cloud exhibited greater z values than the neighbouring points, which meant that when virtual transects were used to calculate structural complexity, the 3D distance measure was erroneously large. Given that the published rugosity of sandy substrate is 1.05 (**Table 8.3**) one would expect the 3D distance to be similar to the 2D distance over sandy areas. A likely reason for these erroneously elevated z values could be a result of dynamic patterns caused by movement of the water's surface (**Figure 8.13**). The position of these patterns varies between images, creating issues during the tie point stage in the photogrammetry workflow, as the feature (i.e. the white lines) positions vary in space over time. We consider that the conditions during data acquisition were optimum (like those in Casella et al. (2017)), with minimal wind and wave disturbance and low sun angles. However, we still find that in deeper sandy substrate areas, these artefacts are a prominent feature, unlike the exceptional 'millpond' like conditions presented in Casella et al. (2017). These concentrated light patterns (caused by surface movement on the water) can cause the SfM-MVS processing to incorrectly characterise the benthic structure

in these particular parts of the reef environment (e.g. **Figure 8.5C**). An example of these features can be seen in **Figure 8.13**.

These differences highlight the potential limitations of the technique. Firstly, there is an indication that weather conditions must be optimal in order to achieve data useable for SfM-MVS processing, and secondly, the technique may only be suitable for areas with certain topographic traits (i.e. bommy dominated lagoon areas) as opposed to areas with higher percentages of coral cover.



**Figure 8.13: Subset of a single image captured from ~30 m altitude over a mixture of sandy substrate and hard coral structures.**

### 8.5.2 Variations in ground sampling distance and the addition of oblique image data

As it was unfeasible to position ground control points (GCPs) and measure them with a high-accuracy (sub-decimeter) GNSS device, the native images captured at 30 m resolution were resampled to coarser resolutions so that multiple point clouds could be constructed with the same spatial positioning. We sought to investigate at which altitudes structural complexity estimations deteriorated and whether there was an optimum ground sampling distance where point cloud density wasn't compromised. Contrary to a similar investigation in a terrestrial forest system (Fraser and Congalton, 2018) where optical data captured at 100 m yielded similar cloud densities to data captured at 50 m, we found large reductions in point cloud density as altitude/ground sampling distance increased (**Table 8.2**). Although our data consisted of resampled images, our results indicate that finer spatial resolution data may be required as an input to the photogrammetry workflow to more accurately represent topographic variation in the resultant point clouds.

The inclusion of oblique image data has been shown to improve the quality of topographic models produced in a photogrammetry workflow (James and Robson, 2014). Our rationale in this study was that structurally complex tropical reefs contain topographic features such as overhanging structures that cannot be fully captured in nadir images. Increasing the number of viewing angles of a given feature should aid in resolving its full structural dimensions in a point cloud. This has been demonstrated with images captured during *in-situ* snorkel surveys of individual coral bommies (Raoult et al., 2017). The similarity in overall point cloud counts (considering the inclusion and exclusion of oblique images) is likely a

result of settings in Agisoft Photoscan. However, when focussing on the AOI, the ~45% increase in the number of points within the dense reef area, shows that more features were matched in the SfM-MVS process with the inclusion of oblique images. We therefore recommend that off-nadir images are a valuable addition when creating topographic reef maps with this methodology. Furthermore, moving a sensor to an off-nadir position when capturing images over water has been shown to reduce glint in the resulting data (Joyce et al., 2018), which in turn should increase the number of tie points associated with submerged features, rather than artefacts on the waters surface.

### 8.5.3 Differences between morphometric types/cover classes

Our results show that the structural complexity calculations result in similar values for all morphometric types analysed (**Figure 8.10**). It may be that this technique is only suitable for certain types of corals, and it could potentially be focussed on key, more easily identifiable parts of the reef ecosystems. For example, tabular corals are thought to constitute keystone structures for fish on reefs (Kerry and Bellwood, 2015), and therefore monitoring their size or presence/absence could be a useful management tool. Our results show that contrary to the published literature, the mean structural complexity estimation for sand (1.39) was the highest out of all cover classes measured (**Figure 8.10**). This is most likely due to patterns caused by movement in the water's surface (discussed in section 8.5.2). Water column correction is a long-standing issue in coral reef remote sensing using satellite and airborne images (Zoffoli et al., 2014) and continues to remain a barrier to successful data collection with drones. However, promising developments are being made to correct distortions by utilising multiple frames

from video footage rather than still images to filter out obscure values caused by motion in the water (Chirayath and Earle, 2016; Partama et al., 2018).

Orthomosaics created with a photogrammetry workflow as shown in this study, provide a wealth of spectral information about the tropical reef environment. Morphometric types, families and species of corals can be identified from such data if spatial resolution and sea conditions are suitable during data capture (see section 8.4.4). As is evident in the subset areas presented in this work, a lot of the coral structures on Kandahalagala reef are in poor condition, having suffered multiple bleaching events in recent years (Perry and Morgan, 2017a, 2017b). Spectrally, this makes them less distinct due to the expulsion of living algae from their carbonate structures, leading to homogenous grey and brown cover across the reef environment. Drones have been used to assess the extent of bleached coral cover on reefs (Levy et al., 2018), but the lack of diversity in the spectral domain makes it difficult to undertake analyses such as object-based image analysis (OBIA), which has been utilised with satellite derived optical imagery in reef environments (Roelfsema et al., 2013). A more spectrally diverse environment (i.e. with healthy corals) will likely be much better suited for investigations utilising techniques such as OBIA, but also for photogrammetry based point cloud generation. The SfM-MVS methodology partially relies on spectral information, and having a greater spectral diversity could aid in the scene reconstruction process.

#### 8.5.4 *In-situ* transects

ReefBudget transects have been used to estimate the rugosity of reef environments, to then be used in further carbonate budget calculations (Perry et

al., 2012). Typically, a series of parallel 10 m transects are swum (by snorkellers or scuba divers) and the cover type (e.g. sand, coral species/type, algae cover, encruster) along with the distance covered (using a flexible tape measure) for each 1 m segment. These surveys can provide rich information on the biodiversity found within the reef as well as the health of particular parts of the ecosystem. However, due to the costs involved, time taken to survey and requirement for trained staff, these surveys are limited in their spatial extent and therefore unrepresentative of the wider reef environment. Furthermore, biases in the identification of cover types/species and the way in which structures such as overhangs or branches are measured can affect reproducibility – a critical component of monitoring programs. Proximal sensing and associated established processing pipelines can reduce the negative impacts of these biases, by scaling up structural complexity measurements. However, that is not to say *in-situ* transect surveys are not required. For every drone survey validation is required in order to understand the quality of the data collected. In an ideal world, these two techniques would be employed in tandem, where proximal sensing techniques provide data on larger spatial extents, underpinned with *in-situ* data from select areas of the reef environment. Furthermore, multi-dimensional *in-situ* data would make more suitable validation data for point cloud based analysis. For example, multiple transect measures over a section of reef (e.g. 5 × 5 m), as opposed to single line transects (as seen in the ReefBudget methodology).

#### 8.5.5 Future work

Future work could focus on a fusion between aerial data captured by drone platforms and *in-situ* underwater image data. This could provide an improved way

to measure structural complexity, particularly in areas with steep vertical variation and overhanging features (Goatley and Bellwood, 2011). SfM-MVS has been used to map marine vertical structures (Robert et al., 2017) and with enough overlap could be combined with data captured from the air. Furthermore, metrics such as structural complexity shown in this study could be combined with ecological datasets describing abundance and diversity of reef dwelling organisms. This has already been demonstrated on intertidal reefs using drone-derived optical data (Murfit et al., 2017). Alternatively, with large and diverse enough sample sizes, one could potentially establish modelled relationships between the surface planar area of individual morphometric types of coral, and the 3D distance. Both of these measurements could be collected *in-situ* and grouped by morphometric type (e.g. tabular corals) and by region (e.g. the Indo-Pacific). Given that estimates of surface planar area can be obtained from photogrammetry data products such as the georeferenced orthomosaic, one could potentially infer what the structural complexity is using the modelled relationship between the two measures. Ferrari et al. (2016) found a linear relationship between underwater SfM derived rugosity and traditional chain and tape measures of structural complexity. Future work should continue trying to establish a relationship using drone derived SfM-MVS data products over greater spatial scales than is achievable in snorkel surveys.

## 8.6 Conclusions

Given the degrading state of tropical coral reef systems in many places globally (Hughes et al., 2018), it is imperative to develop cost-effective ways to track changes in these ecosystems over time. Drones offer a flexible data collection technique that can be employed in often remote and logistically challenging

environments (Joyce et al., 2018). The ability to remotely sense an ecosystem when environmental conditions are optimal (i.e. low sun angles and minimal wind) makes drone technology a promising technique for monitoring shallow tropical reef systems. Furthermore it is a minimally invasive technique (Reichert et al., 2016) causing little disturbance within the reef environment. The data produced in SfM-MVS workflows is also rich and can be manipulated and analysed in many ways. For example, a multitude of structural complexity measures can be obtained (Leon et al., 2015) at user-defined spatial scales (Yanovski et al., 2017).

This study also highlights a shortfall in published data of rugosity estimates at the colony level. With increased availability in these data, the feasibility of this technique can be better tested and across a greater variety of morphometric types. An increase in the availability of such validation data will help further test the feasibility of using proximal sensing with drones and consumer grade cameras to calculate estimations of reef structural complexity.

## 9 Discussion

This thesis has detailed multiple new contributions to scientific knowledge regarding proximal sensing of coastal environments using lightweight drones and kites. Each of the empirical studies detail pioneering methodologies namely i) utilising kites and consumer grade cameras to track fine spatial scale changes in dune structure over time, ii) measuring within-meadow variation of intertidal seagrass with a lightweight drone and consumer grade camera and iii) testing the effect that variation in flight planning attributes has on the ability to measure structural complexity within coral reef environments. Each of these empirical chapters contains its own detailed discussion. This chapter highlights the main findings, and discusses common themes emerging across the chapters, and the challenges and opportunities that potentially lie ahead for proximal sensing in the coastal environment.

### 9.1 Research aims

The overarching aim of this thesis (as stated in chapter 2) was **to develop new approaches using novel proximal sensing platforms such as lightweight drones and kites, that could deliver advances in the quantitative understanding of coastal processes**. This aim was primarily answered through empirical investigations within three key coastal ecosystems (dunes, intertidal seagrass and tropical coral reefs), each of which involved primary data collection and analysis. The more focussed aims relating to each chapter were to:

- (4) Evaluate the challenges of operating drones in demanding environments

- (5) Review and assess the role of kites as an environmental monitoring tool
- (6) Assess topographic changes in coastal dunes using kites and SfM-MVS
- (7) Map within-meadow intertidal seagrass coverage using lightweight drones
- (8) Quantitatively measure structural complexity of coral reefs using drone derived data

The proceeding sections will cover general remarks (with methodological considerations drawn from the thesis as a whole), followed by discussion of each empirical chapter. Lastly, I provide thoughts and opinion on the future of proximal sensing technology.

## 9.2 General remarks

Coastal environments and their associated processes are hugely diverse, each presenting a range of possible research questions and methodological challenges. The coastal zone has provided a well-suited proving ground for kites and drones to test methodologies and ultimately advance the understanding of coastal processes.

### 9.2.1 Drones and kites – different platforms for different situations

Drones and kites possess different attributes that make them advantageous for collecting fine grained remote sensing data at the land-sea interface. Some of these attributes have been demonstrated within the empirical work in this thesis (chapters 6, 7 & 8). For example, the absence of moving or mechanical parts makes kite platforms well suited for sandy environments, whereas the

autonomous nature of lightweight drones makes them well suited for capturing data from areas difficult to access on foot, such as soft substrate in intertidal seagrass meadows. The drone is a more flexible proximal platform and will often be the first choice over alternatives such as kites, blimps or balloons, given their ease of use. However, kites lend themselves as a useful backup platform to drones owing to the ease in which they can be transported and their low cost. As shown in chapter 6, where data collected from both drones and kites was compared, drone derived point clouds exhibited greater precision than the comparison kite dataset. However, the precision estimates for the kite derived data were still suitable for the tracking of dune structural change. This demonstrates the clear need to assess which proximal platforms are suitable for particular research questions or monitoring programs.

### 9.2.2 The coast as a 'natural' laboratory

As described at the very start of this thesis, globally, many people live within and use the coastal zone, both economically and recreationally. While there remain many remote and uninhabited coastal areas which are well suited for studying coastal processes and anthropogenic influence in a natural setting, it is not always financially or logistically feasible to conduct research in these areas. I found this especially during the empirical studies at St. Gothian dunes and intertidal seagrass meadows in Pembrokeshire, where I had to navigate interactions with stakeholders. These ranged from asking beachgoers to relocate so that they did not appear in captured images, to informing the management of oil refineries of intentions to map seagrass near their infrastructure. The simple occurrence of these interactions indicates the intertwine of the natural environment with human activity. This raises two questions. Firstly, how

representative are the choices of study system for coastal studies? And subsequently are certain locations chosen for their 'ease of study' or absence of human activity? Decisions surrounding the location of study systems are dictated by multiple factors including the research questions being posed and the logistical feasibility of undertaking research in that particular place. A key component of study design should include consideration of how representative chosen study systems are.

### 9.2.3 Integrating proximal sensing with other remote sensing data products

Integrating proximal sensing data with satellite and airborne remote sensing data products could provide new insights and potential scalability to coastal studies. One such example of this, is the use of drone derived data to validate and support habitat classification using Worldview-3 (1.24 m spatial resolution) data in a heterogenous estuarine environment (Gray et al., 2018). This technique looks promising for applications that utilise purely spectral data, and could potentially be applied to intertidal environments such as seagrass meadows. In chapter 7, I collected data at 50 m altitude over a river channel. This part of the intertidal zone contained a mixture of bare sediment, seagrass and macroalgae (**Figure 7.7**). These three broad cover types occur in a heterogenous fashion, which would likely appear as mixed pixels in satellite data. Utilising a drone in such environments would help inform habitat classification over greater spatial extents (Koh and Wich, 2012).

Considering the SfM-MVS techniques demonstrated within coastal dunes and coral reefs in chapters 8 and 10 respectively, there is no obvious and direct combination between the ultra-fine spatial resolution dense point clouds and

optical airborne or satellite data. However, these proximal sensing datasets would be compatible with topographic data obtained with active sensors such as LiDAR. Much like the spectral validation shown in Gray et al. (2018), SfM-MVS derived data could be used to validate airborne LiDAR data collected over greater spatial extents.

#### 9.2.4 The sky's the limit – or is it?

In the past decade, proximal sensing technology has begun to revolutionise remote sensing methodologies in a variety of fields. The hyperbole surrounding proximal sensing (especially drones) and the desire to apply this novel technology to capture fine spatial and temporal resolution data can sometimes lead to a mismatch between the research question at hand and the selected methodology. An important point to highlight is that, drones and kites will not outright replace satellite, airborne and other *in-situ* sensing techniques (Tang and Shao, 2015). Often, proximal sensing platforms will offer the opportunity to create complimentary datasets that assist in answering research questions and monitoring efforts (Anderson, 2016; Koh and Wich, 2012). Also, they can be used to capture data in order to answer specific research questions, tailored to their virtues. There are still many applications, especially at the coast, where existing remote sensing techniques are better suited (reef mapping of broad-scale geomorphic zones over 100s km<sup>2</sup> (e.g. (Roelfsema et al., 2018)). The greatest benefits are to be found where sensible and realistic questions are asked, and not where there are mismatches between platform capability, data and question. However, it is important to note that as with any new methodology or technology, trial and error is a natural part of developing and honing the use of a technique for scientific research. Discovering that an application for proximal sensing

platforms is unfeasible may only be achievable by trying to collect data for a stated question (see chapter 4).

### 9.3 The renaissance of kites and the logistical challenges surrounding drone operations

In chapter 5 I reviewed and assessed the utility of kites for environmental research. This involved exploration of the historical use of kite-based data capture, and also how they have been used in the modern era. I concluded that the technological advancements that have contributed to the rise of drone technology in scientific research are also set to benefit kites. These include reduced size and weight of consumer grade cameras, and the ready availability of GNSS equipped devices and components. This chapter also frames kite-based research in relation to alternatives such as blimps, balloons and drones, highlighting its niche as a low cost and easy to operate proximal sensing platform.

Through collaboration with other scientists that utilise drone technology for their research, I collated and presented a series of case studies and methodological advice with a specific focus on operating in challenging environments. This work is presented in chapter 4. Logistically demanding environments such as the coast, polar and tropical forest ecosystems unveil some of the limitations of lightweight drone technology. These limitations are often omitted from the scientific literature where there is a focus on novel and successful research. This work brought together disparate advice, consolidating this information into informative and useful guidance for researchers and practitioners looking to use drones.

## 9.4 Empirical discussion and future research questions

### 9.4.1 Coastal dunes

In chapter 6 I found that sub-decimetre changes in coastal dune topography could be tracked over time using kites, consumer grade cameras and SfM-MVS processing. This empirical work also reinforces my conclusions in chapter 5 – stating that kites are viable proximal platforms for environmental monitoring purposes. Furthermore, this study was one of the first applications of the M3C2-PM methodology since its publication in 2017 (James et al., 2017b), and to my knowledge the first such application with data collected from a kite platform. I also demonstrated that with such fine spatial resolution data, significant changes within specific dune features such as the beach, foredunes and paths can be tracked over time. This is a significant development on other methods of tracking topographic change, such as Difference of DEM approaches (DoD), which due to the nature of the 2-Dimensional data, may struggle to capture changes of complex topographic features, often found in coastal dunes. M3C2-PM is a computationally intensive analysis technique, but with the increasing availability of low-cost, high performance hardware either *in-situ* or on the cloud, it is likely that it will be more widely adopted in future. This will likely be the case for data captured from proximal platforms, such as drones and kites, which are often processed with a photogrammetry workflow (such as SfM-MVS) and result in the production of dense point clouds – a critical component of M3C2-PM analysis.

This study also provided information on the practicalities of kite flying for environmental monitoring purposes. As with the lightweight drone literature, this process is not well reported in published studies (see chapter 4). For example, I

had to utilise two different types of kite (**Table 6.1**). On one occasion the smallest kite was not feasible to fly due to low levels of wind and therefore I had to utilise a kite with greater surface area in order to provide a stable platform from which to mount a sensor. Another key methodological consideration was the presence of beachgoers such as dog walkers and holidaymakers at the study site. The presence of moving objects introduces error in the SfM-MVS workflow, and therefore images captured with these features are not useable for analysis purposes (Westoby et al., 2012). Depending on the time of year and the wind conditions on the survey date, data could not always be captured at times to minimise the presence of people and animals. To account for this, an excess number of images were captured on each survey which were then manually filtered, removing images with problematic features. Another issue to account for, was the placement of GCPs in an area regularly used by members of the public. During a pilot study, one GCP was tampered with, and this resulted in the positioning of notices asking for them not to be moved. Small methodological details such as these are often omitted from the scientific literature but can provide time and cost savings for other researchers wishing to use the similar techniques. Chapter 4 attempts to fill this void in relation to drones, but for kites the knowledge gap still exists.

As evidenced in chapter 1, published work utilising remote sensing data has investigated developments in dune feature formation (e.g. between 1977-1999; Ojeda et al., 2005). This particular study explored multi-decadal change using just two aerial photographs of the study site. The authors also presented crude estimations of volumetric change over the 22 year time period. While this approach has merit for quantifying coastal processes on broad temporal and

spatial scales, it lacks the ability to improve understanding of dune development at fine temporal resolutions (e.g. inter and intra annual). In these scenarios, proximal sensing, utilising platforms such as kites excels, enabling regular and routine monitoring, in effect capturing intra-annual topographic changes. This is especially useful in relation to monitoring where managers/authorities can carefully track the dynamics in dune systems in relation to natural and anthropogenic pressures. Furthermore, the combination of nadir and oblique images and SfM-MVS workflows are likely to create more accurate estimations of volumetric changes, compared to those obtained from 2D photographs. However, this is yet to be rigorously tested and could inform a further strand of research in this area.

### **Future research**

Key research questions which build on the empirical work presented in chapter 6 are:

- How does survey design and therefore sensor positioning during KAP surveys affect the quality and accuracy of photogrammetry data products?
- Do DoD approaches using data from satellite or airborne sensors (e.g. airborne LiDAR) produce similar results to M3C2-PM change analysis with data from a proximal platform?
- Can KAP be used to quantify topographic changes in dune systems immediately after high energy disturbance events (e.g. storms)?

#### 9.4.2 Intertidal seagrass

In chapter 7, I used a lightweight drone and optical sensors to capture very fine spatial resolution images of intertidal seagrass meadows and compare coverage estimations between remotely sensed and *in-situ* methods. I found that estimations made from a classified orthomosaic in more sparsely populated meadows were closer to *in-situ* measurements when compared to a meadow with higher density of seagrass shoots (**Figure 7.5**). Typically, remote sensing has been used to identify the position and quantify the extent of seagrass meadows, while lacking focus on within meadow coverage. This is often due to the coarse spatial resolution of data being used in these studies (e.g. ~30 m for data from the Landsat program (Dekker et al., 2006)). Studies working on broad spatial extents (e.g. 10s of km<sup>2</sup>) are useful for creating thematic maps to assess change in meadow boundaries over time, which can be a crude indicator of ecosystem health (Kirkman, 1996). The work in chapter 7 is a significant development, working with data at spatial resolutions that start to reveal the dynamics within seagrass meadows. Lightweight drones can produce more representative data than a typical *in-situ* quadrat based approach could. The technique demonstrated in chapter 7 is a form of 'virtual quadrat sampling' replicating *in-situ* measures across wider areas.

The ability to quantify *Zostera noltii* coverage at very fine spatial resolutions (e.g. 4.3 mm in chapter 7), could lead to improved estimations of the levels of blue carbon present in intertidal seagrass meadows. Blue carbon is an umbrella term for the sequestration of carbon by plants in the marine environment. Seagrass accumulates carbon through *in-situ* production and sedimentation of particulate carbon from the water column (Greiner et al., 2013). Whilst allometric data linking

above ground biomass or coverage with the below ground carbon storage for *Zostera noltii* is not available, the collection of such data could provide a dataset to link with fine spatial resolution optical image data, such as that collected by sensors on-board a proximal platform. This combination could lead to more accurate estimates of blue carbon storage, by considering the within meadow coverage heterogeneity and how this relates to the amount of carbon stored in the sediment beneath the seagrass leaves.

Data collection for this chapter was methodologically challenging due to the tidal cycle and the flat topography of intertidal seagrass meadows. This meant that on incoming tides, there was limited time until large parts of the meadow were submerged. This was further complicated by the placement of GCPs with associated D-GNSS working, along with multiple quadrat measures of coverage during short tidally accessible periods. Improvements to the methodology could be the positioning of GCPs that are stable throughout the tidal cycle. They could therefore be measured at any time, leaving more time during the low tide period for *in-situ* quadrat measurements. Methodological considerations such as this could be made simpler in future with the implementation of higher accuracy GNSS systems on-board drones which could reduce the number of GCPs required or potentially remove the need for them completely. More discussion about this technology can be found in section 9.5.1.

### **Future research**

Key research questions which build on the empirical work presented in chapter 7 are:

- Can consumer grade optical sensors on-board lightweight drones capture information about the health of seagrass shoots? (i.e. detect wasting disease)
- Can intra-annual proximal sensing surveys be used to detect seasonal variations in within-meadow seagrass coverage?
- How could within meadow coverage estimates be combined with environmental data to predict future changes in plant density (e.g. in response to pollution or run-off?)
- Can fine grained optical proximal sensing data be combined with allometric measures to predict below ground carbon storage based on above ground seagrass coverage?

#### 9.4.3 Coral reefs

In chapter 8, I used a lightweight drone with a variety of flight parameters, to produce SfM-MVS derived point clouds from which to measure the structural complexity of the benthic environment. This work built on the limited published literature in this field (e.g. (Casella et al., 2017) by exploring the use of dense point cloud data as opposed to 2-dimensional DEMs to measure topographic variation in tropical reefs. The technique was partially successful in that variation in measured complexity from the proximal sensing data was present. However, in the comparisons between parts of the reef with differing densities of coral structures, the technique virtual transecting of the point cloud did not produce expected results. For example, in dense reef areas, known to be structurally complex, virtual transects yielded generally low measures of structural complexity. I also explored the use of 15 m altitude data with the same 16 MP optical sensor which yielded promising results, where virtual complexity

measures were clearly different in areas with coral bommies compared to bare sand in the lagoon part of the reef. However, data collection at this altitude greatly limits the spatial extent, and therefore choosing a consumer grade camera with a larger sensor whilst maintaining a higher flight altitude may be a sensible improvement on the methodology. One of the main issues experienced, was the false presence of structure over flat areas of bare sand. This was caused by issues with glint type artefacts in the images collected. The following section discusses this further.

### **Optical sensing of submerged environments**

One of the main challenges that I encountered in chapter 8, was the difficulty of capturing optical data of features through the water column. This is not a trivial issue for proximal sensing applications in the marine environment. For example, Hodgson et al. (2013) were still able to identify dugongs in images collected from an SLR camera mounted on a drone. However, for applications where multiple images of the same features are required (e.g. for SfM-MVS point cloud construction), ensuring features remain visibly identical between scenes is critical. This is achievable when weather conditions are at their absolute optimum, as has been seen in Casella et al. (2017). However, realistically, even in conditions deemed optimal, both refraction and artefacts caused by movement on the waters' surface can likely be found in images collected. Chirayath and Earle (2016) have presented a promising 'Fluid Lensing' algorithm which aims to reduce the distortion caused by movement on the waters' surface. The technique utilises multiple frames from high frame-rate uncompressed video data to calculate and account for the changes in the scene over short periods of time. The authors demonstrate its application in both intertidal and submerged reefs

and claim that it could potentially be applied to submerged environments with <10 m of clear water. The 'Fluid Lensing' methodology also requires significant computer power to process the data. A similar technique that utilised multiple frames from a short video at set GNSS-guided waypoints has been demonstrated within an intertidal rocky shore environment (Partama et al., 2018). The authors applied a temporal minimum filter, aligning 60 images of the same scene, and calculating the darkest pixel values for each pixel in the image. The results show that point clouds increased in density due to the reduction of over-bright features in the input images for SfM-MVS workflows. This work was conducted in environments ranging from 0-2.5 m in depth. Both studies show that promising work is underway to assist in making drones suitable and useful platforms for submerged coastal environment monitoring. There are, however, issues with data storage and processing requirements, as 100 GBs of data are typically produced for < 1 km<sup>2</sup> spatial extent surveys.

### **Future research**

Key research questions which build on the empirical work presented in chapter 8 are:

- How do *in-situ* colony scale measurements compare to proximal sensing derived surface area calculations?
- Identify the optimal altitude and sensor combination to obtain dense point clouds from which structural complexity measures can be derived.
- Does a combination of aerial derived and underwater images and SfM-MVS processing create more accurate estimations of structural complexity than either technique individually?

## 9.5 Technology – challenges and opportunities

Technological developments of drone technology is fast-moving. In the ~4 year timescale of this thesis both the hardware and software used for data capture and processing have greatly developed and improved. This section will reflect on a limited selection of technological challenges and opportunities that potentially lie ahead for drone technology and associated hardware and software, with a specific focus on environmental monitoring applications.

### 9.5.1 Hardware

Batteries are one of the key components currently limiting the effectiveness of drone systems for environmental monitoring. Their longevity is limiting on the amount of time a drone can be flown, in turn constraining the spatial extent and duration of surveys that can be undertaken. Currently, typical flight times (inclusive of sensor payload) range from ~12 minutes for a 3DR Solo (used for empirical work in this thesis), to ~25 minutes for a DJI Phantom 4 and ~50 mins for the eBee classic (a fixed wing drone). Flight duration, driven by battery life is a battleground for drone manufacturers in the commercial realm. This have driven improvement in flight times over recent years, alongside other innovations such as tethered devices, wireless recharging and in-built photovoltaic cells for on-the-fly charging.

High accuracy GNSS systems involving real time kinematic (RTK) or post-processing kinematic (PPK) techniques are a desirable addition to drone survey toolkits due to their ability to help produce data products with centimetre level accuracy. This has typically been achieved with ground control points (GCPs) (see chapters 6 & 7) and a ground based system often with a base and rover

setup (James et al., 2017b). These systems are now becoming integrated with drone autopilot and sensor components, where the drone itself is the rover in the GNSS setup. This means that data captured from the drone platform (such as optical images) can be tagged with the position (to cm accuracy) of the drone. An example of this technology are the Emlid M+ and Reach RS components. Forlani et al. (2018) studied the accuracy of an on-board RTK system compared to a more traditional high-accuracy GNSS survey. They found that without GCPs, the horizontal accuracy was comparable, but there were still issues with accuracy in the vertical domain. However, they found that with the addition of GCP, results were comparable to a full ground-based set of GCPs. This study shows promise and that the need for GCPs could soon become redundant, hence removing a logistical barrier and broadening the opportunity to more easily study coastal ecosystems such as coral reefs with greater confidence and accuracy.

The miniaturisation of sensors and on-board computational power are providing the platform for more capable and advanced drone operations. On such example is, sense and avoid technology (Yu and Zhang, 2015), which could involve both co-operative (i.e. swarming) and non-cooperative (i.e. individual) methods. Developments such as sense and avoid may expand the variety of challenging environments that can be surveyed using a drone such as forest environments or complex topographic areas such as coastal cliffs.

#### 9.5.2 Software

As has been shown in chapters 6 & 8 SfM-MVS can be a suitably quantitative way in which to measure the size, structure, or position of features found within the natural environment. Currently, several software packages are available to

process images to create point clouds, orthomosaics and DEMs – data products which are useful for researchers and managers alike. Photogrammetry software packages include Agisoft Photoscan, Autodesk Recap, MicMac, Microsoft Photosynth, OpenDroneMap and Pix4D. Choice of software can be dictated by several factors. First, price - for the proprietary SfM-MVS software packages, the cost of a licence can sometimes exceed the combined cost of a lightweight drone and consumer grade sensor. For example, Pix4D charge ~£2800 per year (as of 26/10/18), whereas a 3DR Solo and Ricoh GR11 can be purchased for ~£1000. In contrast, OpenDroneMap and MicMac are free to use and the latter has been used in peer-reviewed scientific research (e.g. (Gonçalves et al., 2018)). Second, flexibility and/or access to processing parameters – this is particularly important in scientific research, where transparency in the processing is a desire of some researchers (Smith et al., 2015). Many of these photogrammetry software packages have undergone regular updates and improvements recent years. This is largely driven by the demand for new features such as multispectral point cloud construction and volumetric calculation tools. From a research perspective I hope that the open-source packages continue to develop and mature as robust tools for processing proximal sensing data without large overheads for software licences.

## 9.6 Concluding remarks

Kites and lightweight drones have great potential to improve monitoring efforts at the coast. There are a multitude of coastal ecosystems present on Earth each experiencing complex sets of dynamic natural and often additional anthropogenic driven processes. Furthermore, they each present unique logistical challenges with regards to capturing data, both *in-situ* and remotely. I have demonstrated the capability of these proximal sensing platforms to capture data and create novel datasets that can increase the understanding of coastal processes at finer spatial and temporal scales than has been feasible with alternative technologies. By spanning three key environments across the land-sea interface, this work demonstrates the potential to monitor different environments in both the spectral and the structural domains. Moving forward, as rapid improvements in both hardware and software emerge, the implementation of these techniques in the coastal domain is set to grow. Whilst the proximal view of Earth from above is exciting and intriguing, the biggest gains are set to come from well-planned, consistent and integrated monitoring programs which utilise a combination of *in-situ* and/or other remote sensing datasets.

## 10 Appendices

### 10.1 The CAA approved operations manual – manuscript



This paper was published in the International Journal of Remote Sensing in 2016:

Cunliffe, A. M., Anderson, K., DeBell, L. & Duffy J.P. (2016) A UK Civil Aviation Authority (CAA)-approved operations manual for safe deployment of lightweight drones in research. *International Journal of Remote Sensing*, 38, 2737-2744.

## **A UK Civil Aviation Authority (CAA)-approved operations manual for safe deployment of lightweight drones in research**

Andrew M. Cunliffe<sup>1,2</sup>, Karen Anderson<sup>3\*</sup>, Leon DeBell<sup>3</sup>, James P. Duffy<sup>3</sup>

1. School of Geography, University of Exeter, Exeter, UK

2. School of GeoSciences, University of Edinburgh, Edinburgh, UK

3. Environment and Sustainability Institute, University of Exeter, Penryn, UK

*\*Corresponding author*

### 10.1.1 Abstract

The academic literature of late is rich with examples of lightweight drones being used to capture data to support scientific research. Drone science is a blossoming field, but alongside a long-standing public concern about drone safety, the research community and our collaborators are increasingly calling for a ‘code of best practice’ for researchers who fly drones (no matter how small). Researchers who have long enjoyed the freedom of operating separately from ‘hobbyist’ and ‘commercial’ operators are now finding that their institutions and collaborators are demanding evidence of operational competence. In the UK, such competence can be formally accredited by obtaining a UK Civil Aviation Authority (CAA) ‘permission for aerial work’ (PfAW). Part of this process requires that the operators produce an ‘operations manual’ (OM) – a lengthy document explaining protocols for safe drone deployment, alongside maintenance and flight records. This article provides the frontispiece to an OM produced as part of a successful PfAW accreditation process. We share our OM, which is available as supplemental material to this article, in the spirit of research as a collaborative

endeavour, with the aim that it will assist others facing the same stringent checks as ourselves, whilst also serving as a guide to safe flying that can be adapted and adopted by others.

### 10.1.2 Introduction

Lightweight drones, now widely used in environmental science research, are variously referred to as unmanned or unpiloted aerial vehicles (UAV) or systems (UAS) or remotely piloted aircraft systems (RPAS). In this paper we refer to such aircraft systems as RPAS and drones interchangeably, but in all cases we restrict definition to lightweight platforms, in our case with a take-off-mass not exceeding 7 kg.

There are a plethora of scientific projects now utilising lightweight drones as data collection platforms, servicing a diverse range of civilian, scientific and remote sensing applications. Recent examples of such drone use in ecology include surveys of: marine fauna (Hodgson et al., 2013), vegetation structure (Cunliffe et al., 2016; Dandois et al., 2015), biodiversity (Getzin et al., 2012), and wildfires (Merino et al., 2012). In geoscience research, drone-based data collection is increasing, largely because drones can capture data for 'structure-from-motion' photogrammetry (Westoby et al., 2012) which is useful for erosion studies (D'Oleire-Oltmanns et al., 2012; Kaiser et al., 2014), and for quantifying glacial dynamics (Ryan et al., 2014), to provide just a few examples. Indeed this article is published in a special issue of the *International Journal of Remote Sensing* devoted to the use of drones in scientific research and environmental monitoring.

DeBell et al., (2016) chart the rise of the drone in environmental science publications, showing an exponential rise in the number of papers published in

the past decade. This trend of increasing usage is likely to continue, as the capabilities and applications of these systems continue to develop and the cost of hardware decreases (Anderson and Gaston, 2013; Sandbrook, 2015). The expansion in drone use has led to a growing number of works that highlight the need for a safe operational protocol for drone deployment. Some papers have already sought to determine the effects of drone disturbance on wildlife (Pomeroy et al., 2015; McEvoy et al., 2016) but most recently, work by Hodgson and Koh (Hodgson and Koh, 2016) states that, “there is a need for a code of best practice in the use of UAVs to mitigate or alleviate risks” to third parties. In the context of biological research, this relates primarily to disturbances to wildlife, but such consideration should be given also to safe operations and minimising disturbance in a wide variety of settings. Sandbrook (Sandbrook, 2015), writing about drone use in conservation suggests that, “little attention has been given to their possible social impacts” whilst Hodgson and Koh (Hodgson and Koh, 2016) define the need for work that improves the suitability of drones “as a low impact ecological survey tool”.

Drones look set to play a continued key role in underpinning scientific survey methodologies. With a large international research community now using drones for good purpose the time is ripe for that same community to demonstrate the spectrum of opportunities that this technology can deliver, so as to counter the popular view that drones are simply an operational and social nuisance and/or threat, including a military or terrorist threat. We also argue that a rigorous and carefully designed protocol for drone deployment within the sciences is useful if researchers are to be able to demonstrate competency, safety, and reproducibility of drone operations. A simple step towards this (for all drone

operators including scientists), is to follow agreed procedures such as may be set out in an operations manual, for all flights. Doing so enhances awareness amongst the community of optimal operational procedures, and builds trust amongst colleagues and collaborators that operations are conducted within safe limits and to exacting standards.

As UK-based researchers utilising lightweight (sub-7 kg take off mass) drones, we have enjoyed a period of relative freedom where we were able operate under a separate banner from 'hobbyist' and 'commercial' aerial operators. However, in the past two years we have noticed an increasing number of our collaborators requesting paperwork that provides evidence of our competency to fly, and the airworthiness of our drones. For some research projects, it has become impossible for us to secure permission to fly without providing evidence of accreditation from the UK Civil Aviation Authority (CAA), despite the sites concerned being un-congested and low-risk. Examples have included remote upland moorland sites and areas of lowland rough grassland, hundreds of meters from roads and buildings (and thus un-congested according to the UK CAA's definition), but where the landowner(s) expressed a concern about the use of drones for environmental survey. In response, our research group (comprising the authors) has completed a full accreditation being issued with a 'permission for aerial work' (PFAW) being granted by the UK CAA, for a period of 12-months. Once this accreditation was granted, we found it easier to negotiate with cautious landowners who were then more willing to grant permission for us to fly over their properties. Note that academic drone operators should not normally require PFAW to fly within un-congested areas in the UK (see section 2), but they do require the landowner's permission to fly.

The purpose of this intentionally short manuscript is to provide an introduction to the operations manual (OM) that we produced as part of that accreditation process, and which was formally approved by the UK CAA in August 2016 and which is deposited as supplemental information (SI) related to this paper. This OM is reproduced in both .pdf and .docx formats in the supplemental material to this paper. In what follows in the manuscript, we provide a basic background to airspace regulations, scientific research and permission to fly drones, and the UK procedure for obtaining PfAW, so that readers of this paper can understand the framework within which the shared OM sits.

### 10.1.3 Airspace regulations

Civilian airspace in many countries of the world is regulated by National Aviation Authorities (NAAs), for instance the Civil Aviation Authority (CAA) in the United Kingdom. A directory of NAAs can be found at (“World Aviation Reporting Authorities,” 2016). Use of civilian airspace must be authorised by the relevant NAA for all air users, including unpiloted aircraft, and airspace regulatory frameworks are evolving rapidly to cope with the expansion of civilian drone technologies (CAA, 2015a, 2014a, 2014b, FAA, 2015a, 2015b, 2013, 2012, 2010) as well as in response to calls for innovation in the drone industry. For example, we refer to recent (July 2016) changes to UK airspace regulations to allow Amazon to test beyond-line-of-sight flight and detect-and-avoid capabilities for delivery drones in Cambridgeshire. Presently, authorisations for the use of airspace by lightweight drones commonly cover both recreational and/or commercial operations (CAA, 2015b; FAA, 2015c).

In the UK, recreational authorizations permit the operations of lightweight drones (termed by the UK CAA as “RPAS”) in uncongested airspace, subject to several limitations such as remaining within visual line-of-sight (VLOS) of the operator and not exceeding an altitude of greater than 400 ft (122 m) above ground level. A CAA PFAW is required for operations which are ‘commercial’ (defined by the CAA as “performed for valuable consideration”), or which are undertaken in ‘congested airspace’ (defined by the CAA as “any area which, in relation to a city, town or settlement, is substantially used for residential, industrial, commercial or recreational purposes”) (CAA, 2014b). Furthermore, private landowners are increasingly requiring RPAS operators, including researchers to hold a CAA PFAW in order to conduct operations over their property. Two examples are the National Trust (who own 350 heritage properties and 247 000 ha of land in the UK) (National Trust, 2015) & the Royal Botanical Gardens, Kew, London, UK.

#### 10.1.4 Flying drones for research and CAA permission

In the UK, while some researchers have obtained CAA permission (CAA, 2015a, 2015c) for RPAS operations (Woodget et al., 2015, 2016; Pomeroy et al., 2015), others have operated their RPAS under the existing authorisations granted to hobbyist users (CAA, 2013) which permit researchers to carry out flights in non-congested areas so long as permission from relevant landowners is first obtained (Anderson et al., 2016; Carbonneau and Dietrich, 2017; DeBell et al., 2016; Puttock et al., 2017, 2015). Increasingly, academic researchers utilizing RPAS may deem it necessary to obtain permission from the CAA, codifying their operational competence, in order to (i) comply with institutional insurance requirements (Lloyd’s, 2015), (ii) demonstrate professional standards to collaborators, (iii) operate in congested airspace, and (iv) undertake consultancy

work for monetary reward. We argue, that in instances where a researcher may not be undertaking aerial work for commercial gain, or operating in airspace where special licenses are mandatory, having a working document such as an operations manual will both allow for consistent and safe operation of drones and reassure collaborators and institutions that drone operations are being conducted in a professional manner. This could apply across different organizational scales, from individuals to a research group or an entire research institute. Alongside having a working document, understanding the process by which PfAW is granted can demonstrate the best practice that Hodgson and Koh (Hodgson and Koh, 2016) advocate as the precautionary principle to manage operational risks.

### **Procedure for obtaining PfAW in the UK**

Obtaining a CAA PfAW requires evidence that the RPAS will be operated in a safe manner by the organization concerned (**Figure 10.1**). This evidence normally requires that:

1. The pilot(s) have appropriate theoretical knowledge of air law, flight planning and operational procedures;
2. The organization submit an OM, a comprehensive technical document describing all aspects of RPAS operation including aircraft maintenance and incident reporting procedures;
3. The pilot(s) can demonstrate a good level of practical flight competency, including adherence to the procedures described in the OM.

These three components may be examined by a CAA-authorized entity, and evidence of satisfactory performance during these various assessments may be submitted to the CAA for consideration in support of a PfAW application. Broadly

speaking, although the process varies from one country to another, there are great similarities across many NAAs, including the USA, Canada, Australia, and various EU member states, so the OM shared here has relevance and utility beyond UK borders.

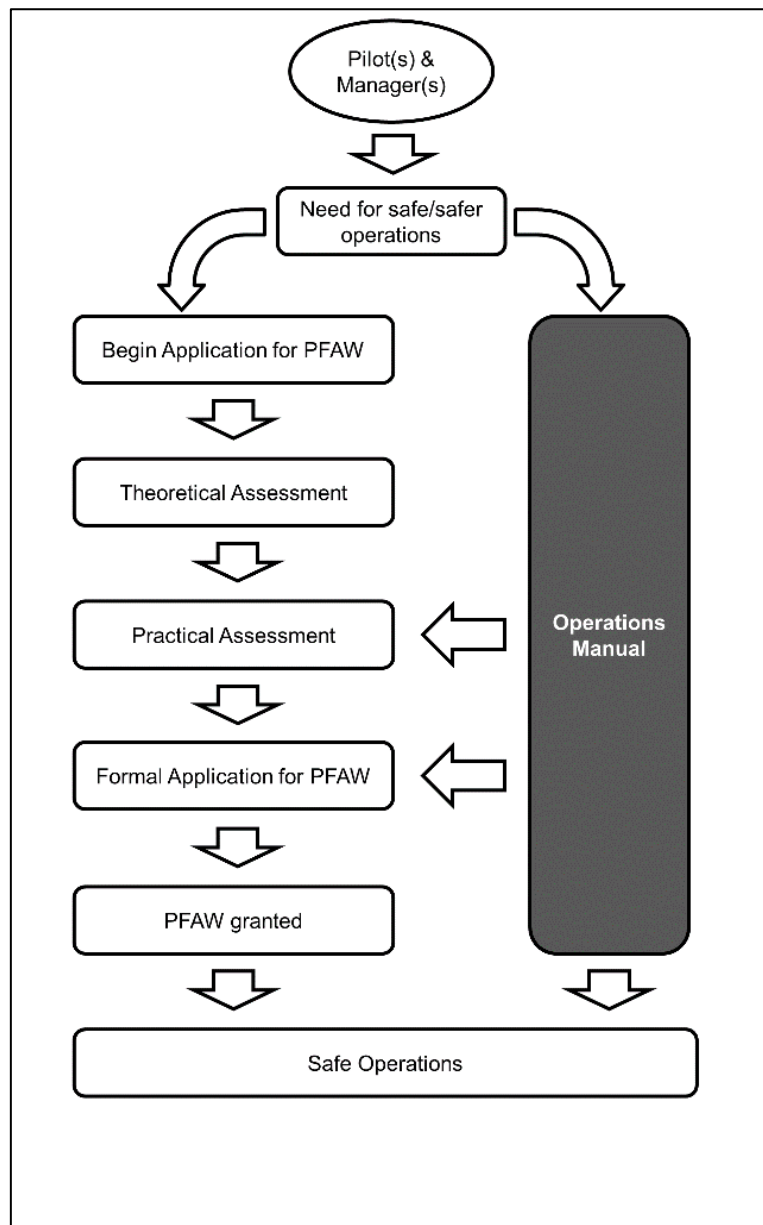


**Figure 10.1: A schematic representation of where the operations manual fits into the typical accreditation process for ‘aerial work’ according to the UK Civil Aviation Authority. Please note that we show two routes for its use. The left-hand part of the flow chart shows the process for CAA accreditation of aerial work which permits RPAS use for commercial operation. However, as we argue in the manuscript, any researcher could use (following adaptation for their specific aircraft and procedures) our operations manual within their flight protocols, to demonstrate to collaborators a competency and safe protocol for drone flights outside of those operations requiring special permission from the CAA for ‘aerial work’.**

### 10.1.5 The operations manual (OM)

Writing and developing the OM is a time-consuming process. The document structure is stringently defined according to criteria on style, organisation and content (CAA, 2011). To produce our OM took several weeks of work and consultations with a CAA-approved assessment centre in the UK. The whole process leading to formal CAA PFAW certification took over one year to complete (**Figure 10.2**) with the majority of time occupied with OM editing whilst waiting for a suitable weather window for the practical flight test.

In sharing this OM we hope that other researchers using drones for their research can benefit from emulating the style and content of the document. It is important to note that we are not arguing that the procedures described in our OM are the *only* way to safely deploy drones for research; rather, it is shared as an example for reference to others in developing their own operational procedures specific to their operational requirements either in the UK or in other countries. This document can also serve as an example of good practice for researchers working in countries with less stringent/developed airspace regulations. Any parts of the shared OM (section 10.2) may be used by other workers, provided this assistance is accredited in any outputs arising from works supported.

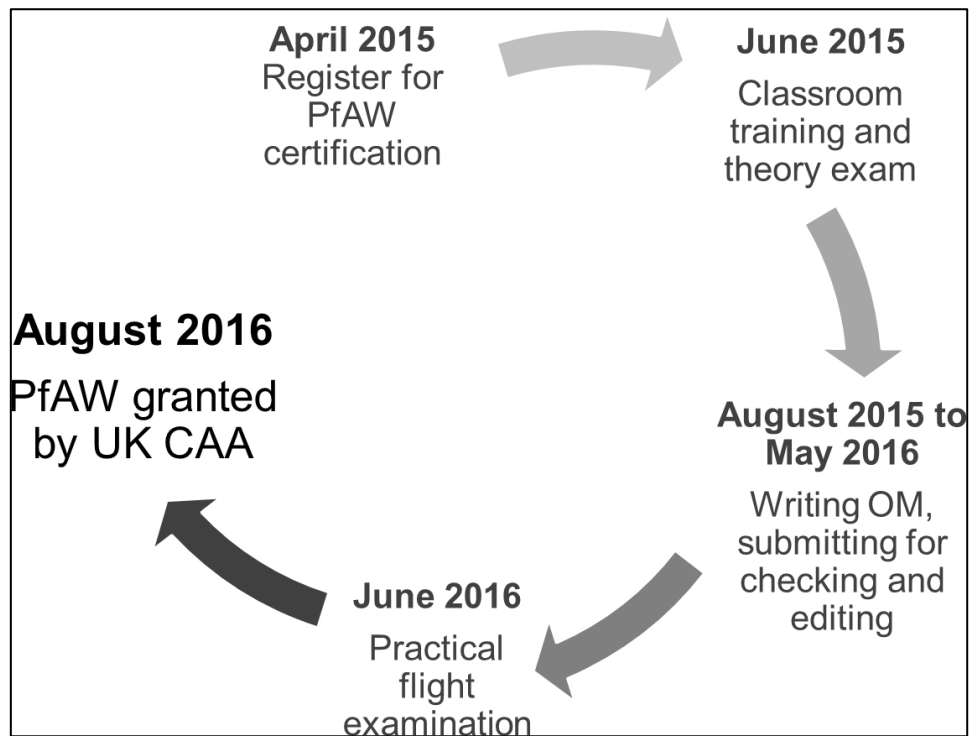


**Figure 10.2: Timeline for PfAW certification experienced by the authors.**

#### 10.1.6 Conclusion

Our OM is shared in the spirit of research as a collaborative endeavour with the aim of assisting other researchers in all areas of environmental or social science, who are using drones as part of their academic practice to follow a safe and CAA-approved protocol for flying. The OM can be downloaded and copied by any researcher wanting to achieve the same levels of accreditation as us. In such cases, researchers would need to substitute the names of their pilots and aircraft and to cross-check and modify (as required) the details of the operational flying procedure to reflect their own practice. In sharing this document, we hope that other researchers can save considerable time by having an approved CAA OM to use as a guide. The document may also provide a useful framework for those applying for accreditation with other national aviation authorities, or for those who are seeking robust operational procedures to follow when flying drones for research.

### 10.1.7 Acknowledgements

This research was supported by a NERC PhD studentship (NE/K500902/1) awarded to AMC. We thank Chris Kasch (from EuroUSC) for comments on earlier versions of the operations manual, and Arthur Cracknell for comments on an earlier version of this frontispiece

## 10.2 The CAA approved operations manual

# ESI DroneLab

## OPERATIONS

## MANUAL



This document is a combined Safety and Operations Manual that covers all of the appropriate aspects of ESI DroneLab required to satisfy the requirements of National Aviation Authority's Permissions for Aerial Work.

Document Reference: DroneLab-Operations Manual

Issue: 1.4 – 9<sup>th</sup> May 2016

Document Authors: Andrew M. Cunliffe, James P. Duffy, Leon DeBell and Karen Anderson

Accountable Manager: Dr Karen Anderson

**Note: This operations manual was compiled by the authors following a style template as recommended by the UAV training company, EuroUSC**

### Amendment Record

Issue Number	Amendment Date	Amendments Incorporated	Signed Off By
1.0	2015-07-20	First edition of ESI DroneLab operations manual.	XXXXXXXXXXXXXXXX
1.1	2015-10-01	Amended following review by Chris Kasch at EuroUSC.	XXXXXXXXXXXXXXXX
1.2	2015-10-13	Amended following review by Chris Kasch at EuroUSC.	XXXXXXXXXXXXXXXX
1.3	2016-02-25	Amended following internal review.	XXXXXXXXXXXXXXXX
1.4	2016-05-09	Amended following internal review.	XXXXXXXXXXXXXXXX

### Commitment of Accountable Manager

This Operations Manual describes the organisation, aircraft systems, personnel, flight operations and procedures by which ESI DroneLab carries out its Small Unmanned Aircraft operations.

It is accepted that the contents of this document do not override the necessity of reviewing and complying appropriately with any new or amended regulation published from time to time by the relevant National Aviation Authorities addressed by this document.

Signed: XXXXXXXXXXXX

Date: 9<sup>th</sup> May 2016

Accountable Manager: Dr Karen Anderson, University of Exeter, ESI DroneLab

For and on behalf of XXXXXXXX

Enquiries regarding the content of this document should be addressed to: XXXXXXXXXXX

## **Contents**

<b><u>Section</u></b>	<b><u>Page</u></b>
Amendment Record .....	1
Commitment of Accountable Manager .....	1
Section Page.....	2
<b>PART A – SAFETY AND ORGANISATIONAL LAYOUT .....</b>	<b>5</b>
1. Purpose .....	5
2. Scope.....	5
2.1. Safety Policy and National Perspective.....	5
2.2. Safety Goals.....	5
2.3. Safety Assurance .....	5
2.4. Organisational and Safety Training .....	5
3. Definitions and Abbreviations .....	6
4. Document Control and Amendment Process .....	6
5. Referenced Documents .....	7
6. Organisation and Personnel .....	7
6.1. Organisation.....	7
6.2. Nominated Personnel .....	7
6.3. Responsibilities.....	8
<b>PART B – AIRCRAFT AND OPERATIONAL CONTROL .....</b>	<b>9</b>
7. Aircraft Technical Specifications.....	9
7.1. Photos of UAVs.....	11
7.2. Operating Limitations and Conditions .....	13
7.3. Types of Operation.....	14
8. Maintenance Principles and Regime.....	15
8.1. Routine Maintenance.....	15
8.2. Software and Firmware Update Policy .....	15
9. Supervision of Unmanned Aerial System (UAS) .....	16
10. Incident Investigation and Mandatory Occurrence Reporting .....	16
10.1. Incident Handling .....	16
10.2. Incident Logging .....	16
10.3. Investigation Procedure.....	16
10.4. Mandatory Occurrence Reporting .....	17
11. Operation of Multiple Aircraft .....	17
12. Flight Team .....	18
12.1. Qualification Requirements and Currency.....	18
12.2. Crew Health.....	18
13. Logs and Records.....	18

<b>PART C – FLIGHT PLANNING AND PREPARATION (Pre-Site)</b> .....	<b>19</b>
14. Determination of Intended Task and Feasibility .....	19
15. Operating Site Location and Assessment .....	19
16. Risk Management .....	19
17. Communications .....	19
18. Pre-Notification .....	19
19. Site Permissions .....	19
20. Weather Forecasts.....	20
21. Preparation and Serviceability of Equipment.....	20
<b>PART D – OPERATING PROCEDURES (On-Site)</b> .....	<b>21</b>
22. On-Site Assessment Survey .....	21
23. Selection of Operating Areas .....	21
24. Weather Checks .....	21
25. Crew Briefing .....	22
26. Crew Clothing .....	22
27. Cordon Procedure .....	22
28. Aircraft Communications .....	22
29. Charging and Fitting of Batteries .....	23
30. Loading of Equipment .....	24
31. Pre-Flight and Post-Flight Checks .....	24
32. Flight Procedures .....	25
32.1. Start-up Procedure.....	25
32.2. Take-off Procedure Multi-rotors.....	26
32.3. Take-off Procedure Fixed Wing.....	26
32.4. In-flight Procedure .....	26
32.5. Landing Procedure for Multi-rotor.....	27
32.6. Landing Procedure for Fixed Wing.....	27
32.7. Shut-down Procedure .....	27
33. Emergency Procedures .....	27
33.1. Flight Controller Failsafes.....	27
33.2. Crew Emergency Procedures .....	30
Appendix A Permission for Aerial Work .....	33
Appendix B Insurance Document .....	34
Appendix C Operational Forms.....	35
Risk Assessment Form .....	35
Job Specification Form .....	38
Pre-Site Assessment Form .....	39
On-Site Assessment Form .....	43

Appendix D Checklists .....	44
Embarkation Checklist .....	44
Pre-Flight Checklist .....	45
Post-Flight Checklist .....	46
Minor Level Service Checklist .....	47
Major Level Service Checklist .....	48
Appendix E Logbooks .....	49
Data recorded in Battery Identification Chart .....	49
- Battery ID .....	49
- Manufacturer .....	49
- Model .....	49
- Type .....	49
- Capacity .....	49
- Cells .....	49
- Discharge C .....	49
- Charge C .....	49
- Date purchased .....	49
- Supplier .....	49
Data recorded in Battery Logbook (individual batteries) .....	49
- Date of change in charge .....	49
- Type of change in charge .....	49
- Pre-change voltage .....	49
- Post-change voltage .....	49
- Notes .....	49
Data recorded in Maintenance Logbook (each aircraft) .....	49
- Date of maintenance .....	49
- Reason for maintenance .....	49
- Work completed .....	49
- Completed by .....	49
- Test flight signature .....	49
- Notes .....	49
Data recorded Pilot and Aircraft Hours Logbook .....	49

## **PART A – SAFETY AND ORGANISATIONAL LAYOUT**

### **1. Purpose**

The purpose of this document is to detail the items to be covered for the safe operation of Unmanned Aerial Systems (UAS) by ESI DroneLab personnel.

### **2. Scope**

This operations manual applies to all ESI DroneLab personnel involved in the safe operation of the UAS detailed in the Aircraft Technical Specifications section.

#### **2.1. Safety Policy and National Perspective**

ESI DroneLab adopts best industry practice to ensure that all of its flight operations using small unmanned aircraft systems (SUAS) as previously detailed are carried out as safely as possible. This document addresses ESI DroneLab operations in the United Kingdom, as regulated by the UK Civil Aviation Authority (CAA).

#### **2.2. Safety Goals**

It is the goal of ESI DroneLab to operate UAS without harm, injury or damage to any persons or property. The ESI DroneLab Pilot-in-Command (PIC) will comply with all of the safety requirements and limitations of the Permission for Aerial Work (PfAW) issued by the UK CAA to ESI DroneLab

#### **2.3. Safety Assurance**

ESI DroneLab is committed to maintaining the highest standards of flight safety and aims to minimise harm to any persons or property by undertaking thorough risk assessment, site surveys, crew training and ensuring aircraft are in operational condition through regular inspection and maintenance regimes. By these processes ESI DroneLab assures safety at all times whilst carrying out flight operations.

#### **2.4. Organisational and Safety Training**

All ESI DroneLab crew members will undertake in-house training by qualified ESI DroneLab personnel, and must follow specific procedures set out in this Operations Manual. The training course will include a brief technical overview of the aircraft currently in service, limitations to be considered for operation, and organisational procedures. Any ESI DroneLab PIC will hold the relevant, current qualification as stated in the qualification requirements section in order to operate the specific aircraft. Crew performance will be monitored, assessed and refresher training may be given if required. All incidents will be recorded, analysed and any findings will be fed back to the crew as training to form a basis of Continual Professional Development. Operational flight logs will be kept by the DroneLab, detailing every flight operation (successful or otherwise) undertaken by any ESI DroneLab PIC.

### 3. Definitions and Abbreviations

Below is a list of abbreviations used in this Operations Manual;

Reference	Full Title
AAIB	Air Accident Investigation Branch
AOI	Area of Interest
CAA	Civil Aviation Authority
CS	Consequence Score
ESI	Environment & Sustainability Institute
ESC	Electronic Speed Controller
FBWA	Fly-By-Wire A mode
FC	Flight Controller
FHSS	Frequency Hopping Spread Spectrum
GCS	Ground Control Station
CoG	Centre of Gravity
GNSS	Global Navigation Satellite System (e.g., GPS, Glonass, Galileo, Bei Dou)
HUD	Heads-up-Display (information screen displayed on the GCS)
LiPo	Lithium Polymer (battery)
LS	Likelihood Score
MTOM	Maximum Take-Off Mass
NAA	National Aviation Authority
NOTAM	Notice to Airmen
PiC	Pilot in Command
PfAW	Permission for Aerial Work
PDoP	Position (3D) - Dilution of Precision
RS	Risk Score
RTL	Return to Launch
Rx	Receiver
SUAS	Small Unmanned Aircraft Systems
Tx	Transmitter
UAS	Unmanned Aircraft Systems
UAV	Unmanned Aerial Vehicle
VLOS	Visual Line of Sight

### 4. Document Control and Amendment Process

All amendments to this Operations Manual are to be made by XXXXXXXXXX and must be recorded in the [Amendment Record Page](#) found at the front of this document. Each amendment is identified with an Amendment Number, Amendment Date, Amendments Incorporated and Incorporated by information header. EuroUSC and all relevant NAAs will be informed of all major updates such as new aircraft or pilots. All ESI DroneLab employees will be informed of any changes to this Operations Manual and they must maintain a current up-to-date version either in electronic or paper format. All amendments will be signed off by the Accountable Manager Dr Karen Anderson.

## 5. Referenced Documents

Reference	Full Title	Issue Number and Date
CAP 382	Mandatory Occurrence Reporting Scheme	9th Edition – 18 <sup>th</sup> March 2011
CAP 393	Air Navigation: <i>The Order and Regulations</i>	4th Edition – 1 <sup>st</sup> April 2015
CAP 722	Unmanned Aircraft System Operations - <i>Guidance</i>	6 <sup>th</sup> Edition – 31 <sup>st</sup> March 2015
CAA- IN2015/008	Small Unmanned Aircraft – Acceptable Forms of Evidence for the Grant of a CAA Permission and Changes to the Approval Requirements for UK National Qualified Entities	1 <sup>st</sup> Edition – 6 <sup>th</sup> March 2015

## 6. Organisation and Personnel

### 6.1. Organisation

Organisation Name: ESI DroneLab

Organisation Type: Research and Commercial Environmental Surveying

Organisation Registration Number: RC000653

Country of Registration: UK

The ESI DroneLab is a non-complex operation, headed by Dr. Karen Anderson within the University of Exeter at the Environment & Sustainability Institute. Predominantly for remote sensing research, it now includes a spin-off enterprise to address the national commercial interest in ESI DroneLab's environmental surveying expertise. All research works will be conducted under the University of Exeter with all commercial work will be carried out either through the University of Exeter Consultancy Ltd. or through another third party commercial entity.

ESI DroneLab has third Party Public Liability Insurance as outlined below:-

Insurer: XXXXXXXXXXXX  
 Insurance Policy Number: XXXXXXXXXXXX  
 Insured amount: XXXXXXXXXXXX  
 Insurance Expiry Date: XXXXXXXXXXXX

### 6.2. Nominated Personnel

Any one of the following listed personnel may be PIC, observer or spotter. Other personnel may be deployed as observers or spotters, after receiving suitable training from the PIC. ESI DroneLab does not use payload operators because our payloads operate autonomously (e.g. are triggered by autopilot software), and thus do not require any significant level of in-flight operator input (in contrast to UAS deploying FPV). ESI DroneLab does not typically undertake cinematography surveys. All data collected from ESI DroneLab UAVs are from science-grade imaging or non-imaging systems.

Remote Pilot Name:	XXXXXXXXXX	XXXXXXXXXX	XXXXXXXXXX
Qualification:	XXXXXXXXXX	XXXXXXXXXX	XXXXXXXXXX
Telephone number:	XXXXXXXXXX	XXXXXXXXXX	XXXXXXXXXX
E-mail address:	XXXXXXXXXX	XXXXXXXXXX	XXXXXXXXXX

### 6.3. Responsibilities

UAS deployments will typically use two operators, a PiC and an observer, this can be extended to include 'spotters' if additional crew are available (i.e. a client on site) or where a complex mission requires it. It can also be appropriate and safe to use a single operator under the following conditions:

- Where lone working is deemed safe.
- Deployment is in non-congested areas (i.e., remote farmland and uplands).
- Where survey flights are autonomous (enabling PiC to also monitor GCS status, facilitated by audible updates regularly given by the accompanying laptop).

When only a single operator is present roles will be combined, but when two operators are present, roles will be allocated as follows:

PiC;

- The PiC on the day is responsible for supervising the operation of the UAS.
- Ensure all crew members are aware of their responsibilities by giving a Crew Briefing prior to flight.
- Ensuring the on-site assessment is completed correctly.
- Ensuring the aircraft is only operated within the stated limitations for that particular aircraft.
- Ensuring all commercial work is completed within the limitations stated on the permission for aerial work document.
- Ensuring that the aircraft used is airworthy by completing the pre-flight checklist.
- Ensuring that the welfare of themselves or others is not compromised by any planned operations.
- Ensuring that they are of sound body and mind to operate the aircraft.
- Ensuring the camera is securely mounted and safely fixed to the UAV.
- Ensuring all required paperwork is completed (e.g., pilot & aircraft hours, battery log).

Observer;

- Ensuring the camera is operational. (battery has sufficient power for planned operation, empty memory card fitted, lens clean, trigger mechanism enabled and working)
- Ensure the camera is rotated to the stored position for take-off and landing procedures.
- Maintain constant visual look-out for public and aircraft encroachments into the flight zone.
- Ensure the position of the UAS is known at all times.
- Be prepared at all times to activate the failsafe function on the UAS should the PiC become incapacitated.

Spotter;

- Supporting the observer to ensure the position of the UAS is known at all times.
- Supporting the observer to maintain constant visual look-out for public and aircraft encroachments into the flight zone.

## PART B – AIRCRAFT AND OPERATIONAL CONTROL

### 7. Aircraft Technical Specifications

The table below shows specifications for UAS. Note that every component of these systems can be replaced or upgraded, provided changes are fully documented in the maintenance log for each UAS.

Item	UAS Details			
	XXXXXXX	XXXXXXX	XXXXXXX	XXXXXXX
Platform	XXXXXXX	XXXXXXX	XXXXXXX	XXXXXXX
Registered Keeper	XXXXXXX	XXXXXXX	XXXXXXX	XXXXXXX
Manufacturer Name	XXXXXXX	XXXXXXX	XXXXXXX	XXXXXXX
Distributor Name	XXXXXXX	XXXXXXX	XXXXXXX	XXXXXXX
Airframe Make	3D Robotics	3D Robotics	3D Robotics	Tarot
Airframe Model	Y6-B(2013)	Y6-B(2013)	IRIS + (2014)	650
Serial Number	XXXXXXX	XXXXXXX	XXXXXXX	XXXXXXX
LUASS™ Registration Number	XXXXXXX	XXXXXXX	XXXXXXX	XXXXXXX
Airframe Type	Y6 (Coaxial Hexacopter)	Y6 (Coaxial Hexacopter)	Quad Copter	Quad Copter
Span/Diameter [m]	XXXXXXX	XXXXXXX	XXXXXXX	XXXXXXX
Un-laden Weight [kg]	XXXXXXX	XXXXXXX	XXXXXXX	XXXXXXX
[Maximum Take-Off Mass [kg]	XXXXXXX	XXXXXXX	XXXXXXX	XXXXXXX
Propulsion Type	Electric	Electric	Electric	Electric
Number of Motors	6	6	4	4
Motor Size	2212 multiphase brushless outrunner	2212 multiphase brushless outrunner	2212 multiphase brushless outrunner	4822 multiphase brushless outrunner
Motor [Kv]	850	850	920	690
ESC	3DR 20A 2-4S 2A@5V BEC running SimonK firmware	3DR 20A 2-4S 2A@5V BEC running SimonK firmware	3DR 4 in 1 20A 2-4S 2A@12V BEC running SimonK firmware	Afro 30A 2-4S 0.5A@5V BEC running BLHeli firmware
Flight Battery Type	LiPo	LiPo	LiPo	LiPo
Flight Battery Capacity	4S 5,000 mAh - 10,000 mAh	4S 5,000 mAh - 10,000 mAh	3S 3,000 mAh - 5,200 mAh	4S 5,000 mAh - 12,000 mAh
Propeller Size	10 x 4.7	10 x 4.7	9.5 x 4.5	12 x 4.7
Flight Control System	APM 2.6	Pixhawk	Pixhawk	Pixhawk
Flight Controller Serial Number	XXXXXXX	XXXXXXX	XXXXXXX	XXXXXXX

Flight Control Power Supply	3DR Power Module	Dual system 3DR Power Module + 5V BEC	Dual system 3DR Power Module + 5V BEC	Dual system 3DR Power Module + 5V BEC
Flight Control Software	ArduCopter (v3.2.1)	ArduCopter (v3.3)	ArduCopter (v3.3)	ArduCopter (v3.3)
Navigation Unit	3DR Ublox LEA-6 GNSS+Compass module	3DR Ublox LEA-6 GNSS+Compass module	3DR Ublox LEA-6 GNSS+Compass module	Drotek Ublox M8N GNSS+Compass module
Transmitter Make and Model	FrSky Taranis X9D	FrSky Taranis X9D	FrSky Taranis X9D	FrSky Taranis X9D
Transmitter Serial Number	XXXXXXXXXX	XXXXXXXXXX	XXXXXXXXXX	XXXXXXXXXX
Receiver Make and Model	FrSky X8R	FrSky X8R	FrSky D4II	FrSky X8R
Receiver Serial Number	NA	NA	NA	NA
Aircraft Control Frequency and Power	2.4 GHz 100 mW			
Ground Station Type	Active	Active	Active	Active
Ground Station Make and Model	Any laptop running OS Windows 7 or above OR android tablet	Any laptop running OS Windows 7 or above OR android tablet	Any laptop running OS Windows 7 or above OR android tablet	Any laptop running OS Windows 7 or above OR android tablet
Ground Station Software and version	Mission Planner V1.3.34 (on Windows platform) OR Tower (on Android platform)	Mission Planner V1.3.37 (on Windows platform) OR Tower (on Android platform)	Mission Planner V1.3.37 (on Windows platform) OR Tower (on Android platform)	Mission Planner V1.3.37_ (on Windows platform) OR Tower (on Android platform)
Ground Station Telemetry Link Make and Model	3DR radio v2	3DR radio v2	3DR radio v2	3DR radio v2
Ground Station Telemetry Control Frequency and Power	433 MHz (using MAVlink protocol, <b>Net ID: 10</b> SIK1.9 Firmware, up to 10 mW)	433 MHz (using MAVlink protocol, <b>Net ID: 97</b> SIK1.9 Firmware, up to 10 mW)	433 MHz (using MAVlink protocol, <b>Net ID: 46</b> SIK1.9 Firmware, up to 10 mW)	433 MHz (using MAVlink protocol, <b>Net ID: 01</b> SIK1.9 Firmware, up to 10 mW)

**7.1. Photos of UAVs**

Aircraft - XXXXX



Aircraft - XXXXX



Aircraft - XXXXX



Aircraft - XXXXX



## 7.2. Operating Limitations and Conditions

### Centre of Gravity (CoG)

For the safe operation of aircraft, it is imperative that the aircraft is not unbalanced to the extent that handling characteristics are significantly reduced. To maintain the balance of the aircraft, payload and batteries must be mounted sufficiently close to the CoG. CoG for fixed wing airframes are stated by manufacturers and adhered to during the build process. Multi-rotor platforms centre of gravity (CoG) is at the centre of the airframe (in the X,Y,Z axes). On all aircraft described in this operating manual, the CoG is marked on the underside of each airframe by a blue sticker.

### Balance Limitation

The balance limitation is the distance between the CoG (marked by a blue sticker) and the centre of balance (CoB) when the all components are loaded (battery, payload and any appropriate counterweights). The balance limitations for each aircraft are given in the table below. In the case of these ArduPilot controlled multi-rotor aircraft, autotuning can be undertaken to automatically adjust thrust generation from the motors to optimise the safe flight operation when the centre of balance is not aligned exactly with the CoG. To an extent, this eases the balance limitations to the value specified in the table below. These multi-rotor platforms will be considered significantly unbalanced – and therefore not capable of safe flight operations – if simply maintaining altitude requires >75% of the maximum thrust output for any single motor, as insufficient thrust from the more loaded motors to support safe flight operations.

The table below shows the UAS operational limitations

Limitation	Units	Platform			
		XXXXXXX	XXXXXXX	XXXXXXX	XXXXXXX
Operational Endurance <sup>1</sup>	minutes	XXXXXXX	XXXXXXX	XXXXXXX	XXXXXXX
Maximum	m s <sup>-1</sup>	15	15	10	15
Permissible Airspeed	knots	29.2	29.2	20	29.2
Maximum Outside Air Temperature	°C	40°C	40°C	40°C	40°C
Minimum Outside Air Temperature <sup>2</sup>	°C	-20°C	-20°C	-20°C	-20°C
Maximum	m s <sup>-1</sup>	13.4	13.4	9	13.4
Permissible Wind Speed Including Gusts <sup>3</sup>	knots	26.0	26.0	17.5	26.0
Maximum	m s <sup>-1</sup>	4.47	4.47	4.47	4.47
Permissible Wind Gusts, over constant, up to maximum permissible	knots	8.7	8.7	8.7	8.7
Operational Ceiling <sup>4</sup>	M amsl	2,000	2,000	2,000	2,000
	Ft amsl	6,562	6,562	6,562	6,562
Broadcast Frequency Signal Strength <sup>5</sup>		2.4 GHz @ 100 mW, & 433 MHz @ 10 mW	2.4 GHz @ 100 mW, & 433 MHz @ 10 mW	2.4 GHz @ 100 mW, & 433 MHz @ 10 mW	2.4 GHz @ 100 mW, & 433 MHz @ 10 mW
Balance Limitation		40 mm in all directions			

<sup>1</sup> NB. Operational endurance will vary depending on payload weight and battery capacity.

<sup>2</sup> If flight operations are planned for outside air temperatures below -5°C, careful attention should be paid to the crew's clothing and their ability to safely operate the equipment (including for Tx and GCS).

<sup>3</sup> 13.4 m s<sup>-1</sup> = 48 kph = 30 mph = 26 kn. 10 m s<sup>-1</sup> = 36 kph = 22.5 mph = 20 kn. Wind speeds are typically higher at flying altitudes compared with ground level, so an approximation is considered of an increase of up to 10% at the (UK VLOS maximum) flying height of 121.9 m, combined with dynamic site assessment of wind conditions in relation to local topography.

<sup>4</sup> Air density is critical for the operation of all aircraft. Air density is inversely related with altitude, air temperature and moisture content of air. The operational ceiling is given as the altitude below which the platform handling characteristics will not normally be greatly impacted by changes in air density. Within the constraints of VLOS operations (i.e., within 121.9 m of the ground surface), flight operations above 2000 m amsl are possible, but platform endurance and carrying capacity will be reduced, particularly for multi-rotor UAVs. This reduction may be approximated as a 1% reduction in flight time per 100 m of altitude.

<sup>5</sup> NB. The transmission of control and telemetry signals at the 2.4Ghz and 433Mhz frequencies can be greatly impeded by moisture in the atmosphere; for further details on remission frequencies and powers, please refer to the aircraft technical specification in section 7.

### 7.3. Types of Operation

Operation Type	UAS Utilised	Payload Fitted
VLOS – Terrestrial Survey	XXXXX, XXXXX, XXXXX, XXXXX	<b>Compact Cameras:</b> E.g. Canon Powershot S100/S110/D30, Panasonic Lumix LX5, Panasonic GF3, Ricoh GR, GoPro. <b>SLRs:</b> E.g. Nikon D800. <b>Thermal Cameras:</b> E.g. FLIR Tau2640, Optris PI450. <b>Multispectral Cameras:</b> E.g. Tetracam Micro MCA. <b>Hyperspectral Cameras:</b> E.g. Tetracam.
VLOS – Sea Survey	XXXXX, XXXXX, XXXXX, XXXXX	<b>Compact Cameras:</b> E.g. Canon Powershot S100/S110/D30, Panasonic Lumix LX5, Panasonic GF3, Ricoh GR, GoPro. <b>SLRs:</b> E.g. Nikon D800. <b>Thermal Cameras:</b> E.g. FLIR Tau2640, Optris PI450. <b>Multispectral Cameras:</b> E.g. Tetracam Micro MCA. <b>Hyperspectral Cameras:</b> E.g. Tetracam.
VLOS – Animal Survey	XXXXX, XXXXX, XXXXX, XXXXX	<b>Compact Cameras:</b> E.g. Canon Powershot S100/S110/D30, Panasonic Lumix LX5, Panasonic GF3, Ricoh GR, GoPro. <b>SLRs:</b> E.g. Nikon D800. <b>Thermal Cameras:</b> E.g. FLIR Tau2640, Optris PI450. <b>Multispectral Cameras:</b> E.g. Tetracam Micro MCA. <b>Hyperspectral Cameras:</b> E.g. Tetracam.

## **8. Maintenance Principles and Regime**

Only ESI DroneLab staff or ESI DroneLab trained technicians can carry out maintenance to unpiloted aerial systems. In all cases the UAS maintenance logbook must be filled in to reflect any work completed and a flight test which tests all functions must be carried out by a registered, qualified ESI DroneLab pilot. All ESI DroneLab logbooks are stored in an online directory.

### **8.1. Routine Maintenance**

The ESI DroneLab splits routine maintenance into 3 sections.

- Firstly, there are the Pre-Flight and Post-Flight checklists as shown in Appendix D. These will be carried out by an ESI DroneLab pilot every time an ESI DroneLab aircraft is operated.
- Secondly, there is the minor level service also shown in Appendix C. This type of service is performed every time a vehicle has been operated for five hours, or when deemed necessary. These will be carried out by an ESI DroneLab pilot or an ESI DroneLab trained technician.
- Finally, there is the major level service also shown in Appendix C. This type of service is performed either yearly or every fifteen hours of flight time, whichever comes first. These will be carried out by an ESI DroneLab pilot or an ESI DroneLab trained technician.

Minor and major level services will be recorded in each UAS' maintenance logbook along with any findings. Any issues identified must be remedied and the aircraft must undergo a full flight test before the aircraft is returned to operational status.

If any issues or problems are identified then the aircraft must not be allowed to fly until the issue has been remedied. If minor problems (damaged propeller, faulty battery pack etc.) are identified and remedied and the PiC believes the aircraft is suitable to return to operational status then the work completed should be noted in the UAS maintenance logbook. If major issues are identified (unserviceable motor, damaged airframe etc.) then the aircraft must undergo a full flight test regime as shown below once the identified fault has been remedied:-

#### FULL FLIGHT TEST

The system must have all functions thoroughly tested with a minimum of ten minutes flight time by a qualified ESI DroneLab pilot, with any abnormalities recorded in each aircraft's operating hours logbook. If the PiC deems the aircraft safe then they will sign the UAS operating hours logbook as fit for operational use. If any doubts exist as to the new upgrade then the aircraft should be subjected to further testing to isolate and rectify the problem, or downgraded to the previous firmware and the flight test procedure repeated.

### **8.2. Software and Firmware Update Policy**

From time to time it will be necessary to update the software used by various components of the UAS. In all circumstances the upgrade should only be performed by trained ESI DroneLab personnel. All upgrade information such as version numbers and new functions must be recorded in the UAS maintenance logbook.

Any upgraded system must then have all functions thoroughly tested with a minimum of ten minutes flight time by a qualified ESI DroneLab pilot, with any abnormalities recorded in the UAS operating hours logbook. If the PiC deems the aircraft safe then they will sign the UAS operating hours logbook as fit for operational use. If any doubts exist as to the new upgrade then the aircraft should be subjected to further testing to isolate and rectify the problem, or downgraded to the previous firmware and the flight test procedure repeated.

## **9. Supervision of Unmanned Aerial System (UAS)**

When in-flight the ESI DroneLab PIC on the day is responsible for supervising the operation of the ESI DroneLab UAS.

## **10. Incident Investigation and Mandatory Occurrence Reporting**

Any incidents or occurrences will be dealt with by ESI DroneLab as follows:-

### **10.1. Incident Handling**

In the event of any incident, the severity must be assessed. The following lists should help to identify minor and major incidents:-

#### Minor Incidents

- Any unusual or unexpected flight behaviour from the aircraft which does not result in damage or loss.
- Any failure of any aircraft system which does not result in damage or loss.

#### Major Incidents

- Any unusual or unexpected flight behaviour from the aircraft which results in damage or loss.
- Any significant damage to the aircraft caused by an aircraft system failure.
- Any significant danger or damage to persons, possessions or property during flight operations.
- Any public encroachments or aircraft incursions which required preventative measures to avoid.

### **10.2. Incident Logging**

All MINOR incidents should be logged in the Aircraft Operating Hours Logbook. Upon noting a minor incident the logbook should be checked for similar occurrences. If a minor incident occurs three times then an investigation should be initiated to identify the cause and consider implementing steps to reduce the likelihood of this incident occurring again.

All MAJOR incidents require an investigation as outlined in the Investigation Procedure section (10.3) and the Incident Logbook should be completed.

### **10.3. Investigation Procedure**

Any investigations undertaken by ESI DroneLab will follow the procedure shown below. EuroUSC™ will be advised initially of any occurrence with a simple statement of the known facts such as date, time, location, aircraft involved, PIC, damage sustained and a brief description of the occurrence. EuroUSC™ will also then receive a copy of the final investigation report once completed.

#### Introduction

The introduction contains the context for the Incident and confirms the major facts as to the companies and people involved, why they were present and the reason for the flights being carried out.

#### Description of Events

This is a factual account of the events leading up to and immediately after the incident as well as the incident itself. Its aim is to provide an agreed basis upon which the analysis is carried out.

Importantly any assumptions should be clearly stated and all data provided should have its authenticity and derivation stated. If there are doubts then these should also be clearly articulated so that future analysis can take this into account.

### Analysis

The analysis of events sets out to find explanations for what is described in the description of events. Wherever possible the analysis draws upon known concepts, models and physical understanding to ensure that the events as described have a logical explanation.

The analysis should set the scene for any conclusions and provide traceability from the facts to the conclusions in a logical and auditable way.

### Conclusions

The conclusions are derived from the analysis, which themselves are based upon the facts in the description of events or the facts as they pertain to concepts, models and physical understanding exposed within the analysis. A strong conclusion is one where this traceability is good and can stand up to scrutiny.

### Recommendations

The aim of the recommendations is to provide the organisations or personnel identified for the report with those items and actions that can lead to a safer operation and which address the short-comings highlighted through the investigation process. These may cover anything however the key issue of safety must be addressed and is the primary concern of EuroUSC.

## **10.4. Mandatory Occurrence Reporting**

Mandatory Occurrence Reporting will be completed as required by the National Aviation Authority for the particular country of operation. For example, when operating in the United Kingdom the compliance document is the UK Air Navigation Order CAP382 which states "*Any incident which endangers or which, if not corrected, would endanger an aircraft, its occupants or any other person*" is a reportable occurrence. Reporting will be carried out utilising the form SRG 1601 (available from <https://www.caa.co.uk/application.aspx?catid=33&pagetype=65&appid=11&mode=detail&id=5080>).

In the event that a person is injured or killed the PiC or other nominated ESI DroneLab personal will also contact the UK Air Accident Investigation Branch (AAIB): the AAIB operates a 24 hour hotline, +441252 512299, and following registration of the incident the AAIB will advise you whether anything additional is required. This complies with CAP 393 – Section 226.

## **11. Operation of Multiple Aircraft**

Not applicable at present time, due to CAA restrictions.

## **12. Flight Team**

### **12.1. Qualification Requirements and Currency**

All personnel operating as PiC for ESI DroneLab must be at least eighteen years of age and have undertaken the following:-

- BNUC-S™ Qualification (assessed through Theory Examination & Flight Operations Examination)
- ESI DroneLab Operational Training

ESI DroneLab pilots are required to maintain operational currency standards by ensuring that they operate a remotely piloted platform or for at least thirty minutes flight time in every two calendar months. This may be completed with training flights or in circumstances such as periods of adverse weather conditions a flight simulator may be permitted. All ESI DroneLab pilots maintain an up-to-date pilot hours logbook, on an online repository, is available for submitting to EuroUSC™ once a year if requested.

### **12.2. Crew Health**

It is the responsibility of the individual to determine if they are in a physically and mentally fit condition to operate as part of the Flight Crew for ESI DroneLab. All Flight Crew members must be capable of clearly reading a vehicle registration number plate from twenty metres distance. ESI DroneLab Flight Crew members shall not operate if they are under the influence of alcohol. All Flight Crew members taking prescription drugs should seek professional guidance and also advise the PiC. Any Flight Crew members should advise the PiC or Observer if an aircraft is in flight immediately if they feel unable to continue with their assigned responsibilities. All ESI DroneLab Pilots are limited to a maximum of four hours flight time in any twenty four hour period.

## **13. Logs and Records**

ESI DroneLab will maintain up-to-date information and operational logbooks for:-

- Aircraft and Pilot Operating Hours Logbook
- Battery Logbook
- UAS maintenance Logbook
- Incident / Accident Logbook

Please see Appendix E for details of the information recorded in these logbooks.

## **PART C – FLIGHT PLANNING AND PREPARATION (Pre-Site)**

### **14. Determination of Intended Task and Feasibility**

Initial customer enquiries should be captured using the job specification form found in Appendix C. A pre-site survey form, risk assessment form and an on-site survey form should also be combined with this Initial contact form to produce a 'job file', a hard copy of which will be taken On-Site whilst the Flight Operations are undertaken. This job file will be retained for at least three years for future reference if required.

### **15. Operating Site Location and Assessment**

The pre-site assessment survey form found in Appendix C should be completed by any trained ESI DroneLab personnel:

### **16. Risk Management**

Hazards potentially affecting normal flight operations will be evaluated by ESI DroneLab personnel, using the risk assessment forms found in Appendix C. This risk assessment, and identified controls to mitigate risks are recorded in Appendix C.

### **17. Communications**

Contact telephone numbers for the following must be recorded on the On-Site Survey Form which can be found in Appendix C before embarkation to the site. This task is best carried out at the planning stage whilst the Pre-Site Survey form is being completed. When on-site all ESI DroneLab crew members must carry a mobile phone.

### **18. Pre-Notification**

Pre-Notification is required if a planned flight operation is to take place within two and a half nautical miles of any aerodrome (*in the UK*). The PIC should contact the local control tower to advise the controller of the planned flight operation at least twenty four hours before the planned flight. If applicable, contact details for the tower will be recorded on the relevant pre-site assessment form.

If the planned flight operation is to take place in areas where there is likely to be members of the public, it may be appropriate to inform the local police. The contact number can be found on the On-Site Assessment form.

If the flight operation is to take place in highly congested areas such as housing estates a leaflet drop must be considered at least seven days in advance to advise members of the public of proposed flight operations. For operations in public areas where public address systems are available, it is desirable for an ESI DroneLab employee to announce planned flight operations at least one hour before commencement.

### **19. Site Permissions**

ESI DroneLab will obtain prior permission from all land owners over which flight operations are to be conducted. The permission will preferably be obtained by e-mail as part of the pre-site assessment process, though in some instances it may be necessary to obtain the clients written signature from the client on site. No flight operations will commence without permission from all relevant landowners. If

operations are within a congested area, landowner permission should also be obtained from any properties within 50 m of the proposed flight path.

## **20. Weather Forecasts**

In the week leading up to any flight operation ESI DroneLab will obtain long range weather forecasts. Twenty four hours before the proposed flight operations a further weather forecast will be obtained. The PiC will then review the weather forecast and, based on the aircraft limitations, make a decision about the feasibility of the planned flight operations. If possible, clients should be informed at least twenty four hours in advance if flight operations are to be postponed. Weather forecasts are available from the following websites:-

- UK Meteorological Office (<http://www.metoffice.gov.uk/public/weather/forecast>)
- Norwegian Meteorological Office ([http://m.yr.no/place/United\\_Kingdom/England/](http://m.yr.no/place/United_Kingdom/England/))
- MetCheck (<http://www.metcheck.com/UK/>)

## **21. Preparation and Serviceability of Equipment**

ESI DroneLab will ensure that all aircraft are kept in a serviceable condition through routine maintenance and the following checklists which can be found in Appendix D:

- Embarkation Checklist
- Arrival Checklist
- Pre-Flight Checklist
- Post-Flight Checklist
- Minor Level Service Checklist
- Major Level Service Checklist

The ESI DroneLab PiC on the day is responsible for ensuring that all checklists are completed correctly. The ESI DroneLab PiC must check the Aircraft Maintenance Logbook for any issues and ensure that all required flight batteries are fully charged and ready to use before arriving at the operations site location.

## PART D – OPERATING PROCEDURES (On-Site)

### 22. On-Site Assessment Survey

Upon arrival at the operating site location, the ESI DroneLab PiC will carry out an on-site assessment survey to familiarise themselves with the local geography of the site. This is completed by physically walking around the site to assess any hazards marked on the Pre-Site Assessment Form. If additional crew are present, it is advisable to carry out this procedure with all present, so that all issues can be discussed as they are found. All findings should be recorded using the on-site assessment form found in appendix C. To facilitate crew orientation and assist with flight operations, it may be helpful to use a smart phone running the GPS test application (available from [https://play.google.com/store/apps/details?id=com.eclipsimgpsstatus2&hl=en\\_GB](https://play.google.com/store/apps/details?id=com.eclipsimgpsstatus2&hl=en_GB)). This complies with CAP 722 – Appendix A3/A4.

### 23. Selection of Operating Areas

The ESI DroneLab PiC should select a position from which to launch, land and operate the UAS; this position should ensure full VLOS over the AOI and preferably positioned between the AOI and the sun, to avoid visual impairment during UAS operation. This position should be discussed with the observer, when present.

The ESI DroneLab PiC should select a take-off/landing zone and, where available, backup landing area. This zone should be discussed with the observer, when present, and should:

- Be clear of physical obstacles (e.g., overhanging trees, rocks, buildings, power lines etc.)
- Be on level terrain (avoiding steep slopes)
- Consider effects such as wind shear (caused by vegetation, buildings, cliffs etc.)
- All buildings and persons not under the control of the PiC must remain 30 metres away from the aircraft for take-off and landing, and 50 metres away during flight.

### 24. Weather Checks

The ESI DroneLab PiC for the operation must assess the local weather conditions. Predicted wind speed (in  $m/s^3$ ), precipitation or humidity and outside air temperature will be monitored in the days leading up to the operation. If weather conditions are forecast as suitable then further weather checks will be undertaken on-site obtained by both visual assessment and using a handheld anemometer. The wind direction can be obtained using a compass or compass feature of a smart phone. The Rain Today application (<http://www.raintoday.co.uk/>) could also be consulted for operations in the UK, this gives information about the path rain has taken and predictions can be made from this. The on-site weather information should be recorded on the on-site survey form.

The 'K' index describes the interference electromagnetic ranges from 0-9, 0-3 is fine for flight operations, 4-5 caution is advised when working with GNSS guided modes, 6-9 expect poor GNSS performance (do not commence flight operations relying on GNSS guided-modes).

## **25. Crew Briefing**

If possible, details of the mission should be issued to the observer at least twenty four hours prior to the planned mission. Where an observer is present, the ESI DroneLab PiC will give a briefing before any flight operations take place. The briefing must cover the criteria listed below.

- Advise Observer of Take-Off, Landing, Emergency and Operating areas.
- Confirm flight plan with the crew, including expected flight times, durations and quantities.
- Ensure Observer is familiar with the GCS & Tx failsafe function.
- Check that the crew are happy to proceed.
- Issue two-way radio communication devices if required and state channel to use.

## **26. Crew Clothing**

All ESI DroneLab flight crew members should check the weather forecast before the planned flight operation and be wearing suitable footwear and clothing (that as a minimum covers at least part of the body) to the operating site. Whilst on site, photo identification (e.g., University of Exeter Identity Card, or UK driving licence) must be carried. The use of high visibility clothing by members of the flight crew should be considered by the PiC prior to flight operations.

## **27. Cordon Procedure**

The pre-site assessment should have identified if a cordon is required, but this decision will be re-evaluated on-site by the ESI DroneLab PiC. If large numbers of the public are expected then a cordon should be established fifty metres around the planned flight path. This cordon should be set out using cones and safety tape. Signs should be placed every 40 metres advising members of the public that UAS flight operations are in progress. Extra spotters may be required to be positioned at gates or on public footpaths to advise members of the public about the dangers of entering the area. Gates may be closed, access may be restricted but spotters may not detain any members of the public or prevent them from accessing public rights of way. The spotters are there to advise on the dangers of entering restricted areas and to advise the PiC about public encroachments. If the location is set in a more rural area then a local cordon around the take-off and landing area may be utilised, this can be as little as four markers set out into a five metre square. It is the responsibility of the spotter to ensure that the PiC is aware of any encroachment from a member of the public. As previously explained, the autonomous UAS operations enables some interaction of the PiC with the observer while sufficiently supervising the aircraft.

## **28. Aircraft Communications**

As part of the on-site assessment survey the ESI DroneLab PiC will ascertain the quality of the positional solution afforded by the GNSS by using the GCS, and consideration should be given to buildings and structures which could block or distort (e.g., multipathing) GNSS signals. The GCS will notify the PiC of the number of satellites detected and the PDOP value. All airframes are fitted with an ArduPilot enabled flight controller that have GNSS pre-flight check inbuilt, whereby a minimum of 6 satellites producing a PDOP signal value of 2.5 or less is required for the UAS to arm for flight.

Because the UAV flight controller has a sensor suite (including barometer, accelerometers and magnetometer) that support flight operations, if the GNSS-derived position solution does not meet the requirements of the pre-arm flight check, due to insufficient signal strength from the available satellite constellation, it may be appropriate in some cases (e.g. small survey areas in remote locations where horizon view may be obscured by topography and/or vegetation) for the PiC to override this pre-flight check in order to undertake a manual flight to complete the task at hand. This will restrict lost-link failsafe options to 'land' immediately, rather than the standard 'return-to-launch'.

The aircraft controlling link is established on the 2.4GHz frequency at 100 mw. These frequencies can be susceptible to interference from other devices, particularly in urban areas. In all instances, all Wi Fi

enabled devices (included phones, laptops and cameras) in the proximity of flight operations should have the WiFi turned off for the duration of flight operations. Importantly, the primary control link (Tx – FrSky Taranis and Rx – FrSky X8R combination) use a frequency hopping spread spectrum (FHSS) method, ensuring a robust and virtually interference free 2.4 Ghz link. They also use (EU) ETSI EN 300 328 compliant listen-before-talk firmware.

GCS telemetry is communicated on the 433 Mhz frequency using SiK Radio (3DR's version 2) HM-TRP radios flashed with SiK 1.9 firmware and the MAVlink communication protocol at 10mw power on a 10 hz cycle (OfCom IR2030/1/10 compliant). As with the FrSky equipment, they also utilise FHSS and listen-before-talk to ensure robust communication and EU compliance. If the 2.4 GHz primary control link becomes inoperable for any reason (e.g., Tx malfunction or interference), the GCS telemetry link can be used as a backup control link, allowing redirection of the UAV to a safe landing site (should the RTL home location become unsafe, for example, due to encroachment by puppies). These procedures are compliant with CAP 722 –Section 5.

## 29. Charging and Fitting of Batteries

The ESI DroneLab trained personnel are responsible for charging the battery packs. All battery packs should be checked as part of the embarkation checklist found in Appendix D. All ESI DroneLab battery packs will be identified by a unique identification code, written on each battery pack. These battery identification codes are recorded in the battery charge logbook, which is stored on an internal directory. The ESI DroneLab's protocols for safe storage, charging, transportation and discharging are intended to significantly reduce the risk of Lithium Polymer (LiPo) battery failure. The main causes of LiPo batteries failure are: over-discharging (below 3.2 V per cell), over-charging (above 4.2 V per cell) and excessive heat (> 60°C; typically due to excessive current draw or charging too rapidly, especially when ambient temperatures are high). Relevant battery information will be recorded in the battery charge logbook, an example of which can be found in Appendix E. The ESI DroneLab parameters for use of LiPo batteries are as follows:

- Charging
  - o Battery packs will be charged to a maximum of **4.2 V per cell** (i.e. 3S = 12.6 V; 4S = 16.8 V).
    - A **balance charger** will be used for every charge cycle (to avoid unequal charging of cells).
    - Battery packs will be charged at a **rate of 1C** for packs with a discharge rate of <20C, and a rate of up to 2C for packs with a discharge rating of ≥20C. Charge rate can be calculated as  $Charging\ Amps = \frac{battery\ capacity\ (mAh)}{1000} \times C$  (e.g., 6000 mAh capacity battery @ 1C = 6 A, 6000 mAh @ 2C = 12 A, etc.).
  - o The procedure for flight battery charging is:-
    - Check the battery voltage using a voltage meter.
    - Select the appropriate settings on the charger for the battery.
    - Connect the battery to the charger charge lead and balance lead.
    - Place the battery pack into a Lipo-Safe bag and start the charge cycle.
    - Charging battery must never be left unattended.
    - When battery is charged record the V level in the charge logbook.
    - Switch off the charger and disconnect the battery pack and place in the "ready to use" Lipo-Safe bag.
- Storage
  - o Batteries will be stored with a charge of between 40 to 70% (between 3.5 V to 3.9 V).
  - o All batteries will be stored in Lipo-Safe bags.
  - o Where available, batteries will be stored in a fridge (NB. LiPo batteries should be allowed to warm before charging).
  - o If a battery pack is not used in any three month period it must be checked and topped up to storage or flight capacity as required.

- Use
  - o Before any battery is to be used in flight, the voltage must be checked using the battery checker, and the indicated capacity should be sufficient for the planned flight
  - o Balance of battery pack cells to be checked pre-flight charging with a battery checker
  - o Battery packs must NEVER be discharged below 3.2 V per cell
  
- Replacement
  - o Battery packs can be used commercially for up to 150 cycles or 3 years, whichever comes first
  - o Battery packs will be suspended from use if there is (i) a noticeable drop in capacity (manifesting as noticeable drop in flight endurance), (ii) the charge cannot be balanced to within 0.1 V across the cells, or (iii) if any signs of physical deterioration are observed (e.g., puncturing of the battery pack casing, or puffing).
  - o Suspended batteries will be disposed of, through the recognised battery disposal area at the local authority refuse site. For safety reasons, it's best that LiPo cells are fully discharged before disposal (however, if physically damaged it is NOT recommended to discharge LiPo cells before disposal).

### 30. Loading of Equipment

The ESI DroneLab Observer (or PiC if no Observer) is responsible for ensuring that the payload is ready to use. If the payload is a camera the memory card should have sufficient space for the mission and the battery should be charged.

The ESI DroneLab PiC is responsible for ensuring that the aircraft does not operate in excess of the stated maximum take-off mass. The PiC is responsible for ensuring that the payload is securely fitted to the airframe; all payloads require two mechanical fixings such as a retaining bolt, a safety lanyard or another fixing such as a Velcro strap before flight operations can commence. The PiC should ensure that when the payload and battery is loaded, the center of balance complies with the balance limitations stated for each platform (balance limitations for each platform are described in section 7.2). Under no circumstances should the aircraft fly if the balance is impeded.

### 31. Pre-Flight and Post-Flight Checks

The ESI DroneLab PiC on the day must complete the following checklists as required:

The **Embarkation Checklist** must be completed in advance of departure before the equipment is brought to site

The **Arrival Checklist** must be completed as soon as the PiC reaches the intended flight operation location.

The **Pre-flight Checklist** must be completed immediately prior to any flight operation.

The **Post-flight Checklist** must be completed immediately after landing.

All Checklists can be found in Appendix D. If any fault or problem is found which can't be remedied then the intended flight operations must be postponed until a solution is found. Any interrupted checklist procedure must be restarted from the beginning.

All airframes are fitted with an ArduPilot (both ArduCopter and ArduPlane) enabled flight controller. This software includes a series of automatic pre-arm safety checks, which will prevent the vehicle from arming if any problems are identified. These checks include (but are not limited to):

- Missed Tx to Rx calibration

- Missed magnetometer (compass) calibration or compass error
- Bad IMU sensor data
- Barometer failure
- PDOP in excess of 2.5
- Error with dual accelerometer error
- Error with dual gyroscope data
- Error in power supply to flight controller

There is also a pre-flight check for GNSS position solution, which requires a minimum of 6 satellites producing a PDOP signal value of 2.5 or less is required for the UAV to arm. If the position solution does not meet the requirements of the pre-arm flight check, due to insufficient signal strength from the satellite constellation, and because the flight controller has a sensor suite (such as barometer, accelerometers and magnetometer) that enable flight via dead-reckoning, it may be appropriate in some cases (e.g. as small survey areas in remote locations with high topographic relief which occludes the horizon and thus GNSS constellations) for the PiC to override this pre-flight check in order to undertake a manual flight to complete the task at hand.

## **32. Flight Procedures**

The following procedures are basic guidelines for ESI DroneLab flight crew. As far as practically possible these procedures must be complied with. The ESI DroneLab PiC on the day is responsible for supervising the operation whilst the aircraft is in flight, and organising the safe distribution of supporting operatives before the aircraft is in flight.

### **32.1. Start-up Procedure**

The following procedure is to be completed by the PiC

- Check flight battery pack with battery checker, ensure cells are balanced and voltage is sufficient to complete the mission safely.
- Record battery pack identification code and voltage in the battery logbook
- Switch on the aircraft control Tx and ensure Tx battery level is sufficient to complete the mission
- Ensure aircraft is level and stable, then fit the flight battery and allow the flight controller to perform calibration checks whilst untouched. If using a fixed wing, ensure aircraft is facing into wind.
- Connect UAS to GCS to ensure pre-arm checks passed.
- Ensure ALL switches on the aircraft control Tx are set correctly.
- Read waypoints from flight controller to ensure mission is correct and ready.
- Test camera trigger if applicable.
- Test camera gimbal operation and move to take-off position if applicable.
- If flying a fixed wing, arm UAS via safety switch to test flight control surfaces from both the Tx and in flight controller stabilized modes. Disarm UAS via safety switch until ready to launch.

### 32.2. Take-off Procedure Multi-rotors

The following procedure is to be completed by the PIC for Multi-rotors

- Make a 360° visual sweep of the area (*Pay particular attention to airspace and public encroachments*)
- Confirm with the observer that it is clear to take off
- Check and note the time
- Call "Taking Off" and start the motors (*Move the left transmitter stick to bottom right*)
- Check throttle response between 0-30%
- If flying a fully autonomous mission and depending on weather, take a final look above the aircraft and switch to auto mode, then apply greater than 30% throttle to start autonomous mission.
- If taking off in stabilized mode, take a final look above the aircraft and power up to ¾ power (*Use a rapid movement*). This assertive take-off minimises destabilisation due to ground cushion effects.
  - o Climb to approximately 5-10 m and engage altitude hold or loiter to test function
  - o Test yaw and cyclic controls (*Use small gentle movements and ensure aircraft reacts correctly*)
- Check battery status and number of satellites being tracked
- Confirm with observer that the planned flight operation is still good to go ahead

### 32.3. Take-off Procedure Fixed Wing

The following procedure is to be completed by the PIC for Fixed Wing

- Make a 360° visual sweep of the area (*Pay particular attention to airspace and public encroachments*)
- Confirm with the observer that it is clear to take off
- Check and note the time
- Observer to arm via safety switch and hand launch aircraft
- Call "Taking Off" and start the motors (*Move the left transmitter stick to bottom right*)
  - o Check throttle response between 0-30%
- If flying a fully autonomous mission, take a final look above the aircraft and switch to auto mode, then apply 50% throttle, then hand launch to start mission.
- If taking off in FBWA (Fly-By-Wire A mode – this is the fixed wing equivalent to AltHold mode in ArduCopter) mode, take a final look above the aircraft and power to 50% power (*Use a gradual movement*). Observer will then count down from 3 to hand launch. PIC will apply additional control input or throttle after UAS has been hand launched.
- Climb to approximately 30 metres and reduce power to cruise
- Test roll, pitch and yaw controls (*Use small gentle movements and ensure aircraft reacts correctly*)
- Check battery status and number of satellites being tracked
- Confirm with observer that the planned flight operation is still good to go ahead
- Engage auto and advise observer, observer to confirm that UAS is heading to waypoint 1

### 32.4. In-flight Procedure

The following procedure is to be completed by the PIC and, where applicable, observer. This complies with (complying with CAP 393 and CAP 722).

- PIC to keep aircraft within visual line of sight (VLOS), within a 500 m wide by 121 m high bubble
- PIC to maintain primary focus on the aircraft and immediate surroundings
- PIC to ensure they can hear audio notification from GCS for key flight parameters (telemetry status, UAV position, distance to next waypoint, flight battery voltage, PDOP, altitude, flight mode, triggered failsafe). Where an observer is present, this information could also be monitored by the observer.
- Observer to maintain visual lookout for public encroachments and airspace incursions.

Page 26

### 32.5. Landing Procedure for Multi-rotor

The following procedure is to be completed by the PiC, and observer

- If observer is present, PiC to confirm of intention to land in an autonomous or manually piloted mode.
- PiC and observer to visually check landing area to ensure it is safe to land
- If the UAS is in RTL, the UAS will automatically land at the designated home location, with a brief period of hover at 10 metres altitude to allow PiC to make any last minute adjustments to position or to take manual control of UAS for landing.
- PiC to take a final look below the aircraft and call "Landing"
- If in RTL mode, PiC must cut power to throttle 1 m above the ground to allow the flight controller to disengage motors.
- If in a manual mode, PiC to reduce power and land the aircraft (*Be aware of ground effect*)

### 32.6. Landing Procedure for Fixed Wing

The following procedure is to be completed by the PiC, and observer

- PiC to confirm with observer if in an RTL or auto land mode.
- PiC to advise observer of intention to land if in a manual mode.
- Observer to visually check landing area to ensure it is safe to land
- PiC (manual) or observer (auto) to take a final look below the aircraft and call "Landing"
- If the UAS is in auto land mode, the UAS will fly an approach into wind and auto land.
- If the UAS is in RTL, the UAS will return to take-off location and enter circle mode.
- PiC will fly UAS on landing approach into wind
- If in a manual mode, PiC to reduce power and land the aircraft

### 32.7. Shut-down Procedure

The following procedure is to be completed by the PiC

- Upon touchdown stop the motors (*Move the left transmitter stick to the bottom left corner*)
- Approach the aircraft, disarm UAS via safety switch, disconnect the flight battery pack and call "Aircraft Safe"
- Turn off camera
- Check and note the time
- Switch off the aircraft control Tx
- Disconnect GCS link with UAS
- Check flight battery pack voltage with battery checker
- Fill in pilot, aircraft hours and battery logbook

## 33. Emergency Procedures

Below is a list of Emergency Procedures for various scenarios which should be adhered to by the ESI DroneLab PiC. Spotters may need to utilise two way radios to communicate with the PiC to ensure that their calls can be heard by the rest of the crew. Any emergency situation should be recorded in the Aircraft Hours Logbook under the "notes" section. Refer to [Section 10](#) for Incident Handling Procedures.

### 33.1. Flight Controller Failsafes

#### Tx or Rx failsafe (not compatible with G-UAV-IRIS)

The failsafe will trigger if:

- The Tx is turned off
- The vehicle travels outside of RC range (usually at around 500 m ~ 700 m)
- The Rx loses power (unlikely)
- The wires connecting the receiver to the flight controller are broken (unlikely).

When a radio failsafe is triggered one of the following will happen:

- Nothing if the vehicle is already disarmed
- Motors will be immediately disarmed if the vehicle is landed OR in stabilize mode and the throttle is at zero
- If the UAV is armed, has a GNSS lock and is more than 2 meters from the home position, the flight controller will initiate return-to-launch (RTL)
- If the UAV is armed but has no GNSS lock, the flight controller will initiate land

None of these UAS are currently fitted with retractable landing gear. If the failsafe clears (i.e. transmitter and receiver regain contact) while in flight, the autopilot will remain in the current flight mode – RTL. It will not automatically return to the flight mode that was active before the failsafe was triggered. To change the flight mode, the pilot will need to actively the flight mode switch to another position.

### **Battery failsafe**

The failsafe will trigger if:

- The main battery voltage drops below 3.6 volts per cell (i.e. 10.8V for a 3S and 14.4V for a 4S) for more than 10 seconds. Note that the PiC may decide to increase these limits if they believe that the operating environment requires an increased safety margin (for example, operations over water, in congested airspace or in windy conditions).

When the failsafe is triggered one of the following will happen:

- Nothing if the vehicle is already disarmed
- Disarm motors if the vehicle is in Stabilize and the throttle is at zero OR the vehicle is landed
- Return-to-Launch (RTL) if the FS\_BATT\_ENABLE param is set to "2" ("RTL") OR the vehicle is in AUTO mode, has a GNSS lock and are at least 2 meters from your home position
- Land in all other cases

### **GNSS/EKF failsafe**

- APM 2.5 with ArduCopter 3.2:

The GNSS failsafe will trigger if the UAS losses GNSS lock or experience a GNSS Glitch for 5 seconds while in a mode that requires the GNSS (Auto, Guided, Loiter, RTL, Circle, Position or Drift) mode. If triggered the GNSS failsafe will of the following will happen it will initiate an AltHold, and not allow a change of flight mode to a mode requiring GNSS.

- Pixhawk with ArduCopter >3.3:

The GNSS failsafe is now described as an Extended Kalman Filter (EKF) failsafe.

ArduCopter and ArduPlane can use an EKF algorithm to estimate vehicle position, velocity and angular orientation based on rate gyroscopes, accelerometer, magnetometer, GPS, airspeed and barometric pressure measurements. The advantage of the EKF over the simpler complementary filter algorithms is that by fusing all available measurements it is better able to reject measurements with significant errors. This makes the vehicle less susceptible to faults that affect a single sensor, such as the not uncommon

GNSS glitches. EKF also enables measurements from optional sensors such as optical flow and laser range finders to be used to assist navigation.

The failsafe will trigger if:

- EKF's compass and velocity "variance" are higher than 0.8 (configurable with EKF\_CHECK\_THRESH parameter) for one second. This "variance" increases as the estimates become untrustworthy. 0 = very trustworthy, >1.0 = very untrustworthy. If both variances climb above the EKF\_CHECK\_THRESH parameter (default is 0.8) the EKF/Inav failsafe triggers.

When the failsafe is triggered the following will happen:

- The Pixhawk's LED will flash red-yellow, the tone-alarm will sound, EKF/DCM error will be recoded to the dataflash logs, and if telemetry is attached "EKF variance" will appear on the GCS heads-up-display (HUD).
- If flying in a flight mode that does not require GNSS nothing further will happen but the system will be unable to switch into an autopilot flight mode (Loiter, PosHold, RTL, Guided, Auto) until the failure clears (this applies to both multi-rotors and fixed wing).
- If flying in a mode that requires GNSS (Loiter, PosHold, RTL, Guided, Auto)
  - o Multi-rotor, it will switch to AltHold, allowing the pilot to bring the vehicle home.
  - o Fixed wing, it will go into a Loiter at its current location (altitude and speed are not affected due to the use of analogue systems for barometric pressure and airspeed). This gives the vehicle the chance to regain a GNSS lock and then continue on its mission, but in cases where this may not happen, it also gives the pilot the option to revert to a manual flight mode (e.g., Stabilize) to bring the vehicle home.

#### **Ground Control Station - THIS FAILSAFE IS NOT USED**

Due to low strength and cycle limits permitted on the 433MHz band in the UK, the GCS telemetry link frequently fails during flight operations; consequently this failsafe is disabled on all ESI DroneLab platforms, and the procedure outlined in the relevant 'Action Required' section in the table below is followed.

### 33.2. Crew Emergency Procedures

Emergency Type	Action Required	Responsibility Delegated to
<b>Tx/Comm Link/Rx Failure Frequency Interference</b>	Call " <i>Radio Failsafe</i> " so that the crew understand the situation and observe the aircrafts flight path. Upon transmitter failure or frequency interference the aircraft will enter the 'Failsafe' mode as described above.	<b>PiC/Observer</b>
	Upon seeing or hearing the call " <i>Radio Failsafe</i> " ensure that the take-off site is clear of all persons as the aircraft will be returning to its initial 'power up' coordinates.	<b>PiC/Observer/Spotter</b>
<b>Loss of Propulsion Motor or Propeller Failure Aircraft Battery Failure</b>	Call " <i>Dead Drone</i> " and assess if the aircraft is controllable, if sufficient control is maintained head directly to either the landing site or alternate landing site whichever is closest. If control is compromised try to execute a controlled descent.	<b>PiC</b>
	Upon hearing the call " <i>Dead Drone</i> " identify the closest safe landing position to the aircraft and advise the PiC.	<b>Observer</b>
	Upon hearing the call " <i>Dead Drone</i> " immediately clear any persons directly underneath or in the path of the aircraft to either the landing site or alternate landing site whichever is closest. Maintain visual contact with the aircraft once the area is clear.	<b>Observer / Spotters</b>
<b>Ground Control Station Failure</b>	The Observer will call " <i>GCS Failsafe</i> ", informing the PiC of the last known voltage of the UAS and mission time and whether there has been a complete failure of the GCS, or whether it is a signal dropout, allowing the PiC to base the next decision on remaining UAS capability. If the UAS is flying in an auto mode, the PiC can choose to allow the aircraft to continue on as the PiC and the crew are all aware of the flight plan and can observe for any deviation such as the UAS flying off course (as a result of mode change due to another failsafe, i.e. GNSS failure mode change to althold). If in a non-auto mode such as stabilize or althold/FBWA, the PiC can choose to continue flying. Both of these scenarios will allow for the telemetry link to recover in a case whereby there has not been a complete loss of GCS or whereby a laptop battery swap could recover the GCS. The PiC can also choose to end the mission, call " <i>Landing</i> " and carry out the standard landing procedure.	<b>Observer / PiC</b>
<b>Loss of GNSS Signal</b>	Call " <i>GPS Failsafe</i> " and confirm that the UAS has entered into Althold mode	<b>Observer (PiC if no Observer)</b>
	Upon hearing the call " <i>GPS Failsafe</i> " and confirmation that UAS is in Althold mode, head directly to either the landing site or alternate landing site whichever is closest. If Althold mode has not been initialized automatically by the flight controller, switch mode to either Althold/FBWA or stabilize, before commencing the landing procedure. If control is compromised try to execute a controlled descent.	<b>PiC</b>
	Upon hearing the call " <i>GPS Failsafe</i> " proceed to clear any persons from the possible path of the aircraft. Maintain visual contact with the aircraft once the area is clear.	<b>Observer / Spotters</b>

<b>Public Encroachment</b>	Call "Public" and approach the member of the public asking them to follow you to safety as they are currently in an extremely dangerous situation.	<b>Spotter</b>
	Upon identifying an encroachment from a member of the public or hearing the call "Public" advise the PIC by using the relevant phrase ("Public Below", "Public Left" or "Public Right"). Identify the nearest available landing site away from the encroachment and advise the PIC. Once the PIC confirms they understand, if there is no Observer present dealing with the situation approach the member of the public asking them to follow you to safety as they are currently in an extremely dangerous situation.	<b>Observer</b>
	Upon being advised by the Observer of a public encroachment immediately hold position and wait for further instruction. The Observer will advise which the safest area to land is and confirmation should be given that the instruction has been understood. Immediately proceed to the advised landing site.	<b>PIC</b>
<b>Aircraft Incursions</b>	Upon identifying an imminent aircraft incursion within the 400ft, 500 metre bubble call the relevant phrase ("Aircraft Ahead", "Aircraft Behind", "Aircraft Left" or "Aircraft Right") and maintain visual contact with the approaching aircraft.	<b>Spotter</b>
	Upon identifying an imminent aircraft incursion within the 400ft, 500 metre bubble or hearing the call "Aircraft ..." identify the approaching aircraft. Advise the PIC to take a voiding action by using the phrase "Aircraft, Descend". Once the intruding aircraft has passed by then Advise the PIC by using the phrase "Aircraft Clear".	<b>Observer</b>
	Upon being advised by the Observer of an aircraft incursion immediately hold position and look beneath the aircraft to identify hazards. Descend the aircraft to around 10 m above the ground or any structure. Once the Observer advises the incursion no longer exists the planned operation may resume. It should be noted that descending a multi-rotor too quickly can result in a crash due to dropping through dirty air, if it is safe to do so and is absolutely necessary, a PIC may choose to take a rapid descent risk to avoid an air collision.	<b>PIC</b>
<b>Fly Away Actions</b>	Activate the RTL failsafe function, if no response from the UAS, switch to a non-GNSS mode such as 'AltHold' and try to manually fly the UAS. If still no response, switch back to RTL in case communication is re-established and maintain direct visual contact with the aircraft for as long as possible. If visual contact is lost make a note of estimated altitude, speed, remaining battery endurance and heading. Once the Observer confirms actual information contact the local air traffic control and local police using the contact numbers found on the on-site assessment form to advise them of the situation. If the aircraft is seen to make contact with the ground or a structure, execute the shutdown procedure and walk over to the crash site. Take photographs at the crash site, contact details and statements from anyone present and recover the aircraft. Leave contact details for any property damaged as a result.	<b>PIC</b>
	If the UAS has breached the GeoFence and the appropriate failsafe has not been triggered as highlighted in the failsafe section, call "Fly Away" so that the crew understand the situation.	<b>Observer</b>

	Upon hearing "Fly Away" immediately monitor the aircraft telemetry data and make a note of the aircrafts actual heading, speed and altitude. Upon the PiC's instruction, try to activate the RTL or land functions on the ground station. Continue to monitor the telemetry data for as long as the connection remains and advise the PiC of the actual information so that the local air traffic control can be advised by the PiC.	<b>Observer</b>
	Upon hearing "Fly Away" maintain direct visual contact with the aircraft for as long as possible and advise the PiC of an estimated heading.	<b>Spotter</b>
<b>Pilot Incapacitation</b>	Upon feeling as though incapacitation is imminent call "Man down" and activate the failsafe function.	<b>PiC</b>
	Upon noticing the PiC has become incapacitated activate the RTL failsafe via the Tx or GCS (if Tx is unreachable) and call "Man down". Ensure that the PiC is not in any imminent danger from a returning aircraft and then ensure that the take-off site is clear of all persons as the aircraft will be returning to its initial 'power up' coordinates. Call for the emergency services if required. Once the aircraft lands and shuts down, disconnect the flight battery.	<b>Observer</b>
<b>Fire (Ground Equipment)</b>	Upon noticing fire call "Fire". If the fire is a Lithium Polymer battery fire do not try to extinguish, allow the battery to burn out and then extinguish any additional fires. If the fire cannot easily be extinguished and increases in size call the emergency services.	<b>All Crew</b>
<b>Fire (Aircraft in Flight)</b>	Upon noticing an aircraft fire call "Aircraft Fire" and wait for instruction from the Observer. Upon hearing "Aircraft Fire", proceed directly as instructed by the Observer to the safest available landing point. Upon landing disarm the motors.	<b>PiC</b>
	Upon identifying an aircraft fire call "Aircraft Fire". Upon hearing "Aircraft Fire" immediately identify the nearest safe landing point and advise the PiC. Approach the aircraft with a fire extinguisher if available and continue as per the Fire (Ground Equipment) procedure	<b>Observer</b>
	Upon identifying an aircraft fire call "Aircraft Fire". Upon hearing "Aircraft Fire" wait for the aircraft to land and then treat the emergency as per the Fire (Ground Equipment) procedure.	<b>Spotter / Remaining Crew</b>

**Appendix A Permission for Aerial Work**

***Insert a valid copy of the Permission for Aerial Work here.***

**Appendix B Insurance Document**

***Insert a valid copy of Insurance Document here.***

## Appendix C Operational Forms

### Risk Assessment Form

Table 1: Consequence Score

Consequence Score	1	2	3	4	5
<b>Description</b>	<b>Insignificant</b> Minor injury not requiring first aid	<b>Minor</b> Minor injury or illness, first aid treatment needed	<b>Moderate</b> Person absent for more than 3 days / bad sprain / broken bone	<b>Major</b> Major injuries, or long term incapacity / disability (loss of limb)	<b>Catastrophic</b> Death or major permanent incapacity

Table 2 - Likelihood Score

Descriptor	1	2	3	4	5
<b>Frequency</b>	<b>Rare</b> Not expected to occur in 100 flights	<b>Unlikely</b> Expected to occur at least every 100 flights	<b>Possible</b> Expected to occur at least every 20 flights	<b>Likely</b> Expected to occur at least every five flights	<b>Almost Certain</b> Expected to occur at least every two flights
<b>Probability</b>	< 1% Will only occur in exceptional circumstances	1 - 5% Unlikely to occur	6 - 20% Reasonable chance of occurring	21 - 50% Likely to occur	> 50% More likely to occur than not

Table 3 - Risk Scoring (RS) Matrix

Likelihood	Consequence				
	1 Insignificant	2 Minor	3 Moderate	4 Major	5 Catastrophic
1 - Rare	1	2	3	4	5
2 - Unlikely	2	4	6	8	10
3 - Possible	3	6	9	12	15
4 - Likely	4	8	12	16	20
5 - Almost Certain	5	10	15	20	25

Table 4. Grading Risk Factors

Score	Descriptor
1 to 6	Low Risk: acceptable and operation can commence
7 to 12	Moderate Risk: mitigation should be considered
13 to 18	High Risk: unacceptable without mitigation
19 to 25	Unacceptable Risk: operation can't be cleared

Table 5. Risk Assessment

What is the hazard (e.g. low temperature, falling rocks)	CS	LS	RS	Action to be taken to control the risk	Residual Risk (risk remaining once controls are in place)		
					CS	LS	RS
Loss of control due to failure of primary control link (Tx-comms.-Rx)	3	1	3	Autopilot programmed to RTL and land in the event of loss of primary control telemetry (2.4 GHz). Ground control station utilizes secondary telemetry link (433 MHz in UK) which can be used to redirect autopilot.	2	1	2
Loss of aircraft control due to insufficient power	3	3	9	Battery status monitored by flight controller and reported to ground control station (with audio low voltage alerts enabled). Autopilot programmed to automatically initiate RTL in event of low power.	3	1	3
Loss of aircraft control in guided autopilot modes due to loss of GNSS fix	3	4	12	Infrequent GNSS glitches can 'disorientate' UAS in guided modes, resulting in 'fly-away' behaviour. Managing this requires continual monitoring by PiC, ready to revert to manual control. The likelihood and impact of GNSS glitches can be further reduced by enabling Extended Kalman Filtering (EKF) on compatible flight controllers (i.e. 32 bit PixHawk). GNSS fix status is monitored continually by flight controller and relayed to ground control station. Simultaneous failure of both primary control telemetry and GNSS solution initiates automatic landing.	3	2	6
Loss of aircraft control due to mechanical failure	3	2	6	Use in remote areas. All craft are small UAVs (<7 Kg). Some multicopter platforms (e.g., Y6, X8), have redundancy in thrust units, allowing control in event of failure of any single thrust unit. Fixed wing aircraft are typically flown at 100 m and are capable of gliding without motor power.	3	2	6

Collision with or interference with other airspace users	5	1	5	Check websites for restrictions on airspace. Operate in authorised airspace, below threshold height (130 m in UK). Check area for other air users (e.g., hobbyist flyers) and only fly if deemed clear.	5	1	5
Fly-away	2	3	6	Continual monitoring by PiC ready to revert to manual control. RTL behaviour programmed in event of primary communications failure. GeoFence normally enabled, restricting horizontal & vertical range of the UAV.	2	1	2
Battery damage on landing leading to fire	4	1	4	Craft under continual supervision of PiC, any crash landings immediately investigated. If vegetation is very dry, a fire extinguisher (preferably powder, for safe use with electrical fires and better protection against reignition compared to CO <sub>2</sub> ) should be available.	2	1	2
Collision with obstacles/operator/spectators during take-off and landing	2	3	6	Avoid flying in high wind speeds in excess of platform limits. The 'home' location should be selected to be clear of obstacles. Brief spectators to remain clear of 'home' and intended landing location (if different to 'home'). When landing in auto mode, PiC should remain ready to retake manual control at all times.	2	2	4
LiPo Battery Fire (detached from drone)	3	2	6	LiPo batteries will be kept in fireproof and waterproof containers while on board a boat or just fireproof containers on land.	1	2	2
Detachment of UAS components during flight	5	2	10	All UAS to be regularly serviced and pre-flight checks to include checking tightness of fittings. Always use at least two mechanical attachments on any payload.	5	1	5
Laceration by propeller blade	3	2	6	Only PiC or Observer (in close communication with PiC) to handle the aircraft when armed.	3	1	3

**Job Specification Form**

<b><u>Client Details</u></b>	<b><u>Date Received:</u></b>
<b><u>Client Name:</u></b>	<b><u>Date Required:</u></b>
<b><u>Address:</u></b>	<b><u>Job Number:</u></b>
	<b><u>Quoted Price</u></b> <u>£</u>
<b><u>Contact</u></b> <b><u>E-mail:</u></b>	<b><u>Site visit</u></b> <u>Yes / No</u> <b><u>requested?</u></b>
<b><u>Number:</u></b>	<b><u>Landowner details</u></b>
<b><u>Area of Interest</u></b> <b><u>Latitude:</u></b>	
<b><u>Longitude:</u></b>	
<b><u>Description of work required:</u></b>	
<b><u>Other relevant information (including other nearby air users if known):</u></b>	

## Pre-Site Assessment Form

### Initial Check

Job: \_\_\_\_\_ Date Completed: \_\_\_\_\_ Completed by: \_\_\_\_\_

Task	Information Source	Completed (initial)	Notes
Review job specification and location (latitude and longitude)	Client information		
Check relevant aeronautical datasets for permanent airspace restrictions, local private airfields, danger areas and no fly zones.	Google Earth 3D Airspace (download .kxz fields from <a href="http://3dairspace.org.uk/airspace.html">http://3dairspace.org.uk/airspace.html</a> ) or Sky Vector ( <a href="https://skyvector.com/">https://skyvector.com/</a> )		Identify whether the planned flight operation occurs within 4.6 km (2.5 nautical miles) of any UK aerodrome; if so, look up local contact number for local control tower.
Identify airspace type			
Obtain Landowner Permission	Possibly client information. If flight operation is in congested area, obtain permission from all landowners within 50 m of planned flight path.		
Check for bird conservation areas	EU nature areas: <a href="http://ec.europa.eu/environment/nature/natura2000/db_gis/index_en.htm">http://ec.europa.eu/environment/nature/natura2000/db_gis/index_en.htm</a>		
Check for temporary airspace restrictions	NOTAMs (Notice to Airmen) ( <a href="http://notaminfo.com/ukmap">http://notaminfo.com/ukmap</a> )		
Check for features of significant to proposed flight operation	Google Earth ( <a href="https://www.google.co.uk/intl/en_uk/earth/">https://www.google.co.uk/intl/en_uk/earth/</a> )		
Consider whether a cordon is necessary to control public encroachment of the operations area			
If in new region (esp. high latitudes), consider checking GNSS satellite coverage	( <a href="https://in-the-sky.org/satmap.php">https://in-the-sky.org/satmap.php</a> )		
Consider Site Access / logistics	Google Maps ( <a href="https://www.google.co.uk/maps">https://www.google.co.uk/maps</a> )		
Advise public	If flight operation is in congested area (e.g., housing estate), consider leaflet drop for public information.		

	If flight operations in area frequented by the public, consider informing local police station of activities.		
Contact information	Pilot Contact Number		
	Client Contact Number (if applicable)		
	Local Air Traffic Control Contact Number ( <a href="http://www.azworldairports.com/airports">http://www.azworldairports.com/airports</a> )		
	Police contact number		Non-emergency: 101
Verify aircraft maintenance status	Maintenance log		

**7 Day check**

Job: \_\_\_\_\_ Date Completed: \_\_\_\_\_ Completed by: \_\_\_\_\_

<b>Task</b>	<b>Information Source</b>	<b>Completed (initial)</b>	<b>Notes</b>
Check weather forecast	Met Office ( <a href="http://www.metoffice.gov.uk/public/weather/forecast">http://www.metoffice.gov.uk/public/weather/forecast</a> ) Yr.No ( <a href="http://m.yr.no/place/United%20Kingdom/England/">http://m.yr.no/place/United Kingdom/England/</a> ) MetCheck ( <a href="http://www.metcheck.com/UK/">http://www.metcheck.com/UK/</a> )		
Check for temporary airspace restrictions	NOTAMs (Notice to Airmen) ( <a href="http://notaminfo.com/ukmap">http://notaminfo.com/ukmap</a> )		
Prefetch maps onto GCS	Mission Planner / Droid Planner		
Design flight plans and load onto GCS	Mission Planner / Droid Planner		

24 hours check

Job: \_\_\_\_\_ Date Completed: \_\_\_\_\_ Completed by: \_\_\_\_\_

<b>Task</b>	<b>Information Source</b>	<b>Completed (initial)</b>	<b>Notes</b>
Check Weather Forecast	Met Office ( <a href="http://www.metoffice.gov.uk/public/weather/forecast">http://www.metoffice.gov.uk/public/weather/forecast</a> ) Yr.No ( <a href="https://www.yr.no/place/United_Kingdom/">https://www.yr.no/place/United_Kingdom/</a> ) MetCheck ( <a href="http://www.metcheck.com/UK/">http://www.metcheck.com/UK/</a> )		If there is a possibility of rain, it is advisable to also continually check the Rain Today Application ( <a href="http://www.raintoday.co.uk/">http://www.raintoday.co.uk/</a> ) for the latest precipitation observations. These may help to identify a suitable weather window for a planned flight operation.
Check for temporary airspace restrictions, including <b>low level military flights (frequently applicable to operations in remote areas, esp. &gt;60 m AGL).</b>	NOTAMs (Notice to Airmen) ( <a href="http://notaminfo.com/ukmap">http://notaminfo.com/ukmap</a> )		
	UK MoD low level advisory service +44800515544). They can issue a NOTAM to advise other air users.		
If the planned flight operation occurs within 4.6 km (2.5 nautical miles) of any UK aerodrome, advise the local control tower.			
Confirm maps prefetched to GCS for offline use			
Confirm flight plans saved on GCS			

**On-Site Assessment Form**

<b>Job Number:</b>		<b>Date completed:</b>	
<b>Personnel:</b>		<b>Weather (temp, wind speed, direction):</b>	
<b>Task</b>		<b>Notes</b>	<b>Check</b>
<b>1.</b>	Confirm pre-site assessment forms are completed and hard copies present.		
<b>2.</b>	Confirm landowner permission obtained if applicable.		
<b>3.</b>	Confirm whether ATC has been notified if required.		
<b>4.</b>	If possible, walk-over survey around AOI to check for obstructions, visual limitations or other hazards		
<b>5.</b>	Locate safest take-off/landing areas		
<b>6.</b>	Confirm flight plan is safe and appropriate and brief crew/client		
<b>7.</b>	If required, ensure safety clothing equipment has been issued		
<b>8.</b>	Unload equipment		
<b>9.</b>	If work is in an area with public access: Set up cordon if required? Check for public address system to announce planned mission?		
<b>10.</b>	Check for 'K' index (e.g. via app such as 'Hover'). K index of 0-3 is fine for flight operations, 4-5 caution is advised when working with GNSS guided modes, 6-9 do not commence flight operations relying on GNSS guided-modes.	Record K index:	



**Pre-Flight Checklist**

Job: \_\_\_\_\_ Date Completed: \_\_\_\_\_ Completed by: \_\_\_\_\_

<b>Task</b>	<b>Check</b>
1. Crew/client briefing	
2. All crew under control of the PiC to switch off WiFi capability on all capable devices within 50 m of the launch / land and flight operation	
3. Check for damage, wear, tightness of fittings, condition and secure fitment of propellers	
4. Note battery number in battery logbook, check voltage with battery checker (to ensure cells are balanced and that there is sufficient voltage for planned flight). Fit battery into airframe.	
5. Switch on GCS, and initiate Mission Planner program	
6. Switch on Tx, check battery power is at least 60%, ensure correct UAV profile selected.	
7. Switch on Camera, ensure battery power is sufficient for mission (and at least 40%), activate script (if being used), secure to airframe.	
8. Ensure aircraft is on stable level ground at desired take-off location and connect flight battery	
9. Wait for ArduPilot to complete its self-diagnostics and accelerometer calibration (~10 seconds)	
10. Connect USB Telemetry and establish a MAVlink connection between the drone and GCS.	
11. Confirm drone heading is correct (cross-check with compass or smartphone GPS app).	
12. Confirm GCS sound enabled (and programmed to announce audio notification of: telemetry status, waypoint tracking, flight battery voltage, PDOP, altitude, triggered failsafe, etc.)	
13. GCS confirm all pre-arm checks are enabled. <i>If planning flights using GNSS guided modes</i> - Confirm six satellites visible and PDOP value is $\leq 2.5$	
14. Check RTL altitude is appropriate for site obstacles	
15. Check GeoFence parameters, consider whether appropriate to modify to constrain for AOI	
16. Confirm 3D fix and other calibrations/diagnostics are complete with relevant indication from ArduPilot device.	
17. Load flight plan from ground station onto drone (if required)	
18. Read flight plan back from drone, in order to check that the flight plan has been correct uploaded.	
19. Check flight modes	
20. Ensure everyone is in correct safe positions	
21. Does this flight have clearance from ATC, if required	
22. If applicable, arm the safety switch on the drone, and return to safe distance.	
23. Final check of immediate area for new hazards	
24. Arm the motors with the transmitter (left stick to bottom right).	
25. Check throttle response	

**Clear to Launch**

**Post-Flight Checklist**

Job: \_\_\_\_\_ Date Completed: \_\_\_\_\_ Completed by: \_\_\_\_\_

<b>Task</b>	<b>Check</b>
1. Upon touchdown, disarm the UAV (Left transmitter stick to bottom left corner)	
2. Disarm UAV (left stick to bottom left and/or by pressing safety switch)	
3. Disconnect flight battery	
4. Recover aircraft from landing area (if appropriate)	
5. Turn off Camera	
6. Switch off Tx transmitter	
7. Record pilot and other flight details in relevant logbook	
8. Remove battery from drone, check voltage with battery checker and record details in logbook	
9. Remove memory card from camera and back data up onto GCS	
10. Review images with crew and client, evaluating whether further data collection is required	
11. Shut down GCS (if no further flights are to be undertaken)	
12. Download image data from sensor memory cards	
13. Download flight logs from flight controller	

**Minor Level Service Checklist**

UAS:: \_\_\_\_\_ Date Completed: \_\_\_\_\_ Completed by: \_\_\_\_\_

	<b><u>Task</u></b>	<b><u>Check (initial)</u></b>
<u>Logs</u>	If available (Pixhawk-based systems) Check last flight log for vibration levels as this will help inform maintenance procedure (e.g. high vibrations may be rectified by cleaning of props).	
<u>Airframe</u>	On returning to base, remove propellers if necessary	
	Inspect the airframe for any damage, unusual marks and tightness of fixings	
	Inspect propellers and check for condition and clean if dirty or replace if damaged	
	Check locknuts on propellers replace or tighten if appropriate	
	Inspect electrical wiring for condition, unusual marks or discolouration and terminal fittings and plugs for secure attachment and general condition	
	Check payload mounting, ensuring it is secure and undamaged. Re-mount or change fixings if necessary	
	Check legs for any damage, especially snapped bolts into spacers	
	Clean motors with compressed air and lubricate with WD40	
<u>Camera(s)</u>	Inspect camera equipment, ensuring it functions correctly	
	Check len(s) for scratches/dirt. Clean and/or replace as necessary	
<u>GCS</u>	Ensure the GCS is in good working condition and that the screen and speakers are working correctly	
<u>Tx</u>	Check that all sticks, sliders and switches move to all positions as expected	

**Major Level Service Checklist**

UAS: \_\_\_\_\_ Date Completed: \_\_\_\_\_ Completed by: \_\_\_\_\_

	<b>Task</b>	<b>Check (initial)</b>
Logs	Check last flight log for vibration levels as this will help inform maintenance procedure (e.g. high vibrations may be rectified by cleaning of propellers)	
Airframe	Strip down the airframe, reducing it to its constituent parts	
	Inspect all parts for any damage, unusual marks and tightness of fixings	
	Inspect propellers condition and replace if damaged/clean if dirty	
	Inspect electrical wiring for condition, unusual marks or discolouration and terminal fittings and plugs for secure attachment and general condition	
	Check payload mounting, ensuring it is secure and undamaged. Re-mount or change fixings if necessary	
	Check legs for any damage, especially snapped bolts into spacers	
Motors	Check bell housings for excessive play. Replace motors if exceeding fifty hours flight time.	
	Clean motors with compressed air and lubricate with WD40	
Camera(s)	Inspect camera equipment, ensuring it functions correctly	
	Check lens for scratches/dirt. Clean and/or replace as necessary	
GCS	Ensure the GCS is in good working condition and that the screen and speakers are working correctly	
	Check that latest stable version of Mission Planner is installed and if not, update as required	
Tx	Check that all sticks, sliders and switches move to all positions as expected	
	Check for latest stable firmware and install if appropriate	
Rx:	Check for latest stable firmware and install if appropriate	
	Check the condition and positioning of antenna and replace or reposition if appropriate	
Flight Controller	Check for latest stable firmware version and update if appropriate	
Telemetry	Check for latest stable firmware version and update if appropriate	
	Check that NetID does not conflict with any others that are being used in ESI DroneLab	
Power module:	Re-calibrate the voltage sensor, ensuring a correct voltage reading is being passed from the module to the autopilot	
Calibration	Re-calibrate compass and accelerometers and Tx	
Test Flight	An ESI DroneLab qualified pilot must then perform a ten minute test flight, testing all flight modes and failsafes.	

**Appendix E Logbooks****Data recorded in Battery Identification Chart**

- Battery ID
- Manufacturer
- Model
- Type
- Capacity
- Cells
- Discharge C
- Charge C
- Date purchased
- Supplier

**Data recorded in Battery Logbook (individual batteries)**

- Date of change in charge
- Type of change in charge
- Pre-change voltage
- Post-change voltage
- Notes

**Data recorded in Maintenance Logbook (each aircraft)**

- Date of maintenance
- Reason for maintenance
- Work completed
- Completed by
- Test flight signature
- Notes

**Data recorded Pilot and Aircraft Hours Logbook**

- Flight number
- Date
- Take-off time
- Flight duration
- Aircraft registration
- Aircraft system name
- Pilot-in-command
- Venue (inc. Location name, Latitude & Longitude)
- Weather
- Observer name
- Purpose of flight
- Comment and minor incidents

Data recorded in Incident Logbook

- Date
- Location
- Pilot-in-command
- UAS
- Damage / Injuries sustained
- Brief description of incident
- Action taken

## 10.3 Appendix for Chapter 6 – St. Gothian sands dune system, Cornwall, UK

### 10.3.1 Agisoft photoscan and M3C2-PM workflow

#### **Software**

Agisoft Photoscan Version: 1.3.2 64bit.

R 3.3.3 64bit

SfM\_georef Version 3.0

CloudCompare Version 2.10

#### **Foreword**

This procedure closely follows those found in the supplementary information guide “Precision maps for 3-D uncertainty-based topographic change detection with structure-from-motion photogrammetry” in (James et al., 2017b).

#### **Data preparation**

- 1) Manually sort photos, removing unusable images from data set
- 2) Add all useable images to Photoscan
- 3) Run ‘Align Photos’ [accuracy:[low] / generic preselection:[x] / reference:preselection[x] / key point limit [100000] / tie point limit:[0] / adaptive camera model fitting [x]]
- 4) Export estimated camera positions as .txt file
- 5) Using *nearest\_neighbour\_camera\_aoi\_points.R* along with a regular point pattern in GDAL supported vector format, the exported camera positions, and the useable survey images, select the images which fall closest in 2D space to points in the regular point pattern

6) Now you should have a new folder with a subset selection of photos with  
n = no. points in regular point pattern

### **Data processing**

- 1) Add subset of images to Photoscan
- 2) Run 'Align Photos' [accuracy:[low] / generic preselection:[x] / reference:preselection[x] / key point limit [100000] / tie point limit:[0] / adaptive camera model fitting [x]]
- 3) Run 'Build Mesh' [surface type:[height field] / source data:[sparse cloud] / face count:[medium] / interpolation:[enabled]]
- 4) Manually locate and position all ground control points (GCPs). Ensure they are positioned correctly across all images
- 5) Import coordinates from differential-global navigational satellite system (D-GNSS) used to record the position of GCPs
- 6) Uncheck images and a subset of GCPs to be used as validation/check points. Ensure that the remaining GCPs are checked
- 7) Run 'Align Photos' [accuracy:[high] / generic preselection:[x] / reference:preselection[x] / key point limit [100000] / tie point limit:[0] / adaptive camera model fitting [x]]
- 8) In 'Reference Settings' set the [image coord accuracy:marker accuracy (pix)] to the chunks RMS reprojection error (as per James et al., 2017b)
- 9) In 'Reference Settings' set the [measurement accuracy:marker accuracy (m)] to that of the D-GNSS system (0.01 m )
- 10) Run 'Optimise Cameras'
- 11) Run 'Build Dense Cloud' [quality:[high] / depth filtering:[aggressive]]

- 12) Use 'Gradual Selection' to remove points with a reprojection error greater than 0.8
- 13) Export dense cloud as .txt (ASCII) file
- 14) Remove dense cloud, leaving sparse cloud in place
- 15) Save project as Photoscan Project (.psz)
- 16) Set bounding box to encompass all points in the sparse cloud with plenty of room as a buffer
- 17) Run `precision_estimate_example_script.py` (James et al., 2017b).
- 18) Continue with M3C2-PM procedure utilising `sfm_georef` and CloudCompare.

### 10.3.2 Figures

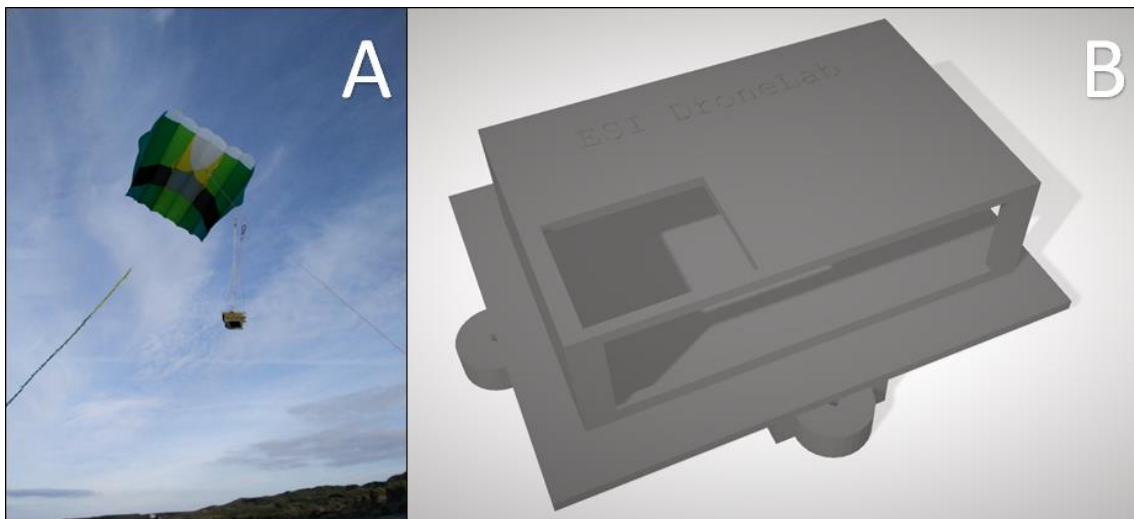


**Figure 10.3: (A) The KAP equipment in the field, with the picavet mount (containing camera) suspended from the single kite line using two carabiners. (B) 3D model of the picavet mount that can be produced with a 3D printer.**

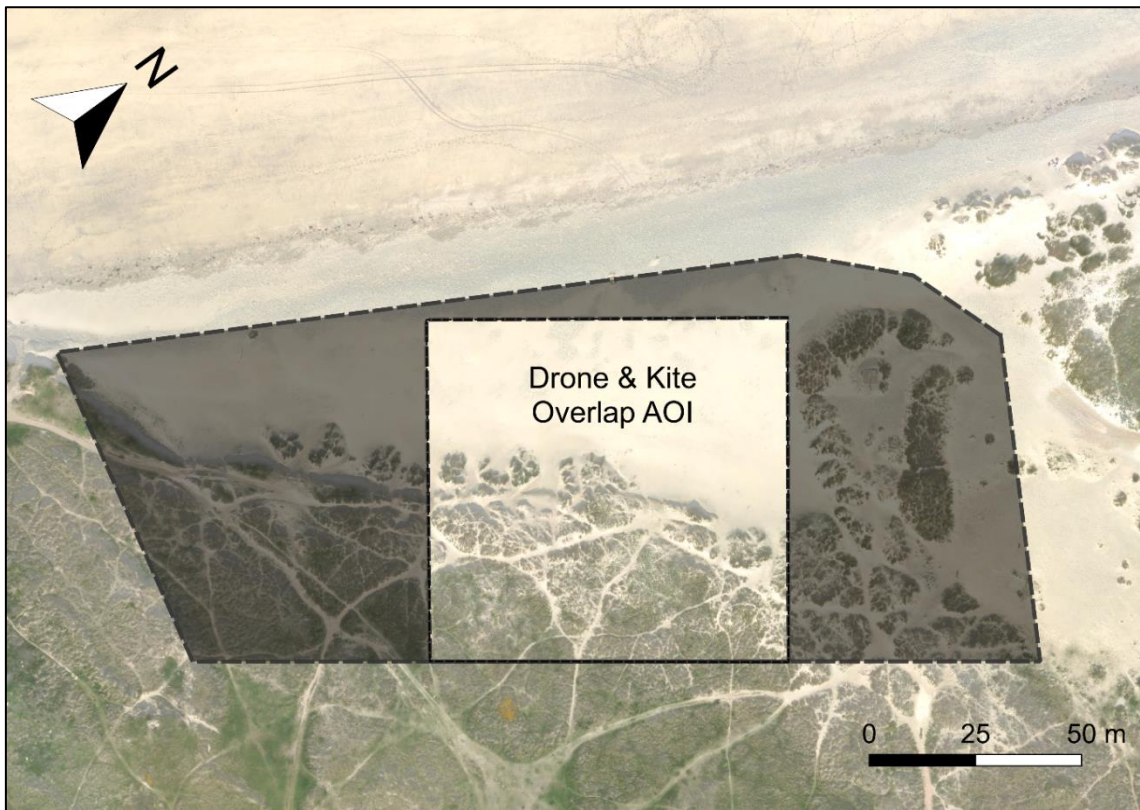


**Figure 10.4: The subset area of interest (AOI) used for the drone and kite comparison analysis. Dark grey shaded area shows whole study system AOI.**

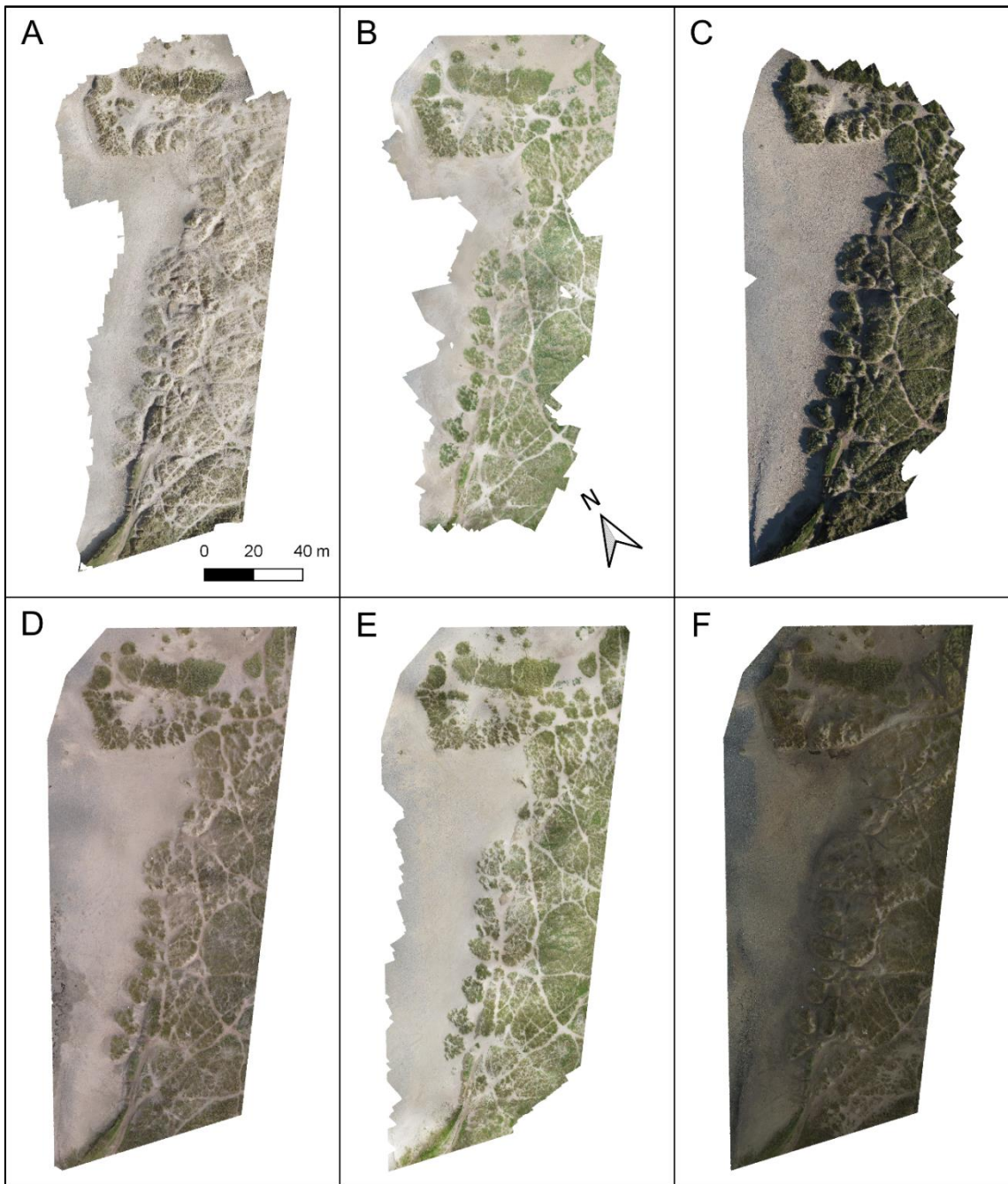


**Figure 10.5: Orthomosaics constructed with images from each of the six KAP surveys. Products from surveys 1-6 represented by A-F respectively. All mosaics cropped to the study area of interest (Figure 6.1).**

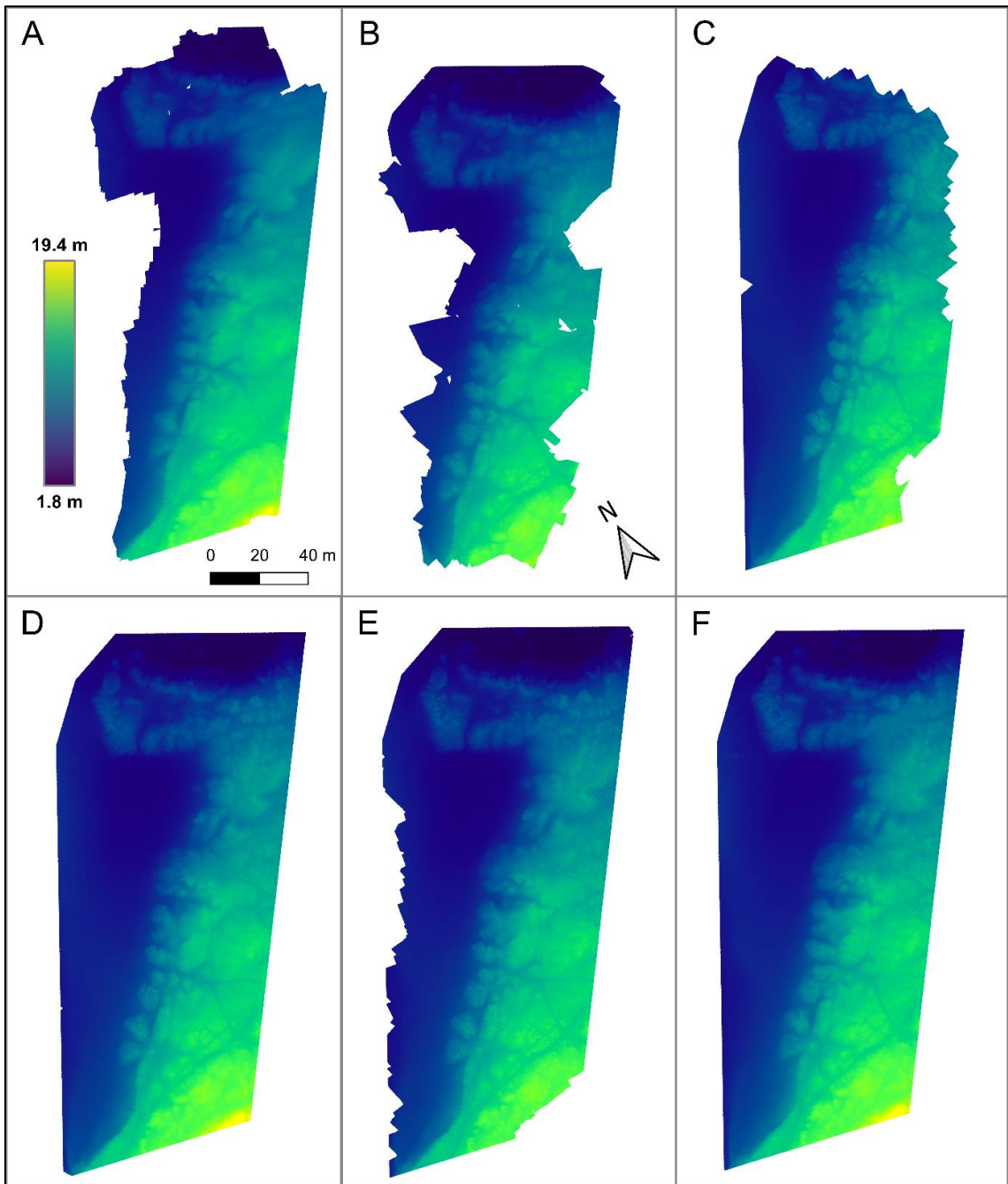


**Figure 10.6: Digital elevation models (DEMs) for each of the six KAP surveys. Products from surveys 1-6 represented by A-F respectively. All models colour scaled to the minimum and maximum found across models. All rasters cropped to the study area of interest (Figure 6.1).**

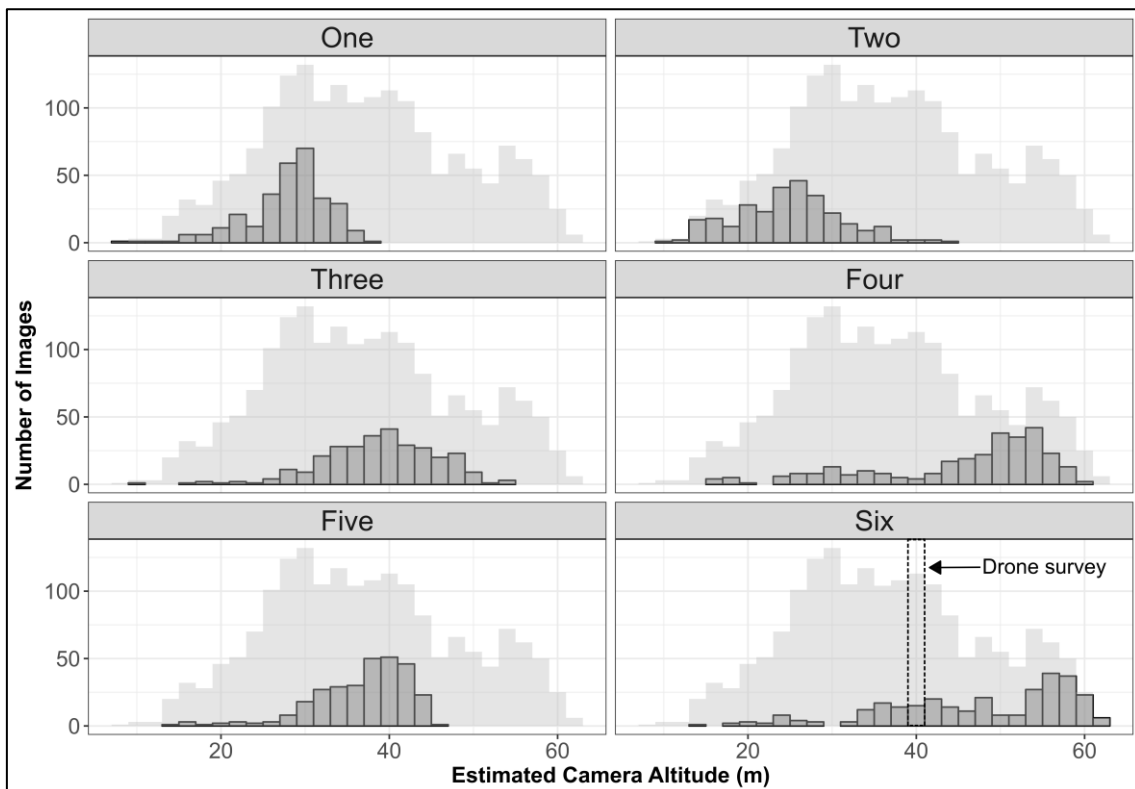


**Figure 10.7: The distribution of estimated altitudes of the camera when images were captured for each of the six surveys. Additional drone survey altitude included with KAP survey six. Altitude estimates calculated in Agisoft Photoscan after sparse cloud construction. Darker grey bars show each surveys bins, whereas distribution incorporating all six surveys is shown in lighter grey.**

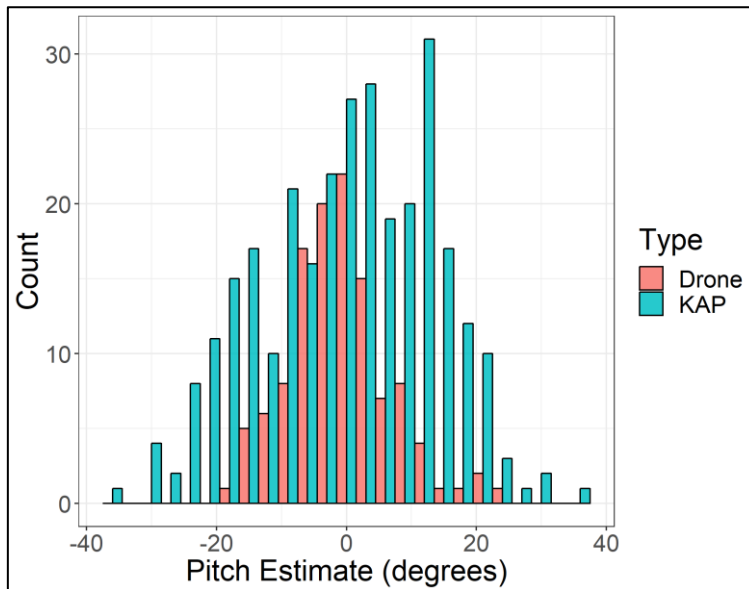


**Figure 10.8: Pitch estimations for each camera position as calculated by Photoscan for both the drone and KAP survey 6 data.**

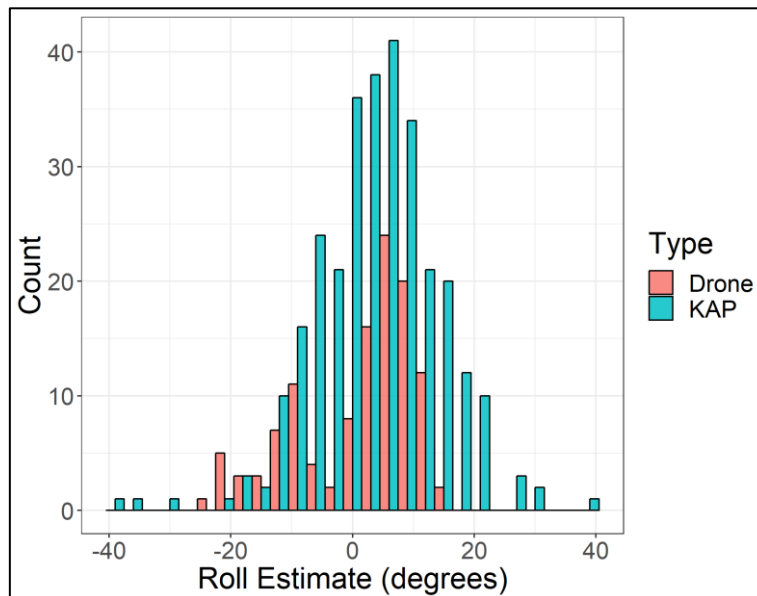


**Figure 10.9: Roll estimations for each camera position as calculated by Photoscan for both the drone and KAP survey 6 data.**

### 10.3.3 Tables

**Table 10.1: Number of Monte Carlo sparse cloud iterations and accuracy values used as seeds in Agisoft Photoscan for each dataset. Marker and tie point accuracy set as the same values within each processing set. This process is part of the workflow presented in (James et al., 2017).**

<b>Survey</b>	<b>No. of Monte Carlo iterations</b>	<b>Marker accuracy (pix)</b>	<b>Tie point accuracy (pix)</b>
1	1500	0.726856	0.726856
2	3000	0.909417	0.909417
3	1900	0.696732	0.696732
4	1800	1.21223	1.21223
5	1800	1.23705	1.23705
6	1800	1.14533	1.14533
Drone	2500	1.16428	1.16428

**Table 10.2: Check point (n=4) errors for each survey. Check points were a subset of GCPs positioned within the SfM-MVS model, but excluded from the point cloud creation stages in the photogrammetry workflow.**

Survey ID	Check Point	Error (mm)			RMSE (mm)
		Easting	Northing	Altitude	
1	1	9.02	31.25	26.92	18.88
	2	40.57	0.83	-3.94	
	3	1.22	-13.49	14.43	
	4	-5.06	6.13	-19.47	
2	1	3.72	-24.13	9.53	15.90
	2	10.15	22.46	-3.36	
	3	-8.22	-11.93	4.18	
	4	18.47	2.71	-33.95	
3	1	-0.14	-15.45	-3.37	16.84
	2	-2.93	4.21	-14.45	
	3	15.21	-13.15	-28.21	
	4	24.67	0.13	33.31	
4	1	9.37	-0.74	-10.01	39.66
	2	-56.85	29.34	117.43	
	3	-3	-21.07	6.27	
	4	-8.78	6.84	-13.54	
5	1	-9.69	15.01	-45.88	43.99

	2	-16.8	3.33	-46.81	
	3	-14.03	52.25	41.13	
	4	11.75	-44.18	-107.71	
6	1	-29.09	-9.04	-13.31	16.64
	2	-10.46	-15.35	10.82	
	3	-3.85	2.44	-14.19	
	4	31.07	1.28	-23.76	

#### 10.3.4 Photoscan reports

# day11\_drone

Processing Report  
14 June 2018



## Survey Data

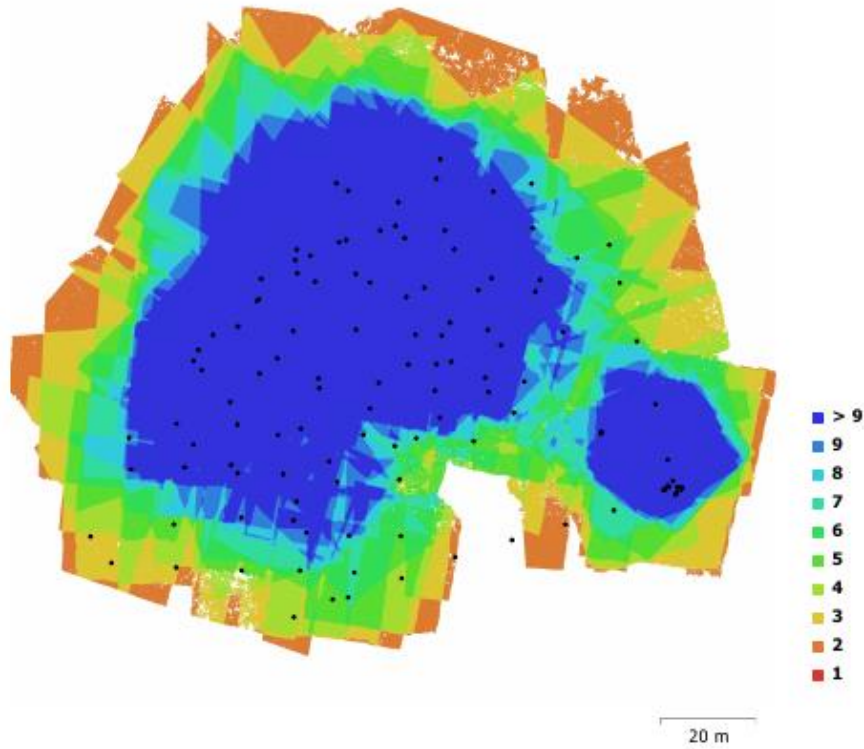


Fig. 1. Camera locations and image overlap.

Number of images:	118	Camera stations:	118
Flying altitude:	32.8 m	Tie points:	370,378
Ground resolution:	9.43 mm/pix	Projections:	1,088,322
Coverage area:	0.0149 km <sup>2</sup>	Reprojection error:	1.14 pix

Camera Model	Resolution	Focal Length	Pixel Size	Precalibrated
Canon PowerShot D30 (5 mm)	4000 x 3000	5 mm	1.55 x 1.55 $\mu$ m	No

Table 1. Cameras.

## Camera Calibration

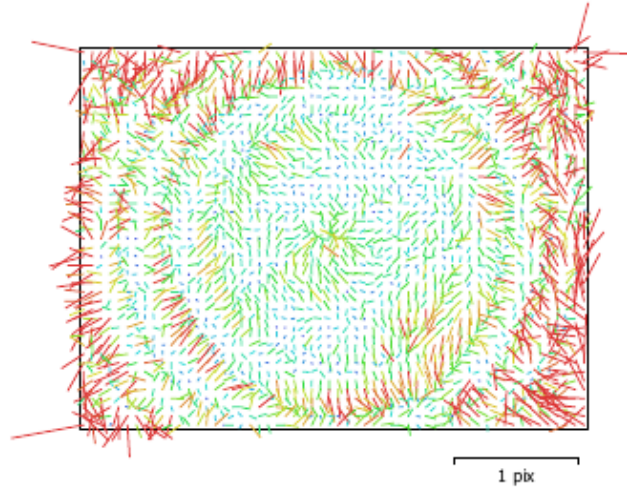


Fig. 2. Image residuals for Canon PowerShot D30 (5 mm).

### Canon PowerShot D30 (5 mm)

118 images

Type Resolution Focal Length Pixel Size  
**Frame 4000 x 3000 5 mm 1.55 x 1.55  $\mu\text{m}$**

	Value	Error	F	Cx	Cy	B1	B2	K1	K2	K3	P1	P2
<b>F</b>	<b>3281.51</b>	0.18	1.00	0.12	-0.05	-0.03	0.13	0.07	0.05	-0.04	0.14	-0.13
<b>Cx</b>	<b>-13.9734</b>	0.07		1.00	-0.02	0.15	-0.18	0.04	-0.02	0.02	0.79	-0.04
<b>Cy</b>	<b>-5.16352</b>	0.069			1.00	0.26	0.18	-0.00	-0.01	0.01	-0.01	0.73
<b>B1</b>	<b>-0.966119</b>	0.014				1.00	-0.03	0.02	-0.03	0.03	0.09	0.10
<b>B2</b>	<b>1.08468</b>	0.015					1.00	0.01	0.00	-0.00	-0.05	0.08
<b>K1</b>	<b>0.00494249</b>	9.5e-05						1.00	-0.94	0.89	0.04	-0.01
<b>K2</b>	<b>-0.0355456</b>	0.00043							1.00	-0.98	-0.01	-0.01
<b>K3</b>	<b>0.0323457</b>	0.00059								1.00	0.01	0.01
<b>P1</b>	<b>-0.00116071</b>	6.3e-06									1.00	-0.03
<b>P2</b>	<b>0.000453444</b>	5.8e-06										1.00

Table 2. Calibration coefficients and correlation matrix.

# Ground Control Points

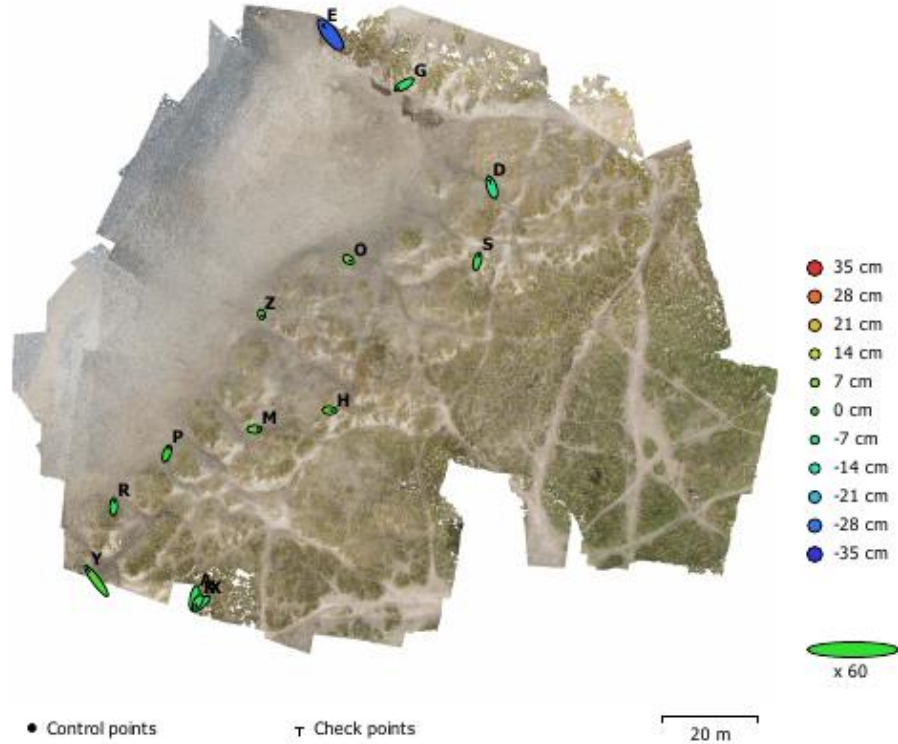


Fig. 3. GCP locations and error estimates.

Z error is represented by ellipse color. X,Y errors are represented by ellipse shape.

Estimated GCP locations are marked with a dot or crossing.

Count	X error (cm)	Y error (cm)	Z error (cm)	XY error (cm)	Total (cm)
10	2.17594	3.15434	3.47633	3.83204	5.17392

Table 3. Control points RMSE.  
X - Easting, Y - Northing, Z - Altitude.

Count	X error (cm)	Y error (cm)	Z error (cm)	XY error (cm)	Total (cm)
4	4.27913	5.98025	16.1209	7.35352	17.7189

Table 4. Check points RMSE.  
X - Easting, Y - Northing, Z - Altitude.

<b>Label</b>	<b>X error (cm)</b>	<b>Y error (cm)</b>	<b>Z error (cm)</b>	<b>Total (cm)</b>	<b>Image (pix)</b>
S	0.966257	3.92157	-1.83595	4.43656	1.212 (15)
Z	0.218434	-0.961926	0.389668	1.06059	1.403 (18)
G	-4.32196	-2.54333	-4.53279	6.75974	1.184 (5)
O	1.22915	-0.820305	3.83885	4.11345	1.178 (20)
M	2.64928	0.0100555	1.85231	3.23262	1.081 (14)
P	1.25889	3.62272	-0.843933	3.92698	1.838 (13)
R	0.149885	3.58828	-2.18832	4.20558	1.759 (4)
A	-1.20168	-5.95171	-4.79524	7.73701	1.533 (2)
X	-3.7543	-3.13988	-4.67913	6.77111	1.169 (2)
K	-1.41809	-2.18429	-5.31248	5.91647	0.995 (2)
<b>Total</b>	<b>2.17594</b>	<b>3.15434</b>	<b>3.47633</b>	<b>5.17392</b>	<b>1.354</b>

Table 5. Control points.  
X - Easting, Y - Northing, Z - Altitude.

<b>Label</b>	<b>X error (cm)</b>	<b>Y error (cm)</b>	<b>Z error (cm)</b>	<b>Total (cm)</b>	<b>Image (pix)</b>
D	-1.65312	5.14976	-8.85262	10.3741	0.976 (10)
H	2.22492	-0.153786	3.96201	4.54658	1.280 (12)
Y	-6.30383	8.47052	2.1798	10.7814	1.513 (3)
E	-5.08157	6.6903	-30.6712	31.801	0.195 (2)
<b>Total</b>	<b>4.27913</b>	<b>5.98025</b>	<b>16.1209</b>	<b>17.7189</b>	<b>1.157</b>

Table 6. Check points.  
X - Easting, Y - Northing, Z - Altitude.

## Digital Elevation Model

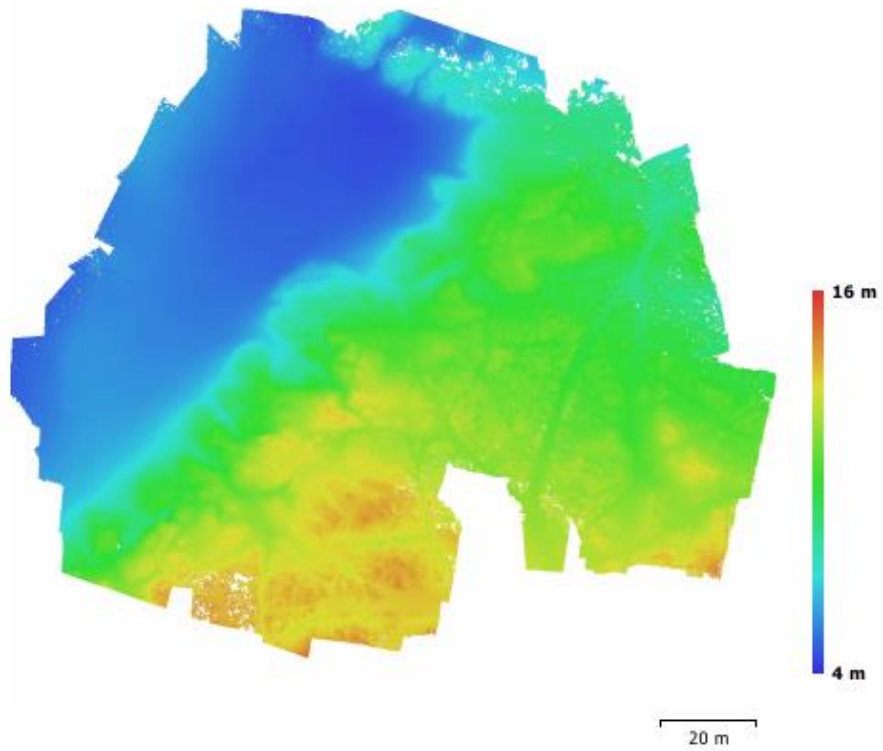


Fig. 4. Reconstructed digital elevation model.

Resolution: unknown  
Point density: unknown

# Processing Parameters

## General

Cameras	118
Aligned cameras	118
Markers	14
Coordinate system	OSGB 1936 / British National Grid (EPSG::27700)
Rotation angles	Yaw, Pitch, Roll

## Point Cloud

Points	370,378 of 388,631
RMS reprojection error	0.225874 (1.13716 pix)
Max reprojection error	1.22988 (46.0722 pix)
Mean key point size	5.0279 pix
Effective overlap	3.05623

## Alignment parameters

Accuracy	High
Generic preselection	Yes
Reference preselection	Yes
Key point limit	100,000
Tie point limit	0
Adaptive camera model fitting	Yes
Matching time	37 minutes 7 seconds
Alignment time	6 minutes 5 seconds

## Optimization parameters

Parameters	f, b1, b2, cx, cy, k1-k3, p1, p2
Fit rolling shutter	No
Optimization time	19 seconds

## Dense Point Cloud

Points	48,277,528
--------	------------

## Reconstruction parameters

Quality	High
Depth filtering	Aggressive
Depth maps generation time	1 hours 57 minutes
Dense cloud generation time	37 minutes 40 seconds

## Software

Version	1.3.2 build 4205
Platform	Windows 64

# Day 5 (Survey 1)

Processing Report

13 February 2018



## Survey Data

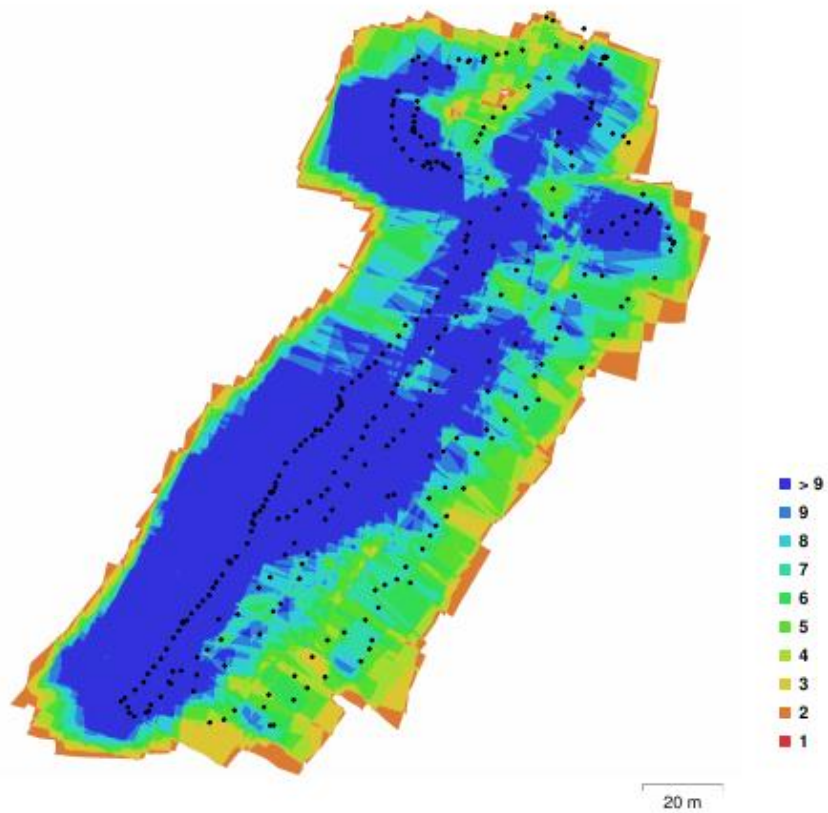


Fig. 1. Camera locations and image overlap.

Number of images:	298	Camera stations:	297
Flying altitude:	21 m	Tie points:	1,856,820
Ground resolution:	6.04 mm/pix	Projections:	6,235,153
Coverage area:	0.0161 km <sup>2</sup>	Reprojection error:	0.727 pix

Camera Model	Resolution	Focal Length	Pixel Size	Precalibrated
Canon PowerShot D30 (5 mm)	4000 x 3000	5 mm	1.55 x 1.55 $\mu$ m	No

Table 1. Cameras.

# Camera Calibration

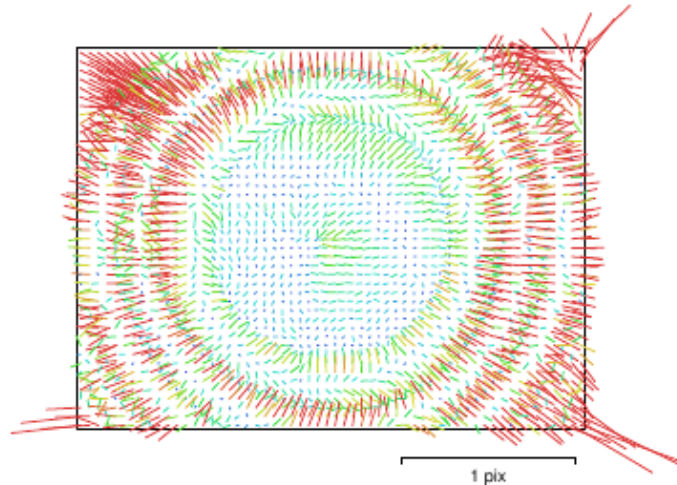


Fig. 2. Image residuals for Canon PowerShot D30 (5 mm).

## Canon PowerShot D30 (5 mm)

298 images

Type Resolution Focal Length Pixel Size  
**Frame 4000 x 3000 5 mm 1.55 x 1.55  $\mu$ m**

	Value	Error	F	Cx	Cy	B1	B2	K1	K2	K3	K4	P1	P2
<b>F</b>	<b>3293.92</b>	0.042	1.00	-0.09	-0.05	-0.13	-0.01	-0.07	0.13	-0.12	0.12	-0.24	0.03
<b>Cx</b>	<b>-32.2416</b>	0.052		1.00	-0.02	-0.36	0.05	-0.04	0.02	-0.03	0.04	0.92	-0.01
<b>Cy</b>	<b>3.08695</b>	0.05			1.00	-0.02	-0.35	-0.00	-0.01	0.02	-0.02	-0.03	0.92
<b>B1</b>	<b>-1.45392</b>	0.0087				1.00	-0.05	0.03	-0.02	0.02	-0.02	-0.39	0.00
<b>B2</b>	<b>0.543809</b>	0.0083					1.00	-0.00	0.01	-0.01	0.01	0.02	-0.43
<b>K1</b>	<b>-0.00469349</b>	4.1e-05						1.00	-0.96	0.92	-0.86	-0.04	-0.00
<b>K2</b>	<b>0.0464851</b>	0.00028							1.00	-0.99	0.96	0.02	-0.01
<b>K3</b>	<b>-0.169397</b>	0.00077								1.00	-0.99	-0.02	0.01
<b>K4</b>	<b>0.168952</b>	0.00072									1.00	0.03	-0.02
<b>P1</b>	<b>-0.00371738</b>	3.8e-06										1.00	-0.04
<b>P2</b>	<b>-0.000954705</b>	3.6e-06											1.00

Table 2. Calibration coefficients and correlation matrix.

# Ground Control Points

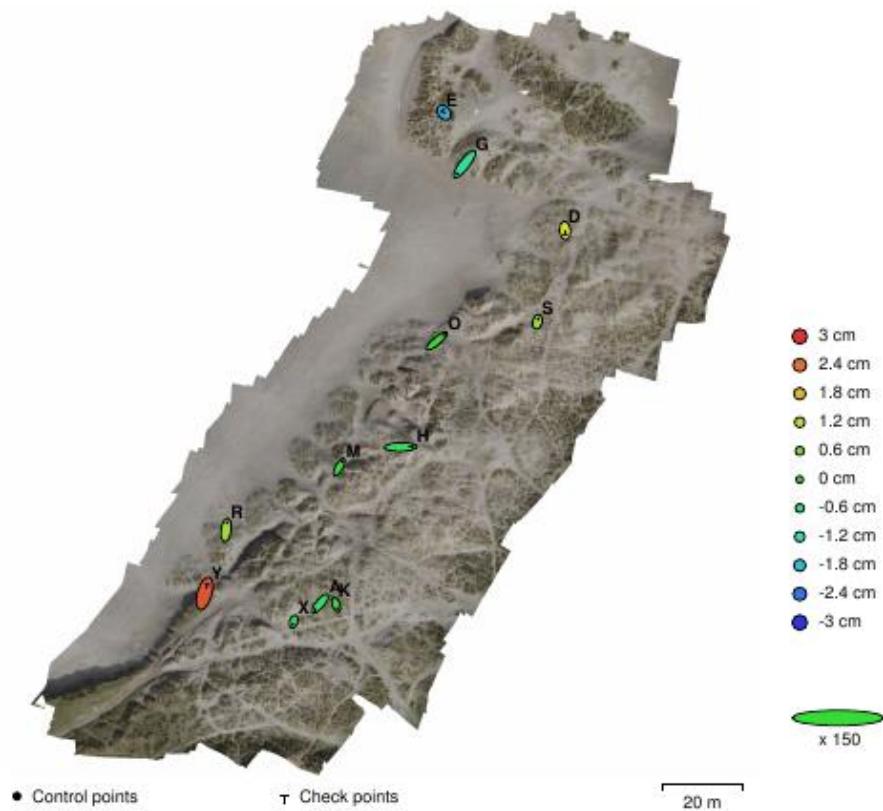


Fig. 3. GCP locations and error estimates.

Z error is represented by ellipse color. X,Y errors are represented by ellipse shape.

Estimated GCP locations are marked with a dot or crossing.

Count	X error (cm)	Y error (cm)	Z error (cm)	XY error (cm)	Total (cm)
8	1.43372	1.98663	0.584657	2.44995	2.51875

Table 3. Control points RMSE.

X - Easting, Y - Northing, Z - Altitude.

Count	X error (cm)	Y error (cm)	Z error (cm)	XY error (cm)	Total (cm)
4	2.09432	1.72981	1.82185	2.71633	3.27071

Table 4. Check points RMSE.

X - Easting, Y - Northing, Z - Altitude.

Label	X error (cm)	Y error (cm)	Z error (cm)	Total (cm)	Image (pix)
A	-1.71726	-2.0915	-0.376565	2.73225	0.410 (8)
G	-2.43147	-3.14958	-0.9572	4.09244	0.779 (16)
K	0.455657	-1.27709	-0.129827	1.36215	1.198 (7)
M	1.05183	1.92906	-0.0232849	2.19731	0.678 (21)
O	2.451	2.05947	0.0214492	3.20145	0.601 (13)
R	0.35565	2.45972	0.91559	2.64859	0.207 (18)
S	0.208919	0.908351	0.842774	1.25659	0.606 (11)
X	-0.302993	-0.900308	-0.331857	1.00622	0.422 (8)
<b>Total</b>	<b>1.43372</b>	<b>1.98663</b>	<b>0.584657</b>	<b>2.51875</b>	<b>0.639</b>

Table 5. Control points.  
X - Easting, Y - Northing, Z - Altitude.

Label	X error (cm)	Y error (cm)	Z error (cm)	Total (cm)	Image (pix)
D	0.121741	-1.34942	1.44302	1.97941	0.483 (8)
E	-0.505649	0.613345	-1.94736	2.10335	0.669 (9)
H	4.05717	0.0832759	-0.393885	4.07709	0.531 (18)
Y	0.901995	3.12489	2.69199	4.22201	0.419 (12)
<b>Total</b>	<b>2.09432</b>	<b>1.72981</b>	<b>1.82185</b>	<b>3.27071</b>	<b>0.527</b>

Table 6. Check points.  
X - Easting, Y - Northing, Z - Altitude.

## Digital Elevation Model

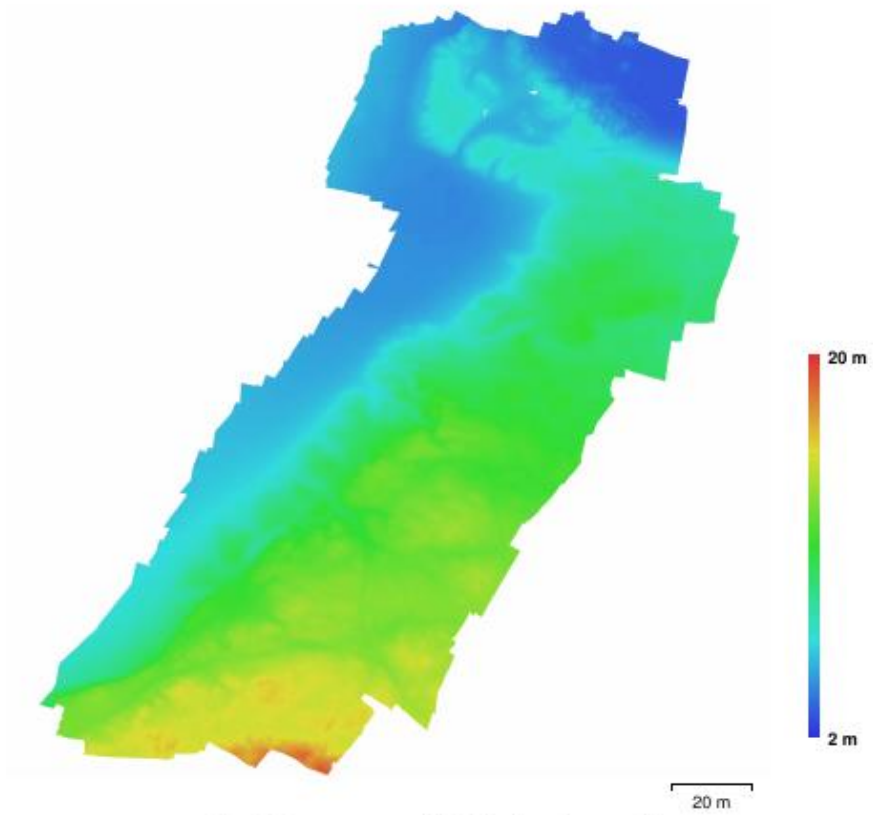


Fig. 4. Reconstructed digital elevation model.

Resolution: 1.21 cm/pix  
Point density: 68.6 points/cm<sup>2</sup>

# Processing Parameters

<b>General</b>	
Cameras	298
Aligned cameras	297
Markers	12
Coordinate system	OSGB 1936 / British National Grid (EPSG::27700)
Rotation angles	Yaw, Pitch, Roll
<b>Point Cloud</b>	
Points	1,856,820 of 1,978,333
RMS reprojection error	0.150065 (0.726912 pix)
Max reprojection error	0.556412 (34.8039 pix)
Mean key point size	4.5717 pix
Effective overlap	3.52432
<b>Alignment parameters</b>	
Accuracy	High
Generic preselection	Yes
Reference preselection	Yes
Key point limit	100,000
Tie point limit	0
Adaptive camera model fitting	Yes
Matching time	47 minutes 25 seconds
Alignment time	11 minutes 54 seconds
<b>Optimization parameters</b>	
Parameters	f, b1, b2, cx, cy, k1-k4, p1, p2
Fit rolling shutter	No
Optimization time	35 seconds
<b>Depth Maps</b>	
Count	297
<b>Reconstruction parameters</b>	
Quality	High
Filtering mode	Aggressive
Processing time	6 hours 29 minutes
<b>Dense Point Cloud</b>	
Points	130,432,521
<b>Reconstruction parameters</b>	
Quality	High
Depth filtering	Aggressive
Depth maps generation time	6 hours 29 minutes
Dense cloud generation time	1 hours 3 minutes
<b>Model</b>	
Faces	25,784,033
Vertices	12,903,469
<b>Reconstruction parameters</b>	
Surface type	Height field
Source data	Dense
Interpolation	Enabled
Quality	High
Depth filtering	Aggressive
Face count	26,086,504
Processing time	12 minutes 1 seconds
<b>Orthomosaic</b>	
Size	28,940 x 31,625
Coordinate system	OSGB 1936 / British National Grid (EPSG::27700)
Channels	3, uint8
<b>Reconstruction parameters</b>	
Blending mode	Mosaic
Surface	Mesh

Enable color correction	No
Enable hole filling	Yes
Processing time	46 minutes 8 seconds
<b>Software</b>	
Version	1.3.2 build 4205
Platform	Linux 64

# Day 7 (Survey 2)

Processing Report  
13 February 2018



## Survey Data

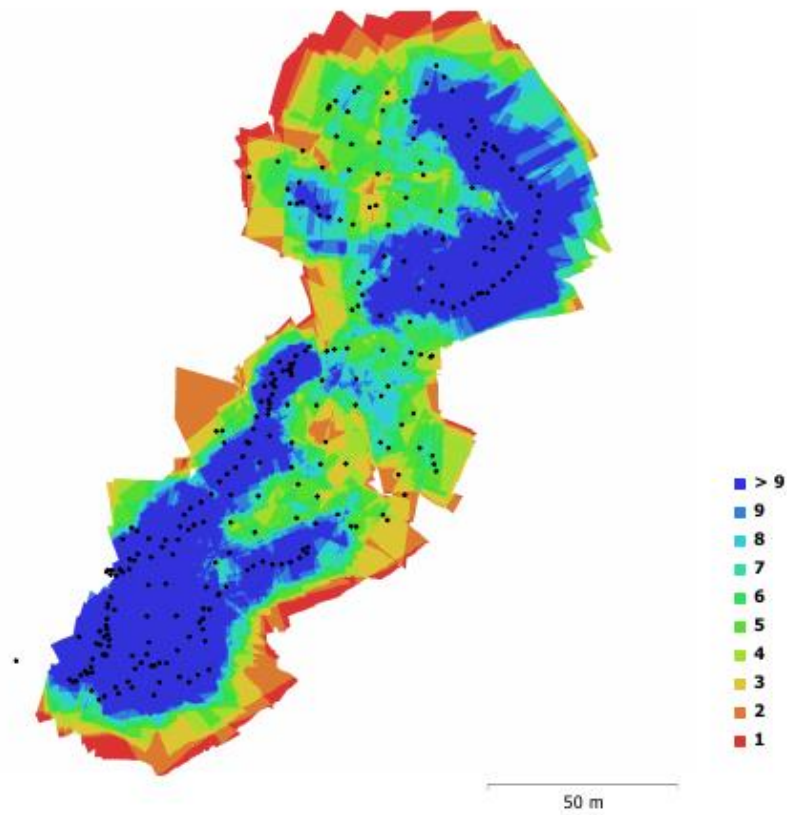


Fig. 1. Camera locations and image overlap.

Number of images:	298	Camera stations:	287
Flying altitude:	18.1 m	Tie points:	819,098
Ground resolution:	5.21 mm/pix	Projections:	2,184,711
Coverage area:	0.0138 km <sup>2</sup>	Reprojection error:	0.91 pix

Camera Model	Resolution	Focal Length	Pixel Size	Precalibrated
Canon PowerShot D30 (5 mm)	4000 x 3000	5 mm	1.55 x 1.55 $\mu$ m	No

Table 1. Cameras.

## Camera Calibration

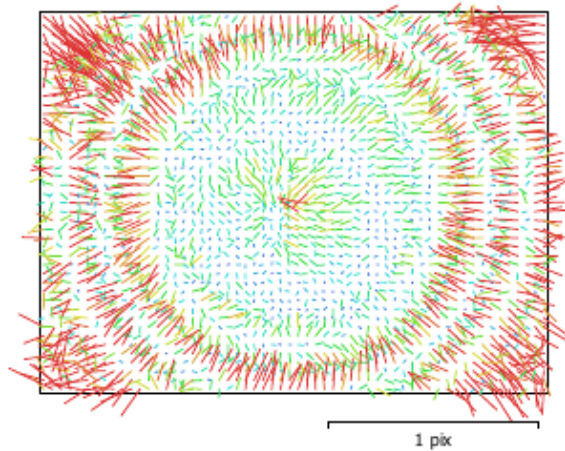


Fig. 2. Image residuals for Canon PowerShot D30 (5 mm).

### Canon PowerShot D30 (5 mm)

298 images

Type	Resolution	Focal Length	Pixel Size
<b>Frame</b>	<b>4000 x 3000</b>	<b>5 mm</b>	<b>1.55 x 1.55 <math>\mu\text{m}</math></b>

	Value	Error	F	Cx	Cy	B1	B2	K1	K2	K3	P1	P2
<b>F</b>	<b>3291.46</b>	0.1	1.00	-0.18	-0.06	0.09	-0.15	0.07	0.07	-0.06	-0.11	0.01
<b>Cx</b>	<b>-31.9629</b>	0.071		1.00	0.03	0.08	0.14	-0.03	0.00	-0.00	0.81	0.02
<b>Cy</b>	<b>1.70773</b>	0.067			1.00	-0.17	0.11	0.01	-0.01	0.01	0.03	0.80
<b>B1</b>	<b>-1.38809</b>	0.014				1.00	-0.04	0.01	-0.03	0.03	-0.05	-0.05
<b>B2</b>	<b>0.104723</b>	0.014					1.00	0.02	-0.02	0.02	0.02	-0.08
<b>K1</b>	<b>0.00302047</b>	5.4e-05						1.00	-0.93	0.87	-0.04	-0.01
<b>K2</b>	<b>-0.0147195</b>	0.00023							1.00	-0.98	0.00	0.00
<b>K3</b>	<b>0.00591995</b>	0.0003								1.00	-0.00	0.00
<b>P1</b>	<b>-0.00374929</b>	5.5e-06									1.00	0.01
<b>P2</b>	<b>-0.0011377</b>	4.8e-06										1.00

Table 2. Calibration coefficients and correlation matrix.

# Ground Control Points

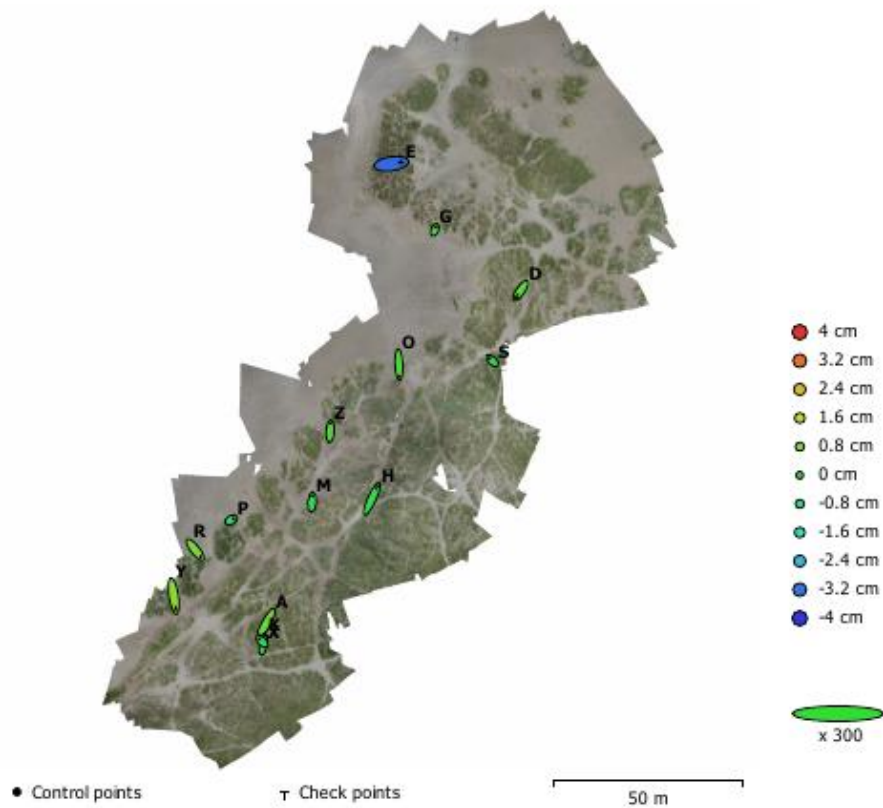


Fig. 3. GCP locations and error estimates.

Z error is represented by ellipse color. X,Y errors are represented by ellipse shape.

Estimated GCP locations are marked with a dot or crossing.

Count	X error (cm)	Y error (cm)	Z error (cm)	XY error (cm)	Total (cm)
10	0.530832	1.25371	0.44003	1.36146	1.4308

Table 3. Control points RMSE.

X - Easting, Y - Northing, Z - Altitude.

Count	X error (cm)	Y error (cm)	Z error (cm)	XY error (cm)	Total (cm)
4	1.14617	1.75806	1.78344	2.09868	2.75411

Table 4. Check points RMSE.

X - Easting, Y - Northing, Z - Altitude.

<b>Label</b>	<b>X error (cm)</b>	<b>Y error (cm)</b>	<b>Z error (cm)</b>	<b>Total (cm)</b>	<b>Image (pix)</b>
Z	0.0890405	1.36501	0.222941	1.38596	0.529 (16)
M	0.0887304	1.07675	-0.48812	1.18555	0.526 (9)
P	0.387269	0.21898	-0.671327	0.805363	0.446 (6)
R	0.952563	-1.22008	0.719306	1.70686	0.392 (11)
O	0.0912239	-2.10231	0.16655	2.11087	0.535 (8)
A	-1.11638	-2.04337	0.571341	2.39752	0.882 (17)
K	0.223874	1.40887	-0.0535979	1.42756	0.613 (18)
X	-0.427673	0.411495	-0.454801	0.747714	0.564 (18)
G	0.183539	0.457546	0.112829	0.505733	0.569 (6)
S	-0.47258	0.447236	-0.321873	0.725916	0.103 (4)
<b>Total</b>	<b>0.530832</b>	<b>1.25371</b>	<b>0.44003</b>	<b>1.4308</b>	<b>0.594</b>

Table 5. Control points.  
X - Easting, Y - Northing, Z - Altitude.

<b>Label</b>	<b>X error (cm)</b>	<b>Y error (cm)</b>	<b>Z error (cm)</b>	<b>Total (cm)</b>	<b>Image (pix)</b>
Y	0.371833	-2.41316	0.953075	2.62106	0.632 (21)
H	1.01465	2.24576	-0.335715	2.4871	0.542 (5)
D	-0.822169	-1.19286	0.417623	1.50774	0.741 (12)
E	1.8469	0.27081	-3.39518	3.87448	0.676 (4)
<b>Total</b>	<b>1.14617</b>	<b>1.75806</b>	<b>1.78344</b>	<b>2.75411</b>	<b>0.660</b>

Table 6. Check points.  
X - Easting, Y - Northing, Z - Altitude.

## Digital Elevation Model

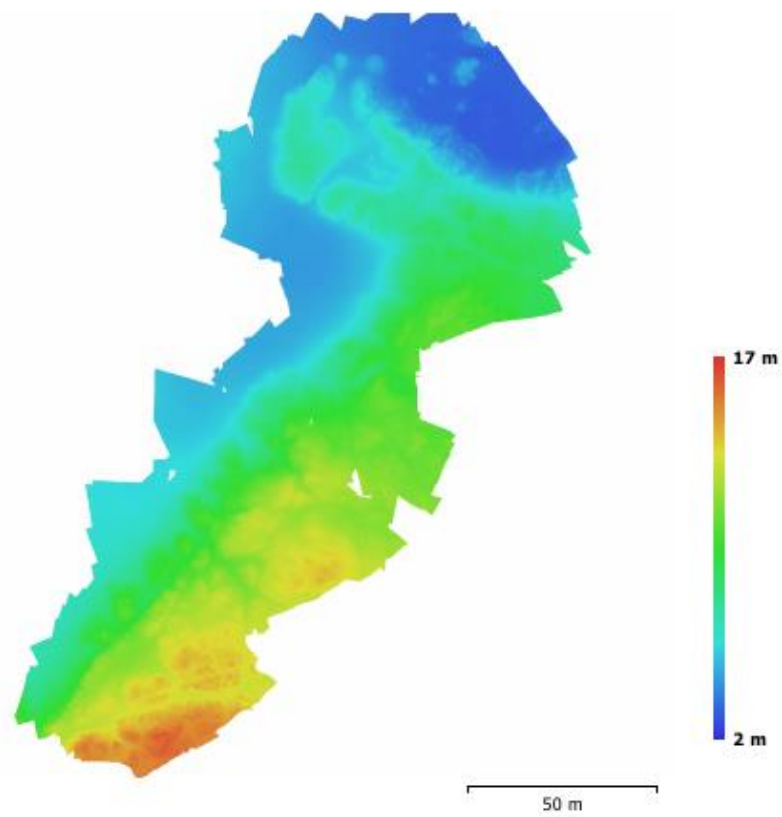


Fig. 4. Reconstructed digital elevation model.

Resolution: 1.04 cm/pix  
Point density: 92 points/cm<sup>2</sup>

# Processing Parameters

## General

Cameras	298
Aligned cameras	287
Markers	14
Coordinate system	OSGB 1936 / British National Grid (EPSG::27700)
Rotation angles	Yaw, Pitch, Roll

## Point Cloud

Points	819,098 of 916,493
RMS reprojection error	0.140989 (0.909653 pix)
Max reprojection error	0.587212 (41.1404 pix)
Mean key point size	5.95078 pix
Effective overlap	2.75146

## Alignment parameters

Accuracy	High
Generic preselection	Yes
Reference preselection	Yes
Key point limit	100,000
Tie point limit	0
Adaptive camera model fitting	Yes
Matching time	1 hours 0 minutes
Alignment time	8 minutes 17 seconds

## Optimization parameters

Parameters	f, b1, b2, cx, cy, k1-k3, p1, p2
Fit rolling shutter	No
Optimization time	15 seconds

## Dense Point Cloud

Points	129,471,939
--------	-------------

## Reconstruction parameters

Quality	High
Depth filtering	Aggressive
Depth maps generation time	3 hours 9 minutes
Dense cloud generation time	1 hours 1 minutes

## Model

Faces	8,569,457
Vertices	4,292,311
Texture	4,096 x 4,096, uint8

## Reconstruction parameters

Surface type	Height field
Source data	Dense
Interpolation	Enabled
Quality	High
Depth filtering	Aggressive
Face count	8,631,462
Processing time	12 minutes 26 seconds

## Texturing parameters

Mapping mode	Orthophoto
Blending mode	Mosaic
Texture size	4,096 x 4,096
Enable color correction	No
Enable hole filling	Yes
UV mapping time	2 minutes 53 seconds
Blending time	7 minutes 23 seconds

## DEM

Size	24,536 x 28,941
Coordinate system	OSGB 1936 / British National Grid (EPSG::27700)

## Reconstruction parameters

Source data	Dense cloud
Interpolation	Enabled
Processing time	21 minutes 27 seconds
<b>Orthomosaic</b>	
Size	31,552 x 38,626
Coordinate system	OSGB 1936 / British National Grid (EPSG::27700)
Channels	3, uint8
<b>Reconstruction parameters</b>	
Blending mode	Mosaic
Surface	Mesh
Enable color correction	No
Enable hole filling	Yes
Processing time	31 minutes 50 seconds
<b>Software</b>	
Version	1.3.2 build 4205
Platform	Windows 64

# Day 8 (Survey 3)

Processing Report  
13 February 2018



## Survey Data

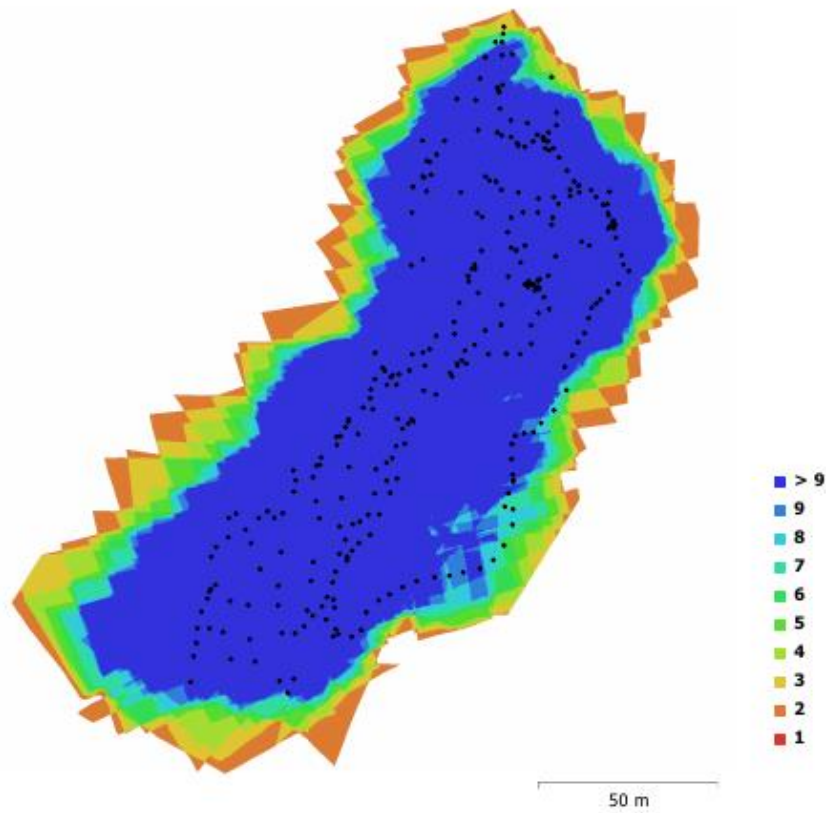


Fig. 1. Camera locations and image overlap.

Number of images:	298	Camera stations:	298
Flying altitude:	34.5 m	Tie points:	1,452,172
Ground resolution:	9.78 mm/pix	Projections:	8,002,133
Coverage area:	0.0202 km <sup>2</sup>	Reprojection error:	0.697 pix

Camera Model	Resolution	Focal Length	Pixel Size	Precalibrated
Canon PowerShot D30 (5 mm)	4000 x 3000	5 mm	1.55 x 1.55 $\mu$ m	No

Table 1. Cameras.

# Camera Calibration

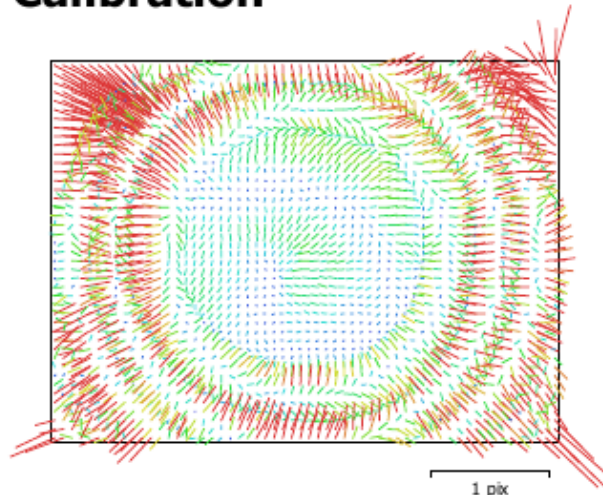


Fig. 2. Image residuals for Canon PowerShot D30 (5 mm).

## Canon PowerShot D30 (5 mm)

298 images

Type Resolution Focal Length Pixel Size  
**Frame 4000 x 3000 5 mm 1.55 x 1.55  $\mu$ m**

	Value	Error	F	Cx	Cy	B1	B2	K1	K2	K3	K4	P1	P2
<b>F</b>	<b>3292.85</b>	0.029	1.00	0.39	-0.09	-0.25	0.09	-0.08	0.13	-0.14	0.14	0.17	-0.14
<b>Cx</b>	<b>-28.2538</b>	0.032		1.00	0.03	-0.50	-0.14	0.02	0.03	-0.04	0.04	0.92	0.01
<b>Cy</b>	<b>3.39421</b>	0.03			1.00	0.14	-0.46	0.00	-0.01	0.01	-0.00	0.04	0.95
<b>B1</b>	<b>-1.48238</b>	0.004				1.00	-0.01	-0.00	-0.02	0.02	-0.02	-0.34	0.13
<b>B2</b>	<b>0.0530544</b>	0.0039					1.00	0.01	-0.00	0.00	-0.00	-0.14	-0.33
<b>K1</b>	<b>-0.004668</b>	2.7e-05						1.00	-0.97	0.92	-0.87	0.02	-0.01
<b>K2</b>	<b>0.0444225</b>	0.00019							1.00	-0.99	0.96	0.03	-0.01
<b>K3</b>	<b>-0.170559</b>	0.00051								1.00	-0.99	-0.03	0.00
<b>K4</b>	<b>0.172414</b>	0.00048									1.00	0.04	-0.00
<b>P1</b>	<b>-0.00343529</b>	2.1e-06										1.00	0.03
<b>P2</b>	<b>-0.00104095</b>	2.1e-06											1.00

Table 2. Calibration coefficients and correlation matrix.

# Ground Control Points

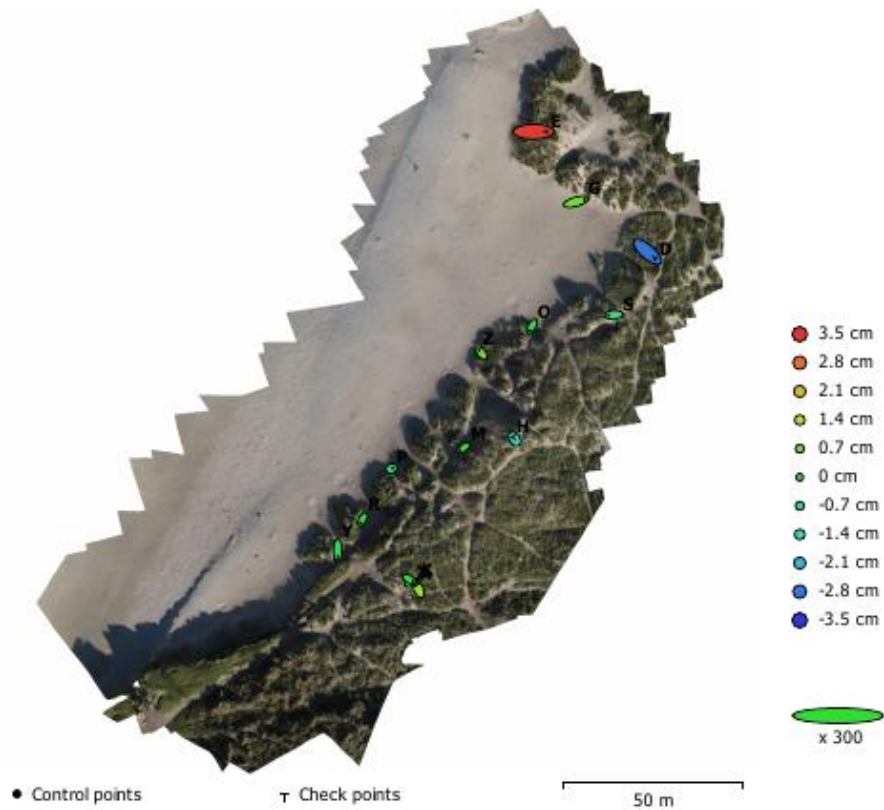


Fig. 3. GCP locations and error estimates.

Z error is represented by ellipse color. X,Y errors are represented by ellipse shape.

Estimated GCP locations are marked with a dot or crossing.

Count	X error (cm)	Y error (cm)	Z error (cm)	XY error (cm)	Total (cm)
10	0.759989	0.498983	0.572202	0.909158	1.07424

Table 3. Control points RMSE.  
X - Easting, Y - Northing, Z - Altitude.

Count	X error (cm)	Y error (cm)	Z error (cm)	XY error (cm)	Total (cm)
4	1.45671	1.03598	2.30506	1.78753	2.91695

Table 4. Check points RMSE.  
X - Easting, Y - Northing, Z - Altitude.

<b>Label</b>	<b>X error (cm)</b>	<b>Y error (cm)</b>	<b>Z error (cm)</b>	<b>Total (cm)</b>	<b>Image (pix)</b>
A	-0.36921	0.816325	1.0617	1.38921	1.263 (15)
G	1.54452	0.440257	0.683828	1.74556	0.652 (39)
K	0.898336	0.285822	-0.0256907	0.94306	1.166 (15)
M	-0.661162	-0.437746	-0.0353339	0.793728	1.201 (16)
O	-0.405125	-0.721398	-0.27356	0.871422	0.706 (51)
P	0.194715	0.0974953	-0.885361	0.911748	1.024 (36)
R	-0.405051	-0.642786	-0.102975	0.76671	0.822 (35)
S	-1.00736	-0.072878	-0.728787	1.24548	0.846 (26)
X	0.653102	-0.334027	-0.179462	0.755197	0.866 (16)
Z	-0.449907	0.544366	0.494743	0.862277	0.600 (38)
<b>Total</b>	<b>0.759989</b>	<b>0.498983</b>	<b>0.572202</b>	<b>1.07424</b>	<b>0.866</b>

Table 5. Control points.  
X - Easting, Y - Northing, Z - Altitude.

<b>Label</b>	<b>X error (cm)</b>	<b>Y error (cm)</b>	<b>Z error (cm)</b>	<b>Total (cm)</b>	<b>Image (pix)</b>
D	1.52118	-1.31507	-2.82067	3.46405	0.686 (17)
E	2.46744	0.0132225	3.33091	4.14529	0.575 (30)
H	-0.292531	0.420601	-1.44513	1.53326	0.692 (10)
Y	-0.0144473	-1.54485	-0.337088	1.58126	0.859 (34)
<b>Total</b>	<b>1.45671</b>	<b>1.03598</b>	<b>2.30506</b>	<b>2.91695</b>	<b>0.725</b>

Table 6. Check points.  
X - Easting, Y - Northing, Z - Altitude.

## Digital Elevation Model

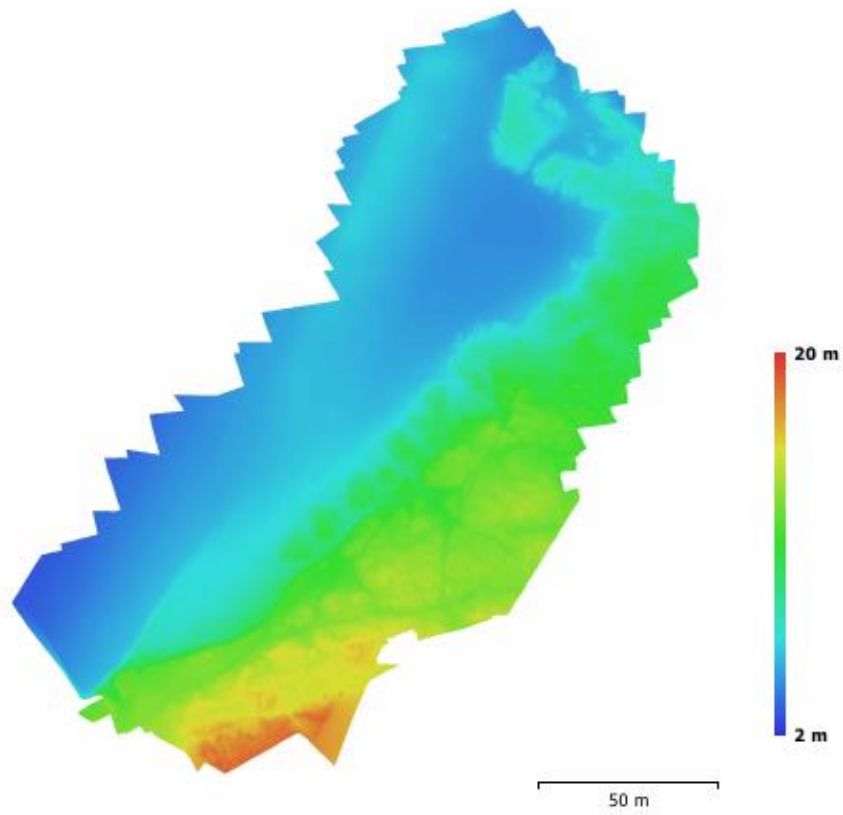


Fig. 4. Reconstructed digital elevation model.

Resolution: 1.96 cm/pix  
Point density: 26.1 points/cm<sup>2</sup>

# Processing Parameters

## General

Cameras	298
Aligned cameras	298
Markers	14
Coordinate system	OSGB 1936 / British National Grid (EPSG::27700)
Rotation angles	Yaw, Pitch, Roll

## Point Cloud

Points	1,452,172 of 1,644,555
RMS reprojection error	0.184159 (0.696765 pix)
Max reprojection error	0.66681 (41.6067 pix)
Mean key point size	3.53177 pix
Effective overlap	6.86049

## Alignment parameters

Accuracy	High
Generic preselection	Yes
Reference preselection	Yes
Key point limit	100,000
Tie point limit	0
Adaptive camera model fitting	Yes
Matching time	7 hours 58 minutes
Alignment time	1 hours 50 minutes

## Optimization parameters

Parameters	f, b1, b2, cx, cy, k1-k4, p1, p2
Fit rolling shutter	No
Optimization time	1 minutes 15 seconds

## Dense Point Cloud

Points	60,423,393
--------	------------

## Reconstruction parameters

Quality	High
Depth filtering	Aggressive
Depth maps generation time	13 hours 2 minutes
Dense cloud generation time	2 hours 29 minutes

## Model

Faces	3,983,909
Vertices	1,996,638

## Reconstruction parameters

Surface type	Height field
Source data	Dense
Interpolation	Enabled
Quality	High
Depth filtering	Aggressive
Face count	4,028,221
Processing time	2 minutes 49 seconds

## Orthomosaic

Size	19,554 x 21,782
Coordinate system	OSGB 1936 / British National Grid (EPSG::27700)
Channels	3, uint8

## Reconstruction parameters

Blending mode	Mosaic
Surface	Mesh
Enable color correction	No
Enable hole filling	Yes
Processing time	28 minutes 59 seconds

## Software

Version	1.3.2 build 4205
Platform	Windows 64

# Day 9 (Survey 4)

Processing Report  
13 February 2018



## Survey Data

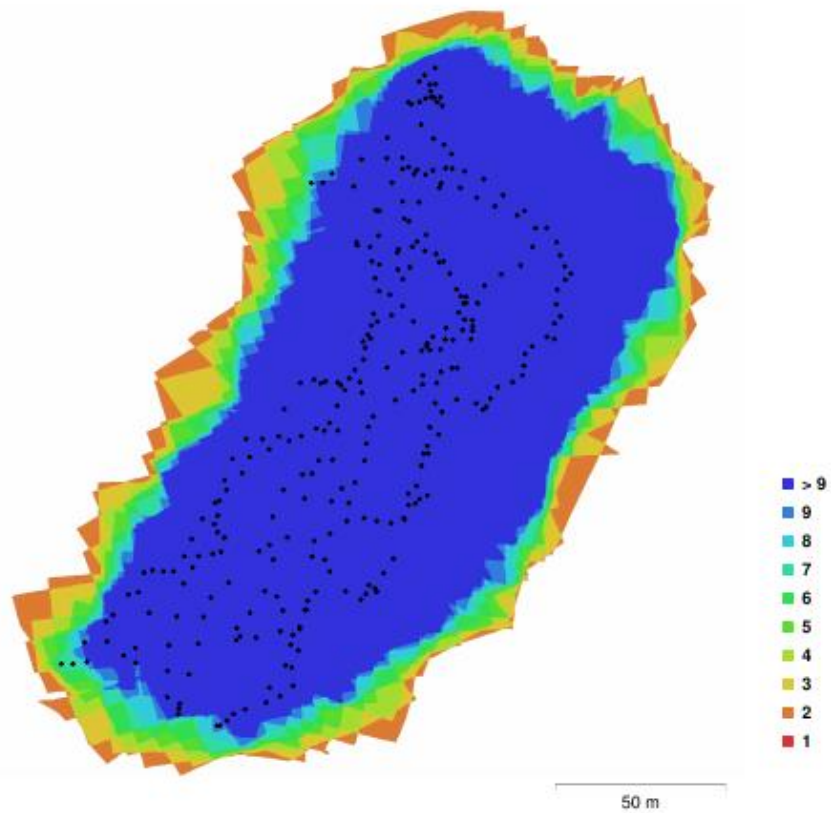


Fig. 1. Camera locations and image overlap.

Number of images:	298	Camera stations:	298
Flying altitude:	40.1 m	Tie points:	1,232,351
Ground resolution:	1.16 cm/pix	Projections:	4,215,961
Coverage area:	0.0264 km <sup>2</sup>	Reprojection error:	1.21 pix

Camera Model	Resolution	Focal Length	Pixel Size	Precalibrated
Canon PowerShot D30 (5 mm)	4000 x 3000	5 mm	1.55 x 1.55 $\mu$ m	No

Table 1. Cameras.

# Camera Calibration

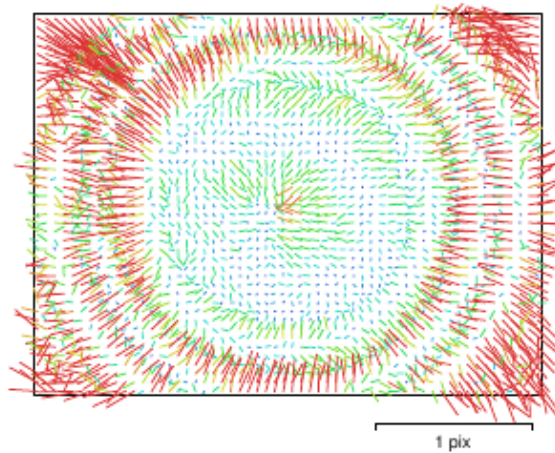


Fig. 2. Image residuals for Canon PowerShot D30 (5 mm).

## Canon PowerShot D30 (5 mm)

298 images

Type Resolution Focal Length Pixel Size  
**Frame 4000 x 3000 5 mm 1.55 x 1.55  $\mu\text{m}$**

	Value	Error	F	Cx	Cy	B1	B2	K1	K2	P1	P2
<b>F</b>	<b>3293.36</b>	0.09	1.00	0.09	-0.26	0.04	0.21	0.24	-0.01	-0.09	-0.00
<b>Cx</b>	<b>-30.3648</b>	0.064		1.00	-0.02	-0.31	0.36	0.02	-0.02	0.89	-0.02
<b>Cy</b>	<b>2.23319</b>	0.075			1.00	-0.39	-0.40	-0.10	0.02	0.05	0.88
<b>B1</b>	<b>-1.68816</b>	0.0082				1.00	0.03	-0.01	-0.00	-0.30	-0.21
<b>B2</b>	<b>0.430692</b>	0.0083					1.00	0.05	-0.01	0.15	-0.31
<b>K1</b>	<b>0.00222779</b>	1.8e-05						1.00	-0.82	0.01	-0.11
<b>K2</b>	<b>-0.00683801</b>	3.2e-05							1.00	-0.01	0.01
<b>P1</b>	<b>-0.00354208</b>	4.6e-06								1.00	-0.01
<b>P2</b>	<b>-0.00108885</b>	5.1e-06									1.00

Table 2. Calibration coefficients and correlation matrix.

# Ground Control Points

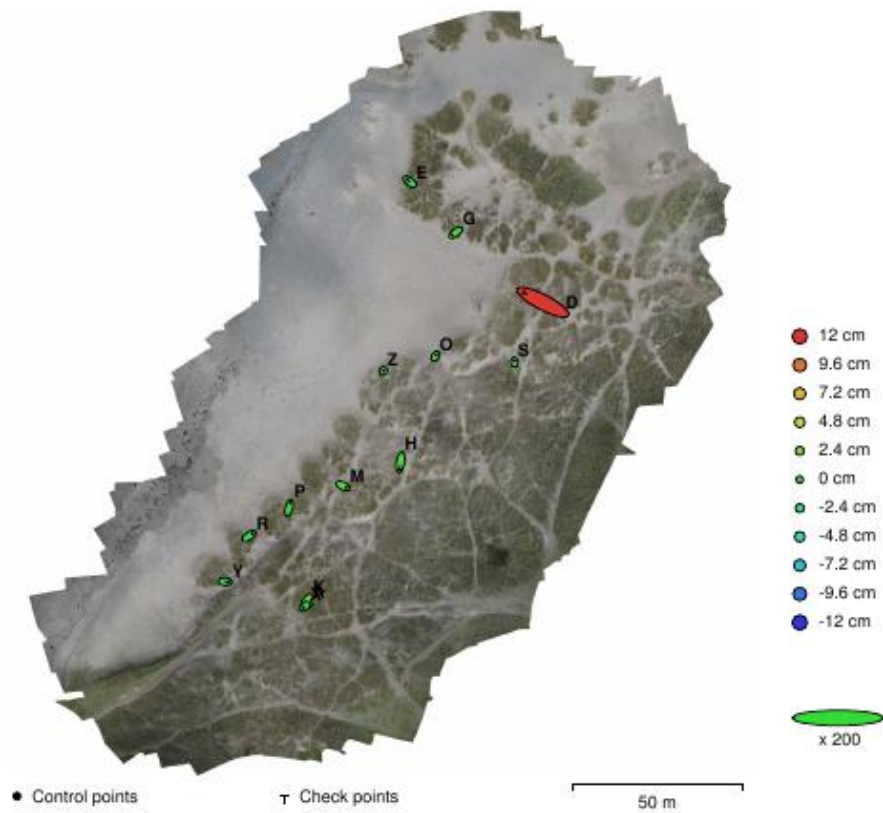


Fig. 3. GCP locations and error estimates.

Z error is represented by ellipse color. X,Y errors are represented by ellipse shape.

Estimated GCP locations are marked with a dot or crossing.

Count	X error (cm)	Y error (cm)	Z error (cm)	XY error (cm)	Total (cm)
10	0.660104	0.746251	0.577163	0.996307	1.15141

Table 3. Control points RMSE.

X - Easting, Y - Northing, Z - Altitude.

Count	X error (cm)	Y error (cm)	Z error (cm)	XY error (cm)	Total (cm)
4	2.9182	1.83849	5.93999	3.44905	6.86873

Table 4. Check points RMSE.

X - Easting, Y - Northing, Z - Altitude.

Label	X error (cm)	Y error (cm)	Z error (cm)	Total (cm)	Image (pix)
A	-0.563179	-0.357057	-0.0585325	0.669393	0.871 (28)
G	-0.94114	-0.760243	0.540041	1.3249	0.694 (41)
K	-0.807629	-1.1674	0.957036	1.71202	0.761 (29)
M	1.00121	-0.475247	0.934028	1.44937	0.845 (28)
O	0.251217	0.413633	-0.370993	0.609786	0.728 (63)
P	0.393816	1.50042	0.0944458	1.55412	0.610 (33)
R	1.0483	0.709096	-0.587199	1.39519	0.798 (26)
S	-0.0387573	0.404595	-0.290728	0.499722	0.701 (42)
X	-0.415086	-0.417487	-0.592608	0.83533	0.822 (27)
Z	0.094058	0.107665	-0.566313	0.584079	0.705 (43)
<b>Total</b>	<b>0.660104</b>	<b>0.746251</b>	<b>0.577163</b>	<b>1.15141</b>	<b>0.746</b>

Table 5. Control points.  
X - Easting, Y - Northing, Z - Altitude.

Label	X error (cm)	Y error (cm)	Z error (cm)	Total (cm)	Image (pix)
D	-5.68546	2.93355	11.7433	13.3729	4.193 (57)
E	-0.878407	0.683758	-1.35404	1.75287	0.661 (27)
H	-0.300451	-2.10748	0.626811	2.21915	0.432 (32)
Y	0.93658	-0.0742056	-1.00147	1.37318	0.594 (26)
<b>Total</b>	<b>2.9182</b>	<b>1.83849</b>	<b>5.93999</b>	<b>6.86873</b>	<b>2.692</b>

Table 6. Check points.  
X - Easting, Y - Northing, Z - Altitude.

## Digital Elevation Model

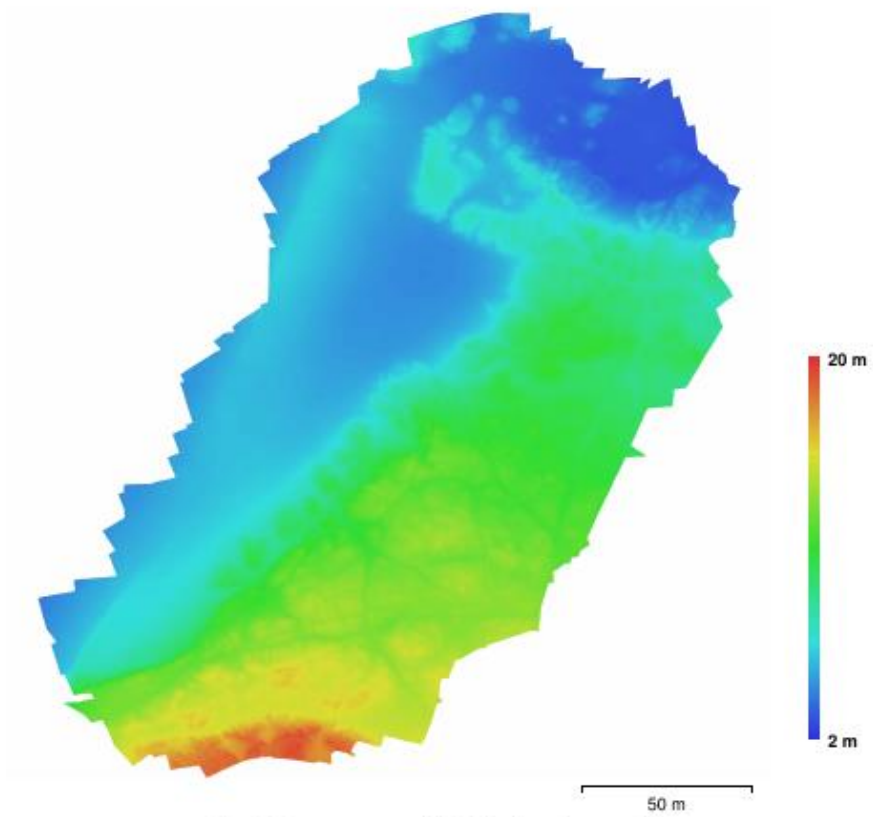


Fig. 4. Reconstructed digital elevation model.

Resolution: 2.32 cm/pix  
Point density: 18.5 points/cm<sup>2</sup>

# Processing Parameters

<b>General</b>	
Cameras	298
Aligned cameras	298
Markers	14
Coordinate system	OSGB 1936 / British National Grid (EPSG::27700)
Rotation angles	Yaw, Pitch, Roll
<b>Point Cloud</b>	
Points	1,232,351 of 1,310,465
RMS reprojection error	0.197978 (1.21227 pix)
Max reprojection error	0.715523 (47.0986 pix)
Mean key point size	5.49004 pix
Effective overlap	3.84492
<b>Alignment parameters</b>	
Accuracy	High
Generic preselection	Yes
Reference preselection	Yes
Key point limit	100,000
Tie point limit	0
Adaptive camera model fitting	Yes
Matching time	1 hours 35 minutes
Alignment time	10 minutes 57 seconds
<b>Optimization parameters</b>	
Parameters	f, b1, b2, cx, cy, k1, k2, p1, p2
Fit rolling shutter	No
Optimization time	29 seconds
<b>Depth Maps</b>	
Count	298
<b>Reconstruction parameters</b>	
Quality	High
Filtering mode	Aggressive
Processing time	1 days 0 hours
<b>Dense Point Cloud</b>	
Points	58,411,074
<b>Reconstruction parameters</b>	
Quality	High
Depth filtering	Aggressive
Depth maps generation time	1 days 0 hours
Dense cloud generation time	4 hours 0 minutes
<b>Model</b>	
Faces	11,581,895
Vertices	5,797,224
<b>Reconstruction parameters</b>	
Surface type	Height field
Source data	Dense
Interpolation	Enabled
Quality	High
Depth filtering	Aggressive
Face count	11,682,211
Processing time	4 minutes 14 seconds
<b>Orthomosaic</b>	
Size	17,737 x 19,316
Coordinate system	OSGB 1936 / British National Grid (EPSG::27700)
Channels	3, uint8
<b>Reconstruction parameters</b>	
Blending mode	Mosaic
Surface	Mesh

Enable color correction	No
Enable hole filling	Yes
Processing time	43 minutes 38 seconds
<b>Software</b>	
Version	1.3.2 build 4205
Platform	Linux 64

# Day 10 (Survey 5)

Processing Report  
13 February 2018



## Survey Data

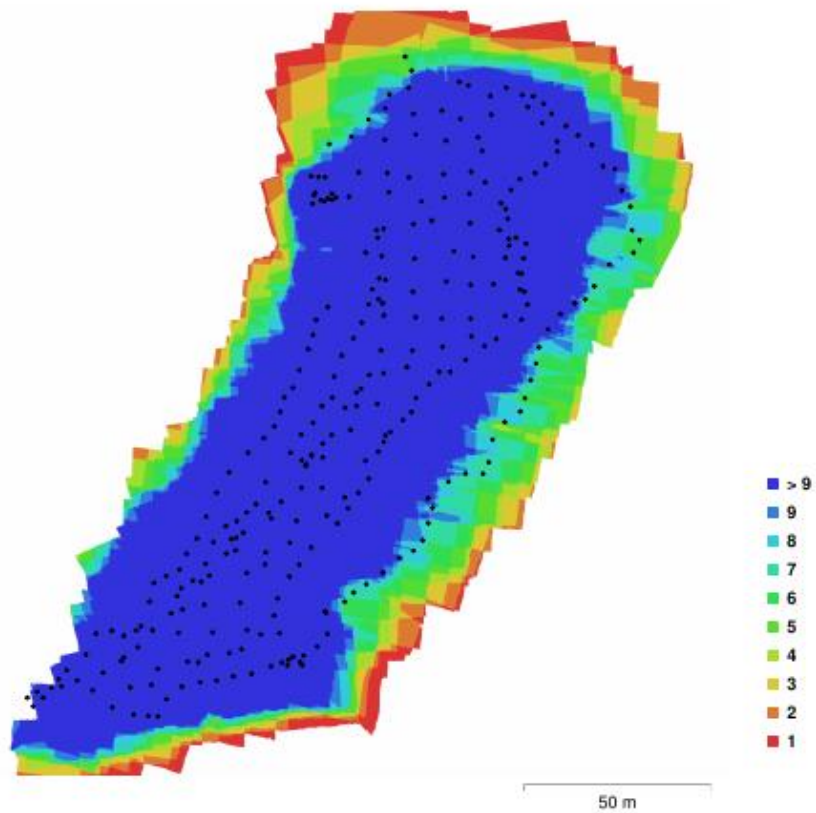


Fig. 1. Camera locations and image overlap.

Number of images:	298	Camera stations:	298
Flying altitude:	30.4 m	Tie points:	1,166,275
Ground resolution:	8.79 mm/pix	Projections:	3,931,742
Coverage area:	0.02 km <sup>2</sup>	Reprojection error:	1.24 pix

Camera Model	Resolution	Focal Length	Pixel Size	Precalibrated
Canon PowerShot D30 (5 mm)	4000 x 3000	5 mm	1.55 x 1.55 $\mu$ m	No

Table 1. Cameras.

# Camera Calibration

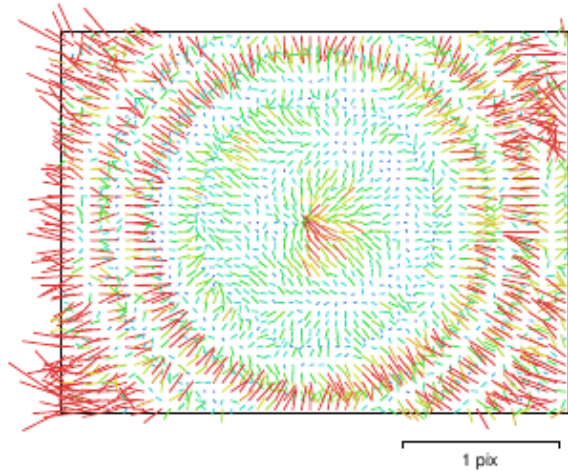


Fig. 2. Image residuals for Canon PowerShot D30 (5 mm).

## Canon PowerShot D30 (5 mm)

298 images

Type Resolution Focal Length Pixel Size  
**Frame 4000 x 3000 5 mm 1.55 x 1.55  $\mu\text{m}$**

	Value	Error	F	Cx	Cy	B1	B2	K1	K2	K3	P1	P2
F	3276.74	0.092	1.00	-0.15	-0.13	0.02	-0.02	0.03	0.06	-0.05	-0.23	-0.08
Cx	-15.4309	0.087		1.00	0.01	-0.26	0.03	-0.02	-0.01	0.01	0.92	0.01
Cy	-8.66948	0.092			1.00	-0.02	-0.32	-0.02	-0.00	0.00	0.01	0.93
B1	-0.996932	0.011				1.00	-0.02	0.04	-0.04	0.04	-0.30	-0.02
B2	0.583552	0.01					1.00	0.01	-0.01	0.00	0.05	-0.36
K1	0.00243633	4.2e-05						1.00	-0.94	0.89	-0.02	-0.02
K2	-0.027078	0.00018							1.00	-0.98	-0.01	-0.00
K3	0.0235598	0.00023								1.00	0.01	0.00
P1	-0.00173149	6.2e-06									1.00	0.00
P2	-0.000270998	6.3e-06										1.00

Table 2. Calibration coefficients and correlation matrix.

# Ground Control Points

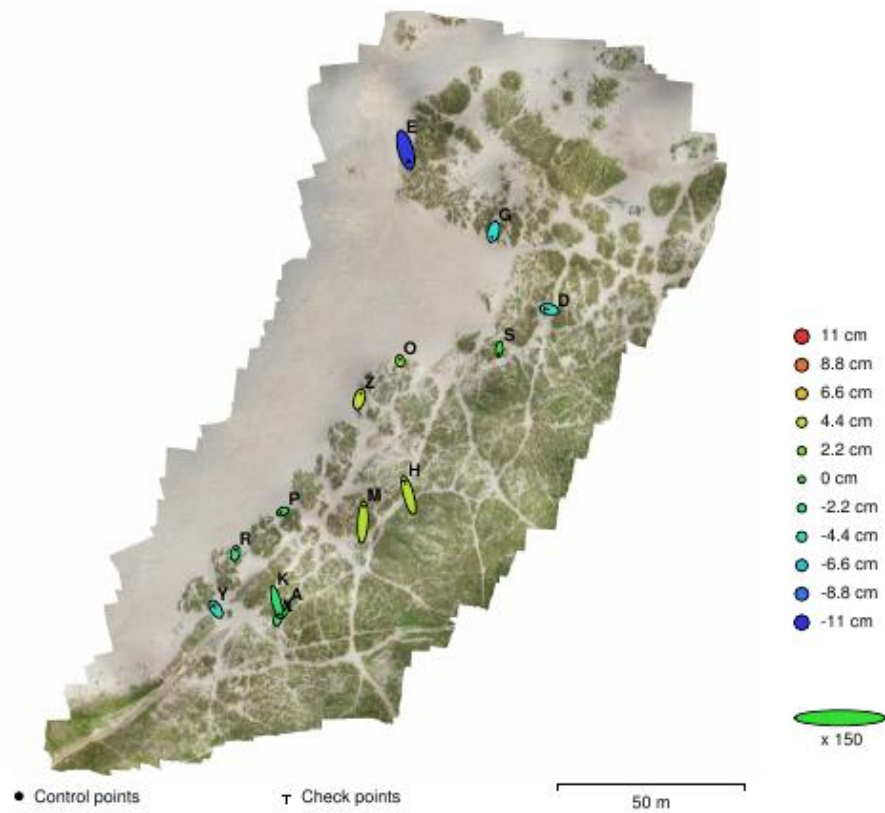


Fig. 3. GCP locations and error estimates.

Z error is represented by ellipse color. X,Y errors are represented by ellipse shape.

Estimated GCP locations are marked with a dot or crossing.

Count	X error (cm)	Y error (cm)	Z error (cm)	XY error (cm)	Total (cm)
10	0.620125	2.60326	2.9376	2.6761	3.97379

Table 3. Control points RMSE.

X - Easting, Y - Northing, Z - Altitude.

Count	X error (cm)	Y error (cm)	Z error (cm)	XY error (cm)	Total (cm)
4	1.33332	3.50651	6.63098	3.75145	7.61861

Table 4. Check points RMSE.

X - Easting, Y - Northing, Z - Altitude.

Label	X error (cm)	Y error (cm)	Z error (cm)	Total (cm)	Image (pix)
Z	0.578724	2.05706	4.47689	4.96074	0.939 (25)
O	-0.0947407	0.575537	2.48116	2.5488	0.916 (29)
S	-0.23013	-1.62764	0.236824	1.6608	1.449 (22)
R	0.223678	1.13781	-2.4126	2.6768	0.862 (30)
G	-0.49421	-1.945	-5.46838	5.82499	1.024 (24)
M	0.33432	5.6629	4.24731	7.0866	1.231 (25)
P	-0.788089	-0.386959	0.532849	1.02701	0.902 (27)
A	-1.0725	-1.95393	-0.616591	2.31264	0.919 (22)
X	0.280116	0.836835	-1.38049	1.63845	0.873 (23)
K	1.09217	-4.32938	-1.92529	4.86242	0.898 (22)
<b>Total</b>	<b>0.620125</b>	<b>2.60326</b>	<b>2.9376</b>	<b>3.97379</b>	<b>1.009</b>

Table 5. Control points.  
X - Easting, Y - Northing, Z - Altitude.

Label	X error (cm)	Y error (cm)	Z error (cm)	Total (cm)	Image (pix)
E	1.17514	-4.41802	-10.7705	11.7006	1.186 (18)
D	-1.68041	0.33325	-4.68066	4.98432	1.029 (21)
Y	-0.968789	1.50093	-4.58784	4.92337	1.042 (26)
H	-1.40276	5.22491	4.11322	6.79603	1.904 (17)
<b>Total</b>	<b>1.33332</b>	<b>3.50651</b>	<b>6.63098</b>	<b>7.61861</b>	<b>1.294</b>

Table 6. Check points.  
X - Easting, Y - Northing, Z - Altitude.

## Digital Elevation Model

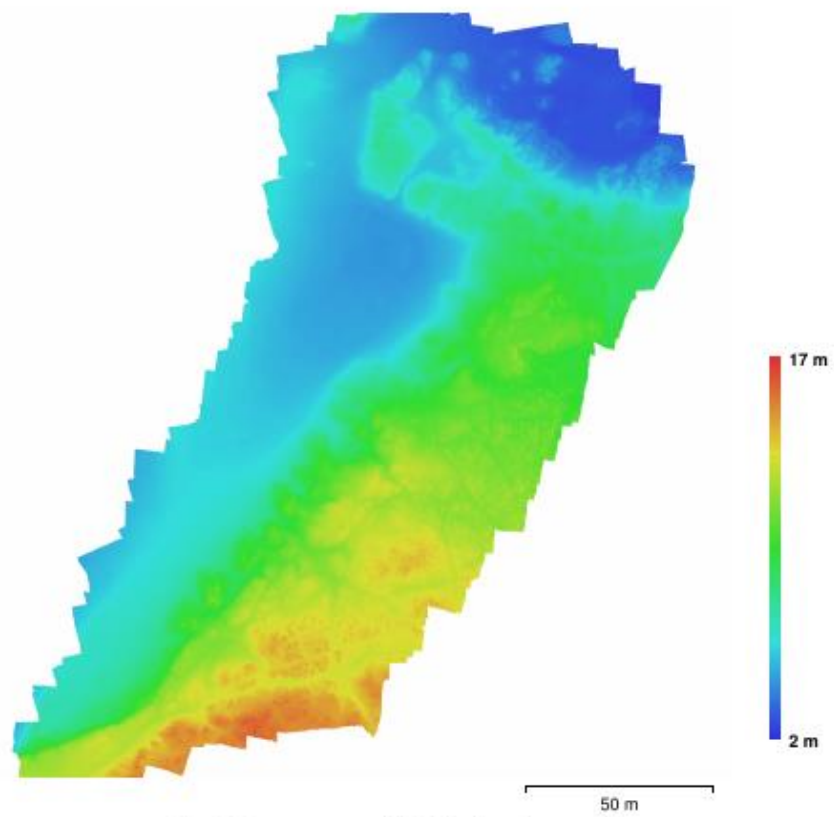


Fig. 4. Reconstructed digital elevation model.

Resolution: 1.76 cm/pix  
Point density: 32.3 points/cm<sup>2</sup>

# Processing Parameters

<b>General</b>	
Cameras	298
Aligned cameras	298
Markers	14
Coordinate system	OSGB 1936 / British National Grid (EPSG::27700)
Rotation angles	Yaw, Pitch, Roll
<b>Point Cloud</b>	
Points	1,166,275 of 1,242,920
RMS reprojection error	0.214948 (1.23753 pix)
Max reprojection error	0.764277 (41.2374 pix)
Mean key point size	5.55455 pix
Effective overlap	3.62198
<b>Alignment parameters</b>	
Accuracy	High
Generic preselection	Yes
Key point limit	100,000
Tie point limit	0
Adaptive camera model fitting	Yes
Matching time	1 hours 20 minutes
Alignment time	11 minutes 45 seconds
<b>Optimization parameters</b>	
Parameters	f, b1, b2, cx, cy, k1-k3, p1, p2
Fit rolling shutter	No
Optimization time	44 seconds
<b>Depth Maps</b>	
Count	298
<b>Reconstruction parameters</b>	
Quality	High
Filtering mode	Aggressive
Processing time	13 hours 13 minutes
<b>Dense Point Cloud</b>	
Points	84,385,355
<b>Reconstruction parameters</b>	
Quality	High
Depth filtering	Aggressive
Depth maps generation time	13 hours 13 minutes
Dense cloud generation time	2 hours 50 minutes
<b>Model</b>	
Faces	16,744,417
Vertices	8,380,179
<b>Reconstruction parameters</b>	
Surface type	Height field
Source data	Dense
Interpolation	Enabled
Quality	High
Depth filtering	Aggressive
Face count	16,877,068
Processing time	6 minutes 33 seconds
<b>DEM</b>	
Size	14,699 x 17,680
Coordinate system	OSGB 1936 / British National Grid (EPSG::27700)
<b>Reconstruction parameters</b>	
Source data	Dense cloud
Interpolation	Enabled
Processing time	7 minutes 54 seconds
<b>Orthomosaic</b>	

Size	22,500 x 23,302
Coordinate system	OSGB 1936 / British National Grid (EPSG::27700)
Channels	3, uint8
<b>Reconstruction parameters</b>	
Blending mode	Mosaic
Surface	DEM
Enable color correction	No
Enable hole filling	Yes
Processing time	6 minutes 34 seconds
<b>Software</b>	
Version	1.3.2 build 4205
Platform	Linux 64

## **Day 11 (Survey 6)**

**Processing Report  
13 February 2018**



## Survey Data

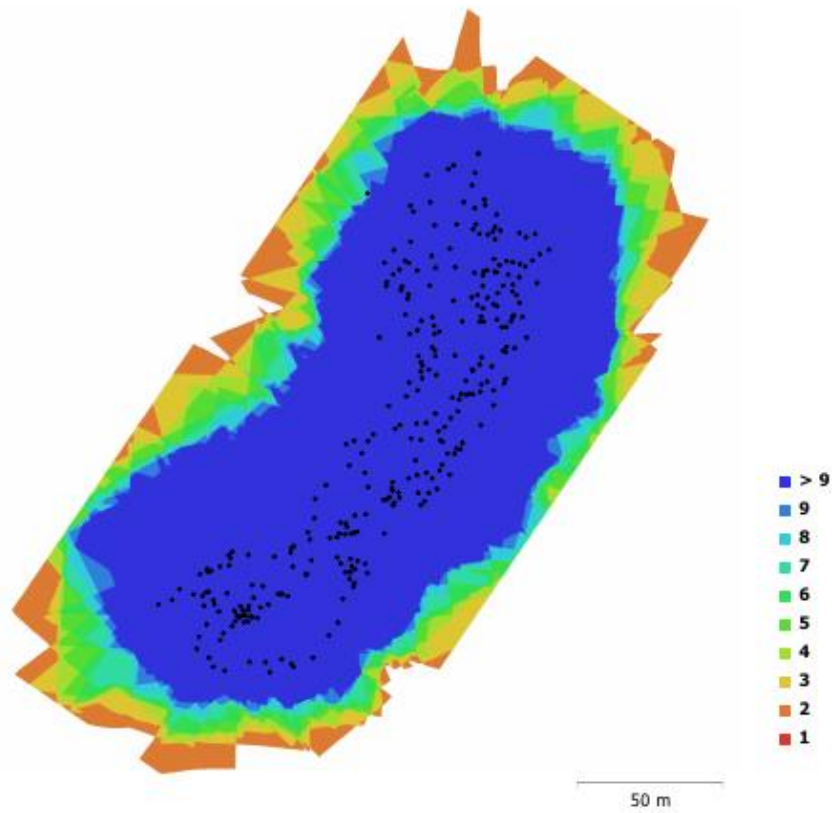


Fig. 1. Camera locations and image overlap.

Number of images:	298	Camera stations:	298
Flying altitude:	42.9 m	Tie points:	1,218,213
Ground resolution:	1.26 cm/pix	Projections:	4,514,338
Coverage area:	0.0324 km <sup>2</sup>	Reprojection error:	1.15 pix

Camera Model	Resolution	Focal Length	Pixel Size	Precalibrated
Canon PowerShot D30 (5 mm)	4000 x 3000	5 mm	1.55 x 1.55 $\mu$ m	No

Table 1. Cameras.

# Camera Calibration

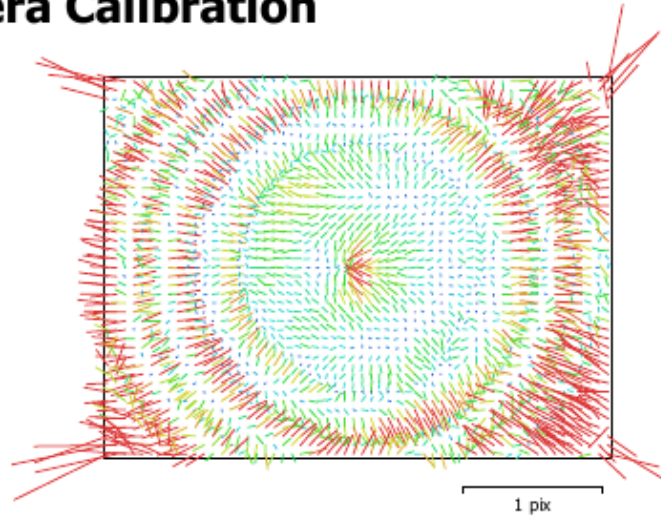


Fig. 2. Image residuals for Canon PowerShot D30 (5 mm).

## Canon PowerShot D30 (5 mm)

298 images

Type Resolution Focal Length Pixel Size  
**Frame 4000 x 3000 5 mm 1.55 x 1.55  $\mu$ m**

	Value	Error	F	Cx	Cy	B1	B2	K1	K2	K3	K4	P1	P2
<b>F</b>	<b>3280.17</b>	0.052	1.00	-0.41	0.11	-0.33	-0.06	-0.10	0.14	-0.14	0.13	-0.16	0.11
<b>Cx</b>	<b>-18.2098</b>	0.05		1.00	-0.07	0.49	0.03	-0.04	0.01	-0.00	0.00	0.89	-0.08
<b>Cy</b>	<b>-6.95172</b>	0.045			1.00	-0.04	0.34	0.02	-0.01	0.00	-0.00	-0.02	0.93
<b>B1</b>	<b>-0.940386</b>	0.0055				1.00	0.02	-0.01	-0.01	0.00	-0.00	0.26	-0.06
<b>B2</b>	<b>0.398266</b>	0.0052					1.00	0.00	0.00	0.00	-0.00	0.04	0.16
<b>K1</b>	<b>-0.00255726</b>	6.5e-05						1.00	-0.97	0.92	-0.87	-0.05	0.02
<b>K2</b>	<b>0.0179736</b>	0.00048							1.00	-0.99	0.95	0.01	-0.01
<b>K3</b>	<b>-0.137336</b>	0.0014								1.00	-0.99	-0.00	0.01
<b>K4</b>	<b>0.173831</b>	0.0014									1.00	0.00	-0.00
<b>P1</b>	<b>-0.00194867</b>	3.5e-06										1.00	-0.04
<b>P2</b>	<b>-1.86849e-06</b>	3.3e-06											1.00

Table 2. Calibration coefficients and correlation matrix.

# Ground Control Points

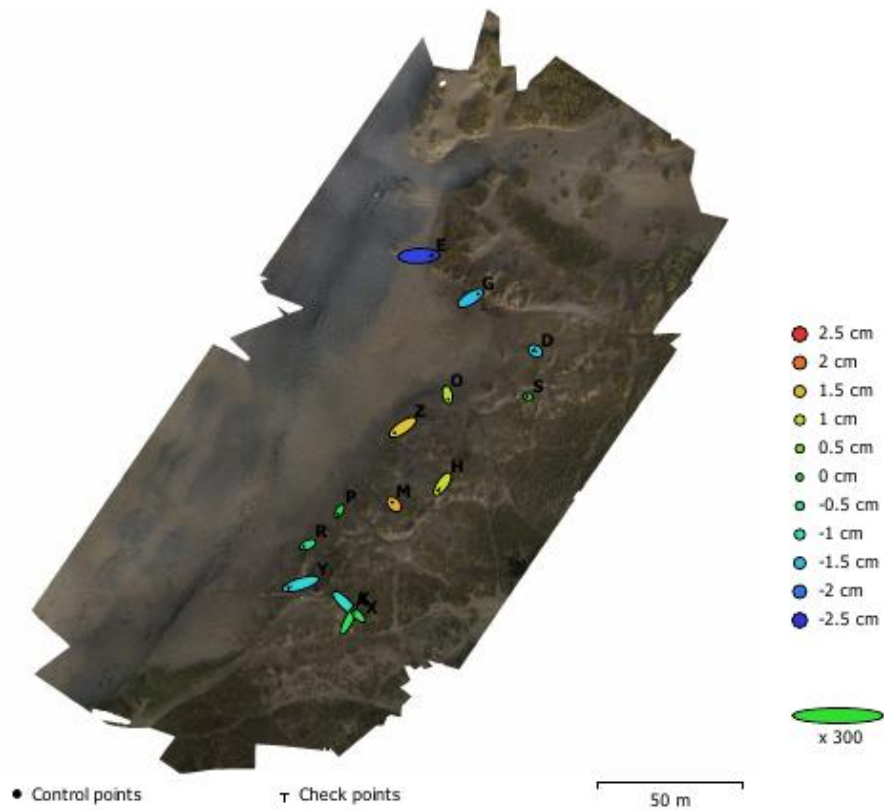


Fig. 3. GCP locations and error estimates.

Z error is represented by ellipse color. X,Y errors are represented by ellipse shape.

Estimated GCP locations are marked with a dot or crossing.

Count	X error (cm)	Y error (cm)	Z error (cm)	XY error (cm)	Total (cm)
10	1.14238	1.19191	0.966502	1.65096	1.91306

Table 3. Control points RMSE.  
X - Easting, Y - Northing, Z - Altitude.

Count	X error (cm)	Y error (cm)	Z error (cm)	XY error (cm)	Total (cm)
4	2.1998	0.901373	1.62794	2.37731	2.88128

Table 4. Check points RMSE.  
X - Easting, Y - Northing, Z - Altitude.

<b>Label</b>	<b>X error (cm)</b>	<b>Y error (cm)</b>	<b>Z error (cm)</b>	<b>Total (cm)</b>	<b>Image (pix)</b>
A	1.71783	-1.69026	-1.03774	2.62389	1.014 (25)
G	1.67708	1.02382	-1.52479	2.48713	0.918 (49)
K	1.27052	2.46023	-0.304412	2.78561	1.104 (23)
M	-0.430292	0.471066	1.61898	1.74016	1.249 (30)
O	0.212763	-0.988092	0.901675	1.35448	0.958 (44)
P	-0.441874	-0.681316	-0.0429745	0.813198	0.957 (40)
R	-0.878742	-0.399331	-0.573623	1.12281	0.803 (29)
S	-0.252691	0.0699665	0.109829	0.284272	0.974 (34)
X	-0.909347	0.907262	-0.268237	1.31225	1.068 (23)
Z	-1.89315	-1.26434	1.41339	2.6796	0.816 (33)
<b>Total</b>	<b>1.14238</b>	<b>1.19191</b>	<b>0.966502</b>	<b>1.91306</b>	<b>0.982</b>

Table 5. Control points.  
X - Easting, Y - Northing, Z - Altitude.

<b>Label</b>	<b>X error (cm)</b>	<b>Y error (cm)</b>	<b>Z error (cm)</b>	<b>Total (cm)</b>	<b>Image (pix)</b>
D	-0.385398	0.243911	-1.41884	1.49035	0.936 (48)
E	3.10685	0.127864	-2.37568	3.91315	0.914 (37)
H	-1.04566	-1.53513	1.08229	2.14974	0.830 (39)
Y	-2.90895	-0.904114	-1.33131	3.32443	1.063 (46)
<b>Total</b>	<b>2.1998</b>	<b>0.901373</b>	<b>1.62794</b>	<b>2.88128</b>	<b>0.945</b>

Table 6. Check points.  
X - Easting, Y - Northing, Z - Altitude.

## Digital Elevation Model

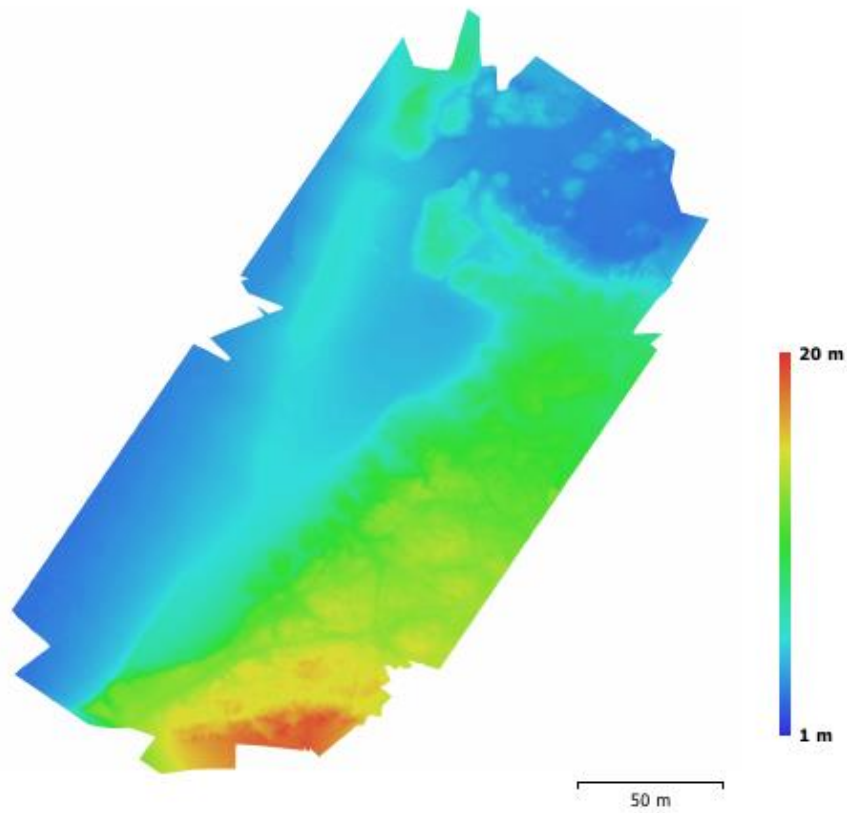


Fig. 4. Reconstructed digital elevation model.

Resolution: 2.52 cm/pix  
Point density: 15.7 points/cm<sup>2</sup>

# Processing Parameters

## General

Cameras	298
Aligned cameras	298
Markers	14
Coordinate system	OSGB 1936 / British National Grid (EPSG::27700)
Rotation angles	Yaw, Pitch, Roll

## Point Cloud

Points	1,218,213 of 1,301,800
RMS reprojection error	0.21012 (1.14538 pix)
Max reprojection error	0.759971 (59.6604 pix)
Mean key point size	4.94085 pix
Effective overlap	4.16971

## Alignment parameters

Accuracy	High
Generic preselection	Yes
Reference preselection	Yes
Key point limit	100,000
Tie point limit	0
Adaptive camera model fitting	Yes
Matching time	2 hours 7 minutes
Alignment time	11 minutes 50 seconds

## Optimization parameters

Parameters	f, b1, b2, cx, cy, k1-k4, p1, p2
Fit rolling shutter	No
Optimization time	31 seconds

## Dense Point Cloud

Points	52,596,413
--------	------------

## Reconstruction parameters

Quality	High
Depth filtering	Aggressive
Depth maps generation time	13 hours 58 minutes
Dense cloud generation time	4 hours 16 minutes

## Model

Faces	3,485,896
Vertices	1,745,198

## Reconstruction parameters

Surface type	Height field
Source data	Dense
Interpolation	Enabled
Quality	High
Depth filtering	Aggressive
Face count	3,506,419
Processing time	2 minutes 43 seconds

## Orthomosaic

Size	18,942 x 20,811
Coordinate system	OSGB 1936 / British National Grid (EPSG::27700)
Channels	3, uint8

## Reconstruction parameters

Blending mode	Mosaic
Surface	Mesh
Enable color correction	No
Enable hole filling	Yes
Processing time	30 minutes 57 seconds

## Software

Version	1.3.2 build 4205
Platform	Windows 64

## 10.4 Appendix for chapter 7 – intertidal seagrass meadows, Pembrokeshire, UK

### 10.4.1 Supplementary methods

#### **Segmentation & support vector machine classification/OBIA**

In an effort to keep the analysis of this data as open-source and replicable as possible, the `'i.segment.uspo'`, `'i.segment'` and `'i.segment.stats'` and `'v.class.mlr'` functions were used in Geographic Resources Analysis Support System (GRASS) 7.0 (GRASS Development Team, 2015) software package.

This particular set of segmentation and classification tools utilises region growing and merging algorithms with a user input difference threshold (0-1, where 0 would allow for the merging of only identical pixels into a segment, and 1 would allow every pixel in the image to merge as one segment). An optimum threshold was determined for each orthomosaic by examining within- and between-segment heterogeneity on subsets of the spectral data, calculated with the `'i.segment.uspo'` tool. This unsupervised process was run on two subset regions which incorporated the variety of landcover types found at each site. For Angle Bay, the subset areas were both 100 m<sup>2</sup> and for Garron Pill they were 234 m<sup>2</sup> and 42 m<sup>2</sup> respectively. The suggested optimum parameters for both sites were a segmentation threshold of 0.1 and minimum segment size of 10 pixels. Using these parameters, the data were segmented with the `'i.segment'` tool. The next process involved attributing geometric and spectral data with each segment, which can be achieved with the `'i.segment.stats'` tool. For each of the six layers (red, green, blue, and three chosen texture layers (described in Section 3: Results)) the following statistics were calculated for each segment: min, max,

range, mean, standard deviation, variance and sum. The following extent calculations were also made per segment: area, perimeter, compact circle and Fourier descriptor. The next stage involved manual selection of a training set of segments (multiple segments for each class). Each set of segments was assigned a value relating to its class, and then used as an input for the 'v.class.mIR' tool which uses various classification techniques (including support vector machine) to assign objects to each of the classes.

### **Exploration of quadrat sampling bias**

As each quadrat was positioned and recorded, a photograph was also taken with the Ricoh GR II from approximately chest height, with the whole quadrat in view. Due to variation in lighting conditions and issues with the focussing of the camera, not all of the photos are of high enough quality to be used in the analysis. However, a selection of 10 photos (5 from each site) with varying seagrass coverage were deemed high enough quality to be used for classification. A two-class unsupervised k-means classification was applied to the pixels within each quadrat and the resulting classified groups labelled as seagrass and non-seagrass based on user discretion. The classifications were produced using the RStoolbox (Leutner and Horning, 2016) package in R (R Core Team, 2016b). The resulting percentage coverage values could then be compared to values observed by eye and classified in the mosaics from the aerial data.

## 10.4.2 Supplementary results

### Quadrat sampling bias

Nine out of ten of the classified photos showed higher seagrass coverage estimates than the values observed by eye (**Figure 10.10**). The mean of the differences between observed and classified coverage was 15%.

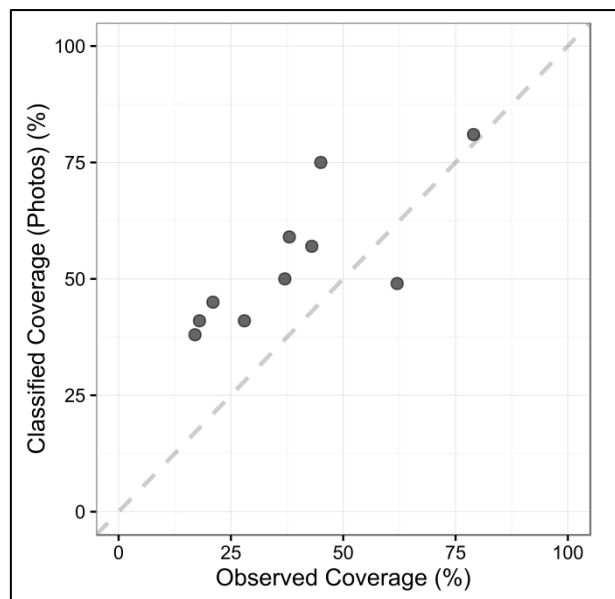


**Figure 10.10: Ten photographs of quadrats were split into two classes and the % coverage of seagrass compared to observed coverage estimations.**

## Classified maps

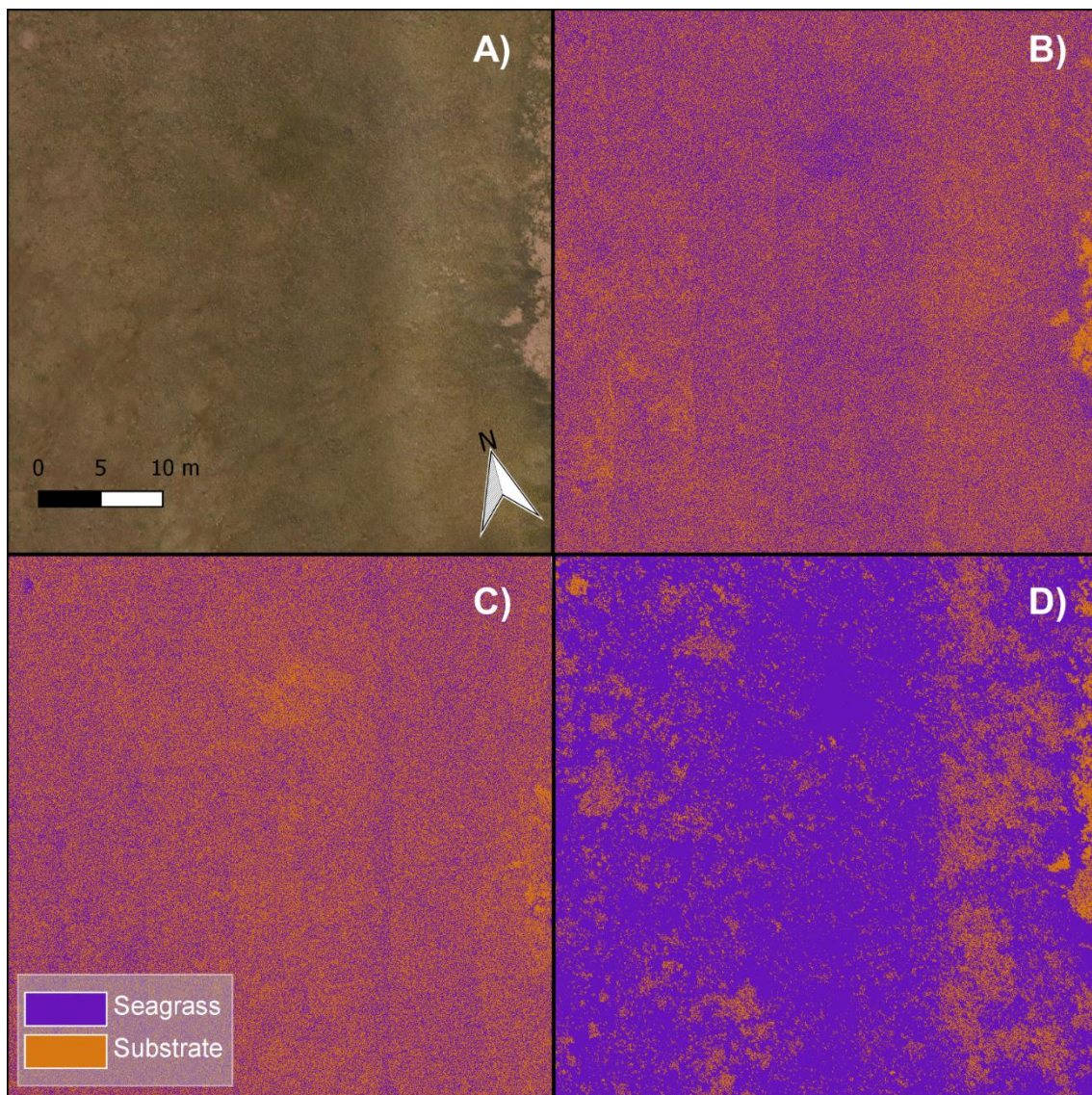


**Figure 10.11: Angle Bay orthomosaic A), unsupervised classification using RGB B), unsupervised classification using RGB and texture layers C) and OBIA based classification D).**

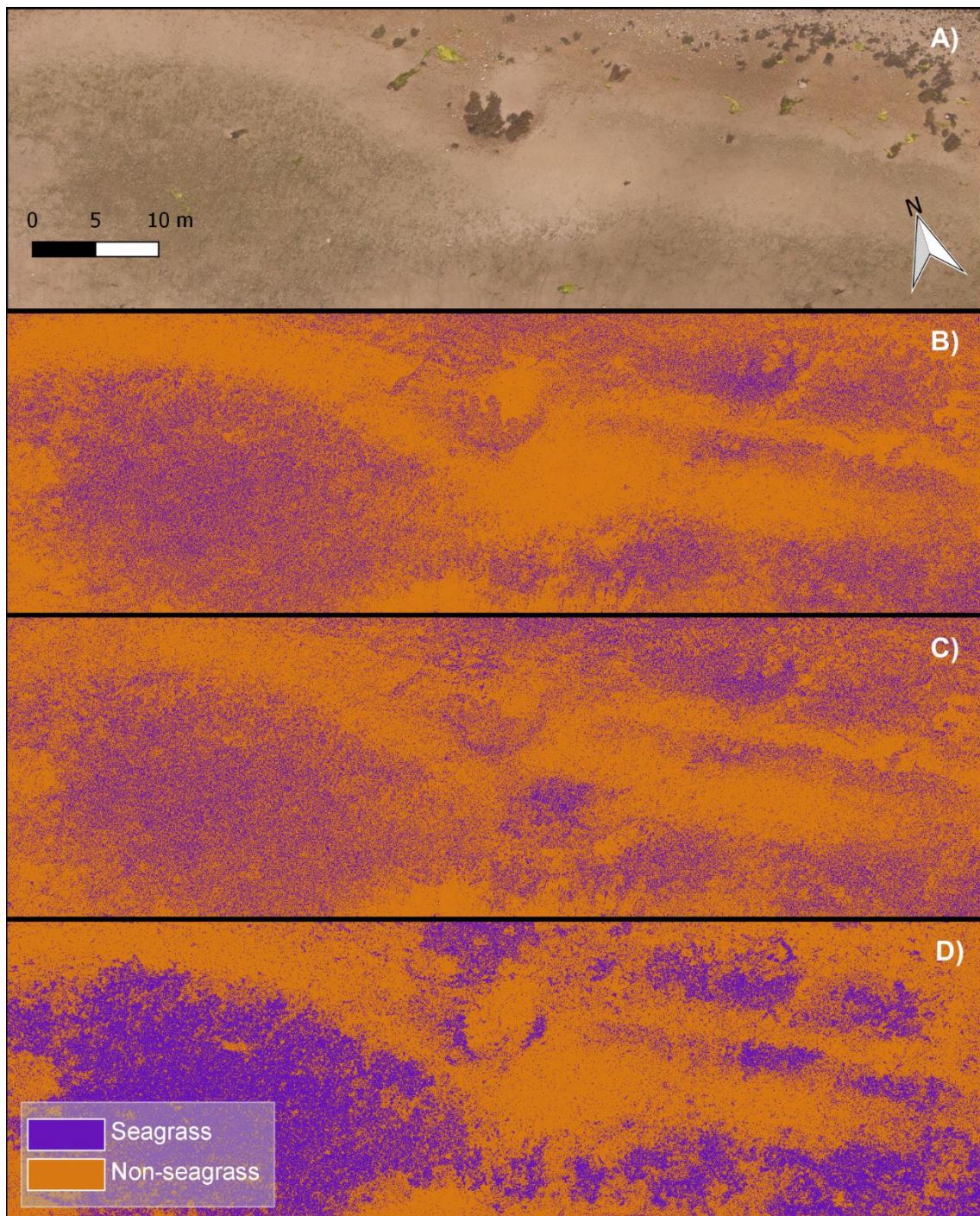


**Figure 10.12: Garron Pill orthomosaic A), unsupervised classification using RGB B), unsupervised classification using RGB and texture layers C) and OBIA based classification D). Non-seagrass class encompasses substrate, macroalgae and gravel cover types.**

**Table 10.3: Specifications for sensors used in the study.**

<b>Camera</b>	<b>Megapixels</b>	<b>Image Dimensions</b>	<b>Sensor Size</b>	<b>Focal Length</b>	<b>Dimensions</b>	<b>Weight</b>
Ricoh GR II	16.2 (effective)	4922 (W) x 3280 (H)	23.7 x 15.7 mm	18.3 mm (~28mm at 35 mm equivalent)	117.0 mm (W) x 62.8 mm (H) x 34.7 mm (D)	251 g (with battery and SD card)
AgroCam RGB	15.9 (effective)	4608 (W) x 3456 (H)	6.16 x 4.62 mm	2.7 mm (~24mm at 35mm equivalent)	60.4 mm (W) x 42 mm (H) x 21.2 mm (D)	78 g (with battery and SD card)

### 10.4.3 Photoscan reports

# Agisoft PhotoScan

Processing Report  
31 August 2016



## Survey Data

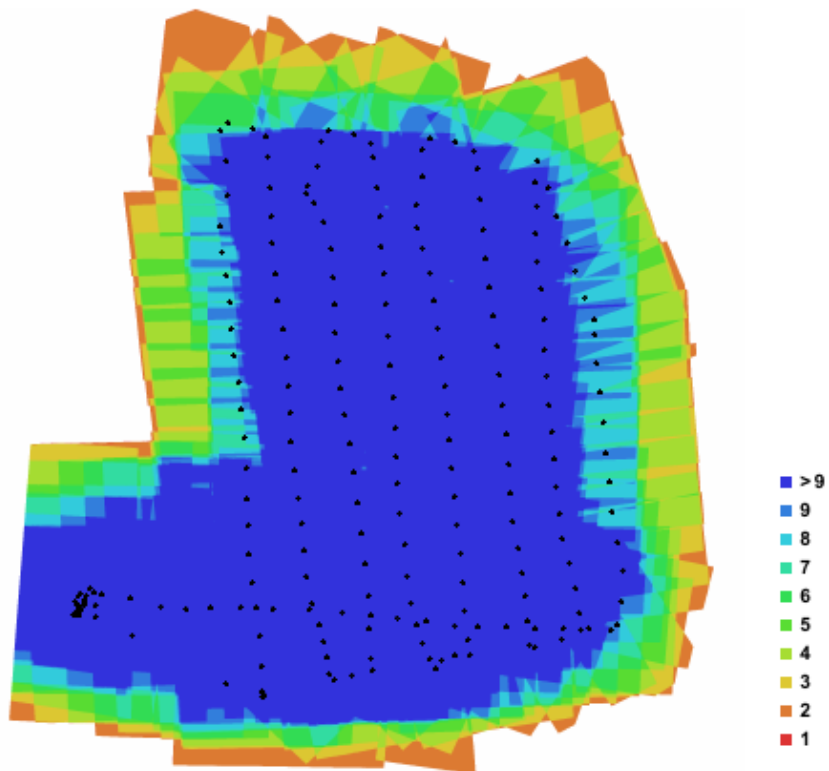


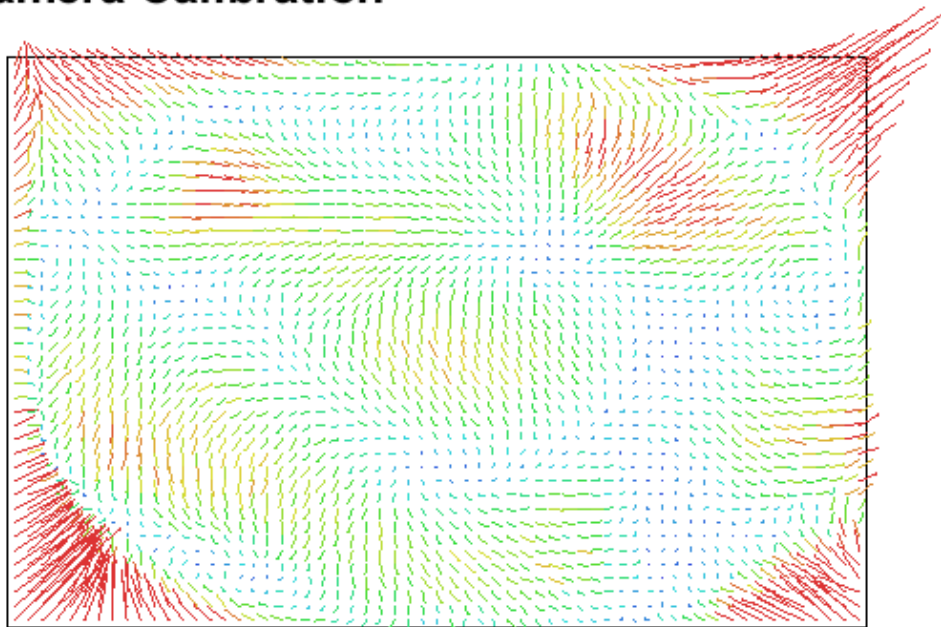
Fig. 1. Camera locations and image overlap.

Number of images:	220	Camera stations:	220
		Tie points:	7,125,119
		Projections:	20,534,671
		Reprojection error:	0.316 pix

Camera Model	Resolution	Focal Length	Pixel Size	Precalibrated
GR II (18.3 mm)	4928 x 3264	18.3 mm	4.78 x 4.78 $\mu\text{m}$	No

Table 1. Cameras.

## Camera Calibration



1 pix  
Fig. 2. Image residuals for GR II (18.3 mm).

### GR II (18.3 mm)

220 images

Resolution	Focal Length	Pixel Size	Precalibrated
<b>4928 x 3264</b>	<b>18.3 mm</b>	<b>4.78 x 4.78 <math>\mu\text{m}</math></b>	<b>No</b>
Type:	Frame	F:	3839.91
Cx:	-16.2496	B1:	0.134767
Cy:	9.36225	B2:	0.148121
K1:	-0.0748161	P1:	-0.000236546
K2:	0.104579	P2:	-0.000145956
K3:	-0.0520816	P3:	0
K4:	0.0244806	P4:	0

## Digital Elevation Model



Fig. 3. Reconstructed digital elevation model.

# Processing Parameters

<b>General</b>	
Cameras	220
Aligned cameras	220
Markers	8
Coordinate system	OSGB 1936 / British National Grid (EPSG:27700)
<b>Point Cloud</b>	
Points	7,125,119 of 7,404,604
RMS reprojection error	0.146299 (0.31587 pix)
Max reprojection error	0.584575 (23.0578 pix)
Mean keypoint size	1.85097 pix
Effective overlap	3.01867
<b>Alignment parameters</b>	
Accuracy	Highest
Pair preselection	Reference
Key point limit	0
Tie point limit	100,000
Constrain features by mask	No
Adaptive camera model fitting	Yes
Matching time	5 hours 19 minutes
Alignment time	40 minutes 48 seconds
<b>Optimization parameters</b>	
Parameters	f, b1, b2, cx, cy, k1-k4, p1, p2
Optimization time	1 minutes 56 seconds
<b>Depth Maps</b>	
Count	220
<b>Reconstruction parameters</b>	
Quality	High
Filtering mode	Mild
Processing time	3 hours 28 minutes
<b>Dense Point Cloud</b>	
Points	92,400,863
<b>Reconstruction parameters</b>	
Quality	High
Depth filtering	Mild
Depth maps generation time	3 hours 28 minutes
Dense cloud generation time	27 minutes 8 seconds
<b>Model</b>	
Faces	18,382,521
Vertices	9,197,484
Texture	8,192 x 8,192, uint8
<b>Reconstruction parameters</b>	
Surface type	Height field
Source data	Dense
Interpolation	Enabled
Quality	High
Depth filtering	Mild
Face count	18,480,139
Processing time	3 minutes 51 seconds
<b>Texturing parameters</b>	
Mapping mode	Orthophoto
Blending mode	Mosaic
Texture size	8,192 x 8,192
Enable color correction	No
Enable hole filling	Yes
UVmapping time	2 minutes 52 seconds
Blending time	4 minutes 40 seconds

**Software**  
Version  
Platform

1.2.5 build 2735  
Windows 64 bit

Processing Report  
08 September 2016



## Survey Data

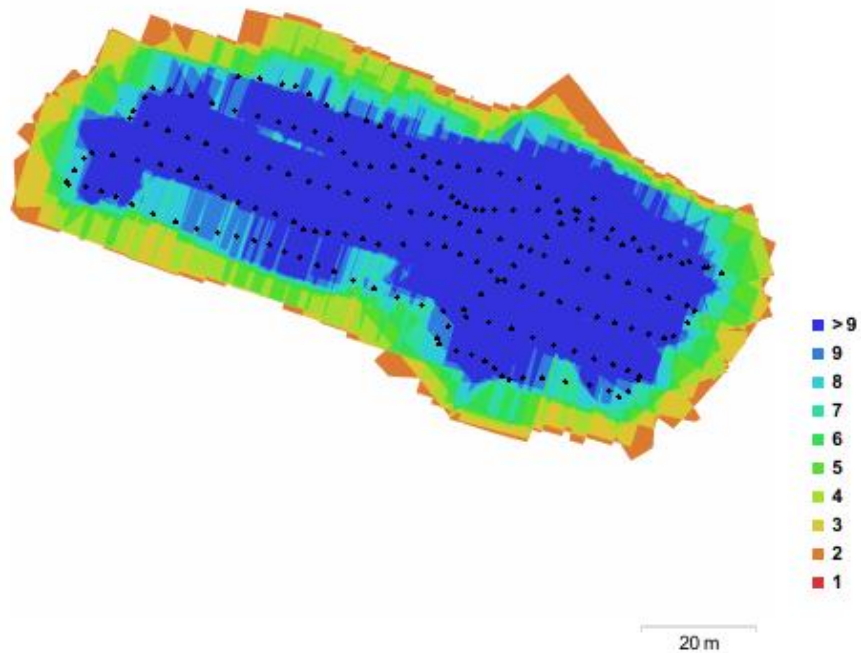


Fig. 1. Camera locations and image overlap.

Number of images:	191	Camera stations:	191
Flying altitude:	17.8 m	Tie points:	4,810,191
Ground resolution:	4.31 mm/pix	Projections:	18,194,592
Coverage area:	5.98e+03 m <sup>2</sup>	Reprojection error:	0.318 pix

Camera Model	Resolution	Focal Length	Pixel Size	Precalibrated
GR II (18.3 mm)	4928 x 3264	18.3 mm	4.78 x 4.78 $\mu\text{m}$	No

Table 1. Cameras.

## Camera Calibration

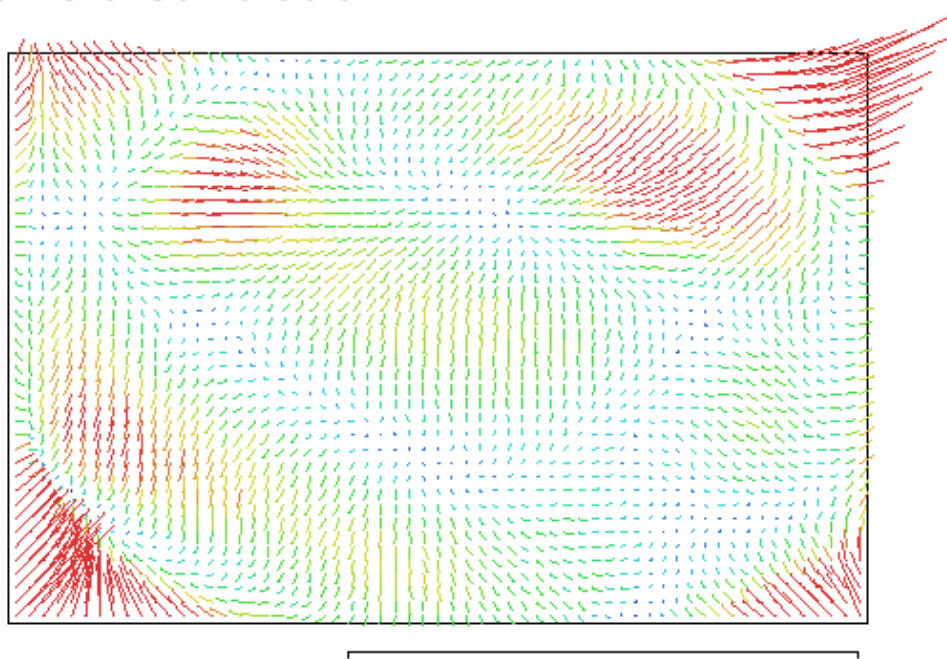


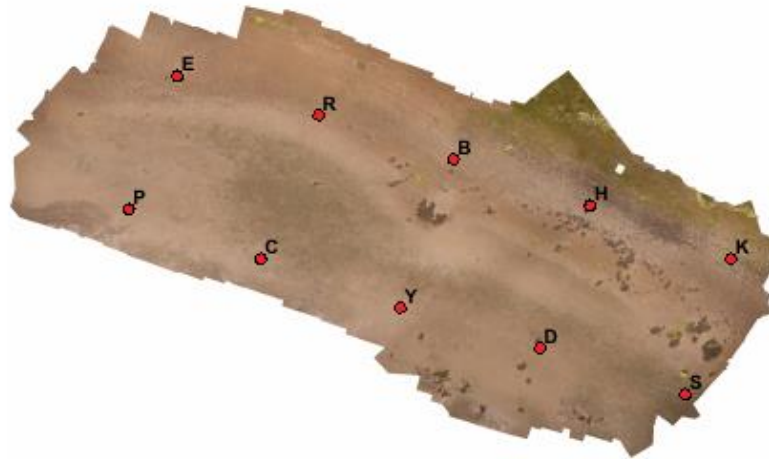
Fig. 2. Image residuals for GR II (18.3 mm).

### GR II (18.3 mm)

191 images

Resolution	Focal Length	Pixel Size	Precalibrated
<b>4928 x 3264</b>	<b>18.3 mm</b>	<b>4.78 x 4.78 <math>\mu\text{m}</math></b>	<b>No</b>
Type:	Frame	F:	3848.9
Cx:	-20.138	B1:	0.195995
Cy:	4.74607	B2:	-0.0399393
K1:	-0.0751586	P1:	-0.000224683
K2:	0.10655	P2:	-8.62649e-05
K3:	-0.0548324	P3:	0
K4:	0.0257545	P4:	0

## Ground Control Points



● Control points

▲ Check points

20 m

Fig. 3. GCP locations.

Count	X error (cm)	Y error (cm)	Z error (cm)	XY error (cm)	Total (cm)	Image (pix)
10	1.1535	2.30185	0.901827	2.5747	2.72807	0.461

Table 2. Control points RMSE.

<b>Label</b>	<b>X error (cm)</b>	<b>Y error (cm)</b>	<b>Z error (cm)</b>	<b>Total (cm)</b>	<b>Image (pix)</b>
B	-0.733446	-3.33897	0.0374561	3.41878	0.419 (14)
C	1.17281	-1.92933	0.49954	2.31244	0.145 (9)
D	-0.0763425	-1.23066	1.07798	1.6378	0.607 (11)
E	0.495544	2.54804	-0.769606	2.70746	0.390 (10)
H	2.17776	-2.35106	1.18599	3.41712	0.595 (17)
K	0.776005	4.40475	-0.306704	4.48308	0.469 (6)
P	0.268742	1.96603	-0.479175	2.04135	0.806 (6)
R	-1.78601	-0.586043	-0.022453	1.87983	0.163 (13)
S	-1.41106	0.895462	-2.02981	2.62927	0.230 (3)
Y	-0.736807	-0.409137	0.526086	0.993501	0.207 (6)
<b>Total</b>	<b>1.1535</b>	<b>2.30185</b>	<b>0.901827</b>	<b>2.72807</b>	<b>0.461</b>

Table 3. Control points.

## Digital Elevation Model

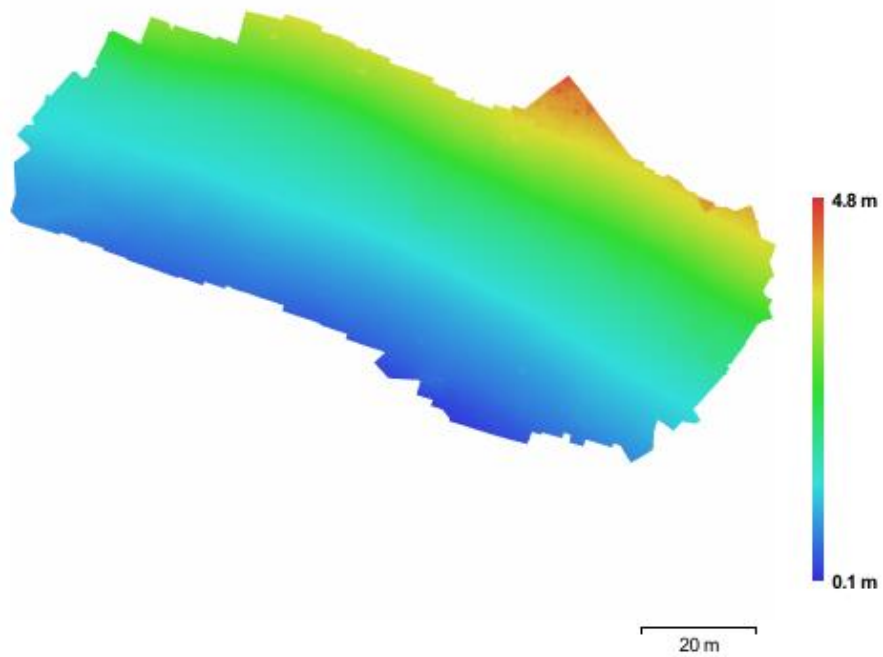


Fig. 4. Reconstructed digital elevation model.

Resolution: 8.62 mm/pix  
Point density: 1.35 points/cm<sup>2</sup>

# Processing Parameters

<b>General</b>	
Cameras	191
Aligned cameras	191
Markers	10
Coordinate system	OSGB 1936 / British National Grid (EPSG:27700)
<b>Point Cloud</b>	
Points	4,810,191 of 5,066,668
RMS reprojection error	0.160825 (0.317932 pix)
Max reprojection error	0.581449 (17.2401 pix)
Mean keypoint size	1.79132 pix
Effective overlap	3.94727
<b>Alignment parameters</b>	
Accuracy	Highest
Pair preselection	Reference
Key point limit	0
Tie point limit	100,000
Constrain features by mask	No
Adaptive camera model fitting	Yes
Matching time	5 hours 43 minutes
Alignment time	35 minutes 55 seconds
<b>Optimization parameters</b>	
Parameters	f, b1, b2, cx, cy, k1-k4, p1, p2
Optimization time	1 minutes 34 seconds
<b>Depth Maps</b>	
Count	191
<b>Reconstruction parameters</b>	
Quality	High
Filtering mode	Mild
Processing time	3 hours 36 minutes
<b>Dense Point Cloud</b>	
Points	87,428,601
<b>Reconstruction parameters</b>	
Quality	High
Depth filtering	Mild
Depth maps generation time	3 hours 36 minutes
Dense cloud generation time	25 minutes 30 seconds
<b>Model</b>	
Faces	17,302,515
Vertices	8,658,405
<b>Reconstruction parameters</b>	
Surface type	Height field
Source data	Dense
Interpolation	Enabled
Quality	High
Depth filtering	Mild
Face count	17,485,720
Processing time	5 minutes 46 seconds
<b>Orthomosaic</b>	
Size	30,956 x 18,298
Coordinate system	OSGB 1936 / British National Grid (EPSG:27700)
Channels	3, uint8
Blending mode	Mosaic
<b>Reconstruction parameters</b>	
Surface	Mesh
Enable color correction	No
Processing time	8 minutes 0 seconds

**Software**  
Version  
Platform

1.2.5 build 2735  
Windows 64 bit

## 11 References

- Aber, J., Marzloff, I., Ries, J., 2010. *Small-Format Aerial Photography*. Elsevier, Amsterdam.
- Aber, J.S., Aber, S.W., Leffler, B., 2001. Challenge of Infrared Kite Aerial Photography. *Trans. Kansas Acad. Sci.* 104, 18–27.  
doi:10.1660/062.112.0205
- Aber, J.S., Gałazka, D., 2000. Potential of kite aerial photography for Quaternary investigations in Poland. *Geol. Quaterly* 44, 33–38. doi:10.1111/j.1477-9730.2009.00535.x
- Acosta, A., Carranza, M.L., Izzi, C.F., 2009. Are there habitats that contribute best to plant species diversity in coastal dunes? *Biodivers. Conserv.* 18, 1087–1098. doi:10.1007/s10531-008-9454-9
- Agisoft LLC, 2017. *Photoscan Professional* (1.3.1)
- Agisoft LLC, 2016. *Photoscan Professional* (1.2.5)
- Alvarez-Filip, L., Dulvy, N.K., Gill, J.A., Watkinson, A.R., Co, I.M., 2009. Flattening of Caribbean coral reefs: region-wide declines in architectural complexity. *Proc. R. Soc. B Biol. Sci.* 276, 1–7.  
doi:10.1098/rspb.2009.0339
- Anderson, K., 2016. Integrating multiple scales of remote sensing measurement – from satellites to kites. *Prog. Phys. Geogr.* 40, 187–195.  
doi:10.1177/0309133316639175
- Anderson, K., Gaston, K.J., 2013. Lightweight unmanned aerial vehicles will revolutionize spatial ecology. *Front. Ecol. Environ.* 11, 138–146.  
doi:10.1890/120150
- Anderson, K., Griffiths, D., DeBell, L., Hancock, S., Duffy, J.P., Shutler, J.D., Reinhardt, W., Griffiths, A., 2016. A grassroots remote sensing toolkit using live coding, smartphones, kites and lightweight drones. *PLoS One* 11, e0151564. doi:10.1371/journal.pone.0151564
- Andrews, B.D., Gares, P.A., Colby, J.D., 2002. Techniques for GIS modeling of coastal dunes. *Geomorphology* 48, 289–308. doi:10.1016/S0169-555X(02)00186-1
- Armstrong, R.A., 1993. Remote sensing of submerged vegetation canopies for biomass estimation. *Int. J. Remote Sens.* 14, 621–627.  
doi:10.1080/01431169308904363
- Aronson, R.B., Precht, W.F., 2001. White-band disease and the changing face of Caribbean coral reefs. *Hydrobiologia* 460, 25–38.  
doi:https://doi.org/10.1023/A:1013103928980

- Arrowsmith, R., 2002. *Kite Photography-The 1906 San Francisco Earthquake*. [Online]. [Accessed 1/3/2016]. Available from: <http://activetectonics.la.asu.edu/kites/06eq.html>
- Asner, G.P., 2001. Cloud cover in Landsat observations of the Brazilian Amazon. *Int. J. Remote Sens.* 22, 3855–3862. doi:10.1080/01431160010006926
- Asner, G.P., Martin, R.E., Mascaro, J., 2017. Coral reef atoll assessment in the South China Sea using Planet Dove satellites. *Remote Sens. Ecol. Conserv.* 3, 57–65. doi:10.1002/rse2.42
- Auby, I., Labourg, P., 1996. Seasonal Dynamics of *Zostera Noltii* Hornem in The Bay of Arcachon (France). *J. Sea Res.* 35, 269–277. doi:[http://dx.doi.org/10.1016/S1385-1101\(96\)90754-6](http://dx.doi.org/10.1016/S1385-1101(96)90754-6)
- Auguie, B., 2017. gridExtra: Miscellaneous Functions for "Grid" Graphics. R package version 2.3. <https://CRAN.R-project.org/package=gridExtra>
- Aurbach, D., Talyosef, Y., Markovsky, B., Markevich, E., Zinigrad, E., Asraf, L., Gnanaraj, J.S., Kim, H., 2004. Design of electrolyte solutions for Li and Li-ion batteries: a review. *Electrochim. Acta* 50, 247–254. doi:10.1016/j.electacta.2004.01.090
- Autret, R., Dodet, G., Suanez, S., Roudaut, G., Fichaut, B., 2018. Long-term variability of supratidal coastal boulder activation in Brittany (France). *Geomorphology* 304, 184–200. doi:10.1016/j.geomorph.2017.12.028
- Baddeley, A., Rubak, E., Turner, R., 2015. *Spatial Point Patterns: Methodology and Applications with R*. Chapman and Hall/CRC Press, London.
- Balsley, B.B., Jensen, M.L., Frehlich, R.G., 1998. The use of state-of-the-art kites for profiling the lower atmosphere. *Boundary-Layer Meteorol.* 87, 1–25. doi:10.1023/A:1000812511429
- Bar Massada, A., Gabay, O., Perevolotsky, A., Carmel, Y., 2008. Quantifying the effect of grazing and shrub-clearing on small scale spatial pattern of vegetation. *Landsc. Ecol.* 23, 327–339. doi:10.1007/s10980-007-9189-0
- Barbier, E.B., Hacker, S.D., Kennedy, C., Koch, E.W., Stier, A.C., Silliman, B.R., 2011. The value of estuarine and coastal ecosystem services. *Ecol. Monogr.* 81, 169–193. doi:10.1890/10-1510.1
- Bargain, A., Robin, M., Méléder, V., Rosa, P., Menn, E.L., Harin, N., Barillé, L., 2013. Seasonal spectral variation of *Zostera noltii* and its influence on pigment-based Vegetation Indices. *J. Exp. Mar. Bio. Ecol.* 446, 86–94. doi:10.1016/j.jembe.2013.04.012
- Barrell, J., Grant, J., 2015. High-resolution, low-altitude aerial photography in physical geography: A case study characterizing eelgrass (*Zostera marina* L.) and blue mussel (*Mytilus edulis* L.) landscape mosaic structure. *Prog. Phys. Geogr.* 39, 440–459. doi:10.1177/0309133315578943

- Barrell, J., Grant, J., Hanson, A., Mahoney, M., 2015. Evaluating the complementarity of acoustic and satellite remote sensing for seagrass landscape mapping. *Int. J. Remote Sens.* 36, 4069–4094. doi:10.1080/01431161.2015.1076208
- Baumstark, R., Duffey, R., Pu, R., 2016. Mapping seagrass and colonized hard bottom in Springs Coast, Florida using WorldView-2 satellite imagery. *Estuar. Coast. Shelf Sci.* 181, 83–92. doi:10.1016/j.ecss.2016.08.019
- Bazzichetto, M., Malavasi, M., Acosta, A.T.R., Carranza, M.L., 2016. How does dune morphology shape coastal EC habitats occurrence? A remote sensing approach using airborne LiDAR on the Mediterranean coast. *Ecol. Indic.* 71, 618–626. doi:10.1016/j.ecolind.2016.07.044
- Beaumont, N.J., Austen, M.C., Mangi, S.C., Townsend, M., 2008. Economic valuation for the conservation of marine biodiversity 56, 386–396. doi:10.1016/j.marpolbul.2007.11.013
- Beaumont, N.J., Jones, L., Garbutt, A., Hansom, J.D., Toberman, M., 2014. The value of carbon sequestration and storage in coastal habitats. *Estuar. Coast. Shelf Sci.* 137, 32–40. doi:10.1016/j.ecss.2013.11.022
- Bejarano, S., Mumby, P.J., Sotheran, I., 2011. Predicting structural complexity of reefs and fish abundance using acoustic remote sensing (RoxAnn). *Mar. Biol.* 158, 489–504. doi:10.1007/s00227-010-1575-5
- Bernard, G., Boudouresque, C.F., Picon, P., 2007. Long term changes in *Zostera* meadows in the Berre lagoon (Provence, Mediterranean Sea). *Estuar. Coast. Shelf Sci.* 73, 617–629. doi:10.1016/j.ecss.2007.03.003
- Bertelli, C.M., Robinson, M.T., Mendzil, A.F., Pratt, L.R., Unsworth, R.K.F., 2018. Finding some seagrass optimism in Wales, the case of *Zostera noltii*. *Mar. Pollut. Bull.* 134, 216–222. doi:10.1016/j.marpolbul.2017.08.018
- Bertelli, C.M., Unsworth, R.K.F., 2014. Protecting the hand that feeds us: Seagrass (*Zostera marina*) serves as commercial juvenile fish habitat. *Mar. Pollut. Bull.* 83, 425–429. doi:10.1016/j.marpolbul.2013.08.011
- Bivand, R., Keitt, T., Rowlingson, B., 2017. rgdal: Bindings for the Geospatial Data Abstraction Library. R package version 1.3-6. <https://CRAN.R-project.org/package=rgdal>
- Bivand, R., Rundel, C., 2017. rgeos: Interface to Geometry Engine - Open Source ('GEOS'). R package version 0.4-1. <https://CRAN.R-project.org/package=rgeos>
- Blaschke, T., 2010. Object based image analysis for remote sensing. *ISPRS J. Photogramm. Remote Sens.* 65, 2–16. doi:10.1016/j.isprsjprs.2009.06.004
- Boike, J., Yoshikawa, K., 2003. Mapping of Periglacial Geomorphology using Kite/Balloon Aerial Photography. *Permafr. Periglac. Process.* 14, 81–85.

doi:10.1002/ppp.437

- Boucher, P., 2015. Domesticating the Drone: The Demilitarisation of Unmanned Aircraft for Civil Markets. *Sci. Eng. Ethics* 21, 1393–1412. doi:10.1007/s11948-014-9603-3
- Bowman, D., Ferri, S., Pranzini, E., 2007. Efficacy of beach dewatering - Alassio, Italy. *Coast. Eng.* 54, 791–800. doi:10.1016/j.coastaleng.2007.05.014
- Breckenridge, R.P., Dakins, M., Bunting, S., Harbour, J.L., White, S., 2011. Comparison of Unmanned Aerial Vehicle Platforms for Assessing Vegetation Cover in Sagebrush Steppe Ecosystems. *Rangel. Ecol. Manag.* 64, 521–532. doi:10.2111/REM-D-10-00030.1
- Brewin, R.J.W., de Mora, L., Jackson, T., Brewin, T.G., Shutler, J., 2015. On the Potential of Surfers to Monitor Environmental Indicators in the Coastal Zone. *PLoS One* 10, e0127706. doi:10.1371/journal.pone.0127706
- Brock, J.C., Wright, C.W., Clayton, T.D., Nayegandhi, A., 2004. LIDAR optical rugosity of coral reefs in Biscayne National Park, Florida. *Coral Reefs* 23, 48–59. doi:10.1007/s00338-003-0365-7
- Brock, J.C., Wright, C.W., Kuffner, I.B., Hernandez, R., Thompson, P., 2006. Airborne lidar sensing of massive stony coral colonies on patch reefs in the northern Florida reef tract. *Remote Sens. Environ.* 104, 31–42. doi:10.1016/j.rse.2006.04.017
- Brodie, J., Ash, L. V, Tittley, I., Yesson, C., 2018. A comparison of multispectral aerial and satellite imagery for mapping intertidal seaweed communities. *Aquat. Conserv. Mar. Freshw. Ecosyst.* 28, 872–881. doi:10.1002/aqc.2905
- Brown, A.C., McLachlan, A., 2002. Sandy shore ecosystems and the threats facing them: some predictions for the year 2025. *Environ. Conserv.* 29, 62–77. doi:10.1017/S037689290200005X
- Brown, D.G., Arbogast, A.F., 1999. Digital photogrammetric change analysis as applied to active coastal dunes in Michigan. *Photogramm. Eng. Remote Sens.* 65, 467–474.
- Bryson, M., Duce, S., Harris, D., Webster, J.M., Thompson, A., Vila-Concejo, A., Williams, S.B., 2016. Geomorphic changes of a coral shingle cay measured using Kite Aerial Photography. *Geomorphology* 270, 1–8. doi:10.1016/j.geomorph.2016.06.018
- Bryson, M., Johnson-Roberson, M., Murphy, R.J., Bongiorno, D., 2013. Kite Aerial Photography for Low-Cost, Ultra-high Spatial Resolution Multi-Spectral Mapping of Intertidal Landscapes. *PLoS One* 8, e73550. doi:10.1371/journal.pone.0073550
- Buckley, S.J., Howell, J.A., Enge, H.D., Kurz, T.H., 2008. Terrestrial laser

scanning in geology: data acquisition, processing and accuracy considerations. *J. Geol. Soc. London.* 165, 625–638. doi:10.1144/0016-76492007-100

- Bukart, A., Hecht, V.L., Kraska, T., Rascher, U., 2018. Phenological analysis of unmanned aerial vehicle based time series of barley imagery with high temporal resolution. *Precis. Agric.* 19, 134–146. doi:10.1007/s11119-017-9504-y
- Burke, L., Kura, Y., Kassem, K., Revenga, C., Spalding, M., McAllister, D., 2001. *Pilot Assessment of Global Ecosystems: Coastal Ecosystems.* World Resources Institute, Washington, DC.
- Burningham, H., French, J., 2017. Understanding coastal change using shoreline trend analysis supported by cluster-based segmentation. *Geomorphology* 282, 131–149. doi:10.1016/j.geomorph.2016.12.029
- Burns, J.H.R., Delparte, D., Gates, R.D., Takabayashi, M., 2015. Utilizing Underwater Three-Dimensional Modeling To Enhance Ecological and Biological Studies of Coral Reefs, in: *The International Archives of the Photogrammetry.* doi:10.5194/isprsarchives-XL-5-W5-61-2015
- CAA, 2015a. IN–2015/008 Small Unmanned Aircraft – Acceptable Forms of Evidence for the Grant of a CAA Permission and Changes to the Approval Requirements for UK National Qualified Entities.
- CAA, 2015b. Flying drones [WWW Document]. URL <https://www.caa.co.uk/Consumers/Model-aircraft-and-drones/Flying-drones/> (accessed 6.14.16).
- CAA, 2015c. CAP 722: Unmanned Aircraft System Operations in UK Airspace - Guidance.
- CAA, 2014a. IN–2014/190 Small Unmanned Aircraft operations within London and Other towns and cities.
- CAA, 2014b. IN–2014/184 Small Unmanned Aircraft: Congested Areas Operating Safety Case (CAOSC).
- CAA, 2013. CAP 658: Model Aircraft: A Guide to Safe Flying. 4th Edition Amendment 1.
- CAA, 2011. CAP 789: Requirements and Guidance Material for Operators.
- Cabaço, S., Cabaço, S., Santos, R., 2007. Effects of burial and erosion on the seagrass *Zostera noltii*. *J. Exp. Mar. Bio. Ecol.* 340, 204–212. doi:10.1016/j.jembe.2006.09.003
- Cambridge, M.L., McComb, A.J., 1984. The loss of seagrasses in Cockburn Sound, Western Australia. I. The time course and magnitude of seagrass decline in relation to industrial development. *Aquat. Bot.* 20, 229–243.

doi:10.1016/0304-3770(84)90089-5

Capolsini, P., Andréfouët, S., Rion, C., Payri, C., 2003. A comparison of Landsat ETM+, SPOT HRV, Ikonos, ASTER, and airborne MASTER data for coral reef habitat mapping in South Pacific islands. *Can. J. Remote Sens.* 29, 187–200. doi:10.5589/m02-088

Carboni, M., Carranza, M.L., Acosta, A., 2009. Assessing conservation status on coastal dunes: A multiscale approach. *Landsc. Urban Plan.* 91, 17–25. doi:10.1016/j.landurbplan.2008.11.004

Carbonneau, P.E., Dietrich, J.T., 2017. Cost-effective non-metric photogrammetry from consumer-grade sUAS: implications for direct georeferencing of structure from motion photogrammetry. *Earth Surf. Process. Landforms* 42, 473–486. doi:10.1002/esp.4012

Carrivick, J.L., Smith, M.W., Quincey, D.J., 2016. *Structure from Motion in the Geosciences*. Wiley-Blackwell, Chichester, UK.

Casella, E., Collin, A., Harris, D., Ferse, S., Bejarano, S., Parravicini, V., Hench, J.L., Rovere, A., 2017. Mapping coral reefs using consumer-grade drones and structure from motion photogrammetry techniques. *Coral Reefs* 36, 269–275. doi:10.1007/s00338-016-1522-0

Casella, E., Rovere, A., Pedroncini, A., Stark, C.P., Casella, M., Ferrari, M., Firpo, M., 2016. Drones as tools for monitoring beach topography changes in the Ligurian Sea (NW Mediterranean). *Geo-Marine Lett.* 36, 151–163. doi:10.1007/s00367-016-0435-9

Catano, L.B., Gunn, B.K., Kelley, M.C., Burkepile, D.E., 2015. Predation Risk, Resource Quality, and Reef Structural Complexity Shape Territoriality in a Coral Reef Herbivore. *PLoS One* 10, e0118764. doi:10.1371/journal.pone.0118764

Chabot, D., Bird, D.M., 2013. Small unmanned aircraft: precise and convenient new tools for surveying wetlands. *J. Unmanned Veh. Syst.* 24, 15–24. doi:10.1139/juvs-2013-0014

Chabot, D., Carignan, V., Bird, D.M., 2014. Measuring Habitat Quality for Least Bitterns in a Created Wetland with Use of a Small Unmanned Aircraft. *Wetlands* 34, 527–533. doi:10.1007/s13157-014-0518-1

Chabot, D., Craik, S.R., Bird, D.M., 2015. Population census of a large common tern colony with a small unmanned aircraft. *PLoS One* 10, e0122588. doi:10.1371/journal.pone.0122588

Chavez, P.S.J., 1996. Image-based atmospheric corrections- revisited and improved. *Photogramm. Eng. Remote Sensing* 62, 1025–1035. doi:0099-1112/96/6209-1025

- CHDK Development Team, 2018. Canon Hack Development Kit.  
<http://chdk.wikia.com/wiki/CHDK>
- Chianucci, F., Disperati, L., Guzzi, D., Bianchini, D., Nardino, V., Lastri, C., Rindinella, A., Corona, P., 2016. Estimation of canopy attributes in beech forests using true colour digital images from a small fixed-wing UAV. *Int. J. Appl. Earth Obs. Geoinf.* 47, 60–68. doi:10.1016/j.jag.2015.12.005
- Chirayath, V., Earle, S.A., 2016. Drones that see through waves – preliminary results from airborne fluid lensing for centimetre-scale aquatic conservation. *Aquat. Conserv.* 26, 237–250. doi:10.1002/aqc.2654
- Christiansen, F., Dujon, A.M., Sprogis, K.R., Arnould, J.P.Y., Bejder, L., 2016. Noninvasive unmanned aerial vehicle provides estimates of the energetic cost of reproduction in humpback whales. *Biosphere* 7, e01468.
- Christie, K.S., Gilbert, S.L., Brown, C.L., Hatfield, M., Biology, A., Fairbanks, A., Koyokuk, N., 2016. Unmanned aerial systems in wildlife research: current and future applications of a transformative technology. *Front. Ecol. Environ.* 14, 241–251. doi:10.1002/fee.1281
- Chust, G., Galparsoro, I., Borja, Á., Franco, J., Uriarte, A., 2008. Coastal and estuarine habitat mapping, using LIDAR height and intensity and multi-spectral imagery. *Estuar. Coast. Shelf Sci.* 78, 633–643.  
doi:10.1016/j.ecss.2008.02.003
- CloudCompare (version 2.10) [GPL software], 2017.  
<https://www.danielgm.net/cc/>
- Conlin, M., Cohn, N., Ruggiero, P., 2018. A Quantitative Comparison of Low-Cost Structure from Motion (SfM) Data Collection Platforms on Beaches and Dunes. *J. Coast. Res.* 34, 1341–1357. doi:10.2112/JCOASTRES-D-17-00160.1
- Costanza, R., Pérez-Maqueo, O., Martinez, M.L., Sutton, P., Anderson, S.J., Mulder, K., 2008. The value of coastal wetlands for hurricane protection. *Ambio* 37, 241–248. doi:10.1579/0044-7447(2008)37[241:tvocwf]2.0.co;2
- Cox, C., Munk, W., 1954. Measurement of the Roughness of the Sea Surface from Photographs of the Sun's Glitter. *J. Opt. Soc. Am.* 44, 838.  
doi:10.1364/JOSA.44.000838
- Crocker, J., 2017. ReefBudget Transect Data from Kandahalagala. Personal Communication.
- Csillik, O., 2017. Fast Segmentation and Classification of Very High Resolution Remote Sensing Data Using SLIC Superpixels. *Remote Sens.* 9, 243.  
doi:10.3390/rs9030243
- Cuevas-Jimenez, A., Ardisson, P.L., Condal, A.R., 2002. Mapping of shallow coral reefs by colour aerial photography. *Int. J. Remote Sens.* 23, 3697–

- Cunha, A.H., Santos, R.P., Gaspar, A.P., Bairros, M.F., 2005. Seagrass landscape-scale changes in response to disturbance created by the dynamics of barrier-islands: A case study from Ria Formosa (Southern Portugal). *Estuar. Coast. Shelf Sci.* 64, 636–644. doi:10.1016/j.ecss.2005.03.018
- Cunliffe, A.M., 2016. Understanding Structure and Function in Semiarid Ecosystems: Implications for Terrestrial Carbon Dynamics in Drylands PhD Thesis. University of Exeter, Exeter, UK.
- Cunliffe, A.M., Anderson, K., Debell, L., Duffy, J.P., 2017. A UK Civil Aviation Authority (CAA)-approved operations manual for safe deployment of lightweight drones in research. *Int. J. Remote Sens.* 38, 2737–2744. doi:10.1080/01431161.2017.1286059
- Cunliffe, A.M., Brazier, R.E., Anderson, K., 2016. Ultra-fine grain landscape-scale quantification of dryland vegetation structure with drone-acquired structure-from-motion photogrammetry. *Remote Sens. Environ.* 183, 129–143. doi:10.1016/j.rse.2016.05.019
- Currier, K., 2015. Mapping with strings attached: Kite aerial photography of Durai Island, Anambas Islands, Indonesia. *J. Maps* 11, 589–597. doi:10.1080/17445647.2014.925839
- Cuvillier, A., Villeneuve, N., Cordier, E., Kolasinski, J., Maurel, L., Farnier, N., Frouin, P., 2016. Causes of seasonal and decadal variability in a tropical seagrass seascape (Reunion Island, South Western Indian Ocean). *Estuar. Coast. Shelf Sci.* 184, 90–101. doi:10.1016/j.ecss.2016.10.046
- D'Oleire-Oltmanns, S., Marzloff, I., Peter, K.D., Ries, J.B., 2012. Unmanned Aerial Vehicle (UAV) for Monitoring Soil Erosion in Morocco. *Remote Sens.* 4, 3390–3416. doi:10.3390/rs4113390
- Dandois, J., Olano, M., Ellis, E., 2015. Optimal Altitude, Overlap, and Weather Conditions for Computer Vision UAV Estimates of Forest Structure. *Remote Sens.* 7, 13895–13920. doi:10.3390/rs71013895
- Dandois, J.P., Ellis, E.C., 2013. High spatial resolution three-dimensional mapping of vegetation spectral dynamics using computer vision. *Remote Sens. Environ.* 136, 259–276. doi:10.1016/j.rse.2013.04.005
- Danovaro, R., Bongiorno, L., Corinaldesi, C., Giovannelli, D., Damiani, E., Astolfi, P., Greci, L., Pusceddu, A., 2008. Sunscreens Cause Coral Bleaching by Promoting Viral Infections. *Environ. Health Perspect.* 116, 441–447. doi:10.1289/ehp.10966
- Darling, E.S., Graham, N.A.J., Januchowski-hartley, F.A., Nash, K.L., Pratchett, M.S., Wilson, S.K., 2017. Relationships between structural complexity, coral traits, and reef fish assemblages. *Coral Reefs* 36, 561–575.

doi:10.1007/s00338-017-1539-z

- Davenport, J., Davenport, J.L., 2006. The impact of tourism and personal leisure transport on coastal environments: A review. *Estuar. Coast. Shelf Sci.* 67, 280–292. doi:10.1016/j.ecss.2005.11.026
- Davidson-Arnott, R., Hesp, P., Ollerhead, J., Walker, I., Bauer, B., Delgado-Fernandez, I., Smyth, T., 2018. Sediment budget controls on foredune height: Comparing simulation model results with field data. *Earth Surf. Process. Landforms* 43, 1798–1810. doi:10.1002/esp.4354
- de la Torre-Castro, M., Rönnbäck, P., 2004. Links between humans and seagrasses—an example from tropical East Africa. *Ocean Coast. Manag.* 47, 361–387. doi:10.1016/j.ocecoaman.2004.07.005
- DeBell, L., Anderson, K., Brazier, R.E., King, N., Jones, L., 2016. Water resource management at catchment scales using lightweight UAVs: current capabilities and future perspectives. *J. Unmanned Veh. Syst.* 4, 7–30. doi:dx.doi.org/10.1139/juvs-2015-0026
- Defeo, O., McLachlan, A., Schoeman, D.S., Schlacher, T.A., Dugan, J., Jones, A., Lastra, M., Scapini, F., 2009. Threats to sandy beach ecosystems: A review. *Estuar. Coast. Shelf Sci.* 81, 1–12. doi:10.1016/j.ecss.2008.09.022
- Dekker, A., Brando, V., Anstee, J., Fyfe, S., Malthus, T., Karpouzli, E., 2006. Remote Sensing of Seagrass Ecosystems: Use of Spaceborne and Airborne Sensors, in: *Seagrasses: Biology, Ecology and Conservation*. Springer, pp. 347–359. doi:10.1007/978-1-4020-2983-7
- Delord, K., Roudaut, G., Guinet, C., Barbraud, C., Bertrand, S., Weimerskirch, H., 2015. Kite aerial photography: a low-cost method for monitoring seabird colonies. *J. F. Ornithol.* 86, 173–179. doi:10.1111/jof.12100
- Dennison, W.C., Orth, R.J., Moore, K.A., Stevenson, J.C., Carter, V., Kollar, S., Bergstrom, P.W., Batiuk, R.A., 1993. Assessing Water Quality with Submersed Aquatic Vegetation Habitat requirements as barometers of Chesapeake Bay health. *Bioscience* 43, 86–94. doi:https://doi.org/10.2307/1311969
- Dines, W.H., 1903. Scientific Kite Flying. *Nature* 68, 154–155.
- Dines, W.H., 1906. Balloons and Kites in the Service of Meteorology. *Nature* 74, 35–36.
- Ditmer, M.A., Vincent, J.B., Werden, L.K., Tanner, J.C., Laske, T.G., Iazzo, P.A., Garshelis, D.L., Fieberg, J.R., 2015. Bears Show a Physiological but Limited Behavioral Response to Unmanned Aerial Vehicles. *Curr. Biol.* 25, 1–6. doi:10.1016/j.cub.2015.07.024
- Dowle, M., Srinivasan, A., 2017. data.table: Extension of `data.frame`. Version 1.11.8. <https://CRAN.R-project.org/package=data.table>

- Downing, J.A., Anderson, M.R., 1985. Estimating the Standing Biomass of Aquatic Macrophytes. *Can. J. Fish. Aquat. Sci.* 42, 1860–1869. doi:10.1139/f85-234
- Duarte, C.M., 2002. The future of seagrass meadows. *Environ. Conserv.* 29, 192–206. doi:10.1017/S0376892902000127
- Duarte, C.M., 1991. Seagrass depth limits. *Aquat. Bot.* 40, 363–377. doi:10.1016/0304-3770(91)90081-F
- Duarte, C.M., Dennison, W.C., Orth, R.J.W., Carruthers, T.J.B., 2008. The Charisma of Coastal Ecosystems: Addressing the Imbalance. *Estuaries and Coasts* 31, 233–238. doi:10.1007/s12237-008-9038-7
- Duarte, C.M., Middelburg, J.J., Caraco, N., 2005. Major role of marine vegetation on the oceanic carbon cycle. *Biogeosciences* 2, 1–8. doi:10.5194/bgd-1-659-2004
- Duffy, J.P., Anderson, K., 2016. A 21st-century renaissance of kites as platforms for proximal sensing. *Prog. Phys. Geogr.* 40, 352–361. doi:10.1177/0309133316641810
- Duffy, J.P., Cunliffe, A.M., Debell, L., Sandbrook, C., Wich, S.A., Shutler, J.D., Myers-smith, I.H., Varela, M.R., Anderson, K., 2018a. Location, location, location: considerations when using lightweight drones in challenging environments. *Remote Sens. Ecol. Conserv.* 4, 7–19. doi:10.1002/rse2.58
- Duffy, J.P., Pratt, L., Anderson, K., Land, P.E., Shutler, J.D., 2018b. Spatial assessment of intertidal seagrass meadows using optical imaging systems and a lightweight drone. *Estuar. Coast. Shelf Sci.* 200, 169–180. doi:10.1016/j.ecss.2017.11.001
- Dumas, P., Bertaud, A., Peignon, C., Léopold, M., Pelletier, D., 2009. A “quick and clean” photographic method for the description of coral reef habitats. *J. Exp. Mar. Bio. Ecol.* 368, 161–168. doi:10.1016/j.jembe.2008.10.002
- Dumbauld, B.R., McCoy, L.M., 2015. Effect of oyster aquaculture on seagrass *Zostera marina* at the estuarine landscape scale in Willapa Bay, Washington (USA). *Aquac. Environ. Interact.* 7, 29–47. doi:10.3354/aei00131
- Dustan, P., Doherty, O., Pardede, S., 2013. Digital Reef Rugosity Estimates Coral Reef Habitat Complexity. *PLoS One* 8, e57386. doi:10.1371/journal.pone.0057386
- Eklöf, J.S., De La Torre Castro, M., Adelsköld, L., Jiddawi, N.S., Kautsky, N., 2005. Differences in macrofaunal and seagrass assemblages in seagrass beds with and without seaweed farms. *Estuar. Coast. Shelf Sci.* 63, 385–396. doi:10.1016/j.ecss.2004.11.014
- El-Askary, H., Abd El-Mawla, S.H., Li, J., El-Hattab, M.M., El-Raey, M., 2014.

- Change detection of coral reef habitat using Landsat-5 TM, Landsat 7 ETM+ and Landsat 8 OLI data in the Red Sea (Hurghada, Egypt). *Int. J. Remote Sens.* 35, 2327–2346. doi:10.1080/01431161.2014.894656
- Eltner, A., Baumgart, P., Maas, H., Faust, D., 2015. Multi-temporal UAV data for automatic measurement of rill and interrill erosion on loess soil. *Earth Surf. Process. Landforms* 40, 741–755. doi:10.1002/esp.3673
- Environment Agency, 2016. Environment Agency LIDAR data: Technical Note.
- Eulie, D.O., Walsh, J.P., Corbett, D.R., 2013. High-resolution analysis of shoreline change and application of balloon-based aerial photography, Albemarle-Pamlico Estuarine System, North Carolina, USA. *Limnol. Oceanogr. Methods* 11, 151–160. doi:10.4319/lom.2013.11.151
- Everard, M., Jones, L., Watts, B., 2010. Have we neglected the societal importance of sand dunes? An ecosystem services perspective. *Aquat. Conserv. Mar. Freshw. Ecosyst.* 20, 476–487. doi:10.1002/aqc.1114
- FAA, 2015a. Unmanned Aircraft Operations in the National Airspace System (NAS). US Department of Transportation, Federal Aviation Administration
- FAA, 2015b. Fact Sheet Unmanned Aircraft Systems (UAS). US Department of Transportation, Federal Aviation Administration
- FAA, 2015c. Unmanned Aircraft Systems [Online] [Accessed 1/2/2016]. Available from <https://www.faa.gov/uas/>. US Department of Transportation, Federal Aviation Administration
- FAA, 2013. Integration of Civil Unmanned Aircraft Systems (UAS) in the National Airspace System (NAS) Roadmap. US Department of Transportation, Federal Aviation Administration
- FAA, 2012. FAA Modernization and Reform Act. US Department of Transportation, Federal Aviation Administration
- FAA, 2010. FAA Safety Briefing: The Wings of Change. US Department of Transportation, Federal Aviation Administration
- Fabricius, K.E., 2005. Effects of terrestrial runoff on the ecology of corals and coral reefs: Review and synthesis. *Mar. Pollut. Bull.* 50, 125–146. doi:10.1016/j.marpolbul.2004.11.028
- Fastie, C., 2014. *Picavet- Thingiverse*. [Online]. [Accessed 1/4/2015]. Available from: <http://www.thingiverse.com/thing:281677>
- Feagin, R.A., Figlus, J., Zinnert, J.C., Sigren, J., Martínez, M.L., Silva, R., Smith, W.K., Cox, D., Young, D.R., Carter, G., 2015. Going with the flow or against the grain? The promise of vegetation for protecting beaches, dunes, and barrier islands from erosion. *Front. Ecol. Environ.* 13, 203–210. doi:10.1890/140218

- Feagin, R.A., Williams, A.M., Popescu, S., Stukey, J., Washington-Allen, R.A., 2014. The Use of Terrestrial Laser Scanning (TLS) in Dune Ecosystems: The Lessons Learned. *J. Coast. Res.* 30, 111–119. doi:10.2112/JCOASTRES-D-11-00223.1
- Ferguson, R.L., Korfmacher, K., 1997. Remote sensing and GIS analysis of seagrass meadows in North Carolina, USA. *Aquat. Bot.* 58, 241–258. doi:doi.org/10.1016/S0304-3770(97)00038-7
- Ferrari, R., McKinnon, D., He, H., Smith, R.N., Corke, P., Gonzalez-Rivero, M., Mumby, P.J., Upcroft, B., 2016. Quantifying multiscale habitat structural complexity: A cost-effective framework for underwater 3D modelling. *Remote Sens.* 8, 113. doi:10.3390/rs8020113
- Feurer, D., Planchon, O., Maaoui, M.A., Slimane, A. Ben, Boussema, M.R., Pierrot-Deseilligny, M., Raclot, D., 2018. Using kites for 3-D mapping of gullies at decimetre-resolution over several square kilometres: a case study on the Kamech catchment, Tunisia. *Nat. Hazards Earth Syst. Sci.* 18, 1567–1582. doi:doi.org/10.5194/nhess-18-1567-2018
- Figueira, W., Ferrari, R., Weatherby, E., Porter, A., Hawes, S., Byrne, M., 2015. Accuracy and Precision of Habitat Structural Complexity Metrics Derived from Underwater Photogrammetry. *Remote Sens.* 7, 16883–16900. doi:10.3390/rs71215859
- Forlani, G., Dall’Asta, E., Diotri, F., di Cella, U.M., Roncella, R., Santise, M., 2018. Quality Assessment of DSMs Produced from UAV Flights Georeferenced with On-Board RTK Positioning. *Remote Sens.* 10, 311. doi:10.3390/rs10020311
- Fourqurean, J.W., Duarte, C.M., Kennedy, H., Marbà, N., Holmer, M., Mateo, M.A., Apostolaki, E.T., Kendrick, G.A., Krause-Jensen, D., McGlathery, K.J., Serrano, O., 2012. Seagrass ecosystems as a globally significant carbon stock. *Nat. Geosci.* 5, 505–509. doi:10.1038/ngeo1477
- Fraser, B.T., Congalton, R.G., 2018. Issues in Unmanned Aerial Systems (UAS) Data Collection of Complex Forest Environments. *Remote Sens.* 10, 908. doi:10.3390/rs10060908
- Fraser, W.R., Carlson, J.C., Duley, P.A., Holm, E.J., Patterson, D.L., 1999. Using Kite-Based Aerial Photography for Conducting Adélie Penguin Censuses in Antarctica. *Waterbirds* 22, 435–440.
- Friedman, A., Pizarro, O., Williams, S.B., Johnson-Roberson, M., 2012. Multi-Scale Measures of Rugosity, Slope and Aspect from Benthic Stereo Image Reconstructions. *PLoS One* 7, e50440. doi:10.1371/journal.pone.0050440
- Fyfe, S.K., 2003. Spatial and temporal variation in spectral reflectance: Are seagrass species spectrally distinct? *Limnol. Oceanogr.* 48, 464–479. doi:10.4319/lo.2003.48.1\_part\_2.0464

- Gardner, T.A., Cote, I.M., Gill, J.A., Grant, A., Watkinson, A.R., 2005. Hurricanes and Caribbean Coral Reefs: Impacts, Recovery Patterns, and Role in Long-term Decline. *Ecology* 86, 174–184. doi:doi.org/10.1890/04-0141
- Garpe, K.C., Yahya, S.A.S., Lindahl, U., Öhman, M.C., 2006. Long-term effects of the 1998 coral bleaching event on reef fish assemblages. *Mar. Ecol. Prog. Ser.* 315, 237–247. doi:doi:10.3354/meps315237
- Geoghegan, J.L., Pirootta, V., Harvey, E., Smith, A., Buchmann, J.P., Ostrowski, M., Eden, J., Harcourt, R., Holmes, E.C., 2018. Virological Sampling of Inaccessible Wildlife with Drones. *Viruses* 10, 300. doi:10.3390/v10060300
- Getzin, S., Wiegand, K., Schöning, I., 2012. Assessing biodiversity in forests using very high-resolution images and unmanned aerial vehicles. *Methods Ecol. Evol.* 3, 397–404. doi:10.1111/j.2041-210X.2011.00158.x
- Ghermandi, A., Nunes, P.A.L.D., 2013. A global map of coastal recreation values: Results from a spatially explicit meta-analysis. *Ecol. Econ.* 86, 1–15. doi:10.1016/j.ecolecon.2012.11.006
- Giesen, W.B.J.T., van Katwijk, M.M., den Hartog, C., 1990. Eelgrass condition and turbidity in the Dutch Wadden Sea. *Aquat. Bot.* 37, 71–85. doi:10.1016/0304-3770(90)90065-S
- Goatley, C.H.R., Bellwood, D.R., 2011. The Roles of Dimensionality, Canopies and Complexity in Ecosystem Monitoring. *PLoS One* 6, e27307. doi:10.1371/journal.pone.0027307
- Goebel, M.E., Perryman, W.L., Hinke, J.T., Krause, D.J., Hann, N.A., Gardner, S., LeRoi, D.J., 2015. A small unmanned aerial system for estimating abundance and size of Antarctic predators. *Polar Biol.* 38, 619–630. doi:10.1007/s00300-014-1625-4
- Gonçalves, G.R., Pérez, J.A., Duarte, J., 2018. Accuracy and effectiveness of low cost UASs and open source photogrammetric software for foredunes mapping. *Int. J. Remote Sens.* 39, 5059–5077. doi:10.1080/01431161.2018.1446568
- Gonçalves, J.A., Henriques, R., 2015. UAV photogrammetry for topographic monitoring of coastal areas. *ISPRS J. Photogramm. Remote Sens.* 104, 101–111. doi:10.1016/j.isprsjprs.2015.02.009
- Gotceitas, V., Fraser, S., Brown, J.A., 1997. Use of eelgrass beds (*Zostera marina*) by juvenile Atlantic cod (*Gadus morhua*). *Can. J. Fish. Aquat. Sci.* 54, 1306–1319. doi:10.1139/f97-033
- Graham, N.A.J., Nash, K.L., 2013. The importance of structural complexity in coral reef ecosystems. *Coral Reefs* 32, 315–326. doi:10.1007/s00338-012-0984-y

- GRASS Development Team, 2015. Geographic Resources Analysis Support System (GRASS) 7.0.
- Gray, P.C., Ridge, J.T., Poulin, S.K., Seymour, A.C., Schwantes, A.M., Swenson, J.J., Johnston, D.W., 2018. Integrating drone imagery into high resolution satellite remote sensing assessments of estuarine environments. *Remote Sens.* 10. doi:10.3390/rs10081257
- Grech, A., Coles, R.G., 2010. An ecosystem-scale predictive model of coastal seagrass distribution. *Aquat. Conserv. Mar. Freshw. Ecosyst.* 20, 437–444. doi:10.1002/aqc.1107
- Green, E.P., Mumby, P.J., Edwards, A.J., Clark, C.D., Ellis, A.C., 1998. The Assessment of Mangrove Areas Using High Resolution Multispectral Airborne Imagery. *J. Coast. Res.* 14, 433–443.
- Greenberg, J.A., Mattiuzzi, M., 2015. gdalUtils: Wrappers for the Geospatial Data Abstraction Library (GDAL) Utilities. R package version 2.0.1.7. <https://cran.r-project.org/web/packages/gdalUtils/index.html>
- Greiner, J.T., McGlathery, K.J., Gunnell, J., McKee, B.A., 2013. Seagrass Restoration Enhances “Blue Carbon” Sequestration in Coastal Waters. *PLoS One* 8, e72469. doi:10.1371/journal.pone.0072469
- Gross, J.W., Heumann, B.W., 2016. A Statistical Examination of Image Stitching Software Packages For Use With Unmanned Aerial Systems. *Photogramm. Eng. Remote Sens.* 82, 419–425. doi:10.14358/PERS.82.6.419
- Guichard, F., Bourget, E., Agnard, J., 2000. High-resolution remote sensing of intertidal ecosystems: A low-cost technique to link scale-dependent patterns and processes. *Limnol. Oceanogr.* 45, 328–338. doi:10.4319/lo.2000.45.2.0328
- Gullström, M., Lundén, B., Bodin, M., Kangwe, J., Öhman, M.C., Mtolera, M.S.P., Björk, M., 2006. Assessment of changes in the seagrass-dominated submerged vegetation of tropical Chwaka Bay (Zanzibar) using satellite remote sensing. *Estuar. Coast. Shelf Sci.* 67, 399–408. doi:10.1016/j.ecss.2005.11.020
- Gutierrez-Heredia, L., Benzoni, F., Murphy, E., Reynaud, E.G., 2016. End to End Digitisation and Analysis of Three-Dimensional Coral Models, from Communities to Corallites. *PLoS One* 11, e0149641. doi:10.1371/journal.pone.0149641
- Halpern, B.S., Walbridge, S., Selkoe, K. a, Kappel, C. V, Micheli, F., D’Agrosa, C., Bruno, J.F., Casey, K.S., Ebert, C., Fox, H.E., Fujita, R., Heinemann, D., Lenihan, H.S., Madin, E.M.P., Perry, M.T., Selig, E.R., Spalding, M., Steneck, R., Watson, R., 2008. A global map of human impact on marine ecosystems. *Science.* 319, 948–952. doi:10.1126/science.1149345

- Hamylton, S.M., 2017. Mapping coral reef environments: A review of historical methods, recent advances and future opportunities. *Prog. Phys. Geogr.* 41, 803–833. doi:10.1177/0309133317744998
- Hamylton, S.M., Duce, S., Vila-Concejo, A., Roelfsema, C.M., Phinn, S.R., Carvalho, R.C., Shaw, E.C., Joyce, K.E., 2017. Estimating regional coral reef calcium carbonate production from remotely sensed seafloor maps. *Remote Sens. Environ.* 201, 88–98. doi:10.1016/j.rse.2017.08.034
- Han, Q., Bouma, T.J., Brun, F.G., Suykerbuyk, W., Katwijk, M.M. Van, 2012. Resilience of *Zostera noltii* to burial or erosion disturbances. *Mar. Ecol. Prog. Ser.* 449, 133–143. doi:10.3354/meps09532
- Hanley, M.E., Hoggart, S.P.G., Simmonds, D.J., Bichot, A., Colangelo, M.A., Bozzeda, F., Heurtefeux, H., Ondiviela, B., Ostrowski, R., Recio, M., Trude, R., Zawadzka-Kahlau, E., Thompson, R.C., 2014. Shifting sands? Coastal protection by sand banks, beaches and dunes. *Coast. Eng.* 87, 136–146. doi:10.1016/j.coastaleng.2013.10.020
- Haralick, R.M., Shanmugam, K., Dinstein, I., 1973. Textural Features for Image Classification. *IEEE Trans. Syst. Man. Cybern.* 3, 610–621. doi:10.1109/TSMC.1973.4309314
- Hardisty, J., 1994. Beach and nearshore sediment transport, in: Pye, K. (Ed.), *Sediment Transport and Depositional Processes*. Blackwell, London, UK, pp. 216–255.
- Harris, D.L., Rovere, A., Casella, E., Power, H., Canavesio, R., Collin, A., Pomeroy, A., Webster, J.M., Parravicini, V., 2018. Coral reef structural complexity provides important coastal protection from waves under rising sea levels. *Sci. Adv.* 4, eaao4350.
- Hartigan, J.A., Wong, M.A., 1979. Algorithm AS 136: A K-Means Clustering Algorithm. *J. R. Stat. Soc. Ser. C (Applied Stat.)* 28, 100–108. <https://doi.org/10.2307/2346101>
- Harvey, P., 2018. Exiftool: Read, Write and Edit Meta Information! Version 11. <https://www.sno.phy.queensu.ca/~phil/exiftool/>
- Hedley, J., Roelfsema, C., Koetz, B., Phinn, S., 2012. Capability of the Sentinel 2 mission for tropical coral reef mapping and coral bleaching detection. *Remote Sens. Environ.* 120, 145–155. doi:10.1016/j.rse.2011.06.028
- Hedley, J.D., Harborne, A.R., Mumby, P.J., 2005. Technical note: Simple and robust removal of sun glint for mapping shallow-water benthos. *Int. J. Remote Sens.* 26, 2107–2112. doi:10.1080/01431160500034086
- Hedley, J.D., Roelfsema, C., Brando, V., Giardino, C., Kutser, T., Phinn, S., Mumby, P.J., Barrilero, O., Laporte, J., Koetz, B., 2018. Coral reef applications of Sentinel-2: Coverage, characteristics, bathymetry and benthic mapping with comparison to Landsat 8. *Remote Sens. Environ.*

- Hedley, J.D., Roelfsema, C.M., Chollett, I., Harborne, A.R., Heron, S.F., Weeks, S.J., Skirving, W.J., Strong, A.E., Mark Eakin, C., Christensen, T.R.L., Ticzon, V., Bejarano, S., Mumby, P.J., 2016. Remote sensing of coral reefs for monitoring and management: A review. *Remote Sens.* 8, 118. doi:10.3390/rs8020118
- Hernandez, I., Peralta, G., Perez-Llorens, J.L., Vergara, J.J., 1997. Biomass and Dynamics of Growth of *Ulva* Species in Palmones River Estuary. *J. Phycol.* 33, 764–772. doi:10.1111/j.0022-3646.1997.00764.x
- Hesp, P., 2002. Foredunes and blowouts: initiation, geomorphology and dynamics. *Geomorphology* 48, 245–268. doi:10.1016/S0169-555X(02)00184-8
- Hesp, P.A., 2013. A 34 year record of foredune evolution, Dark Point, NSW, Australia. *J. Coast. Res.* 65, 1295–1300. doi:10.2112/SI65-219.1
- Hijmans, R.J., 2015. raster: Geographic Data Analysis and Modeling. R package version 2.5-2. <https://CRAN.R-project.org/package=raster>
- Hodgson, A., Kelly, N., Peel, D., 2013. Unmanned aerial vehicles (UAVs) for surveying Marine Fauna: A dugong case study. *PLoS One* 8, e79556. doi:10.1371/journal.pone.0079556
- Hodgson, J.C., Koh, L.P., 2016. Best practice for minimising unmanned aerial vehicle disturbance to wildlife in biological field research. *Curr. Biol.* 26, R404–R405. doi:10.1016/j.cub.2016.04.001
- Holmlund, C.M., Hammer, M., 1999. Ecosystem services generated by fish populations. *Ecol. Econ.* 29, 253–268. doi:doi.org/10.1016/S0921-8009(99)00015-4
- Hossain, M.S., Bujang, J.S., Zakaria, M.H., Hashim, M., 2014. The application of remote sensing to seagrass ecosystems: an overview and future research prospects. *Int. J. Remote Sens.* 36, 61–114. doi:10.1080/01431161.2014.990649
- Houser, C., Hapke, C., Hamilton, S., 2008. Controls on coastal dune morphology, shoreline erosion and barrier island response to extreme storms. *Geomorphology* 100, 223–240. doi:10.1016/j.geomorph.2007.12.007
- Huang, J., Poor, P.J., Zhao, M.I.N.Q., 2007. Economic Valuation of Beach Erosion Control. *Mar. Resour. Econ.* 22, 221–238. doi:doi.org/10.1086/mre.22.3.42629556
- Hughenoltz, C.H., Levin, N., Barchyn, T.E., Baddock, M.C., 2012. Remote sensing and spatial analysis of aeolian sand dunes: A review and outlook. *Earth Sci. Rev.* 111, 319–334. doi:10.1016/j.earscirev.2011.11.006

- Hughes, A.R., Williams, S.L., Duarte, C.M., Heck, K.L., Waycott, M., 2009. Associations of concern: declining seagrasses and threatened dependent species. *Front. Ecol. Environ.* 7, 242–246. doi:10.1890/080041
- Hughes, T.P., Anderson, K.D., Connolly, S.R., Heron, S.F., Kerry, J.T., Lough, J.M., Baird, A.H., Baum, J.K., Berumen, M.L., Bridge, T.C., Claar, D.C., Eakin, C.M., Gilmour, J.P., Graham, N.A.J., Harrison, H., Hobbs, J.A., Hoey, A.S., Hoogenboom, M., Lowe, R.J., Mcculloch, M.T., Pandolfi, J.M., Pratchett, M., Schoepf, V., Torda, G., Wilson, S.K., 2018. Spatial and temporal patterns of mass bleaching of corals in the Anthropocene. *Science*. 359, 80–83.
- Huh, O.K., Moeller, C.C., Menzel, W.P., Rouse, L.J., Roberts, H.H., 1996. Remote Sensing of Turbid Coastal and Estuarine Waters: A Method of Multispectral Water-Type Analysis. *J. Coast. Res.* 12, 984–995.
- Husson, E., Ecke, F., Reese, H., 2016. Comparison of Manual Mapping and Automated Object-Based Image Analysis of Non-Submerged Aquatic Vegetation from Very-High-Resolution UAS Images. *Remote Sens.* 8, 724. doi:10.3390/rs8090724
- Husson, E., Hagner, O., Ecke, F., 2014. Unmanned aircraft systems help to map aquatic vegetation. *Appl. Veg. Sci.* 17, 567–577. doi:10.1111/avsc.12072
- Huya-Kouadio, F., 2016. Tower. Available from the Google Play Store.
- Inoue, T., Nagai, S., Yamashita, S., Fadaei, H., Ishii, R., Okabe, K., Taki, H., Honda, Y., Kajiwara, K., Suzuki, R., 2014. Unmanned Aerial Survey of Fallen Trees in a Deciduous Broadleaved Forest in Eastern Japan. *PLoS One* 9, e109881. doi:10.1371/journal.pone.0109881
- James, M.R., Robson, S., 2014. Mitigating systematic error in topographic models derived from UAV and ground-based image networks. *Earth Surf. Process. Landforms* 39, 1413–1420. doi:10.1002/esp.3609
- James, M.R., Robson, S., D'Oleire-Oltmanns, S., Niethammer, U., 2017a. Optimising UAV topographic surveys processed with structure-from-motion: Ground control quality, quantity and bundle adjustment. *Geomorphology* 280, 51–66. doi:10.1016/j.geomorph.2016.11.021
- James, M.R., Robson, S., Smith, M.W., 2017b. 3-D uncertainty-based topographic change detection with structure-from-motion photogrammetry: precision maps for ground control and directly georeferenced surveys. *Earth Surf. Process. Landforms* 42, 1769–1788. doi:10.1002/esp.4125
- Jaxion-Harm, J., Saunders, J., Speight, M.R., 2012. Distribution of fish in seagrass, mangroves and coral reefs: Life- stage dependent habitat use in Honduras. *Rev. Biol. Trop.* 60, 683–695. doi:10.15517/rbt.v60i2.3984
- Jennerjahn, T.C., 2012. Biogeochemical response of tropical coastal systems to present and past environmental change. *Earth-Science Rev.* 114, 19–41.

doi:10.1016/j.earscirev.2012.04.005

Jensen, A., Sicard, J., 2010. '*Coordinates: A Resource on Positioning, Navigation and beyond*'. *Challenges for Positioning and Navigation in the Arctic*. [Online]. [Accessed 1 January 2017]. Available from: <http://mycoordinates.org/challenges-for-positioning-and-navigation-in-the-arctic>

Jiao, C., Zhou, D., 2014. Modeling the Spatial Distribution of *Carex pseudocuraica* in a Freshwater Marsh, Northeast China. *Wetlands* 34, 267–276. doi:10.1007/s13157-013-0496-8

Johnston, D.W., 2019. Unoccupied Aircraft Systems in Marine Science and Conservation. *Ann. Rev. Mar. Sci.* 11, 9.1-9.25. doi:doi.org/10.1146/annurev-marine-010318-095323

Jones, B.L., Unsworth, R.K.F., 2016. The perilous state of seagrass in the British Isles. *R. Soc. Open Sci.* 3, 1–14. doi:http://dx.doi.org/10.1098/rsos.150596

Jones, G.P., Pearlstine, L.G., Percival, H.F., 2006. An Assessment of Small Unmanned Aerial Vehicles for Wildlife Research. *Wildl. Soc. Bull.* 34, 750–758. doi:doi.org/10.2193/0091-7648(2006)34[750:AAOSUA]2.0.CO;2

Joyce, K.E., Duce, S., Leahy, S.M., Leon, J., Maier, S.W., 2018. Principles and practice of acquiring drone-based image data in marine environments. *Mar. Freshw. Res.* doi:doi.org/10.1071/MF17380

Ju, J., Roy, D.P., 2008. The availability of cloud-free Landsat ETM+ data over the conterminous United States and globally. *Remote Sens. Environ.* 112, 1196–1211. doi:10.1016/j.rse.2007.08.011

Kachamba, D.J., Ørka, H.O., Gobakken, T., Eid, T., Mwase, W., 2016. Biomass Estimation Using 3D Data from Unmanned Aerial Vehicle Imagery in a Tropical Woodland. *Remote Sens.* 8, 1–18. doi:10.3390/rs8110968

Kaiser, A., Neugirg, F., Rock, G., Müller, C., Haas, F., Ries, J., Schmidt, J., 2014. Small-scale surface reconstruction and volume calculation of soil erosion in complex moroccan Gully morphology using structure from motion. *Remote Sens.* 6, 7050–7080. doi:10.3390/rs6087050

Kandrot, S., Farrell, E., Devoy, R., 2016. The morphological response of foredunes at a breached barrier system to winter 2013/2014 storms on the southwest coast of Ireland. *Earth Surf. Process. Landforms* 41, 2123–2136. doi:10.1002/esp.4003

Karpouzli, E., Malthus, T., 2003. The empirical line method for the atmospheric correction of IKONOS imagery. *Int. J. Remote Sens.* 24, 1143–1150. doi:10.1080/0143116021000026779

Kay, S., Hedley, J.D., Lavender, S., 2009. Sun Glint Correction of High and Low Spatial Resolution Images of Aquatic Scenes: a Review of Methods for

Visible and Near-Infrared Wavelengths. *Remote Sens.* 1, 697–730.  
doi:10.3390/rs1040697

Kelly, I., Leon, J.X., Gilby, B.L., Olds, A.D., Schlacher, T.A., 2017. Marine turtles are not fussy nesters: a novel test of small-scale nest site selection using structure from motion beach terrain information. *PeerJ* 5, e2770.  
doi:10.7717/peerj.2770

Kendrick, G.A., Aylward, M.J., Hegge, B.J., Cambridge, M.L., Hillman, K., Wyllie, A., Lord, D.A., 2002. Changes in seagrass coverage in Cockburn Sound, Western Australia between 1967 and 1999. *Aquat. Bot.* 73, 75–87.  
doi:10.1016/S0304-3770(02)00005-0

Kennedy, H., Beggins, J., Duarte, C.M., Fourqurean, J.W., Holmer, M., Marbá, N., Middelburg, J.J., 2010. Seagrass sediments as a global carbon sink: Isotopic constraints. *Global Biogeochem. Cycles* 24, 1–8.  
doi:10.1029/2010GB003848

Kerry, J.T., Bellwood, D.R., 2015. Do tabular corals constitute keystone structures for fishes on coral reefs? *Coral Reefs* 34, 41–50.  
doi:10.1007/s00338-014-1232-4

Kilminster, K., McMahon, K., Waycott, M., Kendrick, G.A., Scanes, P., McKenzie, L., O'Brien, K.R., Lyons, M., Ferguson, A., Maxwell, P., Glasby, T., Udy, J., 2015. Unravelling complexity in seagrass systems for management: Australia as a microcosm. *Sci. Total Environ.* 534, 97–109.  
doi:10.1016/j.scitotenv.2015.04.061

Kim, M., Warner, T.A., Madden, M., Atkinson, D.S., 2011. Multi-scale GEOBIA with very high spatial resolution digital aerial imagery: scale, texture and image objects. *Int. J. Remote Sens.* 32, 2825–2850.  
doi:10.1080/01431161003745608

Kirkman, H., 1996. Baseline and monitoring methods for seagrass meadows. *J. Environ. Manage.* 47, 191–201. doi:10.1006/jema.1996.0045

Kiszka, J.J., Mourier, J., Gastrich, K., Heithaus, M.R., 2016. Using unmanned aerial vehicles (UAVs) to investigate shark and ray densities in a shallow coral lagoon 560, 237–242. doi:10.3354/meps11945

Klauser, F., Pedrozo, S., 2015. Power and space in the drone age: a literature review and politico-geographical research agenda. *Geogr. Helv.* 70, 285–293. doi:10.5194/gh-70-285-2015

Klemas, V., 2011. Remote Sensing Techniques for Studying Coastal Ecosystems: An Overview. *J. Coast. Res.* 27, 2–17.  
doi:10.2112/JCOASTRES-D-10-00103.1

Knudby, A., Ledrew, E., 2007. Measuring Structural Complexity on Coral Reefs, in: *Proceedings of the American Academy of Underwater Sciences 26th Symposium*. pp. 181–188.

- Knudby, A., Newman, C., Shaghude, Y., Muhando, C., 2010. Simple and effective monitoring of historic changes in nearshore environments using the free archive of Landsat imagery. *Int. J. Appl. Earth Obs. Geoinf.* 12, 116–122. doi:10.1016/j.jag.2009.09.002
- Koch, E., Barbier, B., Silliman, D., Reed, G., Perillo, S., Hacker, E., Granek, J., Primavera, N., Muthiga, S., Polasky, B., Halpern, C., Kennedy, C., Kappel, E., Wolanski, E., 2009. Non-linearity in ecosystem services: temporal and spatial variability in coastal protection. *Front. Ecol. Environ.* 7, 29–37. doi:10.1890/080126
- Koch, M., Bowes, G., Ross, C., Zhang, X.-H., 2013. Climate change and ocean acidification effects on seagrasses and marine macroalgae. *Glob. Chang. Biol.* 19, 103–132. doi:10.1111/j.1365-2486.2012.02791.x
- Koh, L.P., Wich, S.A., 2012. Dawn of drone ecology: low-cost autonomous aerial vehicles for conservation. *Trop. Conserv. Sci.* 5, 121–132. doi:WOS:000310846600002
- Kovalskyy, V., Roy, D.P., 2013. The global availability of Landsat 5 TM and Landsat 7 ETM+ land surface observations and implications for global 30m Landsat data product generation. *Remote Sens. Environ.* 130, 280–293. doi:10.1016/j.rse.2012.12.003
- Kutser, T., Vahtmae, E., Roelfsema, C., Metsamaa, L., 2007. Photo-library method for mapping seagrass biomass. *Estuar. Coast. Shelf Sci.* 75, 559–563. doi:10.1016/j.ecss.2007.05.043
- Lague, D., Brodu, N., Leroux, J., 2013. Accurate 3D comparison of complex topography with terrestrial laser scanner: Application to the Rangitikei canyon (N-Z). *ISPRS J. Photogramm. Remote Sens.* 82, 10–26. doi:10.1016/j.isprsjprs.2013.04.009
- Lamb, J.B., Water, J.A.J.M. Van De, Bourne, D.G., Altier, C., Hein, M.Y., Fiorenza, E.A., Abu, N., Jompa, J., Harvell, C.D., 2017. Seagrass ecosystems reduce exposure to bacterial pathogens of humans, fishes, and invertebrates. *Science*. 355, 731–733.
- Land, P.E., 2018. Glint correction algorithm. Personal Communication.
- Lauer, M., Aswani, S., 2010. Indigenous Knowledge and Long-term Ecological Change: Detection, Interpretation, and Responses to Changing Ecological Conditions in Pacific Island Communities. *Environ. Manage.* 45, 985–997. doi:10.1007/s00267-010-9471-9
- Leatherman, S.P., 1979. Beach and dune interactions during storm conditions. *Q. J. Eng. Geol. Hydrogeol.* 12, 281–290. doi:10.1144/GSL.QJEG.1979.012.04.05
- Lee, J., Jeon, J., Ihm, B., Myeong, H., 2012. The classification of biotope type and characteristics of naturalized plant habitat on the coastal sand dune

ecosystem. *J. Ecol. F. Biol.* 35, 167–175. doi:10.5141/JEFB.2012.020

- Lega, M., Kosmatka, J., Ferrara, C., Russo, F., Napoli, R.M.A., Persechino, G., 2012. Using Advanced Aerial Platforms and Infrared Thermography to Track Environmental Contamination. *Environ. Forensics* 13, 332–338. doi:10.1080/15275922.2012.729002
- Lemauviel, S., Rozé, F., 2003. Response of Three Plant Communities to Trampling in a Sand Dune System in Brittany (France). *Environ. Manage.* 31, 227–235. doi:10.1007/s00267-002-2813-5
- Leon, J., Woodroffe, C.D., 2011. Improving the synoptic mapping of coral reef geomorphology using object-based image analysis. *Int. J. Geogr. Inf. Sci.* 25, 949–969. doi:10.1080/13658816.2010.513980
- Leon, J.X., Roelfsema, C.M., Saunders, M.I., Phinn, S.R., 2015. Measuring coral reef terrain roughness using ‘Structure-from-Motion’ close-range photogrammetry. *Geomorphology* 242, 21–28. doi:10.1016/j.geomorph.2015.01.030
- Leutner, B., Horning, N., Schwalb-Willmann, J., 2018. RStoolbox: Tools for Remote Sensing Data Analysis. R package version 0.2.3. <https://CRAN.R-project.org/package=RStoolbox>
- Levin, N., Tsoar, H., Maia, L.P., Sales, V.C., Herrmann, H., 2007. Dune whitening and inter-dune freshwater ponds in NE Brazil. *Catena* 70, 1–15. doi:10.1016/j.catena.2006.06.006
- Levy, J., Hunter, C., Lukaczyk, T., Franklin, E.C., 2018. Assessing the spatial distribution of coral bleaching using small unmanned aerial systems. *Coral Reefs* 37, 373–387. doi:10.1007/s00338-018-1662-5
- Li, J., Roy, D.P., 2017. A Global Analysis of Sentinel-2A, Sentinel-2B and Landsat-8 Data Revisit Intervals and Implications for Terrestrial Monitoring. *Remote Sens.* 9, 902. doi:10.3390/rs9090902
- Liang, X., Kankare, V., Hyypä, J., Wang, Y., Kukko, A., Haggrén, H., Yu, X., Kaartinen, H., Jaakkola, A., Guan, F., Holopainen, M., Vastaranta, M., 2016. Terrestrial laser scanning in forest inventories. *ISPRS J. Photogramm. Remote Sens.* 115, 63–77. doi:10.1016/j.isprsjprs.2016.01.006
- Liquete, C., Piroddi, C., Drakou, E.G., Gurney, L., Katsanevakis, S., Charef, A., Egoh, B., 2013. Current Status and Future Prospects for the Assessment of Marine and Coastal Ecosystem Services: A Systematic Review. *PLoS One* 8, e67737. doi:10.1371/journal.pone.0067737
- Liu, P.L., Lynett, P., Fernando, H., Jaffe, B.E., Fritz, H., Higman, B., Morton, R., Goff, J., Synolakis, C., 2005. Observations by the International Tsunami Survey Team in Sri Lanka. *Science*. 308, 1595. doi:10.1126/science.1110730

- Lloyd's, 2015. Drones Take Flight (Emerging Risk Report), 2015 Innovation Series. Lloyd's.
- Lohrer, A.M., Townsend, M., Hailes, S.F., Rodil, I.F., Cartner, K., Pratt, D.R., Hewitt, J.E., 2016. Influence of New Zealand cockles (*Austrovenus stutchburyi*) on primary productivity in sandflat-seagrass (*Zostera muelleri*) ecotones. *Estuar. Coast. Shelf Sci.* 181, 238–248. doi:10.1016/j.ecss.2016.08.045
- Long, N., Millescamps, B., Guillot, B., Pouget, F., Bertin, X., 2016. Monitoring the Topography of a Dynamic Tidal Inlet Using UAV Imagery. *Remote Sens.* 8, 387. doi:10.3390/rs8050387
- Lorenz, R.D., Scheidt, S.P., 2014. Compact and inexpensive kite apparatus for geomorphological field aerial photography, with some remarks on operations. *GeoResJ* 3–4, 1–8. doi:10.1016/j.grj.2014.06.001
- Lovett, G.M., Burns, D.A., Driscoll, C.T., Jenkins, J.C., Mitchell, M.J., Rustad, L., Shanley, J.B., Likens, G.E., Haeuber, R., 2007. Who needs environmental monitoring? *Front. Ecol. Environ.* 5, 253–260. doi:10.1890/1540-9295(2007)5[253:WNEM]2.0.CO;2
- Luscier, J.D., Thompson, W.L., Wilson, J.M., Gorham, B.E., Dragut, L.D., 2006. Using digital photographs and object-based image analysis to estimate percent ground cover in vegetation plots. *Front. Ecol. Environ.* 4, 408–413. doi:10.1890/1540-9295(2006)4[408:UDPAOI]2.0.CO;2
- Lyons, M., Roelfsema, C., Kovacs, E., Samper-Villarreal, J., Saunders, M., Maxwell, P., Phinn, S., 2015. Rapid monitoring of seagrass biomass using a simple linear modelling approach, in the field and from space. *Mar. Ecol. Prog. Ser.* 530, 1–14. doi:10.3354/meps11321
- Macleod, R.D., Congalton, R.G., 1998. Quantitative comparison of change-detection algorithms for monitoring eelgrass from remotely sensed data. *Photogramm. Eng. Remote Sensing* 64, 207–216.
- Macreadie, P.I., Baird, M.E., Trevathan-Tackett, S.M., Larkum, A.W.D., Ralph, P.J., 2014. Quantifying and modelling the carbon sequestration capacity of seagrass meadows – A critical assessment. *Mar. Pollut. Bull.* 83, 430–439. doi:10.1016/j.marpolbul.2013.07.038
- Madurapperuma, B., Close, P., Fleming, S., Collin, M., Thuresson, K., Lamping, J., Dellysse, J., Cortenbach, J., 2018. Habitat Mapping of Ma-le'i Dunes Coupling with UAV and NAIP imagery. *Proceedings* 2, 368. doi:10.3390/ecrs-2-05182
- Madurapperuma, B.D., Dellysse, J.E., 2018. Coastal Fringe Habitat Monitoring using Kite Aerial Photography: A Remote Sensing-based Case Study. *J. Trop. For. Environ.* 8, 25–35. doi:10.31357/jtfe.v8i1.3480
- Malthus, T.J., Karpouzli, E., 2003. Integrating field and high spatial resolution

satellite-based methods for monitoring shallow submersed aquatic habitats in the Sound of Eriskay, Scotland, UK. *Int. J. Remote Sens.* 24, 2585–2593. doi:10.1080/0143116031000066314

- Mancini, F., Dubbini, M., Gattelli, M., Stecchi, F., Fabbri, S., Gabbianelli, G., 2013. Using Unmanned Aerial Vehicles (UAV) for High-Resolution Reconstruction of Topography: The Structure from Motion Approach on Coastal Environments. *Remote Sens.* 5, 6880–6898. doi:10.3390/rs5126880
- Marbà, N., Duarte, C.M., 2010. Mediterranean warming triggers seagrass (*Posidonia oceanica*) shoot mortality. *Glob. Chang. Biol.* 16, 2366–2375. doi:10.1111/j.1365-2486.2009.02130.x
- Martínez, M.L., Gallego-Fernández, J.B., García-Franco, J.G., Moctezuma, C., Jiménez, C.D., 2006. Assessment of coastal dune vulnerability to natural and anthropogenic disturbances along the Gulf of Mexico. *Environ. Conserv.* 33, 109–117. doi:10.1017/S0376892906002876
- Martínez, M.L., Intralawan, A., Vázquez, G., Pérez-maqueo, O., 2007. The coasts of our world: Ecological, economic and social importance. *Ecol. Econ.* 63, 254–272. doi:10.1016/j.ecolecon.2006.10.022
- Martinez, M.L., Psuty, N.P., Lubke, R.A., 2004. A perspective on coastal dunes, in: Martinez, M.L., Psuty, N.P. (Eds.), *Coastal Dunes - Ecology and Conservation*. Springer-Verlag, Berlin, pp. 3–10.
- Martins, I., Neto, J.M., Fontes, M.G., Marques, J.C., Pardal, M.A., 2005. Seasonal variation in short-term survival of *Zostera noltii* transplants in a declining meadow in Portugal. *Aquat. Bot.* 82, 132–142. doi:10.1016/j.aquabot.2005.03.006
- Marzloff, I., Poesen, J., 2009. The potential of 3D gully monitoring with GIS using high-resolution aerial photography and a digital photogrammetry system. *Geomorphology* 111, 48–60. doi:10.1016/j.geomorph.2008.05.047
- McCormick, M.I., 1994. Comparison of field methods for measuring surface topography and their associations with a tropical reef fish assemblage. *Mar. Ecol. Prog. Ser.* 112, 87–96. doi:10.3354/meps112087
- McEvoy, J.F., Hall, G.P., McDonald, P.G., 2016. Evaluation of unmanned aerial vehicle shape, flight path and camera type for waterfowl surveys: disturbance effects and species recognition. *PeerJ* 4, e1831. doi:10.7717/peerj.1831
- McGarey, P., Saripalli, S., 2014. AUTOKITE: Experimental use of a low cost autonomous kite plane for aerial photography and reconnaissance. *J. Intell. Robot. Syst.* 74, 363–370. doi:10.1007/s10846-013-9974-8
- McGlathery, K.J., Reynolds, L.K., Cole, L.W., Orth, R.J., Marion, S.R., Schwarzschild, A., 2012. Recovery trajectories during state change from

bare sediment to eelgrass dominance. *Mar. Ecol. Prog. Ser.* 448, 209–221. doi:10.3354/meps09574

McGranahan, G., Balk, D., Anderson, B., 2007. The rising tide: assessing the risks of climate change and human settlements in low elevation coastal zones. *Environ. Urban.* 19, 17–37. doi:10.1177/0956247807076960

Mckenzie, L.J., 2003. Guidelines for the rapid assessment of seagrass habitats in the western Pacific (QFS, NFC, Cairns).

Mckenzie, L.J., Campbell, S.J., Roder, C.A., 2001. Seagrass-Watch: Manual for Mapping & Monitoring Seagrass Resources by Community (citizen) volunteers. (QFS, NFC, Cairns).

Mcmanus, J.W., Reyes, R.B., Nanola Jr., C.L., 1997. Effects of Some Destructive Fishing Methods on Coral Cover and Potential Rates of Recovery. *Environ. Manage.* 21, 69–78.

Meredith, M., Carrigan, T., Brockman, J., Cloninger, T., Privoznik, J., Williams, J., 2003. Exploring Beowulf Clusters. *J. Comput. Sci. Coll.* 18, 268–284.

Merino, L., Caballero, F., Martínez-De-Dios, J.R., Maza, I., Ollero, A., 2012. An unmanned aircraft system for automatic forest fire monitoring and measurement. *J. Intell. Robot. Syst. Theory Appl.* 65, 533–548. doi:10.1007/s10846-011-9560-x

MicaSense, 2017. *Best practices: Collecting Data with MicaSense RedEdge and Parrot Sequoia*. [Online]. [Accessed 3 July 2017]. Available from: <https://support.micasense.com/hc/en-us/articles/224893167-Best-practices-Collecting-Data-with-MicaSense-RedEdge-and-Parrot-Sequoia>

Minomura, M., Kuze, H., Takeuchi, N., 2001. Adjacency effect in the atmospheric correction of satellite remote sensing data: Evaluation of the influence of aerosol extinction profiles. *Opt. Rev.* 8, 133–141. doi:10.1007/s10043-001-0133-2

Misbari, S., Hashim, M., 2016. Change Detection of Submerged Seagrass Biomass in Shallow Coastal Water. *Remote Sens.* 8, 200. doi:10.3390/rs8030200

Miyamoto, M., Yoshino, K., Nagano, T., Ishida, T., Sato, Y., 2004. Use of Balloon Aerial Photography for Classification of Kushiro Wetland Vegetation, Northeastern Japan. *Wetlands* 24, 701–710. doi:doi.org/10.1672/0277-5212(2004)024[0701:UOBAPF]2.0.CO;2

Moore, K.A., Wilcox, D.J., Orth, R.J., 2000. Analysis of the abundance of submersed aquatic vegetation communities in the Chesapeake Bay. *Estuaries* 23, 115–127. doi:10.2307/1353229

Mumby, P.J., Edwards, A.J., 2002. Mapping marine environments with IKONOS imagery: Enhanced spatial resolution can deliver greater thematic

- accuracy. *Remote Sens. Environ.* 82, 248–257. doi:10.1016/S0034-4257(02)00041-X
- Mumby, P.J., Green, E.P., Clark, C.D., Edwards, A.J., 1998. Digital analysis of multispectral airborne imagery of coral reefs. *Coral Reefs* 17, 59–69.
- Mumby, P.J., Green, E.P., Edwards, A.J., Clark, C.D., 1999. The cost-effectiveness of remote sensing for tropical coastal resources assessment and management. *J. Environ. Manage.* 55, 157–166. doi:10.1006/jema.1998.0255
- Mumby, P.J., Green, E.P., Edwards, A.J., Clark, C.D., 1997. Measurements of seagrass standing crop using satellite and digital airborne remote sensing. *Mar. Ecol. Prog. Ser.* 159, 51–60. doi:10.3354/meps159051
- Mumby, P.J., Skirving, W., Strong, A.E., Hardy, J.T., Ledrew, E.F., Hochberg, E.J., Stumpf, R.P., David, L.T., 2004. Remote sensing of coral reefs and their physical environment. *Mar. Pollut. Bull.* 48, 219–228. doi:10.1016/j.marpolbul.2003.10.031
- Murfitt, S.L., Allan, B.M., Bellgrove, A., Rattray, A., Young, M.A., Ierodiaconou, D., 2017. Applications of unmanned aerial vehicles in intertidal reef monitoring. *Sci. Rep.* 7, 1–11. doi:10.1038/s41598-017-10818-9
- Murray, J.C., Neal, M.J., Labrosse, F., 2007. Development and Deployment of an Intelligent Kite Aerial Photography Platform (iKAPP) for Site Surveying and Image Acquisition. *J. F. Robot.* 30, 288–307. doi:10.1002/rob
- Mutanga, O., Adam, E., Azong, M., 2012. High density biomass estimation for wetland vegetation using WorldView-2 imagery and random forest regression algorithm. *Int. J. Appl. Earth Obs. Geoinf.* 18, 399–406. doi:10.1016/j.jag.2012.03.012
- Myint, S.W., Gober, P., Brazel, A., Grossman-clarke, S., Weng, Q., 2011. Per-pixel vs. object-based classification of urban land cover extraction using high spatial resolution imagery. *Remote Sens. Environ.* 115, 1145–1161. doi:10.1016/j.rse.2010.12.017
- Nash, K.L., Graham, N.A.J., Wilson, S.K., Bellwood, D.R., 2013. Cross-scale Habitat Structure Drives Fish Body Size Distributions on Coral Reefs. *Ecosystems* 16, 478–490. doi:10.1007/s10021-012-9625-0
- National Trust, 2015. National Trust - Drones and unmanned aerial vehicle (UAV) - contractor checklist.
- Natural England, 2018. *St Gothian Sands LNR*. [Online]. [Accessed 10/1/18]. Available from: <https://designatedsites.naturalengland.org.uk/SiteLNRDetail.aspx?SiteCode=L1122976&SiteName=G&countyCode=6&responsiblePerson=&SeaArea=&IFCAAra=>

- Ndzi, D.L., Kamarudin, L.M., Mohammad, E.A.A., Zakaria, A., Ahmad, R.B., Fareq, M.M.A., Shakaff, A.Y.M., Jafaar, M.N., 2012. Vegetation Attenuation Measurements and Modelling In Plantations For Wireless Sensor Network Planning. *Prog. Electromagn. Res. B* 36, 283–301.
- Nedjati, A., Vizvari, B., Izbirak, G., 2016. Post-earthquake response by small UAV helicopters. *Nat. Hazards* 80, 1669–1688. doi:10.1007/s11069-015-2046-6
- Newman, S.P., Meesters, E.H., Dryden, C.S., Williams, S.M., Sanchez, C., Mumby, P.J., Polunin, N.V.C., 2015. Reef flattening effects on total richness and species responses in the Caribbean. *J. Anim. Ecol.* 84, 1678–1689. doi:10.1111/1365-2656.12429
- Nolet, C., Puijenbroek, M. Van, Suomalainen, J., Limpens, J., Riksen, M., 2018. UAV-imaging to model growth response of marram grass to sand burial: Implications for coastal dune development. *Aeolian Res.* 31, 50–61. doi:10.1016/j.aeolia.2017.08.006
- O'Connor, J., Smith, M.J., James, M.R., 2017. Cameras and settings for aerial surveys in the geosciences. *Prog. Phys. Geogr.* 41, 325–344. doi:10.1177/0309133317703092
- Oberthür, T., Cock, J., Andersson, M.S., Naranjo, R.N., Castañeda, D., Blair, M., 2007. Acquisition of low altitude digital imagery for local monitoring and management of genetic resources. *Comput. Electron. Agric.* 58, 60–77. doi:10.1016/j.compag.2006.08.005
- Oborne, M., 2016. Mission Planner. Version 1.3. Available from <http://ardupilot.org/planner/docs/mission-planner-installation.html>
- Obura, D.O., Bigot, L., Benzoni, F., 2018. Coral responses to a repeat bleaching event in Mayotte in 2010. *PeerJ* 6, e5305. doi:10.7717/peerj.5305
- Ojeda, J., Vallejo, I., Malvarez, G.C., 2005. Morphometric evolution of the active dune system of the Doñana National Park (1977-1998), Southern Spain. *J. Coast. Res.* 49, 40–45.
- Orth, R.J., Carruthers, T.J.B., Dennison, W.C., Duarte, C.M., Fourqurean, J.W., Heck, K.L., Hughes, A.R., Kendrick, G.A., Kenworthy, W.J., Olyarnik, S., Short, F.T., Waycott, M., Williams, S.L., 2006. A Global Crisis for Seagrass Ecosystems. *Bioscience* 56, 987–996. doi:10.1641/0006-3568(2006)56[987:AGCFSE]2.0.CO
- Ota, T., Ogawa, M., Shimizu, K., Kajisa, T., Mizoue, N., Yoshida, S., Takao, G., Hirata, Y., Furuya, N., Sano, T., Sokh, H., Ma, V., Ito, E., Toriyama, J., Monda, Y., Saito, H., Kiyono, Y., Chann, S., Ket, N., 2015. Aboveground Biomass Estimation Using Structure from Motion Approach with Aerial Photographs in a Seasonal Tropical Forest. *Forests* 6, 3882–3898. doi:10.3390/f6113882

- Otero, V., Van De Kerchove, R., Satyanarayana, B., Martínez-Espinosa, C., Fisol, M.A. Bin, Ibrahim, M.R. Bin, Sulong, I., Mohd-Lokman, H., Lucas, R., Dahdouh-Guebas, F., 2018. Managing mangrove forests from the sky: Forest inventory using field data and Unmanned Aerial Vehicle (UAV) imagery in the Matang Mangrove Forest Reserve, peninsular Malaysia. *For. Ecol. Manage.* 411, 35–45. doi:10.1016/j.foreco.2017.12.049
- Paneque-Gálvez, J., Mccall, M.K., Napoletano, B.M., Wich, S.A., Koh, L.P., 2014. Small Drones for Community-Based Forest Monitoring: An Assessment of Their Feasibility and Potential in Tropical Areas. *Forests* 5, 1481–1507. doi:10.3390/f5061481
- Partama, I.G.Y., Kanno, A., Ueda, M., Akamatsu, Y., Inui, R., Sekine, M., Yamamoto, K., Imai, T., Higuchi, T., 2018. Removal of water-surface reflection effects with a temporal minimum filter for UAV-based shallow-water photogrammetry. *Earth Surf. Process. Landforms.* doi:10.1002/esp.4399
- Pebesma, E.J., 2004. Multivariable geostatistics in S: The gstat package. *Comput. Geosci.* 30, 683–691. doi:10.1016/j.cageo.2004.03.012
- Pebesma, E.J., Bivand, R., 2005. Classes and methods for spatial data in R. *R News* 5, 9–13.
- Pebezm, E., Bivand, R., Rowlingson, B., Gomez-Rubio, V., Hijmans, R., Sumner, M., MacQueen, D., Lemon, J., O'Brien, J., O'Rourke, J., 2018. sp: Classes and Methods for Spatial Data. R package version 1.2-5.
- Pereira da Silva, C., Nogueira Mendes, R., Moutinho, G., Mota, V., Fonseca, C., 2016. Beach carrying capacity and protected areas: management issues in Arrábida Natural Park, Portugal. *J. Coast. Res.* 75, 680–684. doi:10.2112/SI75-136.1
- Pergent-Martini, C., Buia, M., Fernandez Torquemada, Y., 2015. *Zostera noltii*. *The IUCN Red List of Threatened Species* [Online]. [Accessed 1/6/2016]. Available from: <https://www.iucnredlist.org/species/173361/6999224>
- Perry, C.T., Edinger, E.N., Kench, P.S., Murphy, G.N., Smithers, S.G., Steneck, R.S., Mumby, P.J., 2012. Estimating rates of biologically driven coral reef framework production and erosion: A new census-based carbonate budget methodology and applications to the reefs of Bonaire. *Coral Reefs* 31, 853–868. doi:10.1007/s00338-012-0901-4
- Perry, C.T., Morgan, K.M., 2017a. Bleaching drives collapse in reef carbonate budgets and reef growth potential on southern Maldives reefs. *Sci. Rep.* 7, 40581. doi:10.1038/srep40581
- Perry, C.T., Morgan, K.M., 2017b. Post-bleaching coral community change on southern Maldivian reefs: is there potential for rapid recovery? *Coral Reefs* 36, 1189–1194. doi:10.1007/s00338-017-1610-9

- Perry, C.T., Murphy, G.N., Kench, P.S., Edinger, E.N., Smithers, S.G., Steneck, R.S., Mumby, P.J., 2014. Changing dynamics of Caribbean reef carbonate budgets: emergence of reef bioeroders as critical controls on present and future reef growth potential. *Proc. R. Soc. B Biol. Sci.* 281, 20142018.
- Philippart, C.J.M., Dijkema, K.S., 1995. Wax and wane of *Zostera noltii* Hornem in the Dutch Wadden Sea. *Aquat. Bot.* 49, 255–268. doi:10.1016/0304-3770(94)00431-K
- Phinn, S., Roelfsema, C., Dekker, A., Brando, V., Anstee, J., 2008. Mapping seagrass species, cover and biomass in shallow waters: An assessment of satellite multi-spectral and airborne hyper-spectral imaging systems in Moreton Bay (Australia). *Remote Sens. Environ.* 112, 3413–3425. doi:10.1016/j.rse.2007.09.017
- Phinn, S.R., Roelfsema, C.M., Mumby, P.J., 2012. Multi-scale, object-based image analysis for mapping geomorphic and ecological zones on coral reefs. *Int. J. Remote Sens.* 33, 3768–3797. doi:10.1080/01431161.2011.633122
- Pikelj, K., Ružić, I., Ilić, S., James, M.R., Kordić, B., 2018. Implementing an efficient beach erosion monitoring system for coastal management in Croatia. *Ocean Coast. Manag.* 156, 223–238. doi:10.1016/j.ocecoaman.2017.11.019
- Pittman, S.J., Costa, B.M., Battista, T.A., 2009. Using Lidar Bathymetry and Boosted Regression Trees to Predict the Diversity and Abundance of Fish and Corals. *J. Coast. Res.* 53, 27–38. doi:10.2112/SI53-004.1
- Pizarro, O., Friedman, A., Bryson, M., Williams, S.B., Madin, J., 2017. A simple, fast, and repeatable survey method for underwater visual 3D benthic mapping and monitoring. *Ecol. Evol.* 7, 1770–1782. doi:10.1002/ece3.2701
- Pomeroy, P., O'Connor, L., Davies, P., 2015. Assessing use of and reaction to unmanned aerial systems in gray and harbor seals during breeding and molt in the UK. *J. Unmanned Veh. Syst.* 3, 102–113. doi:10.1139/juvs-2015-0013
- Puttock, A.K., Cunliffe, A.M., Anderson, K., Brazier, R.E., 2015. Aerial photography collected with a multicopter drone reveals impact of Eurasian beaver reintroduction on ecosystem structure. *J. Unmanned Veh. Syst.* 3, 123–130. doi:10.1139/juvs-2015-0005
- Puttock, A.K., Graham, H., Cunliffe, A.M., Elliott, M., Brazier, R.E., 2017. Eurasian beaver activity increases water storage, attenuates flow and mitigates diffuse pollution from intensively-managed grasslands. *Sci. Total Environ.* 576, 430–443. doi:10.1016/j.scitotenv.2016.10.122
- R Core Team, 2017. R: A language and environment for statistical computing. Version 3.3.3

- R Core Team, 2016a. R: A language and environment for statistical computing. Version 3.1.3
- R Core Team, 2016b. R: A language and environment for statistical computing. Version 3.2.3
- Rader, A.M., Pickart, A.J., Walker, I.J., Hesp, P.A., Bauer, B.O., 2018. Fore-dune morphodynamics and sediment budgets at seasonal to decadal scales: Humboldt Bay National Wildlife Refuge, California, USA. *Geomorphology* 318, 69–87. doi:10.1016/j.geomorph.2018.06.003
- RAF, 2011. *Making Landings Safer* [Online]. [Accessed 1/2/2016]. Available from: <http://www.raf.mod.uk/news/archive.cfm?storyid=DF79349-5056-A318-A8DBA7DB432A0454>
- Rajasuriya, A., Öhman, M.C., Svensson, S., 1998. Coral and Rock Reef Habitats in Southern Sri Lanka; Patterns in the Distribution of Coral Communities. *Ambio* 27, 723–728. doi:doi.org/10.1579/0044-7447-31.7.558
- Raoult, V., Gaston, T.F., 2018. Rapid biomass and size-frequency estimates of edible jellyfish populations using drones. *Fish. Res.* 207, 160–164. doi:10.1016/j.fishres.2018.06.010
- Raoult, V., Reid-Anderson, S., Ferri, A., Williamson, J.E., 2017. How Reliable Is Structure from Motion (SfM) over Time and between Observers? A Case Study Using Coral Reef Bommies. *Remote Sens.* 9, 740. doi:10.3390/rs9070740
- Rapinel, S., Clément, B., Magnanon, S., Sellin, V., Hubert-Moy, L., 2014. Identification and mapping of natural vegetation on a coastal site using a Worldview-2 satellite image. *J. Environ. Manage.* 144, 236–246. doi:10.1016/j.jenvman.2014.05.027
- Ratcliffe, N., Guihen, D., Robst, J., Enderlein, P., 2015. A protocol for the aerial survey of penguin colonies using UAVs. *J. Unmanned Veh. Syst.* 3, 95–101.
- Reichert, J., Schellenberg, J., Schubert, P., Wilke, T., 2016. 3D scanning as a highly precise, reproducible, and minimally invasive method for surface area and volume measurements of scleractinian corals. *Limnol. Oceanogr. Methods* 14, 518–526. doi:10.1002/lom3.10109
- Richardson, L.E., Graham, N.A.J., Hoey, A.S., 2017. Cross-scale habitat structure driven by coral species composition on tropical reefs. *Sci. Rep.* 7, 7557. doi:10.1038/s41598-017-08109-4
- Ries, J.B., Marzloff, I., 2003. Monitoring of gully erosion in the Central Ebro Basin by large-scale aerial photography taken from a remotely controlled blimp. *Catena* 50, 309–328. doi:10.1016/S0341-8162(02)00133-9
- Rieucou, G., Kiszka, J.J., Carlos, J., Johann, C., Boswell, K.M., Heithaus, M.R.,

2018. Using unmanned aerial vehicle (UAV) surveys and image analysis in the study of large surface-associated marine species: a case study on reef sharks *Carcharhinus melanopterus* shoaling behaviour. *J. Fish Biol.* 93, 119–127. doi:10.1111/jfb.13645
- Robbins, B.D., 1997. Quantifying temporal change in seagrass areal coverage: The use of GIS and low resolution aerial photography. *Aquat. Bot.* 58, 259–267. doi:10.1016/S0304-3770(97)00039-9
- Robert, K., Huvenne, V.A.I., Georgiopolou, A., Jones, D.O.B., Marsh, L., Carter, D.O.G., Chaumillon, L., 2017. New approaches to high-resolution mapping of marine vertical structures. *Sci. Rep.* 7, 1–14. doi:10.1038/s41598-017-09382-z
- Roberts, C.M., McClean, C.J., E, V.J., Hawkins, J.P., Allen, G.R., McAllister, D.E., Mittermeier, C.G., Schueler, F.W., Spalding, M., Wells, F., Vynne, C., Werner, T.B., 2002. Marine Biodiversity Hotspots and Conservation Priorities for Tropical Reefs. *Science.* 295, 1280–1285.
- Roelfsema, C., Kovacs, E., Carlos, J., Wol, N.H., Callaghan, D., Wettle, M., Ronan, M., Hamylton, S.M., Mumby, P.J., Phinn, S., 2018. Coral reef habitat mapping: A combination of object-based image analysis and ecological modelling. *Remote Sens. Environ.* 208, 27–41. doi:10.1016/j.rse.2018.02.005
- Roelfsema, C., Lyons, M., Dunbabin, M., Kovacs, E.M., Phinn, S., 2015. Integrating field survey data with satellite image data to improve shallow water seagrass maps: the role of AUV and snorkeller surveys? *Remote Sens. Lett.* 6, 135–144. doi:10.1080/2150704X.2015.1013643
- Roelfsema, C., Phinn, S., Jupiter, S., Comley, J., Albert, S., 2013. Mapping coral reefs at reef to reef-system scales, 10s–1000s km<sup>2</sup>, using object-based image analysis. *Int. J. Remote Sens.* 34, 6367–6388. doi:10.1080/01431161.2013.800660
- Roelfsema, C.M., Lyons, M., Kovacs, E.M., Maxwell, P., Saunders, M.I., Samper-Villarreal, J., Phinn, S.R., 2014. Multi-temporal mapping of seagrass cover, species and biomass: A semi-automated object based image analysis approach. *Remote Sens. Environ.* 150, 172–187. doi:10.1016/j.rse.2014.05.001
- Roelvink, D., Reniers, A., van Dongeren, A., van Thiel de Vries, J., McCall, R., Lescinski, J., 2009. Modelling storm impacts on beaches, dunes and barrier islands. *Coast. Eng.* 56, 1133–1152. doi:10.1016/j.coastaleng.2009.08.006
- Rogers, A., Blanchard, J.L., Mumby, P.J., 2018. Fisheries productivity under progressive coral reef degradation. *J. Appl. Ecol.* 55, 1041–1049. doi:10.1111/1365-2664.13051
- Rogers, A., Blanchard, J.L., Mumby, P.J., 2014. Vulnerability of Coral Reef

Fisheries to a Loss of Structural Complexity. *Curr. Biol.* 24, 1000–1005.  
doi:10.1016/j.cub.2014.03.026

- Rogers, C.S., 1990. Responses of coral reefs and reef organisms to sedimentation. *Mar. Ecol. Prog. Ser.* 62, 185–202.
- Russ, G.R., Alcalá, A.C., Maypa, A.P., Calumpong, H.P., White, A.T., 2004. Marine reserve benefits local fisheries. *Ecol. Appl.* 14, 597–606.  
doi:doi.org/10.1890/03-5076
- Ryan, J.C., Hubbard, A.L., Box, J.E., Todd, J., Christoffersen, P., Carr, J.R., Holt, T.O., Snooke, N., 2015. UAV photogrammetry and structure from motion to assess calving dynamics at Store Glacier, a large outlet draining the Greenland ice sheet. *Cryosph.* 9, 1–11. doi:10.5194/tc-9-1-2015
- Ryan, J.C., Hubbard, A.L., Todd, J., Carr, J.R., Box, J.E., Christoffersen, P., Holt, T.O., Snooke, N., 2014. Repeat UAV photogrammetry to assess calving front dynamics at a large outlet glacier draining the Greenland Ice Sheet. *Cryosph. Discuss.* 8, 2243–2275. doi:10.5194/tc-9-1-2015
- Sagar, S., Roberts, D., Bala, B., Lymburner, L., 2017. Extracting the intertidal extent and topography of the Australian coastline from a 28 year time series of Landsat observations. *Remote Sens. Environ.* 195, 153–169.  
doi:10.1016/j.rse.2017.04.009
- Salameh, Z.M., Kim, B.G., 2009. Advanced Lithium Polymer Batteries, in: *Power & Energy Society General Meeting, 2009. PES '09. IEEE.*  
doi:10.1109/PES.2009.5275404
- Sallenger, A.H., Krabill, W.B., Swift, R.N., Brock, J., List, J., Hansen, M., Holman, R.A., Manizade, S., Sontag, J., Meredith, A., Morgan, K., Yunkel, J.K., Frederick, E.B., Stockdon, H., 2003. Evaluation of Airborne Topographic Lidar for Quantifying Beach Changes. *J. Coast. Res.* 19, 125–133.
- Sandbrook, C., 2015. The social implications of using drones for biodiversity conservation. *Ambio* 44, 636–647. doi:10.1007/s13280-015-0714-0
- Sander, L., 2014. Kite aerial photography (KAP) as a tool for field teaching. *J. Geogr. High. Educ.* 38, 425–430. doi:10.1080/03098265.2014.919443
- Santoro, R., Jucker, T., Prisco, I., Carboni, M., Battisti, C., Acosta, A.T.R., 2012. Effects of Trampling Limitation on Coastal Dune Plant Communities. *Environ. Manage.* 49, 534–542. doi:10.1007/s00267-012-9809-6
- Schubert, J.E., Gallien, T.W., Majd, M.S., Sanders, B.F., 2015. Terrestrial Laser Scanning of Anthropogenic Beach Berm Erosion and Overtopping. *J. Coast. Res.* 31, 47–60. doi:10.2112/JCOASTRES-D-14-00037.1
- Schweizer, D., Armstrong, R.A., Posada, J., 2005. Remote sensing characterization of benthic habitats and submerged vegetation biomass in Los Roques Archipelago National Park, Venezuela. *Int. J. Remote Sens.*

26, 2657–2667. doi:10.1080/01431160500104111

- Scoffin, T.P., 1982. Reef Aerial Photography from a Kite. *Coral Reefs* 1, 67–69. doi:10.1007/BF00286542
- Scrosati, B., Croce, F., Panero, S., 2001. Progress in lithium polymer battery R & D. *J. Power Sources* 100, 93–100.
- Seddon, S., Connolly, R.M., Edyvane, K.S., 2000. Large-scale seagrass dieback in northern Spencer Gulf, South Australia. *Aquat. Bot.* 66, 297–310. doi:10.1016/S0304-3770(99)00080-7
- Selgrath, J.C., Roelfsema, C., Gergel, S.E., Vincent, A.C.J., 2016. Mapping for coral reef conservation: Comparing the value of participatory and remote sensing approaches. *Ecosphere* 7, 1–17. doi:10.1002/ecs2.1325
- Seymour, A.C., Ridge, J.T., Rodriguez, A.B., Newton, E., Dale, J., Johnston, D.W., 2018. Deploying Fixed Wing Unoccupied Aerial Systems (UAS) for Coastal Morphology Assessment and Management. *J. Coast. Res.* 34, 704–717. doi:10.2112/JCOASTRES-D-17-00088.1
- Shalaby, A., Tateishi, R., 2007. Remote sensing and GIS for mapping and monitoring land cover and land-use changes in the Northwestern coastal zone of Egypt. *Appl. Geogr.* 27, 28–41. doi:10.1016/j.apgeog.2006.09.004
- Shaw, J.A., Nugent, P.W., Kaufman, N.A., Pust, N.J., Mikes, D., Knierim, C., Faulconer, N., Larimer, R.M., Desjardins, A.C., Knighton, W.B., 2012. Multispectral imaging systems on tethered balloons for optical remote sensing education and research. *J. Appl. Remote Sens.* 6, 063613-1-063613-11. doi:10.1117/1.JRS.6
- Sheppard, C.R.C., Davy, S.K., Pilling, G.M., Graham, N.A.J., 2018a. *The Biology of Coral Reefs*, 2nd ed. Oxford University Press.
- Sheppard, C.R.C., Davy, S.K., Pilling, G.M., Graham, N.A.J., 2018b. *The Biology of Coral Reefs*. Oxford University Press.
- Short, F.T., Burdick, D.M., 1996. Quantifying Eelgrass Habitat Loss in Relation to Housing Development and Nitrogen Loading in Waquoit Bay, Massachusetts. *Estuaries* 19, 730–739. doi:10.2307/1352532
- Short, F.T., Carruthers, T.J.R., Waycott, M., Kendrick, G.A., Fourqurean, J.W., Callabine, A., Kenworthy, W.J., Dennison, W.C., 2010. *Zostera noltii*. *The IUCN Red List of Threatened Species 2010* [Online]. [Accessed 22 November 2016]. Available from: <http://www.iucnredlist.org/details/biblio/173361/0> (accessed 11.22.16).
- Short, F.T., Neckles, H.A., 1999. The effects of global climate change on seagrasses. *Aquat. Bot.* 63, 169–196.
- Short, F.T., Polidoro, B., Livingstone, S.R., Carpenter, K.E., Bandeira, S., Bujang,

- J.S., Calumpong, H.P., Carruthers, T.J.B., Coles, R.G., Dennison, W.C., Erftemeijer, P.L.A., Fortes, M.D., Freeman, A.S., Jagtap, T.G., Kamal, A.H.M., Kendrick, G.A., Judson Kenworthy, W., La Nafie, Y.A., Nasution, I.M., Orth, R.J., Prathep, A., Sanciangco, J.C., Tussenbroek, B. van, Vergara, S.G., Waycott, M., Zieman, J.C., 2011. Extinction risk assessment of the world's seagrass species. *Biol. Conserv.* 144, 1961–1971. doi:10.1016/j.biocon.2011.04.010
- Short, F.T., Wyllie-Echeverria, S., 1996. Natural and human-induced disturbance of seagrasses. *Environ. Conserv.* 23, 17–27. doi:10.1017/S0376892900038212
- Siebert, S., Gries, D., Zhang, X., Runge, M., Buerkert, A., 2004. Non-destructive dry matter estimation of *Alhagi sparsifolia* vegetation in a desert oasis of Northwest China. *J. Veg. Sci.* 15, 365–372. doi:10.1658/1100-9233(2004)015[0365:NDMEOA]2.0.CO;2
- Sigren, J.M., Figlus, J., Highfield, W., Feagin, R.A., Armitage, A.R., 2018. The Effects of Coastal Dune Volume and Vegetation on Storm-Induced Property Damage: Analysis from Hurricane Ike. *J. Coast. Res.* 34, 164–173. doi:10.2112/JCOASTRES-D-16-00169.1
- Silver, M., 2013. *Kite Aerial Photography Picavet System - Fun, Simple, and Easy to Build! - Instructables* [Online]. [Accessed 1/4/2015]. Available from: <http://www.instructables.com/id/Kite-Aerial-Photography-Picavet-System-Fun-Simple-/?ALLSTEPS>
- Sklaver, B.A., Manangan, A., Bullard, S., Svanberg, A., Handzel, T., 2006. Technical note and Cover: Rapid imagery through kite aerial photography in a complex humanitarian emergency. *Int. J. Remote Sens.* 27, 4709–4714. doi:10.1080/01431160600784309
- Small, C., Nicholls, R.J., 2003. A global analysis of human settlement in coastal zones. *J. Coast. Res.* 19, 584–599. doi:10.2307/4299200
- Smith, A., Gares, P.A., Wasklewicz, T., Hesp, P.A., Walker, I.J., 2017. Three years of morphologic changes at a bowl blowout, Cape Cod, USA. *Geomorphology* 295, 452–466. doi:10.1016/j.geomorph.2017.07.012
- Smith, M.J., Chandler, J., Rose, J., 2009. High spatial resolution data acquisition for the geosciences: kite aerial photography. *Earth Surf. Process. Landforms* 34, 155–161. doi:10.1002/esp.1702
- Smith, M.W., Carrivick, J.L., Quincey, D.J., 2015. Structure from motion photogrammetry in physical geography. *Prog. Phys. Geogr.* 40, 1–29. doi:10.1177/0309133315615805
- Snavely, N., Seitz, S.M., Szeliski, R., 2008. Modeling the world from Internet photo collections. *Int. J. Comput. Vis.* 80, 189–210. doi:10.1007/s11263-007-0107-3

- Solazzo, D., Sankey, J.B., Sankey, T.T., Munson, S.M., 2018. Geomorphology Mapping and measuring aeolian sand dunes with photogrammetry and LiDAR from unmanned aerial vehicles (UAV) and multispectral satellite imagery on the Paria Plateau, AZ, USA. *Geomorphology* 319, 174–185. doi:10.1016/j.geomorph.2018.07.023
- Spalding, M.D., Ravilious, C., Green, E.P., 2001. *World Atlas of Coral Reefs*, First. ed. University of California Press.
- Stanisci, A., Acosta, A., Carranza, M.L., De Chiro, M., Del Vecchio, S., Di Martino, L., Frattaroli, A.R., Fusco, S., Izzi, C.F., Pirone, G., Prisco, I., 2014. EU habitats monitoring along the coastal dunes of the LTER sites of Abruzzo and Molise (Italy). *Plant Sociol.* 51, 51–56. doi:10.7338/pls2014512S1/07
- Stekoll, M.S., Deysher, L.E., Hess, M., 2006. A remote sensing approach to estimating harvestable kelp biomass. *J. Appl. Phycol.* 18, 323–334. doi:10.1007/s10811-006-9029-7
- Sterckx, S., Knaeps, E., Ruddick, K., 2011. Detection and correction of adjacency effects in hyperspectral airborne data of coastal and inland waters: the use of the near infrared similarity spectrum. *Int. J. Remote Sens.* 32, 6479–6505. doi:10.1080/01431161.2010.512930
- Stockdon, H.F., Sallenger Jr., A.H., List, J.H., Holman, R.A., 2002. Estimation of Shoreline Position and Change Using Airborne Topographic Lidar Data. *J. Coast. Res.* 18, 502–513. doi:10.2307/4299097
- Storlazzi, C.D., Dartnell, P., Hatcher, G.A., Gibbs, A.E., 2016. End of the chain? Rugosity and fine-scale bathymetry from existing underwater digital imagery using structure-from-motion (SfM) technology. *Coral Reefs* 35, 889–894. doi:10.1007/s00338-016-1462-8
- Strahler, A.H., Woodcock, C.E., Smith, J.A., 1986. On the Nature of Models in Remote Sensing. *Remote Sens. Environ.* 20, 121–139.
- Sturdivant, E.J., Lentz, E.E., Thieler, E.R., Farris, A.S., Weber, K.M., Remsen, D.P., Miner, S., Henderson, R.E., 2017. UAS-SfM for Coastal Research: Geomorphic Feature Extraction and Land Cover Classification from High-Resolution Elevation and Optical Imagery. *Remote Sens.* 9, 1020. doi:10.3390/rs9101020
- Suominen, T., Tolvanen, H., 2016. Temporal analysis of remotely sensed turbidity in a coastal archipelago. *Int. J. Appl. Earth Obs. Geoinf.* 49, 188–199. doi:10.1016/j.jag.2016.01.012
- Sykes, J.M., Horrill, A.D., Mountford, M.D., 1983. Use of Visual Cover Assessments as Quantitative Estimators of Some British Woodland Taxa. *J. Ecol.* 71, 437–450. doi:10.2307/2259726
- Tang, L., Shao, G., 2015. Drone remote sensing for forestry research and

- practices. *J. For. Res.* 26, 791–797. doi:10.1007/s11676-015-0088-y
- QGIS Development Team (2018) QGIS Geographic Information System. Open Source Geospatial Foundation Project. <http://qgis.osgeo.org>
- Teixeira, L., Hedley, J., Shapiro, A., Barker, K., 2016. Comparison of two independent mapping exercises in the Primeiras and Segundas archipelago, Mozambique. *Remote Sens.* 8, 52. doi:10.3390/rs8010052
- Thayn, J.B., 2012. Assessing vegetation cover on the date of satellite-derived start of spring. *Remote Sens. Lett.* 3, 721–728. doi:10.1080/2150704X.2012.674227
- Theriault, C., Scheibling, R., Hatcher, B., Jones, W., 2006. Mapping the distribution of an invasive marine alga (*Codium fragile* spp. *tomentosoides*) in optically shallow coastal waters using the compact airborne spectrographic imager (CASI). *Can. J. Remote Sens.* 32, 315–329. doi:doi.org/10.5589/m06-027
- Thomas, A., Byrne, D., Weatherbee, R., 2002. Coastal sea surface temperature variability from Landsat infrared data. *Remote Sens. Environ.* 81, 262–272.
- Thomsen, M.S., Wernberg, T., Engelen, A.H., Tuya, F., Mat, A., Holmer, M., Mcglathery, K.J., Arenas, F., Kotta, J., Brian, R., 2012. A Meta-Analysis of Seaweed Impacts on Seagrasses: Generalities and Knowledge Gaps. *PLoS One* 7, e28595. doi:10.1371/journal.pone.0028595
- Tittensor, D.P., Mora, C., Jetz, W., Lotze, H.K., Ricard, D., Berghe, E. Vanden, Worm, B., 2010. Global patterns and predictors of marine biodiversity across taxa. *Nature* 466, 1098–1101. doi:10.1038/nature09329
- Torres-Sánchez, J., López-Granados, F., De Castro, A.I., Peña-Barragán, J.M., 2013. Configuration and Specifications of an Unmanned Aerial Vehicle (UAV) for Early Site Specific Weed Management. *PLoS One* 8, e58210. doi:10.1371/journal.pone.0058210
- Turner, R.K., Paavola, J., Cooper, P., Farber, S., Jessamy, V., Georgiou, S., 2003. Valuing nature: lessons learned and future research directions. *Ecol. Econ.* 46, 493–510. doi:10.1016/S0921-8009(03)00189-7
- Valle, M., Borja, Á., Chust, G., Galparsoro, I., Mikel, J., 2011. Modelling suitable estuarine habitats for *Zostera noltii*, using Ecological Niche Factor Analysis and Bathymetric LiDAR. *Estuar. Coast. Shelf Sci.* 94, 144–154. doi:10.1016/j.ecss.2011.05.031
- Valle, M., Pala, V., Lafon, V., Dehouck, A., Garmendia, J.M., A, B., Chust, G., 2015. Mapping estuarine habitats using airborne hyperspectral imagery, with special focus on seagrass meadows. *Estuar. Coast. Shelf Sci.* 164, 433–442. doi:10.1016/j.ecss.2015.07.034

- Van Andel, A.C., Wich, S.A., Boesch, C., Koh, L.P.I.N., 2015. Locating Chimpanzee Nests and Identifying Fruiting Trees With an Unmanned Aerial Vehicle. *Am. J. Primatol.* 77, 1122–1134. doi:10.1002/ajp.22446
- van der Meulen, F., Bakker, T.W.M., Houston, J.A., 2004. The costs of our coasts: examples of dynamic dune management from Western Europe, in: Martinez, M.L., Psuty, N.P. (Eds.), *Coastal Dunes - Ecology and Conservation*. Springer-Verlag, Berlin, pp. 259–277.
- van Zanten, B.T., van Beukering, P.J.H., Wagtendonk, A.J., 2014. Coastal protection by coral reefs: A framework for spatial assessment and economic valuation. *Ocean Coast. Manag.* 96, 94–103. doi:10.1016/j.ocecoaman.2014.05.001
- Vas, E., Lescroël, A., Duriez, O., Boguszewski, G., Grémillet, D., 2015. Approaching birds with drones: first experiments and ethical guidelines. *Biol. Lett.* 11, 20140754. doi:doi.org/10.1098/rsbl.2014.0754
- Ventura, D., Bonifazi, A., Gravina, M.F., Belluscio, A., Ardizzone, G., 2018. Mapping and Classification of Ecologically Sensitive Marine Habitats Using Unmanned Aerial Vehicle (UAV) Imagery and Object-Based Image Analysis (OBIA). *Remote Sens.* 10, 1331. doi:10.3390/rs10091331
- Ventura, D., Bruno, M., Jona Lasinio, G., Belluscio, A., Ardizzone, G., 2016. A low-cost drone based application for identifying and mapping of coastal fish nursery grounds. *Estuar. Coast. Shelf Sci.* 171, 85–98. doi:10.1016/j.ecss.2016.01.030
- Verhoeven, G.J.J., 2009. Providing an Archaeological Bird's-Eye View - An Overall Picture of Ground-Based Means to Execute Low-Altitude Aerial Photography (LAAP) in Archaeology. *Archaeol. Prospect.* 16, 233–249. doi:10.1002/arp.354
- Wabnitz, C.C., Andréfouët, S., Torres-Pulliza, D., Müller-Karger, F.E., Kramer, P.A., 2008. Regional-scale seagrass habitat mapping in the Wider Caribbean region using Landsat sensors: Applications to conservation and ecology. *Remote Sens. Environ.* 112, 3455–3467. doi:10.1016/j.rse.2008.01.020
- Wadcock, A.J., Ewing, L.A., Solis, E., Potsdam, M., Rajagopalan, G., 2008. Rotorcraft Downwash Flow Field Study to Understand the Aerodynamics of Helicopter Brownout, in: American Helicopter Society Southwest Region Technical Specialists' Meeting, "Technologies for the Next Generation of Vertical Lift Aircraft." pp. 1–27.
- Wahidin, N., Siregar, V.P., Nababan, B., Jaya, I., 2015. Object-based image analysis for coral reef benthic habitat mapping with several classification algorithms. *Procedia Environ. Sci.* 24, 222–227. doi:10.1016/j.proenv.2015.03.029
- Wang, L., Sousa, W.P., Gong, P., Biging, G.S., 2004. Comparison of IKONOS

- and QuickBird images for mapping mangrove species on the Caribbean coast of Panama. *Remote Sens. Environ.* 91, 432–440. doi:10.1016/j.rse.2004.04.005
- Ward, D.H., Markon, C.J., Douglas, D.C., 1997. Distribution and stability of eelgrass beds at Izembek Lagoon, Alaska. *Aquat. Bot.* 58, 229–240. doi:10.1016/S0304-3770(97)00037-5
- Waycott, M., Duarte, C.M., Carruthers, T.J.B., Orth, R.J., Dennison, W.C., Olyarnik, S., Calladine, A., Fourqurean, J.W., Heck, K.L., Hughes, A.R., Kendrick, G.A., Kenworthy, W.J., Short, F.T., Williams, S.L., 2009. Accelerating loss of seagrasses across the globe threatens coastal ecosystems. *Proc. Natl. Acad. Sci. U. S. A.* 106, 12377–12381. doi:10.1073/pnas.0905620106
- Weijerman, M., Gove, J.M., Williams, I.D., Walsh, W.J., Minton, D., Polovina, J.J., 2018. Evaluating management strategies to optimise coral reef ecosystem services. *J. Appl. Ecol.* 1823–1833. doi:10.1111/1365-2664.13105
- Westoby, M.J., Brasington, J., Glasser, N.F., Hambrey, M.J., Reynolds, J.M., 2012. ‘Structure-from-Motion’ photogrammetry : A low-cost, effective tool for geoscience applications. *Geomorphology* 179, 300–314. doi:10.1016/j.geomorph.2012.08.021
- Westoby, M.J., Lim, M., Hogg, M., Pound, M.J., Dunlop, L., Woodward, J., 2018. Cost-effective erosion monitoring of coastal cliffs. *Coast. Eng.* 138, 152–164. doi:10.1016/j.coastaleng.2018.04.008
- Wickham, H. 2017. tidy: Easily Tidy Data with “spread()” and “gather()” Functions. R Package version 0.8.0. <https://cran.r-project.org/web/packages/tidy/index.html>
- Wickham, H., 2009. ggplot2: Elegant Graphics for Data Analysis. Springer-Verlag, New York.
- Wickham, H., Francois, R., 2016. dplyr: A Grammar of Data Manipulation. R Package version 0.7.5. <https://CRAN.R-project.org/package=dplyr>
- Wilding, T.A., Rose, C.A., Downie, M.J., 2007. A novel approach to measuring subtidal habitat complexity. *J. Exp. Mar. Bio. Ecol.* 353, 279–286. doi:10.1016/j.jembe.2007.10.001
- Williams, G.D., Fraser, A.D., Lucieer, A., Turner, D., Cougnon, E., Kimball, P., Toyota, T., Maksym, T., Singh, H., Nitsche, F., Paget, M., 2016. *Drones in a Cold Climate* [Online]. [Accessed 1/2/2017]. Available from: <https://eos.org/project-updates/drones-in-a-cold-climate>.
- Wobus, C., Anderson, R., Overeem, I., Matell, N., Clow, G., Urban, F., 2011. Thermal Erosion of a Permafrost Coastline: Improving Process-Based Models Using Time-Lapse Photography. *Arctic, Antarct. Alp. Res.* 43, 474–484. doi:10.1657/1938-4246-43.3.474

- Woodget, A.S., Carbonneau, P.E., Visser, F., Maddock, I.P., 2015. Quantifying submerged fluvial topography using hyperspatial resolution UAS imagery and structure from motion photogrammetry. *Earth Surf. Process. Landforms* 40, 47–64. doi:10.1002/esp.3613
- Woodget, A.S., Visser, F., Maddock, I.P., Carbonneau, P.E., 2016. The accuracy and reliability of traditional surface flow type mapping: Is it time for a new method of characterizing physical river habitat? *River Res. Appl.* 32, 1902–1914. doi:10.1002/rra.3047
- Woolard, J.W., Colby, J.D., 2002. Spatial characterization, resolution, and volumetric change of coastal dunes using airborne LIDAR: Cape Hatteras, North Carolina. *Geomorphology* 48, 269–287. doi:10.1016/S0169-555X(02)00185-X
- World Aviation Reporting Authorities 2016 [Online]. [Accessed 14 June 2016]. Available from: [http://www.airlineupdate.com/content\\_subscription/authorities/country\\_index.htm](http://www.airlineupdate.com/content_subscription/authorities/country_index.htm)
- Wundram, D., Löffler, J., 2008. High-resolution spatial analysis of mountain landscapes using a low-altitude remote sensing approach. *Int. J. Remote Sens.* 29, 961–974. doi:10.1080/01431160701352113
- Xu, J., Zhao, J., Li, F., Wang, L., Song, D., Wen, S., Wang, F., Gao, N., 2016. Object-based image analysis for mapping geomorphic zones of coral reefs in the Xisha Islands, China. *Acta Oceanol. Sin.* 35, 19–27. doi:10.1007/s13131-016-0921-y
- Yanovski, R., Nelson, P.A., Abelson, A., 2017. Structural Complexity in Coral Reefs: Examination of a Novel Evaluation Tool on Different Spatial Scales. *Front. Ecol. Evol.* 5, 1–9. doi:10.3389/fevo.2017.00027
- Yu, X., Zhang, Y., 2015. Sense and avoid technologies with applications to unmanned aircraft systems: Review and prospects. *Prog. Aerosp. Sci.* 74, 152–166. doi:10.1016/j.paerosci.2015.01.001
- Zahawi, R.A., Dandois, J.P., Holl, K.D., Nadwodny, D., Reid, J.L., Ellis, E.C., 2015. Using lightweight unmanned aerial vehicles to monitor tropical forest recovery. *Biol. Conserv.* 186, 287–295. doi:10.1016/j.biocon.2015.03.031
- Zarco-Tejada, P.J., González-Dugo, V., Berni, J.A.J., 2012. Fluorescence, temperature and narrow-band indices acquired from a UAV platform for water stress detection using a micro-hyperspectral imager and a thermal camera. *Remote Sens. Environ.* 117, 322–337. doi:10.1016/j.rse.2011.10.007
- Zhang, C., Kovacs, J.M., 2012. The application of small unmanned aerial systems for precision agriculture: a review. *Precis. Agric.* 13, 693–712. doi:10.1007/s11119-012-9274-5

- Zoffoli, M.L., Frouin, R., Kampel, M., 2014. Water Column Correction for Coral Reef Studies by Remote Sensing. *Sensors* 14, 16881–16931. doi:10.3390/s140916881
- Zvoleff, A., 2016. glcm: Calculate Textures from Grey-Level Co-Occurrence Matrices. R Package version: 1.6.1. <http://www.azvoleff.com/glcm>
- Zweig, C.L., Burgess, M.A., Percival, H.F., Kitchens, W.M., 2015. Use of Unmanned Aircraft Systems to Delineate Fine-Scale Wetland Vegetation Communities. *Wetlands* 35, 303–309. doi:10.1007/s13157-014-0612-4